

Proceedings of the  
15<sup>th</sup> International Workshop  
on Laser Ranging

*Extending the Range*

Volume 1

October 15-20, 2006  
Canberra, Australia

**Book Title**

Proceedings of the 15<sup>th</sup> International Workshop on Laser Ranging, Canberra  
Australia, October 2006 (editors J. Luck, C. Moore and P. Wilson).

**Author and Publisher**

EOS Space Systems Pty Limited  
111 Canberra Avenue  
Griffith ACT 2603  
Australia  
Telephone: + 61 2 6222 7900  
Facsimile: + 61 2 6299 7687

**First published**

Feb 2008

**Printer**

QPrint  
24 Markus Clarke St, Canberra City, ACT.  
Contact: [info@qprint.net.au](mailto:info@qprint.net.au)

---

## Sponsors

### International Laser Ranging Service



The International Laser Ranging Service (ILRS) provides global satellite and lunar laser ranging data and their related products to support geodetic and geophysical research activities as well as IERS products important to the maintenance of an accurate International Terrestrial Reference Frame (ITRF). The service develops the necessary global standards/specifications and encourages international adherence to its conventions.

Website: <http://ilrs.gsfc.nasa.gov/>

### Geoscience Australia, Australian Government



Within the portfolio of Industry, Tourism and Resources, Geoscience Australia plays a critical role by producing first-class geo-scientific information and knowledge. This can enable the government and the community to make informed decisions about the exploration of resources, the management of the environment, the safety of critical infrastructure and the resultant wellbeing of all Australians.

Website: <http://www.ga.gov.au/>

### Electro Optic Systems Pty Ltd



EOS is a public company, specialising in the design, development and production of sophisticated laser technologies, including supporting software and electronic sub-systems. EOS' advanced technologies are applied to a variety of sighting and surveillance applications in the aerospace and defence markets.

Website: <http://www.eos-aus.com>

### ACT Government



Website: <http://www.act.gov.au/>



**15<sup>th</sup> INTERNATIONAL WORKSHOP ON LASER RANGING**  
**Canberra, A.C.T., Australia**  
**15 – 21 October 2006**

**ORGANIZATION**

**Theme:** “Extending the Range”

**Venue:** Canberra Convention Centre

**PROGRAM COMMITTEE**

Ben Greene (Chair), Ramesh Govind, Hiroo Kunimori, Ron Noomen, Mike Pearlman, Peter Shelus, Mark Torrence, Georg Kirchner, Ulrich Schreiber

**LOCAL ORGANIZING COMMITTEE**

Ron Thompson (Chair), Jennifer Mullaney (Coordinator), Craig Smith, John Luck, Chris Moore, Ramesh Govind

**SESSION CHAIRS**

Opening Ceremony	Ben Greene
Science Products	Steve Klosko, Gerhard Beutler
Network Performance and Results	Cinzia Luceri, Mark Torrence
Lasers and Detectors	John Degnan, Ivan Prochazka
Altimetry	Frank Lemoine
Kilohertz Systems	Georg Kirchner, Graham Appleby
Timing Systems	Yang Fumin
Multiple Wavelength and Refraction	Erricos Pavlis
Telescopes, Stations and Upgrades	Craig Smith
Advanced Concepts and Time Transfer	Hiroo Kunimori
Transponders	Ulrich Schreiber
Uncooperative Targets	Craig Smith
Software and Automation	Jan McGarry, Werner Gurtner
LLR Systems	Tom Murphy
Targets and Return Signal Strength	Tom Murphy
Overflow	Mike Pearlman
Closing Session	Mike Pearlman

**EDITORIAL COMMITTEE**

John Luck, Chris Moore, Peter Wilson, and Session Chairs

# **PROGRAM**

## **SCIENTIFIC PROGRAM**

Monday 16	09:30	Opening Ceremony
	11:05	Science Products
Tuesday 17	09:00	Network Performance and Results
	14:00	Lasers and Detectors
	14:45	Altimetry
	16:00	Kilohertz Systems
Wednesday 18	09:00	Timing Systems
	11:15	Multiple Wavelength and Refraction
	12:00	Telescopes, Stations and Upgrades
	16:00	Advanced Concepts and Time Transfer
Thursday 17	11:00	Transponders
	12:00	Uncooperative Targets
	14:00	Software and Automation
Friday 18	09:00	LLR Systems
	09:15	Targets and Return Signal Strength
	11:00	Overflow
	14:00	ILRS General Assembly
	15:15	Closing Session

## **SPLINTER MEETINGS**

Sunday 15	15:00	Workshop Program Meeting
Monday 16	13:00	WPLTN Executive;    Eurolas General Meeting
	17:30	Data Formats and Procedures Working Group with Consolidated Predictions Format Study Group
Tuesday 17	13:00	Missions Working Group
	17:30	Refraction Study Group
	19:30	Signal Processing Study Group
Wednesday 18	13:00	Networks and Engineering Working Group with Transponders Study Group
Thursday 19	08:30	ILRS Governing Board
	13:00	WPLTN General Assembly;    T2L2 Planning Meeting
Friday 20	13:00	IERS Working Group 2;        LLR Prediction Algorithm
Saturday 21	09:00	Analysis Working Group

## **SOCIAL PROGRAM**

Sunday 15	17:30	Informal Welcome, Crowne Plaza Hotel
Monday 16	19:30	Official Reception, National Gallery of Australia
Wednesday 18	17:30	Observatory Visit and Barbecue, Mount Stromlo SLR
Thursday 19	19:30	Banquet, Old Parliament House

# TABLE OF CONTENTS

Karel Hamal Obituary <i>I Prochazka</i>	1
Preface <i>J Luck</i>	3
Foreword <i>R Thompson</i>	4
Welcome Note <i>W Gurtner</i>	5
Workshop Summary <i>M Pearlman</i>	7
<b>Science Products Session</b>	
Summary <i>S Klosko</i>	9
Enhanced Modelling of the Non-Gravitational Forces Acting on LAGEOS <i>J Andres, R Noomen</i>	12
Calibrating GNSS Orbits with SLR Tracking Data <i>C Urschl, G Beutler, W Gurtner, U Hugentobler, S Schaer</i>	23
GIOVE-A and GPS-35/36 Orbit Determination and Analysis of Dynamical Properties Based on SLR-only Tracking Data <i>S Melachroinos, F Perosanz, F Deleflie, R Biancalel, O Laurain, P Exertier</i>	27
Orbit Determination and Analysis for Giove-A using SLR Tracking Data <i>R Govind</i>	39
Orbit Determination for GIOVE-A using SLR Tracking Data <i>C Urschl, G Beutler, W Gurtner, U Hugentobler, M Ploner</i>	40
Satellite Laser Ranging in the National (Australian) Collaborative Research Infrastructure Proposal for Geospatial R&D <i>K Lambeck</i>	47
Time-Variable Gravity from SLR and DORIS Tracking <i>F Lemoine, S Klosko, C Cox, T Johnson</i>	48
Global Glacial Isostatic Adjustment: Target Fields for Space Geodesy <i>W Peltier</i>	55
Recent Results from SLR Experiments in Fundamental Physics: Frame Dragging Observed with Satellite Laser Ranging. <i>E Pavlis, I Ciufolini, R Konig</i>	69
A "Web Service" to Compare Geodetic Time Series <i>F Deleflie</i>	79
Least-Square Mean Effect: Application to the Analysis of SLR Time Series <i>D Coulot, P Berio, A Pollet</i>	80
Some Aspects Concerning the SLR Part of ITRF2005 <i>H Mueller, D Angermann</i>	91
Determination of the Temporal Variations of the Earth's Centre of Mass from Multi- Year Satellite Laser Ranging Data <i>R Govind</i>	98
Contribution of Satellite and Lunar Laser Ranging to Earth Orientation Monitoring <i>D Gambis, R Biancalel</i>	99
Station Positioning and the ITRF <i>Z Altamimi</i>	100
Station Coordinates, Earth Rotation Parameters and Low Degree Harmonics from SLR within GGOS-D <i>R Koenig, H Mueller</i>	106
An Original Approach to Compute Satellite Laser Ranging Biases <i>D Coulot, P Berio, O Laurain, D Feraudy, P Exertier</i>	110

Analysis of 13 Years (1993-2005) of Satellite Laser Ranging Data on the Two LAGEOS Satellites for Terrestrial Reference Frames and Earth Orientation Parameters <i>D Coulot, P Berio, O Laurain, D Feraudy, P Exertier, F Deleflie</i>	120
---	-----

## Network Performance and Results Session

Summary <i>C Luceri, M Torrence</i>	131
The SLR Network from a QC Perspective <i>R Noomen</i>	132
The ILRS Standard Products: a Quality Assessment <i>G Bianco, V Luceri, C Sciarretta</i>	141
Systematic Range Bias 2005-06 <i>T Otsubo, N Obara</i>	148
A Reassessment of Laser Ranging Accuracy at SGF Herstmonceux, UK <i>P Gibbs, G Appleby, C Potter</i>	154
The Global SLR Network and the Origin and Scale of the TRF in the GGOS Era <i>E Pavlis</i>	159
FTLRS Ajaccio Campaigns: Operations and Positioning Analysis over 2002/2005 <i>F Pierron, B Gourine, P Exertier, P Berio, P Bonnefond, D Coulot et al</i>	167
SLR-based Evaluation and Validation Studies of Candidate ITRF2005 Products <i>E Pavlis, M Kuzmich-Cieslak, D Pavlis</i>	173
An Optimised Global SLR Network for Terrestrial Reference Frame Definition <i>R Govind</i>	180
Performance of Southern Hemisphere Stations <i>J Luck</i>	181
The Evolution of SLR/LLR in Response to Mission Needs <i>P Shelus</i>	188
Assessment of SLR Network Performance <i>M Torrence, P Dunn</i>	189
Performance of WPLTN Stations <i>J Luck</i>	191
Archiving and Infrastructure Support at the ILRS Data Centers <i>C Noll, M Torrence, W Seemueller</i>	198
Minico Calibration of System Delay Calibration at Mount Stromlo SLR <i>J Luck</i>	202
A Summary of Observations of Giove A, taken from Mt Stromlo SLR Station <i>C Moore</i>	203

## Lasers and Detectors Session

Summary <i>J Degnan, I Prochaska</i>	210
Photon Counting Module for Laser Time Transfer Space Mission <i>K Hamal, I Prochazka, L Kral, Y Fumin</i>	211
Picosecond Lasers with Raman Frequency and Pulsewidth Conversion for Range Finding <i>N Andreev, E Grishin, O Kulagin, A Sergeev, M Valley</i>	217
Advanced Solid State Laser System for Space Tracking <i>Y Gao, Y Wang, B Greene, C Smith, A Chan, A Gray, J Vear, M Blundell</i>	222

## Altimetry Session

Summary <i>F Lemoine</i>	223
Second-Generation, Scanning, 3D Imaging Lidars Based on Photon-Counting <i>J Degnan, D Wells, R Machan, E Leventhal, D Lawrence, Y Zheng, S Mitchell, C Field, W Hasselbrack</i>	224

The BELA - The First European Planetary Laser Altimeter: Conceptional Design and Technical Status <i>H Michaelis, T Spohn, J Oberst, N Thomas, K Seiferlin, U Christensen, M Hilchenbach, U Schreiber</i>	229
Timing System for the Laser Altimeter for Planetary Exploration Technology Demonstrator <i>P Jirousek, I Prochazka, K Hamal, M Fedyszynova, U Schreiber, H Michaelis, Y Fumin, H Peicheng</i>	236
A Compact Low Power Altimetry Laser for Lunar Applications <i>T Varghese, R Burnham</i>	242
Lasercomm at Sea - Trident Warrior 06 <i>R Burris</i>	

## **Kilohertz Session**

Summary <i>G Kirchner, G Appleby</i>	243
Portable Pico Event Timer and SLR Control (P-PET-C) System <i>K Hamal, I Prochazka, Y Fumin</i>	244
Some Early Results of Kilohertz Laser Ranging at Herstmonceux <i>P Gibbs, C Potter, R Sherwood, M Wilkinson, D Benham, V Smith, G Appleby</i>	250
Performance of Liquid Crystal Optical Gate for Suppressing Laser Backscatter in Monostatic Kilohertz SLR Systems <i>J Degnan, D Caplan</i>	259
SLR2000: The Path toward Completion <i>J McGarry, T Zagwodzki</i>	265
Determination of AJISAI Spin Parameters using Graz kHz SLR Data <i>G Kirchner, W Hausleitner, E Cristea</i>	270
New Methods to Determine Gravity Probe-B Spin Parameters using Graz kHz SLR Data <i>G Kirchner, D Kucharski, E Cristea</i>	276
LAGEOS-1 Spin Determination, using Comparisons between Graz kHz SLR Data and Simulations <i>D Kucharski, G Kirchner</i>	285
Measuring Atmospheric Seeing with KHz SLR <i>G Kirchner, D Kucharski, F Koidl, J Weingrill</i>	293

## **Timing Systems Session**

Summary <i>Y Fumin</i>	299
A032-ET Experimental Test on Changchun SLR <i>C Fan, X Dong, Y Zhao, X Han</i>	300
Event Timing System for Riga SLR Station <i>Y Artyukh, V Bepal'ko, K Lapushka, A Rybakov</i>	306
Instrumentation for Creating KHz SLR Timing Systems <i>Y Artyukh, E Boole, V Vedin</i>	311
OCA Event Timer <i>E Samain, J-M Torre, D Albanese, Ph Guillemot, F Para, J Paris, I Petitbon, P Vrancken, J Weick</i>	316
The Model A032-ET of Riga Event Timers <i>V Bepal'ko, E Boole, V Vedin</i>	321
Upgrading of Integration of Time to Digit Converter on a Single FPGA <i>Y Zhang, P Huang, R Zhu</i>	327
High-Speed Enhancement to HTSI Event Timer Systems <i>D McClure, C Steggerda, S Wetzel</i>	331

Low-Noise Frequency Synthesis for High Accuracy Picosecond Satellite Laser Ranging Timing Systems <i>J Kolbl, P Sperber, G Kirchner, F Koidl</i>	338
<b>Multiple Wavelength and Refraction Session</b>	
Summary <i>E Pavlis</i>	340
Analysis of Multi-Wavelength SLR Tracking Data Using Precise Orbits <i>H Mueller</i>	341
Improvement of Current Refraction Modeling in Satellite Laser Ranging (SLR) by Ray Tracing through Meteorological Data <i>G Hulley, E Pavlis</i>	345
Two-Color Calibration of the Zimmerwald SLR System <i>W Gurtner, E Pop, J Utzinger</i>	351
Multi Color Satellite Laser Ranging <i>K Hamal, I Prochazka, J Blazej, Y Fumin, H Jingfu, Z Zhongping, H Kunimori, B Greene, G Kirchner, F Koidl, S Riepfel, W Gurtner</i>	356
<b>Telescopes, Stations and Upgrades Session</b>	
Summary <i>C Smith</i>	358
Grasse Laser Stations in Evolutions to Future and Technological Developments <i>F Pierron, E Samain, J-M Torre, M Pierron, M Furia et al</i>	359
New Russian Systems for SLR, Angular Measurements and Photometry <i>V Burmistrov, N Parkhomenko, V Shargorodsky, V Vasiliev</i>	365
TLRS-3 Return to Operations <i>H Donovan, D McCollums, D Patterson, J Horvath, M Heinick, S Wetzel, D Carter</i>	370
Korean Plan for SLR System Development <i>H-C Lim, J-U Park, S-K Jeong, B-S Kim</i>	375
Study on Servo-Control System of Astronomical Telescopes <i>Z Li, X Zheng, Y Xiong</i>	378
Russian Laser Tracking Network <i>V Burmistrov, A Fedotov, N Parkhomenko, V Pasinkov, V Shargorodsky, V Vasiliev</i>	381
TLRS-4 Deployment to Maui, Hawaii <i>S Wetzell, H Donovan, M Blount, D McCollums, C Foreman, M Heinick</i>	384
New SLR Station Running in San Juan of Argentina <i>T Wang, F Qu, Y Han, W Liu, E Actis, R Podesta</i>	390
System Improvement and GIOVE-A Observation of Changchun SLR <i>Y Zhao, C Fan, X Han, D Yang, N Chen, F Xue, L Geng, C Liu, J Shi, Z Zhang, B Shao, H Zhang, X Dong</i>	399
<b>Advanced Concepts and Time Transfer Session</b>	
Summary <i>H Kunimori</i>	405
Progress on Laser Time Transfer Project <i>Y Fumin, H Peicheng, C Wanzhen, Z Zhongping, W Yuanming, C Juping, G Fang, Z Guangnan, L Ying, I Prochazka, K Hamal</i>	406
T2L2 - Time Transfer by Laser Link <i>E Samain, Ph Guillemot, D Albanese, Ph Berio, F Deleflie, P Exertier, F Para, J Paris, I Petitbon, J-M Torre, P Vrancken, J Weick</i>	414
New Application of KHz Laser Ranging: Time Transfer via Ajisai <i>T Otsubo, H Kunimori, T Gotoh</i>	420
A Satellite Tracking Demonstration on Ground Using 100mm Aperture Optical Antenna for Space Laser Communication <i>H Kunimori, M Okawa, H Watanabe, Y Yasuda</i>	425

The NASA Satellite Laser Ranging Network: Current Status and Future Plans <i>D Carter</i>	430
Possibility of Laser Ranging Support for the Next-Generation Space VLBI Mission, ASTRO-G <i>T Otsubo, T Kubo-oka, H Saito, H Hirabayashi, T Kato, M Yoshikawa, Y Murata, Y Asaki, S Nakamura</i>	434
Electron Multiplying CCD Camera Performance Tests <i>D Lewova, M Nemeč, I Prochazka, K Hamal, G Kirchner, F Koidl, D Kucharski, Y Fumin</i>	438
LIDAR Experiments at the Space Geodesy Facility, Herstmonceux, UK <i>G Appleby, C Potter, P Gibbs, R Jones</i>	441
Possibility of the Near Earth Objects Distance Measurement with Laser Ranging Device <i>M Abele, L Osipova</i>	444
<b>Transponder Session</b>	
Summary <i>U Schreiber</i>	450
Laser Ranging at Interplanetary Distances <i>G Neumann, J Cavanaugh, B Coyle, J McGarry, D Smith, X Sun, M Torrence, T Zagwodski, M Zuber</i>	451
Simulating Interplanetary Transponder and Laser Communications Experiments via Dual Station Ranging to SLR Satellites <i>J Degnan</i>	457
Laser Ranging at Planetary Distances from SLR2000 <i>J McGarry, T Zagwodzki, P Dabney, P Dunn, J Cheek</i>	463
Laser Ranging to the Lunar Reconnaissance Orbiter (LRO) <i>D Smith, M Zuber, M Torrence, J McGarry, M Pearlman</i>	468
<b>Un-cooperative Targets Session</b>	
Summary <i>C Smith</i>	472
The Experimental Laser Ranging System for Space Debris at Shanghai <i>Y Fumin, C Wanzhen, Z Zhongping, C Juping, W Yuanming, K Hamal, I Prochazka</i>	473
Simultaneous Optical and Laser Space Objects Tracking <i>M Nemeč, I Prochazka, K Hamal, G Kirchner, F Koidl, W Voller</i>	479
<b>Software and Automation Session</b>	
Summary <i>W Gurtner, J McGarry</i>	485
A Comparison of Performance Statistics for Manual and Automated Operations at Mt. Stromlo <i>C Moore</i>	486
EOS Software Systems for Satellite Laser Ranging and General Astronomical Observatory Applications <i>M Pearson</i>	490
Electro-Control System of San Juan SLR Station <i>P Wang, T Guo, X Li, Y Han, W Liu, T Wang, F Qu, Y Tan, T Zou</i>	495
Integrated Upgrades of Control System for TROS <i>L Xin, G Tangyong, A Tong, W Peiyuan, T Yechun, X Jiening, Z Yunyao D Ruilin</i>	498
CCD and SLR Dual-use of the Zimmerwald Tracking System <i>W Gurtner, M Ploner</i>	500
Automated Transmitter Beam Size and Divergence Control in the SLR2000 System <i>J Degnan, G Jodor, H Bourges</i>	507
Obtaining the High-resolution Epoch with the FPGA Technology <i>Q Li, F Qu, Z Wei</i>	513

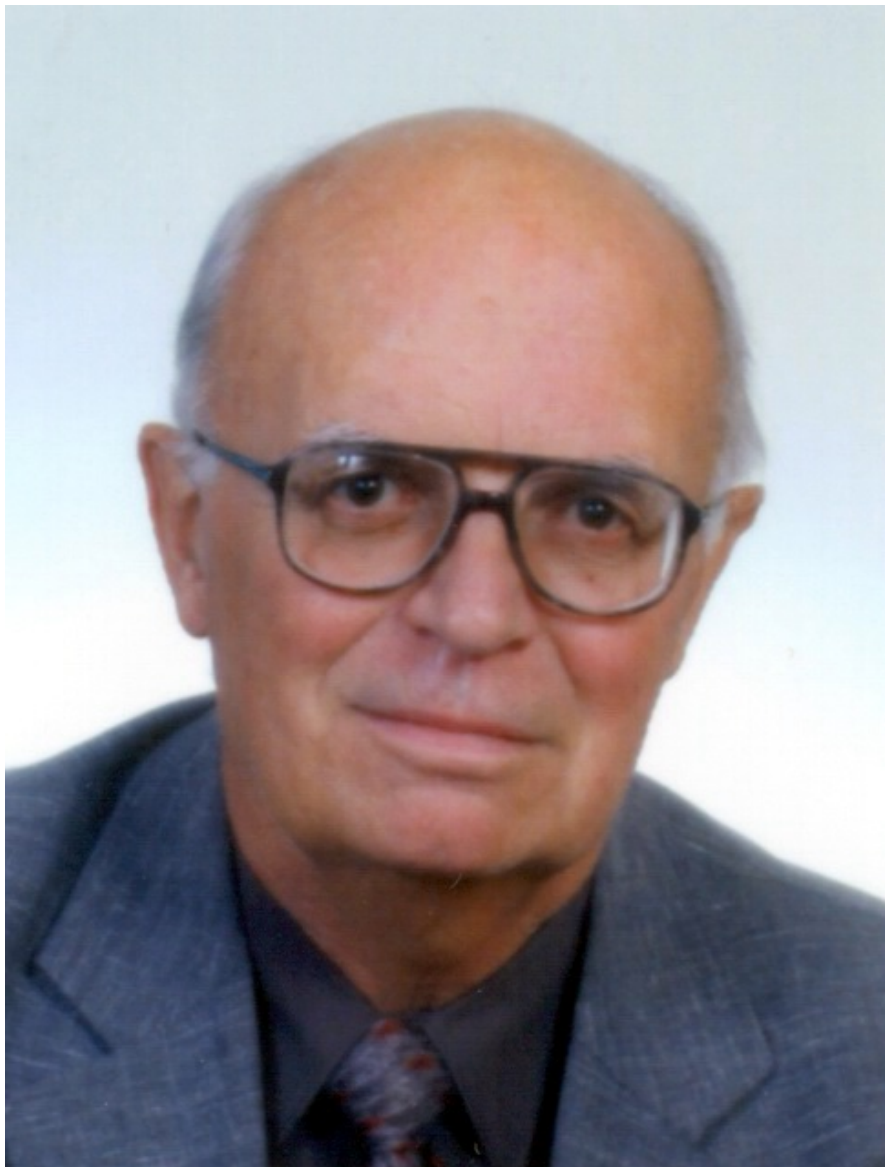
New FTLRS Software Tools for Tuning Observations Schedule and Remote Control <i>M Pierron et al</i>	516
Recursive Filter Algorithm for Noise Reduction in SLR <i>M Heiner, U Schreiber, N Brandl</i>	520
The Impact and Resolution of "Collision Bands" on Tracking Targets at Various Ranges <i>C Moore</i>	526
Web Application for the Engineering Data Files Processing <i>K Salminsh</i>	532
Consolidated Laser Prediction and Data Formats: Supporting New Technology <i>R Ricklefs</i>	535
 <b>Lunar Laser Ranging Session</b>	
Summary <i>T Murphy</i>	539
APOLLO Springs to Life: One-millimeter Lunar Laser Ranging <i>T Murphy, E Adelberger, J Battat, C Hoyle, E Michelsen, C Stubbs, H Swanson</i>	540
 <b>Targets and Return Signal Strength Session</b>	
Summary <i>T Murphy</i>	546
Retroreflector Studies <i>D Arnold</i>	547
The INFN-LNF Space Climatic Facility for LARES and ETRUSCO <i>D Arnold, G Bellettini, A Cantone, I Ciufolini, D Currie, S Dell'Agnello, G Delle-Monache, M Franceschi, M Garattini, N Intaglietta, A Lucantoni, T Napolitano, A Paolozzi, E Pavlis, R Tauraso, R Vittori</i>	550
Absolute Calibration of LLR Signal: Reflector Health Status <i>T Murphy, E Adelberger, J Battat, C Hoyle, E Michelsen, C Stubbs, H Swanson</i>	556
Experimental Return Strengths from Optus-B and GPS <i>J Luck, C Moore</i>	562
Spherical Glass Target Microsatellite <i>V Shargorodsky, V Vasiliev, M Belov, I Gashkin, N Parkhomenko</i>	566
 <b>Overflow Session</b>	
Summary <i>M Pearlman</i>	571
Current Status of "Simeiz-1873" Station <i>A Dmytrotsa, O Minin, D Neyachenko</i>	572
Overview and Performance of the Ukrainian SLR station "Lviv-1831" <i>K Martynyuk-Lototsky, J Blahodyr, A Bilinskiy, O Lohvynenko</i>	575
Results of the TLRS-4/Moblas-7 Intercomparison Test <i>J Horvath, M Blount, C Clarke, H Donovan, C Foreman, M Heinick, A Mann, D Patterson, D McCollums, T Oldham, S Wetzel, D Carter</i>	576
The Accuracy Verification for GPS Receiver of ALOS by SLR <i>N Kudo, S Nakamura, R Nakamura</i>	582
Fulfillment of SLR Daylight Tracking of Changchun Station <i>Y Zhao, X Han, C Fan, T Dai</i>	587
GLONASS Status Update and MCC Activity in GLONASS Program <i>V Glotov, S Revnivkykh, V Mitrikas</i>	593
 <b>PARTICIPANTS</b>	
Attendees	597
Group Photo 19 October 2006	600

## **Obituary**

**KAREL HAMAL, 1932 - 2007**

Professor, Czech Technical University in Prague

Passed away suddenly, 8 February 2007



Karel Hamal joined the Czech Technical University in Prague in 1962 after spending some time working for the Tesla radio communication company. His primary interests at that time were in microwaves and radar. At the university he founded the study of a newly emerging technology – solid state lasers. He established a world class laboratory and formed a team of international collaborators. This lab became world famous both for its scientific and educational results.

In the nineteen seventies and eighties he formed international ties between the Czech Technical University and scientists and labs in other countries and he headed the international network of satellite laser ranging stations under the roof of INTERKOSMOS. Satellite laser ranging was his main interest for more than three decades. He was one of the initiators of the international workshops on laser ranging and was involved in the organization of all the workshops for 35 years. The International Laser Ranging Service represented by its Central Bureau awarded Karel Hamal with the “SLR Pioneer Award” in 2002, for his longstanding contributions the subject, in particular, for his early technical leadership in developing and deploying the INTERKOSMOS systems, which helped to create a truly global satellite laser ranging network. Recently Karel Hamal was involved in research and development of solid state photon counters and their applications in laser ranging and space science, in millimeter precision laser ranging and new trends in information technology. Two deep space probes carried his laser ranging and photon counting devices toward the planet Mars late nineties, another two space mission are under completion in Europe and in China to be launched on Earth orbit soon.

Along with the science, Karel Hamal taught several generations of students Physics, ranging from MSc students, PhDs up to research scientists. In the early nineties, he was the driving force behind the reorganization of education at the university.

The passing of Karel Hamal is a significant loss for the University and to the world scientific community. Education and science are losing an expert and unparalleled organizer, the students are losing an excellent teacher and his colleagues are losing a man, who always erupted with new ideas and human energy.

We all will miss him.

*Ivan Prochazka*

---

## PREFACE

These Proceedings are dedicated to the memory of Karel Hamal, a veritable stalwart of the laser ranging community and one of its prime movers over many years. He attended every International Workshop on Laser Ranging (Instrumentation) since the first at Lagonissi, Greece in 1973. Only Mike Pearlman remains who can match that record. Karel was a great believer in these Workshops and was dynamic on many of their Program Committees. As well as being a brilliant and innovative scientist, he was also a thorough gentleman and a friend to many. Vale Karel.

This volume is being published in three forms:

1. A CD;
2. A book (paper) containing all received papers and some details of the Workshop;
3. On the Internet, most likely on:

<http://ilrs.gsfc.nasa.gov/reports/workshop/>

All papers received are included. Where authors have withdrawn their full papers, or not responded, their abstracts have been included when available.

Nearly all the PowerPoint presentations at the Workshop are available at:

<http://ilrscanberraworkshop2006.com.au>

and are useful adjuncts to the full manuscripts.

Originally, the deadline for submission of papers was set at mid-December 2006, i.e. about six weeks after the Workshop. This was hopelessly idealistic! About 60% of papers were in by the end of February, although not many from the Science Products session. It was felt that this was insufficient to proceed at that time. By 24th August, 113 papers had been received including session summaries, 6 were withdrawn by the authors and 6 were not received at all. I would like to thank the authors, especially those who submitted by the end of February, and the Session Chairs who harassed authors to submit. I also heartily thank Chris Moore, Peter Wilson, Nathan White, Ron Thompson and Jen Mullaney (and her successor, Sarah-Louise McHugh), all of EOS, for their great assistance in the production process.

A “Golden Gong” award was instituted for the last paper to be received and accepted. Several candidates were notified of their eligibility, and competition was fierce. The winner will be formally announced on a suitably sauspicious occasion. Finally, I profusely apologize to all previous editors for my own tardiness in submitting manuscripts. I can now feel that I have been adequately punished!



John Luck  
Editor

## **Foreword**

It is my pleasure to be involved in the 15th International Laser Ranging Service (ILRS) Workshop in Canberra from 15 to 20 October 2006.

This will be the second time in 30 years that Australia has hosted this prestigious meeting of space scientists. This is an honour for Canberra and for Australia, due to the leading role that Australian scientists and technologists play in this field.

I would like to thank all of you who have travelled to our shores to participate in this event, and also those who have made contributions but were not able to be here.

I would particularly like to acknowledge our sponsors whose generosity has made this Workshop possible:

ACT Government  
Geoscience Australia  
Electro Optic Systems Pty Limited

Welcome to our beautiful city. We hope you enjoy your stay and find great benefit in the Workshop discussions.



Ron Thompson  
Chair, Local Organising Committee

15th International Laser Ranging Workshop  
16-20 October 2006-10-13

**Welcome Note**

Werner Gurtner  
Chairman of the ILRS Governing Board

Dear Dr Ben Greene, dear Dr. Williams,  
ladies and gentlemen, dear colleagues,

this is the second time that I have the honor to welcome you to an international laser ranging workshop, and it is also the second time that I attend a laser workshop here in Canberra.

For me it is a special honor to attend this meeting in the country and continent with the top two laser tracking stations of our service: Yarragadee has been leading the chart for years, without danger of ever being relegated to a lower position by any other station. The most recent chart, prepared a few days ago by our Central Bureau, awards Mount Stromlo the silver medal for the number of passes collected during the previous 12 months. All our analysts are extremely pleased with this performance of the Australian stations, because it significantly attenuates the well-known weakness of our tracking network in the southern hemisphere.

We have seen several remarkable achievements since the last workshop in San Fernando, four of which I would like to address:

- With Icesat and Alos we have demonstrated that we can successfully track satellites with vulnerable sensors
- Within a year we have introduced a new orbit prediction system with significant improvements in the satellite acquisition
- We are tracking the first Galileo test satellite, Giove-A, although I think that we have to study how to improve our performance for such weak targets
- I was especially pleased to see the very efficient and fast installation and consolidation of the new Chinese station in San Juan in South America. It will further and significantly improve our coverage of the southern hemisphere.

The two space-geodetic techniques VLBI and SLR still form the basis and nucleus of any research in need of high-precision global positions, especially with regard to the referencing to the center of the earth and the height components or the scale of the earth. It is very disturbing that due to budgetary reasons major contributors to the infrastructure needed to maintain these fundamental activities decide to withdraw their support, as we have learned a few days ago from our Canadian VLBI network, and we also had such experiences in our own ranks.

It is extremely important that we can demonstrate the high quality of our products to our parent organizations to convince them of the necessity of space geodesy for modern research in earth sciences. And we have to carefully avoid any activities or statements that could send wrong signals to the external community. There has to be a

healthy competition among the different space-geodetic techniques, internally, in our groups. However, to publicly play one technique off against the another would be disastrous. We will support our sister service, the International VLBI Service, in its activities to convince the Canadian government to re-evaluate these unfavorable decisions.

I would like to thank the local organizing committee for the excellent preparations for this workshop and the sponsors without which it would not be possible to organize and hold such an event.

I wish you all a fruitful and successful workshop. Please enjoy the various activities prepared for the evenings by our hosts. Some of you may even take the opportunity to append a few days to the workshop to see more of this fascinating country.

# 15th International Workshop on Laser Ranging; Canberra, Australia

---

## Workshop Summary

Michael Pearlman

Electro Optic Systems Pty. Ltd, Geoscience Australia, the Australian Capital Territory Government, and the ILRS sponsored the 15th International Workshop on Laser Ranging in Canberra, Australia during the week of October 16 – 20, 2006. About 111 people from 19 countries participated in the workshop, which included oral and poster presentations on scientific achievements, applications and future requirements, system hardware and software, operations, advanced systems, and analysis.

After the Opening Ceremony, which featured an Aboriginal father-and-son duo welcoming delegates and distinguished guests on didgeridoos, sessions were organized around the following topics:

- Science Achievements, Applications, and Products
- Network Performance and Results
- Lasers and Detectors Session Summary
- Laser Altimetry
- Kilohertz Systems
- Timing Systems
- Multiple Wavelength and Refraction
- Telescopes, Stations, and Upgrades
- Advanced Concepts
- Eye safe Systems
- Laser Transponders
- Uncooperative Targets
- Software and Automation
- Lunar Laser Ranging
- Targets and Return Signal Strength

Some of the key items of interest were:

- Geophysical results through long-term monitoring of SLR data supporting work in gravity field, reference frame, Earth rotation, non-conservative forces on satellites, calibration of GNSS, ocean and ice surface altimetry, lunar science, relativity, and planetary science;
- New event timing systems including the new PICO event timer and control system from TU in Prague;
- Impressive performance (including spin and atmospheric measurements) of the 2 KHz laser at Graz;
- The operation of the new San Juan SLR;
- The SLR progress at Arequipa and Maui;
- Transponder developments for interplanetary ranging;
- Laser altimetry technology and its future application in satellites;

- Automated operations at Stromlo and Zimmerwald;
- Web Application for data engineering files;
- The new climatic facility at INFN for retroreflector array testing;
- Very impressive Lunar Ranging results from the Apollo Station; and
- Systematic time biases in the SR620 counters

Abstracts, most PowerPoint presentations and other information on the workshop can be found at: <http://www.ilrscanberraworkshop2006.com.au/>. Proceedings from the workshop will be available in mid-2007 on CD with selections in hardcopy, and on the web at that address and at <http://ilrs.gsfc.nasa.gov/>.

Workshop participants also had the opportunity to visit the SLR station at Mt. Stromlo which has had an extremely impressive recovery after the devastating forest fire in 2003.

The 16th International Workshop on Laser Ranging will be held in Poznan, Poland in the fall of 2008. A specialized SLR workshop similar to those held in Eastbourne and Koetting will be held in Grasse, France on 24-28 September 2007.

---

## SCIENCE PRODUCTS SESSION SUMMARY

Chairs: Steven Klosko and Gerhard Beutler

The 15th International Laser Ranging Workshop held in Canberra, Australia in October 2006 provided an overview of the state of SLR technologies, campaign activities, and science products. The Science Products Sessions began the meeting and consisted of 16 papers. These presentations demonstrated that satellite laser ranging continues to provide an important resource for satellite orbit determination, verification and validation of active remote sensing systems, and for producing science products that are needed to support a wide range of space geodesy and geodynamic investigations.

A theme of the meeting was the continued contribution of SLR to the progress being made in studying the Earth's system in four dimensions. At the same time, the SLR techniques are being used to both directly provide precision orbits and calibrate precise orbit positioning provided by other tracking systems. And by being a dynamic as opposed to reduced dynamic technique, SLR investigators have contributed significant insight into the intricate force modeling needed to produce cm-level orbit accuracy. All of these topics were discussed during the Science Products Session of the Workshop.

The first set of presentations of the session focused on the orbit determination capabilities of SLR. While GPS analyses benefit from continuous 3-D tracking, which allows "reduced" dynamic orbital techniques, SLR satellites are only observed and directly tracked for a small percentage of the time. Thereby precision orbit determination for SLR requires a high level of sophisticated conservative and non-conservative force modeling.

R. Noomen (1) gave a presentation demonstrating the state of the art in modeling the thermal imbalance and radiative forces acting on the LAGEOS 1 and 2 satellites. These satellites, given their specific design and highly stable orbits, provide an excellent laboratory to study very subtle thermal and drag-like effects acting on these orbits. The thermal perturbations acting on these satellites evolve over time as the satellite spin rate slows and the satellite experiences larger levels of thermal imbalance. R. Noomen presented results obtained at the Delft Technical University of the detailed modeling they have undertaken for the pair of LAGEOS satellites to determine the spin orientation and spin rates for the LAGEOS satellites. In the analysis they account for the complete regime of the spin behavior of the LAGEOS satellites as well as a complete description of the satellites' material composition. This has allowed them to greatly improve the orbit accuracy and fit to the SLR data while reducing the need for empirical correction parameters. SLR provides important and in many cases key independent validation capabilities for a variety of orbit applications. Herein, SLR is complementing GPS and measurements being acquired by these missions to validate orbit accuracy, detect manoeuvres, and provide a back up, fail safe orbit determination capability. Papers given by Urschl (2,5), Govind (4), and Deleflie (3) focused on SLR orbit determination applications that are being applied to study the orbits of GPS-35 and GIOVE-A.

Dedicated SLR satellite missions continue to provide unique long wavelength gravity and decadal time histories of site motions to help establish the geophysical context for many phenomena, a robust reference frame to report these changes within, and place constraints on the geophysical models themselves. Kurt Lambeck (6) gave a paper on the status and future plans for the geodetic network and geospatial modeling framework

within Australia. Australia is moving towards a highly integrated GPS, VLBI, and SLR geodetic reference and geophysical monitoring system. Currently there are two widely e-w separated SLR stations (Yarragadee and Mt Stromlo). Kurt discussed the possibility of deploying a third station in the north central part of the country co-located with VLBI near Katherine.

Contributions are coming from SLR to monitor and better understand long wavelength changes in the Earth's gravity field. Mass flux within the Earth's system over large spatial scales can be observed through the orbit changes they induce on well tracked SLR satellites. The return of the Earth to isostatic equilibrium since the time of the most recent Ice Age is a major source of nearly secular long wavelength gravity field changes. To understand the glacial mass flux apart from the total mass flux dominant over high latitude regions, detailed understanding of the Glacial Isostatic Adjustment (GIA) processes are needed. Dick Peltier of the University of Toronto gave a paper on recent refinements he has instituted to improve GIA modeling (7). Frank Lemoine (8) gave a talk on the long time history of gravity changes obtained from SLR for the longest wavelengths in the field and how they relate to GRACE. To understand contemporary ice sheet mass balance and its contribution to sea level rise, both the high latitude gravity changes and their decoupling from GIA processes are needed.

As knowledge of the long wavelength gravity field has improved, especially with advances coming from the GRACE Mission, further improvements have been made in deriving a constraint on the Lens Thirring effect. Erricos Pavlis (9) of the University of Maryland gave a paper on an improved estimate of the Lens Thirring term. This team has measured the value of this term to approximately 1% of its expected value as predicted by General Relativity. The experiment reported by Ciufolini and Pavlis was based on the long term behavior of the argument of the ascending node of the LAGEOS 1 and 2 satellites. The Lens Thirring predicted "frame-dragging" is seen as an unmodeled node signal for the LAGEOS pair. By evaluating more than eleven years of these data, these authors were able to isolate Lens Thirring from zonal gravity field error sources.

There were a set of papers focused on the reference frame, SLR contributions to the International Terrestrial Reference Frame (ITRF) and www-based tools for comparing time series from different experiments and technologies. D. Delefilie (10) of GRGS gave a presentation on a www-based tool for comparing geodetic times series. D. Coulot (11) of IGN presented a paper on different approaches to accommodate the "least squares mean effect", that is, the effect in a least squares environment of the variation of solved for parameters when a model is imposed on their behavior. H. Mueller of GFZ gave two papers (12 and 16). In the first, he discussed various experiments ongoing to compare SLR solutions using different processes and these results to VLBI and GPS. In the 2nd paper, the authors evaluated the contribution of SLR to the ITRF and presented a comparison of SLR solutions being produced at GFZ with those of IGN. Of high interest in this paper, in contrast to results described below, the GFZ Group is not seeing a scale difference from 2001 onward with their SLR solution and VLBI.

A contrasting paper was given by Z. Altamimi (15) of IGN on the construction and results he derived in computing the ITRF 2005 solution. Therein, this author found a greater than 1 ppb scale difference between SLR and VLBI, and this scale difference seemingly got progressively larger from 2001 onward. Zuheir went into considerable

detail about the use of local survey ties to bring SLR, GPS, and VLBI into a common frame.

The contrast between the IGN and GFZ results with regard to SLR scale, and the decision to use the scale provided by VLBI in the final ITRF 2005 realization caused a great deal of discussion, splinter groups, and involvement of the Analysis Centers in an attempt to better understand, resolve, and develop a strategy for utilizing the ITRF in future SLR analyses.

Also given during this portion of the session were papers by R. Govind (13) who discussed geocenter solutions he has obtained from SLR. This was followed by a paper by D. Gambis (14) of GRGS who presented results for the determination of EOP and Earth rotation using both SLR and LLR and the changing balance of contributions from all technologies over time in the combination solutions produced by IERS.

### References:

- [1] Andres, J. and R. Noomen, Enhanced modeling of the non-gravitational forces acting on LAGEOS.
- [2] Urschl, C., G. Beutler, W. Gurtner, U. Hugentobler, S. Schaer, Calibrating GNSS orbits with SLR tracking.
- [3] Deleflie, F., S. Melachroinos, F. Perosanz, O. Laurain, P. Exertier, GIOVE-A and GPS-35 satellite orbits: analysis of dynamical properties based on SLR-only tracking.
- [4] Govind, R., GIOVE-A using Satellite Laser Ranging Data.
- [5] Urschl, C., G. Beutler, W. Gurtner, U. Hugentobler, M. Ploner, Orbit determination for GIOVE-A using SLR tracking.
- [6] Lambeck, K., Satellite Laser Ranging in the National Collaborative Research Infrastructure Proposal for Geospatial R&D in Australia.
- [7] Lemoine, F., S. Klosko, C. Cox, T. Johnson, Time-variable gravity from SLR and DORIS tracking
- [8] Peltier, W., Global glacial isostatic adjustment: target field for Space Geodesy.
- [9] Pavlis, E., I. Ciufolini, R. Konig, Recent results from SLR experiments in fundamental physics.
- [10] Deleflie, F., A "web-service" to compare geodetic time series.
- [11] Coulot, D. Ph. Berio, A. Pollet, Least-squares mean effect: application to the analysis of SLR time series.
- [12] Mueller, H., D. Angermann, M. Kruegel, Some aspects concerning the SLR part of ITRF2005.
- [13] Govind, R., Determination of the temporal variations of the Earth's centre of mass from a multi-year SLR data.
- [14] Gambis, D., R. Biancale, Contribution of Satellite and Lunar Laser Ranging to Earth orientation monitoring.
- [15] Altamimi, Z., Station positioning and the ITRF.
- [16] Koenig, R. H. Mueller, Station coordinates, earth rotation parameters, and low degree harmonics from SLR with GGOS-D.

---

## Enhanced modelling of the non-gravitational forces acting on LAGEOS

J.I. Andrés<sup>1</sup>, R. Noomen<sup>1</sup>

1. Delft University of Technology, Kluyverweg 1, 2629 HS Delft, The Netherlands.

Contact: [j.i.andres@tudelft.nl](mailto:j.i.andres@tudelft.nl), [r.noomen@tudelft.nl](mailto:r.noomen@tudelft.nl)

### Abstract

*LAGEOS-I and LAGEOS-II orbit Earth since 1976 and 1992 respectively. With 426 Corner Cube Reflectors (CCRs) embedded in a spherical surface and a very low area-to-mass ratio, the LAGEOS satellites are among the best tools for global space geodetic research. By means of SLR observations, geophysical phenomena such as variations of the Terrestrial Reference Frame (TRF) origin w.r.t. the geocenter, global scale, low-degree gravity field terms, Earth Orientation Parameters (EOPs) and plate tectonic motions can be accurately measured, their accuracy directly dependent on that of the ground laser instrumentation and the accuracy of the orbit determination.*

*Intensive orbital analyses yielded a decrease in the semi-major axis of the orbit of LAGEOS-I, at a rate of 1.3 mm/d, shortly after launch; a similar decay has been observed for LAGEOS-II. Various physical processes (or a combination of them) have been proposed as possible causes for this acceleration: radiation pressure from celestial bodies (Earth and Sun) mismodeling, thermal thrust (re-radiation from the satellite itself), together with eclipse dependencies of the (re-)radiation, and ionospheric drag (neutral and charged particles). This decay can be modeled by an empirical along-track acceleration with a mean value of about  $-3.4 \text{ pm/s}^2$ . The modeling efforts done so far have given a partially successful explanation of the non-gravitational perturbations acting on LAGEOS. However, a clear signal is still present in the calculations, due to a lack of precise modeling of the (unique) physical truth.*

*This study has concentrated on an accurate modeling of the major factors which could be responsible of the unexplained signal: the geometrical and optical properties, the rotational dynamics of the spacecraft, and poorly modeled forces. Accurate results have been obtained for the rotational dynamics thus eliminating one of the largest uncertainties still present. In parallel, finite element modeling has permitted a detailed characterization of the various elements of the spacecraft, together with an accurate description of their (time-dependent) geometry w.r.t. radiation sources. This has yielded a numerical answer for the thermal accelerations for all possible spinning regimes. Uncertainties in some physical parameters have been dealt within a sensitivity analysis.*

### Introduction

Although the technique of Satellite Laser Ranging (SLR) dates back more than 40 years [Marshall *et al.*, 1995], it is still one of the main techniques to be used for studying certain elements of System Earth. In particular, global aspects of the terrestrial reference frame, such as origin and scale, are uniquely determined by this technique by virtue of its direct and unambiguous method of observation: the travel time measurements of a pulse of light from a ground station to a satellite and back are typically measurable with high precision, and the various elements that play a role in

converting these 2-way travel times into a 1-way range observation (*e.g.* satellite signature, atmospheric refraction, station delay, etcetera) can be modeled with an accuracy of various mm typically [Otsubo and Appleby, 2005]. To arrive at the best possible solutions for such global parameters, it is mandatory to model the orbit of the satellites as accurately as possible. Typically, the cannonball satellites LAGEOS-1 and LAGEOS-2 (launched in May 1976 and October 1992, respectively) are used for this purpose by virtue of their attractive area-to-mass ratio, making them relatively insensitive to (intrinsically complex to model) surface forces.

In spite of the attractive design of these spacecraft, high-precision orbit determination currently necessitates the estimation of so-called empirical accelerations (typically, in various directions w.r.t. an orbit-referenced frame and with different character – constant or sinusoidal with orbital period). This is a clear indication of the limitations of current analysis models to represent “physical truth” correctly. An illustration of this is given in Figure 1, which shows the residuals of the constant along-track acceleration as observed/estimated for the satellite LAGEOS-1, *i.e.* bi-weekly solutions of such a parameter after subtraction of best known physical mechanisms to explain the acceleration (in reality, the accelerations show a mean value of  $-3.4 \text{ pm/s}^2$ , which can be addressed to a variety of surface forces). The plot clearly illustrates that there is a signal in the residuals at the level of several  $\text{pm/s}^2$ , which needs a physical explanation in order to advance the contributions of LAGEOS-type missions to geophysical studies further. Candidates for the residuals shown here are (1) thermal radiation exerted by the satellite itself, (2) direct radiation forces, (3) charged and neutral particle drag, and others; of course shortcomings in the modeling of any of these individually, and/or a combination of effects can play a role here. This paper will focus on the so-called thermal forces: minute forces that are introduced by the emission of thermal energy by surface elements of a satellite.

First, a model for the rotational behavior of the satellites will be presented. Previous investigations by other authors show that a proper understanding and description of this aspect is crucial for a good modeling of the thermal behavior. The thermal behavior of the satellites will be the next topic of discussion, and a multi-node model of each satellite will be developed and used to simulate actual temperatures. Then, the temperature distribution will be used to compute contributions to thermal forces as exerted by individual surface elements, resulting in a total acceleration. This acceleration will be used in a first-order assessment of its orbital effect. The paper will end with conclusions and recommendations.

### **Rotational dynamics**

Compared to the orbital motion of the spacecraft, the rotational dynamics of LAGEOS-1 and -2 can be considered as a neglected element of the mission: observations of the attitude and spin rate are few, and models of the rotational behavior are hardly available. One of the reasons for this is the absence of any need for such information: the rotation dynamics plays a subtle role in the orbital behavior of the vehicles, which only come into play when the requirements on orbital accuracies arrive at the level of a single cm and below. A recently developed description of the spin behavior of the LAGEOS pair is given in [Andrés *et al.*, 2004].

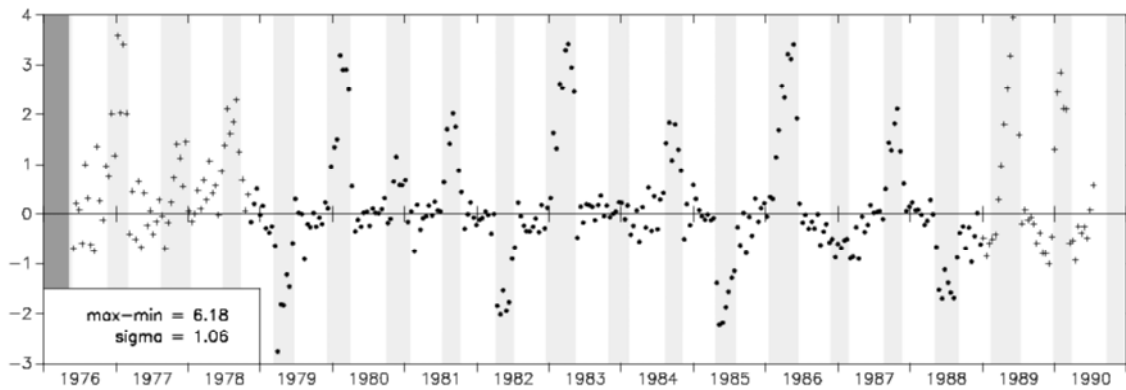


**Figure 1.** Residuals of the along-track accelerations as observed for LAGEOS-1, for the time period 1976-1990. Grey areas indicate the periods when the satellite experienced an umbra while orbiting the Earth [Scharroo *et al.*, 1991].

The LAGEOS Spin Axis Model (LOSSAM) that is developed in this reference is based on a straightforward integration of Euler's equation:

$$\frac{d\vec{L}}{dt} = \vec{M}_{magn} + \vec{M}_{grav} + \vec{M}_{offset} + \vec{M}_{reflec}$$

Here, the external torques represent the influence of the Earth's magnetic field, gravity, a possible difference between the center-of-pressure w.r.t. the center-of-mass, and a possible difference in effective reflectivity between the northern and southern hemisphere of the satellites, respectively. LOSSAM has been obtained after confrontation of the theoretical model as described by the previous equation with independent observations on spin-axis orientation and spin rate taken by a variety of stations and institutes: (i) University of Maryland, USA, (ii) the laser station in Herstmonceux, UK (owned by the Natural Environment Research Council, NERC), (iii) the laser station in Matera, Italy (owned by the Agenzia Spaziale de Italia, ASI) and (iv) Lincoln Laboratory [Sullivan, 1980]. Figures 2 and 3 show the behavior of the spin axis orientation of LAGEOS-1 and -2 according to LOSSAM, respectively (spin rate results are withheld here). The plots also show the independent observations that were used in the derivation of the model, and the level of fit. Clearly visible is that LAGEOS-1 is in a different rotational regime currently than LAGEOS-2: the spin-axis orientation of the former satellite follows a more irregular pattern, which is due to a slowing down from a rotational period of 10.5 s at launch (1976) to about 6000 s now (Figure 2). LAGEOS-2 is still spinning with a period of about 360 s currently. Also visible is the fact that the set of observations on the spin axis that is available for LAGEOS-1 is quite restricted: the last ones were taken at the end of 1996, and effectively one cannot do but make predictions of the current behavior of the satellite; the absence of recent observations is directly related to the fact that the rotation of LAGEOS-1 has almost come to a standstill, which makes it extremely difficult to actually apply currently practiced observation techniques on spin axis orientation and rotation rate. For LAGEOS-2, the situation is much better (cf. Figure 3). The reader is referred to [Andrés *et al.*, 2004] for more details.

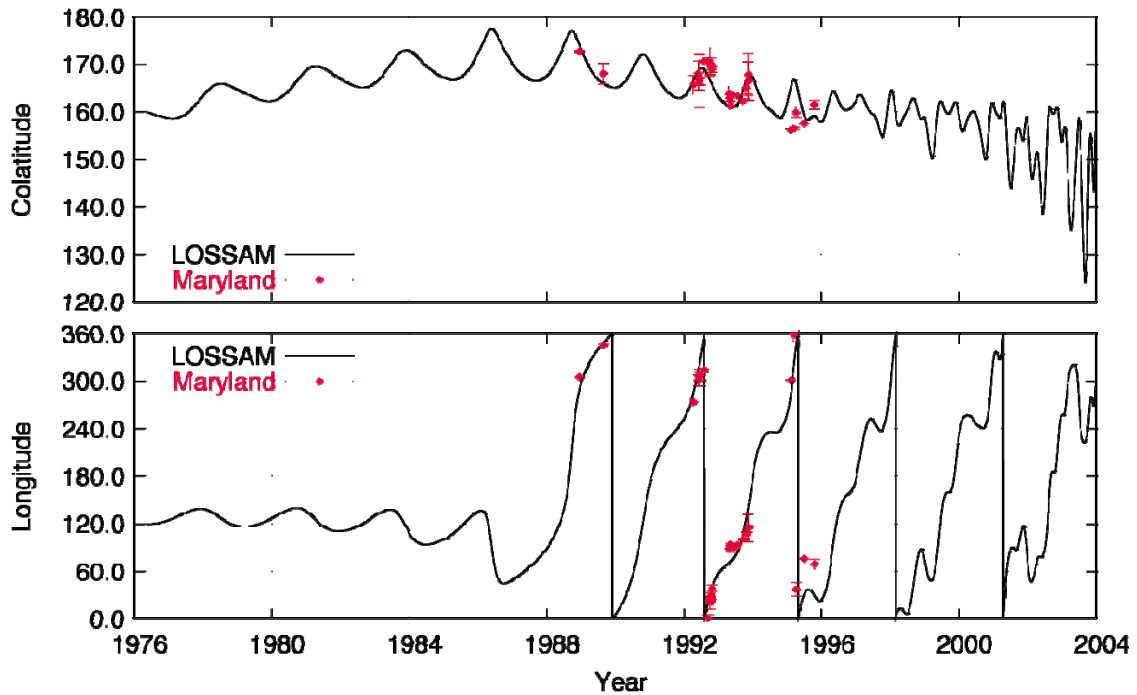


**Figure 2.** The LOSSAM spin orientation behavior of LAGEOS-1 as a function of time, as described by the longitude and co-latitude w.r.t. the J2000 reference frame. The red symbols represent the independent observations that were used to derive this model [Andrés et al., 2004].

### Thermal model

Thermal forces, *i.e.* forces that are generated somehow by either direct or reflected radiation, are known to play an important role in the explanation of the observed decay of the semi-major axis of the LAGEOS pair and, directly related to this, of the solutions for the empirical accelerations; many studies have been done into the effects of direct solar radiation (Yarkovsky effect), albedo radiation, earth infrared radiation, the effect of eclipses (Yarkovsky-Schach effect), etcetera (*e.g.* [Rubincam, 1982], [Anselmo et al., 1983], [Barlier et al., 1986], [Rubincam, 1987a], [Rubincam, 1987b], [Afonso et al., 1989], [Rubincam, 1990], [Martin and Rubincam, 1996], [Slabinski, 1997] and [Vokrouhlický and Métris, 2004]). However, none of these investigations has led to a full description and complete understanding of the actual phenomena that influence the orbital behavior of the LAGEOS satellites; if only because simplifications had to be made in order to arrive at first-order estimates of the effects. Clearly, in view of the slow rotation of LAGEOS-1 and a similar trend for LAGEOS-2, the necessity for a more detailed modeling of the satellite and its interaction with various elements in its environment has arisen. As mentioned in the introduction, this paper addresses one of those elements: the thermal interaction with the various radiation sources, and the resulting accelerations. A detailed discussion of procedures, models and results is given in [Andrés et al., 2006].

To model the interaction in detail, making allowance for potential differences in its reaction to various sources of energy, the satellite model needs to be split up into a number of different components. In recognition of the various mechanisms that are effectively responsible for heat transfer (*i.e.* radiation and conduction; any other can be shown to be insignificant [Andrés et al., 2006]) and the differences in thermal and mechanical properties of the various construction elements, a finite-element model of each LAGEOS satellite has been created, with 2133 elements in total: the inner core

(core and stud), two hemispheres, and 426 retroreflector assemblies each consisting of 5 elements: a retainer ring, an upper ring, a corner-cube reflector, a set of ring posts, and a lower ring.

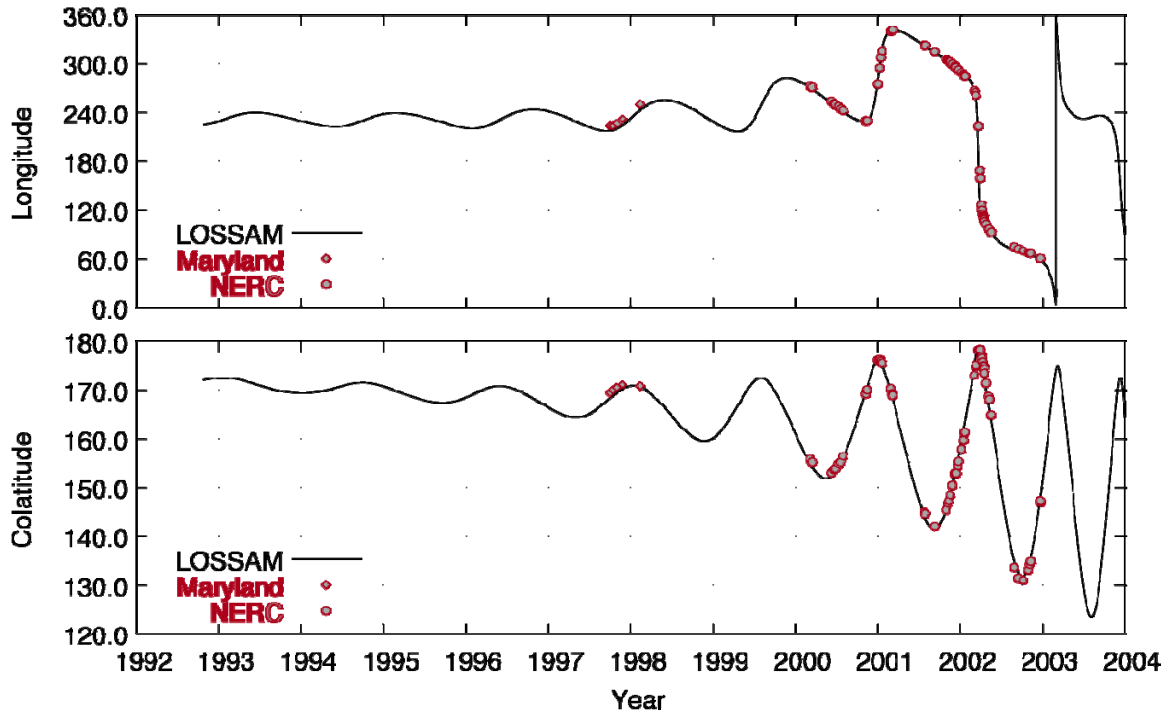


**Figure 3.** The LOSSAM spin orientation behavior of LAGEOS-2 as a function of time, as described by the longitude and co-latitude w.r.t. the J2000 reference frame. The red symbols represent the independent observations that were used to derive this model [Andrés *et al.*, 2004].

For each LAGEOS element  $i$ , the following (abstract) heat equation can be written:

$$H_i \frac{\partial T_i}{\partial t} = Q_{in} - Q_{out}$$

For more details, see [Andrés *et al.*, 2006]. In combination with cm-level accurate solutions for the orbital motion of the satellites (obtained with GEODYN [Pavlis *et al.*, 1998], the positions of sources of radiative energy (Sun, Earth), models for these radiative flows, models for the thermal and mechanical properties of the spacecraft components, and the LOSSAM model for the rotational behavior of the spacecraft [Andrés *et al.*, 2004] this equation can be integrated over time for each element to yield the thermal behavior of each individual element. This has been done for both satellites from the date of launch onwards, with a step-size of 60 s, and taking care that allowance is made for aspects like shadowing, aliasing (when the rotational period and the integration step size are integer multiples) and rotationally averaged radiation input. An illustration of the result is given in Figure 4, which shows the temperature distribution of the various elements of LAGEOS-1 and -2 for the (arbitrary) epoch January 1, 2002, respectively. The plots clearly show the different temperatures of the Germanium reflectors (3 out of 4 are visible in each plot; the thermal absorption and emission coefficients are very different from the quantities for the 422 Silicium reflectors), and, in a similar fashion, the different temperatures for

the retainer rings. In the case of LAGEOS-1 (Figure 4, left), the Sun is more-or-less located over the satellites equator, resulting in a similar temperature for the northern and the southern hemispheres. In the case of LAGEOS-2 (Figure 4, right), the Sun is at an apparent latitude of about  $45^\circ$ , with a higher temperature for the northern hemisphere as a consequence.

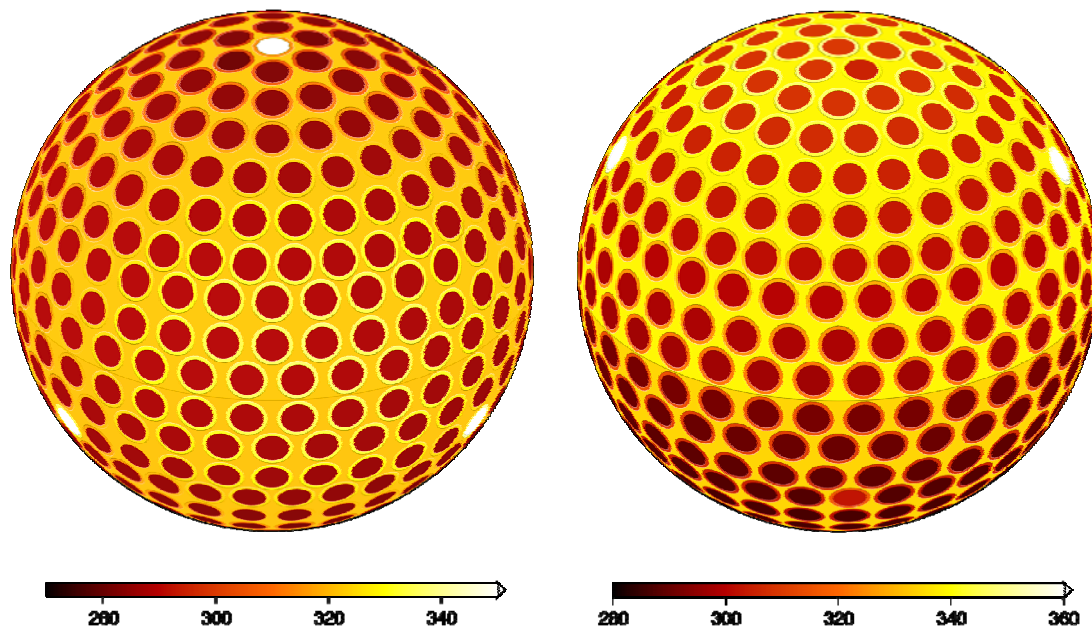


**Figure 4.** Temperature distribution on January 1, 2002, for LAGEOS-1 and -2, respectively. All values are in Kelvin [Andrés *et al.*, 2006].

As an illustration, Figure 5 shows the long-term temperature behavior for a number of elements of LAGEOS-1; a similar behavior has been derived for LAGEOS-2 (not included here; cf. [Andrés *et al.*, 2006]). Figure 5(a) shows the temperatures for representative retainer rings and a Silicon CCR in the northern hemisphere. By virtue of its thermal properties, the CCR has an average temperature which is some 20 K lower than that of the retainer rings. All elements show a variation with time, which is correlated with the occurrence of solar eclipses (indicated by grey bands) and the position of the Sun (the main source of energy) w.r.t. the satellite spin axis; in the case of reflector assembly 89, which is located at a (satellite-fixed) co-latitude of about  $58^\circ$ , temperature variations are relatively humble, but after about 10 years in orbit the attitude of the spacecraft starts to develop into an erratic behavior w.r.t.  $\lambda$  and the spin rate drops off, resulting in extreme temperature variations for the retainer ring located at the satellite's north pole. A similar observation can be made for the retainer rings and the reflectors located in the southern hemisphere of the satellite (Figure 5(b)): the CCRs are typically cooler, show less variation, and big excursions of up to 60 K are visible for the retainer rings closer to the pole (in this case the south pole of the satellite). Figure 5(c), finally, very clearly illustrates the sensitivity of the Germanium CCRs to the actual lighting conditions: the 3 Ge CCRs that are located at co-latitude  $121^\circ$ , show a temperature variation of about 50 K (already large when compared to the behavior of the Si CCRs, cf. Figure 5(a)), but the situation appears to change dramatically for the CCR located at the very north pole of LAGEOS-1: temperature variations of up to 300 K are observed here.

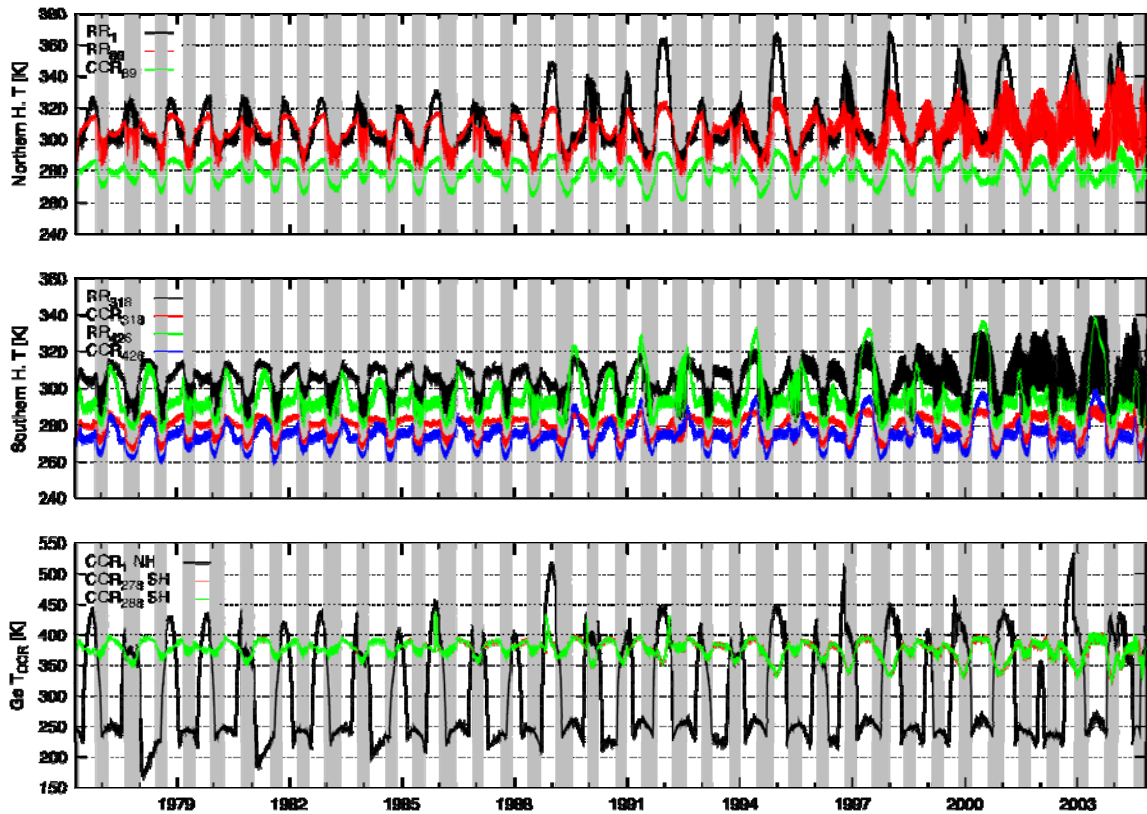


Figure 5. Temperature behavior of several retainer rings and CCRs for LAGEOS-1 since launch [Andrés et al., 2006].

### Accelerations

Having arrived at a time-series of temperatures for the 2133 elements of each LAGEOS finite-element model, it is possible to derive values for the force that each element exerts (cf. [Slabinski, 1997]):

$$d\vec{F}_i = -\frac{2}{3} \frac{\varepsilon_i \sigma T_i^4}{c} dA_i \vec{n}_i$$

Integration of all contributions from all surface elements (clearly, internal elements do not contribute) yields the net thermal acceleration that each satellite experiences. An illustration of that is given in Figure 6: accelerations in the radial, along-track and cross-track directions for one day for LAGEOS-1 and LAGEOS-2, respectively; the right-hand side of the plots zooms in for a particular orbit during that day. It is clearly visible that for both satellites, radial and along-track accelerations of up to 50 pm/s<sup>2</sup> can be obtained (the two follow one another by virtue of the rotation of the orbital, satellite-related reference frame); much larger than the average value of about -3.4 pm/s<sup>2</sup> that is seen in the empirical (constant) accelerations. Since the cross-track orientation of the orbit remains more-or-less constant during one day, this component shows much less of a variation (but can have a very significant value). The plots indicate that an irregular behavior occurs in particular during times of eclipse; in such a situation, the cause for an uneven heating of the satellite disappears (ignoring any

influence from the Earth, that is) and the net acceleration tends to develop towards zero.

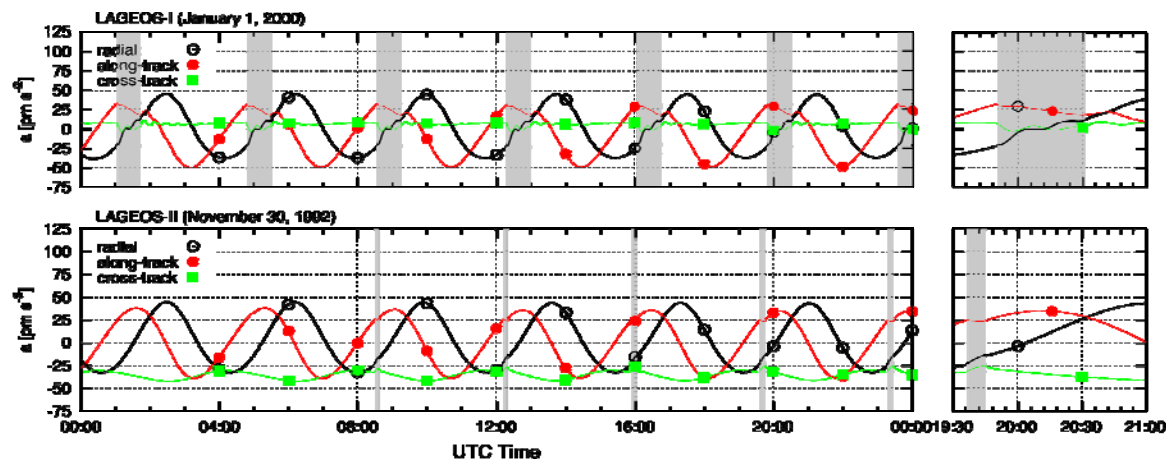


**Figure 6.** Net thermal accelerations for (top) LAGEOS-1 on January 1, 2000, and (bottom) LAGEOS-2 on November 30, 1992. The grey bands indicate the exact periods when the satellites are in eclipse [Andrés et al., 2006].

Extending the presentation to the full lifetime of the satellites (so far), Figure 7 shows the development of the net accelerations as well as the orientation of the Sun in a satellite frame, for each LAGEOS version. Again, the grey bands indicate when eclipses occur (somewhere in the orbit). Starting the discussion with LAGEOS-2 (Figure 7(b)), the long-term behavior is in line with what was shown in Figure 6 already: radial and along-track components interchange by virtue of the definition of the orbital frame, and the variation of the cross-track component is slower. All LAGEOS-2 components have values that go up to about  $50 \text{ pm/s}^2$ . In the situation that the Sun is located in the equatorial plane of the satellite (i.e.  $\beta_{\text{Sun-SA}}$  is equal to  $90^\circ$ ), all 3 components of the net acceleration are effectively zero (by virtue of the rapid rotation of LAGEOS-2). As for LAGEOS-1, a similar story holds (Figure 7(a)), albeit that the relations are a bit more difficult to observe because of the longer time-span covered since launch. Also visible are the larger values for the net accelerations after about 1990, which is due to the specific rotational behavior of the spacecraft (with consequences for the temperature of particular elements of the satellite; cf. Figure 5). Although not included here explicitly, it can be shown that the model for the rotational behavior of the satellites plays a crucial role: net accelerations computed with the LOSSAM model (which is regarded as the state-of-the-art representation of the actual rotational behavior) differ by an amount of about  $25 \text{ pm/s}^2$  with the results that would have been obtained with a more traditional (i.e. constant) model for the spin axis [Andrés et al., 2006].

### Orbit computations

As a very first test of the actual usefulness of the results, two types of orbital computations have been done for LAGEOS-2 only (the choice of this satellite is arbitrary). First, weekly orbital fits have been computed using a model that does not include any external acceleration, and in which the solar radiation pressure force scaling parameter  $C_R$  is estimated only (in addition to the state-vector at epoch). Second, similar computations have been done but now with inclusion of the thermal

accelerations as derived by the procedures sketched above (and keeping them fixed at their nominal values). Computations were done for the period October 1993 until

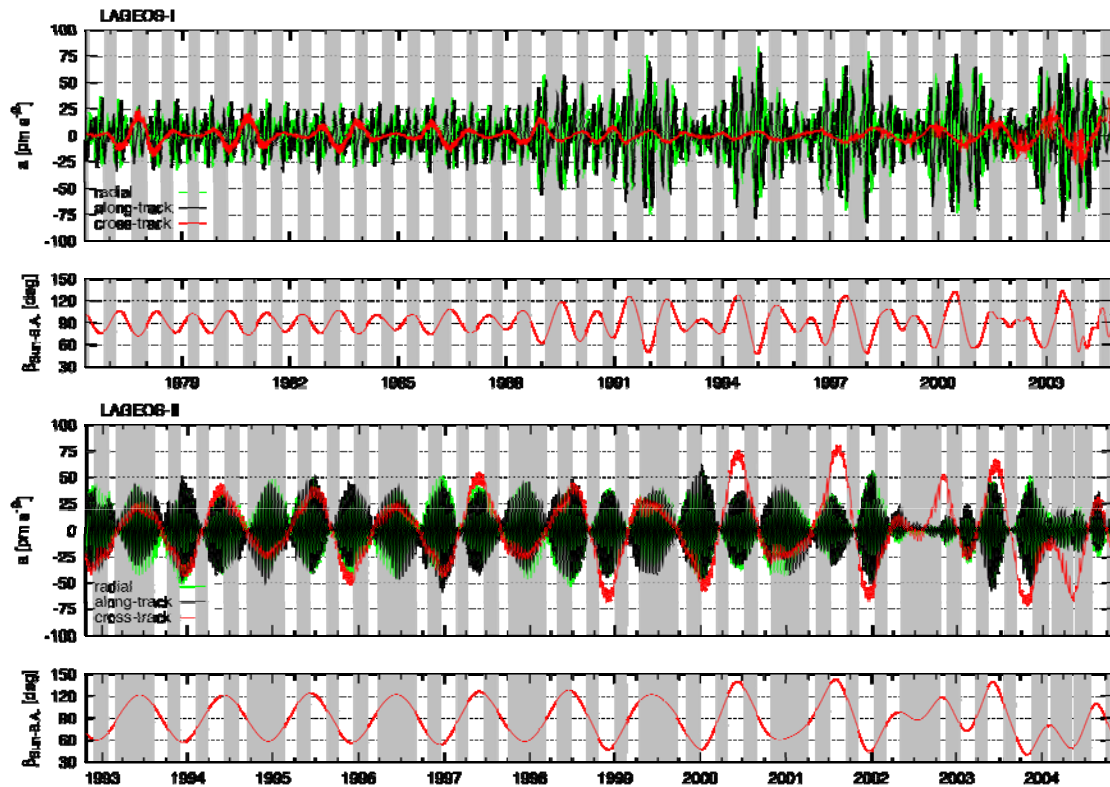


**Figure 7.** Net thermal accelerations and solar co-latitude (i.e. position w.r.t. the satellite north pole) for (top) LAGEOS-1, and (bottom) LAGEOS-2. The grey bands indicate the exact periods when the satellites are in eclipse [Andrés *et al.*, 2006].

December 1994. It should be emphasized here that no effort was done to fine-tune these results, nor to include other (necessary) elements to represent the orbital dynamics of the spacecraft. This explains the relatively high values for the rms-of-fit, which is shown in Figure 8 (typically, one would obtain fits in the order of better than 30 mm (for this period, that is), at the expense of solving for a collection of empirical accelerations; this was explicitly not the purpose of the current test). Figure 8 shows that the use of the thermal accelerations does lead to significant reductions in the quality of the orbit: the fit reduces from a range of 2.5-7.5 cm to a range of 2-4 cm, whereas the stability of the radiation scaling parameter  $C_R$  (a physical parameter, which should be constant rather than time-dependent – ignoring adjustments to the space environment during the first months in orbit [Ries *et al.*, 1997] indeed improves as well. The results shown here are very first results; further fine-tune of the computational model will hopefully result in the situation where the (estimation of) empirical accelerations can be discontinued altogether, without any loss of quality of the orbital solution nor of the derived parameters (origin, scale, station coordinates and such); preferably even an improvement of the latter products can be obtained.

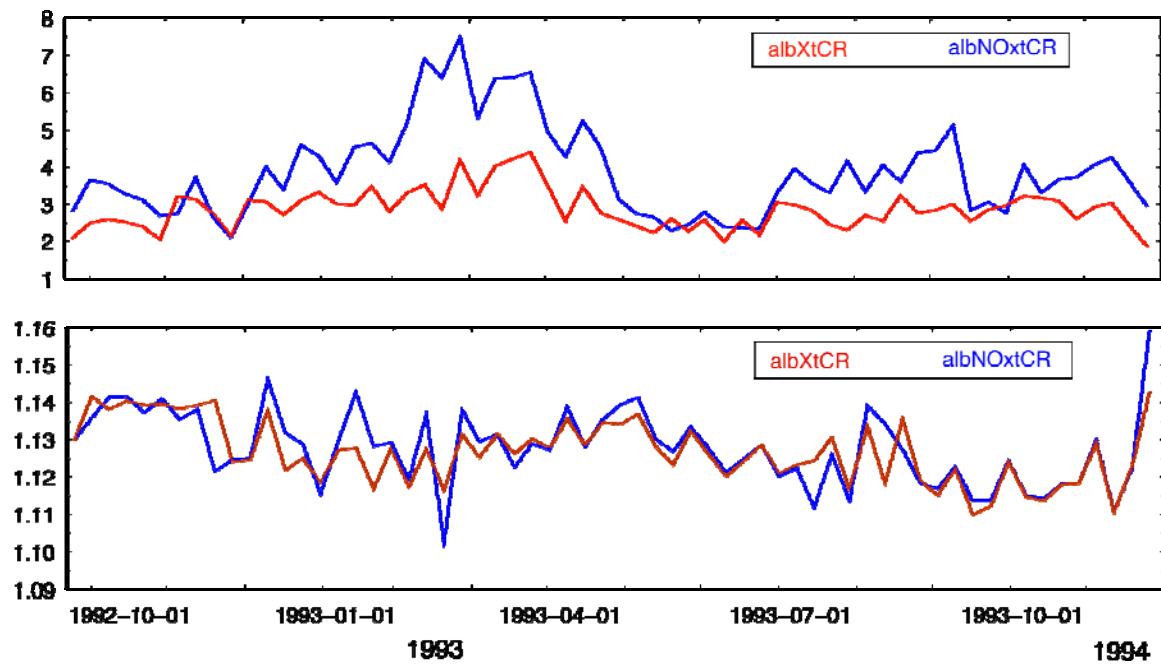


*Figure 8. Rms-of-fit (in cm) and solutions for the solar radiation scaling parameter  $C_R$  as a function of time for LAGEOS-2, with and without inclusion of the nominal thermal accelerations as shown in Figure 7.*

## Conclusions and recommendations

Based on a detailed finite-element representation of the pair of LAGEOS satellites, and in combination with LOSSAM, the state-of-the-art model for the rotational behavior of each satellite, it has been possible to derive a highly accurate and unprecedented model for the thermal behavior of 2133 different components of each satellite: LOSTHERM. The temperatures appear to show a strong correlation with geometry w.r.t. the Sun as the main source of influx of energy. Also, temperature variations of up to several hundreds of Kelvin are observed by virtue of the sensitivity of particular spacecraft components to irradiation (absorption and emission coefficients). The instantaneous temperature distribution of the outer components in particular can be integrated to yield the net thermal acceleration. These accelerations have magnitudes of up to  $75 \text{ pm/s}^2$ , much larger than the average value that is typically obtained from orbital computations. The results clearly shows that the rotational behavior of the satellites plays a decisive role in the actual values of these accelerations, and underlines the necessity of including such formulations in the most demanding orbital computations. It also underpins the need for continuation of independent observations of the rotational behavior of LAGEOS-2, and an answer to the challenge of doing similar things for LAGEOS-1.

## References

- [1] Afonso, G., F. Barlier, M. Carpino, P. Farinella, F. Mignard, A. Milani and A.M. Nobili, Orbital effects of LAGEOS seasons and eclipses, *Ann. Geophys.*, 7(5), 501-514, 1989.
- [2] Andrés, J.I., G. Bianco, D. Currie, R. Noomen and T. Otsubo, The spin axis behavior of the LAGEOS satellites. *J. Geophys. Res.*, 109, B06403, doi:10.1029/2003JB002692, 2004.
- [3] Andrés, J.I., R. Noomen and S. Vecellio None, Numerical simulation of the LAGEOS thermal behavior and thermal accelerations, *J. Geophys. Res.*, 111, B09406, doi:10.1029/2005JB003928, 2006.
- [4] Anselmo, L., P. Farinella, F. Mignard, A. Milani and A.M. Nobili, Effects of the Earth reflected sunlight on the orbit of the LAGEOS satellite, *Astron. Astrophys.*, 117, 3-8, 1983.

- [5] Barlier, F., M. Carpino, P. Farinella, F. Mignard, A. Milani and A. Nobili, Non-gravitational perturbations on the semimajor axis of LAGEOS, *Ann. Geophys., Ser. A*, 4, 193-210, 1986.
- [6] Farinella, P., D. Vokrouhlický and F. Barlier, The rotation of LAGEOS and its long-term semimajor axis decay, *J. Geophys. Res.*, 101(B8), 17,861-17,892, 1996.
- [7] Marshall, J.A., S.M. Klosko and J.C. Ries, Dynamics of SLR tracked satellites, *Reviews of Geophysics*, 33(S1), 353-360, 1995.
- [8] Martin, C.F., and D.P. Rubincam, Effects of Earth albedo on the LAGEOS-1 satellite, *J. Geophys. Res.*, 101(B2), 3215-3226, 1996.
- [9] Otsubo, T., and G. Appleby, Centre-of-Mass Correction Issues: Towards mm-Ranging Accuracy, in: Garate, J., J.M. Davila, C. Noll and M. Pearlman (eds.), *Proceedings 14th International Laser Ranging Workshop*, San Fernando, Spain, June 2004, Boletín ROA No. 5, Ministerio de Defensa, Real Instituto y Observatorio de la Armada en San Fernando, Spain, 467-472, 2005.
- [10] Pavlis, D.E. et al., *GEODYN-II systems description*, NASA Goddard Space Flight Center, Greenbelt, Maryland, USA, 1998.
- [11] Ries, J.C., R.J. Eanes, G. Métris and D. Vokrouhlický, Anomalous variations in the LAGEOS and LAGEOS-2 eccentricity, presented at the AGU Fall Meeting, San Diego, California, USA, 1997.
- [12] Rubincam, D.P., On the secular decrease in the semimajor axis of LAGEOS' orbit, *Celestial Mech.*, 26, 361-382, 1982.
- [13] Rubincam, D.P., LAGEOS orbit decay due to infrared radiation from Earth, *J. Geophys. Res.*, 92(B2), 1287-1294, 1987a.
- [14] Rubincam, D.P., Earth anisotropic reflection and the orbit of LAGEOS, *J. Geophys. Res.*, 92(B11), 11,662-11,668, 1987b.
- [15] Rubincam, D.P., Drag on the LAGEOS satellite, *J. Geophys. Res.*, 95(B4), 4881-4886, 1990.
- [16] Scharroo, R., K.F. Wakker, B.A.C. Ambrosius and R. Noomen, On the along-track acceleration of the LAGEOS satellite, *J. Geophys. Res.*, 96(B1), 729-740, 1991.
- [17] Sullivan, L.J., Infrared coherent radar, *Proc. Soc. Photo Opt. Instrum. Eng.*, 227(148), 1980.
- [18] Vokrouhlický, D., and G. Métris, LAGEOS asymmetric reflectivity and corner cube reflectors, *J. Geophys. Res.*, 109, B10401, doi:10.1029/2003JB002921, 2004

---

## Calibrating GNSS orbits with SLR tracking data

C. Urschl<sup>1</sup>, G. Beutler<sup>1</sup>, W. Gurtner<sup>1</sup>, U. Hugentobler<sup>2</sup>, S. Schaer<sup>3</sup>

1. Astronomical Institute, University of Bern, Switzerland
2. Institute of Astronomical and Physical Geodesy, Technical University of Munich, Germany
3. Federal Office of Topography, swisstopo, Wabern, Switzerland

Contact: [claudia.urschl@aiub.unibe.ch](mailto:claudia.urschl@aiub.unibe.ch)

### Abstract

*SLR tracking data allow for a completely independent validation of GNSS orbits that are derived from microwave data. SLR validation results show mean range residuals of several centimeters for both, GPS and GLONASS satellites, as well as significant seasonal variations for the two GPS satellites that are equipped with retroreflector arrays. It was, however, not clear whether these systematic effects could be assigned to orbit modeling deficiencies or to SLR tracking biases. We present new SLR validation results, which point to serious GPS orbit modeling problems. Moreover, we address the question, whether it would make sense to perform a combined analysis of microwave and SLR data for GNSS orbit determination. With the available low number of SLR observations no significant improvement of the orbit accuracy is found. An a priori variance-covariance analysis shows an improvement of the situation, if continuous SLR tracking data of already a very small number of globally distributed SLR sites were available.*

### 1. Introduction

The International Laser Ranging Service (ILRS) provides Satellite Laser Ranging (SLR) tracking data of Global Navigation Satellite Systems (GNSS, at present consisting of GPS and GLONASS). Two GPS satellites that are equipped with laser retroreflector arrays (LRAs), and a subset of three GLONASS satellites (all GLONASS satellites carry LRAs) are tracked by SLR.

SLR data allow for an independent validation of GNSS orbits that are derived from microwave data. In Section 2 we present recent SLR validation results, covering about four years of SLR data.

SLR observations may contribute to the GNSS orbit determination in a combined analysis of microwave and SLR observations. The possible improvement of the orbit accuracy is demonstrated on the basis of an a priori variance-covariance analysis in Section 3.

The main results of this work were already presented at the COSPAR 36<sup>th</sup> Scientific Assembly in Beijing. As this analysis is of a particular interest for the ILRS community, we will briefly introduce and sum up the most important results. We refer to (Urschl et al., 2007) for a detailed discussion.

### 2. GNSS orbit validation using SLR

For orbit validation we compare the SLR range measurements with the ranges derived from GNSS orbits. We used SLR normal points provided by the ILRS (Pearlman et al., 2002), and final orbits of CODE (Center for Orbit Determination in Europe). CODE is one of the analysis centers of the International GNSS Service (IGS) generating daily orbit solutions for all active GNSS satellites. The orbit determination is based on GNSS microwave observation provided by the IGS (Dow et al., 2005).

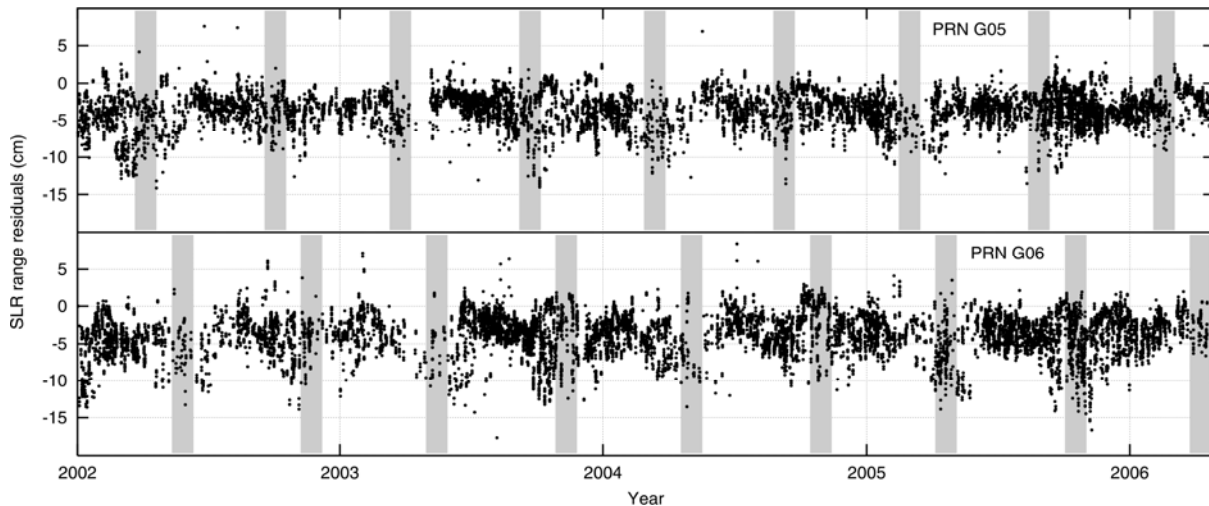


**Figure 1.** SLR range residuals in cm for GPS satellites PRN G05 and G06, derived from CODE final orbits. The shaded areas indicate eclipse seasons

The resulting range residuals indicate the GNSS orbit accuracy, but mainly in radial direction due to the observation geometry. SLR data of about four years starting 2002 were used for the range residual analysis.

Figure 1 shows the range residuals for the two GPS satellites. A standard deviation of the range residuals of 2 cm and 5 cm was estimated for the GPS and GLONASS satellites, respectively. The GPS orbits have a better accuracy compared to the GLONASS orbits due to the much denser GPS microwave tracking network. The GPS range residuals show a mean bias of about  $-3$  to  $-4$  cm. This bias is already known from previous studies, but its origin still remains unexplained. A wrong value for the retroreflector offset, giving the distance from the LRA's center to the satellite's center of mass, could be a possible explanation. It is interesting to note that there is no significant mean bias for the GLONASS satellites.

As part of the analysis, systematic variations were found in the SLR residuals of the GPS satellites, correlated to eclipsing seasons and with amplitudes of up to 10 cm. The largest residuals occur when the satellite is observed within the Earth's shadow during eclipsing seasons (indicated with shaded areas in Figure 1).

We could attribute the periodic signature to orbit modeling problems by displaying the range residuals in the  $(\beta, u)$ -coordinate system.  $\beta$  is the Elevation of the Sun above the orbital plane, and  $u$  is the argument of latitude of the satellite with respect to the argument of latitude of the Sun.

Figure 2 shows the range residuals in the  $(\beta, u)$ -system. The residuals are color-coded according to their values. The dependency of the range residuals on the satellite's position within the orbital plane is visible, and rules out SLR tracking biases. The pattern is rather caused by the microwave analysis, indicating attitude or orbit modelling problems.

### 3. Combined analysis of microwave and SLR data for GNSS orbit determination

Beside the validation purpose, SLR data can be used for GNSS orbit determination in a combined analysis together with microwave observations. But does this make sense in terms of orbit improvement? To answer this question an a priori variance-covariance analysis is performed.

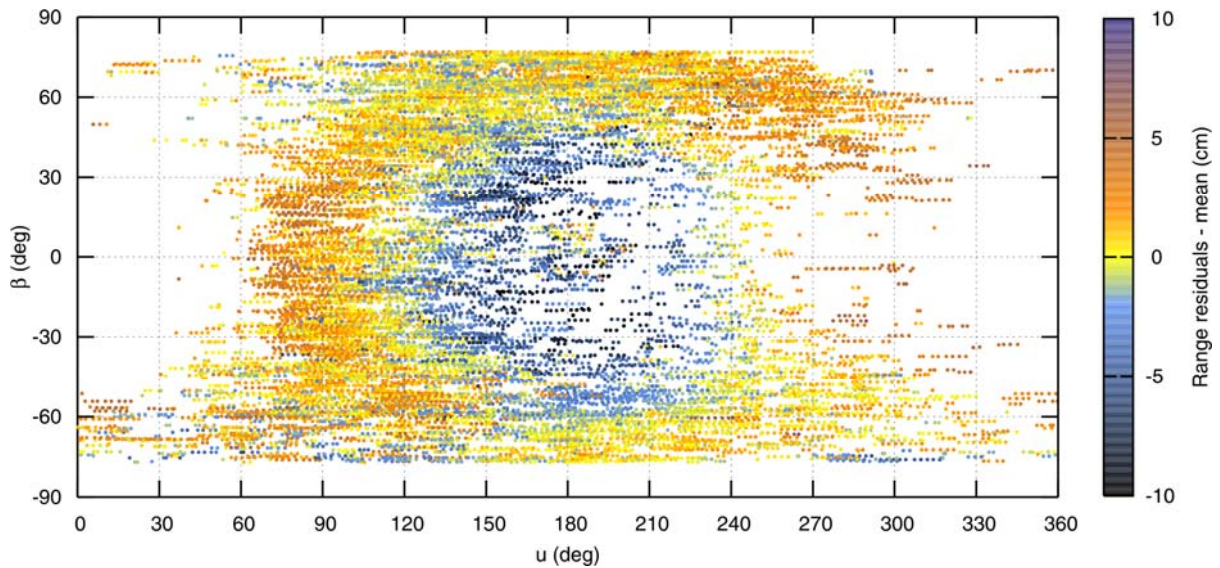


**Figure 2.** Color-coded SLR range residuals in cm minus mean value for the GPS satellites PRN05 and PRN06, derived from CODE final orbits

We used microwave phase observations of about 150 IGS sites and SLR data of 13 ILRS sites. For the variance-covariance analyses only the number, the temporal distribution, and an error model of the observations are needed. The a priori formal errors of the orbit components can be derived from the covariance matrices.

Several experiments were performed using different SLR observation weights. In the first experiment the SLR observation weight is set to zero by setting the a priori sigma of the SLR observations  $\sigma_{\text{SLR}}$  to infinity. Thus, the first experiment corresponds to a pure microwave solution. In the second experiment  $\sigma_{\text{SLR}}$  is set to 1 cm, similar to that of the microwave observations. In the third experiment the weight of SLR is increased by setting  $\sigma_{\text{SLR}}$  to 1 mm.

We compare the a priori formal errors of the orbital parameters of the different experiments. The a priori formal errors only decrease with very strong SLR observation weights ( $\sigma_{\text{SLR}} = 1$  mm) and only around epochs, where SLR observations are available. When using real SLR observations, no significant improvement of the orbit accuracy was found, as SLR tracking data of GNSS satellites are very sparse and not well distributed.

But the situation changes, if SLR data would cover the entire satellite arc. Evenly distributed SLR observations have been simulated with an accuracy of 5 mm, equally spaced at 15 min interval, for altogether four globally distributed SLR tracking sites. SLR data of four sites can cover as much as 90% of a GNSS satellite arc. The a priori formal errors of the orbit parameters decrease significantly for SLR observations with 1 cm accuracy, and even more for SLR observations with increased weighting.

Two additional experiments have been performed using SLR data of only two or three SLR sites. With the data of two sites about 50% of a GNSS satellite arc can be covered, with three sites about 75%. The a priori formal errors in radial orbit component decrease by about 20% including additional SLR data of two sites into orbit determination. The formal error decreases even more if data of three sites are used. Data of the fourth site leads to no further improvement.

For the GLONASS satellites the a priori formal errors of the radial orbit component decrease by about 50%. The impact of additional SLR data on GLONASS orbit determination is larger than for GPS satellites as the number of GLONASS microwave observations is much smaller.

#### 4. Conclusion

The quality of GNSS orbits can be validated using SLR observations of GNSS satellites. An orbit accuracy of about 2 cm and 5 cm was estimated for the GPS and GLONASS orbits, respectively, from a 4-year time series of range residuals covering 2002-2006. A mean bias of -3 to -4 cm for the GPS satellite orbits remains still unexplained. Periodic variations of the GPS range residuals were found, which are highly correlated with eclipsing seasons. We could demonstrate that these variations are not caused by SLR tracking data, but due to deficiencies in the GNSS orbit modeling. An improved solar radiation pressure model might solve the problem. Radiation pressure caused by Earth albedo was not considered in the GNSS orbit determination, but it may have a non-negligible effect on the orbit. Attitude modeling problems might also cause similar periodic variations in the range residuals. Further studies will follow to understand the source of the systematic residual pattern.

The combined analysis of microwave and SLR observations could improve GNSS orbit determination, assuming that the SLR observations are evenly distributed over the entire arc. Already a small network of three globally distributed SLR sites tracking the GNSS satellites continuously may contribute significantly to GNSS orbit improvement.

#### References

- [1] Dow, J.M., R.E. Neilan, G. Gendt, et al.: "The International GPS Service (IGS): Celebrating the 10th anniversary and looking to the next decade", *Adv. Space Res.*, 36(6),pp. 320-326, 2005.
- [2] Pearlman, M.R., J.J. Degnan, J.M. Bosworth: "The International Laser Ranging Service", *Adv. Space Res.*, 30(2), pp. 135-143, 2002.
- [3] Urschl, C. , G. Beutler, W. Gurtner, U. Hugentobler, S. Schaer: "Contribution of SLR tracking data to GNSS orbit determination", *Adv. Space Res.*, in press.

---

## **GIOVE-A and GPS-35/36 orbit determination and analysis of dynamical properties based on SLR-only tracking data**

Stavros A. Melachroinos<sup>1</sup>, Felix Perosanz<sup>1,3</sup>, Florent Deleflie<sup>2</sup>, Richard Biancale<sup>1,3</sup>,  
Olivier Laurain<sup>2</sup>, Pierre Exertier<sup>2</sup>

1. Groupe de Recherche en Géodésie Spatiale/LDTP-UMR5562
2. Groupe de Recherche en Géodésie Spatiale-OCA/GEMINI, Grasse, France
3. Centre National d'Etudes Spatiales, 18 avenue Edouard Belin, 31400 Toulouse, France

Contact: [stavros@calc-gen3-ci.cst.cnes.fr](mailto:stavros@calc-gen3-ci.cst.cnes.fr)

### **Abstract**

*SLR tracking data provided by the ILRS (International Laser Ranging Service) network are used to compute orbits of radio-navigation satellites equipped with laser retroreflectors : GPS-35 and GPS-36 for the American GPS constellation, and the first European GIOVE-A (Galileo In-Orbit Validation Element) satellite, launched in December 2005. The equations of motion are computed through an exhaustive dynamical model and is propagated with the two orbit determination softwares of the French GRGS (Groupe de Recherche de Géodésie Spatiale) group: GINS (for high frequency analyses), and CODIOR (for secular orbital elements analyses).*

*For each of these satellites, a set of SLR (Satellite Laser Ranging) data is processed and the results of the post-fit residuals analysis are shown. The orbit validation for GIOVE-A is based on overlaps between 2-day, 10-day and 30-day arcs calculated with the GINS software. The resulting 3D rms and radial residuals are the primary criteria for the internal accuracy of SLR orbits and may indicate possible dynamical perturbations such as orbit or attitude control manoeuvres. For GPS-35/36 satellites we compare two 10-day arcs to the precise IGS (International Global Navigation Satellite Systems Service) sp3 microwave final orbits. An offset of 2-3 cm in the radial direction appears between the two solutions and may reflect the effect of the non-homogeneity of the SLR tracking network. "Mean observed elements" are also provided.*

**Keywords:** GNSS, GIOVE-A, Satellite Laser Ranging, Solar radiation pressure modeling, mean orbital elements

### **1. Introduction**

GIOVE-A is the first satellite of the future GALILEO global navigation system. It has been developed by Surrey Satellite Technology Ltd and the ESA (European Space Agency) . It was launched from Baikonur Cosmodrome on 28 December 2005 and placed into a MEO (Medium Earth Orbit) with a semi major axis of 29600 km, an inclination of 56° and an eccentricity of 0.002. GIOVE-A is equipped with a LRR (Laser Retro Reflector) array having 76 corner cubes with a diameter of 27 mm each (ESA-EUING-TN/10206), which provides 40 % more return energy than GPS-35/36 LRR arrays (ILRS). The final constellation of Galileo will consist of 27 operational spacecrafts equipped with such identical LRR arrays. After the launch of GIOVE-A, ESA has requested ILRS an SLR campaign support during spring and summer 2006

(<http://www.esa.int>). The purpose of these campaigns is to provide data for the characterization of the satellite's on-board clock

The first of these campaigns has taken place between 22 May and 24 July 2006, with the participation of 13 globally distributed SLR stations. This paper presents the results of the GIOVE-A orbit determination for this period. The orbit validation is based on overlaps of fitted SLR-only orbits of 2-day, 10-day and 30-day duration arcs.

The ILRS community is also actively tracking the only two GPS (*Global Positioning System*) satellites which have LRR arrays on-board, designated GPS-35 and GPS-36. The GPS satellites are equipped with LRR arrays of 32 corner cubes arranged in a flat panel of 19x29 cm (*Degnan and Pavlis, 1994; ILRS, 2004; Urschl et al., 2005*). The altitude of GPS 35 and 36 is that of 20,195 km and 20,030 km respectively, with a 0.000 and 0.006 eccentricity and a 54 ° inclination for both.

In this study we are using 10 days of SLR data, for the two GPS satellites, in the period of 6<sup>th</sup> till 16<sup>th</sup> of June 2006. In this period most of the SLR stations were pointing to the GIOVE-A satellite and the SLR tracking data for the two GPS satellites have always been sparse. In this investigation the challenge consists in discovering the achievable orbit accuracy with sparse tracking data for the two GPS satellites. The analysis of SLR orbits of both GPS satellites is based on overlaps wrt the precise IGSsp3 orbits and the examination of difference residuals in the radial, normal and along-track direction. Transformation parameters between the fitted SLR arcs and the IGSsp3 orbits are adjusted.

Moreover, a propagation of the mean equations of motion, accounting for only the long periodic effects acting on the GIOVE-A orbit, has been led. This study provides the values of the mean observed elements, giving a mean value of each orbital parameter, and of the angles in particular (ascending node, argument of perigee, mean anomaly) for the 10-day arc.

The paper is organized such as follows. The analysis of the SLR-orbit estimation strategy and the solar radiation pressure modeling is outlined in Section 2. Section 3 describes the data set being used for GIOVE-A and GPS-35 and GPS-36 satellites. Section 4 analyses the results of the GIOVE-A internal orbit overlaps. Section 5 makes the analysis of the differences of the estimated SLR orbits of GPS-35/36 wrt IGSsp3 final microwave orbits for the period in question. Section 6 is dedicated to the analysis of GIOVE-A and GPS-35/36 orbit mean elements. Section 7 derives the necessary conclusions and summarizes the results.

## **2. SLR orbit estimation strategy**

Our motivation to process the GIOVE-A and GPS-35/36 satellite SLR data on the period of June 2006 is two-fold: firstly we want to evaluate the implementation of the new box-and-wing SRP (Solar Radiation Pressure) model of GIOVE-A in our software GINS 6.1, and secondly to test the performances of SLR-only orbit determination for these 3 GNSS (Global Navigation Satellite System) satellites.

Our estimation strategy is based on a weighted least squares scheme. The present analysis is made by the orbit determination and analysis software package GINS 6.1 developed by the CNES (Centre National d'Etudes Spatiales) geodetic team of. In table (1) the ad-hoc models and estimated parameters are summarized.

The attitude model used for all three s/c is illustrated in Fig. 1. and corresponds to the following coordinate frame :

- The **Y-axis** points along the solar panels
- The **D-axis** points towards the sun
- The **X-axis** completes the system

For GIOVE-A and GPS-35/36 we have implemented a box and wing solar radiation pressure model including respectively 8 and 19 surfaces with a-priori reflectivity and specularity coefficients

<i>GINS 6.1 soft. package</i>	<i>GPS 35/36</i>	<i>GIOVE-A</i>
Datum definition	ITRF 2000, EOPC04	ITRF 2000, EOPC04
Tidal displacements	IERS03	IERS03
Gravity field	EIGEN_GL04S(20x20)	EIGEN_GL04S(20x20)
Atmospheric loading	ECMWF	ECMWF
Ocean loading	FES2004 (K2 cor.)	FES2004 (K2 cor.)
Troposphere	Marini-Murray	Marini-Murray
Solar Radiation Pressure	Box-and-wing	Box-and-wing
Albedo and infra-red	Analytical model (10°x10°)	Analytical model (10°x10°)
Satellite's retro-reflector offsets	x=-0.863, y=-0.524, z=-0.658	x=0.828, y=-0.655, z=-0.688
Attitude model	X, Y, D	X, Y, D
Numerical integration	Cowell 8 <sup>th</sup> order, step size 180s	Cowell 8 <sup>th</sup> order, step size 180s
Parameter adjustment	6 orbital parameters, 1 SRP coeff., 1 Y-bias, 1 X, D per revolution (cos, sin)	6 orbital parameters, 1 SRP coeff., 1 Y-bias, 1 X, D per-revolution (cos, sin)

**Table 1.** SLR-only orbit processing parameters for GPS-35/36 and GIOVE-A

We have processed a set of 2-day, 10-day and 30-day arcs for the GIOVE-A satellite and two 10-day arcs for the GPS-35/36 satellites. Depending on the length of each arc, we include 1 per revolution terms for 2-day arcs (with constraints) and 5 per revolution terms (1 every 2d) for 10-day arcs in X, D directions. An additional acceleration along the s/c's Y-axis, the so-called Y-bias, is also adjusted.

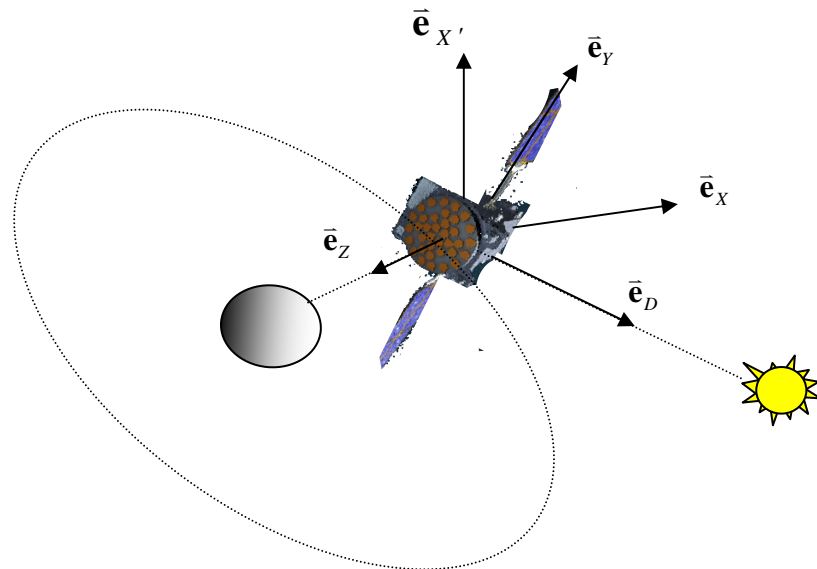


*Fig. 1. The GIOVE-A and GPS-35/36 attitude model*

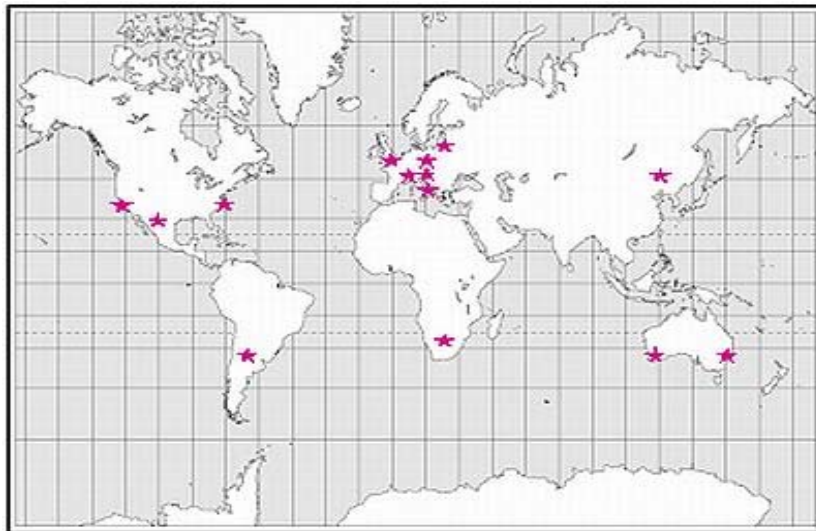


*Fig. 2. The 13 SLR network stations distributed globally (ESA courtesy)*

### 3. Data set

Fourteen laser ranging stations (Fig. 2) participated in a campaign to track ESA's GIOVE-A satellite during spring and summer of 2006, providing invaluable data for the characterization of the satellite's on-board clock. The campaign was coordinated by ILRS and the GIOVE Processing Centre at ESA-ESTEC.

See [www.esa.int/esaNA/SEM8QOKKKSE\\_index\\_2.html](http://www.esa.int/esaNA/SEM8QOKKKSE_index_2.html).

GIOVE-A satellite data from June to August 2006 used in this study have been processed. Figure 2 illustrates the distribution of the SLR tracking network. The total number of normal SLR points for this period arises up to 2311.

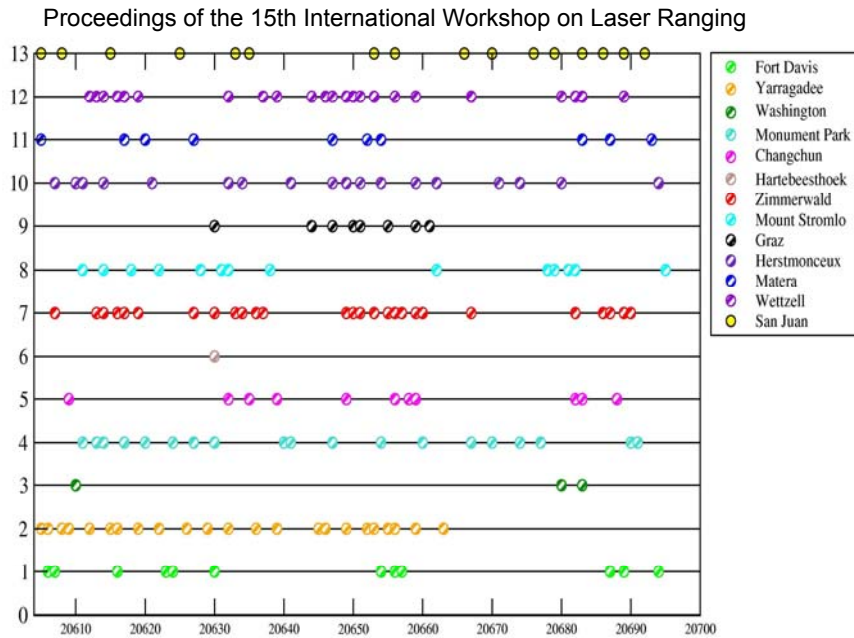


*Fig. 3. 3 months (in Julian days 1950) of GIOVE-A SLR data from global tracking stations*

For GPS-35/36 we processed data from the period of June 2006 corresponding to a set of 306 and 402 normal points respectively. For the same period the amount of normal points for GIOVE-A is 900.

#### 4. Orbit analysis of GIOVE-A

In this section we are examining:

- 1-day overlapping SLR-only sessions for GIOVE-A, from JULD50 (Julian day 1950) 20612 (2006/06/05) till JULD50 20623 (2006/06/19),
- a 10-day arc (2006/06/01.5-2006/06/11.5) over a 30-day arc (2006/06/01.5-2006/06/30.5)
- the overlaps with a 90-day arc expanding over the whole period of 3 months.

The illustration of the overlapping strategy is shown in Fig. 4.

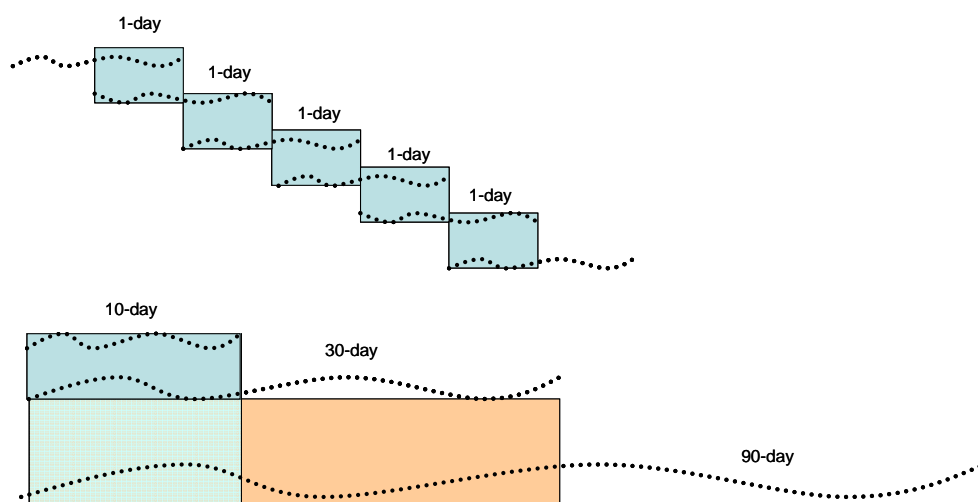


*Fig. 4. The overlapping periods of successive SLR arcs*

The evaluation criteria of the estimated orbit used are the root mean square misfit (RMS) (Eq. 1) and standard deviation (SD) of overlapping periods of successive arcs. An orbit overlap is defined by the comparison of the satellite's position vector between the common time-span of the two successive orbits (e.g. 1-day overlaps over 2 successive 2-day arcs).

$$rms_{misfit} = \sqrt{\frac{(\mathbf{x}^{arc1} - \mathbf{x}^{arc2})^2}{n}} \quad (1)$$

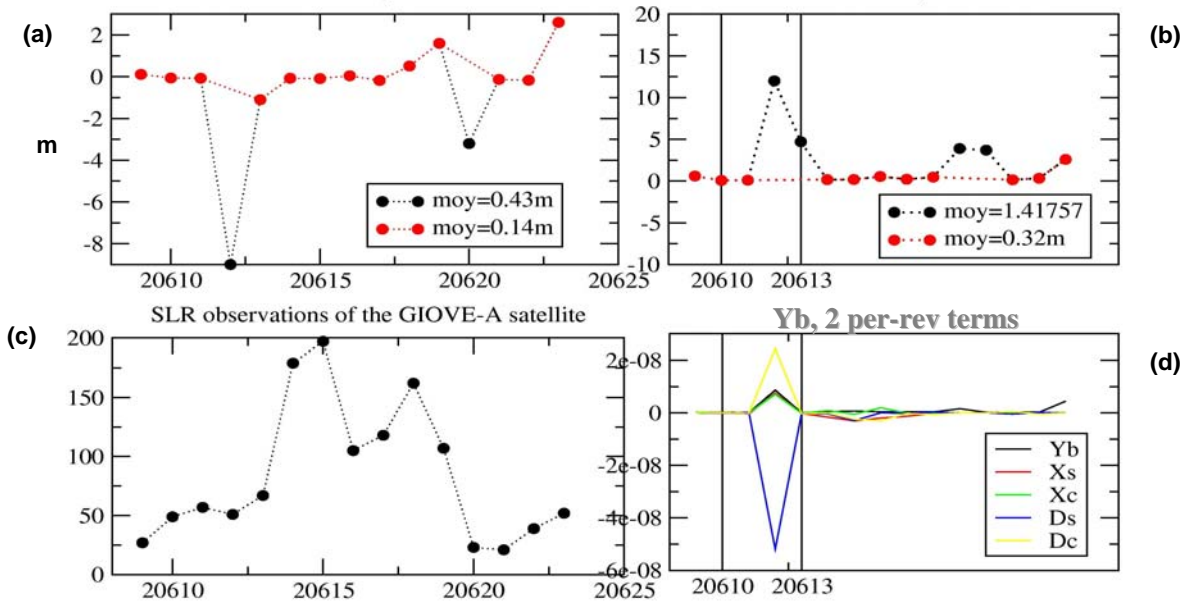
$$rms_{3D} = \sqrt{rms_{Radial}^2 + rms_{Along}^2 + rms_{Cross}^2}$$

Figure 5 shows the statistical results of the overlapping period of 2-day successive arcs.

For the arcs between JULD50 20611 (2006/06/08) and JULD50 20613 (2006/06/10), there is a significant change in the estimated accelerations, as well in the overlap mean difference and RMS. This implies that a dynamic perturbation like a manoeuvre occurred. In addition, a degradation of the mean difference of the SLR residuals appears at JJULD50 20620 (2006/06/16). This effect could be related to a reduction in the number of tracking stations for that epoch especially in the southern hemisphere.

The overlapping mean difference for the 2-day arcs is 43 cm in the Radial direction. Without accounting for the possible manoeuvre period it falls down to 14 cm. The same effect can be seen on the residual SD which decreases from 1.41 m to 32 cm for both 2 cases respectively.

Table 2 shows the orbit overlap misfit between a 10-day and a 30-day arc for the



**Fig. 5** statistical results of the overlapping period of 2-day successive arcs: In (a) and (b) are illustrated the mean difference and the RMS misfit in the radial direction respectively. In black are the mean values (in m) including the perturbation days and in red are the mean values without the perturbation days. In (c) is the number of observations for every day and in (d) is the values of the empirical accelerations. Y-b is the Y bias, Xs and Xc are the sin and cos revolution terms in X direction, Dc and Ds are the sin and cos revolution terms in D direction. The perturbation has a stronger influence in the D direction revolution terms.

period JULD50 20605 (2006/06/01) to 20615 (2006/06/11). The RMS of the satellite positions projected in the radial, normal and tangential directions are respectively 8cm, 45cm and 37cm.

The SLR residuals of a 10-day, 30-day and a 90-day arc are given figure 6 and lead to the same conclusions about the perturbations dates. All arcs agree in the residual level. Outliers up to 8m, verify the existence of dynamical perturbation event and appear in all arcs.

**GIOVE-A RMS Misfits (cm)**

Earth Along (Tangential)	45.64
Earth Normal	37.46
Earth Radial	8.96

*Table 2. GIOVE-A 10-day orbit overlaps from 2006/06/01.5 to 2006/06/11.5 over a 30-day arc from 2006/06/01.5 – 2006/06/30.5*

**5. Orbit analysis of GPS 35/36**

One 10-day SLR-only arc has been computed for GPS-35/ 36. The SLR data set spans from JULD50 20610 (2006/06/06) to 20620 (2006/06/16). As already mentioned, this period corresponds to a SLR campaign giving the priority to GIOVE-A tracking. This validation method has been very well known in the last 10 years and many studies, like Pavlis(1995), Appleby and Otsubo (2000), Hujsak et al. (1998) have investigated the undergoing problems of SLR sparse tracking orbit determination.

Tables 3(a) and 3(b) compare the adjusted orbits to the IGSsp3 final precise orbits in terms of position differences in the radial, normal and tangential directions. The RMS is at the level of 3 cm in radial, 47 cm in cross-track and 23 cm in along-track direction for GPS-35.

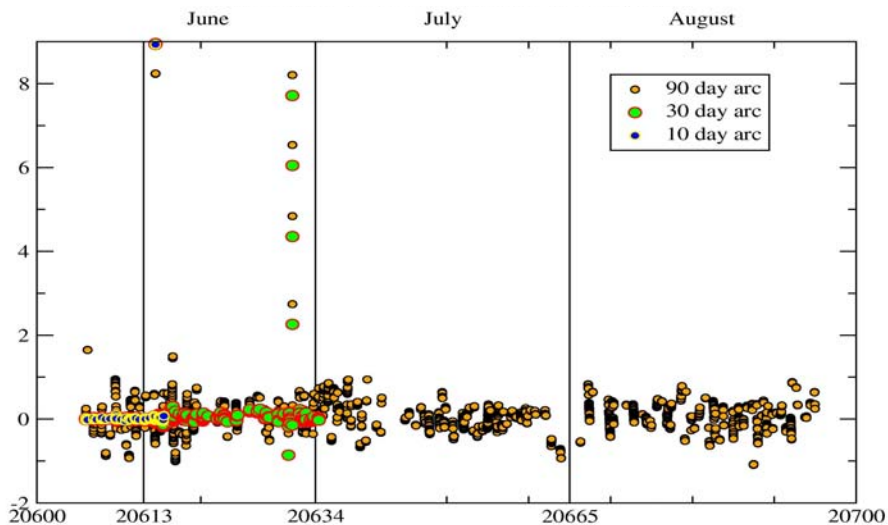


*Fig. 6: SLR residuals for the 10-day, 30-day and 90-day arcs from the 1<sup>st</sup> of June*

**GPS-35 RMS Misfits (cm)**

Earth Along (Tangential)	23.81
Earth Normal	47.25
Earth Radial	3.24

*Table 3 (a). GPS-35 10-day SLR arc overlap wrt IGSp3 final orbits*

**GPS-36 RMS Misfits (cm)**

Earth Along (Tangential)	9.55
Earth Normal	25.75
Earth Radial	2.03

*Table 3 (b). GPS-36 10-day SLR arc overlap wrt. IGSp3 final orbits*

For the case of GPS-36 the level of agreement in comparison with the IGSp3 radiometric orbits, is respectively in the radial, along-track, cross-track directions: 2-9-25 cm. Obviously, for GPS-35 and GPS-36, this result reflects the poor geographical distribution of SLR tracking stations. When one station in the southern hemisphere tracks GPS-36, for the same period, the factor of disagreement wrt IGSp3 orbits drops down by a factor of 2.

<b>Tx</b>	<b>-7.8 +/- 9.</b>
<b>Ty</b>	<b>-.4 +/- .9</b>
<b>Tz</b>	<b>59.8 +/- 9.</b>
<b>S (ppb)</b>	<b>.620124 x 10<sup>-9</sup> +/- .375 x 10<sup>-9</sup></b>
<b>S (m)</b>	<b>16.5 +/- 10</b>
<b>Rx</b>	<b>-.3 +/- .1</b>
<b>Ry</b>	<b>.01 +/- .1</b>
<b>Rz</b>	<b>-2.4 +/- .1</b>

*Table 4 (a). Helmert transformation wrt. the IGS microwave orbits for GPS-35 JJULD 20610-20620 in mm*

In order to further quantify any RF (Reference Frame) systematic differences, we applied a 7-parameter Helmert transformation between SLR-only orbits and IGSp3 solutions. Table 4 (a) and 4 (b) summarize the statistics from this comparison.

Both translation coefficients in Z for GPS 35/36 are significant with 60 mm ( $\pm 10$  mm) and 45 mm ( $\pm 5$  mm) respectively. This offset may reflect systematic problems

in either or both types of orbit as a result of non-homogeneity of SLR tracking stations in the global networks. In addition there is a factor of 8 in scale differences for GPS 35 and GPS 36 wrt the RF defined by IGSsp3 orbit. This statement is probably related to the poor number of southern tracking SLR tracking stations.

Tx	2.2 +/- 5.3
Ty	.8 +/- 5.3
<b>Tz</b>	<b>45.3 +/- 5.3</b>
S (ppb)	.712820 x 10 <sup>-10</sup> +/- .2 x 10 <sup>-9</sup>
<b>S (m)</b>	<b>1.9 +/- 5.</b>
Rx	-.3 +/- .05
Ry	.04 +/- .05
<b>Rz</b>	<b>-1.4 +/- .05</b>

*Table 4 (b). Helmert transformation wrt. the IGS microwave orbits for GPS-36 JJULD 20610-20620 in mm*

Furthermore, the overall agreement of SLR-only orbits with sparse data wrt. the radiometric IGSsp3 final orbits, is 2 to 3 cm radially. The consistency of the RF arises up to 6-4 cm in translation along the z-axis.

## 6. Mean observed elements

A complementary study has been led to give the value of the mean elements of the orbits of GIOVE-A, GPS-35 and GPS-36, namely : the mean semi-major axis, the mean eccentricity and inclination for the metric variables (those providing the computation of secular effects induced on the angles), the mean ascending node, mean perigee and mean “mean anomaly”. Such an approach leads up to an evaluation of the long term validity of gravitational and non gravitational models, and requires a data processing strategy where short periodic effects are removed from the osculating orbit, on each orbital element. This filtering approach has been carried out following the analytic part of the method, developed in (Exertier, 1990). The formulation of (Kaula, 1966) has been used to express the short period acting on the semi major axis, inclination, ascending node, and the one developed in (Deleflie, 2006) for the components of the eccentricity vector, because the investigated orbits are nearly circular.

Figures 7, 8, 9 show the temporal evolution of the mean metric elements of the GIOVE-A, GPS-35 and GPS-36 orbits, respectively. Table 5 gathers up some of these main elements, and Table 6 the main dynamic characteristics of these orbits which can be deduced from this study.

## 7. Conclusion and perspectives

The capability to estimate SLR-only orbits for GIOVE-A s/c has been implemented and evaluated in the GINS 6.1 CNES/GRGS software. The generated orbits are internally accurate to the level of 5-10 cm radially. This is the case when we are taking into account longer arc periods where orbit dynamics can absorb uniformly in the least square process a possible un-mapped perturbation such as s/c manoeuvres. Unknown manoeuvres are a critical issue for the s/c orbit determination.

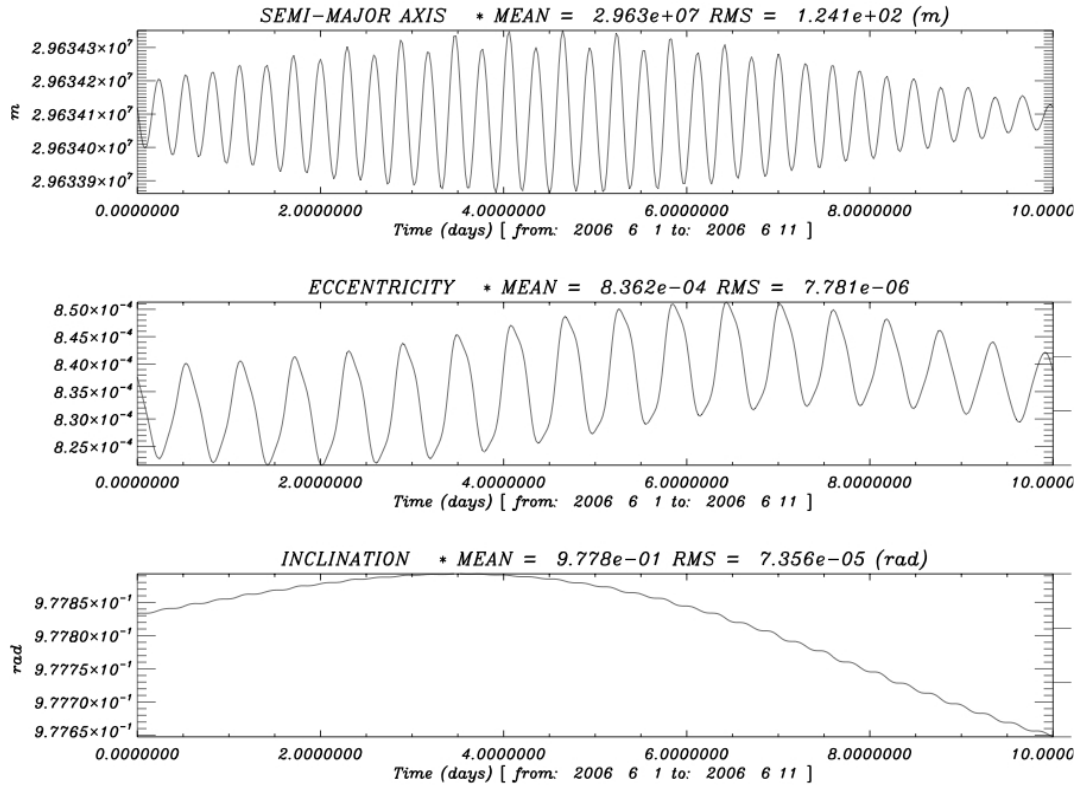


**Fig 7.** Temporal evolution of the mean metric elements of the GIOVE-A orbit, from 2006, 1<sup>st</sup> of June to 2006, 11<sup>th</sup> of June

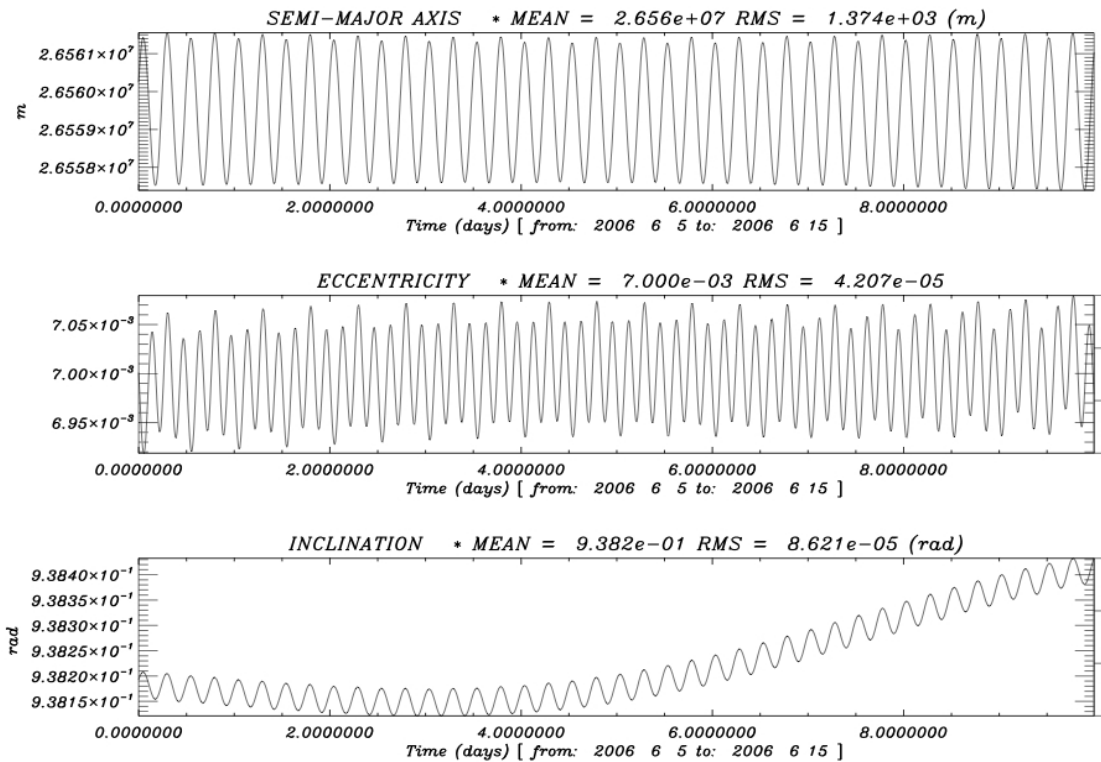


**Fig 8.** Temporal evolution of the mean metric elements of the GPS-35 orbit, from 2006, 6<sup>th</sup> of June to 2006, 15<sup>th</sup> of June

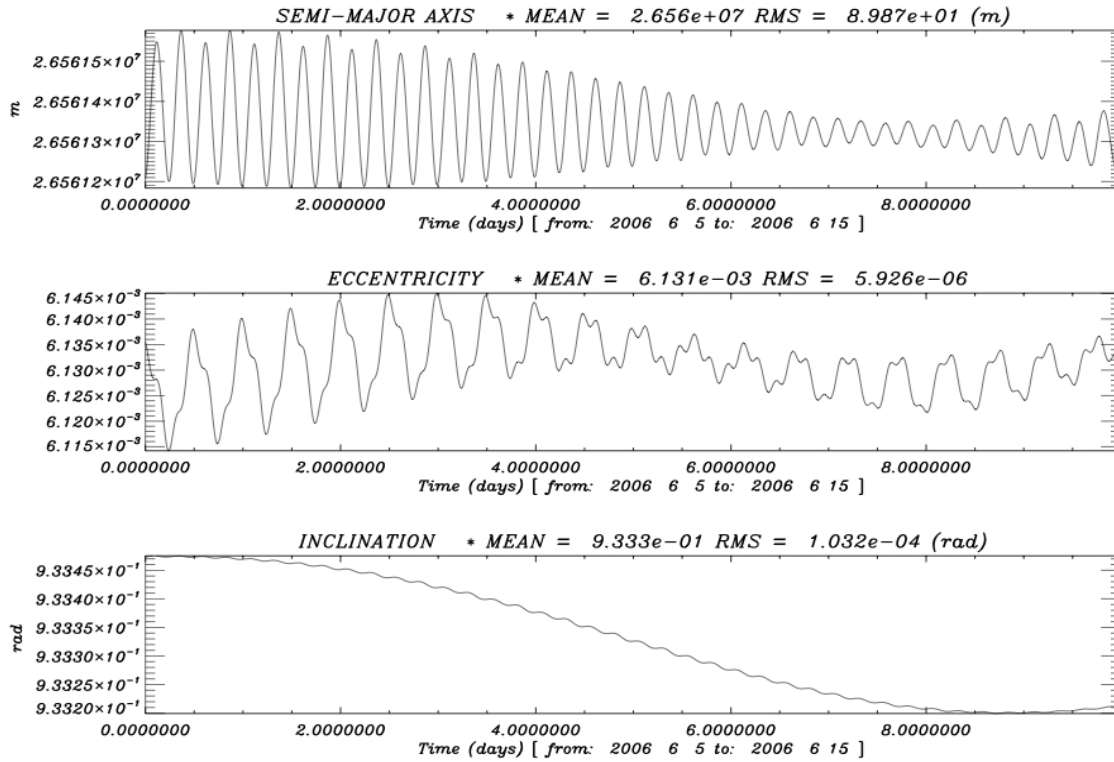


**Fig 9.** Temporal evolution of the mean metric elements of the GPS-36 orbit, from 2006, 6th of June to 2006 15th of June

By comparing the results for the 90-day, 30-day, 10-day and 2-day orbits we believe that 2-day orbits are the most appropriate for further orbit dynamics investigation. Another critical aspect in the orbit determination of GIOVE-A s/c is the solar radiation pressure model (SRP). We are using an analytical box-and-wing SRP model with approximate specularity and reflectivity coefficients.

	Epoch. (Julian Days 1950)	Semimajor Axis (m)	Eccentricity	Inclination °	Ascending node (rad)	Argument of perigee (rad)	Mean anomaly (rad)
<b>GIOVE-A</b>	20605,5	0.29634118E+08	0.83763674E-03	56.025730°	0.32550034E+01	0.57163824E+01	0.11332092E+01
	20615,5	0.29634120E+08	0.83869966E-03	56.015079°	0.32504105E+01	0.57263379E+01	0.12404609E+01
<b>GPS-35</b>	20609,5	0.26560245E+08	0.70009131E-02	53.754485°	0.24052494E+01	0.10521913E+01	0.19530670E+01
	20619,5	0.26561274E+08	0.69619513E-02	53.768426°	0.23981146E+01	0.10572299E+01	0.23138993E+01
<b>GPS-36</b>	20609,5	0.26561208E+08	0.61354695E-02	53.484095°	0.35019663E+01	0.44620688E+01	0.31748379E+01
	20619,5	0.26561276E+08	0.61312841E-02	53.469107°	0.34948338E+01	0.44640863E+01	0.35254203E+01

**Table 5.** Mean observed elements for three orbits, deduced from an analytical filtering of the short periodic terms inside the osculating orbit adjusted on SLR-data.

	Secular effects induced on			Period of revolution of			Altitude of	
	Asc. Node (rad/s)	Perigee (rad/s)	Mean anomaly (rad/s)	Asc. Node (day)	Perigee (day)	Mean anomaly (min)	Perigee (km)	Apogee (km)
<b>GIOVE-A</b>	-0.520220E-08	0.261182E-08	0.123762E-03	13979	27843	846	23231	23280
<b>GPS-35</b>	-0.807674E-08	0.510770E-08	0.145861E-03	9003	14238	718	19995	20367
<b>GPS-36</b>	-0.812694E-08	0.525981E-08	0.145852E-03	8948	13826	718	20020	20345

**Table 6.** Main characteristics of motion.

A further improvement would be the adjustment of these coefficients in at least one year period time by making use, as well, of the most accurate radiometric observations in L1 and E5. Though an empirical model like those used by CODE orbit analysis center and implemented in the Bernese GPS software, would be further investigated

For GPS 35/36 the presented comparison to the IGSsp3 final orbits for the two 10-day arcs shows a high quality of SLR-only orbits derived with sparse data. RMS residuals are of the order of 2-3 cm radially, 5-10 cm in along and 25-40 cm in cross-track. The systematic patterns of the translation and scale parameters of the RF demonstrate the dependencies in the geographic distribution of the SLR network.

Finally, only two s/c of the GPS constellation are equipped with LRR arrays for orbit validation and the end of their life time could be within the next year. Nevertheless Europe's satellite navigation system Galileo will offer this valuable opportunity of independent orbit validation procedures since all s/c of the constellation will be equipped with LRR arrays.

## References

- [1] Appleby, G., Otsubo, T. Comparison of SLR measurements and orbits with GLONASS and GPS microwave orbits, in : Proceedings of the 12th International Workshop on Laser Ranging, Matera Italy, 13-17 November 2000
- [2] C. Urschl, W. Gurtner, U. Hugentobler, S. Schaer, G. Beutler, Validation of GNSS orbits using SLR observations, *Advances in Space Research* 36 (2005) 412 – 417
- [3] Degnan, J.J., Pavlis, E.C., Laser ranging to GPS satellites with centimeter accuracy. *GPS World* 62-70, 1994
- [4] Deleflie, F., Métris, G., Exertier, P., An analytical solution of the lagrange equations valid also for very low eccentricities. Influence of a central potential, *Celest. Mech.* 94, 1, 105-134, 2006
- [5] European Space Agency, Specifications of Galileo and GSTB-V2 space segment properties relevant for satellite laser ranging, ESA-EUING-TN/10206, Technical note, 2005
- [6] Exertier, P., Precise determination of mean orbital elements from osculating elements , by semi-analytical filtering, -V 15, pp 115-123, 1990
- [7] Hujsak, R. S., Gilbreath, G. C., Sequential Orbit Determination for GPS-35 and GPS-36 using SLR data from NRL@SOR “ SPIE Proceedings, 3380 (32), April 1998
- [8] International Laser Ranging Service, GIOVE-A, <http://ilrs.gsfc.nasa.gov>
- [9] Kaula, W. M., Theory of Satellite Geodesy. Blaisdell publ. Co., New York, 1996
- [10] Pavlis, E.C, Comparison of GPS S/C orbits determined from GPS and SLR tracking data, *Adv. Space Res.* Vol. 16, No. 12, pp (12)55-(12)58, 1995

## **Orbit Determination and Analysis of Giove-A using SLR Tracking Data.**

Ramesh Govind<sup>1</sup>

1. Geoscience Australia, Canberra, Australia

### **Abstract**

*Using the early available SLR data since its launch, precise orbit determination of the GIOVE-A satellite was undertaken in weekly arcs. A description of the contributing data set, the computation process and the initial results of the orbit quality are presented. From these solutions, the inferred data quality from the individual stations is summarised. Using one estimate of the state vector from these solutions, a spectral analysis of the orbit perturbations due to the Earth's gravity field is shown.*

---

## Orbit determination for GIOVE-A using SLR tracking data

C. Urschl<sup>1</sup>, G. Beutler<sup>1</sup>, W. Gurtner<sup>1</sup>, U. Hugentobler<sup>2</sup>, M. Ploner<sup>1</sup>

1. Astronomical Institute, University of Bern, Switzerland
2. Institute of Astronomical and Physical Geodesy, Technical University of Munich, Germany

Contact: [claudia.urschl@aiub.unibe.ch](mailto:claudia.urschl@aiub.unibe.ch)

### Abstract

*The first European navigation test bed satellite GIOVE-A was launched on 28 December 2005. SLR observations of GIOVE-A, collected from the ILRS tracking network, are available since 21 May 2006. SLR data are primarily needed for the validation of the microwave-based orbit. As no microwave tracking data are available until now, the orbit determination based on SLR data is of high interest. We present GIOVE-A orbit determination results based on SLR-only data. In addition, the contribution of SLR data to the microwave-based orbit determination is demonstrated.*

*For the SLR-based orbit determination of GIOVE-A SLR data of the first GIOVE-A SLR tracking campaign were used. Orbits with different arc lengths were determined, as well as orbit predictions. Orbit overlaps were derived to assess the orbit quality. SLR-based orbits of 9-days arc length were determined with an accuracy of about 10 cm in radial orbit component, and about 0.5 m and 1 m in along-track and out-of-plane components.*

*The microwave-based GIOVE-A orbits as well as the first Galileo orbits in the In Orbit Validation (IOV) phase will rely on microwave tracking data of a very limited number of stations. Therefore, SLR would give an important contribution to the orbit determination through a combined analysis of microwave and SLR data. The possible improvement of the orbit accuracy including SLR observations is demonstrated on the basis of an a priori variance-covariance analysis. For this purpose SLR range measurements and simulated microwave data of GIOVE-A are used.*

### 1. Introduction

Galileo, the European global navigation satellite system (GNSS), is presently being developed. The first of two “Galileo In-Orbit Validation Element” test satellites, GIOVE-A (GSTB/V2A), was successfully launched on 28 December 2005. It carries a retroreflector array and can thus be observed by Satellite Laser Ranging (SLR). For evaluating the characterization of the on-board atomic clocks a first SLR tracking campaign on GIOVE-A was initiated. Between 22 May and 24 July 2006, 14 globally distributed SLR stations participated in the campaign.

As no microwave tracking data are available for scientific use, the orbit determination based on SLR is of high interest. In Section 2, we present first results of the GIOVE-A orbit determination using SLR data of the tracking campaign. Different orbit solutions with varying arc-length were determined. In order to assess the orbit quality, orbit overlaps were computed and compared with each other. In addition, orbit predictions were generated and evaluated by comparing the predicted orbits with the orbits derived from real tracking data.

Orbit determination of GIOVE-A (and the first Galileo satellites as well) based on microwave observations will rely on data of a very limited number of microwave tracking receivers in the beginning. In view of this situation, SLR data would give an

important contribution for precise orbit determination. SLR data may significantly improve the orbit estimates used in addition to the microwave data in a combined analysis. Section 3 shows results of an a priori variance-covariance analysis, demonstrating the possible positive impact of additional SLR data on GIOVE-A orbit determination. For this purpose, simulated microwave data and real SLR data from the tracking campaign were used.

## 2. GIOVE-A orbit determination using SLR observations

In this Section, we present first GIOVE-A orbit determination results based on SLR data only. SLR data collected during the first GIOVE-A SLR tracking campaign lasting nine weeks (May 22 – July 24, 2006) were used. The SLR data are provided by the International Laser Ranging Service (ILRS) (Pearlman et al., 2002). The triangles in Figure 1 indicate the geographical location of the 11 SLR sites that were included in our analysis. Note that we did not use SLR measurements of San Juan (located in South America), as no official terrestrial reference frame coordinates have been available at the time of analysis.

The temporal distribution of the SLR tracking data is shown in Figure 2. Each line represents 24 hours of a particular day. SLR observation epochs are indicated with a bar. The varying data coverage is clearly visible. Thus, the quality of the orbits derived from these data will vary, depending on the available SLR data.

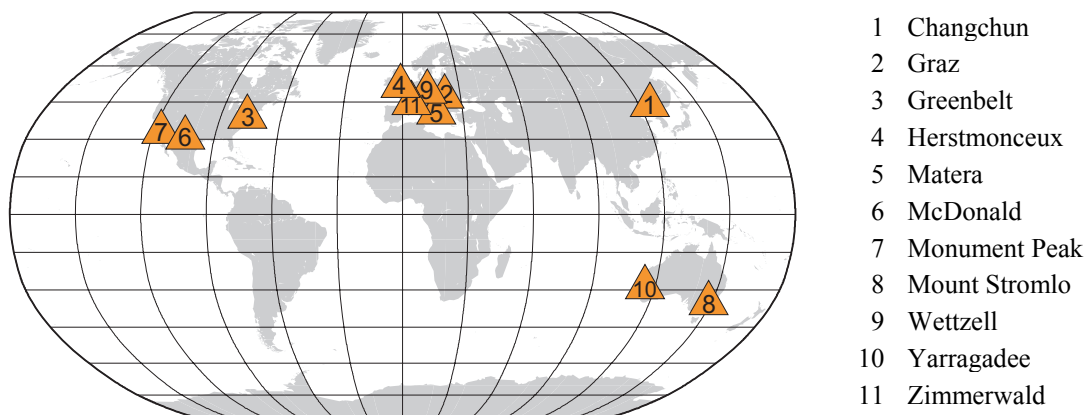


*Figure 1. Geographical location of the 11 SLR sites used for orbit determination*

In each orbit determination process six osculating elements and nine dynamical orbit parameters were estimated. The dynamical parameters represent solar radiation pressure (SRP) parameters defined in the SRP frame (D,Y,X). The SRP frame origin corresponds to the satellite's center of mass. The D-axis points towards the Sun, the Y-axis points along the solar panel axis, and the X-axis completes the right-handed system. The nine estimated SRP parameters are three constant acceleration (in D,Y, and, X direction) as well as six once per orbit revolution sinusoidal accelerations (sine and cosine in D, Y, and X direction).

Different orbits solutions were prepared using arc-lengths of n-days (n = 5, 7, 9, 11, 14) in order to estimate the arc-length that leads to the best possible orbit quality. The Bernese GPS Software Version 5.0 (Hugentobler et al., 2005) was used for the parameter estimation.

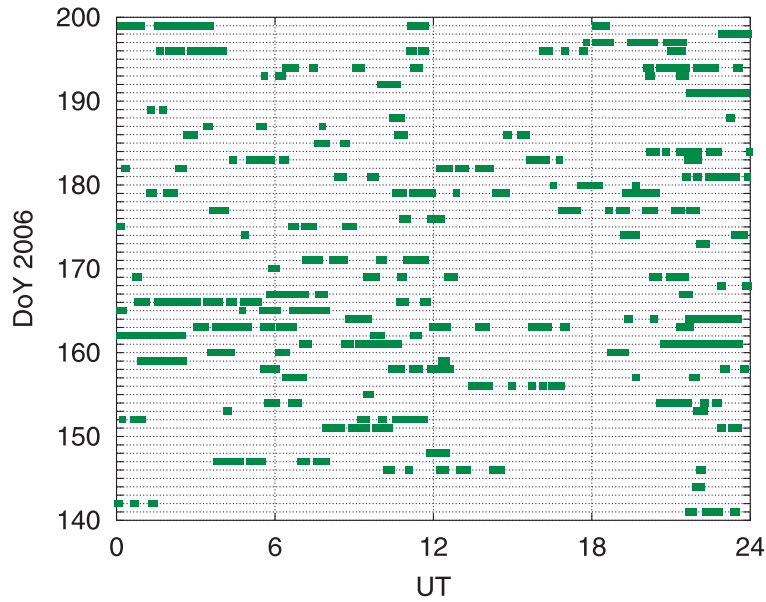


**Figure 2.** SLR data coverage of the GIOVE-A SLR tracking campaign

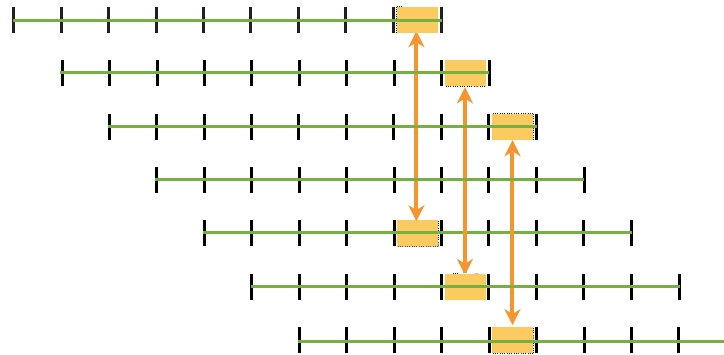


**Figure 3.** Sketch illustrating the generation of orbit overlaps for 9-day arcs; orbit overlap is the orbit difference between last and central day

For each solution we generated between 32 and 50 n-day arcs within the 60 days interval of the SLR tracking campaign of GIOVE-A. Consecutive n-day arcs are shifted by one day each. Thus, overlapping orbits can be generated. The resulting orbit differences (referred to as orbit overlaps in the following) indicate the orbit quality. Small overlaps indicate a good quality, whereas large overlaps indicate a bad quality of the determined orbit. We assume that the central part of an arc is best defined and that the boundary parts of an arc are worst defined. The overlap analysis concept is to compare the last day of an arc with the corresponding central day of another arc of the same arc-length, as illustrated in Figure 3. In the sketch each line represents a 9-day arc, day boundaries are indicated. The arrows show the orbital parts that are compared with each other.

Figure 4 shows the orbit overlaps of the GIOVE-A 9-day arcs. This arc length of 9 days has proved to be the best one, as the overlaps of the other orbit solutions with arc lengths of 5, 7, 11, or 14 days are larger. The orbit overlaps vary significantly, as the orbit quality is highly correlated with the number and temporal distribution of the SLR observations. Arcs with less or badly distributed observations are determined worse. Satellite maneuvers might also cause problems, if they are not considered in the orbit model. The radial orbit overlaps (top chart in Figure 4) show values of up to 10 cm. The radial component is best defined, as the SLR ranges represent observations mainly in radial direction. Orbit overlaps in along-track and out-of-plane components vary up to

1 m and 2 m, respectively. For arcs with a good temporal distribution of SLR data the orbit overlaps are smaller with values up to 0.5 m in along-track and 1 m in out-of-plane component. The formal errors of the satellite positions in the orbit system (radial, along-track, out-of-plane) show corresponding magnitudes similar to the overlap values.

Figure 5 displays the range residuals derived from the 9-day arc solution. The standard deviation of the residuals is about 2 cm, which is within the range of the accuracy of the SLR observations. SLR observations are assumed to be accurate at the 1-2 cm level.

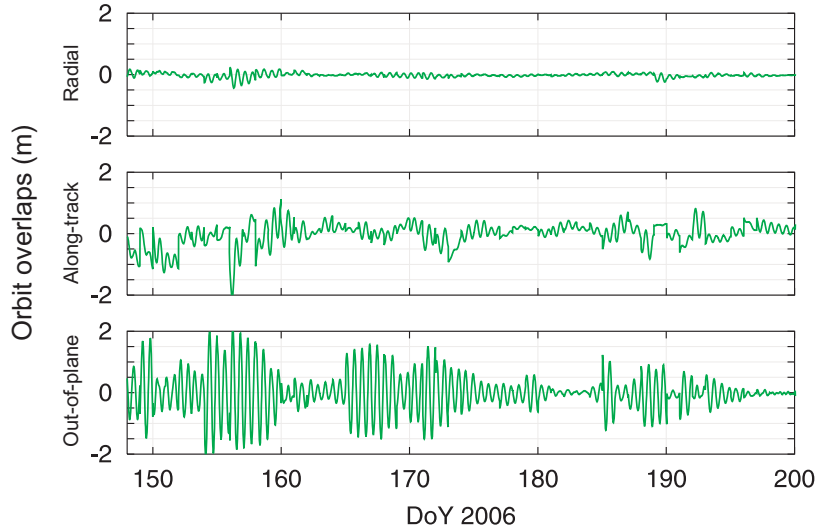


**Figure 4.** Orbit overlaps of SLR-based 9-day arcs of GIOVE-A; orbit overlaps are the orbit differences between the central days and the last days of the corresponding 9-day arcs

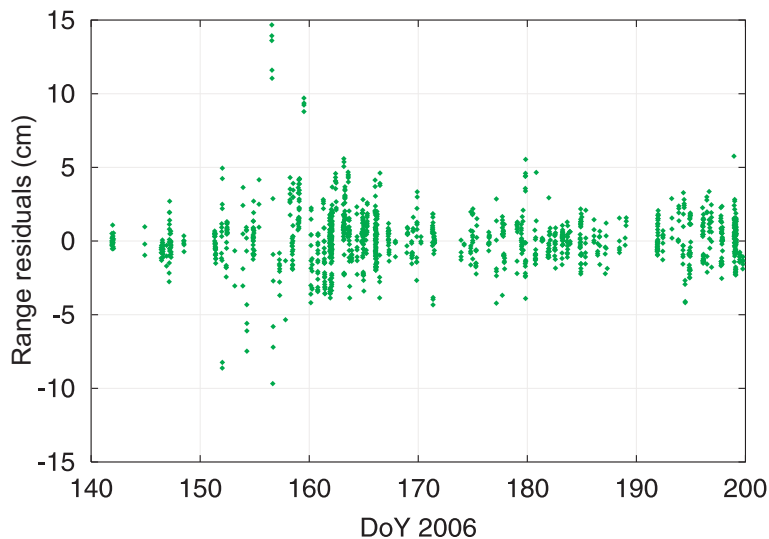
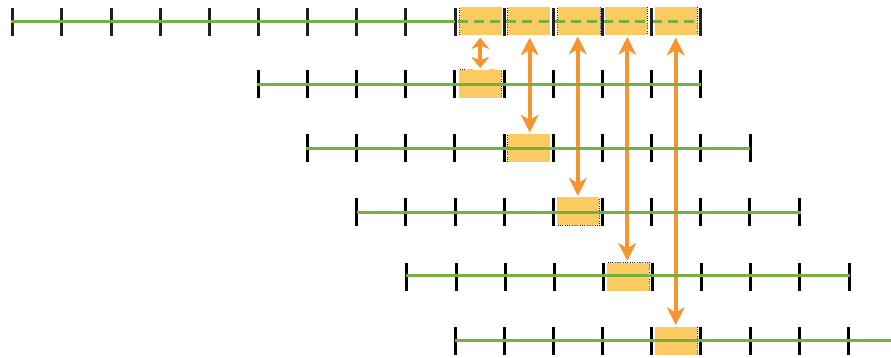


**Figure 5.** Range residuals derived from SLR-based 9-day arcs of GIOVE-A

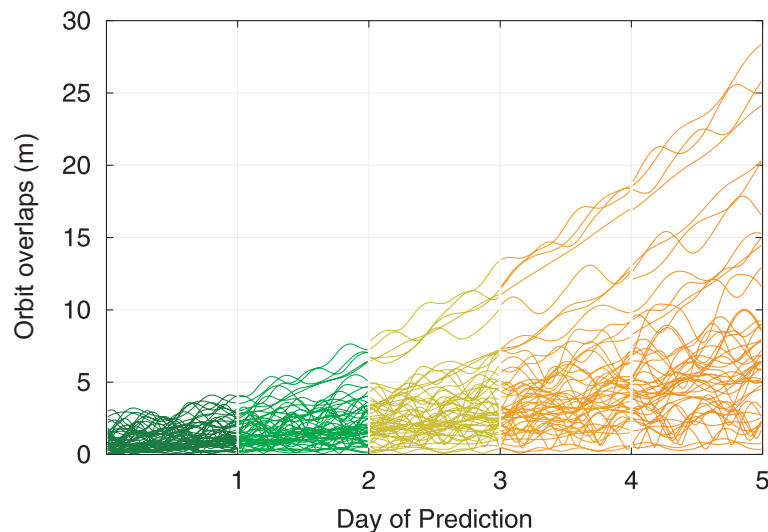
In addition to the SLR-based 9-day arcs, we computed consecutive 5-day orbit predictions. For the overlap computation, each predicted day is compared with the corresponding central day of the orbit part covered by SLR observations, as illustrated in Figure 6. Thus, for each 9-day arc overlaps of the five prediction days are generated.

Figure 7 shows the orbit overlaps for all prediction days of all orbital arcs. The predictions are getting worse in time due to the accumulated orbit errors. The computed prediction overlaps are dominated by the along-track error of the orbital arc, as this

error increases exponential in time. The overlaps indicate a potential orbit accuracy of about 20-30 m after 5 days of prediction.



**Figure 6.** Sketch illustrating the generation of orbit overlaps for 9-day arcs with 5 day predictions; orbit overlap is the orbit difference between each prediction day and the corresponding central day of the orbit part covered by SLR observations



**Figure 7.** Orbit overlaps of 5-day predictions based on GIOVE-A 9-day arcs; orbit overlaps are the orbit differences between the prediction days and the central days of the corresponding 9-day arcs

### 3. Combined analysis of SLR and microwave observation for GIOVE-A orbit determination

This Section demonstrates the possible contribution of SLR to GIOVE-A orbit determination through a combined analysis of microwave and SLR data. As no microwave tracking data of GIOVE-A were available at the time of our analyses, we performed an a priori variance-covariance analysis. For such an analysis the observations are not needed, rather the number and temporal distribution and the assumed a priori error of the observations. Note that model deficiencies are not considered here.

Microwave phase observations were simulated for 13 GIOVE-A tracking sites, which are chosen similar to the proposed sites of the first Galileo tracking network. Their global distribution is indicated with circles in Figure 8. In addition we used the SLR true observations of the SLR sites represented with triangles.

The microwave phase observations are sampled with 30 s and have an accuracy of 1 mm. Observation equations were set up for microwave phase zero difference observations and SLR normal points. Satellite clocks, ambiguities, and orbit parameters were included in the parameter estimation. Other parameters, as station coordinates,

receiver clocks, tropospheric zenith path delays, and Earth orientation parameters are assumed to be known accurately, as for example from a global analysis of GPS and GLONASS data.

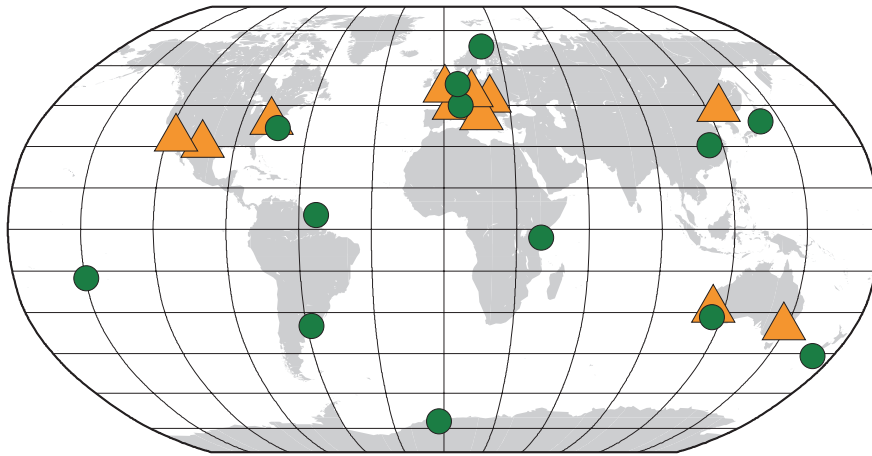


**Figure 8.** GIOVE-A tracking sites (circles) and SLR tracking sites (triangles)

The *a priori* variance-covariance matrix is derived from the obtained normal equation system. The *a priori* formal errors of the orbit parameters are then computed from the variance-covariance matrix. We used the same orbit parameters as in Section 2, i.e. six osculating elements and nine solar radiation pressure parameters in D,Y,X- direction. In summary 57 orbital arcs of 3 days length were determined, shifted by one day each.

To assess the impact of additional SLR observation on GIOVE-A orbit determination, we performed three different analysis with different SLR observation weight scenarios. The first solution corresponds to a pure microwave solution. The SLR observation weight is set to zero by setting the *a priori* sigma  $\sigma_{\text{SLR}}$  to infinity. In the second case,  $\sigma_{\text{SLR}}$  is set to 1cm. In the third case, the SLR observation weight is increased (with  $\sigma_{\text{SLR}} = 1 \text{ mm}$ ), and corresponds to the microwave observation weight.

We calculate the *a priori* formal errors of the satellite position in the inertial system from the *a priori* formal orbit errors by applying the law of error propagation. Figure 9 shows the *a priori* formal errors of the satellite position in radial, along-track, and out-of plane component for the three different solutions of a GIOVE-A 3-day arc. The absolute error values must be considered to be much too optimistic, as the error scales with the number of observations. We used 30 s sampled microwave data, but did neglect any temporal correlations between consecutive observations. A sampling rate of 180 s should rather be used for further studies.

The introduced parameters (e.g., station coordinates, troposphere parameters), which are assumed to be known from the GPS/GLONASS analysis, are not error free. Neglecting the formal errors of the introduced parameters, and of temporal correlations between observations causes too optimistic formal errors. However, in this analysis we are not interested in the absolute values of the formal orbit errors, but rather in the relative difference of the formal orbit errors between the three solutions. We may from this assess the impact of additional SLR observations on GIOVE-A (or Galileo) orbit determination in terms of orbit improvement.

The major impact of additional SLR data on the resulting orbit accuracy is given in the radial orbit component. A possible improvement of the radial orbit accuracy of about 60-80% may be feasible, depending on the SLR weight and the number and distribution of SLR observations. The formal orbit error in along-track and out-of-plane components

decreases with strong SLR weights, only. A good temporal distribution of the SLR observations over the entire arc is always necessary. Otherwise, if e.g. SLR observations are only available at the beginning of an orbital arc, the orbital errors as well as the orbit positions will show periodic variations.

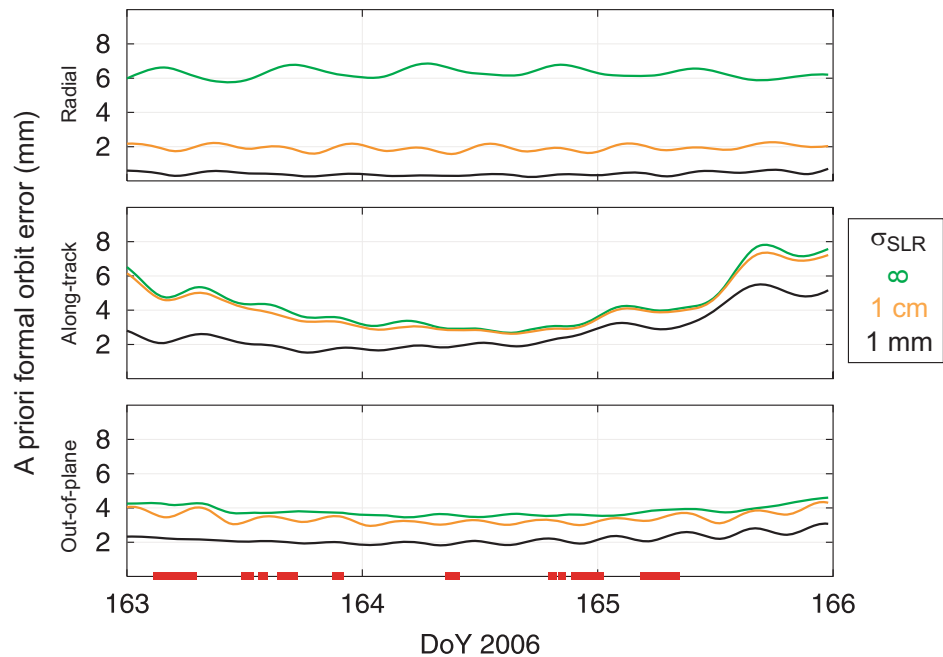


**Figure 9.** *A priori formal orbit errors in the inertial system; the three lines indicate the different orbit solutions using different a priori sigmas  $\sigma_{SLR}$  for the SLR observations; the bars on the horizontal axis indicate the SLR observation epochs*

#### 4. Summary

We presented GIOVE-A orbit determination results based on SLR observations of the first GIOVE-A SLR tracking campaign. Orbits of several arc-length were determined and compared with each other. Nine-day arcs proved to provide the best possible orbits with the used orbit model. No a priori solar radiation pressure model was introduced in the orbit determination, but constant accelerations and once-per orbit revolution accelerations were estimated. The orbit accuracy of a 9-day arc is about 10 cm, 0.5 m, and 1 m in radial, along-track, and out-of-plane component, unless the observation coverage of the orbit is poor. If SLR observations are very sparse and not well distributed over the entire arc, the orbit quality decreases. Orbit predictions are at the 20-30 m accuracy level after five days.

The impact of SLR observations used in addition to microwave observations for precise orbit determination of GIOVE-A was demonstrated. An a priori variance-covariance analysis shows a significant orbit improvement mainly in radial direction of about 60%, if additional and well distributed SLR observations are used. This can be addressed to the very low number of microwave tracking sites for the upcoming Galileo system in the very beginning of the system implementation.

#### References

- [1] Pearlman, M.R., J.J. Degnan, J.M. Bosworth: "The International Laser Ranging Service", Adv. Space Res., 30(2), pp. 135-143, 2002.
- [2] Hugentobler, U., P. Fridez, S. Schaer: "Bernese GPS Software Version 5.0", Druckerei der Universität Bern, Switzerland, 2005.

**Satellite Laser Ranging in the National (Australian) Collaborative  
Research Infrastructure Proposal for Geospatial R&D**

Kurt Lambeck<sup>1</sup>

1. The Australian National University, Canberra, Australia

The presentation is at:

<http://www.ilrscanberraworkshop2006.com.au/workshop/day2/Monday1400.pdf>

---

## Time-variable gravity from SLR and DORIS tracking

Frank G. Lemoine<sup>1</sup>, Steven M. Klosko<sup>2</sup>, Christopher M. Cox<sup>3</sup>, Thomas J. Johnson<sup>4</sup>

1. Planetary Geodynamics Laboratory, NASA Goddard Space Flight Center, Greenbelt, Maryland, USA
2. SGT, Inc., Greenbelt, Maryland, USA
3. Raytheon Integrated Defense Systems, Arlington, Virginia, USA
4. National Geospatial-Intelligence Agency, Reston, Virginia, U.S.A.

### Abstract

*One of the significant strengths of the tracking of satellites with satellite laser ranging (SLR) is the long time base of data available. This has been exploited to provide us with monthly snapshots of the variations of the low-degree field from approximately 1980 to the present. The analysis of these data by Cox and Chao [2002] revealed an anomaly in the zonal rate for  $J_2$ . Cox and Chao [2002] clearly indicated that the contributions to this zonal rate from the cryosphere and surface hydrology, such as glacier melt and ground water storage, are just as important as post-glacial rebound. In this paper, we extend the time series of low degree variations through 2006, describing the satellite data incorporated into the solutions, the method of analysis, and the satellite performance. We compare the SLR/DORIS recovered low-degree variations with those derived from GRACE from 2003 to 2005, through degree four, and investigate the climatological and geophysical connections revealed by the new time series.*

### Introduction

Although GRACE provides us with a valuable source of high-resolution data for assessment of surface mass transport, the analysis of SLR and DORIS tracking data to low Earth orbiting satellites still provides valuable information. Intercomparison of the GRACE and independent SLR & DORIS results can provide a validation of the GRACE results where the data overlap after launch of GRACE, and an improvement in the quality of the time series through improvements in the dynamic modeling, for example through usage of the GRACE-derived geopotential. In this manner, the joint analysis of GRACE and the SLR and DORIS tracking data can help to leverage these data into the pre-GRACE era. In this manner we can obtain a snapshot of surface mass transport on the Earth over the past 25 years.

### Data and Processing

The gravity solutions are based on data to nine satellites: Lageos 1 & 2, Starlette, Stella, Ajisai, Westpac, GFZ-1, TOPEX/Poseidon, and BE-C. The temporal coverage of the tracking data is depicted in Figure 1. For most of the 1980's, only three satellites are available. From the 1990's onward, between six and nine satellites are used, including the SLR & DORIS tracking data to TOPEX/Poseidon.

The modeling applied the ITRF2000 reference frame [Altamimi *et al.*, 2002] with corrections for certain stations, derived principally by the TOPEX/POD team (N. Zelensky, NASA GSFC, personal communications). The GGM01C GRACE-derived gravity model was used [Tapley *et al.*, 2004]. The IERS2003 solid Earth tides were applied including anelasticity [McCarthy and Petit, 2004]. The GOT00.2 T/P-derived ocean tide model was applied [Ray, 1999]. The atmospheric gravity was forward modeled using atmospheric pressure data from NCEP to 20x20, with an inverse

barometer correction assumed over the oceans. The observed annual gravity terms to 4x4 were forward modeled a priori, based on a previous SLR time series solution. After 1992, the daily arcs are 10 days in length, and constructed to be commensurate with the start and stop times of the near-ten day ground track cycle of TOPEX/Poseidon. Prior to 1992, the arc length was 30 days for Lageos-1, and 15-days for Starlette and Ajisai. For all the arcs, global station biases are adjusted for the SLR data. The gravity solutions consisted of a 30x30 static field, a 6x6 field for the secular rates of the geopotential, annual and semi-annual terms to 4x4, and a 4x4 monthly time series.

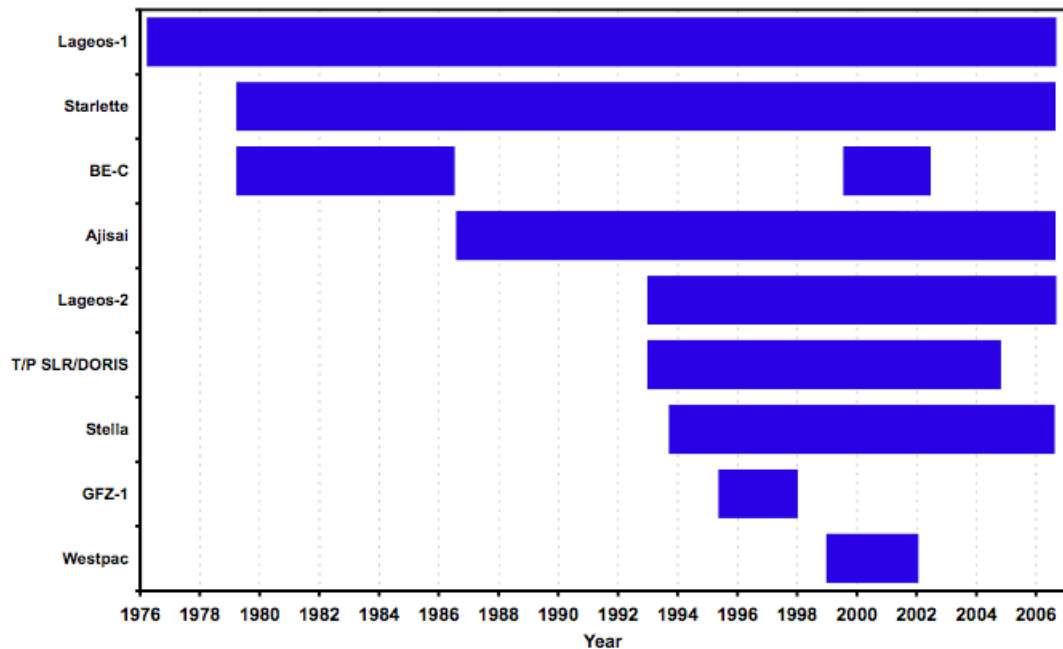


*Figure 1. Temporal coverage of SLR and DORIS tracking data used in the monthly gravity solutions, the solutions for the annual and semi-annual harmonics and the solutions for the secular rates.*

### Analysis of the $J_2$ signal

The full time series is depicted in Figure 2, with respect to the GGM01C. The 1998  $J_2$  ( $-C_{20}$ ) anomaly discussed in *Cox and Chao* [2002], appears as an inter-annual variation. The slope in  $J_2$  obtained from 1980 to 1997 of  $1.34 \times 10^{-11}$ /year is similar to the post 1997 slope of  $1.36 \times 10^{-11}$ /year. It now appears, especially after the application of an annual filter, that a similar interannual variation was observed in 1987-1988. The  $J_2$  time series is visibly much noisier before 1983. The addition of Starlette to the solution, especially after 1983, acts to stabilize the solutions for  $J_2$  and the other low degree harmonics. An additional consideration is that the strength of the network and the quality of the data for 1983 and later is far superior to the pre-1983 SLR data. For reference, we note that a  $\pm 1 \times 10^{-10}$  in  $J_2$  corresponds to a  $\pm 2$  mm change for the geoid in a zonal sense from pole to equator.

In Figure 3 we compare the  $C_{20}$  time series for GRACE, and from the SLR & DORIS solutions from 2002 to 2006. We show the comparisons for the CSR Release 01 fields (constrained and unconstrained), the NASA GSFC GRACE solutions based solely on GRACE K Band Range-Rate data (KBRR) from *Luthcke et al.* [2006], and the corresponding SLR & DORIS solution. The unconstrained CSR release 01 (RL01)

$C_{20}$  data have the worst agreement, especially around the period in late 2004 when GRACE entered a deep resonance driven by a close ground track repeat. The solutions lightly constrained by a Kaula constraint are smoother in their performance. The  $C_{20}$  from the NASA GSFC spherical harmonic time series is smoother, but still does not have good agreement with the SLR & DORIS solution. We conclude that the GRACE spacecraft are not a good sensor of this very long wavelength harmonic.

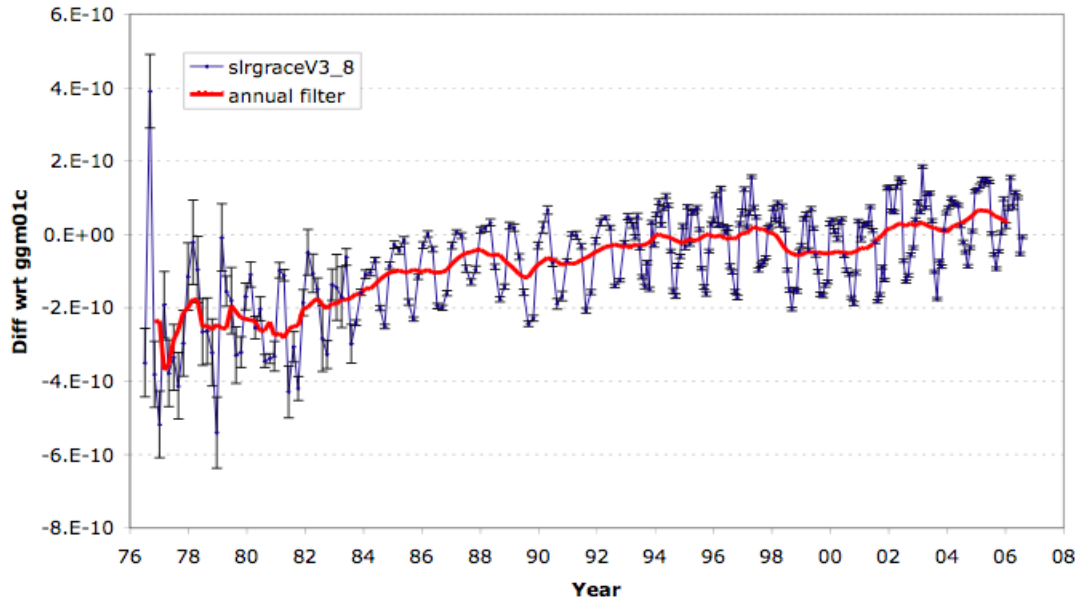


**Figure 2.** Monthly  $J_2$  solutions from SLR and DORIS tracking from 1976 through 2006. The solutions are shown w.r.t. the GGM01C solution, and with the application of an annual filter (red line).

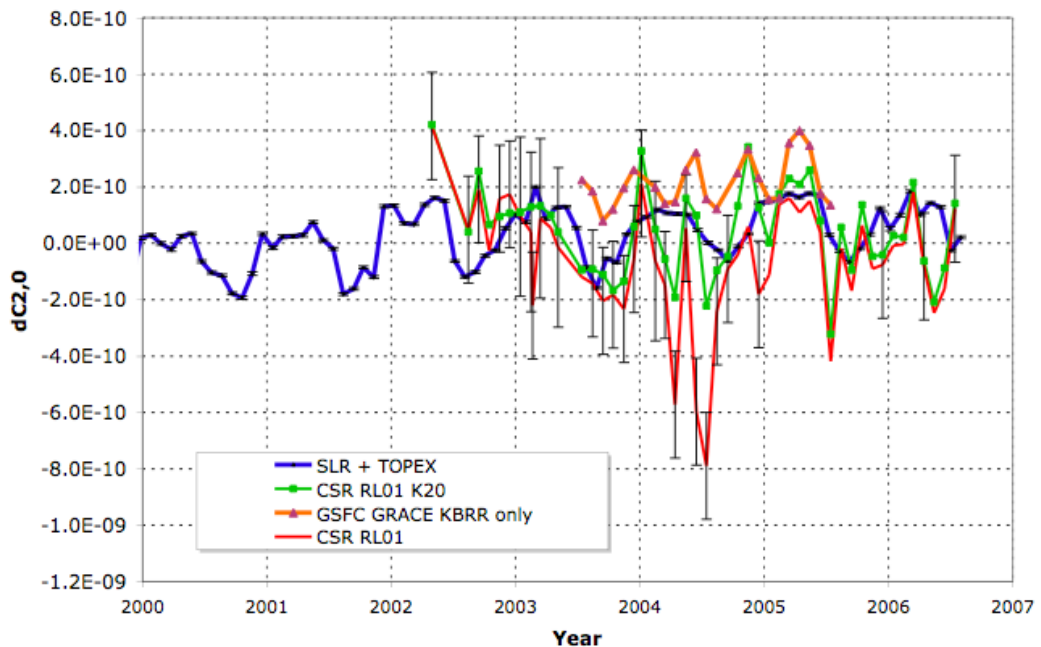


**Figure 3.** Comparison of solutions for  $C_{20}$  from the SLR and DORIS solutions, and from GRACE.

### Comparison of Other Low Degree Harmonics

The SLR and DORIS monthly time series is compared to the GRACE solutions in Figure 4 for the other low degree harmonics ( $C_{21}$ ,  $S_{21}$ ,  $C_{22}$ ,  $S_{22}$ ,  $C_{30}$  and  $C_{40}$ ). For  $C_{21}$  and  $S_{22}$ , the agreement is exceptionally good; For  $S_{21}$  and  $C_{22}$  there is some agreement on the amplitude of the variation, but the phases really do not match. For  $C_{30}$  we obtain the interesting result that the time series for the two GRACE solutions (CSR RL01, and NASA GSFC, KBRR-only) agree perfectly. The SLR and DORIS time series matches more closely the GRACE  $C_{30} + C_{50}$  solutions, suggesting that for the  $C_{30}$  harmonic, what the SLR and DORIS time series discerns is really a lumped harmonic. In contrast for the  $C_{40}$  harmonic, the GRACE solutions completely fail to discern the variations that are visible in the SLR and DORIS time series. We conclude that for  $C_{40}$ , just as for  $C_{20}$ , the GRACE spacecraft are simply not good sensors of this harmonic.

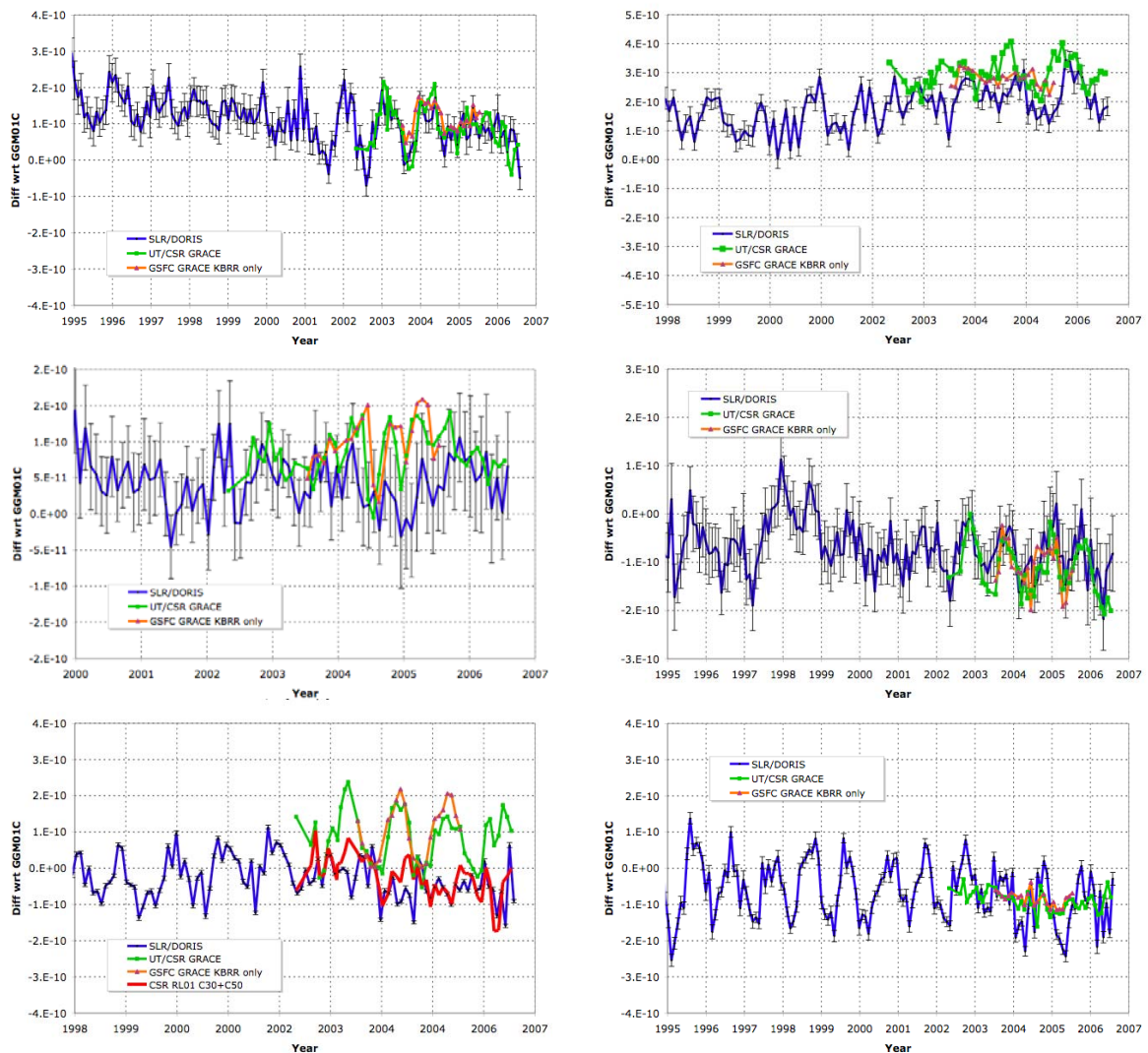


**Figure 4.** Comparison time series for the low-degree harmonics between GRACE and the SLR and DORIS solutions ( $C_{21}$ ,  $S_{21}$ ;  $C_{22}$ ,  $S_{22}$ ;  $C_{30}$ ,  $C_{40}$ ). We show the formal errors for the SLR/DORIS solutions. The agreement is exceptionally good for the  $C_{21}$  and  $S_{22}$  harmonics. For the two GRACE solutions tested, the variations in the  $C_{40}$  harmonic cannot be properly resolved.

### Recovery of Annual and Semiannual Harmonics

We are able to use the entire time series of SLR and DORIS data to recover the annual variations in the geopotential through degree six, and the semiannual variations through degree four. In Figure 5, the signal of the annual harmonics recovered from the CSR RL01 GRACE series, is compared to the signal recovered from the SLR & DORIS time series, and the formal uncertainties of the SLR and DORIS recovery. Thus, from this comparison of the degree variances, the SLR and DORIS data can recover signals between degrees five and six.

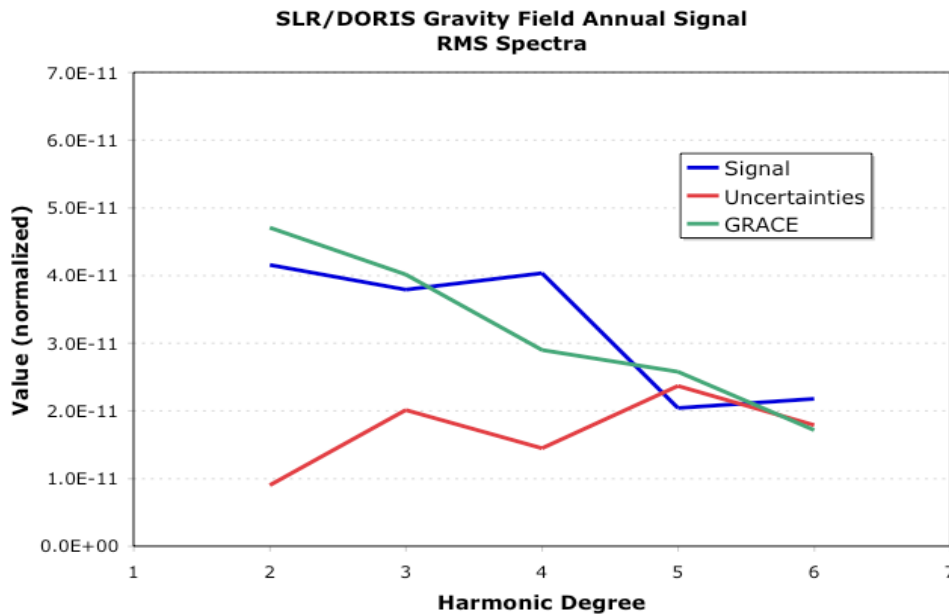


*Figure 5. Degree variances of the annual harmonics recovered from the SLR and DORIS data, and from the GRACE monthly solutions, compared to the formal uncertainties in the SLR/DORIS solutions. The SLR & DORIS time series can resolve the annual variations in the geopotential through degree five over a period of 25 years.*

The SLR/DORIS time series is sufficiently long that we can reliably recover annual and semiannual harmonics over different time scales. For example, if we compare the time-variable gravity variations for two SLR/DORIS solutions (1979-1997, and 1998-2005), we can observe for the most part overall similarities between the solutions. Both show the same patterns of geoid highs and geoid lows in the Amazon region, and Southeast Asia associated with the expected hydrology variations. If we compare the 1998-2005 SLR/DORIS solution to the annual and semiannual harmonics recovered from GRACE (in this case the CSR RL01), both observe the geoid highs in the Amazon in April and May, and the geoid lows in south east Asia and the Bay of Bengal. In addition, both data sets observe the same phase of the Southeast Asia monsoon with a prominent high in August and September over the Bay of Bengal, Bangladesh and the Indian subcontinent. The geoid low observed over the Amazon in November with the GRACE results is more prominent than with the SLR/DORIS observed variations.

### Recovery of Secular Geoid Rates

The long time series of SLR and DORIS data allows to solve for secular rates in the geopotential, not just with the zonal harmonics, but for all coefficients through degree

six. The recovered geoid rates are illustrated in Figure 6 for the period from 1979 through 1997. In this figure, the general pattern of post-glacial rebound is observed over Antarctica, Greenland and the Arctic consistent with post-glacial rebound models. Globally the scale of the variations is  $\pm 1$  mm/year, with an error of 0.14 mm/year. Secular geoid changes occur in other regions, for example over the Indian subcontinent (+0.5 mm/yr). While we may ascribe the secular changes in the polar regions for the most part to changes in the solid Earth (cf. post-glacial rebound), in other regions, other considerations (long-term hydrology or ocean mass variations) may also play a role. If secular solutions are obtained on shorter time scales (five years) the solutions differ considerably, indicating that on those time scales, annual and inter-annual variations in the geopotential are more prominent than the secular variations.

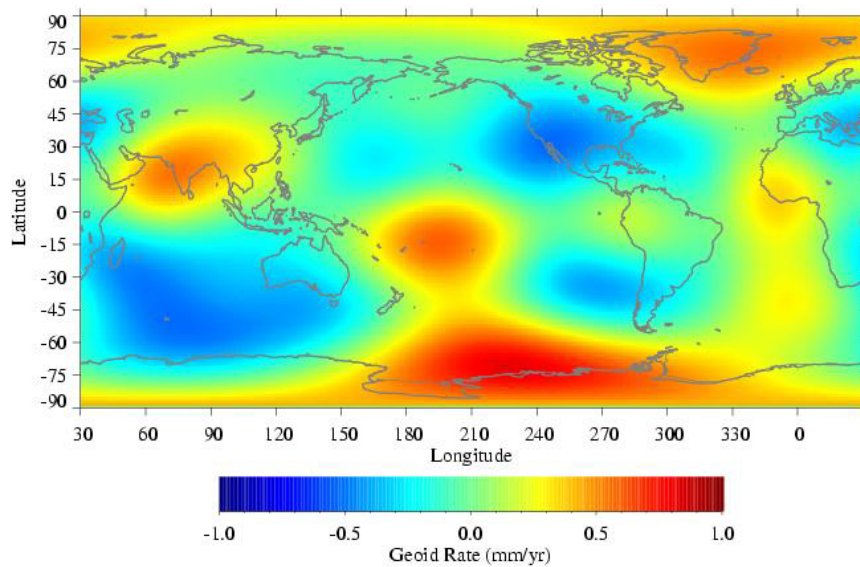


**Figure 6.** Geoid rates observed from 1979 through 1997 from SLR and DORIS data. The global error is 0.14 mm/yr.

## Summary

The long time series of SLR and DORIS data allow us to resolve periodic time variations on the time scale of months, and secular variations over the period of many years. These data allow us a window into geophysical mass flux variability over a period prior to the launch of GRACE. We discern that that 1998  $C_{20}$  anomaly was in fact an interannual variation, and that similar variations are observable over the course of the 25-year time series. The GRACE solutions for the low degree even zonals do not agree with those obtained from SLR and DORIS data, although in an overall sense the annual variations observed are similar. The SLR and DORIS data have sufficient strength to resolve secular changes in the geopotential through degree 6 corresponding to a spatial scale of 3300 km.

## Acknowledgements

The authors acknowledge the ILRS [Pearlman *et al.*, 2002] and the IDS [Tavernier *et al.*, 2006] for making the SLR and DORIS data available for this study as well as for overseeing the networks and the stations responsible for providing the data. Jennifer

Wiser Beall (Raytheon Corp, Upper Marlboro, MD) performed most of the GEODYN processing for the SLR and DORIS solutions.

## References

- [1] Altamimi Z., P. Sillard, and C. Boucher, ITRF2000: A new release of the International Terrestrial Reference Frame for earth science applications, *J. Geophys. Res.*, 107(B10), 2214, doi:10.1029/2001JB000561.
- [2] Cox, C.M., and B.F. Chao, Detection of a large-scale mass redistribution in the terrestrial system since 1998, *Science*, 297, 831, Aug. 2., 2002.
- [3] Luthcke, S.B., D.D. Rowlands, F. G. Lemoine, S.M. Klosko, D. Chinn, and J.J. McCarthy, Monthly spherical harmonic gravity field solutions determined from GRACE inter-satellite range-rate data alone, *Geophys. Res.Lett.*,33, L02402,
- [4] doi:10.1029/2005GL024846.
- [5] McCarthy, D.D., and G. Petit (Eds.), IERS Conventions, IERS Tech. Note, vol. 32, Verl. Des Bundesamts für Kartogr. Und Geod., Frankfurt am Main, Germany, 2003.
- [6] Pearlman, M.R., J. Degnan, and J.M. Bosworth (2002), The International Laser Ranging Service (ILRS), *Adv. Space Research*, 30, 135-143, 2002.
- [7] Ray, R.D., A global ocean tide model from TOPEX/Poseidon altimetry: GOT99.2, *NASA Technical Memo. 209478*, NASA Goddard Space Flight Center, 58 pp., 1999.
- [8] Tapley, B.D., S. Bettadpur, M. Watkins, and C. Reigber, The gravity recovery and climate experiment: Mission overview and early results, *Geophys. Res. Lett.*, 31, L09607, doi:10.1029/2004GL019920, 2004.
- [9] Tavernier, G. et al., The International DORIS Service: Genesis and early achievements, *J. Geodesy*, 80, 403-417, doi:10.1007/S00190-006-0082-4, 2006.

---

## Global Glacial Isostatic Adjustment: Target Fields for Space Geodesy

W.R. Peltier<sup>1</sup>

1. Department of Physics, University of Toronto, Toronto, Ontario, Canada M5S-1A7.

Contact: [peltier@atmosp.physics.utoronto.ca](mailto:peltier@atmosp.physics.utoronto.ca)

### Abstract

*A very detailed theory of the global process of glacial isostatic adjustment (GIA) is now available that is being employed to address a number of significant problems in both solid Earth geophysics and climate dynamics. A recent focus of the work in this area has been upon the impact of changes in the Earth's rotational state upon postglacial sea level history and the modern field of geoid height time dependence that is being measured by the GRACE dual satellite system that is now in space. Satellite laser ranging continues to play a critical role in the understanding of these processes. This paper summarizes recent progress in modelling the impact of the GIA process upon Earth's rotational state.*

### Introduction

The origins of highly significant anomalies in the Earth's rotational state, respectively the so-called non-tidal acceleration of the rate of axial rotation and the secular drift (true polar wander) of the pole of rotation relative to the surface geography, have been associated for some time with the influence of the glacial isostatic adjustment (GIA) process. The non-tidal acceleration is equivalent to a value for the time dependence of the degree 2 zonal coefficient in the spherical harmonic expansion of Earth's gravitational field, commonly represented as  $\dot{J}_2$  of  $(-2.67 \pm 0.15) \times 10^{-11}$  year<sup>-1</sup> (e.g. Cheng et al. 1989). The value for the rate of polar wander reported by Vincente and Yumi (1969, 1970) using the data of the International Latitude Service (ILS) was  $(0.95 \pm 0.15)$  degree/million years, a value that is close to the most recent estimation by Argus and Gross (2004) of 1.06 degree/million years. The latter authors have suggested that the observed direction and speed of polar wander should be corrected for the influence of plate tectonic motions and that this could be a significant effect, depending upon the assumptions on the basis of which the correction is made (see Table 1 of Argus and Gross, 2004).

The development of theoretical explanations for the above discussed anomalies in Earth rotation has been dominated by work over the past two decades that has suggested a close connection of them both to GIA. The earliest discussion of the impact upon polar wander that should be expected due to time dependent surface loading of a visco-elastic model of the Earth was that of Munk and MacDonald (1960) who employed a simple homogeneous model to suggest that wander of the pole could only occur in response to simultaneous variability in the surface mass load. This point was obscured in the later papers by Nakiboglu and Lambeck (1980, 1981) and Sabadini and Peltier (1981) whose analysis was based upon the application of a homogeneous viscoelastic model similar to that employed by Munk and MacDonald (1960). These authors, however, suggested that polar wander would continue on a homogeneous visco-elastic model of the Earth even after all temporal variations of the surface mass load had ceased. This significant error of interpretation was corrected in Peltier (1982) and Wu and Peltier (1984) who showed that, in the case of cyclic loading and unloading, as is appropriate for the computation of the GIA

effect following the series of glacial loading and unloading events that have characterized the Late Quaternary period of Earth history (e.g. Broecker and van Donk, 1970), there would be no polar wander effected once the cycle ended. The homogeneous visco-elastic model of the planet would therefore exhibit no memory of the past history of loading and unloading as correctly pointed out by Munk and McDonald. This was traced to the fact that, specifically for the homogeneous visco-elastic model, there exists an exact annihilation of the polar wander forced by the internal redistribution of mass due to the free relaxation of Earth's shape and that forced by the deformation due to the changing rotation itself (see e.g. Figure 2 of Wu and Peltier 1984).

Based upon the prior analysis of Peltier (1974, 1976), however, it was known that realistic viscoelastic models of the planetary interior were significantly more complex than could be accommodated by the homogeneous visco-elastic model of Munk and MacDonald (1960). Whereas the relaxation under surface forcing of a homogeneous visco-elastic model of the Earth is described by a single relaxation time that is unique for each spherical harmonic degree in the deformation spectrum, realistically layered spherical visco-elastic models have a much more complex relaxation spectrum, a unique spectrum consisting of an (often essentially) finite number of modes for each spherical harmonic degree. In Peltier (1982) and Wu and Peltier (1984) it was demonstrated that this realistic level of complexity endowed the Earth model with a memory of its history of surface loading and unloading such that the pole of rotation would continue to wander even after the surface load had ceased to vary. Deep sea core oxygen isotopic data based upon  $\delta^{18}O$  measurements on benthic foraminifera were employed as basis for the construction of a model of cyclic ice-sheet loading and unloading of the continents following the interpretation of such data as proxy for the variation of continental ice volume through time (Shackleton 1967, Shackleton and Opdyke 1973). Analysis based upon the application of rather crude models of the growth and decay of the Laurentide, Fennoscandian and Antarctic ice sheets then demonstrated that both the speed and direction of true polar wander as well as the non-tidal acceleration of rotation could be fit by the model and that the radial visco-elastic structure required to fit both of these observations was essentially the same. This was construed to strongly suggest that both anomalies might to be entirely explained as a consequence of the ongoing global process of glacial isostatic adjustment.

A recent objection to this interpretation was raised in the paper by Mitrovica, Wahr et al. (2005; hereafter MW) who have suggested that the theoretical formulation employed in Peltier (1982) and Wu and Peltier (1984) was mathematically "unstable" insofar as the computation of the polar wander component of the response to the GIA process is concerned. This objection appears to be based upon an error of mathematical comprehension as explicit analyses to be presented in what follows will demonstrate.

### **Computation of the rotational response of the Earth to the GIA process**

The time dependent impact on the Earth's rotational state of the glacial isostatic adjustment process is determined as a solution of the classical Euler equation describing the conservation of angular momentum of a system subjected to no external torques, as:

$$\frac{d}{dt} (J_{ij} \omega_i) + \epsilon_{ijk} \omega_j J_{k\ell} \omega_\ell = 0 \quad (1)$$

in which the  $J_{ij}$  are the elements of the moment of inertia tensor, the  $\omega_i$  are as previously and  $\epsilon_{ijk}$  is the Levi-Civita (alternating) tensor. Restricting attention to small departures from the modern state of steady rotation with angular velocity  $\Omega_o$ , we may construct a solution to (1), accurate to first order in perturbation theory, by expanding:

$$\omega_i = \Omega_o (\delta_{i3} + m_i); m_i = \omega_i / \Omega_o \quad (2a)$$

$$J_{11} = A + I_{11} \quad (2b)$$

$$J_{22} = B + I_{22} \quad (2c)$$

$$J_{33} = C + I_{33} \quad (2d)$$

$$J_{ij} = I_{ij}, i \neq j \quad (2e)$$

Substitution of these expansions into equation (1), keeping only terms of first order, leads to the standard set of governing equations for polar wander and the length of day, respectively (see Munk and McDonald, 1960), as:

$$\left. \begin{aligned} \frac{dm_1}{dt} + \frac{(C-B)}{A} \Omega_o m_2 &= \Psi_1 \\ \frac{dm_2}{dt} + \frac{(C-A)}{B} \Omega_o m_1 &= \Psi_2 \end{aligned} \right\} \text{polar wander} \quad (3a,b)$$

$$\left. \frac{dm_3}{dt} = \Psi_3 \right\} \text{length of day} \quad (3c)$$

in which the ‘‘excitation functions’’ are defined as:

$$\Psi_1 = \left( \frac{\Omega_o}{A} \right) I_{23} - \frac{(dI_{13}/dt)}{A} \quad (4a)$$

$$\Psi_2 = - \left( \frac{\Omega_o}{B} \right) I_{13} - \frac{(dI_{23}/dt)}{B} \quad (4b)$$

$$\Psi_3 = - \left( \frac{I_{33}}{C} \right) \quad (4c)$$

Now it is critical to recognize that there exist perturbations  $I_{ij}$  to the inertia tensor due to two distinct causes, namely due to the direct influence of change in the mass distribution of the planet that accompanies the change in planetary shape due to surface loading and unloading and that due to the additional deformation induced by the changing rotation triggered by the surface mass loading and unloading process. The contribution due to the former process may be represented as (e.g. Peltier, 1982):

$$I_{ij}^{GIA} = \left( 1 + k_2^L(t) \right) * I_{ij}^R(t) \quad (5)$$

in which  $k_2^L(t)$  is the surface mass load Love number of degree 2 and the  $I_{ij}^R$  are the perturbations of inertia that would obtain due to the variation in surface mass load if the Earth were rigid. The symbol \* in equation (5) represents the convolution operation. The contribution to the perturbations of inertia due to the changing rotation

follows from an application of a linearized version of MacCullagh's formula (e.g. see Munk and MacDonald, 1960) as:

$$I_{13}^{\text{ROT}} = \left( \frac{k_2^T * a^5 \omega_1 \omega_3}{3G} \right) = \left( \frac{k_2^T}{k_f} \right) * m_1 (C - A) \quad (6a)$$

$$I_{23}^{\text{ROT}} = \left( \frac{k_2^T * a^5 \omega_2 \omega_3}{3G} \right) = \left( \frac{k_2^T}{k_f} \right) * m_2 (C - A) \quad (6b)$$

with 
$$k_f = \left( \frac{3G}{a^5 \Omega_0^2} \right) (C - A) \quad (6c)$$

the value of which is determined entirely by the observed flattening of the Earth's figure. Assuming the validity of the data in Yoder (1995) as listed on the web site: ([www.agu.org/references/geophys/4\\_Yoder.pdf](http://www.agu.org/references/geophys/4_Yoder.pdf)), one obtains the value  $k_f \cong 0.9414$ , a value that deviates somewhat from the value of 0.9382 employed in MW.

### The General Solution for the Rotational Response in the Laplace Transform Domain

Since the solution of equation (3c) for the change in the axial rate of rotation is uncomplicated, it will suffice to focus first in what follows on the solution of (3a) and (3b) for the polar wander component of the response to surface loading. Substitution of (6a) and (6b) into (3a,b), the Laplace-transformed forms of the equations that follow are simply:

$$s m_1 + \sigma \left( 1 - \frac{k_2^T(s)}{k_f} \right) m_2 = \Psi_1(s) \quad (7a)$$

$$s m_2 + \sigma \left( 1 - \frac{k_2^T(s)}{k_f} \right) m_1 = \Psi_2(s) \quad (7b)$$

where 
$$\sigma = \Omega_0 \frac{(C - A)}{A} \quad (7c)$$

is the Chandler Wobble frequency of the rigid Earth, "s" is the Laplace transform variable, and again A=B has been assumed. The Laplace-transformed forms of the excitation functions in (4a) and (4b) are simply:

$$\Psi_1(s) = \left( \frac{\Omega_0}{A} \right) I_{23}(s) - \left( \frac{s}{A} \right) I_{13}(s) \quad (8a)$$

$$\Psi_2(s) = \left( \frac{\Omega_0}{A} \right) I_{13}(s) - \left( \frac{s}{A} \right) I_{23}(s) \quad (8b)$$

with 
$$I_{ij}(s) = \left( 1 + k_2^L(s) \right) I_{ij}^{\text{Rigid}}(s) \quad (8c)$$

Now equations (7a) and (7b) are elementary algebraic equations for  $m_1(s)$  and  $m_2(s)$  and these may be solved exactly to write:

$$m_1(s) = \frac{1 + k_2^L(s)}{s^2 + \sigma^2 \left(1 + \frac{k_2^T(s)}{k_f}\right)^2} \left[ \left( \frac{\Omega_o \sigma}{A} \right) \left( 1 - \frac{k_2^T(s)}{k_f} \right) - \frac{s^2}{A} \right] I_{13}^{\text{Rigid}}(s) \quad (9a)$$

$$m_2(s) = \frac{1 + k_2^L(s)}{s^2 + \sigma^2 \left(1 + \frac{k_2^T(s)}{k_f}\right)^2} \left[ \left( \frac{\Omega_o \sigma}{A} \right) \left( 1 - \frac{k_2^T(s)}{k_f} \right) - \frac{s^2}{A} \right] I_{23}^{\text{Rigid}}(s) \quad (9b)$$

If we now neglect terms of order  $s^2/\sigma^2$  in (9a,b), which delivers a highly accurate approximation free of the influence of the Chandler wobble, we obtain:

$$m_1(s) = \left( \frac{\Omega_o}{A \sigma} \right) \frac{1 + k_2^L(s)}{1 - \frac{k_2^T(s)}{k_f}} I_{13}^{\text{Rigid}}(s) = H(s) I_{13}^{\text{Rigid}}(s) \quad (10a)$$

$$m_2(s) = H(s) I_{23}^{\text{Rigid}}(s) \quad (10b)$$

A convenient short-hand form for the solution vector  $(m_1, m_2) = \underline{m}$  is to write:

$$\underline{m}(s) = \frac{\underline{\Psi}^L(s)}{\begin{bmatrix} 1 - \frac{k_2^T(s)}{k_f} \end{bmatrix}} = H(s) \left( I_{13}^{\text{Rigid}}(s), I_{23}^{\text{Rigid}}(s) \right) \quad (11a)$$

$$\text{where } \underline{\Psi}^L(s) = \left[ \left( \frac{\Omega_o}{A \sigma} \right) (1 + k_2^L(s)) \left( I_{13}^{\text{Rigid}}(s), I_{23}^{\text{Rigid}}(s) \right) \right] \quad (11b)$$

### An Exact Inversion of the Laplace Transform Domain Solution

From equations (11) it will be clear that the polar wander solution  $m(s)$  will depend critically upon the ratio  $k_2^T(s)/k_f$ . This fact was more fully exposed in the analysis of Peltier (1982) and Wu and Peltier (1984) who re-wrote the Laplace transform domain forms of  $k_2^T(s)$  and  $k_2^L(s)$  as (e.g. see equation 61 of Wu and Peltier 1984):

$$k_2^T(s) = k_2^T(s=0) - s \sum_{j=1}^N \frac{(q'_j/s_j)}{(s + s_j)} \quad (12a)$$

$$k_2^L(s) = (-1 + \ell_s) - s \sum_{j=1}^N \frac{(q_j/s_j)}{(s + s_j)} \quad (12b)$$

in which the superscript  $\ell=2$  on  $q_j^2, r_j^2, s_j^2$  has been suppressed for convenience. Substituting (12a) into (11a) this may be re-written as:

$$\underline{m}(s) = \frac{\underline{\Psi}^L(s)}{\left[ 1 - \frac{k_2^T(s=0)}{k_f} \right] + \frac{s}{k_f} \sum_{j=1}^N \frac{(q'_j / s_j)}{(s + s_j)}} \quad (13)$$

In their discussion of the formal inversion of (13) into the time domain, Peltier (1982) and Wu and Peltier (1984) made the approximation that the term in square brackets in the denominator of 13 could be safely neglected. In MW it is claimed that this renders the numerical structure employed to compute the time domain response unstable. This appears to be connected to a misunderstanding of the Tauberian Theorem (eg Widmer, 1983) which asserts that the infinite time limit of  $\mathbf{m}(t)$  will be equal to the  $s \rightarrow 0$  limit of the product  $s\mathbf{m}(s)$ . Clearly the approximation in which the square bracketed term in the denominator of (13) is neglected, in which case one is assuming that  $k_2^T(s=0) = k_f$ , the multiplication by “s” on the lhs of (13) cancels the “s” in the denominator of (13), thus rendering the infinite time limit of the approximate form of (13) entirely stable. In this brief paper my purpose is to

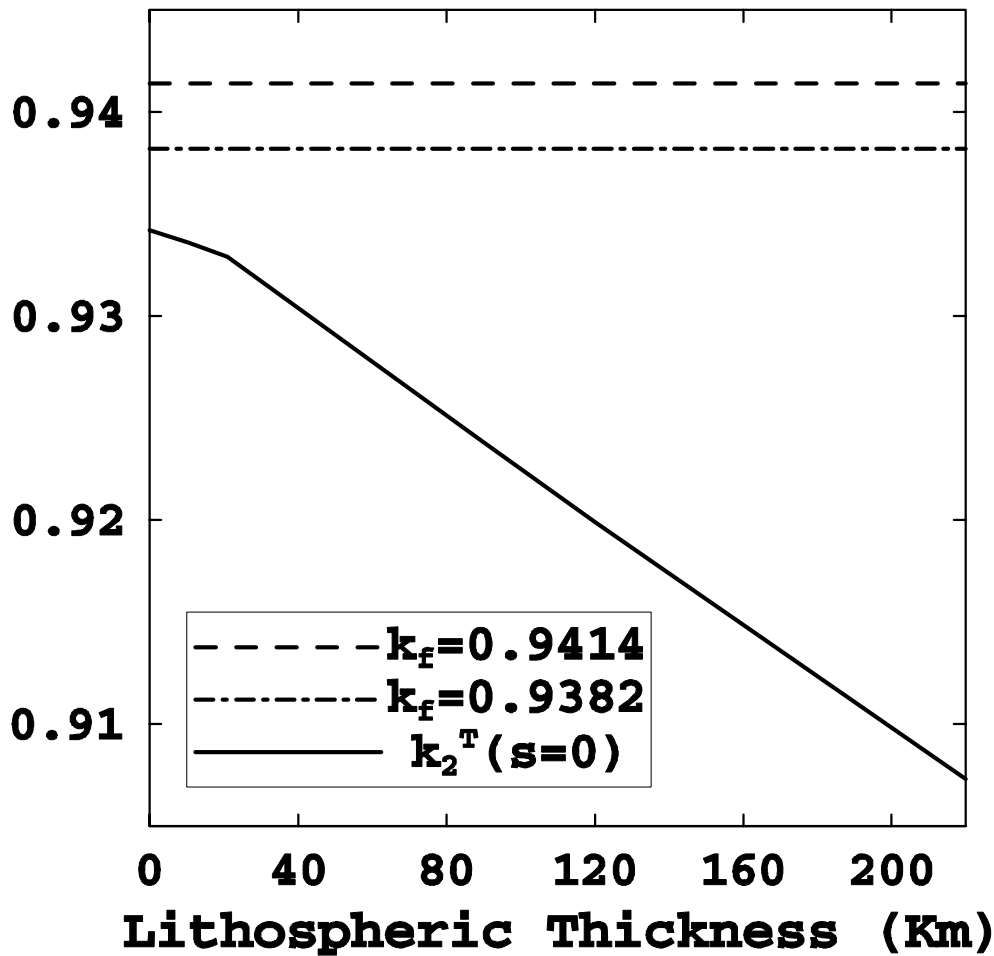


*Figure 1. Compares the value of the degree 2 “tidal Love number” in the limit of zero frequency ( $s=0$ ) with the two estimates of the “fluid Love number” discussed in the text*

demonstrate this fact by computing exact solutions for the inverse of (13) without making the approximation involved in the neglect of the term in square brackets in the denominator of (13). It is nevertheless useful to start this process by showing explicitly that this term is small. This is demonstrated in Figure 1 where I show  $k_2^T(s=0)$  as a function of lithospheric thickness “L”. It will be clear by inspection of this Figure, on which the two previously cited values for  $k_f$  are also shown, that in the limit of zero lithospheric thickness the approximation made in the analyses of Peltier (1982) and Wu and Peltier (1984) becomes increasingly more valid. That the Earth might be expected to respond to the GIA process such that the flattening of its figure was accurately predictable by the infinite time limit of the first order linear visco-elastic field theory of Peltier (1974) is entirely expected. The fact that it is not “exactly” predictable by this field theory (see Figure 1) is also entirely expected because processes other than the basic rotation of the object, such as mantle convection, may also contribute to this flattening. To demonstrate the impact of the approximation previously made in constructing the solutions for the polar wander speed and direction caused by the GIA process we must invert the Laplace transform domain solution (13) exactly. This was not done in MW and this appears to have clouded their judgement as to what the impact might be.

When the assumption  $k_2^T(s=0) = k_f$  is abandoned, the Laplace transform domain impulse response may then be written in the form:

$$H(s) = \left( \frac{\Omega_o}{A\sigma} \right) \frac{1 + k_2^L(s)}{k_f \sum_{j=1}^N \frac{(q_j/s_j)}{(s + s_j)} + \varepsilon} \quad (14a)$$

where

$$\varepsilon = 1 - \frac{k_2^T(s=0)}{k_f}. \quad (14b)$$

As will become clear, even though  $\varepsilon$  is a small quantity (especially in the case that the finite thickness of the lithosphere may be neglected in the limit  $t \rightarrow \infty$ ), retaining it in expression (14a) for the impulse response could have a significant impact upon the solution as the rotational stability of the system would be modified. Now the construction of the solution for the time-domain form of the impulse response  $H(t)$  proceeds in this case as in the case based upon the Equivalent Earth Model assumption, although the result differs somewhat from a physical perspective. In this case it is useful to make the distinction between the Chandler wobble frequency of a rigid Earth  $\sigma$  and the Chandler wobble frequency of the visco-elastic Earth  $\sigma_o$ , by employing the definition:

$$\sigma_o = \frac{(k_2^T(s=0) - k_2^{TE})}{k_2^T(s=0)} \sigma. \quad (15)$$

We must then re-write the expression for  $H(s)$  as:

$$H(s) = \left( \frac{\Omega}{A\sigma_o} \right) \frac{(1 + k_2^L(s))}{\left( (1 - \varepsilon)s \sum_{i=1}^N \frac{g_j}{s + s_j} \right) + \varepsilon'} \quad (16a)$$

with

$$\varepsilon' = \varepsilon \frac{\sigma}{\sigma_0}, \quad (16b)$$

and,

$$g_j = \frac{q'_j/s_j}{\sum_j (q'_j/s_j)}. \quad (16c)$$

The inversion of  $H(s)$  into the time domain now proceeds by expanding the sum in the denominator of (16a) in the form:

$$\sum_{j=1}^N \frac{g_j}{(s+s_j)} = \frac{Q_{N-1}(s)}{\prod_{j=1}^N (s+s_j)} = \frac{\prod_{j=1}^{N-1} (s+\lambda_j)}{\prod_{j=1}^N (s+s_j)} \quad (17)$$

since  $\sum_j g_j \equiv 1$ . Then we have, suppressing for the moment the factor  $(\Omega_0 / A\sigma_0)$ ,

$$H(s) = \frac{\prod_{j=1}^N (s+s_j) [1+k_2^L(s)]}{(1-\varepsilon)s \prod_{i=1}^{N-1} (s+\lambda_i) + \varepsilon' \prod_{j=1}^N (s+s_j)}. \quad (18)$$

Now substituting for the function  $1+k_2^L(s)$  from (12b) we obtain:

$$H(s) = \frac{\prod_{j=1}^N (s+s_j) \ell_s}{(1-\varepsilon)s \prod_{i=1}^{N-1} (s+\lambda_i) + \varepsilon' \prod_{i=1}^N (s+s_i)} + \sum_{j=1}^N \frac{(-q_j/s_j)s \prod_{i \neq j}^N (s+s_i)}{(1-\varepsilon)s \prod_{i=1}^{N-1} (s+\lambda_i) + \varepsilon' \prod_{i=1}^N (s+s_i)} \quad (19a)$$

$$= \frac{\prod_{j=1}^N (s+s_j) \ell_s}{(1-\varepsilon+\varepsilon') \prod_{i=1}^N (s+\kappa_i)} + \sum_{j=1}^N \frac{(-q_j/s_j)s \prod_{i \neq j}^N (s+s_i)}{(1-\varepsilon+\varepsilon') \prod_{i=1}^N (s+\kappa_i)}. \quad (19b)$$

Where now the  $\kappa_i$  are the  $N$  roots of the polynomial in the denominator of the 2 terms in (19a). This expression for the impulse response may be further reduced by re-writing the ratios of products as follows:

$$\frac{\prod_{j=1}^N (s+s_j)}{\prod_{j=1}^N (s+\kappa_j)} = 1 - \frac{q'(s)}{\prod_{i=1}^N (s+\kappa_i)} \quad (20a)$$

where now 
$$q'(s) = \prod_{j=1}^N (s+\kappa_j) - \prod_{j=1}^N (s+s_j) \quad (20b)$$

$$\text{and} \quad \frac{s \prod_{i \neq j}^N (s + s_i)}{\prod_{j=1}^N (s + \kappa_j)} = 1 - \frac{R'_j(s)}{\prod_{i=1}^N (s + \kappa_i)} \quad (21a)$$

$$\text{with} \quad R'_j(s) = \prod_{i=1}^N (s + \kappa_i) - s \prod_{i \neq j}^N (s + s_i) \quad (21b)$$

We then have, for the Laplace transform of the impulse response, the expression:

$$H(s) = \frac{\ell_s}{(1 - \varepsilon + \varepsilon')} \left\{ 1 - \frac{q'(s)}{\prod_{i=1}^N (s + \kappa_i)} \right\} + \frac{1}{(1 - \varepsilon + \varepsilon')} \sum_{j=1}^N \left( -\frac{r_j}{s_j} \right) \left\{ 1 - \frac{R'_j(s)}{\prod_{i=1}^N (s + \kappa_i)} \right\} \quad (22a)$$

or

$$H(s) = \frac{\ell_s - \sum_{j=1}^N r_j / s_j}{(1 - \varepsilon + \varepsilon')} - \frac{\ell_s q'(s)}{(1 - \varepsilon + \varepsilon') \prod_{i=1}^N (s + \kappa_i)} + \frac{1}{(1 - \varepsilon + \varepsilon')} \sum_{j=1}^N \frac{(q_j / s_j) R'_j(s)}{\prod_{i=1}^N (s + \kappa_i)} \quad (22b)$$

Denoting  $\ell_s - \sum_{j=1}^N r_j / s_j = 1 + k_2^{LE} = D_1$ , say, then we may further reduce the expression for the impulse response to:

$$H(s) = \frac{D_1}{(1 - \varepsilon + \varepsilon')} - \frac{1}{(1 - \varepsilon + \varepsilon')} \left\{ \frac{\ell_s q'(s) - \sum_{j=1}^N (q_j / s_j) R'_j(s)}{\prod_{i=1}^N (s + \kappa_i)} \right\} \quad (23)$$

The inverse Laplace transform of this expression is such that the solution in the present case, in which  $k_2^T(s=0) \neq k_f$ , is just:

$$m_1(t) = \frac{1}{(1 - \varepsilon + \varepsilon')} \left( \frac{\Omega_o}{A \sigma_o} \right) \left\{ \left[ \ell_s - \sum_{j=1}^N \frac{r_j}{s_j} \right] I_{13}^{\text{Rigid}}(t) + \sum_{i=1}^N E'_i e^{-\kappa_i t} * I_{13}^{\text{Rigid}}(t) \right\} \quad (24a)$$

$$m_2(t) = \frac{1}{(1 - \varepsilon + \varepsilon')} \left( \frac{\Omega_o}{A \sigma_o} \right) \left\{ \left[ \ell_s - \sum_{j=1}^N \frac{r_j}{s_j} \right] I_{23}^{\text{Rigid}}(t) + \sum_{i=1}^N E'_i e^{-\kappa_i t} * I_{23}^{\text{Rigid}}(t) \right\} \quad (24b)$$

where

$$E'_i = \left\{ -\ell_s q'(-\kappa_i) + \sum_{j=1}^N \frac{r_j}{s_j} R'_j(-\kappa_i) \right\} / \prod_{i=j}^N (\kappa_j - \kappa_i). \quad (24c)$$

The polar wander velocity vector components are obtained simply by time differentiation of equations (24a) and (24b). It is useful to compare the result in (24) to the solutions that obtain under the approximation previously employed. In the limit  $\varepsilon \rightarrow 0$  we have  $\kappa_N = 0$  and  $\kappa_i = \lambda_i$  the N-1 relaxation times that govern the system in this limit. In this case, the parameter  $E'_N$  in the above becomes:

$$E'_N = - \frac{\ell_1 q(0)}{\prod_{j=1}^{N-1} (\kappa_j - \kappa_N)} = - \frac{\ell_s q(0)}{\prod_{j=1}^{N-1} \lambda_j} \quad (25)$$

And the previous approximate result is fully recovered.

In order to compare the temporal histories of the rotational anomalies in the two cases, it will be important to proceed by keeping as many features of the Earth model fixed as possible. To this end and for the remainder of this paper, I will focus entirely upon the nature of the solutions that obtain when the recently published ICE-5G model of the glaciation and deglaciation process of Peltier (2004) is employed to determine the rotational excitation functions required for the evaluation of the solution (24). In the next section results will be discussed for a sequence of simple two layered viscosity structures as a function of the parameter  $\varepsilon$  in order to explicitly demonstrate the highly stable nature of the solution in the limit that this parameter vanishes.

## Results

Of particular importance for the purpose of this paper is the sensitivity of the predictions of polar wander speed to the assumption that  $k_2^T(s=0)$  may be assumed to be equal to  $k_f$ . When this assumption is not made, then the solution is given by equation (24). In the latter, there appears the quantity  $(1 - \varepsilon + \varepsilon')$ , the values in which for the Earth model (VM2) in question are respectively 0.034, 0.05, and 1.017 (for  $\varepsilon$ ,  $\varepsilon'$  and  $1 - \varepsilon + \varepsilon'$ ) when the thickness of the lithosphere is taken to be 90 km. In Figure 2 (bottom) are plotted the predictions of polar wander speed based upon equations (24) as a function of the viscosity of the lower mantle with the upper mantle viscosity held fixed to the value in the VM2 model of Peltier (1996). Results are also shown for several different values of a parameter  $\Delta = \varepsilon / 0.034$  including the value  $\varepsilon = 0.034$  ( $\Delta = 1$ ) which is appropriate for the VM2 model with a lithospheric thickness of 90 km, in which case  $k_2^T(s=0) = 0.9263$ , but also for significantly smaller values of  $\varepsilon$  including the value  $\varepsilon = 0$  ( $\Delta = 0$ ) so as to investigate the “smoothness” of the transition from the value  $\varepsilon = 0$  which obtains when  $k_2^T(s=0)$  is assumed to be equal to  $k_f$ . The two intermediate values of  $\Delta$  for which results are shown on Figure 2 correspond to the two values of  $k_f$  shown on Figure 1 when the lithospheric thickness  $L$  is assumed to be equal to zero. Also shown on Figure 2 (top) is the dependence of the predicted value of the non-tidal acceleration as a function of lower mantle viscosity.

Inspection of Figure 2 clearly demonstrates the fact that the solutions for polar wander speed that obtain in the limit  $\Delta = 0$  are almost identical to those that obtain for either of the two non-zero values that correspond to zero lithospheric thickness. This demonstrates that the formulation of Peltier (1982) and Wu and Peltier (1984) based upon the approximation  $k_2^T(s=0) = k_f$  was not mathematically unstable as claimed in WM. In fact, careful inspection of Figure 2 will show that the preferred solution for BOTH the non-tidal acceleration and polar wander speed is the model

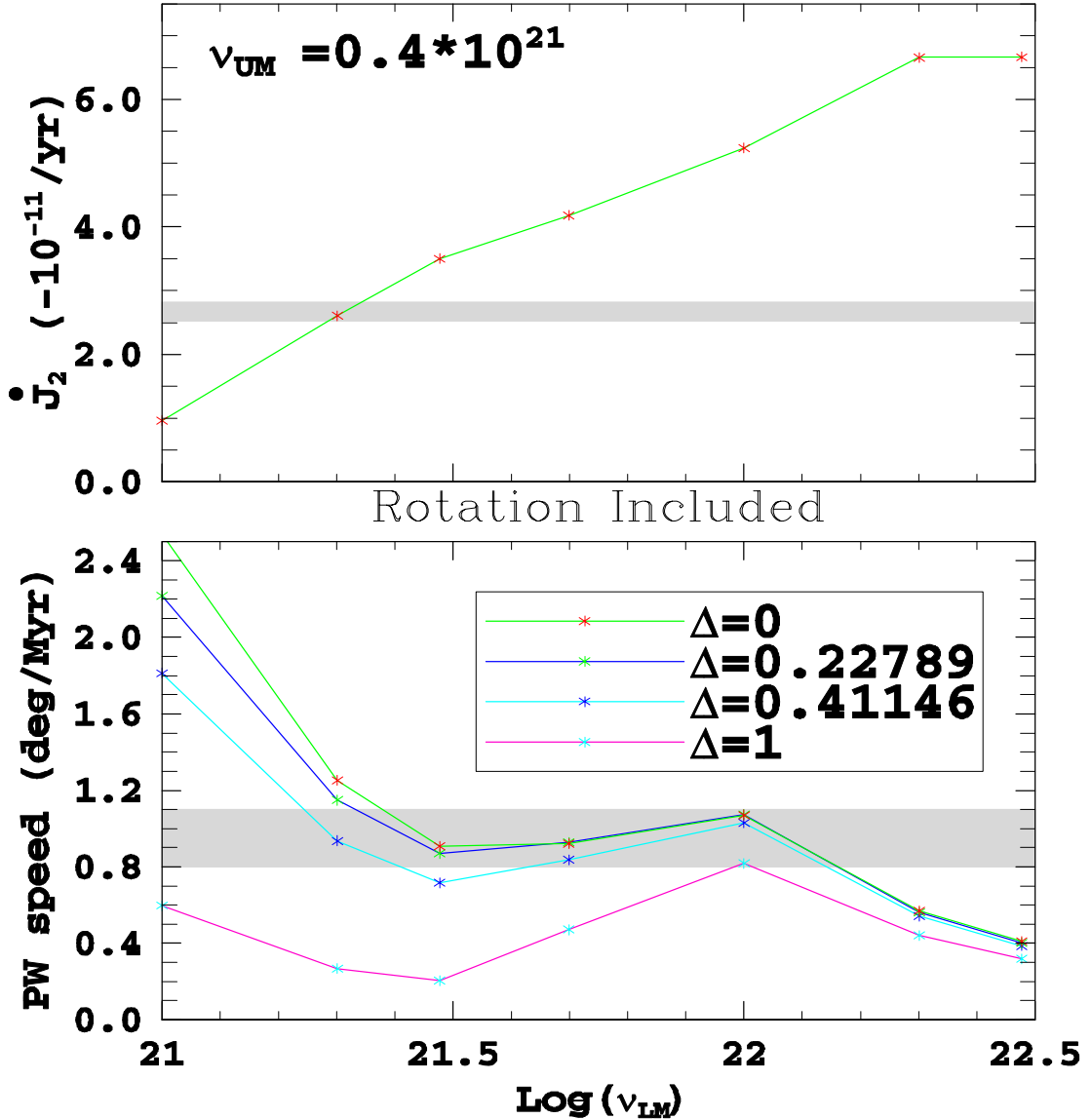


**Figure 2.** This Figure compares model predictions of the non-tidal acceleration of rotation (top) and of the speed of polar wander (bottom) as a function of the viscosity of the lower mantle when the upper mantle viscosity is held fixed to the value in the VM2 viscosity model of Peltier (1996). The polar wander speed predictions are shown for several values of the parameter  $\Delta$  which measures the importance of the difference between the fluid Love number  $k_f$  and  $k_2^T(s=0)$ . The two values of  $\Delta$  that are less than unity, 0.22789 and 0.41146, correspond respectively to the  $k_f$  values of 0.9382 and 0.9414 and are those that obtain in the limit of vanishing lithospheric thickness. The value  $\Delta = 1$  is the value appropriate for a finite lithospheric thickness of 90 km.

with  $\Delta = 0.41146$  AND  $L=0.0$ . This solution amounts to a very modest adjustment of the earlier result obtained with  $\Delta = 0.0$  and  $L=0.0$ . The results for finite non-zero lithospheric thickness cannot fit the observed polar wander speed except, marginally, for a model with an upper mantle-lower mantle viscosity contrast that is incompatible with the observed non-tidal acceleration. Such high contrast viscosity models are also firmly rejected by relative sea level data from the previously ice covered area of North America.

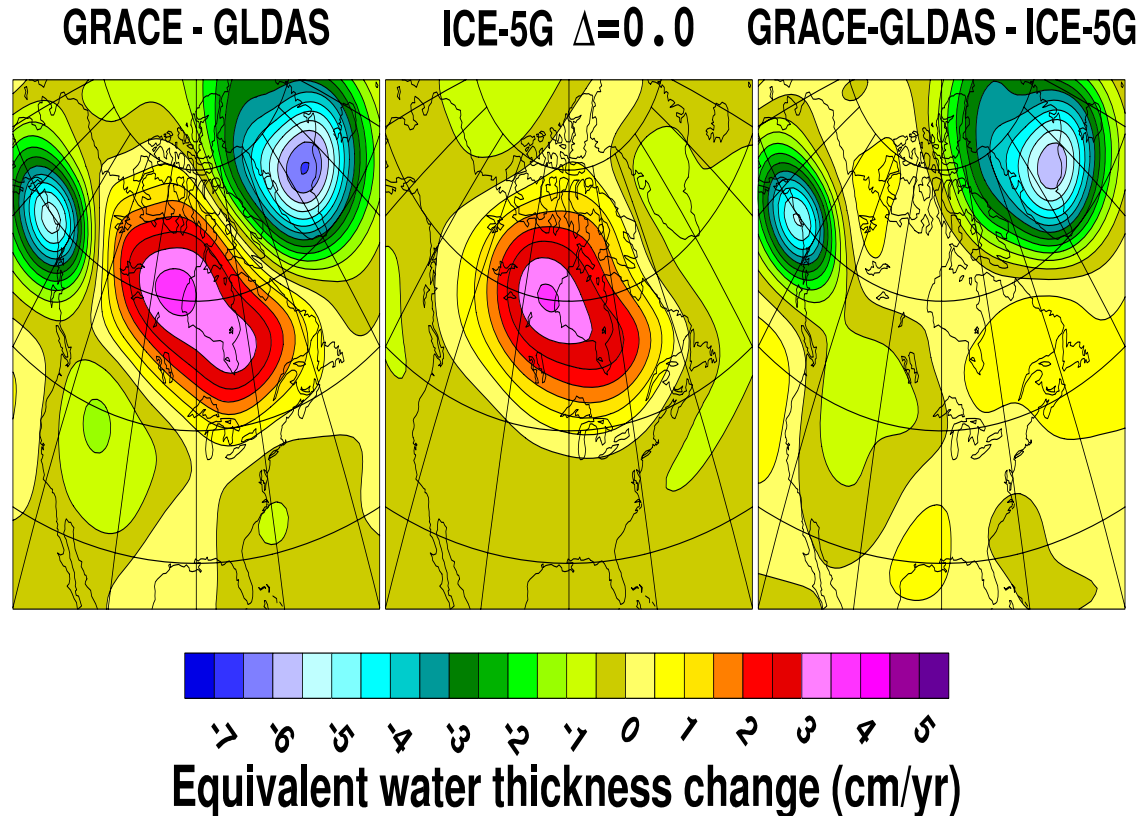


*Figure 3. Demonstrates the ability of the GIA model of Peltier(2004) to accurately explain the observed time dependence of the gravity field over the North American continent. This field is represented by the time rate of change of the thickness of an equivalent layer of water at the earth's surface. This analysis is based upon the level 2 release of the GRACE Stokes coefficients. In this comparison, the degree 2 terms have been excluded, a consequence of the fact that GRACE does not provide accurate measures of these coefficients.*

The quality of this low contrast model is also strongly re-enforced by the recently obtained time dependent gravity field data from the GRACE satellite system. Figure 3 compares the GRACE observed and hydrology corrected GRACE time dependent gravity field observations with the ICE-5G(VM2) GIA model prediction of the same field. In the third frame of Figure 3 the difference between these two data sets is also shown, thus demonstrating the extremely high quality of the ICE-5G(VM2) model. The neglect of the degree 2 coefficients, which are very large for the ICE-5G(VM2) model, as demonstrated in Peltier (2004), is required by virtue of the inability of GRACE to accurately observe these coefficients..

**Conclusion**

The analyses described in the previous sections of this paper have considerably extended the previously published theory that is employed to compute the response of

the earth's rotational state to the global process of glacial isostatic adjustment. These analyses suffice to refute the claim in MW that the formalism described in Peltier (1982) and Wu and Peltier (1984) was fundamentally unstable mathematically. This error of interpretation appears to have been due to a lack of understanding of the Tauberian Theorem that may be employed to predict the infinite time limit of a solution from the Laplace transform of this solution. The extended version of the theory described herein has allowed a direct investigation of the question of the extent to which the finite thickness of a globally continuous and unbroken lithosphere may contribute to the rotational response to surface mass load forcing. These analyses demonstrate that, in this long timescale limit, the most accurate representation of the rotational response of the Earth is that based upon the assumption of vanishing lithospheric thickness. This is understandable on the basis of the fact that the lithosphere of the planet is "broken" into a series of weakly coupled plates. For planets whose lithospheres are not unbroken in this way, the same assumption would clearly not be appropriate.

## References

- [1] Argus, D.F. & Gross, R.S. An estimate of motion between the spin axis and the hotspots over the past century. *Geophys. Res. Lett.* **31**, L06614, doi:10.1029/2004GL019657,2004
- [2] Broecker, W.S. & Van Donk, J. Insolation changes, ice volumes, and the  $\delta^{18}\text{O}$  record in deep sea cores. *Geophys. Space Phys.* **8**, 169-198, 1970.
- [3] Cheng, Mik, Eanes, R.J., Shum, C.K., Schutz, B.E. & Tapley, B.D. Temporal variations in low degree zonal harmonics from Starlette orbit analysis. *Geophys. Res. Lett.* **16**, 393-396, 1989.
- [4] Clark, J.A., Farrell, W.E. & Peltier, W.R. Global changes in postglacial sea levels: A numerical calculation. *Quat. Res.* **9**, 265-287, 1978.
- [5] Dahlen, F.A. The passive influence of the oceans upon the rotation of the Earth. *Geophys. J.R. Astron. Soc.* **46**, 663-406, 1976.
- [6] Domack, E., Duran, D., Leventer, A., Ishman, S., Doane, S., McCullum, S., Amblas, D. Ring, J. Gilbert, R. & Prentice, M. Stability of the Larsen B ice shelf on the Antarctic Peninsula during the Holocene epoch. *Nature* **436**, 681-685, 2005.
- [7] Dziewonski, A.M. & Anderson, D.L. Preliminary reference Earth model. *Phys. Earth Planet. Int.* **25**, 297-356, 1981.
- [8] Farrell, W.E. Deformation of the Earth by surface loads. *Rev. Geophys.* **10**, 761-797, 1972.
- [9] Farrell, W.E. & Clark, J.A. On postglacial sea level. *Geophys. J.R. Astron. Soc.* **46**, 647-667, 1976.
- [10] Imbrie, J., Hays, J.D., Martinson, D.G., McIntyre, A., Mix, A.C., Morley, J.J., Pisias, N.G., Prell, W.L. & Shackleton, N.J. The orbit theory of Pleistocene climate: Support from a revised chronology of the marine  $\delta^{18}\text{O}$  record in Milankovitch and Climate, edited by A. Berger et al., pp. 269-306. D. Reidel, Norwell, Mass., 1984.
- [11] Lambeck, K. & Chappell, J. Sea level change through the last glacial cycle. *Science* **292**(5517), 679-686, 2001.
- [12] Mitrovica, J.X., Wahr, J., Matsuyama, I. & Paulson, A. The rotational stability of an ice-age Earth. *Geophys. J. Int.* **161**, 491-506, 2005.
- [13] Nakiboglu, S.M. & Lambeck, K. Deglaciation effects on the rotation of the Earth. *Geophys. J.R. Astron. Soc.* **62**, 49-58, 1980.
- [14] Nakiboglu, S.M. & Lambeck, K. Deglaciation related features of the Earth's gravity field. *Tectonophysics* **72**, 289-303, 1981.
- [15] Peltier, W.R. The impulse response of a Maxwell Earth. *Rev. Geophys. Space Physics.* **12**, 649-669, 1974.
- [16] Peltier, W.R. Glacial isostatic adjustment, II: The inverse problem. *Geophys. J. Roy. Astron. Soc.* **46**, 669-706, 1976.
- [17] Peltier, W.R. Dynamics of the ice-age Earth. *Advances in Geophysics*, **24**, 1-146, 1982.

- [18] Peltier, W.R. The LAGEOS constraint on deep mantle viscosity: Results from a new normal mode method for the inversion of visco-elastic relaxation spectra. *J. Geophys. Res.* **90**, 9411-9421, 1985.
- [19] Peltier, W.R. Ice-age paleotopography. *Science* **265**, 195-201, 1994.
- [20] Peltier, W.R. Mantle viscosity and ice-age ice-sheet topography. *Science* **273**, 1359-1364, 1976.
- [21] Peltier, W.R. Postglacial variations in the level of the sea: implications for climate dynamics and solid-Earth geophysics. *Rev. Geophys.* **36**, 603-689, 1998.
- [22] Peltier, W.R. Comments on the paper of Yokoyama et al. (2000) entitled "Timing of the last glacial maximum from observed sea level minima" *Quat. Sci. Rev.* **21**, 409-414, 2002a.
- [23] Peltier, W.R. One eustatic sea level history, Last Glacial Maximum to Holocene. *Quat. Sci. Rev.* **21**, 377-396, 2002b.
- [24] Peltier, W.R. Global glacial isostatic adjustment: paleo-geodetic and space-geodetic tests of the ICE-4G (VM2) model. *J. Quat. Sci.* **17**, 491-510, 2002c.
- [25] Peltier, W.R. On the hemispheric origins of meltwater pulse 1a. *Quat. Sci. Rev.* **24**, 1655-1671, 2005.
- [26] Peltier, W.R., Farrell, W.E., & Clark, J.A. Glacial isostasy and relative sea-level: a global finite element model. *Tectonophysics*, **50**, 81-110, 1978.
- [27] Peltier, W.R. & Jiang, X. Glacial isostatic adjustment and Earth rotation: Refined constraints on the viscosity of the deepest mantle. *J. Geophys. Res.* **101**, 3269-3290, 1996 (Correction, *J. Geophys. Res.* **102**, 10,101-10,103, 1997).
- [28] Peltier, W.R., Shennan, I., Drummond, R. & Horton, B. On the postglacial isostatic adjustment of the British Isles and the shallow visco-elastic structure of the Earth. *Geophys. J. Int.*, **148**, 443-475, 2002.
- [29] Peltier, W.R. & Fairbanks, R.G. Global glacial ice-volume and Last Glacial Maximum duration from an extended Barbados Sea Level record. *Quat. Sci. Rev.*, 2006.
- [30] Sabadini, R. & Peltier, W.R. Pleistocene deglaciation and the Earth's rotation: implications for mantle viscosity. *Geophys. J. Roy. Astron. Soc.* **66**, 553-578, 1981.
- [31] Stephenson, E.R. & Morrison, L.V. Long term fluctuations in the Earth's rotation: 700 B.C. to A.D. 1990. *Philos. Trans. R. Soc. London, Ser. A*, **351**, 165-202, 1995.
- [32] Shackleton, N.J. Oxygen isotope analysis and Pleistocene temperatures re-addressed. *Nature* **215**, 15-17, 1967.
- [33] Shackleton, N.J. & Opdyke, N.D. Oxygen isotope and paleomagnetic stratigraphy of equatorial Pacific core V28-238: Oxygen isotope temperatures and ice volumes on a  $10^5$ -year time scale. *Quaternary Res.* **3**, 39-55, 1973.
- [34] Vincente, R.O. & Yumi, S. Co-ordinates of the pole (1899-1968) returned to the conventional international origin. *Publ. Int. Latit. Obs. Mizusawa* **7**, 41-50, 1969.
- [35] Vincente, R.O. & Yumi, S. Revised values (1941-1961) of the co-ordinates of the pole referred to the CIO. *Publ. Int. Latit. Obs. Mizusawa* **7**, 109-112, 1970.
- [36] Waelbroecke, C., Labyrie, L., Michel, E., Duplessy, J.-C. McManus, J.F., Lambeck, K., Balbon, E. & Labracherie, M. Sea-level and deep water temperature changes derived from benthic foraminifera isotopic records. *Quat. Sci. Rev.* **21**, (1-3), 295-305, 2002.
- [37] Wu, P. & Peltier, W.R. Pleistocene deglaciation and the Earth's rotation: A new analysis. *Geophys. J. R. astr. Soc.* **76**, 202-242, 1984.
- [38] Yoder, C.F., Williams, J.G., Dickey, J.O., Schutz, B.E., Eanes, R.J. & Tapley, B.D. Secular variation of the Earth's gravitational harmonic  $J_2$  coefficient from LAGEOS and non-tidal acceleration of Earth rotation. *Nature* **303**, 757-762, 1983.
- [39] Yoder, C.F., 1995. [www.agu.org/references/geophys/4\\_Yoder.pdf](http://www.agu.org/references/geophys/4_Yoder.pdf)
- [40] Yokoyama, Y., Lambeck, K., DeDekkar, P., Johnston, P. & Fifield, L.K. Timing of the Last Glacial Maximum from observed sea level minima. *Nature* **406**, 713-716, 2000. (Correction, 2001, *Nature* **412**, 99).

---

## Recent Results from SLR Experiments in Fundamental Physics: Frame Dragging observed with Satellite Laser Ranging.

E. C. Pavlis<sup>1</sup>, I. Ciufolini<sup>2</sup>, R. König<sup>3</sup>

1. Joint Center for Earth Systems Technology (JCET), UMBC, Baltimore, MD, USA.
2. Università degli Studi di Lecce, Lecce, Italy
3. GeoForschungsZentrum (GFZ), Potsdam, Germany.

Contact: [epavlis@JCET.umbc.edu](mailto:epavlis@JCET.umbc.edu) / Fax: +1 410 455 5868

### Abstract

*Satellite laser ranging provided for decades the most precise measurement of positions and velocities of earthbound tracking stations, as well as the most precise orbits of earth-orbiting artificial satellites. While the latter applies to any satellite carrying the appropriate reflectors, the use of these orbits for precise geodetic products requires the use of specially designed target satellites in high altitude orbits, such as the two LAGEOS satellites. To achieve such high quality, the motion of these satellites must be described with equally accurate models, such as those made available recently, thanks to missions like CHAMP and GRACE. This led to the synergistic application of such precise products to devise tests of fundamental physics theories. Nearly twenty years after conceiving and proposing an initial concept for a General Relativity (GR) prediction test, our recent experiment resulted in a positive and convincing measurement of the Lense-Thirring effect, also known as the gravitomagnetic effect of the rotating Earth. Using state-of-the-art Earth gravitational field models based on data from the CHAMP and GRACE missions, we obtained an accurate measurement of the Lense-Thirring effect predicted by GR, analyzing eleven years of LAGEOS and LAGEOS 2 Satellite Laser Ranging (SLR) data. The new result, in agreement with the earlier one based on Earth models JGM-3 and EGM96, is far more accurate and more robust. The present analysis uses only the nodal rates of the two satellites, making NO use of the perigee rate, thus eliminating the dependence on this unreliable element. Using the EIGEN-GRACE02S model, we obtained our optimal result:  $\mu = 0.99$  (vs. 1.0 in GR), with a total error between  $\pm 0.05$  and  $\pm 0.1$ , i.e., between 5% and 10 % of the GR prediction. Results based on processing with NASA and GFZ s/w will be presented, along with preliminary tests with very recent improved GRACE models. Further improvement of the gravitational models in the near future will lead to even more accurate tests. We discuss the LAGEOS results and some of the crucial areas to be considered in designing the future LARES mission dedicated to this test.*

### Introduction

One of the most fascinating theoretical predictions of general relativity is “frame-dragging” (Misner et al. 1973, Ciufolini and Wheeler 1995), also known as the Lense-Thirring effect, after the two Austrian physicists who predicted the effect based on Einstein’s General Relativity (GR) theory (Lense and Thirring, 1918). The equivalence principle, at the basis of Einstein’s gravitational theory, states that “locally”, in a sufficiently small spacetime neighbourhood, in a freely falling frame, the observed laws of physics are the laws of special relativity. However, the axes of these inertial frames where “locally” the gravitational field is “unobservable”, rotate with respect to “distant stars” due to the rotation of a mass or in general due to a

current of mass–energy. In general relativity the axes of a local inertial frame can be realized by small gyroscopes, as shown in Figure 1.

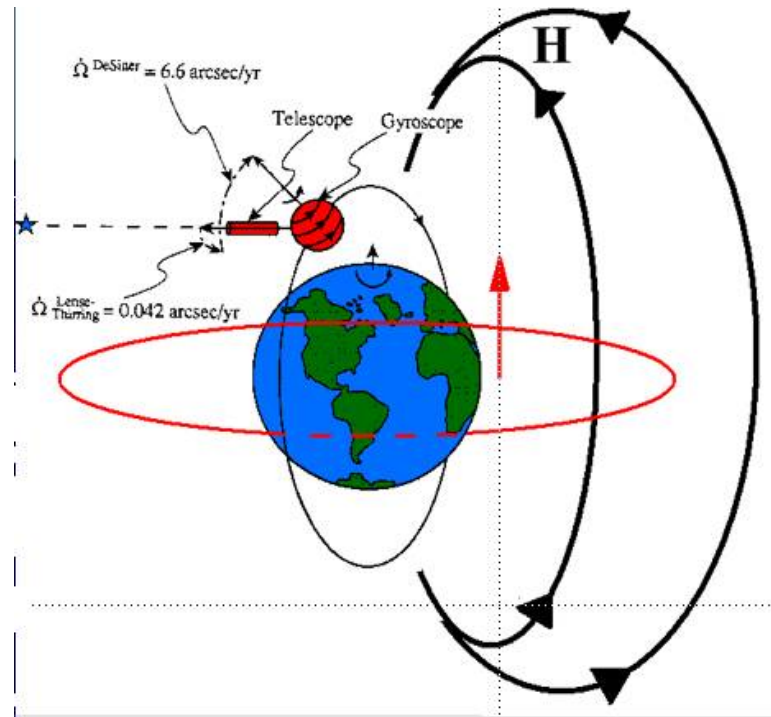


**Figure 1.** The gravitomagnetic field and the mass-energy currents that produce the frame-dragging effect on the node of the orbiting gyroscope.

### Methodology

The gravitomagnetic force is by far smaller than the gravitational monopole, so we can use the tools of celestial mechanics and consider this force as a perturbation on an orbiting satellite. From the integrated (to first order) perturbation equations we obtain the most significant effects on the orbital elements, the secular rates of the node and perigee:

$$\left\{ \begin{array}{l} \dot{\Omega}^{L-T} = \frac{2GJ}{c^2 a^3 (1-e^2)^{3/2}} \\ \dot{\omega}^{L-T} = \frac{-6GJ}{c^2 a^3 (1-e^2)^{3/2}} \cos I \end{array} \right.$$

In the past we used both quantities in our methodology (Ciufolini *et al.*, 1998) due to the lack of accurate enough gravitational models. Since the release of improved models from the CHAMP and GRACE missions though, we only use the node rate in our experiments. Our methodology uses as “source” of the field Earth with its angular momentum, as a test particle the geodetic satellites LAGEOS and LAGEOS 2 at present (and in the future LARES, see more on this later), and our basic observations are the two-way precise ranging with laser pulses from the ground network of the International Laser Ranging Service (ILRS), (Pearlman *et al.*, 2002).

Perturbations due to  $J_2$  are much larger than the Lense-Thirring (LT) effect, so we need to be able to eliminate such uncertainties in order to extract the sought-for LT signal from our data. Thanks to Ciufolini's 1986 idea however, (using a "butterfly" configuration of counter-orbiting satellites in supplementary inclination orbits, Figure 2), the effect of  $J_2$  uncertainties is cancelled.

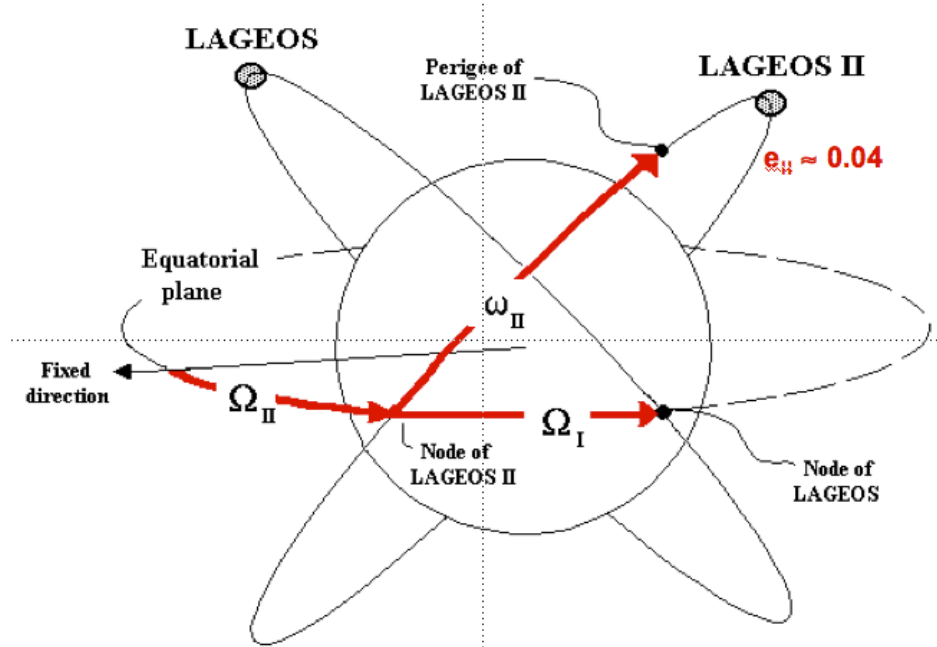


**Figure 2.** The nearly-“butterfly” configuration of the retrograde LAGEOS ( $i = 109.8^\circ$ ) and the prograde LAGEOS 2 ( $i = 52.6^\circ$ ) orbits.

When the two orbits are supplementary, one-half the sum of their nodal rate variations would provide a direct observation of the LT effect. However, Ciufolini (1989) generalized his original idea of the butterfly configuration to configurations of  $N$  nodes of various orbits, to cancel out the effects of the first  $N-1$  even zonals on the nodal rates of these orbits. Using this modified constraint for the case of two orbits in near- (but not exact) butterfly configuration, such as the LAGEOS and LAGEOS 2 orbits, we obtain:

$$\delta\dot{\Omega}_I + k\delta\dot{\Omega}_{II} = 48.2\mu + \text{other errors} \quad [\text{mas/y}]$$

where  $k$  ( $\approx 1/2$ ) is a function of the elements of the two orbits, and  $\mu$  is our LT parameter to be determined. If  $\mu = 1$ , GR is correct, if  $\mu = 0$  the Newtonian physics are correct. Under “other errors” we lump a number of higher order errors and the uncertainty in the background models mapped on the estimated quantity  $\mu$ . Extensive error analysis of the experiment provides bounds on these errors and allows for a realistic error budget for the result (Ciufolini, Pavlis and Peron, 2006). We separate the error sources in two groups, the gravitational and the non-gravitational. A summary of the results published in detail in (*ibid.*) are given in Figures 3 and 4.

This study supports the errors quoted for our most recent published results for  $\mu$ , (Ciufolini and Pavlis, 2004), between 5 and 10% of the expected value of 1 for GR. This improved (in accuracy) result compared to our 1998 result, is a direct consequence of the highly improved gravitational model accuracy, thanks to the use

of gravity mapping data from the CHAMP and GRACE missions (Reigber *et al.*, 2002, 2003, 2005 and Tapley *et al.*, 2002 and 2003). These products are the enabling factors for the success of these experiments. Pavlis (2002) and Ries *et al.* (2003) had already forewarned of this leap in accuracy for these models and proposed the continuation of the LAGEOS experiments in anticipation of their release.

### Gravitational perturbations:

- Even zonal harmonic coefficients  $J_{2n}$  of the geopotential (static part)
- Odd zonal harmonic coefficients  $J_{2n+1}$  (static part)
- Non zonal harmonic coefficients (Tesseral and Sectorial)
- Solid and ocean Earth tides and other temporal variations of Earth gravity field
- Solar, lunar and planetary perturbations
- de Sitter precession
- Other general relativistic effects
- Deviations from geodesic motion

$$\delta\mu^{\text{even zonals}} \leq 3\text{-}4\% \mu^{\text{GR}}$$

$$\delta\mu^{\text{odd zonals}} \leq 10^{-3} \mu^{\text{GR}}$$

$$\delta\mu^{\text{tides}} \leq 1\% \mu^{\text{GR}}$$

$$\delta\mu^{\text{other ...}} \leq 10^{-3} \mu^{\text{GR}}$$

*Figure 3. The calibrated errors on  $\mu$ , due to realistic uncertainties of the gravitational parameters.*

### Non-gravitational perturbations:

- Solar radiation pressure
- Earth albedo
- Anisotropic emission of thermal radiation due to Sun visible radiation (Yarkovsky-Schach effect)
- Anisotropic emission of thermal radiation due to Earth infrared radiation (Yarkovsky-Rubincam effect)
- Neutral and charged particle drag
- Earth magnetic field

$$\delta\mu^{\text{solar rad.}} \leq 10^{-3} \mu^{\text{GR}}$$

$$\delta\mu^{\text{albedo}} \leq 1\% \mu^{\text{GR}}$$

$$\delta\mu^{\text{Y-S}} \leq 1\% \mu^{\text{GR}}$$

$$\delta\mu^{\text{Y-R}} \leq 1\% \mu^{\text{GR}}$$

$$\delta\mu^{\text{Drag-like}} \leq 10^{-3} \mu^{\text{GR}}$$

*Figure 4. The calibrated errors on  $\mu$ , due to realistic uncertainties of the non-gravitational parameters.*

### The 2004 experiment results

The most accurate results on the measurement of the LT effect were published in (Ciufolini and Pavlis, 2004). The methodology and error analysis were subsequently detailed in (Ciufolini, Pavlis and Peron, 2006). These two references describe in detail the technique and the data that were used for the 2004 experiment. The basic points to be noted here are that the analysis covered the period from 1993 (just after the launch of LAGEOS 2) up to 2004, including all SLR data from the two LAGEOS satellites. The data were reduced using 15-day orbital arcs with a one-day overlap. The models used were the most accurate and consistent with the IERS Conventions 2003. All known perturbations were modeled **except** for the LT effect (set to zero). Once all arcs were converged, for each LAGEOS we formed a time series of consecutive arcs' nodal longitude differences, i.e. the nodal longitude at  $t_d^{\text{ARC}=n+1}$  and the same quantity obtained for the same time from the previous arc at  $t_d^{\text{ARC}=n}$ . These were then integrated and combined using our constraint equation to generate a single time series. The secular trend of these series is the sought-for estimate of the  $\mu$  LT parameter. Figure 5 shows the final result for the 2004 experiment.

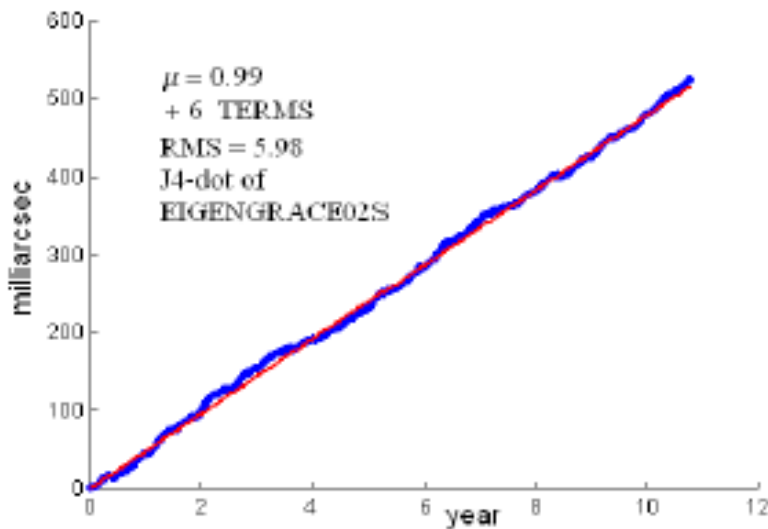


*Figure 5. The linear trend of the LAGEOS and LAGEOS 2 integrated nodal longitude differences time series for the EIGEN-GRACE02S gravitational model. Six periodic signals associated with well-known periods were filtered at the same time.*

We have already discussed the accuracy estimates associated with the 2004 result and the extensive work done to validate these error estimates as much as possible. It is worth noting that the gravitational model improvements from additional years of GRACE data result in an ever-improving estimate of these errors. The converging progression of these accuracy estimates provides a means to validate our quoted accuracy estimates for previous experiments. It is this point that makes the forthcoming new and much improved GRACE model GGM03S so anxiously awaited by all.

### Beyond the 2004 experiment

The LAGEOS experiments are a zero-budget verification experiment for the much more accurate (~0.1%) and expensive (>\$700M) result expected from NASA's Gravity Probe B mission (Buchman et al., 2000). In particular, with the recent

discovery of unanticipated errors in the gyro design of GP-B (Tomlin, 2007), it is doubtful that the GP-B results will ever break the 10% accuracy level (Kahn, 2007), so the LAGEOS experiments may eventually take a totally unforeseen center role in the area of fundamental physics tests.

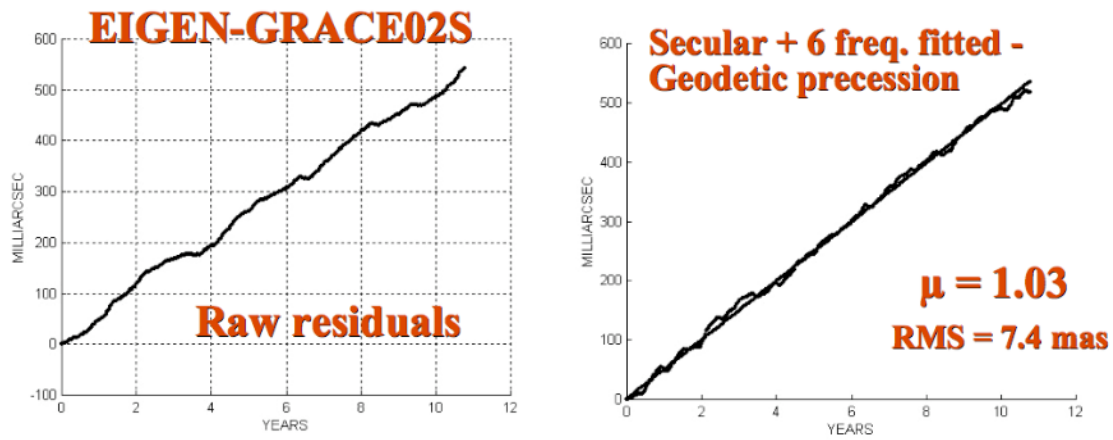


**Figure 6.** Results from the GFZ software package EPOS, replicating the 2004 experiment (preliminary, pending small s/w improvements in the force model).

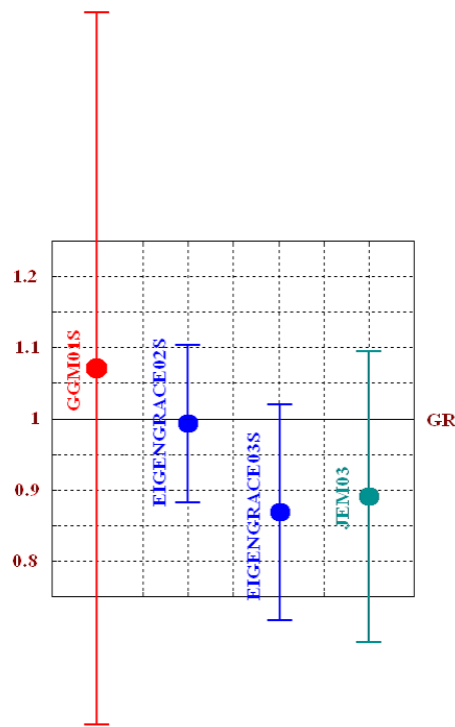


**Figure 7.** Results from the joint analysis for four different gravitational models from GRACE (plotted is the value of the recovered  $\mu$ , with unity signifying GR is correct).

To improve the validation of our results our original group was extended to encompass analysts from other institutions and allow an independent check of the results with multiple software packages and alternate reduction philosophy. So far, the GFZ group has become an integral and active participant with their software package EPOS. First results from their initial attempts to replicate our 2004 experiment are shown in Fig. 6. The small discrepancy with respect to our 2004 result is due to the

fact that their software needs some small improvements to match the modeling that was used in Geodyn. In addition to the test results for 2004, new models developed by various GRACE science team groups were also used to derive new estimates of  $\mu$ . Using different gravitational models we also get a good sense of the variability of the  $\mu$ -estimates due to the change in the model, the development group's strategy and their ability to properly calibrate the errors of their model. The results are shown in a summary plot in Figure 7.

### **LAGEOS results and LLR claims**

It is sometimes claimed that gravitomagnetism, measured already by SLR with the LAGEOS satellites, (might also be detected after refining the GP-B data analysis, see Tomlin, 2007), has already been observed by Lunar Laser Ranging (LLR), (Murphy in these proceedings and Murphy *et al.*, 2007); however the gravitomagnetic effects measured by LLR and the LAGEOS satellites are intrinsically different.

The gravitomagnetic effect measured by LLR depends on the motion of a gyroscope (the Earth-Moon system in the case of the LLR analysis) with respect to a central mass (the mass of the Sun in the LLR analysis) and, by changing the frame of reference used in the analysis, is equivalent to the geodetic precession, already well measured by LLR. The second gravitomagnetic effect measured by the LAGEOS satellites is an intrinsic gravitomagnetic effect (Ciufolini, 1994 and Ciufolini and Wheeler, 1995, Ciufolini 2007) that cannot be eliminated by means of any coordinate transformation.

In general relativity, in the frame in which a mass is at rest the so-called "magnetic" components  $g_{0i}$  of the metric are zero (in standard PPN coordinates). However, if an observer is moving with velocity  $\mathbf{v}$  relative to the mass, the "magnetic" components  $g_{0i}$  are no longer nonzero in his local frame. These "magnetic" components  $g_{0i}$  can be simply eliminated by a Lorentz transformation back to the original frame. This is precisely what has been observed by LLR since the first measurements of the geodetic precession of the lunar orbit. In contrast, a mass object (such as Earth) with angular momentum  $J$  generates a gravitomagnetic field intrinsic to the structure of spacetime that therefore cannot be eliminated by a simple coordinate transformation or choice of reference frame. This is the field producing the LT effect on Earth orbiting satellites such as LAGEOS, measured by SLR.

In general relativity, given explicitly a general metric  $\mathbf{g}$ , with or without magnetic components  $g_{0i}$ , in order to test for intrinsic gravitomagnetism (i.e. which cannot be eliminated with a coordinate transformation), one should use the Riemann curvature tensor  $\mathbf{R}$  and the spacetime invariants built using it (Ciufolini, 1994 and Ciufolini and Wheeler, 1995). Ciufolini and Wheeler (1995) give the explicit expression of the Riemann curvature invariant  $*\mathbf{R}\cdot\mathbf{R}$ , where  $*\mathbf{R}$  is the dual of  $\mathbf{R}$ . Irrespective of the frame of choice, this invariant is non-zero in the case of the Kerr metric generated by the angular momentum and the mass of a rotating body. When however we evaluate it for the Schwarzschild metric generated by the mass of a non-rotating body, it is equal to zero for any frame and coordinate system of choice. In (*ibid.*) it is shown that the gravitomagnetic effect measured by LAGEOS and LAGEOS 2, due to Earth's angular momentum, is intrinsic to the spacetime's curvature and cannot be eliminated by a simple change of frame of reference since the spacetime curvature invariant  $*\mathbf{R}\cdot\mathbf{R}$  is different from zero. However, the effect measured by LLR is just a gravitomagnetic effect that depends on the velocity of the Earth-Moon system and whose interpretation depends on the frame used in the analysis.

Murphy *et al.* (2007) show that on the lunar orbit there is a gravitomagnetic acceleration that changes the Earth-Moon distance by about 5 meters with monthly and semi-monthly periods. In a frame of reference co-moving with the Sun, the lunar gravitomagnetic acceleration in the Moon's equation of motion, is  $\sim \mathbf{v}_M \times (\mathbf{v}_E \times \mathbf{g}_{ME})$ ; where  $\mathbf{v}_M$  and  $\mathbf{v}_E$  are the velocities of Moon and Earth in the frame of reference co-moving with the Sun and  $\mathbf{g}_{ME}$  is the standard Newtonian acceleration vector on the Moon due to the Earth mass; this is the term discussed in (Murphy *et al.*, 2007). However, in a geocentric frame of reference co-moving with Earth, the lunar gravitomagnetic acceleration can be written:  $\sim \mathbf{v}_M \times (\mathbf{v}_S \times \mathbf{g}_{MS})$ : where  $\mathbf{v}_M$  and  $\mathbf{v}_S$  are the velocities of Moon and Sun in the frame of reference co-moving with Earth and  $\mathbf{g}_{MS}$  is the standard Newtonian acceleration vector on the Moon due to the Sun mass. This acceleration can be simply rewritten as a part equivalent to the geodetic precession (Ciufolini 2007) and another one too small to be measured at the present time.

This argument can be made rigorous by using the curvature invariant  $*\mathbf{R} \cdot \mathbf{R}$ . This invariant is formally similar to the invariant  $*\mathbf{F} \cdot \mathbf{F}$  equal to  $\mathbf{E} \cdot \mathbf{B}$  in electromagnetism. In the case of a point-mass metric generated by Earth and Sun, this invariant is:  $\sim \mathbf{G} \cdot \mathbf{H}$ , where  $\mathbf{G}$  is the standard Newtonian electric-like field of the Sun and Earth and  $\mathbf{H}$  the magnetic-like field of the Sun and Earth; this magnetic-like field is  $\sim \mathbf{v} \times \mathbf{G}$  and then clearly, on the ecliptic plane, the invariant  $*\mathbf{R} \cdot \mathbf{R}$  is null. Indeed, this invariant has been calculated (Ciufolini 2007) to be zero on the ecliptic plane, even after considering that the lunar orbit is slightly inclined on the ecliptic plane, this component would only give a contribution to the change of the radial distance too small to be measured at the present time.



**Figure 8.** A 1:2 model of the proposed LARES (Bosco *et al.*, 2006) geodetic satellite for SLR applications in relativistic tests and geodetic TRF development.

### Summary and future plans

The analysis of nearly twelve years of SLR data from LAGEOS and LAGEOS 2 has demonstrated the measurement of the LT effect at the 5-10% level for the first time. This result was possible because of the extremely precise gravitational models developed from the gravity-mapping missions CHAMP and GRACE. The results have been validated with independently developed s/w and our future plans include further additional validation with even more groups.

Interim results are also exchanged and compared with John Ries of Univ. of Texas, who is now using the UTEX software UTOPIA, in a similar reduction approach and obtains similar results. We hope to have UTOPIA results regularly in the near future, as the UTEX group makes time for participation in these experiments. It is our intention to have a new experiment using the new and soon to be released 3<sup>rd</sup>-generation UTEX model GGM03S, using all s/w packages (GEODYN, EPOS and UTOPIA) and groups, extending our LAGEOS data span by several years (3+) to the present, and incorporating many small but significant model improvements, especially in the temporally varying gravitational signals area due to climate change and global mass redistribution.

In a parallel process we are actively pursuing the optimal design and likely contribution of a new dedicated mission, LARES (Bosco *et al.*, 2006), which is currently in pre-phase B and expected to be in orbit in the next two years. Although not identical to LAGEOS, the improved design of LARES will result in a better LT measurement and expand the list of high-accuracy geodetic targets for TRF and low-degree temporal gravity observations. As explained in (*ibid.*), LARES is being designed with the utmost care for the definition of its “signature”, i.e. the precise offset between the effective reflection plane and its CoM, to minimize errors that affect the origin and scale of the TRF. A half-scale model of LARES is shown in

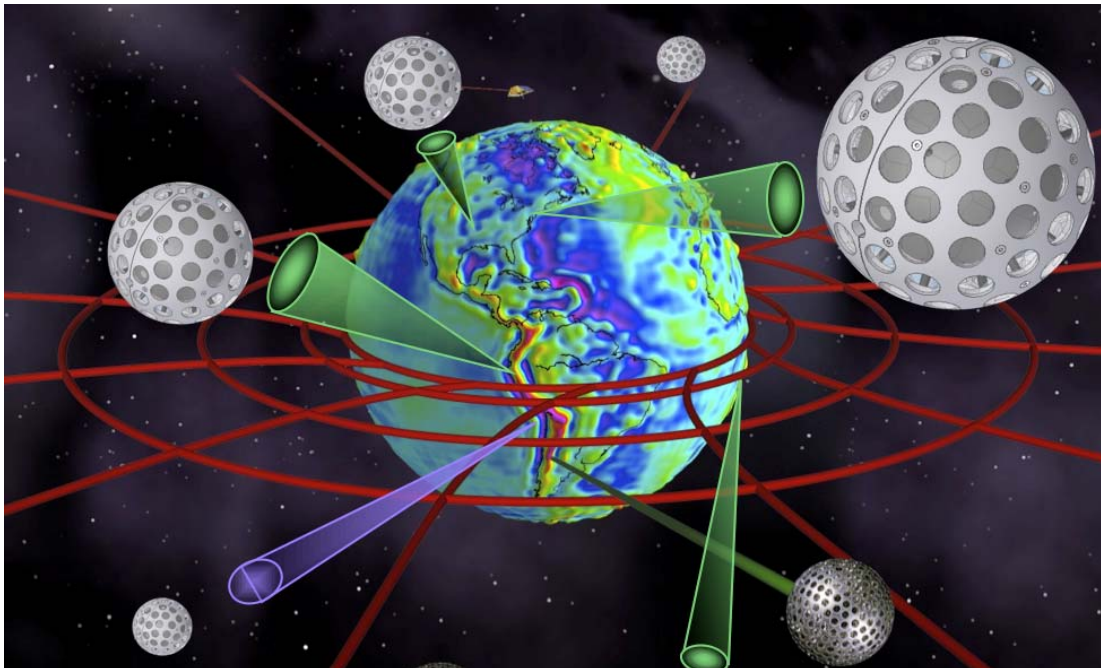


**Figure 9.** A visualization of the LT effect on frame coordinate lines and a constellation of geodetic satellite targets which with a small effort could be a reality by the end of this decade.

Figure 8 along with a mechanical drawing of the current design.

The future launch of LARES and other similar geodetic targets will go a long way towards the development of a “SLR” constellation (Figure 9). The near-continuous availability of targets at all SLR stations and the improved geometry from the mix of inclinations and nodal longitudes, etc., will lead to a more robust set of SLR products for TRF and POD. Improvement of the gravitational static and temporal models and the availability of other data sets from Earth observing missions will soon allow us to use most of the currently available and future geodetic satellites with laser arrays for highly precise geophysical products.

## References

- [1] Bosco, A. *et al.*, 2006. “Probing Gravity in NEO with High-Accuracy Laser-Ranged Test Masses,” proceedings of “*Quantum to Cosmos*” NASA Int. Workshop, Warrenton, VA, USA, May 2006, *Int. J. Mod. Phys. D*, 8.
- [2] Buchman, S. *et al.*, 2000. “The Gravity Probe B Relativity Mission,” *Adv. in Space Res.* 25(6), p. 1177.
- [3] Ciufolini, I., 1989. *Int. J. Mod. Phys. A* 4, 3083.
- [4] Ciufolini, I., 1994. *Class. Quantum Grav.* 11, 958.
- [5] Ciufolini, I. and J.A. Wheeler, 1995. *Gravitation and Inertia*, Princeton University Press, Princeton, New Jersey.
- [6] Ciufolini, I. *et al.*, 1998. *Science* 279, 2100.
- [7] Ciufolini, I. and E. C. Pavlis “A confirmation of the general relativistic prediction of the Lense-Thirring effect”, *Nature*, 431, 958-960, 2004.
- [8] Ciufolini, I., E. C. Pavlis and R. Peron, 2006. Determination of frame-dragging using Earth gravity models from CHAMP and GRACE, *New Astronomy*, 11, 527-550, 10.1016/j.newast.2006.02.001, Elsevier Science B.V., Amsterdam.
- [9] Ciufolini, I., 2007, to be published (arXiv:0704.3338v2).
- [10] Everitt, C.W.F., *et al.*, 1980. Report on a program to develop a gyro test of General Relativity in a satellite and associated technology, Stanford University.
- [11] Kahn, B., 2007. *StanfordNews*, Press release of April 14, 2007, <http://www.stanford.edu/dept/news/pr/>.
- [12] Lense, J., Thirring, H., 1918. *Phys. Z.* 19, 156. See also English translation by Mashhoon, B., Hehl, F.W., Theiss, D.S., 1984. *Gen. Relativ. Gravit.* 16, 711.
- [13] Murphy, T.W., K. Nordtvedt and S.G. Turyshev, 2007. *Phys. Rev. Lett.* 98, 071102.
- [14] Pavlis, E. C., 2002. Geodetic Contributions to Gravitational Experiments in Space, in *Recent Developments in General Relativity, Genoa 2000*, R. Cianci, R. Collina, M. Francaviglia, P. Fré eds., 217-233, Springer-Verlag.
- [15] Pearlman, M.R., Degnan, J.J., and Bosworth, J.M., 2002. "[The International Laser Ranging Service](#)", *Adv. in Space Res.*, Vol. 30, No. 2, pp. 135-143, 10.1016/S0273-1177(02)00277-6.
- [16] Reigber, Ch., *et al.*, 2002. GRACE Orbit and Gravity Field Recovery at GFZ Potsdam - First Experiences and Perspectives, *Eos. Trans. AGU*, 83(47), Fall Meet. Suppl., Abstract G12B-03.
- [17] Reigber, Ch., *et al.*, 2003. The CHAMP-only Earth Gravity Field Model EIGEN-2, *Adv. in Space Res.* 31(8), 1883-1888 (doi: 10.1016/S0273-1177(03)00162-5).
- [18] Reigber, C., Schmidt, R., Flechtner, F., König, R., Meyer, U., Neumayer, K. H., Schwintzer, P., and Zhu, S. Y., 2005. An Earth gravity field model complete to degree and order 150 from GRACE: EIGEN-GRACE02S, *J. Geodyn.* 39, 1.
- [19] Ries, J.C., Eanes, R.J., Tapley, B.D., 2003. In: *Non-Linear Gravitodynamics*, The Lense-Thirring Effect. World Scientific, Singapore.
- [20] Tapley, B. D., 2002. The GRACE Mission: Status and Performance Assessment, *Eos. Trans. AGU*, 83(47), Fall Meet. Suppl., Abstract G12B-01.
- [21] Tapley, B.D., Chambers, D.P., Bettadpur, S., Ries, J.C., 2003. *Geophys. Res. Lett.* 30 (22), 2163.
- [22] Tomlin, S., 2007. Interim view from NASA relativity probe, *Nature*, 446, 19 April 2007.

## A "Web Service" to Compare Geodetic Time Series

Florent Deleflie<sup>1</sup>

1. Geodesie and Mecanique Celeste Team, Grasse, France

### **Abstract**

*We have developed a geodetic database built on the concept of "Virtual Observatory" (<http://www.ivoa.net>). These time series come from our solutions of Earth Orientation Parameters, stations coordinates and velocities, polar motion, and start at the beginning of the 1990's. Solutions deduced from various techniques are available (SLR data, combined or not...)*

*This tool enables one to directly compare, in an easy, homogeneous and coherent way, results coming, for example, from various groups. One of the scientific goals consists in making different results be comparable one from another, and to check, for example, if there is or not systematic differences, or if the used reference frames are fully compatible or not.*

*I will show how this database works (directly through the Web, if it is possible), and I will mention some interesting scientific applications for the future.*

---

## Least-square mean effect: Application to the Analysis of SLR Time Series

D. Coulot<sup>1</sup>, P. Berio<sup>2</sup>, A. Pollet<sup>1</sup>

1. IGN/LAREG - Marne-la-Vallée – France

2. CNRS/OCA/GEMINI - Grasse - France

Contact: [David.Coulot@ensg.ign.fr](mailto:David.Coulot@ensg.ign.fr) Fax: +33-1-64-15-32-53

### Abstract

*In this paper, we evidence an artifact due to the least square estimation method and, in particular, to the current modeling used to derive station position time series from space-geodetic measurements. Indeed, to compute such series, we in fact estimate constant (typically over one week) updates of station positions with respect to a priori models (ITRF2000, solid Earth tides, polar tide and oceanic loading effects). Thus, these estimations must underline the physical models which were not taken into account in the a priori modeling (atmospheric and hydrologic loading effects and even unknown signals, in our case).*

*As shown through the example of the Satellite Laser Ranging measurement processing, it is not the case: the weekly position time series exhibit weekly means of these physical signals but with a supplementary signal at the level of a few millimeters. This is the so-called “least square mean effect”.*

*To avoid this effect, alternative modeling such as periodic series can be used. A method to compute such periodic series for the station positions together with the geocenter motion is also presented in this paper.*

### Introduction

This paper comprises four parts. First of all, we present the least square mean effect from two points of view, theoretical and numerical. Secondly, we propose alternative models to reduce this effect. Then, we study a new method to process Satellite Laser Ranging (SLR) data. This method should help to use alternative modeling for a global network. Finally, we provide some conclusions and prospects.

#### 1. Least square mean effect

The quality presently reached by space-geodetic measurements allows us to study geodetic parameters (Earth Orientation Parameters (EOPs), station positions, Earth’s gravity field, etc.) under the form of time series. The modeling currently used to derive such time series is the following. The physical effects which are well understood are modeled (take as examples solid Earth tides or oceanic loading effects for station positions). These models are used to compute a priori values for the parameters worthy of interest and we compute the parameters with respect to these a priori values. These estimations are supposed to be constant over a given time (typically one day for EOPs and one week for station positions). And these estimations should help us to study the underlying physical effects (atmospheric loading effects, for instance). But, to do so, we need exact and judicious representations. We show that it is not really the case for the current modeling in this section.

##### 1.1. Theoretical considerations

We consider a vector of physical parameters  $\vec{X}$  which vary with time. According to the modeling used, we split this vector in two parts: the modeled effects  $\vec{X}_0$  and the effects we

want to study through time series  $\delta\bar{X}$ ,  $\bar{X}(t) = \bar{X}_0(t) + \delta\bar{X}(t)$ . We know that the vector  $\delta\bar{X}$  varies with time but, in order to get a robust estimation, we suppose it constant over a given interval  $[t_1, t_m]$ . And, doing so, we hope that the constant estimations  $\delta\hat{\bar{X}}$  will correspond to the averages of the underlying physical signals over this interval. The measurements used are modeled with a function  $f(m(t) \equiv f(t, \bar{X}))$  which is linearized

$$m(t) \equiv f(t, \bar{X}_0(t)) + \frac{\partial f}{\partial \bar{X}}(t, \bar{X}_0(t)) \cdot \delta\bar{X} \quad \text{with } \frac{\partial f}{\partial \bar{X}}(t, \bar{X}_0(t)),$$

the partial derivative matrix of  $f$  at the point  $(t, \bar{X}_0(t))$  to get the least square model. Furthermore, we can also linearize the measurements but with respect to the true signal to be studied ( $m(t) \equiv f(t, \bar{X}_0(t)) + \frac{\partial f}{\partial \bar{X}}(t, \bar{X}_0(t)) \cdot \delta\bar{X}(t)$ ).

As a consequence, on one hand, we have a relation between the measurements and the constant updates to be estimated and, on the other hand, a relation between these measurements and the true physical signal to be studied. From these two relations, we get the following observation equation:

$$f(t, \bar{X}_0(t)) + \frac{\partial f}{\partial \bar{X}}(t, \bar{X}_0(t)) \cdot \delta\bar{X} \equiv f(t, \bar{X}_0(t)) + \frac{\partial f}{\partial \bar{X}}(t, \bar{X}_0(t)) \cdot \delta\bar{X}(t)$$

This observation equation allows us to build the following system:

$$A \cdot \delta\bar{X} \equiv \tilde{A} \cdot \delta\hat{\bar{X}}$$

$$\text{with } A = \begin{bmatrix} \frac{\partial f}{\partial \bar{X}}(t_1, \bar{X}_0(t_1)) \\ \frac{\partial f}{\partial \bar{X}}(t_2, \bar{X}_0(t_2)) \\ \vdots \\ \frac{\partial f}{\partial \bar{X}}(t_m, \bar{X}_0(t_m)) \end{bmatrix},$$

$$\tilde{A} = \begin{bmatrix} \frac{\partial f}{\partial \bar{X}}(t_1, \bar{X}_0(t_1)) & 0 & \dots & 0 \\ 0 & \frac{\partial f}{\partial \bar{X}}(t_2, \bar{X}_0(t_2)) & \dots & 0 \\ \vdots & \vdots & \ddots & \vdots \\ 0 & 0 & \dots & \frac{\partial f}{\partial \bar{X}}(t_m, \bar{X}_0(t_m)) \end{bmatrix},$$

$$\text{and } \delta\hat{\bar{X}} = \begin{bmatrix} \delta\bar{X}(t_1) \\ \delta\bar{X}(t_2) \\ \vdots \\ \delta\bar{X}(t_m) \end{bmatrix}.$$

This system is then used to compute the least square solution with a weight matrix  $P$ :

$$\hat{\delta\vec{X}} \cong \delta\vec{X}_{average} + (A^T P A)^{-1} A^T P \tilde{A} (\delta\vec{X} - \delta\vec{X}_{average})$$

$$\text{with } \delta\vec{X}_{average} = \begin{pmatrix} \delta\vec{X}_{average} \\ \delta\vec{X}_{average} \\ \vdots \\ \delta\vec{X}_{average} \end{pmatrix} \text{ and } \delta\vec{X}_{average} = \frac{1}{t_m - t_1} \int_{t_1}^{t_m} \delta\vec{X}(u) du .$$

In this solution, we can see that the estimations effectively contain the averages of the involved signals over the time interval but with a complementary term. We have called this term the “least square mean effect”.

**1.2. Numerical examples**

In this section, we provide some numerical examples based on simulations. Here is the method used to carry out these simulations (cf. Fig.1). The first step is the two LAGEOS satellite orbit computation with GINS software. These orbits are used, in a second step, with ITRF2000 [Altamimi et al., 2002a] and a model for atmospheric loading effects to compute simulated range measurements and partial derivatives of these latter with respect to station positions. Then, we estimate station positions without any atmospheric loading effect in the a priori model. Thus, the estimated positions must reflect these non modeled effects. These estimations are finally compared with the temporal averages of the atmospheric loading effect models. We use real orbits and real SLR measurement epochs in order to get the most realistic simulations. European Center for Medium-range Weather Forecasts (ECMWF, <http://www.ecmwf.int/>) pressure fields were used to derive the atmospheric loading effect models.

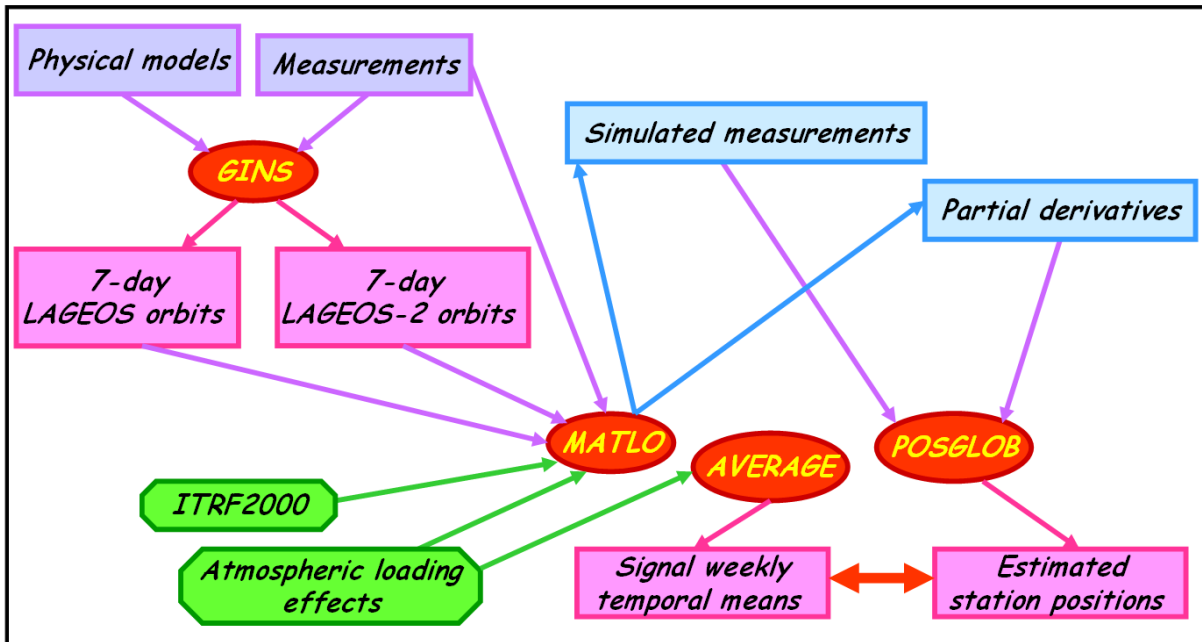
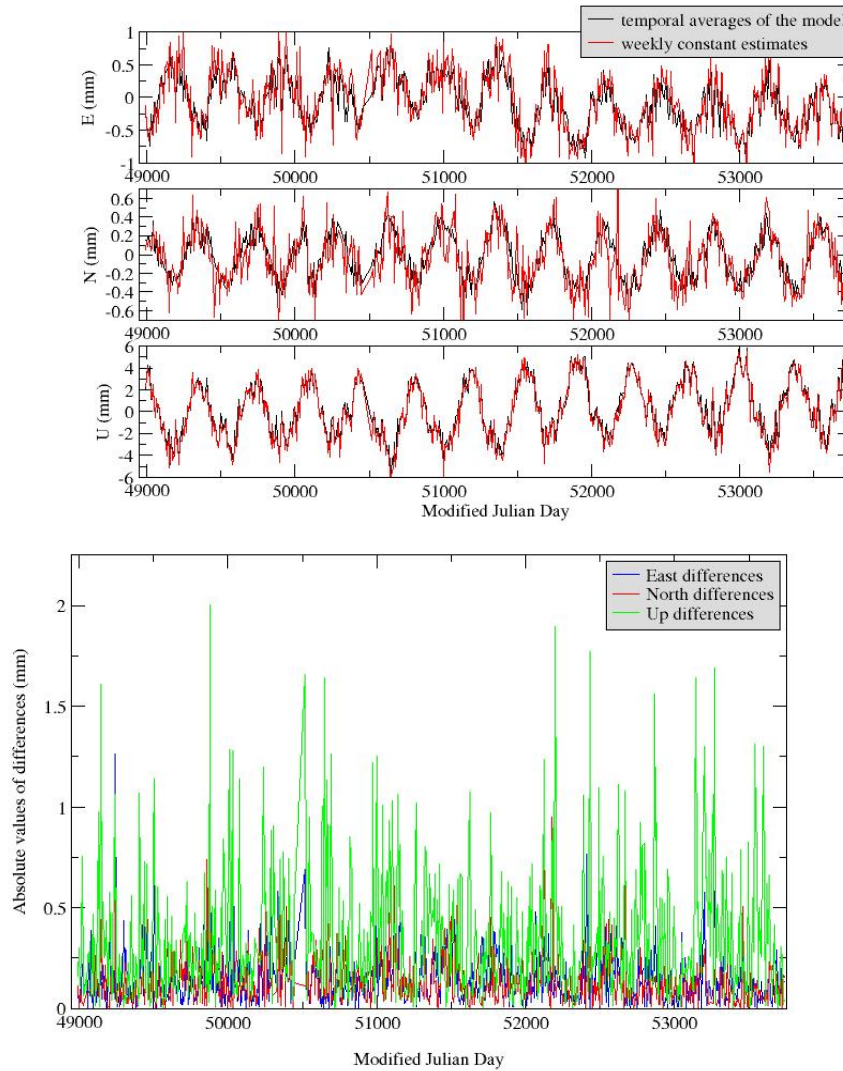


Figure 1. Simulation method.

Fig. 2 shows the results produced for the station Yarragadee (7090) regarding the three components East, North and Up, in mm. In the graphs above, black curves correspond to the weekly temporal averages of the atmospheric loading effects and red curves to the estimated

weekly time series. The graph below shows the absolute differences between black and red curves, so the least square mean effects.

Table 1 provides maximum values of differences of a few millimeters (2 mm for the Up component). And, on average, the least square mean effect is approximately 10 % of the amplitude of the loading effects.



**Figure 2.** Simulation results for the station Yarragadee (7090).  
 Graphs above: black (resp. red) curves correspond to the weekly temporal averages of the atmospheric loading effects (resp. to the estimated weekly time series) in mm.  
 Graph below: absolute values of least square mean effects per component in mm.

**Table 1.** Statistics of the results shown on Fig. 2.

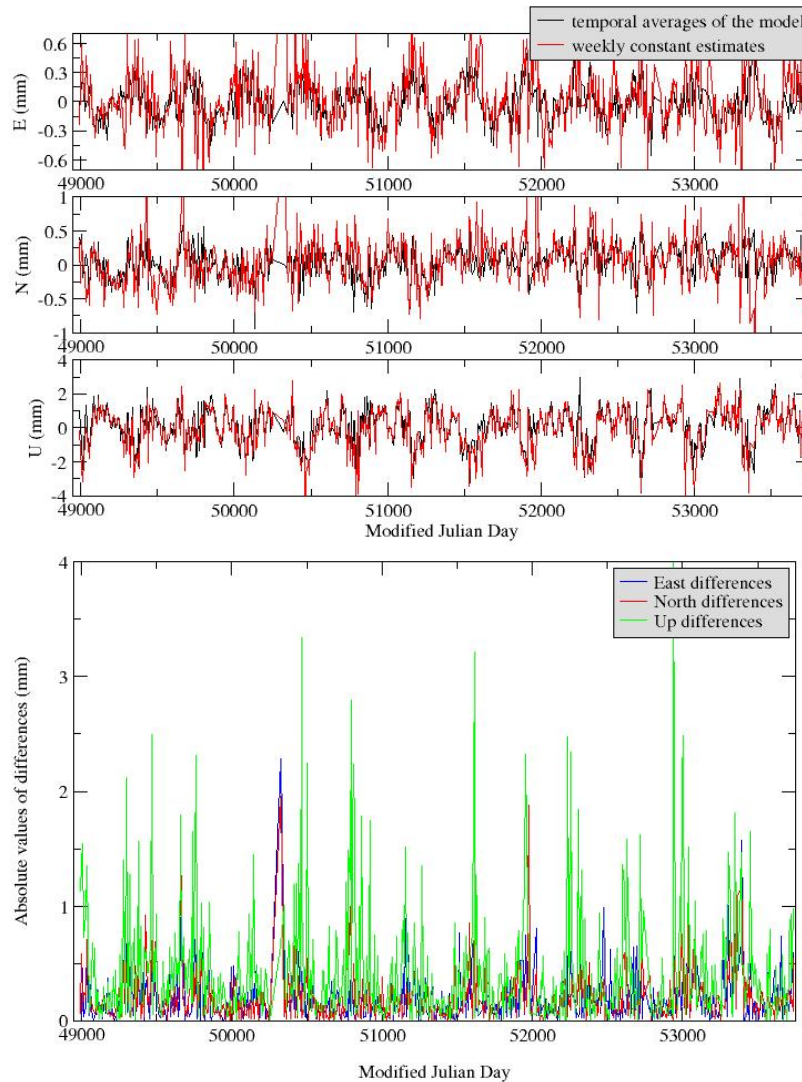
Values (mm)	Minimum	Maximum	Average	RMS
East	2.37 10 <sup>-4</sup>	1.26	0.15	0.13
North	1.86 10 <sup>-5</sup>	0.95	0.13	0.12
Up	2.29 10 <sup>-5</sup>	2.00	0.34	0.32

Fig. 3 shows the equivalent results for the Monument Peak station (7110).

**Table 2.** Statistics of the results shown on Fig. 3.

Values (mm)	Minimum	Maximum	Average	RMS
East	1.57 10 <sup>-4</sup>	2.28	0.19	0.21
North	3.87 10 <sup>-4</sup>	1.96	0.19	0.22
Up	3.14 10 <sup>-5</sup>	4.49	0.42	0.51

As shown in Table 2, the effects are even stronger than those obtained for Yarragadee (see Fig.2 and Tab. 1). Indeed, the maximum effect is 4.5 mm for the Up component.



**Figure 3.** Simulation results for the station Monument Peak (7110).

Graphs above: black (resp. red) curves correspond to the weekly temporal averages of the atmospheric loading effects (resp. to the estimated weekly time series) in mm.

Graph below: absolute values of least square mean effects per component in mm.

Thus, this effect is clearly not negligible and we have to take it into account in a geodynamical framework. Indeed, due to this effect, weekly station position time series can not be directly compared to geodynamical models, [Coulot and Berio, 2004] and [Coulot,

2005]. Furthermore, the results provided in [Penna and Stewart, 2003], [Stewart et al., 2005], and [Penna et al., 2007] show that this effect could create spurious periodic signals in the estimated time series. To reduce this effect, we have studied some alternative models.

## 2. Alternative models

We have studied two alternative modeling. The first one uses periodic terms and the second one is based on wavelets.

### 2.1. Periodic series

The first model is a periodic one. Each of the three positioning components  $\varphi$  is modeled as periodic series:  $\varphi(t) \cong \sum_{i=1}^n a_i \cos(\frac{2\pi}{T_i}t) + b_i \sin(\frac{2\pi}{T_i}t)$  where the periods  $(T_i)_{i=1,n}$  are the characteristic periods of the involved signals. Instead of estimating weekly  $\varphi$  time series, all available measurements are stacked to compute the coefficients  $(a_i)_{i=1,n}$  and  $(b_i)_{i=1,n}$ .

Fig. 4 shows the results (in mm) provided by simulations for the station Yarragadee (7090). The computational scheme is the same than the one shown on Fig. 1 but the simulated measurements are now used to compute the periodic series. On Fig. 4, blue curves correspond to the model of atmospheric loading effects used to compute the simulated measurements and red curves to the estimated periodic series. We can see a good coherence for the Up component and artifacts near the limits of the considered interval for all components. The less satisfying agreement for the horizontal components is certainly due to the low amplitude of the involved signals and to the poorest sensitivity of SLR measurements with respect to horizontal motions.

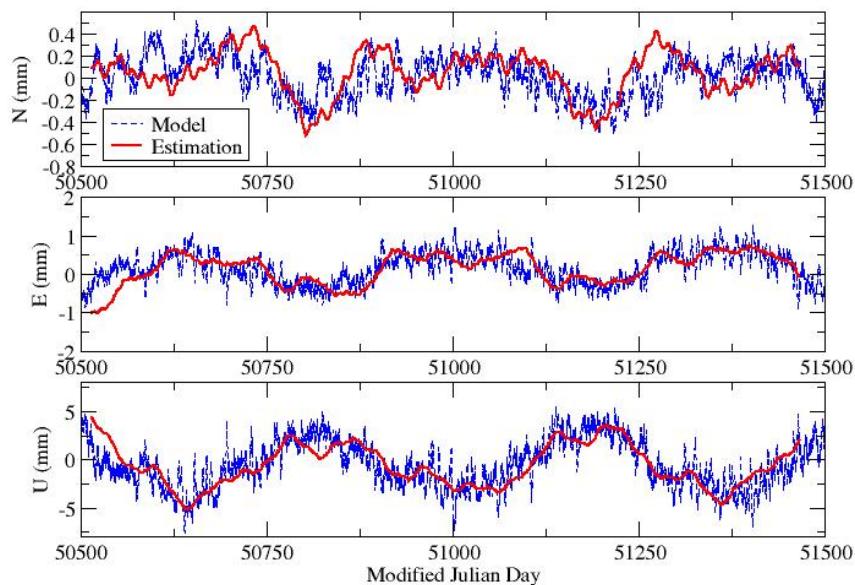


**Figure 4.** Periodic series estimated with simulated measurements for Yarragadee station (7090), in mm. Blue (resp. red) curves correspond to the atmospheric loading effect models used to simulate the range measurements (resp. to the estimated periodic series).

The main advantage of this approach is that no sampling is a priori imposed for estimations but

- the minimal period to be estimated may be imposed by the measurement sampling;

- regarding unknown signals, it will probably be difficult to find the involved periods;
- this model can difficultly take into account discontinuities such as earthquakes.

## 2.2. Wavelets

To go further, we have also studied a model based on wavelets. We have used, as a first test, the simplest wavelet, Haar's wavelet, for which the core function  $\psi$  is defined as follows:

$$\psi(t) = \begin{cases} 1 & \text{if } 0 \leq t < \frac{1}{2} \\ -1 & \text{if } \frac{1}{2} \leq t < 1 \\ 0 & \text{if not} \end{cases} .$$

Each of the three positioning components  $\varphi$  is modeled by the decomposition of the involved

physical signal on the wavelet basis:  $\varphi(t) = \sum_{j=-j_1}^{j_2} \sum_{n=0}^{n_{\max}} a_{j,n} \psi_{j,n}(t)$  with

$$n_{\max} = \begin{cases} 2^j - 1 & \text{if } j < 0 \\ 0 & \text{if not} \end{cases} \text{ and } \psi_{j,n}(t) = \frac{1}{\sqrt{2^j}} \psi\left(\frac{t - 2^j n}{2^j}\right).$$

All available measurements are stacked to compute the coefficients  $a_{j,n}$ . The discontinuities can now be taken into account with the help of this time-frequency representation.

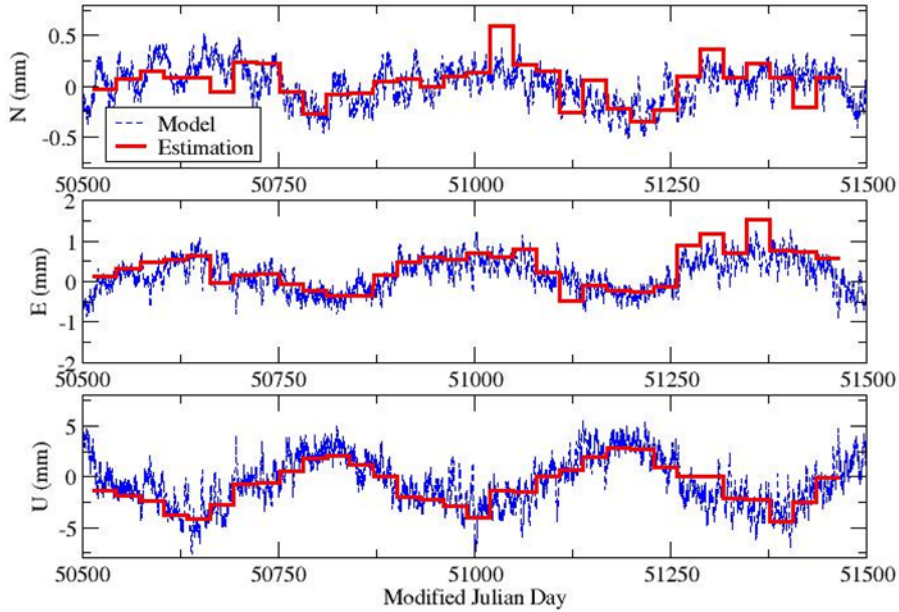


**Figure 5.** Wavelet decompositions estimated with simulated measurements for Yarragadee station (7090), in mm. Blue (resp. red) curves correspond to the atmospheric loading effect models used to simulate the range measurements (resp. to the estimated wavelet decompositions).

Fig. 5 shows the results provided by simulations for Yarragadee station (7090). We can notice the good agreement for the Up component and also the great importance of the smallest scale used for wavelets.

These preliminary results are encouraging but, whatever the model used, we need to guarantee the homogeneity of the involved Terrestrial Reference Frames (TRFs) to carry out such

computations for a station network. Furthermore, we can take the opportunity of such global computation to derive geodynamical signals contained in global parameters such as translations. To reach this goal, we have developed a new approach to process SLR data [Pollet, 2006].

### 3. New model for SLR data processing

#### 3.1. General considerations

In the “classical approach”, the starting point is the observation system  $Y=A.\delta X$  composed by the pseudo measurements  $Y$ , the design matrix  $A$  and the parameters to be computed  $\delta X$ . By applying weak or minimum constraints, we are able to derive weekly solutions [Altamimi et al., 2002b] (usually, daily EOPs together with weekly station positions for the considered network). On the basis of these weekly solutions, with the help of Helmert’s transformation - here are the well-known formulae for station positions and for EOPs [Altamimi et al., 2002a]:

$$\begin{array}{ll}
 \textit{Station positions} & \textit{Earth Orientation Parameters} \\
 \delta X = T + DX_0 + RX_0 & \\
 \textit{with } T = (T_x, T_y, T_z)^T & \left\{ \begin{array}{l} \delta x_p = R_y \\ \delta y_p = R_x \\ \delta UT_1 = -\frac{1}{f} R_z \end{array} \right. \\
 \textit{and } R = \begin{bmatrix} 0 & -R_z & R_y \\ R_z & 0 & -R_x \\ -R_y & R_x & 0 \end{bmatrix} & \textit{with } f = 1.002737909350795
 \end{array}$$

we can compute station positions in the a priori reference frame (ITRF2000, for instance) together with coherent EOPs and also 7-parameter transformation between involved TRFs.

The new model we have developed allows us to compute all these parameters in the same process, directly at the observational level. To derive this new approach, we have directly translated Helmert’s transformations at the level of the previous observation system:  $Y=A.\delta X$  with  $\delta X = \delta XC + T + DX_0 + RX_0$  and  $\delta EOP = \delta EOPC + \epsilon R\{X, Y, Z\}$ . Doing so, we have replaced the parameters  $\delta X$  and  $\delta EOP$  by new ones:  $\delta XC$ ,  $T$ ,  $D$ ,  $R\{X, Y, Z\}$  and  $\delta EOPC$ .

Theoretical considerations and numerical tests with SLR data have shown that the rotations  $R\{X, Y, Z\}$  were not needed at all in this model. We did not keep them.

The normal matrices provided by this new approach present a rank deficiency of 7, coming from:

- the fact that SLR data do not carry any orientation information (deficiency of 3);
- the estimation of three translations and a scale factor (deficiency of 4).

This rank deficiency in fact corresponds to the definition of the totally unknown TRF underlying the estimated  $\delta XC$  for which the seven degrees of freedom need to be defined. To do so, minimum constraints [Sillard and Boucher, 2001] are applied with respect to the ITRF2000 and with the help of a minimum network.

#### 3.2. First results

In this section, we provide the preliminary results produced with this new model for SLR data processing over 13 years.

Fig. 6 shows the minimum network used to apply the minimum constraints to define the homogenous weekly TRFs.



**Figure 6.** Minimum network used to apply the minimum constraints to define the homogeneous weekly TRFs.

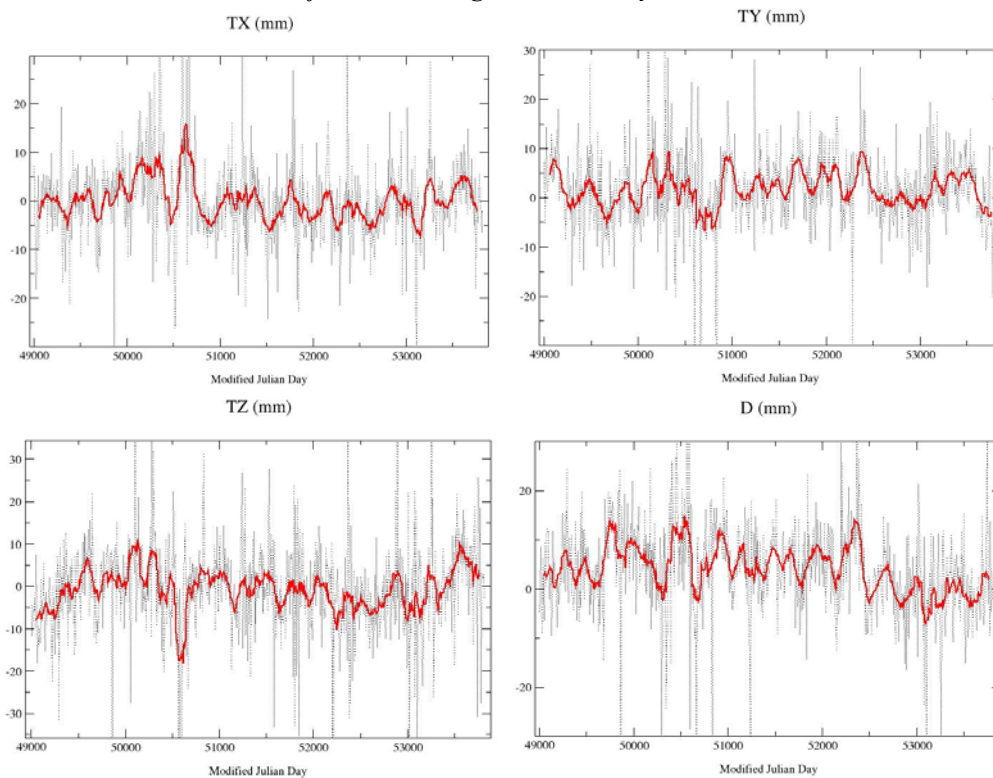


**Figure 7.** Weekly time series of the three translations and the scale factor, in mm. Red curves correspond to running averages.

Fig. 7 shows the four estimated transformation parameters between the weekly TRFs underlying the SLR measurements and directly linked to the two LAGEOS orbit references and the weekly TRFs constrained to be realized in ITRF2000. The three translations exhibit periodic signals (mainly annual) certainly linked to the geocenter motion.

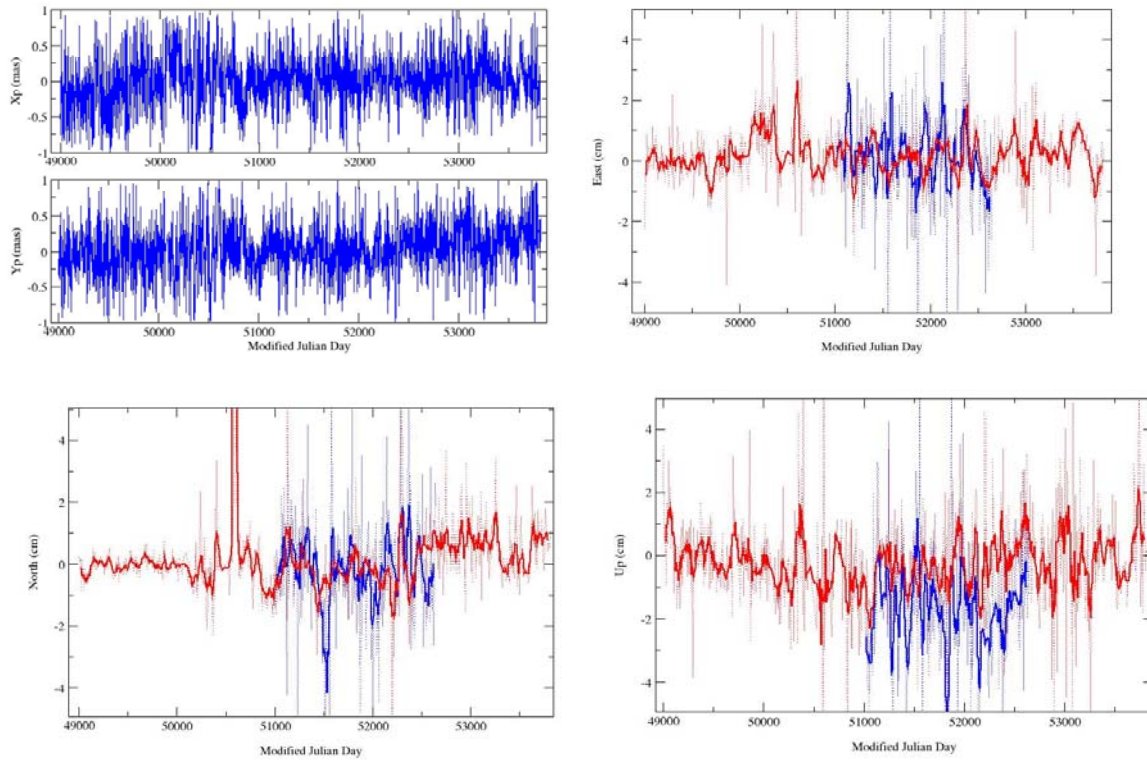


**Figure 8.** Results produced with the new method for EOPs and station positions. Graph up left: EOP residuals (mas) with respect to EOPC04 time series [Gambis, 2004] consistent with the estimated station positions. Three other graphs: Mount Stromlo - 7849, in blue- and Yarragadee - 7090, in red-station three positioning component estimated time series (cm).

Fig. 8 shows the results provided by the new method for EOPs and two Australian SLR stations, Mount Stromlo (blue curves) and Yarragadee (red curves). Regarding EOPs, the weighted biases (resp. the WRMS) are respectively  $5\mu\text{s}$  for  $X_p$  and  $23\mu\text{s}$  for  $Y_p$  (resp.  $280\mu\text{s}$  for  $X_p$  and  $Y_p$ ). Regarding the station position time series, we can notice the similarities between these series. The constant difference between the two Up time series is certainly due to range biases which were not taken into account for these computations.

### 3.3. Toward global estimations over long period

How this new model can help us to reduce the least square mean effect? We can replace the new parameters of the model by previous alternative models such as periodic series in the following example (new parameters to be estimated are underlined in green):

**Observation system :  $Y = A \cdot \delta X'$**   $\longrightarrow$   $\delta X = \delta X_c + T + \underline{DX_0}$

$\delta EOP = \delta EOP_c$

**For each parameter  $\delta Z$ , we can use the model**

$$\delta Z(t) = \underline{\delta Z_0} + \sum_i [\underline{az_i(t)} \cos(2\pi t/T_i) + \underline{bz_i(t)} \cos(2\pi t/T_i)]$$

But, each harmonic estimated on station positions generates new rank deficiencies. Consequently, we have to generalize the minimum constraints for harmonic vectors. Furthermore, the number of involved parameters is very large (close to 50 000 in the next example). Thus, we have to use tools allowing the handling of large normal systems.

As a very preliminary computation, we have used this approach to compute amplitudes of annual signals contained in the four global parameters involved. The computation was carried out over 3 years of data. Amplitudes obtained are relatively satisfying ( $TX$ : 2.1 mm,  $TY$ : 3.6 mm,  $TZ$ : 1.1 mm and  $D$ : 0.9 mm). Moreover, the periodic series really absorb the annual signals as the annual harmonic totally disappears in the residual weekly parameters (the previous parameters called  $\delta Z_0$ ) computed with respect to this annual term.

#### 4. Conclusions and Prospects

All these results are satisfying but we of course need to go further by:

- using this periodic approach not only for global parameters but also for station positions;
- computing periodic series directly linked to oceanic loading effects together with series corresponding to atmospheric and hydrologic loading effects;
- deriving diurnal and semi-diurnal signals affecting EOPs with this approach;
- studying the spurious effects provided by this least square mean effect in the International Laser Ranging Service (ILRS) operational products.

We could also couple periodic series with more complex wavelet bases to get a more robust model and, eventually, with stochastic modeling in a filtering framework.

#### References

- [1] Altamimi, Z., P. Sillard, and C. Boucher: "ITRF2000: a new release of the International Terrestrial Reference Frame for Earth science applications", *J. Geophys. Res.*, 107(B10), 2214, doi: 10.1029/2001JB000561, 2002a.
- [2] Altamimi, Z., C. Boucher, and P. Sillard: "New trends for the realization of the International Terrestrial Reference System", *Adv. Space Res.*, 30(2), p. 175-184, 2002b.
- [3] Coulot, D. and P. Berio: "Effet de moyenne par moindres carrés, application à l'analyse des séries temporelles laser", *Bulletin d'Information Scientifique & Technique de l'IGN*, 75, p. 129-142, IGN (Eds), IGN-SR-03-083-G-ART-DC, 2004.
- [4] Coulot, D.: "Télémétrie laser sur satellites et combinaison de techniques géodésiques. Contributions aux Systèmes de Référence Terrestres et Applications", Ph. D. thesis, Observatoire de Paris, 2005.
- [5] Gambis, D: "Monitoring Earth orientation using space-geodetic techniques: state-of-the-art and prospective", *J. Geod.*, 78, p. 295-305, 2004.
- [6] Penna, N.T. and M.P. Stewart: "Aliased tidal signatures in continuous GPS height time series", *Geophys. Res. Lett.*, 30(23), p. 2184-2187, doi: 10.1029/2003GL018828, 2003.
- [7] Penna, N.T., M.A. King, and M.P. Stewart: "GPS height time series: Short-period origins of spurious long-period signals", *J. Geophys. Res.*, 112, B02402, doi: 10.1029/2005JB004047, 2007.
- [8] Pollet, A.: "Combinaison de mesures de télémétrie laser sur satellites. Contributions aux systèmes de référence terrestres et à la rotation de la Terre.", Master research course report, Observatoire de Paris, 2006.
- [9] Sillard, P. and C. Boucher: "Review of algebraic constraints in terrestrial reference frame datum definition", *J. Geod.*, 75, p. 63-73, 2001.
- [10] Stewart, M.P., N.T. Penna, and D.D. Lichti: "Investigating the propagation mechanism of unmodelled systematic errors on coordinate time series estimated using least squares", *J. Geod.*, 79(8), p. 479-489, doi: 10.1007/s00190-005-0478-6, 2005.

---

## Some Aspects Concerning the SLR Part of ITRF2005

H. Mueller<sup>1</sup>, D. Angermann<sup>1</sup>

1. Deutsches Geodätisches Forschungsinstitut (DGFI) Alfons-Goppel-Str. 11 80539 Muenchen.

Contact: [mueller@dgfi.badw.de](mailto:mueller@dgfi.badw.de) Fax: +49 89 23031 1240

### Abstract

*Two combined solutions for the ITRF2005 were generated independently by two ITRS Combination Centres, IGN, Paris and DGFI, Munich. A comparison of the two ITRF2005P solutions shows in general a good agreement, but the scale and scale rate of the SLR network differs significantly. To investigate this difference a number of tests were performed. It was found that the actual SLR results are consistent with the ITRF2005 solution of DGFI, whereas there is a bias of about 2 ppb compared to the IGN solution. The translation parameters between both ITRF2005 solutions are in good agreement. We also compared the VLBI and SLR scale through co-locations with GPS. This comparison showed the importance of a proper choice and weighting of local ties at co-location sites for the connection of the technique-dependent reference frames. Especially the sites at the southern hemisphere influence the resulting scale of the combined product.*

### Introduction

Within the re-organized IERS structure, there are three Combination Centres for the International Terrestrial Reference System (ITRS) at Deutsches Geodätisches Forschungsinstitut (DGFI), Munich, Institute Géographique National (IGN), Paris, and National Resources Canada (NRCAN), Ottawa. The ITRS Product Center at IGN is coordinating the processing. DGFI and IGN provided each one solution for ITRF2005. Both used their own software and applied their preferred strategy. This guarantees independent results and allows a decisive validation and quality control of the results.

The combination strategy of IGN is based on the solution level by simultaneously estimating similarity transformation parameters w.r.t. the combined frame along with the adjustment of station positions and velocities. The ITRF2005 computations done at DGFI use unconstrained normal equations from the solutions of the different techniques.

This paper briefly summarizes the combination methodology of the ITRS Combination Center at DGFI. Main subject is a comparison of the ITRF2005 solutions of IGN and DGFI. The focus thereby is on the SLR part of ITRF2005.

### Combination methodology of DGFI

The general concept of the ITRS Combination Center at DGFI is based on the combination of normal equations and the common adjustment of station positions, velocities and EOP. The computations are performed with the DGFI Orbit and Geodetic Parameter Estimation Software (DOGS). Details on the combination procedure and the mathematical background are given in various publications (e.g., Angermann et al., 2004; Angermann et al., 2006; Drewes et al., 2006; Krügel and Angermann, 2006; Meisel et al., 2005). Figure 1 shows the data flow and the combination methodology for the ITRF2005 computation.

The combination methodology of DGFI comprises the following major steps:

- Analysis of ITRF2005 input data and generation of normal equations
- Analysis of time series and accumulation per-technique (intra-technique combination)
- Comparison and combination of different techniques (inter-technique combination)
- Generation of the ITRF2005 solution by applying minimum datum conditions

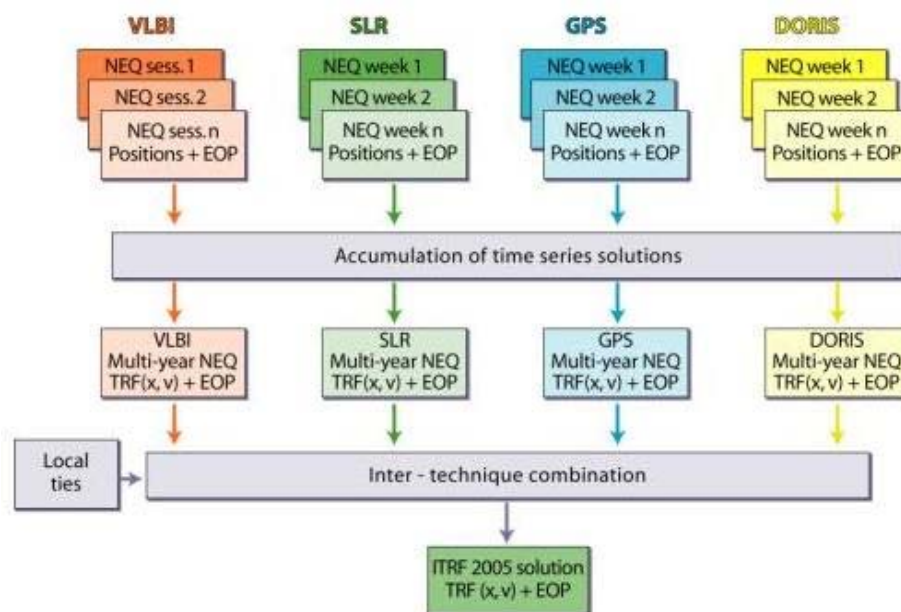


**Figure 1.** Data flow and computation procedure for the ITRF2005 solution of DGFI

The final ITRF2005 solution comprises station positions, velocities and daily EOP estimates as primary results. In addition epoch position residuals and geocenter coordinates are obtained from the time series combination. The reference epoch for station positions is 2000.0. The rather inhomogeneous data quality and quantity of the space geodetic observation stations is reflected in the accuracy and reliability of the ITRF2005 station position and velocity estimations. This holds in particular for a number of SLR and VLBI stations, but also for some GPS and DORIS stations with few observations. Another aspect is that the new type of ITRF2005 solution contains many stations with several solution ID's. As a consequence the station positions and velocities are valid only for a certain period of time, which has to be known and considered by the users. Furthermore co-location sites may have different station velocities for co-located instruments, if their estimated velocities differ significantly.

### Comparison of the ITRF2005 solutions of DGFI and IGN

For comparisons we performed similarity transformations between both solutions. These transformations were done separately for each technique by using good reference stations. The RMS differences for station positions and velocities show a very good agreement (after similarity transformations). This holds in particular for "good" stations with several years of continuous observations without discontinuities (Table 1). For weakly estimated stations (e.g., observation time < 2.5 years, different solutions caused by discontinuities) larger discrepancies do exist, which are in most cases within their standard deviations.

Most of the transformation parameters agree within their estimated standard deviations, except for the scale and its time variation of the SLR network. A significant difference of about 1 ppb (offset) and 0.13 ppb/yr (rate) between the ITRF2005P solutions of DGFI and IGN has been found, which accumulates to nearly 2 ppb in 2006 (see Table 2). The scale difference is not visible in the pure SLR intra-technique solutions of IGN and DGFI. This indicates that the difference between both ITRF2005P solutions is caused within the inter-technique combination.

From these comparisons it is obvious that the major problem of the ITRF2005 is the significant difference in the SLR scale. The analysis of weekly SLR solutions in 2006 has shown that the scale is in good agreement with the ITRF2005P solution of DGFI, whereas

there is a significant scale bias of about 2 ppb w.r.t. the IGN solution (see Figure 2), which is equivalent to a difference of 1.3 cm in SLR station heights. It was argued by IGN that this “scale problem” is a consequence of a scale bias between VLBI and SLR. Because of the apparent discrepancies the scale of the IGN solution was defined by VLBI only, whereas the scale of the DGFI solution is defined by the SLR and VLBI data.

**Table 1.** RMS differences for station positions and velocities between IGN and DGFI solutions for ITRF2005 for “good” Reference stations (25 VLBI, 22 SLR, 57 GPS, 40 DORIS stations).

ITRF2005P DGFI - IGN	Positions [mm]	Velocities [mm/yr]
GPS	0.31	0.14
VLBI	0.79	0.34
SLR	1.82	0.66
DORIS	3.32	1.11

**Table 2.** Scale differences between the pure intra-technique and the ITRF2005P solutions of DGFI and IGN.

	SLR		VLBI	
	offset [ppb]	drift [ppb/yr]	offset [ppb]	drift [ppb/yr]
Pure intra-technique solutions (IGN – DGFI)	-0.17 ± 0.06	0.01 ± 0.02	0.16 ± 0.05	0.01 ± 0.02
ITRF2005 P solutions (IGN – DGFI)	<b>0.86</b> <b>± 0.12</b>	<b>0.13</b> <b>± 0.03</b>	-0.12 ± 0.06	0.03 ± 0.03

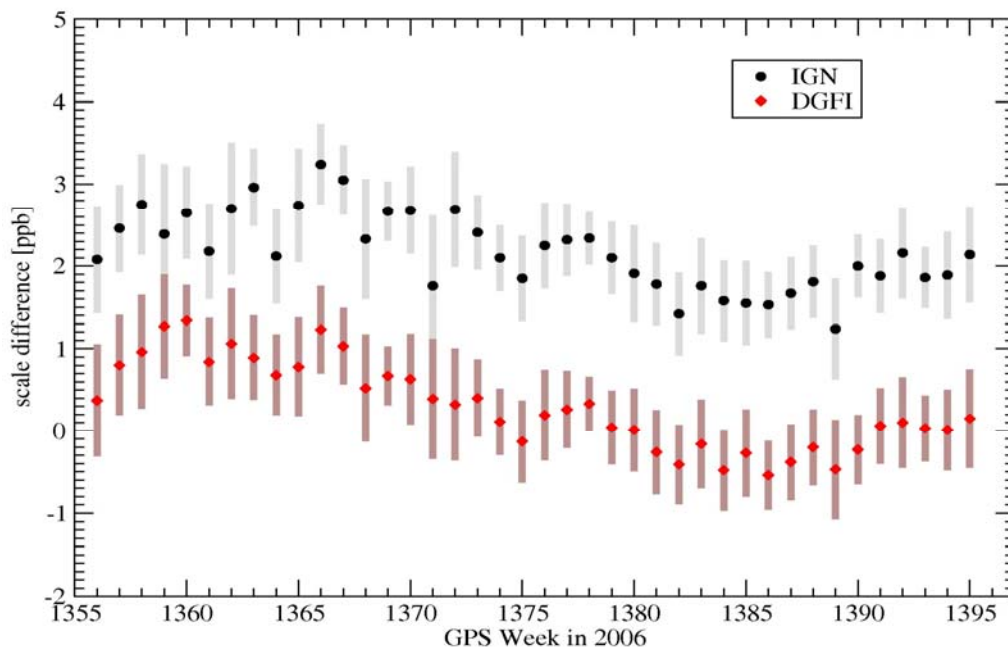


**Figure 2.** Scale of ITRF2005P solutions of IGN and DGFI w.r.t. to the combined SLR solution (ILRSA)

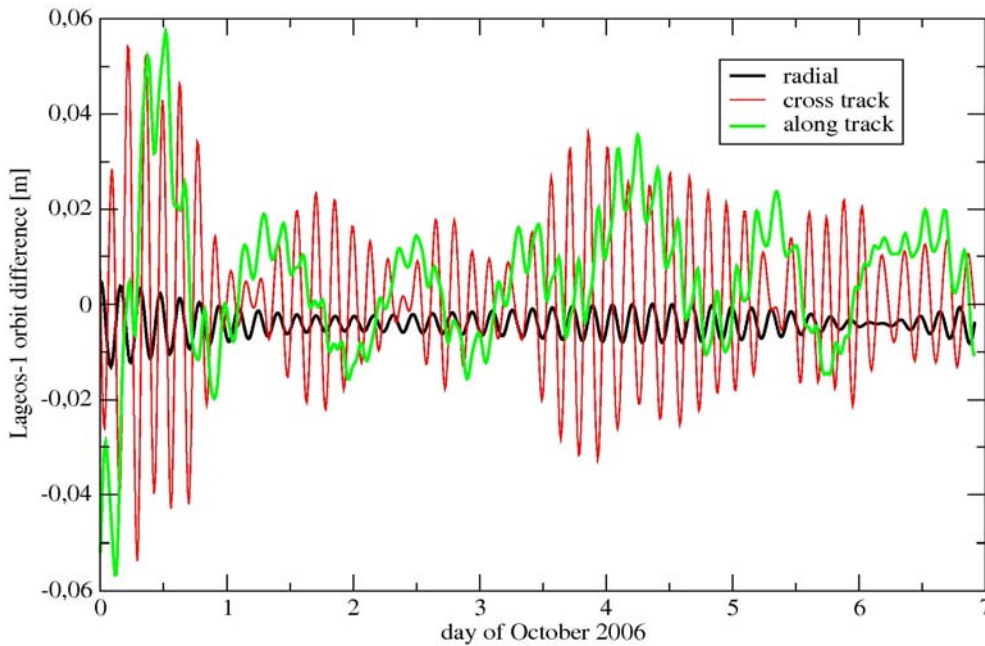


**Figure 3.** Difference between IGN and DGFI solution for a weekly Lagesos-1 orbit.

This scale difference is also reflected in the resulting satellite orbits. For a comparison we solved a weekly Lagesos-1 orbit with fixed station coordinates, one with the DGFI solution, the other with the IGN solution, solving for all internal arc parameters and polar motion (X-, Y- pole and dUT1). The resulting orbits were compared in radial, cross- and along track to investigate the influence of the scale difference. In figure 3 the radial offset of about 5 mm is clearly visible. The cross and along track components only show a revolution dependent signal which results from the radial orbit bias, but there is no systematic error. This comparison indicates that the scale of the IGN solution will produce biased satellite orbits.

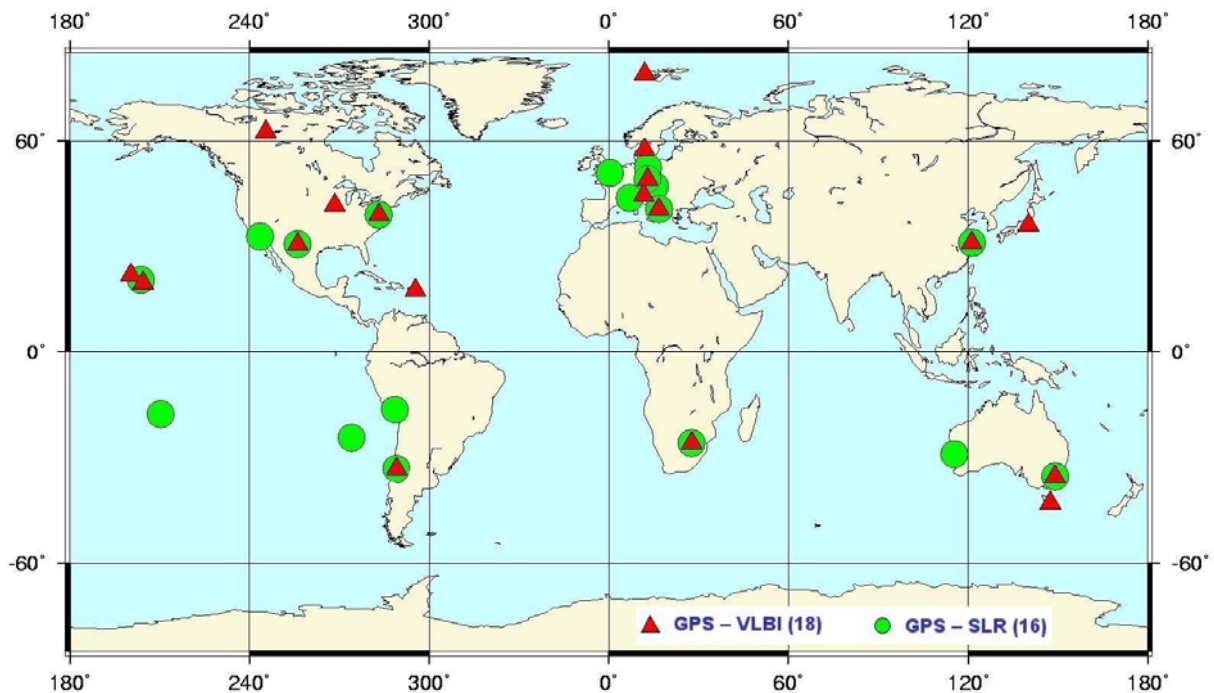


**Figure 4.** Available co-location sites between GPS, SLR and VLBI

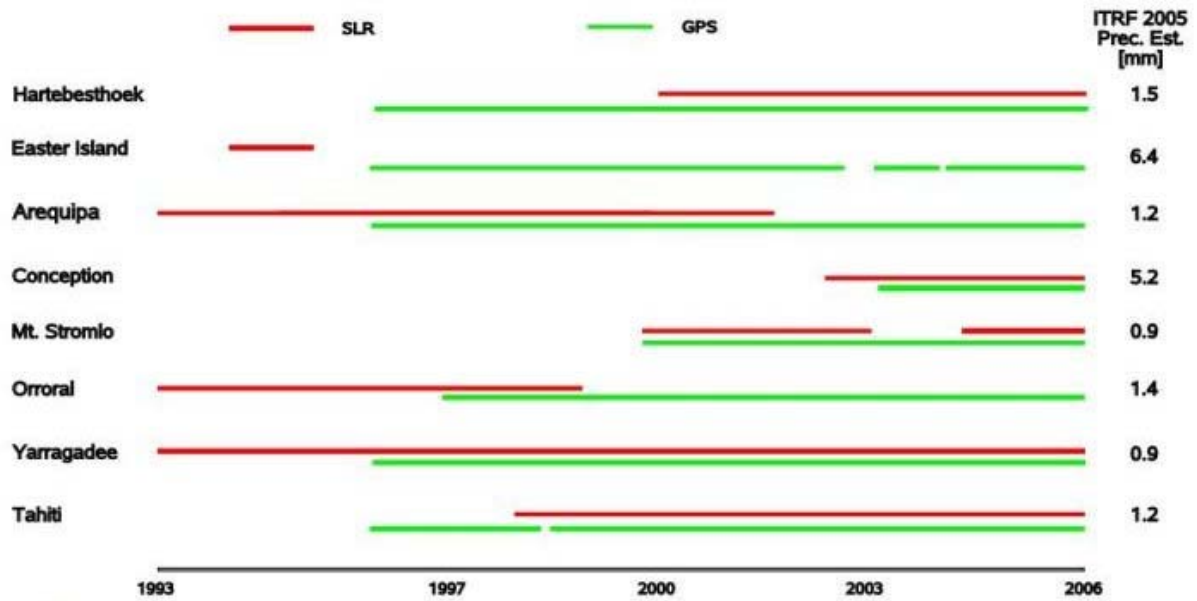


Figure 5. Observation period of southern hemisphere collocation sites

### Investigation of the scale differences

We used the intra-technique solutions of the DGFI combination for ITRF2005 to investigate the scale of VLBI and SLR. Since the number and spatial distribution of good co-location sites between VLBI and SLR is not sufficient to get reliable results for a direct comparison of the scale, we used an "indirect" approach via the GPS network and consider the GPS intra-technique solution as reference for this specific study. We used "good" co-location sites and local ties to refer the VLBI and SLR solutions to an "arbitrary" GPS frame (see Fig. 4).

The geographical distribution and quality of SLR tracking stations is in particular problematic in the Southern hemisphere. Therefore we focus on these stations and on the co-locations with GPS. Fig. 5 shows the GPS and SLR observation periods and the estimated ITRF 2005 precision for 8 SLR-GPS co-location sites on the southern hemisphere. DGFI used for the connection of the reference frames all stations except Easter Island and Concepcion because of poor SLR data. In the IGN solution the Australian sites Yarragadee, Mt. Stromlo, Orroral and Tahiti are down-weighted. Thus the reference frame connection in the IGN solution was realized mainly via the remaining 4 co-location sites on the Southern hemisphere, from which Easter Island and Concepcion are poorly observed by SLR. This indicates that the integration of GPS and SLR networks in the Southern hemisphere is rather poor in the IGN solution.

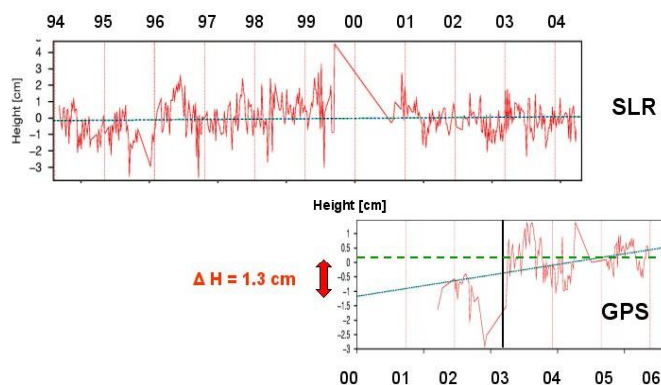


Figure 6. Jump in the Haleakala time series

**Table 3:** Scale difference between SLR and VLBI obtained from DGFI ITRF2005P solution.

	$\Delta$ Scale offset [ppb]	$\Delta$ Scale drift [ppb/yr]
SLR - VLBI	$0.40 \pm 0.42$	$0.04 \pm 0.10$
<b>SLR - VLBI *</b>	<b><math>0.26 \pm 0.41</math></b>	<b><math>0.03 \pm 0.09</math></b>

**\* : Discontinuity for GPS station Maui introduced**

We also investigated the position time series of co-location sites. As an example Fig. 6 shows the GPS and SLR position time series for the co-location site Maui on Hawaii. A clear jump is visible in the GPS time series at the end of 2002, which affects the height estimation by about 1.3 cm. We have introduced a discontinuity for the GPS station Maui and we solved for two solutions. To test the influence of the jump we performed a 14 parameter similarity transformation between the GPS and SLR solutions and compared the resulting residuals. As shown in Fig. 7 the relatively large height residual for Maui disappeared completely.

The scale parameters obtained from the singularity transformations of the SLR and VLBI solutions w.r.t. GPS are arbitrary numbers, but the difference of the scale parameters is independent from the "arbitrary" GPS scale. The estimated scale difference between VLBI and SLR are shown in Table 3. If the discontinuity for GPS station Maui is introduced the scale differences are  $0.26 \pm 0.41$  ppb for the offset and  $0.03 \pm 0.09$  ppb/yr for the drift. Thus the results of the DGFI ITRF2005P solution do not indicate any evidence for a scale bias between VLBI and SLR.

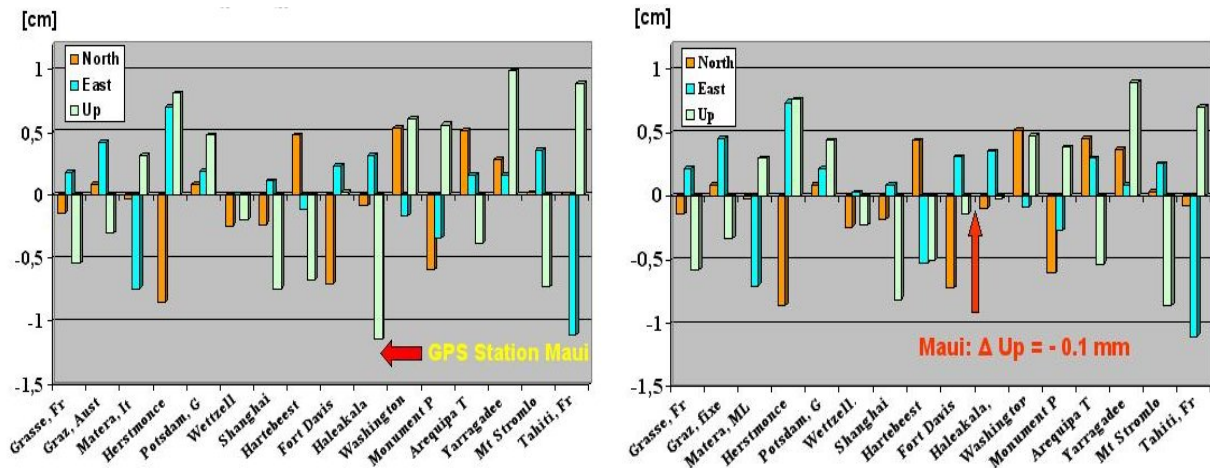


**Figure 7.** Station position residuals for 16 SLR-GPS colocation sites. The left figure shows a height residual for Maui of 1.2 cm, which is reduced to almost zero, if the jump for GPS station is introduced (see right figure).

## Conclusion

The DGFI and IGN for the ITRF2005 are in good agreement for the station positions and velocities (after similarity transformations), but a significant difference has been observed for the scale of the SLR network. As the discrepancies are not visible in the pure SLR intra-technique solutions of IGN and DGFI, they are most likely caused by a different combination procedure and in particular by the implementation of local tie information. Furthermore the IGN solution reveals an apparent difference in SLR and VLBI scales, which led to the exclusion of SLR data for the scale definition of the ITRF2005. The ITRF2005 solution of DGFI does not show this apparent scale difference between SLR and VLBI and it relies on the data of both techniques to define the scale. The analysis of the actual SLR tracking data show a good agreement with the scale of the ITRF2005 solution of DGFI, whereas there is a misfit of about 2 ppb w.r.t. the IGN solution.

## Acknowledgement

The authors thank the ILRS (Pearlman et al,2002) for providing the SLR data and the combined weekly SLR intra-technique solutions. For the investigations on the SLR scale we used also the time series of GPS and VLBI intra-technique solutions kindly provided by the IGS and the IVS, respectively.

## References

- [1] Angermann D, Drewes H, Krügel M, Meisel B, Gerstl M, Kelm R, Müller H, Seemüller W, Tesmer V (2004) ITRS Combination Center at DGFI: A terrestrial reference frame realization 2003, Deutsche Geodätische Kommission, Reihe B, Heft Nr. 313.
- [2] Angermann D, Drewes H, Krügel M, Meisel B (2006) Advances in terrestrial reference computations, IAG Symposia Cairns, Springer.
- [3] Drewes H, Angermann D, Gerstl M, Krügel M, Meisel B, Seemüller W (2006) Analysis and Refined Computations of the International Terrestrial Reference Frame, Observation of the Earth System from Space, Flury, Rummel, Reigber, Rothacher, Boedecker, Schreiber (Eds), 343-356, Springer.
- [4] Krügel M and Angermann D (2006) Frontiers in the combination of space geodetic techniques Proceedings of IAG Symposia Cairns, Springer.
- [5] Meisel B, Angermann D, Krügel M, Drewes H, Gerstl M, Kelm R, Müller H, Seemüller W, Tesmer V (2005) Refined approaches for terrestrial reference frame computations, Adv Space Res 36, 350-357, Elsevier.
- [6] Pearlman, M.R., Degnan, J.J., and Bosworth, J.M., "The International Laser Ranging Service", Advances in Space Research, Vol. 30, No. 2, pp. 135-143, July 2002.

## **Determination of the Temporal Variations of the Earth's Centre of Mass from Multi-Year Satellite Laser Ranging Data**

Ramesh Govind<sup>1</sup>

1. Geoscience Australia, Canberra, Australia

### **Abstract**

*Temporal variation of geodetic parameters (station positions, Earth's gravity field) that are used to monitor global change are referred to a time-varying terrestrial reference system (geocentre, orientation). The time evolution of the geocentre referred to the origin of the terrestrial reference system can be determined from estimates of degree one spherical harmonic representation of the Earth's gravity field. Weekly estimates of the degree one coefficients were undertaken for the period spanning 1993.0 to 2006.8 using SLR data from the global network for four satellites (Lageos-1, Lageos-2, Stella, Starlette). The data set, computation process and results of the geocentre estimates are presented. A comparison of the geocentre estimates from the satellite pairs at two different altitudes is shown. A system to "visualise" the motion of the geocentre as an indicator of mass transport is proposed.*

---

## Contribution of Satellite and Lunar Laser Ranging to Earth Orientation Monitoring

D.Gambis<sup>1</sup>, R. Biancale<sup>2</sup>

1. Paris Observatory, France
2. CNES Toulouse, France

### Abstract

*Lunar and Satellite Laser Ranging have been contributing for several decades to Earth orientation variations monitoring. UT0 derived from LLR was used for the period 1976 to 1982 and made the transition between Astrometry and VLBI techniques. Polar motion derived from Lageos observations has a significant contribution in the IERS combinations, mainly thanks to its long term stability. So far Earth orientation parameters and ITRF are derived separately leading to inconsistencies. Rigorous approaches to simultaneously determine a terrestrial reference frame (TRF) and Earth Orientation Parameters (EOP) are now being developed either using SINEX files derived from the different techniques or at the observation level. We present here the results from a coordinated project within the Groupe de Recherches de Geodesie Spatiale (GRGS). Observations of the different techniques VLBI, SLR, LLR, DORIS and GPS) are separately processed by different Analysis centres using the software package GINS DYNAMO. The strength of the method is the use of a set of identical up-to-date models and standards in unique software. The normal equation matrices obtained by the different groups are then stacked to derive weekly solutions of station coordinates and Earth Orientation Parameters (EOP). Results are made available at the IERS site (ftp iers1.bkg.bund.de) in the form of SINEX files.*

*The analyses we have performed show that for the accuracy and stability of the EOP solution is very sensitive to a number of critical parameters mostly linked to the terrestrial reference frame realization, i.e. minimum constraints application and localities. We present the recent analyses and the latest results obtained.*

---

## Station Positioning and the ITRF

Zuheir Altamimi<sup>1</sup>

1. Institut Geographique National, ENSG/LAREG, 6-8 Avenue Blaise Pascal, 77455 Champs-sur-Marne, FRANCE

### Abstract

*The International Terrestrial Reference Frame (ITRF) as a realization of the International Terrestrial Reference System is one of the scientific products of the International Earth Rotation and Reference Systems Service (IERS). The ITRF is the standard frame recommended for a variety of applications, from surveying to the very fine studies in Earth Sciences. In order to satisfy science requirements, the ITRF should be accurate, reliable and internally consistent over time with unambiguously specified datum definition (origin, scale, orientation and their respective time evolution). Starting with the ITRF2005, the input data requested for the ITRF construction are under the form of time series of station positions and Earth Orientation Parameters (EOPs). Such data do not only allow an appropriate evaluation of the frame accuracy and internal consistency, but also are adequately suited to measure the positioning performance of space geodesy techniques. This paper attempts to review the positioning performance of space techniques via the analysis of the submitted time series to ITRF2005. A special focus will also be given to address the current accuracy level of the ITRF datum definition.*

### Introduction

The concept of reference systems and frames is one of the fundamental mathematical foundations of modern geodesy with the advent of space techniques since the early eighties. We refer to the pioneering work by a certain number of geodesists and astronomers in (Kovalevsky et al., 1989) who established the foundation of the concept of reference systems and frames followed and used as a basis for the ITRF derivation. Indeed, it is fundamental to adopt that clearly defined concept which distinguish between the system as a theoretical inaccessible mathematical model and the frame as the numerical realization of the system. Moreover, the frame is not only accessible to the users but it is also by essence perfectible, being based on and derived from space geodesy observations.

Using the commonly accepted model of 7(14)-parameter euclidian similarity (also known as Helmert or Bursa-Wolf parameters), it becomes then straightforward to estimate discrepancies between solutions over the frame physical parameters. This is the case for instance where large translation components are often found between SLR on one hand and GPS or DORIS solutions on the other hand. Less scattered temporal behavior of the SLR translation components (as seen from time series analysis), compared to GPS or DORIS, leads to privilege SLR for the ITRF origin definition. Regarding the scale, it is of course admitted that from the theoretical and technology point of view, VLBI and SLR techniques should agree on the TRF scale. However, because we have the possibility to check for their scale consistency (or inconsistency), then when comparing their respective solutions, the possible inconsistency is obviously due to some systematic errors that should be investigated.

The ITRF Product Center hosted by the Institut Géographique National, France, together with the contribution of the ITRF combination centers (DGFI and NRCan) released the ITRF2005 solution in October 2006. Contrary to previous ITRF versions,

the ITRF2005 integrates time series of station positions and daily Earth Orientation Parameters (EOP's). The ITRF2005 input time-series solutions are provided in a weekly sampling by the IAG International Services of satellite techniques: the International GNSS Service-IGS (Dow et al. 2005), the International Laser Ranging Service-ILRS (Pearlman et al., 2002) and the International DORIS Service-IDS, (Tavernier et al., 2006), and in a daily (VLBI session-wise) basis by the International VLBI Service-IVS (Schlueter et al., 2002). Each per-technique time-series is already a combination, at a weekly basis, of the individual Analysis Center (AC) solutions of that technique, except for DORIS where two solutions are submitted by two ACs, namely the Institut Géographique National (IGN) in cooperation with Jet Propulsion Laboratory (JPL) and the Laboratoire d'Etudes en Géophysique et Oceanographie Spatiale (LEGOS) in cooperation with Collecte Localisation par Satellite (CLS), designated by (LCA).

Reasons for which it was decided to use time series of station positions and EOPs as input to ITRF2005 include:

- monitoring of non-linear station motions and all kinds of discontinuities in the time series: Earthquake related ruptures, site instability, seasonal loading effects, etc;
- rigorously and consistently including EOPs in the combination and ensuring their alignment to the combined frame;
- examining the temporal behavior of the frame physical parameters, namely the origin and the scale;
- assessing space geodesy positioning performance, through the estimation of the weekly (daily) Weighted Root Mean Scatter (WRMS) with respect to the long-term solution resulting from the stacking of the time series.

In the following sections we will primarily focus on two main issues: the positioning performance of space geodesy techniques and the temporal behavior of the SLR origin and the scale and the VLBI scale of the contributed solutions to the ITRF2005.

### **Combination Methodology**

The approach that is currently adopted for the combination of various TRF solutions provided by a single or several space geodesy techniques is built on the construction of a unique (combined) TRF, making use of the mathematical (7)14-parameter euclidian similarity. It considers defining the combined TRF at a given (arbitrary) reference epoch and adopting a TRF time evolution law that is supposed to be linear (secular). Consequently, 14 degrees of freedom are always necessary to completely ensure the TRF datum definition: 6 for the TRF origin and its rate (time derivative), 2 for the scale and its rate and 6 for the orientation and its rate. The inclusion of EOPs into the combination requires additional equations where the link between the TRF and EOPs is ensured via the 6 orientation parameters. The combination model considered by the ITRF Product Center allows the estimation of station positions and velocities, transformation parameters of each individual TRF solution with respect to the combined TRF and, if included, consistent series of EOPs. The input solutions usually used in this kind of combination are either (1) time series of station positions and EOPs or (2) long-term solutions composed by station positions and velocities and EOPs. In the first case where the combination amounts to rigorously stacking the time series, the un-modeled non-linear part of geodetic parameters are implicitly embedded in the combination output: possible seasonal (e.g. annual or semi-annual) station or/and geocenter motions are respectively left in the output time series of

station residuals and the transformation parameters. For more details, regarding the combination methodology the reader may refer to (Altamimi et al. 2007a, 2007b).

### Positioning Performance

When stacking station positions time series (weekly for satellite techniques and daily for VLBI), global WRMS per week (day) is computed, that is to characterize the internal precision and repeatability over time of each individual position time series. Figure 1 illustrates the WRMS per week (day) for each one of the 4 technique time series over the horizontal and vertical components and Table 1 summarizes the WRMS range. It is to be noted that the WRMS values do not qualify the techniques, but rather the solutions of the techniques which were submitted to the ITRF2005, and they are highly dependent on the quality of each station/instrument. Other factors are also important such as the number of the satellites available, e.g. in case of DORIS it was shown (Altamimi et al. 2006) that the quality (WRMS) improves when the number of satellites increases. However, from Figure 1 and Table 1, we can postulate that the current positioning performance for the best cases is around 2 mm for the horizontal component and around 5 mm for the vertical component.

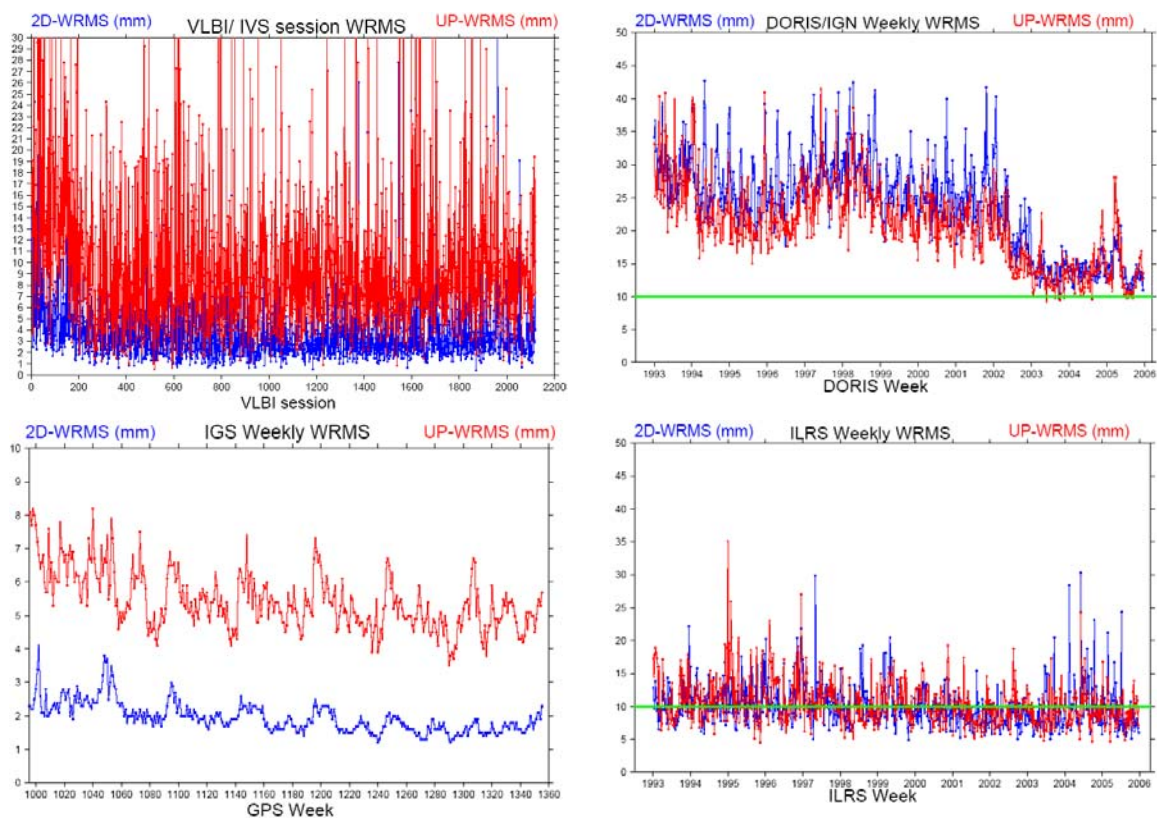


*Figure 1. Weekly (daily) WRMS as results from the time series stacking.*

### Accuracy of the ITRF Origin and Scale

#### *The Origin*

Although it is hard to assess the origin accuracy of the single ILRS solution that is submitted to ITRF2005, we attempt however to evaluate its consistency with respect to ITRF2000. Figure 2 shows the 3 translation time variations with respect to ITRF2000, using a reference set of 12 stations. Given their observation history and good performance, these are the only stations that are usable to link the combined

*Table 1. WRMS range per technique*

Solution	2-D WRMS mm	Up WRMS mm
VLBI	2-3	5-7
SLR	5-10	5-10
GPS	2-3	5-6
DORIS	12-25	10-25

SLR TRF resulting from the stacking of the time series to the ITRF2000 frame. Because the estimated transformation parameters are heavily sensitive to the network geometry, the distribution of the reference set of 12 stations is far from being optimal; only two of them are in the southern hemisphere (Yaragadee, Australia, and Arequipa, Peru). Apart from the seasonal variations that could be estimated over the translation parameters, the linear trends are of great importance to the ITRF origin stability over time. From Figure 2 we can easily see that the most significant trend is that of the Z-translation component, being of the order of 1.8 mm/yr. This bias will therefore exist between ITRF2000 and ITRF2005, and could be regarded as the current level of the origin accuracy as achieved by SLR. From that figure we can also distinguish a "piece-wise" behavior of the Z-translation: between respectively 1993-1996; 1996-2000 and 2000-2006. In our opinion, this is completely related to and correlated with the change of the ILRS network geometry over time. In order to illustrate that effect, we plotted on Figure 3 the number of SLR stations available in each weekly solution. From this plot, one can easily see the decreasing tendency of the number of stations, starting around 2000, which should be correlated with the Tz component that starts to significantly drifting at this same epoch (see Figure 2). In addition, among the approximately 80 SLR stations available in the ITRF2005, approximately 20 of them have sufficient time-span of observations to be considered as core stations for useful and comprehensive analysis.

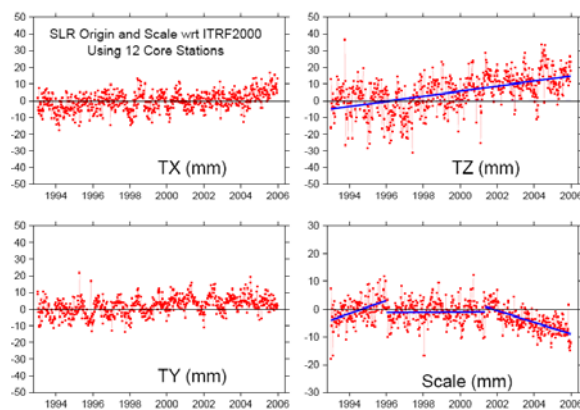


**Figure 2.** Translations and scale variations with respect to ITRF2000 of the ILRS SLR time series submitted to ITRF2005.

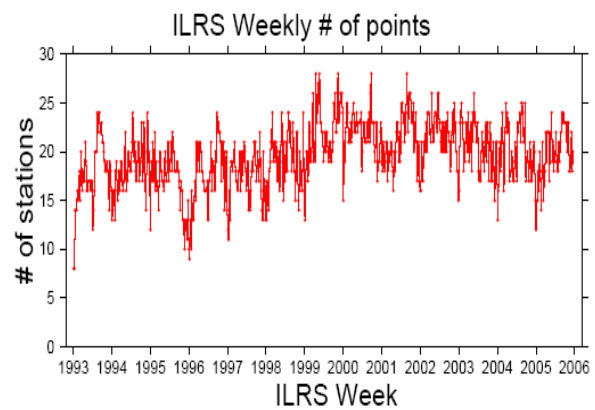


**Figure 3.** Number of stations included in the weekly ILRS SLR time series submitted to the ITRF2005.

### The Scale

The ITRF2005 combination (making use of local ties in co-location sites) revealed a scale bias of 1 ppb between VLBI and SLR solutions at epoch 2000.0 and a scale drift of 0.08 ppb/yr. VLBI scale selected to define that of ITRF2005 is justified by (1) the availability of the full VLBI history of observations (26 years versus 13 for SLR)

embedded in the submitted time series and (2) the the non-linear behavior (discontinuities) observed in the ILRS scale (see Figures 3). In order to illustrate more the inconsistency between the two scales, Figure 4 displays both scales with respect to ITRF2005, showing a clear bias both in the offset and the linear trend.

The accuracy assessment of the ITRF scale is not easy to evaluate, being dependent on several factors, as for instance, the quality and distribution of the local ties, the SLR range bias effect, the tropospheric modeling in case of VLBI and other possible systematic errors of the two techniques. However, given the level of consistency mentioned above between VLBI and SLR scales and despite the optimistic accuracy estimate of the ITRF2000 datum definition as stated in (Altamimi et al., 2002), and to be more conservative, we can postulate that the current level of accuracy of ITRF scale is around 1 ppb and 0.1 ppb/yr.

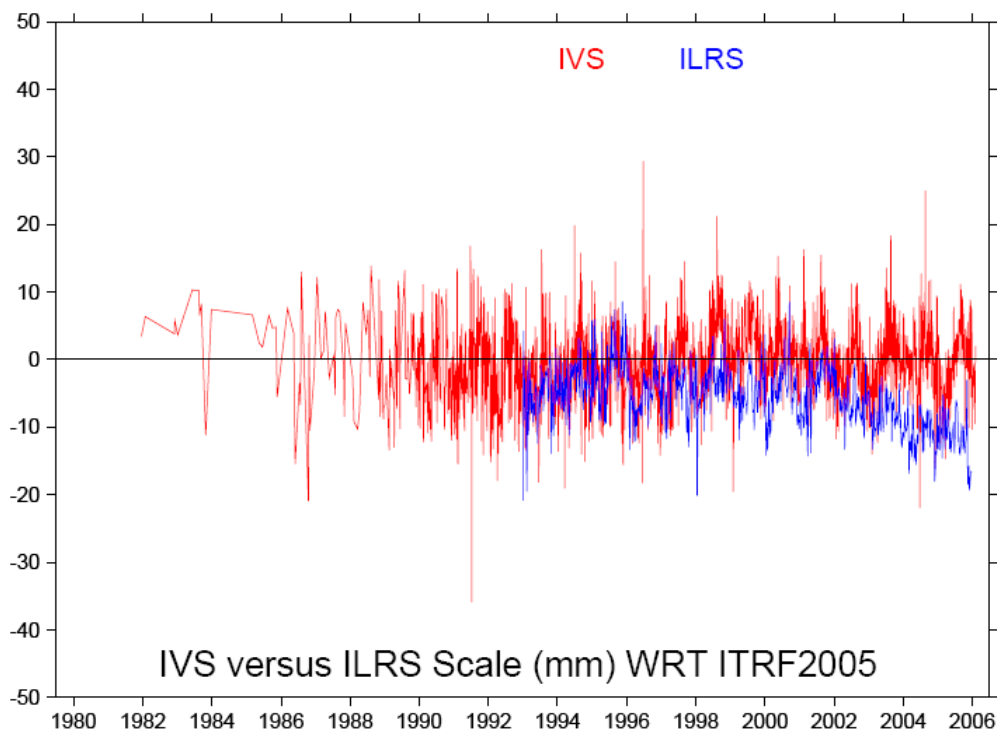


*Figure 4. VLBI and SLR Scale factor variations with respect to ITRF2005.*

## Conclusion

The ITRF2005 experience, using time series as input data, showed how sensitive the frame parameters are to the network geometry and in particular in case of SLR and VLBI and their co-locations. The scale bias between VLBI and SLR solutions revealed by the ITRF2005 combination is most probably due to multiple reasons that include poor VLBI and SLR co-locations, local tie uncertainties, systematic errors and possible differences in correction models (e.g. troposphere, SLR range bias, relativity) employed in the data analysis of both techniques. As results from the ITRF2005 analysis, the positioning performance at the weekly/daily basis, range between 2 to 25 mm, depending on the measurement technique, the instrument quality or station performance.

## References

- [1] Altamimi, Z., P. Sillard and C. Boucher (2002), ITRF2000: A New Release of the International Terrestrial Reference Frame for Earth Science Applications, *Journal of Geophys. Res.*, 107(B10), 2214, doi:10.1029/2001JB000561.
- [2] Altamimi, Z., X. Collilieux and C. Boucher, (2007a), Accuracy assessment of the ITRF datum definition, VI Hotine-Marussi Symposium of Theoretical and Computational Geodesy: Challenge and Role of Modern Geodesy, International Association of Geodesy, in press.
- [3] Altamimi, Z., X. Collilieux J. Legrand, B. Garayt and C. Boucher, (2007b), ITRF2005: A new release of the International Terrestrial Reference Frame based on time series of station positions and Earth Orientation Parameters, *Journal of Geophys. Res.*, in Press.
- [4] Altamimi, Z., X. Collilieux, C. Boucher, 2006, DORIS Contribution to ITRF2005, *Journal of Geodesy*, doi: 10.1007/s00190-006-0065-5.
- [5] Dow J.M, R.E. Neilan and G. Gendt, 2005, The International GPS Service (IGS): Celebrating the 10th Anniversary and Looking to the Next Decade, *Adv. Space Res.* 36 vol. 36, no. 3, pp. 320-326, doi:10.1016/j.asr.2005.05.125.
- [6] Kovalevsky, J., Mueller, I. I., and B. Kolaczek (Eds.), 1989, *It Reference Frames in Astronomy and Geophysics*, 474 pp., Kluwer Academic Publisher, Dordrecht.
- [7] Pearlman, M.R., J.J. Degnan and J.M. Bosworth, 2002, The International Laser Ranging Service, *Adv. Space Res.*, Vol. 30, No. 2, pp. 135-143.
- [8] Schlueter W., E. Himwich, A. Nothnagel, N. Vandenberg, and A. Whitney, 2002, IVS and Its Important Role in the Maintenance of the Global Reference Systems, *Adv. Space Res.*, Vol. 30, No. 2, pp. 145-150.
- [9] Tavernier, G., H. Fagard M. Feissel-Vernier, K. Le Bail, F. Lemoine, C. Noll, R. Noomen, J.C. Ries, L. Soudarin, J.J Valette, and P. Willis, 2006, The International DORIS Service: genesis and early achievements, in DORIS Special Issue, P. Willis (Ed.), *Journal of Geodesy*, 80(8-11):403-417, doi: 10.1007/s00190-006-0082-4.

---

## Station Coordinates, Earth Rotation Parameters, and Low Degree Harmonics from SLR within GGOS-D

R. Koenig<sup>1</sup>, H. Mueller<sup>2</sup>

1. GeoForschungsZentrum Potsdam (GFZ)
2. Deutsches Geodaetisches Forschungsinstitut (DGFI), Alfons-Goppel-Str. 11, 80539 Muenchen.

Contact: [koenigr@gfz-potsdam.de](mailto:koenigr@gfz-potsdam.de)

### Abstract

*Time series of station coordinates, Earth rotation parameters, and low degree harmonics of the gravity field are generated in weekly batches from Satellite Laser Ranging (SLR) measurements by two independent German institutes, the Deutsches Geodaetisches Forschungsinstitut (DGFI) and the GeoForschungsZentrum Potsdam (GFZ) and their two software packages for parameter and orbit determination, DOGS (DGFI Orbit and Geodetic Parameter estimation Software) and EPOS (Earth Parameter and Orbit System) respectively.*

*The products are based on common standards laid down by a consortium of some more German institutes joined in the GGOS-D (Global Geodetic Observing System - Deutschland (Germany)) project. GGOS-D strives for a rigorous and proper combination of the various space-geodetic techniques. The details of the processing and model standards and the differences with the International Laser Ranging Service (ILRS) "pos&eop" products are presented. A first series covering the years 1993 to 2006 has recently been provided by DGFI and GFZ to the project, initial results are shown and compared.*

### Introduction

The overall objective of the GGOS-D project is the investigation of the technological, methodological and information-technological realization of a global geodetic-geophysical observing system. The main fields of research are the development and implementation of data collection and data management systems as well as the generation of consistent and integrated geodetic time series for the description and modelling of the geophysical processes in the Earth system. The time series have to be referred to a unique, extremely accurate reference frame, stable over decades, and should be generated in such a way that they can be made available in near real-time to all users in science and society. Methods for a careful internal and external validation shall guarantee a very high reliability.

The space-geodetic techniques, i.e. Global Positioning System (GPS), SLR, and Very Long Baseline Interferometry (VLBI) with the exception of Doppler Orbitography and Radiopositioning Integrated by Satellite (DORIS), contribute to the processing with the models and as far as possible with the same set of parameters being applied by all the participating institutions, the Forschungsgruppe Satelliten Geodaesie (FSG), the Geodetic Institute of the University of Bonn (GIUB), the GFZ, the Bundesamt fuer Kartografie und Geodaesie (BKG), and the DGFI. The SLR part is covered by two independent contributions from DGFI with its DOGS and from GFZ with its EPOS software packages. The analysis should span the period 1983 until present date. A first solution beginning in 1993 up to early 2007 has recently been provided.

## Processing

Geometric and dynamic models mainly coincide with those recommended for the routine processing of the so-called “pos&eop” product, weekly station coordinates and Earth Orientation Parameters (EOPs) based on SLR, by the ILRS (see Pearlman et al., 2002) analysis centers (DGFI and GFZ being part there as well). In case of the dynamic models however, the ocean tide model FES2004 (Letellier et al., 2007), and the gravity field model EIGEN-GL04S1 (the satellite-only solution of the EIGEN-GL04C model, see Foerste et al., 2006) have been chosen. Also the ocean tide loading site displacements as provided by Bos and Scherneck (2007) corresponding to the FES2004 are applied.

In a first step we processed weekly arcs for the years 1993 to 2006 solving for weekly stations coordinates, daily EOPs, i.e. X-, Y- pole, and UT1 at 0:00 h UTC, all piecewise linear and continuous (in case of “pos&eop” instead X-, Y- pole, and, notably, LOD at 12:00 UTC, all piecewise constant, are solved for). The GFZ solution additionally incorporates the low degree coefficients of the spherical harmonic representation of the Earth's gravity field (shortly “low degree harmonics”) of degree 0 to 2 (in case of “pos&eop” the low degree harmonics are not solved for). In order to overcome the datum defect, the coordinates, the EOPs, and the low degree harmonics are endowed with an a priori sigma of 1 meter or its equivalent.

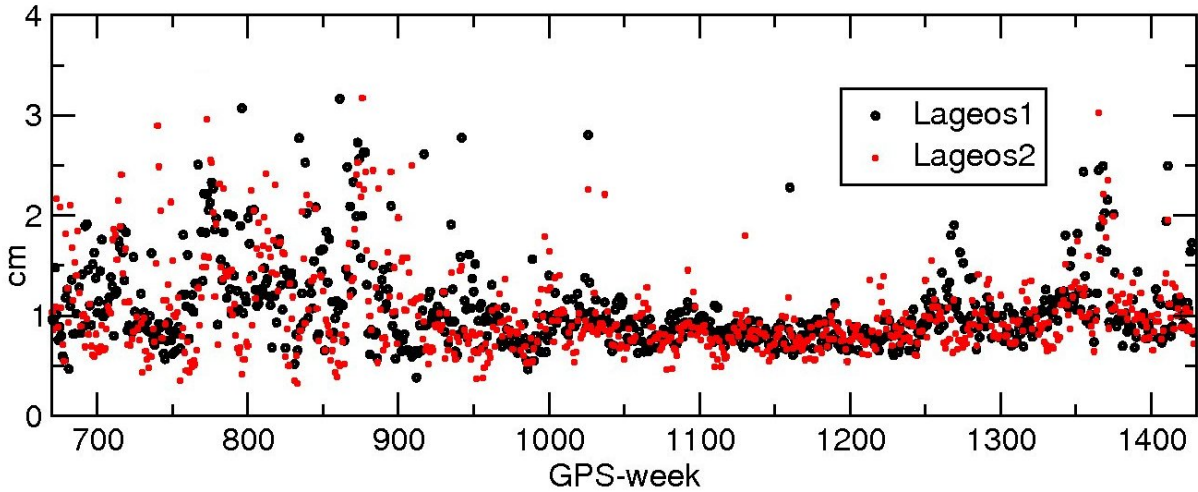
## First Results

The overall orbital fit and statistics for the whole period are shown in Table 1. The intention was to include as many stations as possible in the solutions. As a minimum however, stations should contribute with more than 10 observations per weekly arc. Besides that, iterative editing has been performed according to some criteria chosen individually by both institutes. This becomes evident in the number of observations used for the processing and the resulting orbital fit, and could end up in some differences of the solved-for parameters. In a next step, DGFI and GFZ are going to compare their editing procedures and to analyse the effect on the solution.

*Table 1. Global orbital fit of the two solutions.*

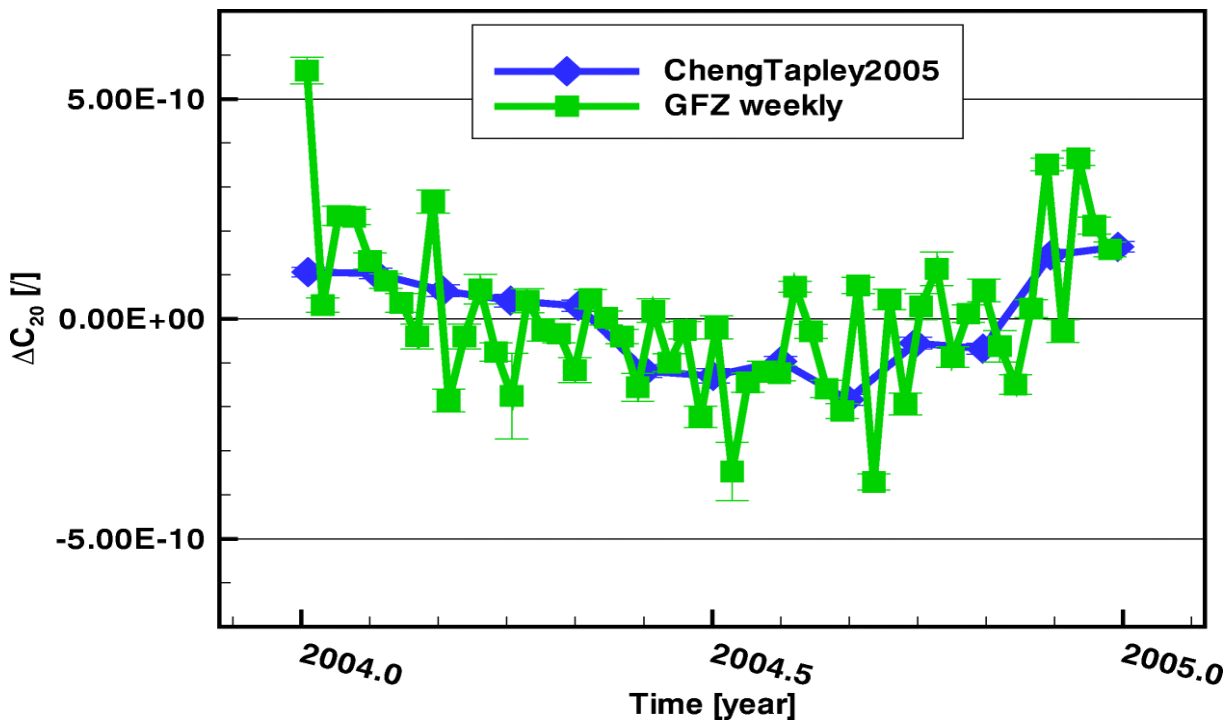
	<b>EPOS</b>	<b>DOGS</b>
<b>No. of Arcs</b>	742	759
<b>Period</b>	25-Oct-1992 - 13-Jan-2007	11-Nov-1992 - 20-May-2007
<b>Global Orbital Fit RMS (cm)</b>	1.04	1.07
<b>No. of Observations</b>	1,749,965	1,997,569
<b>No. of Observations per Arc</b>	2,358	2,632

In Figure 1 the weekly orbital fits of the DGFI solution show that some weeks are determined with worse accuracy, especially prior to 1999 or GPS week 990. This is mainly induced by some poorly performing non-core stations, the orbital fit for the core stations remains stable mostly below 1 cm all over the analysis period. In general, Lageos-1 turns out slightly more accurate than Lageos-2. Once up-to-date corrections for the Stanford-counter range bias problems or for the station dependent centre of mass corrections become available, we expect improved orbits and hence an improved quality of the resulting parameters.



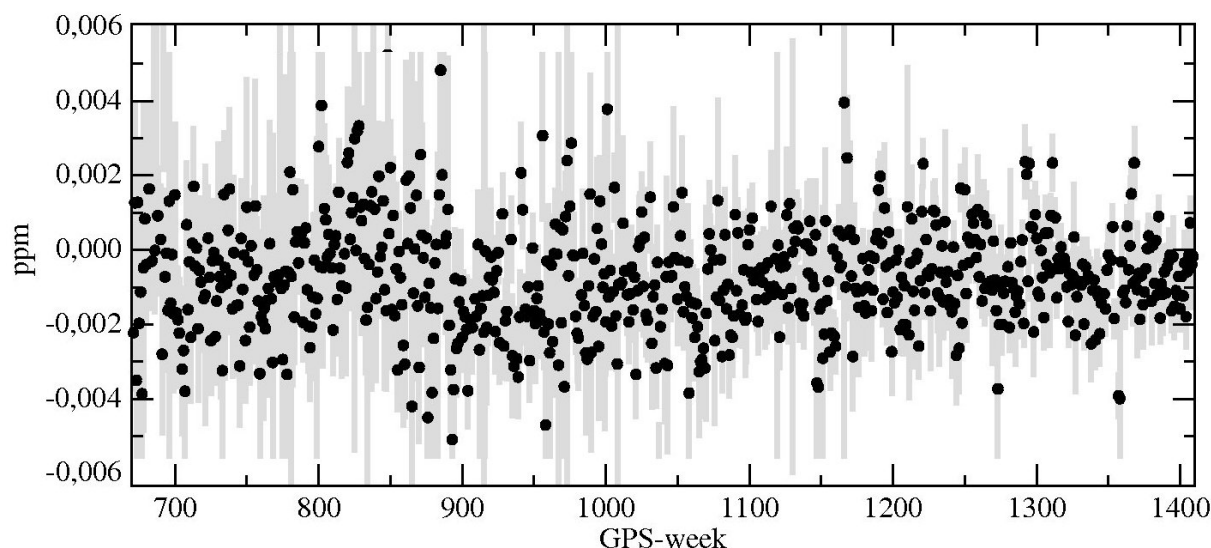
*Figure 1: Weekly orbital fits of the DOGS solutions.*

Figure 2 shows a comparison of the GFZ  $C_{20}$  time series to the recently published series by Cheng and Tapley (2005). Obviously the GFZ series shows a larger scatter, being mainly an effect of the dense resolution of the parameters and of the multitude of solved-for parameters. A generalization of the coordinate and low degree harmonic parameters would presumably stabilize the solution. Underneath the scatter, the general agreement of the curves is visible.



*Figure 2: Comparison of the EPOS  $C_{20}$  time series to the Cheng and Tapley (2005) series.*

The scale differences between the DOGS and the EPOS coordinate solutions are shown in Fig. 3. A small offset of about 1 ppb is visible and may be related to the different editing and to the fact that the GFZ solution has solved in addition for the low degree harmonics including  $C_{00}$ , the dynamic scale parameter. The alignment of the editing criteria for DOGS and EPOS, and solving for the low degree harmonics in the DOGS solution as well, should improve the agreement. Also, Fig. 3 reveals a



**Figure 3:** Scale differences between the DOGS and EPOS coordinate solutions 1993-2007.

decrease of the scatter in the course of time, demonstrating the improvement and stabilization of the SLR technique.

### Conclusions

Within the GGOS-D project, DGFI and GFZ are processing SLR data with their independent software packages DOGS and EPOS based on common, modern standards. In a first iteration, a 14 year long time series of weekly solutions for coordinates, EOPs, and, in case of GFZ, for low degree harmonics, has been generated. The standards adopted here are different with respect to those of the routine ILRS analysis centre processing.

First results show an excellent quality of the two SLR solutions. Some efforts have to be undertaken to harmonize in particular the editing of the weekly arcs and to include the low degree harmonic parameters to the DGFI solution.

The combination of all space-geodetic techniques within GGOS-D is pending, but first preliminary combinations of GPS and VLBI results indicate an excellent agreement, better than that experienced earlier during the ITRF2005 combinations by DGFI (Meisel et al., 2005).

### References

- [1] Bos, M.S., Scherneck, H.-G.: *The free ocean tide loading provider website*. <http://www.oso.chalmers.se/~loading>, modified 02/03/2007.
- [2] Cheng, M., Tapley, B.D.: *Correction to „Variations in the Earth's oblateness during the past 28 years“*. *Journal of Geophysical Research*, 110, B03406, doi:10.1029/2005JB003700, 2005
- [3] Förste, C., Flechtner, F., Schmidt, R., König, R., Meyer, U., Stubenvoll, R., Rothacher, M., Barthelmes, F., Neumayer, H., Biancale, R., Bruinsma, S., Lemoine, J.-M., Loyer, S., *A mean global gravity field model from the combination of satellite mission and altimetry/gravimetry surface data – EIGEN-GLO4C*. *Geophysical Research Abstracts*, 8, 03462, 2006
- [4] Letellier, T., Lyard, F., Lefebvre, F.: *The new global tidal solution: FES 2004*. [http://www.joss.ucar.edu/joss\\_psg/meetings/Archived/TOPEX2004/abstracts/D/Letellier.htm](http://www.joss.ucar.edu/joss_psg/meetings/Archived/TOPEX2004/abstracts/D/Letellier.htm), modified 06/27/2007.
- [5] Meisel B, Angermann D, Krügel M, Drewes H, Gerstl M, Kelm R, Müller H, Seemüller W, Tesmer V: *Refined approaches for terrestrial reference frame computations*. *Advances in Space Research*, Vol. 36, 350-357, Elsevier, 2005
- [6] Pearlman, M.R., Degnan, J.J., Bosworth, J.M.: *The International Laser Ranging Service*. *Advances in Space Research*, 30, 135-143, doi:10.1016/S02731177-(02)00277-6, 2002

---

## An original approach to compute Satellite Laser Range biases

D. Coulot<sup>1</sup>, Ph. Berio<sup>2</sup>, O. Laurain<sup>2</sup>, D. Féraud<sup>2</sup>, P. Exertier<sup>2</sup>

1. IGN/LAREG - Marne-la-Vallée – France
2. CNRS/OCA/GEMINI - Grasse – France

Contact: [David.Coulot@ensg.ign.fr](mailto:David.Coulot@ensg.ign.fr) / Fax: +33-1-64-15-32-53

### Abstract

*Although they are permanently calibrated, the Satellite Laser Ranging (SLR) stations can present residual systematic errors, the well-known “range biases”. These biases must be considered in any SLR data processing. Indeed, they are strongly correlated with the Up component of the station positions. Thus, if they are not computed together with these positions, they can induce jumps in these latter and consequently damage the global scale factor of the underlying Terrestrial Reference Frame with respect to any given reference.*

*On the other hand, estimating range biases together with station positions is not so easy, due to the previously mentioned correlations. In this paper, we describe a new approach to derive range bias values together with station positions: the so-called “temporal de-correlation” approach. This method consists in computing station range biases per satellite over a “long” period of time (determined by instrumental changes) together with weekly station position time series in order to significantly reduce the correlations.*

### Introduction

This paper comprises four parts. First, we provide general considerations about the Satellite Laser Ranging (SLR) technique range biases. Second, we demonstrate the strength of our temporal de-correlation approach through numerical illustrations based on simulations. Then, we analyze the first results produced by this method which has already been used for CALVAL (CALibration/VALidation) experiments and for a SLR data analysis carried out over 12 years. Finally, we describe the recent method improvements, provide the results of this new approach, and produce some conclusions and prospects.

### 1. General considerations

Fig. 1 shows the Grasse SLR station (7835) Up component time series computed in ITRF2000 without considering any range bias. We can clearly detect a jump in these time series and the epoch of this jump (September 1997) corresponds to a modification of the detection system of the station. This detection system modification has certainly modified the station detection and, as a consequence, its associated systematic errors. As shown by this example, a great attention must be paid to the SLR biases.

As shown on Fig. 2, the International Laser Ranging Service (ILRS) monitors these range biases. Indeed, among all the quality criteria used to qualify the tracking stations, two are directly linked to these biases: the short and long-term bias stabilities.

- The short-term stability is computed as the standard deviation about the mean of the pass-by-pass range biases.

- The long-term stability is the standard deviation of the monthly range bias estimates.

Regarding the data analysis, the situation does not seem to be so clear. Indeed, there are various strategies used to take into account these range biases: not to take biases into account, to correct a priori data with estimated bias values, to compute weekly range biases, etc. This paper aims to describe a method close to the instrumental evolutions of the considered stations. This method allows us to derive range biases by taking into account the problems linked to the simultaneous computation of these latter and station positions.

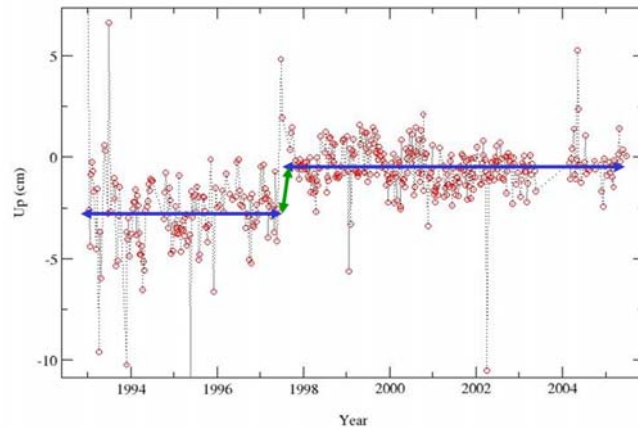


**Figure 1.** Up component time series (in cm) of Grasse SLR station (7835) in ITRF2000. No range bias has been estimated nor applied during this computation.

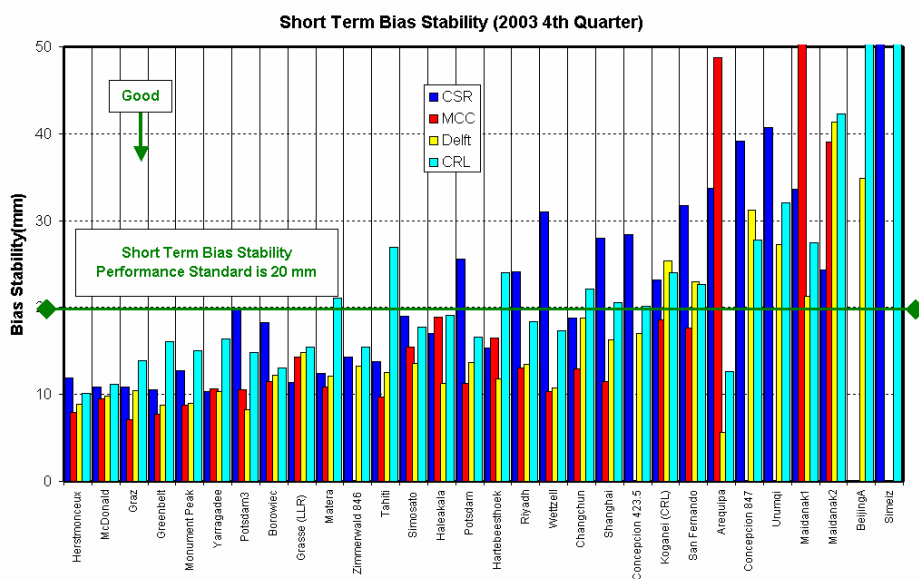


**Figure 2.** Example of short-term range bias stabilities provided by ILRS for 2003.

Source: <http://ilrs.gsfc.nasa.gov>.

## 2. Numerical illustrations

The simulations provided here aims to evidence the impact of range biases on any SLR data processing results. Fig. 3 shows the global simulation scheme. The first step consists in estimating the two LAGEOS satellite orbits. Then, these orbits are used with SLR measurements together with ITRF2000 [Altamimi et al., 2002], a model of atmospheric loading effects, and some range bias values to derive, on one hand, simulated range measurements and, on other hand, the partial derivatives of these simulated data with respect to station positions and, eventually, to range biases.

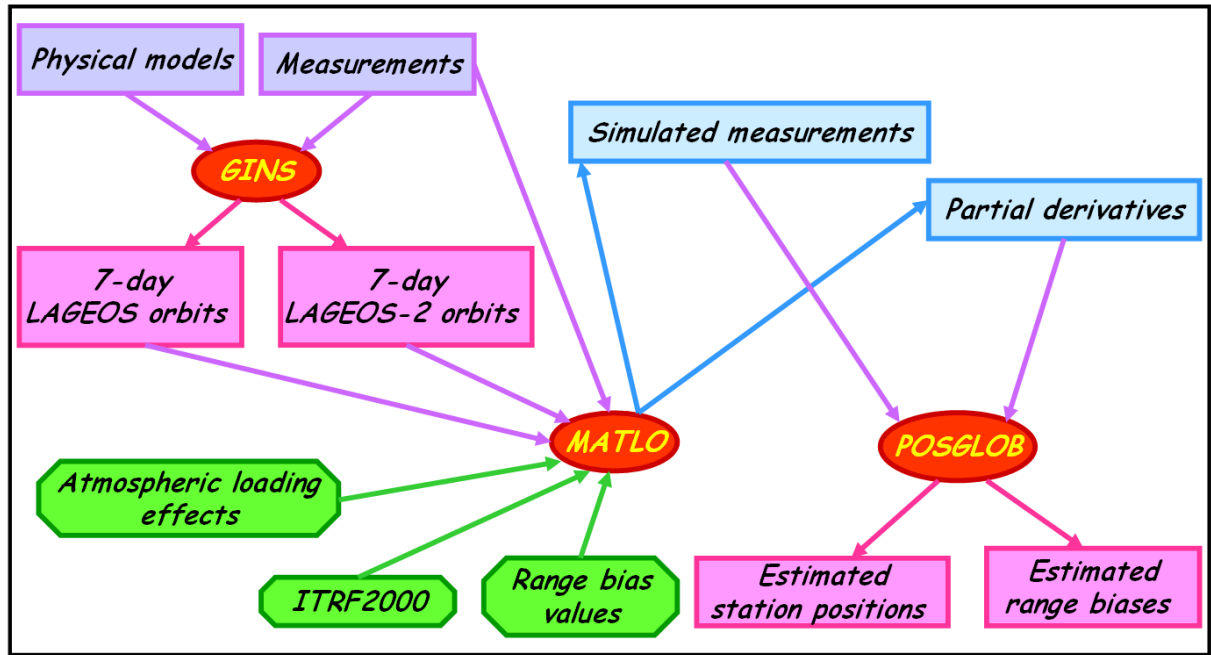


Figure 3. Simulation method.

Real orbital arcs and real SLR measurement epochs are used in order to get the most realistic simulations. Atmospheric loading effects are derived from the European Center for Medium-range Weather Forecasts (ECMWF, <http://www.ecmwf.int/>) pressure grids. As these loading signals are not modeled in the a priori values used, estimated station position time series must evidence them.

For the first simulation (cf. Fig. 4), range biases are applied in simulated measurements but they are not estimated with the Yarragadee SLR station (7090) position time series. The results clearly show that the range biases make a great impact on the Up component time series. Indeed, the time series is completely biased (the mean difference value almost reaches the centimeter level) and is no more stable (the RMS value of the differences is near 5 mm, while the horizontal component RMS values of differences are only at the millimeter level). Thus, range biases must be

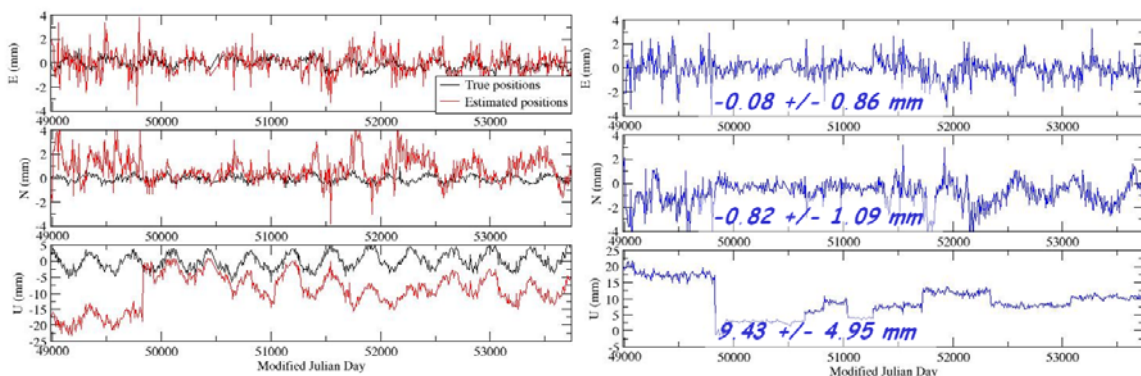


Figure 4. Results of the first simulation carried out for the Yarragadee SLR station (7090). Values are provided in mm for the three positioning components East, North, and Up. Graphs on the left: black (resp. red) curves correspond to the position time series computed without any bias in simulated measurements (resp. the time series computed with biases applied in simulated measurements). Graphs on the right: differences between red and black curves. Numerical values correspond to the mean and the RMS values.

estimated together with station positions.

In a second simulation, range biases are applied in simulated measurements and weekly range biases are estimated with the Yarragadee SLR station weekly position time series.

The results shown on Fig. 5 are clearly improved in comparison with those shown on Fig.4. Indeed, the mean value of the Up component differences is divided by 23 and the RMS value by 3.5. Furthermore, the values are also improved for the horizontal components (the difference RMS values are almost divided by 2), proof that range biases can also make an impact (of course lower than the one on the vertical component) on these components. But,

- we can notice large correlations between estimated bias and Up component values (96% on the average);
- spurious signals clearly appear in the weekly estimated biases, even if these latter have made the piece-wise behavior of the Up component time series disappearing.

Thus, range biases must be estimated over a longer period. For the third and last simulation (see the results on Fig. 6), range biases are still applied in simulated

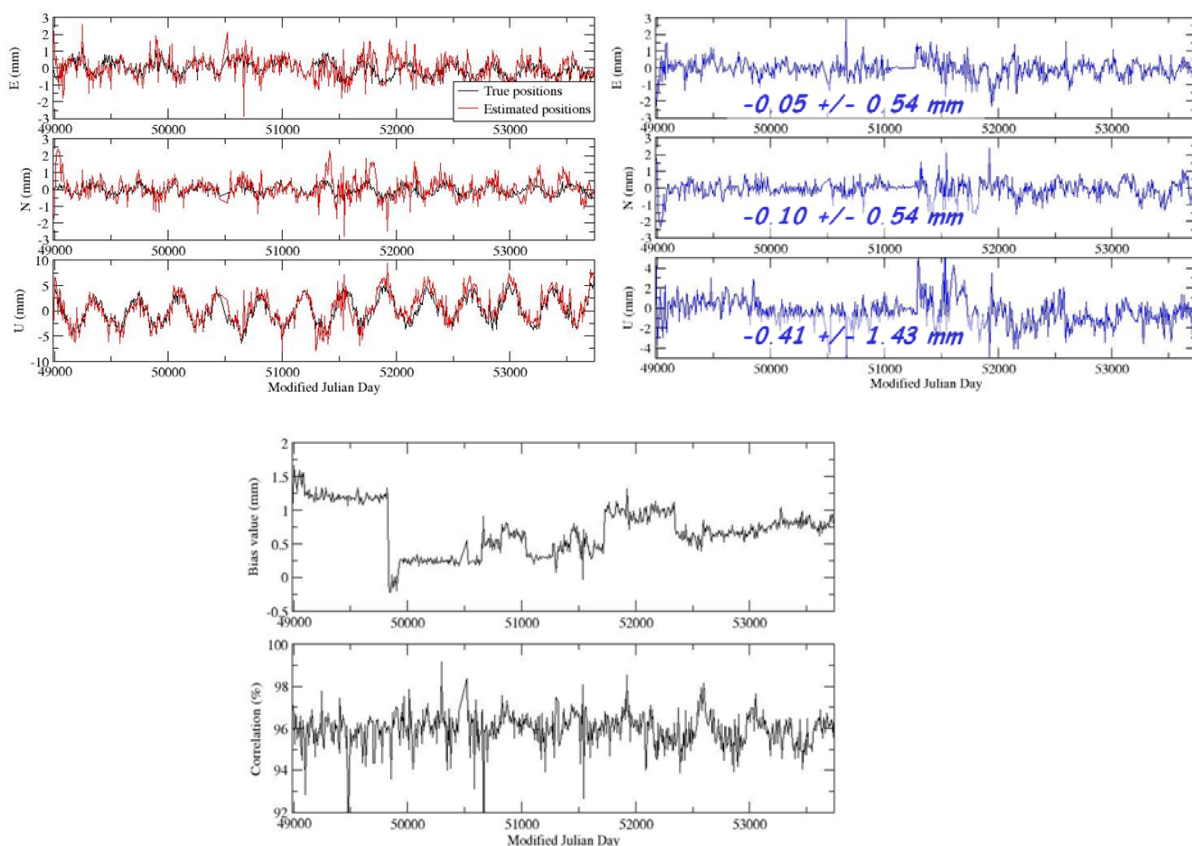


**Figure 5.** Results of the second simulation carried out for the Yarragadee SLR station (7090). Values are provided in mm for the three positioning components East, North, and Up. Graphs on the top left: black (resp. red) curves correspond to the position time series computed without any bias in simulated measurements (resp. the time series computed together with weekly range biases with biases applied in simulated measurements). Graphs on the top right: differences between red and black curves. Numerical values correspond to the mean and the RMS values. Graphs below: weekly computed range biases and correlations between bias and Up component estimated values.

measurements but range biases are now estimated over “long” periods together with the weekly Yarragadee SLR station position time series. The produced results are very satisfying. Indeed, the differences are quite negligible (the mean and the RMS values are below 0.5 mm). Moreover, estimating range biases per satellite allows us to take into account the possible constant signature effects. The correlations have decreased but they are still large (86% on the average).

This approach (that we have called the “temporal de-correlation method”) is the most satisfying one. Moreover, it is fully justified from an instrumental point of view. Indeed, the range biases are directly linked to the tracking instrumentation and we can suppose (at least for the most stable stations) that these instrumentations do not change all the time. As a result, the range biases can be supposed constant over given time intervals.

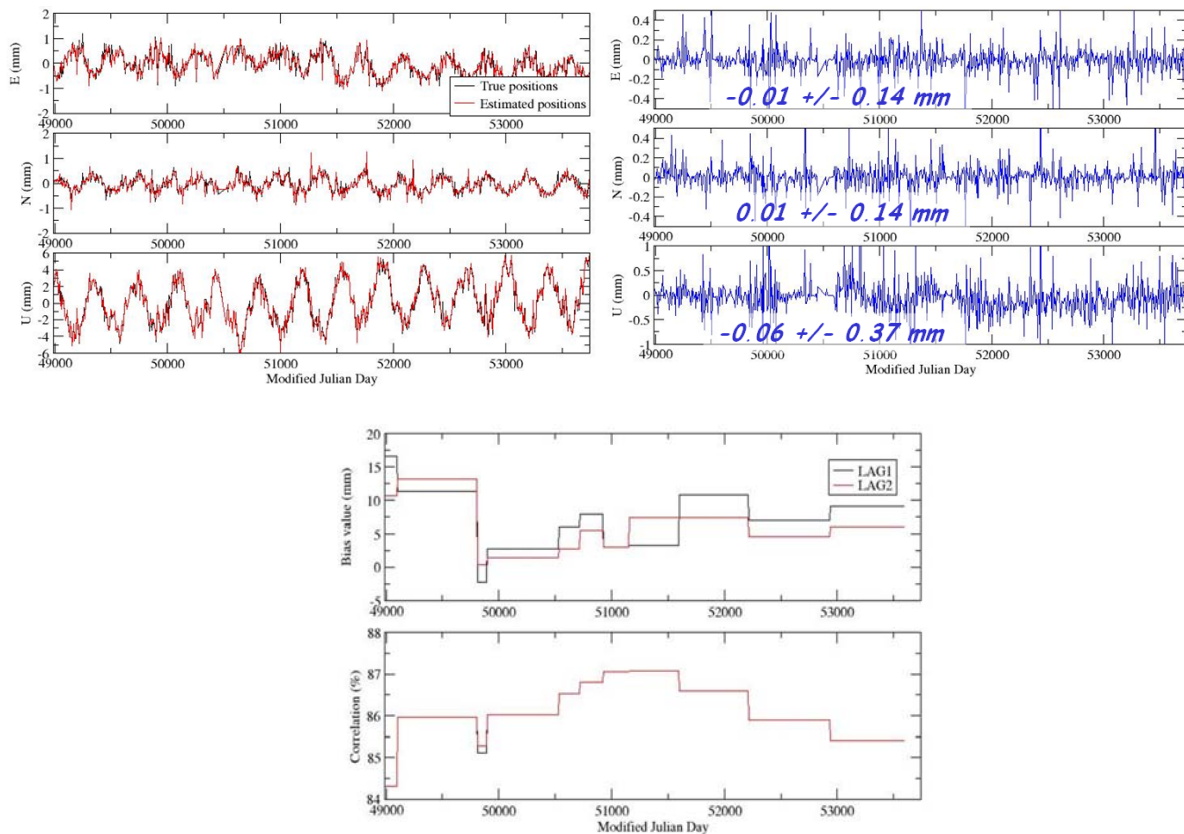


**Figure 6.** Results of the third simulation carried out for the Yarragadee SLR station (7090). Values are provided in mm for the three positioning components East, North, and Up. Graphs on the top left: black (resp. red) curves correspond to the position time series computed without any bias in simulated measurements (resp. the time series computed together with the “long-period” range biases with biases applied in simulated measurements). Graphs on the top right: differences between red and black curves. Numerical values correspond to the mean and the RMS values. Graphs below: “long-period” computed range biases per satellite and correlations between bias and Up component estimated values.

### 3. First results of the temporal de-correlation method

#### 3.1. CALVAL experiment

These experiments were carried out with the French Transportable Laser Ranging System (FTLRS, see [Nicolas, 2000]) in Corsica in 2002 [Exertier et al., 2004] (and, more recently, in 2005) and in Crete in 2003 [Berio et al., 2004]. As an illustration of the use of our temporal de-correlation method, here is the example of the GAVDOS project, e.g. of the Crete campaign carried out in 2003. During such campaign, the FLTRS aims to calibrate the satellite altimeter (see Fig. 7) with the help of a short-arc technique [Bonfond et al., 1995]. Thus, we need the most accurate positioning for this transportable station as well as an exhaustive knowledge of its error budget and, in particular, an accurate estimate of its range bias.

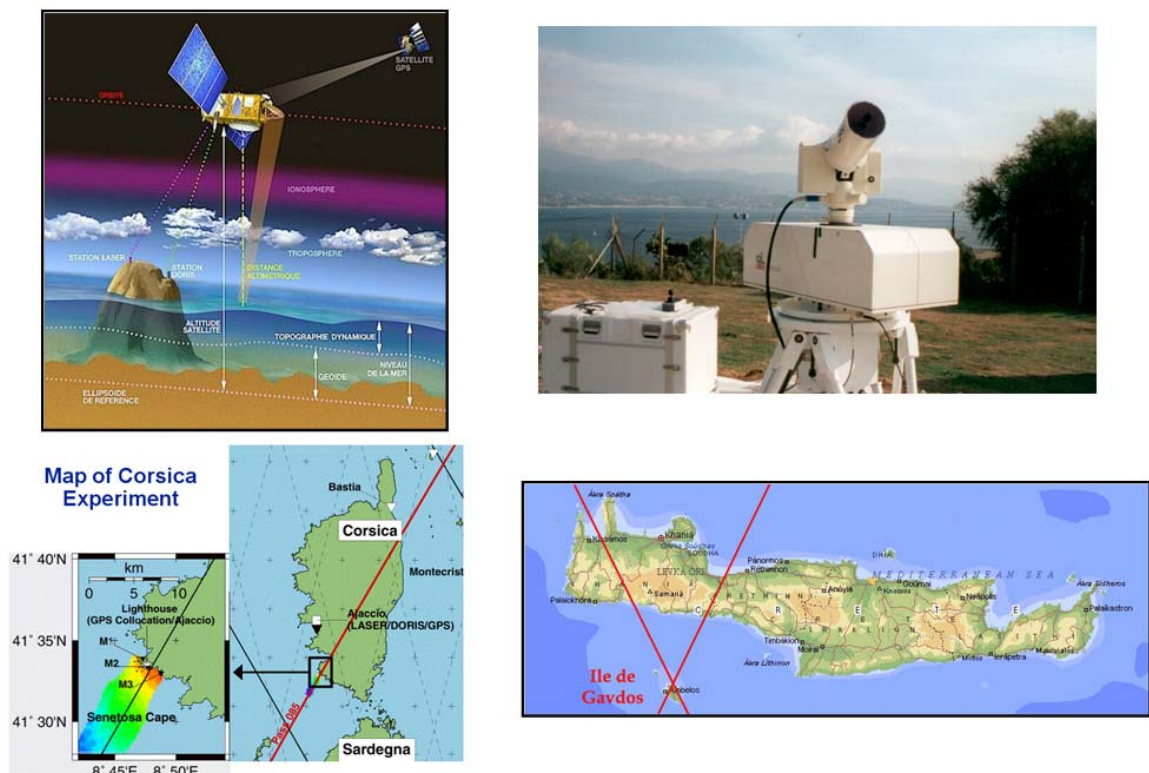


*Figure 7. CALVAL experiments with the FTLRS in Corsica and in Crete.*

Regarding the number of normal points collected on the two LAGEOS satellites by the FTRLRS during this campaign (see Tab. 1), it is clear that we need to use the four satellite data to compute the FTLRS positioning. To do so, we have carried out two kinds of computations:

1. the FTLRS position and the range biases per satellite are computed over the whole period of time;
2. we compute weekly FTLRS positions together with range biases per satellite which are computed over the whole period of time (temporal de-correlation approach).

Satellite	Number of normal points
LAGEOS-1	108
LAGEOS-2	315
STARLETTE	2 902
STELLA	1 479

**Table 1.** Number of normal points collected by the FTLRS during the Crete campaign carried out in 2003.

In the both computations, the FTRLRS positions are computed with respect to the ITRF2000 position [Altamimi et al., 2002] corrected for the solid Earth tides and the solid Earth pole tide in agreement with [McCarthy, 1996]. With the first method, the mean FTLRS position is directly computed, while, with the second approach, the mean FTLRS position is provided as the weighted mean value of the weekly estimated positions. The results produced by these two methods are summarized in Table 2.

The horizontal component estimated values are left unchanged between both approaches. And, the correlation is strongly decreased with the temporal de-correlation method. We can also notice a transfer between the biases and the Up components (the value is close to 1 cm) between both methods. Only the results of the second method are retained and, as a result, the mean FTLRS range bias value is -13,8 mm. [Nicolas et al. 2002] provides - 5 mm. This difference is explained. Indeed, during the whole campaign, the internal and external FTLRS calibrations exhibited a constant 1-cm difference.

Method	East	North	Up	BLAG1	BLAG2	BSTE	BSTA	Corr.
Method 1	2,5	-5,9	0,3	-19,7	-20,6	-28,3	-22,4	0,93
Method 2	1,6	-5,8	12,5	-9,6	-9,7	-20,2	-15,7	0,57
Absolute differences	0,9	0,1	12,2	10,1	10,9	8,1	6,7	.

**Table 2.** Results (in mm) produced by the two methods studied to compute the FTLRS mean position and range bias during the Crete campaign carried out in 2003. The FTLRS mean positions are provided in the ENU local frame. BXXXX corresponds to the FTLRS bias computed for the satellite XXXX and corr. is the maximum value of the correlations between the estimated FTLRS range bias values per satellite and its Up component positioning values.

Finally, we can see differences between the bias estimated values per satellite (both LAGEOS satellites versus STELLA and STARLETTE satellites). These differences could be explained by a radial constant error of 1 cm found for STELLA [Bonnefond, 2006] and by the fact that the signature effects depend on satellite and on detection system [Nicolas, 2000].

### 3.2. 12-year SLR data analysis

The temporal de-correlation method has also been applied over 5-month running windows in the framework of a 12-year SLR LAGEOS satellite data analysis (see [Coulot et al., 2005] and [Coulot, 2005] for more details).

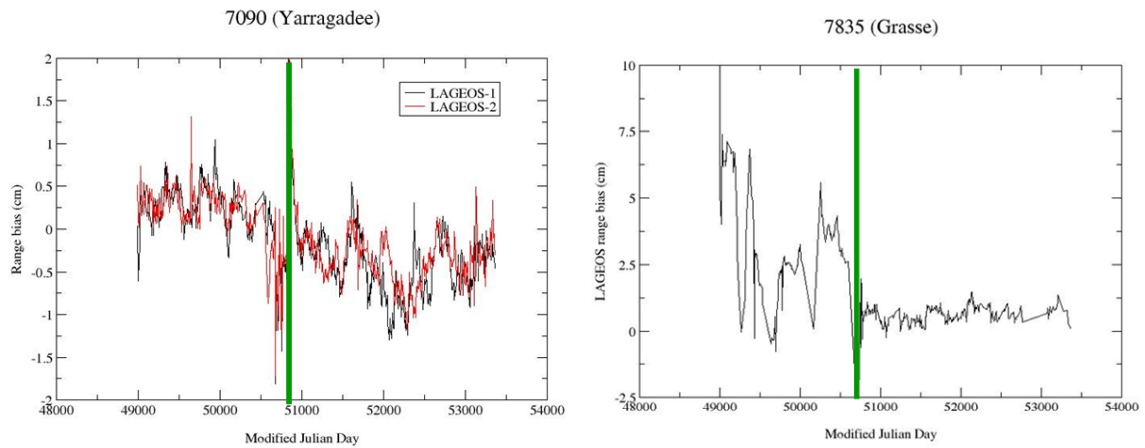


**Figure 8.** Bias (in cm) time series with a 5-month sampling computed for the Yarragadee (on the left) and the Grasse (on the right) SLR stations during the 12-year SLR LAGEOS satellite data analysis.

Fig. 8 provides two examples of bias time series computed during this study. Regarding the Yarragadee (7090) SLR station results, we can first notice that the bias values per satellite are very close: the RMS of the difference is 0.03 mm! A jump is clearly detected in the two time series. And, the epoch of this jump (January 1998) in fact corresponds to a detection system change.

Regarding the Grasse (7835) SLR station results, a jump is also detected in September 1997 and this jump corresponds to the detection system change previously mentioned in section 1 (cf. Fig. 1). We can finally notice the great stabilization of the range biases after this discontinuity. Indeed, the bias RMS value after this latter is 3.0 mm whereas this value is 20.5 mm before the jump!

#### 4. Method improvement

##### 4.1. New approach

Up to now, the limits of the time interval over which biases are supposed to be constant were not rigorously determined. As previously mentioned, range biases are directly linked to SLR instruments. Thus, biases are now supposed to be constant

	<p>8.01 Calibration Type : PRE+POST                  Target Location : EXTERNAL                  Target Type : CORNER CUBE                  Target Structure : CONCRETE PIER                  Target Distance [m]: 150.4229                  Date Measured : 1998-08                  Accuracy (mm) [mm]: 2                  Verification : Local Tie Survey Comparison                  Return-rate Controlled : YES                  Mode of Operation : FEW PHOTON                  Average Cal Interval [min]: 75                  Single Shot RMS [mm]: 4.5                  Edit Criterion 1st Chain : ITERATIVE 3.0 SIGMA                  Edit Criterion 2nd Chain : N.A.                  Application of Cal Data : AVERAGE                  Date Installed : 1992-07-20                  Date Removed : (yyyy-mm-dd)                  Additional Information : (multiple lines)</p>	<p>6.01.01 Primary Chain                  Signal Processing : CFD                  Manufacturer : Tennelec                  Model : TC454                  Date Installed : 1993-04-23                  Date Removed : (yyyy-mm-dd)                  Amplitude Measurement : YES                  Return-rate Controlled: YES                  Mode of Operation : Few to Multi Photons</p> <p>6.02.02 Secondary Chain                  Signal Processing : CFD                  Manufacturer : Tennelec                  Model : TC454                  Date Installed : 1998-08-13                  Date Removed : (yyyy-mm-dd)                  Amplitude Measurement : YES                  Return-rate Controlled: YES                  Mode of Operation : Single to Multi Photons</p>
<p>9. Time and Frequency Standards                  9.01.01 Frequency Standard                  Type : Rubidium disciplined by GPS                  Model : XL-DC 151-358-108-2                  Manufacturer : TrueTime                  Short Term Stab. [e-12]: 10                  Long Term Stab. [e-12]: 3                  Time Reference : GPS                  Synchronization : GPS Epoch                  Accuracy [ns]: &lt;100                  Date Installed : 2000-06-29                  Date Removed : (yyyy-mm-dd)</p>		

**Figure 9.** Examples of instrumental change epochs found in the log file of the Yarragadee SLR station (7090).

between two instrumental changes. We use station log files to determine these changes. Fig. 9 shows examples of instrumental change epochs used for the Yarragadee station (7090). Examples of so computed biases per satellite are provided in [Coulot et al., 2007].

#### 4.2. Results

Fig. 10 compares the results produced with our improved temporal de-correlation method with those produced without considering any range bias during the data processing. Results are satisfying. Indeed, for instance, the scale factor time series is

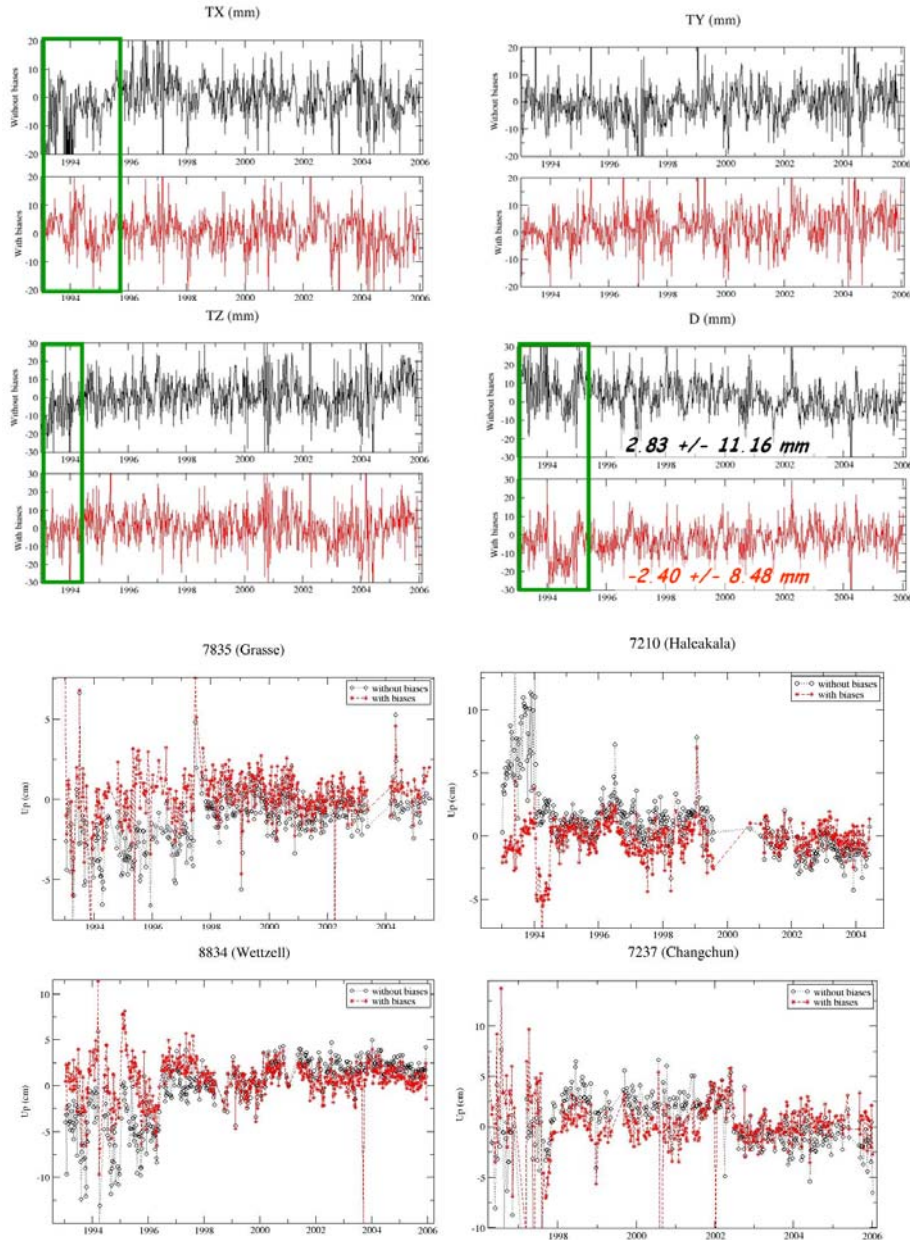


**Figure 10.** Translation and scale factor parameters (in mm) computed between the weekly Terrestrial Reference Frames and ITRF2000 and four station Up component time series computed in ITRF2000 (in cm). Black (resp. red) curves correspond to the computation carried out without considering any bias (resp. the computation for which our improved temporal de-correlation method has been applied).

more stable (RMS value of 8.5 mm to be compared with the 11.2 mm value provided by the computation carried out without bias). Moreover, the drift exhibited by the black scale factor time series disappears when our approach is used. Finally, the station time series are clearly more stable even if some discontinuities are still detected.

## 5. Conclusions and prospects

The two approaches (“running windows” or “instrumental change epochs”) produce very satisfying results. They could be coupled to detect jumps which are not clearly linked to reported instrumental evolutions. Furthermore, it would allow us to rigorously apply the method to “poor quality stations”, e.g.. stations for which biases are not stable.

Our method takes into account the correlation between station position Up components and range biases. We should also pay attention to the correlations with the possible radial orbital errors in the framework of a semi-dynamical approach (see [Coulot et al., 2007]). It would thus require a global estimation of all parameters for the whole network involved.

## References

- [1] Altamimi, Z., P. Sillard, and C. Boucher: “ITRF2000: a new release of the International Terrestrial Reference Frame for Earth science applications”, *J. Geophys. Res.*, 107(B10), 2214, doi: 10.1029/2001JB000561, 2002.
- [2] Berio, P., P. Exertier, F. Pierron, J. Weick, D. Coulot, and O. Laurain: “FTLRS support to the Gavdos project: tracking and positioning”, in *Proceedings of the 14<sup>th</sup> International Laser Ranging Workshop*, 2004.
- [3] Bonnefond, P., P. Exertier, P. Shaeffer, S. Bruinsma, and F. Barlier: “Satellite Altimetry from a Short-Arc Technique: Application to the Mediterranean”, *J. Geophys. Res.*, 100(C12), p. 25 365-25 382, 1995.
- [4] Bonnefond, P., personal communication, 2006.
- [5] Coulot, D., P. Berio, O. Laurain, D. Féraudy, P. Exertier, and K. Le Bail: “Analysis of 12 years (1993-2004) of SLR data”, poster presented at the 2<sup>nd</sup> European Geosciences Union General Assembly, Vienna, Austria, 2005.
- [6] Coulot, D.: “Télémétrie laser sur satellites et combinaison de techniques géodésiques. Contributions aux Systèmes de Référence Terrestres et Applications”, Ph. D. thesis, Observatoire de Paris, 2005.
- [7] Coulot, D., P. Berio, O. Laurain, D. Féraudy, P. Exertier, and F. Deleflie: “Analysis of 13 years (1993-2005) of Satellite Laser Ranging data on the two LAGEOS satellites for Terrestrial Reference Frames and Earth Orientation Parameters”, same issue, 2007.
- [8] Exertier, P., J. Nicolas, P. Berio, D. Coulot, P. Bonnefond, and O. Laurain: “The role of Laser Ranging for calibrating Jason-1: the Corsica tracking campaign”, *Mar. Geod.*, 27, p. 1-8, 2004.
- [9] McCarthy, D.D.: “IERS Conventions”, IERS Technical Note 21, Observatoire de Paris, 1996.
- [10] Nicolas, J.: “La Station Laser Ultra Mobile. De l'obtention d'une exactitude centimétrique des mesures à des applications en océanographie et géodésie spatiales”, Ph. D. thesis, Université de Nice-Sophia-Antipolis, 2000.
- [11] Nicolas, J., P. Bonnefond, O. Laurain, F. Pierron, P. Exertier, and F. Barlier: “Triple laser ranging collocation experiment at the Grasse Observatory, France - September - November 2001-“, in *Proceedings of the 13<sup>th</sup> International Laser Ranging Workshop*, 2002.

---

## **Analysis of 13 years (1993-2005) of Satellite Laser Ranging data on the two LAGEOS satellites for Terrestrial Reference Frames and Earth Orientation Parameters**

D. Coulot<sup>1</sup>, Ph. Berio<sup>2</sup>, O. Laurain<sup>2</sup>, D. Féraud<sup>2</sup>, P. Exertier<sup>2</sup>, F. Deleflie<sup>2</sup>

1. IGN/LAREG - Marne-la-Vallée – France
2. CNRS/OCA/GEMINI - Grasse - France

Contact: [David.Coulot@ensg.ign.fr](mailto:David.Coulot@ensg.ign.fr) /Fax: +33-1-64-15-32-53

### **Abstract**

*The quality presently reached by space-geodetic techniques, regarding precision, accuracy such as spatial and temporal distributions of their measurements, allows us to compute time series of geodetic products.*

*In this context, we have developed a method to compute time series of Earth Orientation Parameters (EOPs) and terrestrial station positions through the analysis of Satellite Laser Ranging (SLR) data. This technique being an important basis for the computation of the International Terrestrial Reference Frame, it is crucial to derive accurate time series with a rigorous approach. Furthermore, this method will be used by the scientific department GEMINI of the Observatoire de la Côte d'Azur when it will become an official IERS analysis center.*

*These time series are obtained with a good accuracy and a reasonable sampling (1 day for EOPs and 1 week for station positions). This good accuracy is ensured by i) a rigorous weighting of SLR measurements per satellite and per station; ii) a kinematic approach to compute orbital residual errors; iii) a rigorous control of range biases which is detailed in [Coulot et al.,2007].*

*In this paper, we first present the two aspects i) and ii) of our method. In a second part, we analyze 13 years (1993-2005) of SLR data on both LAGEOS satellites in order to study the Terrestrial Reference Frames and the EOPs so computed.*

### **Introduction**

This paper comprises four parts. First, we detail the two LAGEOS satellite orbit computation. Second, we provide general considerations about the Satellite Laser Ranging (SLR) data processing, regarding the data weighting, the orbital residual errors, and the range biases. Then, we describe the time series computation method and produce the results and, finally, we provide some conclusions and prospects.

#### **1. Orbit computation**

This section aims to briefly describe the two LAGEOS satellite orbit computation. Tables 1, 2, and 3 respectively show the physical models used for the orbit computations and for the Earth Orientation Parameters (EOPs) and the station positions during these computations.

Fig.1 shows the orbit residual WRMS and the numbers of data used and rejected for both satellites. Tab. 4 provides some statistics of these values. We can see that, on average, the residual WRMS are at the centimeter level for both LAGEOS satellites.

The sampling used for these computations is the GPS week but, in order to reduce the impact of the residual orbital errors, we in fact compute 9-day orbital arcs and only keep the 7-day central arcs. As a result, our orbital arcs provide 2-day overlaps. Fig. 2

shows the bias and the RMS values of the orbit differences so computed in RTN frame for both satellites. Table 5 provides the mean values of these difference bias and RMS values.

*Table 1. Physical models used for the orbit computations.*

Type	Description
Earth's gravity field	GRIM5_C1 [Gruber et al., 2000]
Atmospheric density	DTM94 [Berger et al., 1998]
Planetary ephemerides	DE403 [Standish et al., 1995]
Earth's time varying gravity field	
Solid Earth tides	Model in [McCarthy and Petit, 2004]
Solid Earth pole tide	Model in [McCarthy and Petit, 2004]
Oceanic tides	FES2002 [Le Provost, 2002]
Atmospheric pressure	ECMWF, <a href="http://www.ecmwf.int/">http://www.ecmwf.int/</a>

*Table 2. Physical models used for the EOPs during the orbit computations.*

Type	Description
Reference time series	EOPC04 [Gambis, 2004]
Quasi-diurnal Variations	Model in [McCarthy and Petit, 2004]
Precession	Model [Lieske et al., 1977]
Nutation	Model in [McCarthy, 1996]

*Table 3. Physical models used for the stations positions during the orbit computations.*

Type	Description
Terrestrial Reference Frame	ITRF2000 [Altamimi et al., 2002]
Celestial Reference Frame	ICRF [Arias et al., 1995]
Solid Earth tides	Model in [McCarthy and Petit, 2004]
Solid Earth pole tide	Model in [McCarthy and Petit, 2004]
Oceanic loading (only tidal components)	Computed with FES2002
Atmospheric loading (only non-tidal components)	Computed with ECMWF fields

*Table 4. Statistics of the values shown on Fig. 1.*

Satellite	Mean residual WRMS	Mean number of data used	Mean number of rejected data
LAGEOS	1.11 cm	1433	49
LAGEOS-2	0.95 cm	1320	35

Their interpretation is not easy, and yet these overlaps provide a way of controlling the orbit quality. From Table 5, we can see that the two LAGEOS satellite orbits provide differences with mean RMS values between 1 and 4.5 cm.

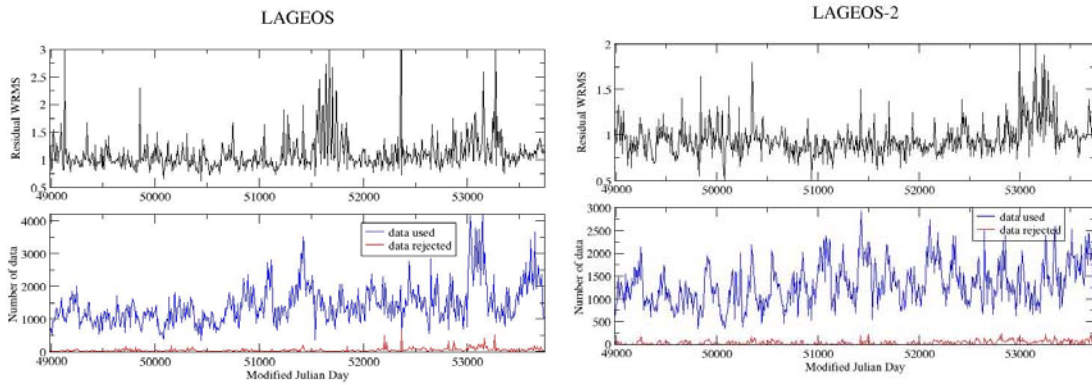


**Figure 1.** Orbit residual WRMS (cm) (black curves) and numbers of data used (blue curves) and rejected (red curves) per orbital arc for both LAGEOS satellites (LAGEOS on the left and LAGEOS-2 on the right).

**Table 5.** Statistics of the values shown on Fig. 2.

Satellite	R (cm)	T (cm)	N (cm)	.
LAGEOS	-0.02	-0.01	0.01	Mean bias
	2.57	4.37	2.59	Mean RMS
LAGEOS-2	0.01	-0.05	0.00	.
	1.32	2.26	2.66	.

## 2. General considerations

The SLR data processing method we have developed is divided in three steps. Fig. 3 shows the global computational scheme. First, GRGS (french Groupe de Recherche en Géodésie Spatiale, Spatial Geodesy Research Group, in English) GINS (Géodésie par Intégration Numérique Simultanée, Geodesy by Simultaneous Numerical Integration, in English) software provides the two LAGEOS satellite orbits with the help of physical models and SLR measurements (see previous section 1). Second, GRGS MATLO (MATHématiques pour la Localisation et l’Orbitographie, MATHEMATICS for Localization and Orbitography, in English) software uses these orbital arcs and the SLR data to compute pseudo measurements as well as partial derivatives of these latter with respect to the parameters worthy of interest. Finally, an estimation software (POSGLOB for POSitionnement GLOBal or GLOBal POSitioning in English) produces parameter estimates from MATLO outputs.

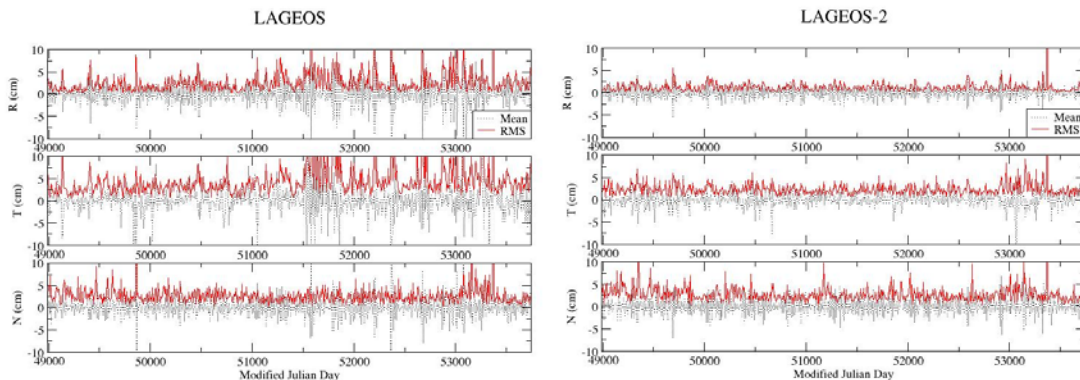


**Figure 2.** Orbit differences (biases - in black - and RMS values - in red -, in cm) in the RTN frame computed over the two overlapping days for both LAGEOS satellites (LAGEOS on the left and LAGEOS-2 on the right).

As shown in green boxes on Fig. 3, there are three critical issues in such computation: the range bias and residual orbital error handling and the data weighting. Thus, we try to build the optimal method to take these issues into account.

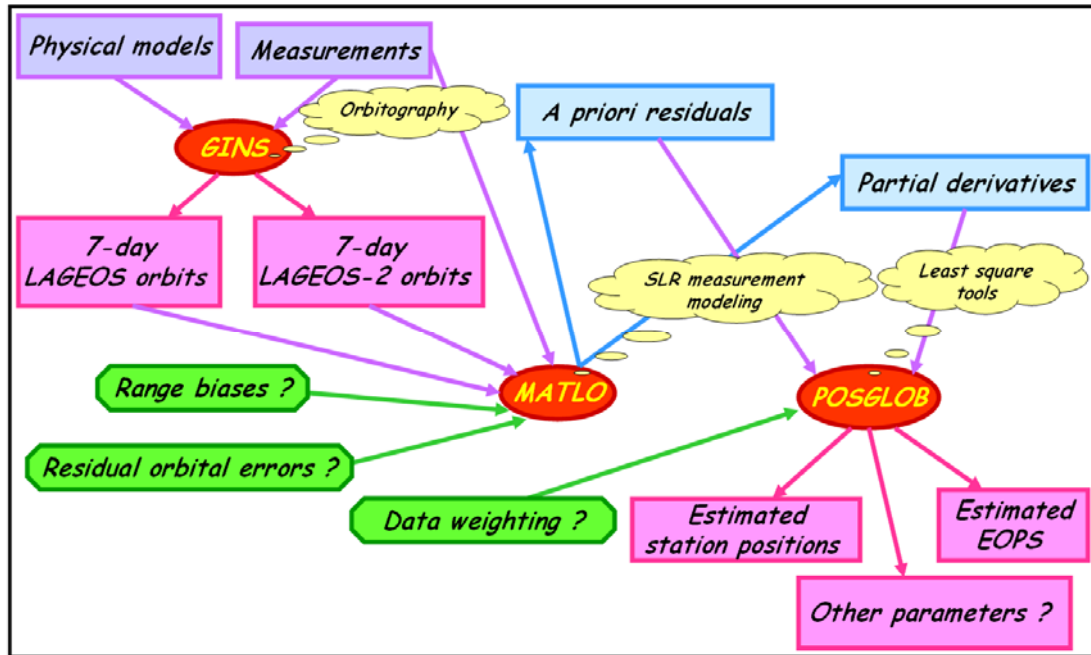


Figure 3. SLR data processing scheme.

### 2.1. Data weighting

SLR stations do not provide measurements of the same quality. As a consequence, we can not use the same weight for all SLR measurements but we have to find weights which really correspond to the quality of these measurements. To do so, we use an optimal variance component analysis method: the degree of freedom method inspired by [Persson, 1982]. The following scheme on Fig. 4 summarizes the method (see [Sillard, 1999] and [Coulot, 2005] for more details).

As shown on Fig.4, this method (as a great part of such variance component analysis method) is based on common parameters for all considered observation groups. In our case, the only real common parameters are EOPs as we consider that observation groups are measurements per station and per satellite. Thus, our variance component analysis approach only relies on these EOPs.

Fig. 5 shows the method used to derive the optimal weighting per station and per satellite. First of all, MATLO software is used to derive pseudo measurements and partial derivatives of these latter with respect to station positions and EOPs from the 7-day LAGEOS satellite orbits and the range biases computed with the temporal de-correlation method (see section 2.3 and [Coulot et al., 2007]). Then, a first computation is carried out with an empirical weighting derived from the mean orbit residual WRMS per station and per satellite.

For this computation, we apply weak constraints on station positions and EOPs. From this data processing results, we get estimated station positions which are used for the second computation. Indeed, for this latter, station positions are held fixed to the previous estimated values and, consequently, the only parameters to be computed are EOPs, the common parameters. From this computation, we then get the weekly

optimal weights per station and per satellite which can now be used for any SLR data processing.

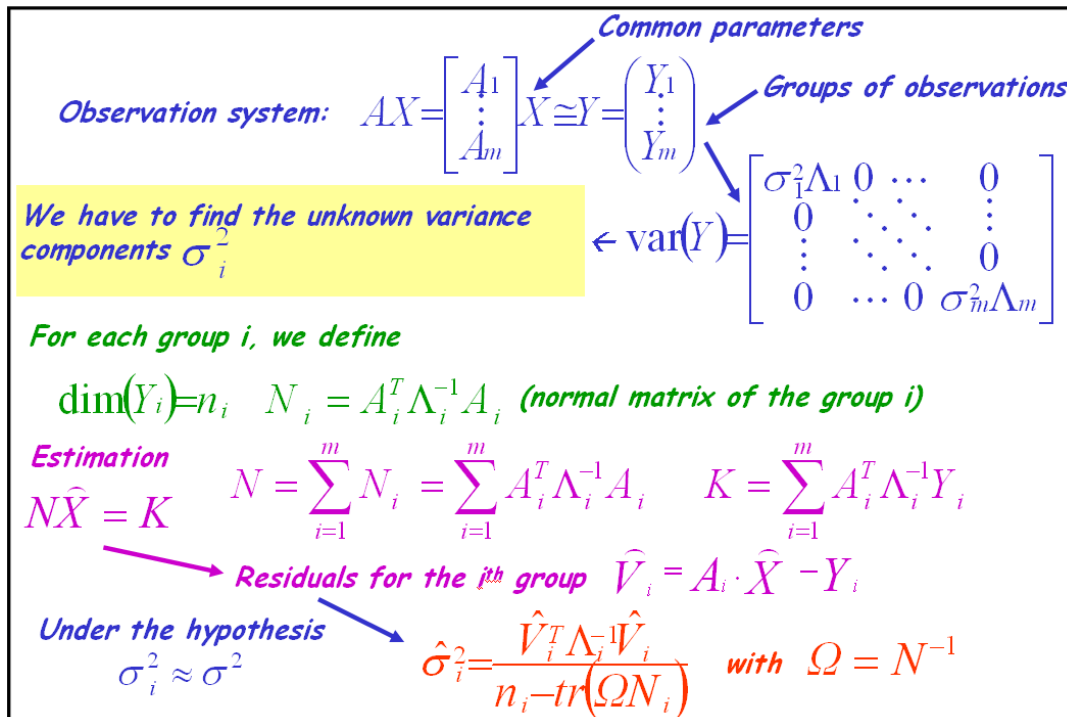


Figure 4. Scheme of the degree of freedom method.

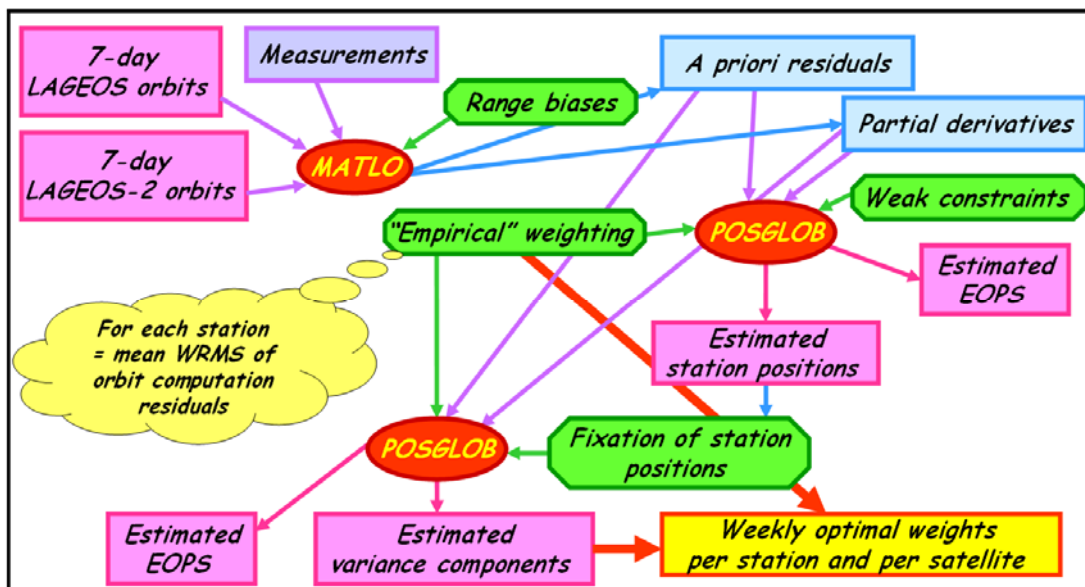


Figure 5. Scheme of weekly optimal weight per station and per satellite computation.

Table 6 provides the mean WRMS values of residuals per station and per satellite computed with the optimal weighting. On the whole, the values are consistent with the a priori knowledge one can have on the SLR network station quality but our approach should be more improved by the use of all the involved parameters to compute the optimal weighting. Indeed, orbital residual error parameters (see next section) are common parameters for measurements per station and we should study the impact of the non common parameters (namely, the station positions) on the results produced by variance component analysis methods. Moreover, these values

also evidence the fact that the model used to compute the optimal weighting does not explain the SLR measurements at the millimeter level (the best values are few millimeters). It is certainly mainly due to the fact that the residual orbital errors were not estimated.

**Table 6.** Mean WRMS (in cm) values of residuals per station and per satellite computed with the weekly optimal weights derived from the method shown in Fig. 5. For each station, the first (resp. second) column corresponds to the mean WRMS for LAGEOS (resp. LAGEOS-2) satellite. Evidenced stations are present in less than 50 weeks over the 13-year time interval.

<b>1824</b>	20.5	20.3	7210	1.0	0.9	<b>7502</b>	2.3	1.9	7840	0.9	0.9
<b>1831</b>	4.0	3.9	<b>7231</b>	5.1	6.2	<b>7505</b>	1.6	2.0	7841	1.1	1.1
<b>1863</b>	2.6	2.5	7236	11.4	10.4	7520	1.5	1.3	7843	1.8	1.6
1864	4.0	3.6	7237	2.0	1.9	7548	11.6	6.8	7845	1.0	0.9
<b>1867</b>	30.9	16.2	7249	5.1	4.5	<b>7597</b>	2.5	3.1	<b>7847</b>	9.9	12.9
1868	9.4	8.1	<b>7295</b>	0.9	0.9	<b>7805</b>	13.2	15.0	<b>7848</b>	2.3	1.9
1873	13.8	14.1	7308	2.0	1.9	<b>7806</b>	1.9	1.5	7849	2.3	1.1
1884	2.3	2.1	<b>7335</b>	1.0	0.9	7810	1.4	1.4	<b>7850</b>	0.7	0.8
<b>1885</b>	8.9	13.0	<b>7337</b>	1.0	2.2	7820	2.3	2.4	<b>7882</b>	0.5	0.6
1893	3.3	3.3	7339	1.2	0.8	<b>7821</b>	2.0	2.9	<b>7883</b>	0.5	0.6
<b>1953</b>	9.9	11.5	<b>7355</b>	4.3	3.7	7824	2.4	2.3	<b>7884</b>	1.2	0.6
7080	1.0	0.8	<b>7356</b>	2.8	2.8	7825	1.8	1.9	<b>7918</b>	0.9	1.1
7090	1.7	1.4	<b>7357</b>	4.9	6.0	<b>7830</b>	1.6	1.5	7939	6.9	6.8
7105	0.9	0.8	<b>7358</b>	5.0	6.9	<b>7831</b>	2.7	2.0	7941	0.9	0.8
<b>7106</b>	7.6	.	7403	1.5	1.1	7832	1.2	1.2	<b>8833</b>	2.8	2.7
7109	0.7	0.6	<b>7404</b>	4.9	1.8	7835	1.0	0.9	8834	1.4	1.4
7110	0.9	0.8	7405	2.7	2.7	7836	1.0	0.9	7811	1.8	1.6
<b>7122</b>	0.7	0.7	<b>7410</b>	0.7	0.6	7837	2.1	2.0			
7124	1.7	1.2	<b>7411</b>	0.5	0.6	7838	1.7	1.6			
<b>7130</b>	1.3	1.4	7501	2.2	2.1	7839	0.8	0.8			

## 2.2. Orbital residual errors

As previously shown in section 1, the LAGEOS satellite orbital arcs may be affected by some residual errors (cf. Fig. 2 and Tab. 5). The integration of Hill’s satellite first-order motion differential equations ([Cretaux et al., 1994] and [Coulot, 2005]) provides the empirical form of such orbital residual errors in the RTN frame:

$$\begin{aligned} \delta R(t) &= a_R t \cos(\bar{n}t) + b_R t \sin(\bar{n}t) + c_R \cos(\bar{n}t) + d_R \sin(\bar{n}t) + e_R + f_R t \\ \delta T(t) &= a_T t \cos(\bar{n}t) + b_T t \sin(\bar{n}t) + c_T \cos(\bar{n}t) + d_T \sin(\bar{n}t) + e_T + f_T t + g_T t^2 \\ \delta N(t) &= a_N t \cos(\bar{n}t) + b_N t \sin(\bar{n}t) + c_N \cos(\bar{n}t) + d_N \sin(\bar{n}t) + e_N \end{aligned}$$

The coefficients evidenced in yellow can be estimated. Thus, doing so, we can carry out a kinematic (or semi-dynamic) estimation of the orbital residual errors; see Fig. 6 for examples.

In order to avoid spurious transfers between the terrestrial and the orbital parameters, we should compute all the involved parameters (station positions, EOPs and orbital residual errors) in a same process. But, doing so gives rise to problems. Indeed, it creates supplementary reference system effects [Sillard and Boucher, 2001] on the third translation and on the scale factor of the underlying Terrestrial Reference Frame

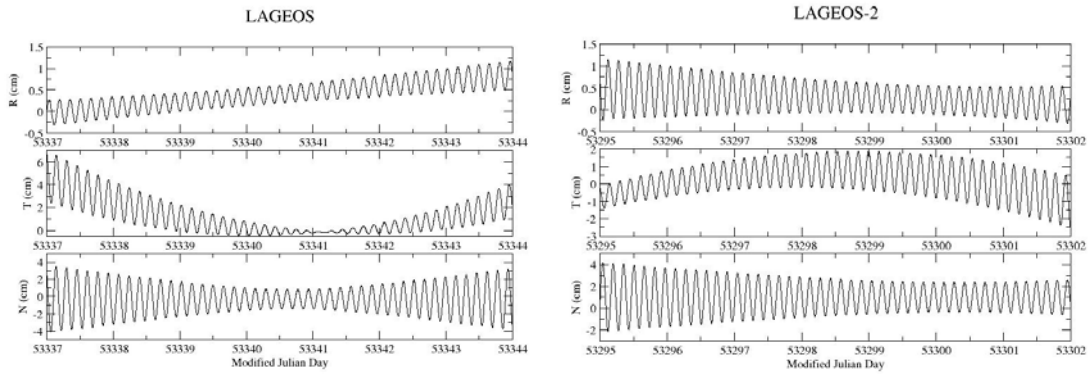


**Figure 6.** Examples of orbital residual errors estimated, in cm, for both LAGEOS satellites in the RTN frame.

(TRF). These parameters are thus damaged and the estimated orbital errors so computed are completely eccentric! Consequently, we have to find a rigorous balance between minimum constraints used to define the weekly TRFs and possible constraints applied on the orbital error coefficients. Furthermore, we have to take into account the physical coupling between the radial and tangential components [Coulot, 2005]. Finally, we have to carry out a sensitivity analysis to determine which coefficients can be optimally computed each week.

### 2.3. Range biases

Regarding range biases, we have developed a temporal de-correlation method in order to get the most accurate and consistent range bias values (see [Coulot et al., 2007] for more details). Fig. 7 provides an extract of the raw output file provided by this method. We can see that, when they are estimated over long periods, biases per satellite are very coherent. In other cases, the differences are at a few millimeter level.

Station	Validity (CNES J. Dates)	Values obtained for LAGEOS (m) Bias + precision	Values obtained for LAGEOS-2 (m) Bias + precision
7835	15340 16544	1.395828547040809E-002	1.158416922784649E-003
7835	16544 16564	3.529396209728985E-002	1.475236139678072E-002
7835	16564 16679	3.320933374887905E-002	3.232516758791523E-003
7835	16679 17413	1.664937112299916E-002	1.430681097343033E-003
7835	17413 18143	-1.971404917293083E-003	3.328628424293636E-004
7835	18143 18873	2.129710997299538E-003	3.360069389674007E-004
7835	18873 19603	9.131760532044128E-003	4.467022182450903E-004
7835	19603 20300	7.851262565453349E-003	9.554258819448195E-004
7845	17521 18305	-4.428851680859768E-003	6.223534556697570E-004
7845	18305 19305	8.113087278820413E-003	4.018334706229168E-004
7845	19305 20035	1.285646431835049E-002	5.459565786674019E-004
7105	15317 16047	-3.746952854385001E-003	4.944474970946950E-004
7105	16047 16777	-1.549706818118012E-002	6.921317933826075E-004
7105	16777 16940	-1.105482201853714E-002	5.900205316694585E-004
7105	16940 17670	-4.330403233925809E-003	3.766190351993729E-004
7105	17670 17877	-8.797353166941418E-003	6.028898715788532E-004
7105	17877 17959	-8.741490387424361E-003	1.310118230413150E-003
7105	17959 18039	-4.648690714335582E-003	8.785822392202415E-004
7105	18039 18666	-5.169111580414628E-003	3.867953242580351E-004
7105	18666 18877	-3.472024871091189E-003	5.657230028905748E-004
7105	18877 19607	-4.193980900330184E-003	3.817904507077791E-004
7105	19607 20337	-6.548560807830205E-003	4.924245800410994E-004
7105	20337 20500	-7.040431351813800E-003	9.396523059811853E-004
			1.234432517595224E-002
			6.300895927387962E-002
			2.891112857748582E-002
			1.540554934193744E-002
			-6.434411963804878E-004
			3.901844189266957E-003
			5.700719983120365E-003
			2.842151050185370E-003
			-1.201192209408536E-003
			7.840983271450021E-003
			1.654336641325428E-002
			-6.864306478378965E-003
			-1.064881791710468E-002
			-7.750502221599706E-003
			2.921756834785135E-003
			-4.826611780213416E-003
			-1.019322123979381E-002
			-2.871015614103231E-003
			-4.312745700605802E-003
			-2.899406111483316E-003
			-5.491238818875488E-003
			-7.645452603994796E-003
			-6.322205532930170E-003

**Figure 7.** Examples of range bias values (m) per station and per satellite computed with the temporal de-correlation method [Coulot et al., 2007]. CNES JD=MJD-33 282.

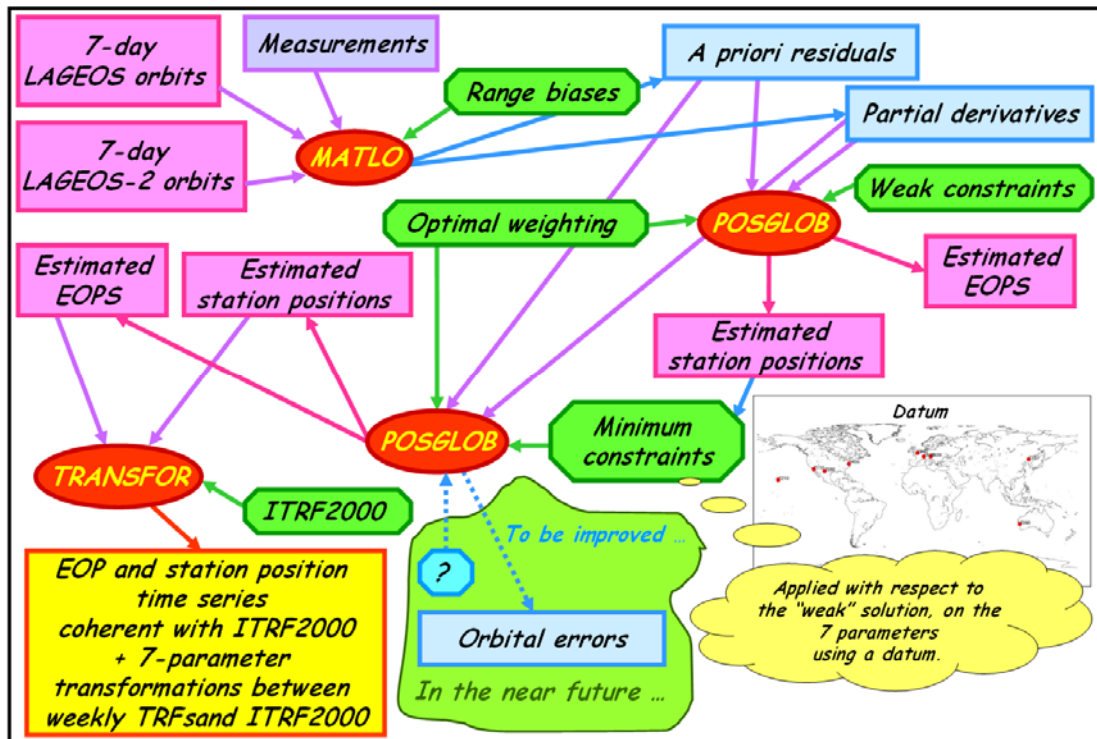


Figure 8. Time series computation method scheme.

### 3. Time series computation

#### 3.1. Method

Fig. 8 shows the global method scheme. For the time series computation, the range bias values computed with our new method as well as our optimal weights are applied. For this first “long period” data processing carried out with MATLO/POSGLOB software, no orbital residual error is estimated nor applied.

#### 3.2 Results

Fig. 9 shows the results produced with TRANSFOR software (cf. Fig. 8) for the three translation parameters. We have carried out frequency analyses of these time series. These analyses have been carried out with FAMOUS (Frequency Analysis Mapping On Unusual Sampling) software developed by F. Mignard (OCA, France) in the framework of the GAIA project [Mignard, 2004]. The TX (resp. TY) time series exhibit a 2.9 mm (resp. 3.2 mm)-amplitude annual signal and the TZ time series exhibit a 2.4 mm-amplitude annual signal as well as a 1.7 mm-amplitude semi-annual signal. Moreover, the scale factor time series are shown in [Coulot et al., 2007], Fig. 10. They exhibit a 2.6 mm-amplitude annual signal. This annual signal may be an artifact due to the SLR network geometry and the fact that the atmospheric loading effects have not been considered in the a priori modeling used for station positions (see next results for these station positions).

Regarding EOPs, the results are shown on Fig. 10. The weighted biases are respectively -119 and 7  $\mu\text{s}$  for  $X_p$  and  $Y_p$  and the WRMS are respectively 299 and 256  $\mu\text{s}$  for  $X_p$  and  $Y_p$ . Moreover, the opposite drifts detected between 2000.0 and 2006.0 certainly come from some network effects.

The station position time series are estimated with respect to the ITRF2000 mean position corrected for plate tectonics (ITRF2000 velocities), Earth solid tides, pole tide and oceanic loading effects in agreement with the IERS conventions [McCarthy

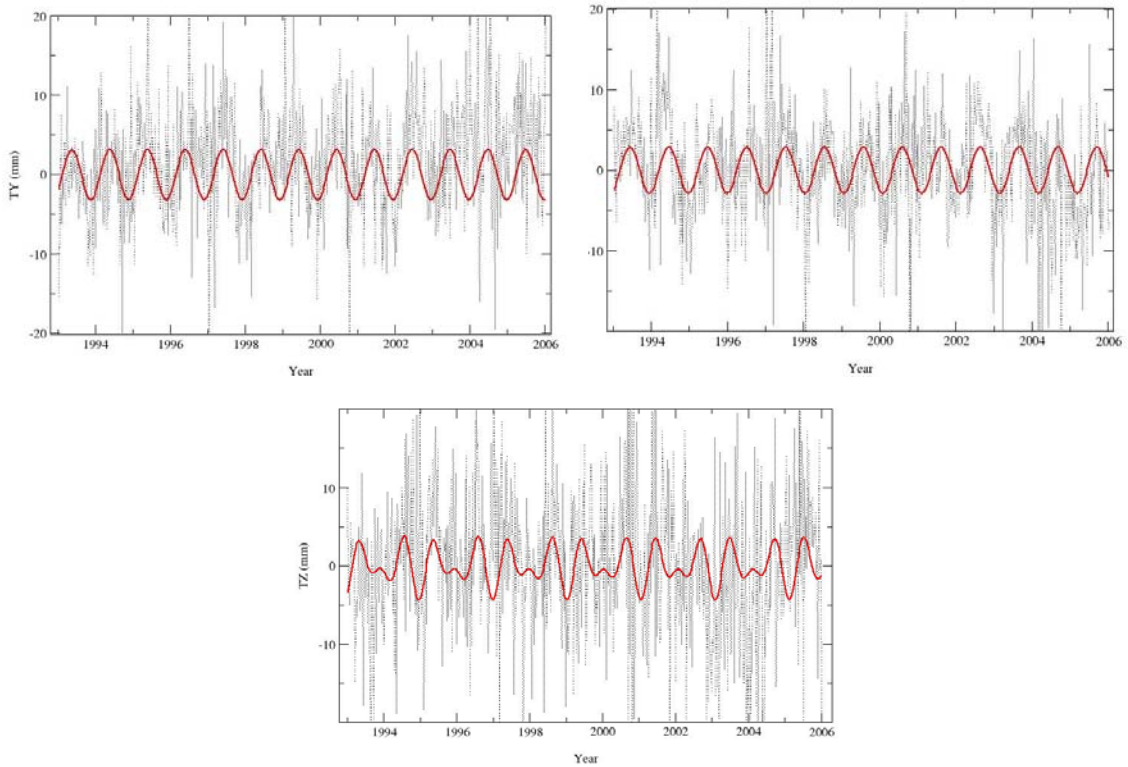


**Figure 9.** Weekly translation parameter time series (mm) between weekly SLR TRFs and ITRF2000. Red curves correspond to the periodic signals detected and estimated with FAMOUS software.

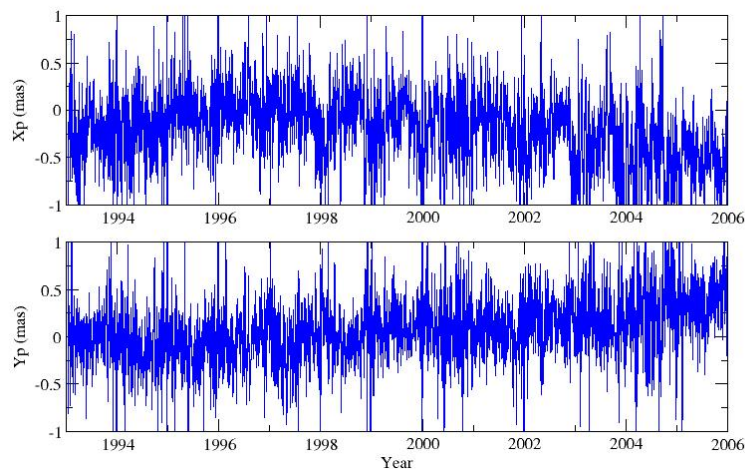


**Figure 10.** Daily EOP time series (mas) computed with respect to the EOPC04 time series.

and Petit, 2004]. These time series must consequently evidence the atmospheric and hydrologic loading effects.

Fig 11 shows 7839 and 7840 SLR station position time series in ITRF2000. Annual and semi-annual signals with amplitudes between 5 mm and 1 cm are detected by FAMOUS software in such Up component time series for some stations. These annual signals may be linked to the previously mentioned loading effects.

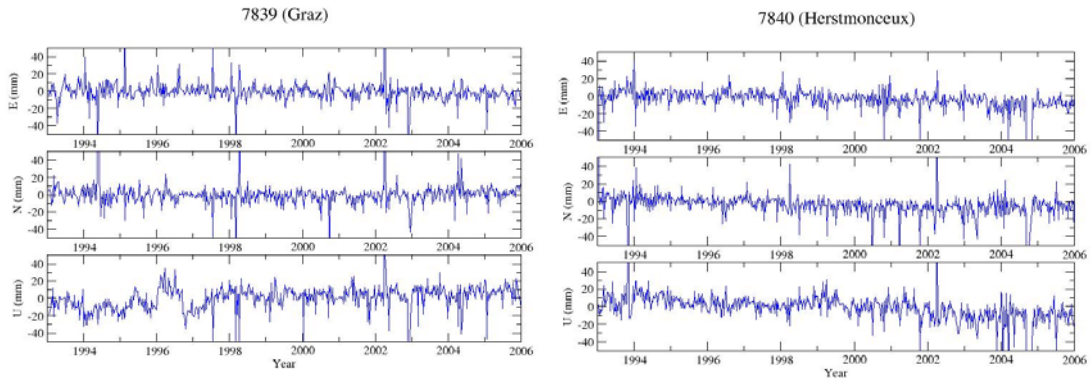


**Figure 11.** Examples of station position time series computed (in mm) in the ENU local frame in ITRF2000. On the left: Graz, 7839. On the right: Herstmonceux, 7840.

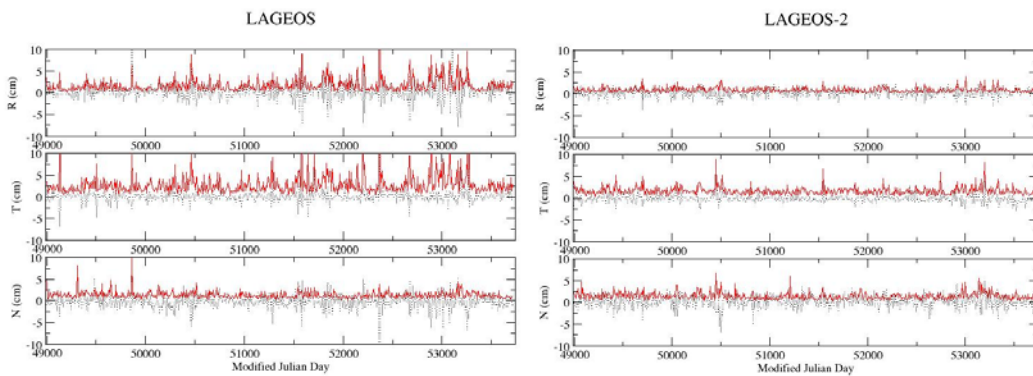


**Figure 12.** Empirical orbital errors (biases - in black - and RMS values - in red -, in cm) in the RTN frame computed with our semi-dynamic approach for both LAGEOS satellites (LAGEOS on the left and LAGEOS-2 on the right).

**Table 7.** Statistics of the values shown on Fig. 12.

Satellite	R (cm)	T (cm)	N (cm)	.
LAGEOS	0.38	0.06	-0.13	Mean of means
	1.71	2.73	1.32	Mean of RMS
LAGEOS-2	0.31	-0.11	0.20	.
	0.90	1.65	1.46	.

Finally, although our global method (cf. Fig. 8) does not provide any orbital error estimate, we have tested our semi-dynamic approach by keeping station positions and EOPs fixed. Almost all effects are included in the a priori modeling then used for station positions: plate tectonics, solid Earth tides, pole tide, and oceanic and atmospheric loading effects (European Center for Medium-range Weather Forecasts - ECMWF, <http://www.ecmwf.int/>- pressure fields were used to derive the atmospheric loading effect models) as well as the range biases provided by the temporal decorrelation method. Fig. 12 shows the bias and the RMS values of the empirical orbital errors so computed in RTN frame for both satellites. Tab. 7 provides the mean values of these error bias and RMS values. These values are coherent with the 2-day LAGEOS overlaps (cf. Fig. 2 and Tab. 5).

#### 4. Conclusions and prospects

Our time series estimation method should be operational soon. To do so, we still have to:

- finalize our method regarding orbital errors;
- use all available common parameters to get optimal weekly weightings;
- go further with our temporal de-correlation approach for range biases [Coulot et al., 2007].

New computations should be carried out with ITRF2005 and the improved EOPC04 time series. And, in the near future, we plan to:

- carry out computations with atmospheric loading effect models in the a priori modeling for station positions to quantify their impact;
- use other satellites and study the impact on the involved TRFs.

#### References

- [1] Altamimi, Z., P. Sillard, and C. Boucher: "ITRF2000: a new release of the International Terrestrial Reference Frame for Earth science applications", *J. Geophys. Res.*, 107(B10), 2214, doi: 10.1029/2001JB000561, 2002.
- [2] Arias, E.F., P. Charlot, M. Feissel, and M.F. Lestrade: "The Extragalactic Reference System of the International Earth Rotation Service, ICRS", *Astron. Astrophys.*, 303, p. 604-608, 1995.
- [3] Berger, C., R. Biancale, M. Ill, and F. Barlier: "Improvement of the empirical thermospheric model DTM: DTM94- a comparative review of various temporal variations and prospects in space geodesy applications", *J. Geod.*, 72(3), p. 161-178, 1998.
- [4] Coulot, D.: "Télemétrie laser sur satellites et combinaison de techniques géodésiques. Contributions aux Systèmes de Référence Terrestres et Applications", Ph. D. thesis, Observatoire de Paris, 2005.
- [5] Coulot, D., P. Berio, O. Laurain, D. Féraud, and P. Exertier: "An original approach to compute satellite laser range biases", same issue, 2007.
- [6] Cretaux, J.F., F. Nouel, C. Valorge, and P. Janniere: "Introduction of empirical parameters deduced from the Hill's equations for satellite orbit determination", *Manuscr. Geod.*, 19, p. 135-156, 1994.
- [7] Gambis, D.: "Monitoring Earth orientation using space-geodetic techniques: state-of-the-art and prospective", *J. Geod.*, 78, p. 295-305, 2004.
- [8] Gruber, T., A. Bode, C. Reigber, P. Schwintzer, R. Biancale, and J.M. Lemoine: "GRIM5-C1: combination solution of the global gravity field to degree and order 120", *Geophys. Res. Lett.*, 27, p. 4005-4008, 2000.
- [9] Le Provost, C.: "FES 2002 - A new version of the FES tidal solution series", paper presented at Jason-1 Science Working Team Meeting, Biarritz, France, 2002.
- [10] Lieske, J.H., T. Lederle, W. Fricke, and B. Morando: "Expressions for the precession quantities based upon the IAU (1976) System of Astronomical Constants", *Astron. Astrophys.*, 58, p. 1-16, 1977.
- [11] McCarthy, D.D.: "IERS Conventions", IERS Technical Note 21, Observatoire de Paris, 1996.
- [12] McCarthy, D.D. and G. Petit: "IERS Conventions", IERS Technical Note 32, Verlag des Bundesamts für Kartographie und Geodäsie, Frankfurt, 2004.
- [13] Mignard, F.: "Overall science goals of the GAIA mission", in Proceedings of the symposium "The Three-Dimensional Universe with GAIA", 2004.
- [14] Persson, C.G.: "Adjustment, weight-testing and detection of outliers in mixed SFF-SFS models", *Manuscr. Geod.*, 7, p. 299-323, 1982.
- [15] Standish, E.M., X.X. Newhall, J.G. Williams, and W.M. Folkner: "JPL planetary and lunar ephemerides, DE403/LE403", *JPL IOM 314.10-127*, 1995.
- [16] Sillard, P. and C. Boucher: "Review of algebraic constraints in terrestrial reference frame datum definition", *J. Geod.*, 75, p. 63-73, 2001

---

## NETWORK PERFORMANCE AND RESULTS SESSION SUMMARY

C. Luceri and M. Torrence, co-chairs

This workshop session was a forum for the assessment of network data production, quality, and ILRS products.

The regular quality control assessments performed by several ILRS analysis centers was discussed by R. Noomen. He showed range bias estimates for LAGEOS 1 and 2 improved in consistency from 2004 through 2006 from 30 to 20 mm level. Other analysis centers contributions to regular and rapid data quality analyses will help the overall assessment of the results as there are, as of this writing, only two AC contributing to this effort. T. Otsubo showed that characterization of possible intensity-dependence station effects should be considered to achieve mm level data accuracy and calibrations may show possible correlations with seasonal loading effects. M. Torrence showed examples of plots of station's data as a function of local time and range measurement.

J. Luck reported on upgrades to the WPLTN sites and reported the data yield from southern hemisphere tracking sites has increased to 40% of the total data available data with the quality generally comparable with the data from the northern hemisphere. Luck also commented that all stations should pay close attention to their system delay and calibrations. A report on mm level bias due to measurement characteristics of the Stanford counter in the data from Herstmonceux was given by P. Gibbs, with the suggestion that all Stanford counters should be characterized. F. Pierron showed results of the FTLRS occupations at the Ajaccio site, achieving stable position estimation from multi-satellite data analyses using the Eigen-Grace03s gravity model for the two occupations (2002 and 2005).

E. Pavlis discussed the global SLR network and the origin and scale of the TRF in the GGOS era and an SLR-based evaluation and validation studies of candidate ITRF2005 products. An assessment of the ILRS-A standard product was presented by G. Bianco. This routine production process is stable and reliable and those ILRS standard products allow monitoring of site coordinates and EOPs. Additionally, the geocenter motion, geometrically derived from the weekly solutions, could be included among the future ILRS standard products. R. Govind showed results of a simulation to evaluate the contribution of an additional SLR station in northern Australia to the Earth center-of-mass determination.

The session concluded with a light-hearted presentation by P. Shelus on "Evolution of SLR/LLR in Response to Mission Needs." From the summary slide: "As scientific experiments become more complicated, greater pressures are placed upon operational logistics in order to perform necessary operations, and yet retain personnel safety and instrumental integrity. Thorny logistical problems have been solved by a combination of computer power, internet communications, orbital dynamics and precisely defined inter-relationships among several reference frames."

There were several posters presented for this session. C. Noll described the laser ranging archive available at the ILRS data centers and plans for future enhancements. J. Luck showed the result of a minico system delay for the Mt. Stromlo site. C. Moore presented a summary of the observations of GioveA taken from Mt Stromlo SLR Station, the identified patterns that have impacts on tracking productivity and the use of Giove A data for an empirical analysis of link budget requirements for potential gain in tracking GioveA, Galileo and similar satellites. T. Otsubo showed plots of intensity-dependent effects for all stations. M. Torrence displayed plots of data as function of local time and range for all stations.

---

## The SLR network from a QC perspective

R. Noomen<sup>1</sup>

1. Delft University of Technology, Kluyverweg 1, 2629 HS Delft, The Netherlands.

Contact: [r.noomen@tudelft.nl](mailto:r.noomen@tudelft.nl) / Fax: +31-15-2785322

### Abstract

*Although it can be considered as a traditional if not classical technique, Satellite Laser Ranging (SLR) (still) plays a crucial role when it comes to assessing and monitoring a number of global aspects of System Earth: scale and origin of the terrestrial reference frame. A proper and timely monitoring of the performance of the network of laser stations is a prerequisite to provide an optimal contribution to the space geodetic community. In order to detect possible data problems at an early stage, a number of analysis centers perform a regular quality control (QC) of the SLR measurements on a variety of satellites. This paper addresses a number of issues relating to that: the development of the global network in terms of stations and their distribution, and the development of the (raw) data quality. The quality and consistency of reported range biases will be studied in this paper as well. Although the analysis done here covers the years 2004-2006 only, the results show an improvement in consistency for most of the QC centers, from about 30 mm in 2004 to about 20 mm in 2006 (total network) or from 25 mm to 15 mm (AWG core network). Two points of concern are the global coverage of the network of SLR stations and the decrease in the number of QC centers.*

### Introduction

With its highly accurate absolute distance measurements between satellites and ground stations, the International Laser Ranging Service (ILRS) supports a wide range of space geodetic missions: gravity field missions, altimetry missions, missions aimed at the assessment and monitoring of the terrestrial reference frame, and others. To obtain the best possible contribution from such SLR observations, a good global coverage of the network of ground stations, a good production rate and a high quality of such observations are prerequisites.

In this paper, both network geometry and data quality aspects are addressed. In particular, the overall development of the network in terms of geometry, data yield and data precision is described. Also, the various possibilities to monitor the quality of these observations and to alert stations in case of systematic errors (range biases) are examined. The paper compares a number of QC institutes, and derives recommendations for the threshold at which a reported bias can be considered to be real. This is primarily done by comparing independent bias estimates for common passes on LAGEOS-1 and on LAGEOS-2.

### SLR network development

Figure 1 shows the number of stations that have tracked the satellites LAGEOS-1 and/or LAGEOS-2, during a particular year. Considering the central role of these two spacecraft, an inventory of the data acquisition on either of these satellites can be considered as a direct measure for the amount of stations that were active in a particular year. It is clearly visible that the number of stations in the global network has increased from about 30 in the mid-1980s to about 40 now; variations and developments in this number are typically related to the operations of transportable SLR stations, and the installation of new stations at various places around the world.

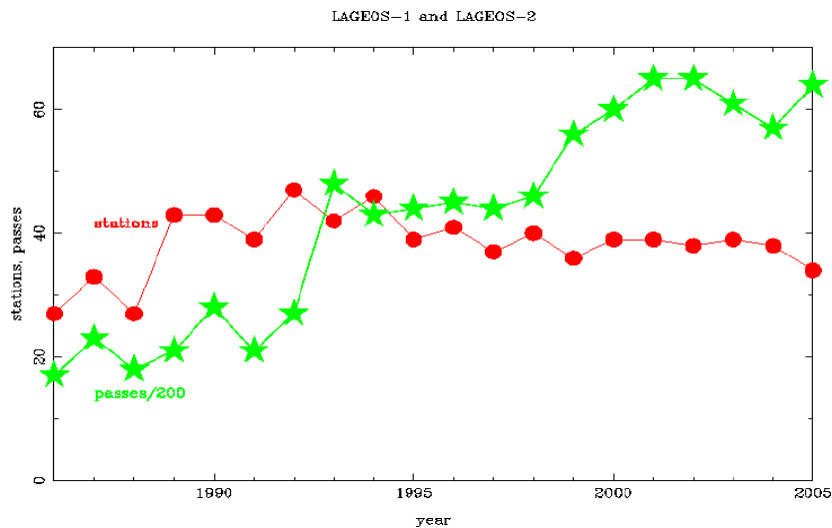


**Figure 1.** The yearly number of stations that tracked LAGEOS-1 and/or LAGEOS-2, and their production in terms of number of passes.

In spite of the reasonable stability of this number over the past decade, the plot shows a remarkable reduction from a recent maximum of 39 in 2003 to 34 in 2005. This will be discussed further shortly.

The figure also shows the total number of passes (on LAGEOS-1 and LAGEOS-2) that have been taken during the same year. In spite of the reduction of the number of stations, the total number of individual passes has been stable if not on the rise: in 2005, about 13,000 passes were obtained, or almost 400 on average per station. Clearly visible is the increase of this number of passes in 1993, the first full year after the launch of LAGEOS-2, on October 25, 1992. Contrary to the decline in number of stations in the past few years, the total data yield of the network appears to be stable (if not increasing). This can be attributed to a higher level of efficiency (automation), improvements in scheduling and increasing number of shifts.

The geometry of the SLR network is illustrated in Figure 2. Here, the tracking network in 2003 is compared to that in 2005; note that no allowance for the number of passes is made. It is clearly visible that the majority of the network has been in operation permanently, whereas a relatively small number of stations (Hawaii, Arequipa/Peru, Chania/Crete and Komsomolsk-na-Amure/Russia; open red circles) did not range in 2005 whereas they did in 2003. New stations in 2005 (or 2004, at least w.r.t. 2003) are Ajaccio/France and Tanegashima/Japan. The plot shows that the distribution of stations has a preference for the Northern Hemisphere, and that the termination of activities in Hawaii and Arequipa has dramatic consequences for the coverage in particular in the Pacific region. In view of the important role of SLR in its unique determination of global parameters of System Earth like geocenter and scale, such flaws in station distribution are an absolute point of concern. Fortunately, the situation has improved again with the installation of new stations in San Juan/Argentina, Hawaii and Arequipa in mid-2006.

To get an idea of the advancement of the technical quality of the network, Figure 3 gives a comparison of single-shot precision values of raw SLR observations. It is clearly visible that these values have improved dramatically in 2002 when compared to 1997. These numbers are to be considered as representative for the current network of stations: on average, the single-shot precision is at the level of a few mm for the major part of the network.

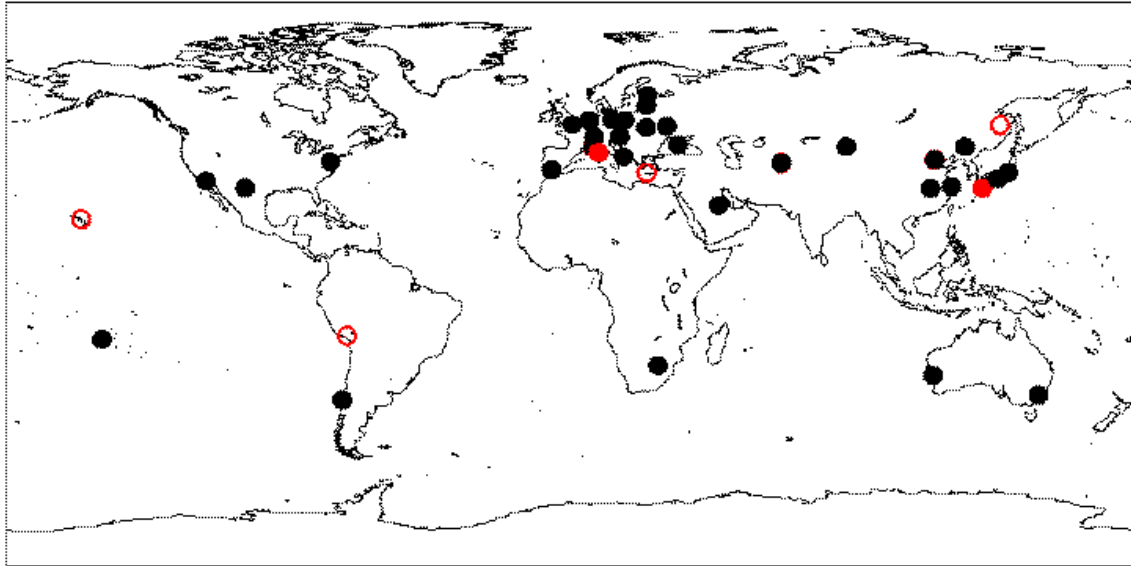


**Figure 2.** The global network of SLR stations, Black circles indicate stations that have been active in both 2003 and 2005. Open red circles represent stations that were active in 2003, but not in 2005. Solid red circles represent stations that were active in 2005, but not in 2003.

### Improvements – Precision (Single Shot RMS)

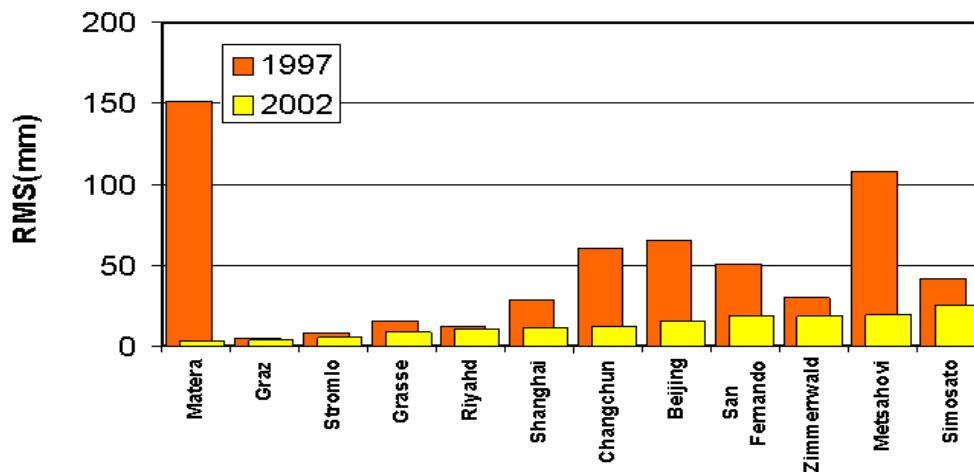


**Figure 3.** A comparison of the single-shot precision of a number of representative SLR stations, in 2002 as compared to 1997 (courtesy Van Husson).

#### Bias detection capability

SLR observations are reputed for their absolute, unambiguous value, and therefore they play an essential role in the determination of the origin and scale of the International Terrestrial Reference Frame (ITRF) (e.g. [Altamimi *et al.*, 2002]). In order to do so properly, it is of utmost importance to monitor the quality of the observations taken by the SLR stations, not only on a precision level (*i.e.* in terms of internal consistency) but especially on absolute accuracy. To this aim, possible systematic errors (range biases) need to be computed and evaluated on a pass-by-pass basis and scrutinized constantly. To do so, a number of options exist. First, one can do so at the tracking station itself; actually the monitoring of such items is already being done, on the basis of orbit predictions and/or short-arc, rapid-return orbit solutions.

Although the capabilities are limited, the stations and analysis centers involved in this are encouraged to continue to do so. The second option is to derive such biases from the official ILRS product; here, a group of 6 analysis centers cooperate in a concerted effort to generate a weekly solution for station coordinates and Earth Orientation Parameters (EOPs) [ILRS, 2006]. A drawback of this technique is that station position and biases become highly correlated below a certain level, and the possibility to monitor range biases at the level of a few mm is therefore not possible. Also, by virtue of the (inherent) scatter in the weekly coordinates solutions for an arbitrary station, the corresponding range biases would also reflect this scatter to say the minimum. The third option is most attractive: a dedicated analysis in which the satellite orbit and related parameters are estimated to come to a most accurate description of the relevant elements of our system, but in which the position of the stations is kept fixed at a highly accurate model value (of course, allowing for temporal effects like crustal deformation, tidal motions, and ocean and atmospheric pressure loading deformation). This paper focuses on results obtained by the latter techniques.

An overview of the analysis centers active in such analyses (not necessarily exhaustive) is given in Table 1. In order to assess the quality of the bias values as reported by these groups on a regular (daily, weekly) basis, only values reported for the satellites LAGEOS-1 and LAGEOS-2 will be treated further here.

<b>Institute</b>	<b>Altimetry, gravity missions</b>	<b>LAGEOS- 1, -2</b>	<b>Navigation missions</b>
<b>Astronomisches Institut Universität Bern, Switzerland</b>			X
<b>Center for Space Research, Texas, USA</b>		X	
<b>Deutsches Geodätisches Forschungs Institut, München, Germany</b>		X	
<b>Delft University of Technology, Netherlands</b>		X	
<b>Mission Control Center, Moscow, Russia</b>		X	
<b>National Institute of Information and Communications Technology, Kashima, Japan</b>	X	X	
<b>Shanghai Astronomical Observatory, China</b>		X	

*Table 1. Overview of the dedicated QC efforts done by various SLR analysis groups.*

Although Table 1 shows that quite a number of analysis centers are involved in the operational QC assessments, and might suggest that the results are consistent, a simple illustration (Figure 4) shows that this is not necessarily the case: differences in the “verdict” for individual passes of up to several tens of millimeter can easily be present, sometimes even exceeding decimeter values. This aspect has been known for quite a number of years already [ILRS, 1999]. One of the main reasons for this is the modeling of the ground station positions: differences in this analysis component will immediately show up as consistent bias differences. To remedy this (aspect of the) situation, QC centers have been urged to use a common representation, which has been put into practice during the last years with reasonable success: at this moment, almost all QC centers use the ITRF2000 [Altamimi *et al.*, 2002] model, with just a single exception: MCC still uses its own set of station coordinates (status October 2006).

The consistency of the reported bias values is the subject of the remainder of this paper. The results as they are included in the weekly so-called ILRS Combined Range Bias Reports [Gurtner, 2006] are used as input for this evaluation. These reports basically merge the information from a number of individual bias reports, and have been available since 2004. An example of (a few lines from) such a report is given in Table 2, for one (arbitrary) station only.

1864 MAIL Maidanak					CSR		DGFI		DUT		MCC		NICT		SAO	
		sc	wl		rb	pr	rb	pr	rb	pr	rb	pr	rb	pr	rb	pr
1864	2005-11-30	19:49	L2	532	-8	6	-72	12			5	5	-27	12	-2	3
1864	2005-11-30	21:03	L1	532	-18	5	-49	23			-14	10	-28	16	13	20
1864	2005-12-01	17:43	L2	532	29	14	-36	11	-10	15	48	6	13	11	23	1
1864	2005-12-01	19:41	L1	532	4	11	-27	12	-54	11	8	5	-15	12	30	12
1864	2005-12-02	19:40	L2	532	-35	0	-91	11	82	4	*	*	-81	5	171	4
1864	2005-12-05	18:10	L2	532	-31	7	29	8	-62	7			-38	7		
1864	2005-12-05	21:07	L1	532	-50	15	19	14	-16	18			-2	16		
1864	2005-12-05	22:19	L2	532	-40	5	4	9	-64	12			-74	6		
1864	2005-12-06	16:15	L2	532	4	7	50	9	-36	6			-17	7		
1864	2005-12-06	16:29	L1	532	12	4	-52	4	-12	3			-6	3		
1864	2005-12-08	14:03	L1	532	-16	13	-55	12	-64	12			-53	13		
1864	2005-12-08	16:35	L2	532	-5	9	10	15	-70	21			-56	13		
1864	2005-12-08	17:12	L1	532	28	1	-80	6	-32	0			-49	9		
1864	2005-12-08	20:36	L1	532	3	10	-3	9	-5	10			-32	10		
1864	2005-12-08	20:42	L2	532	8	7	26	10	-24	11			-27	11		
1864	2005-12-09	16:02	L1	532	10	5	-61	9	-59	9			-29	9		
1864	2005-12-10	14:29	L1	532	22	13	-13	12	-7	12			12	13		
1864	2005-12-10	16:39	L2	532	-5	11	40	27	-54	28			-27	20		
1864	2005-12-10	17:58	L1	532	-5	16	-29	15	-39	15			-28	16		
1864	Average			532	-4	8	-20	12	-38	11	11	6	-29	11	47	8

**Table 2.** An example of an entry in the ILRS Combined Range Bias Report [Gurtner, 2006], for station Maidanak in December 2005. All values are in mm.

To compare the reported biases in a useful fashion, statistics on a large number of values will be derived. In principle, one can do so in two ways. First, it is possible to do a covariance analysis (cf. Figure 5), where common biases from an arbitrary pair of QC centers are plotted against one another and trend line(s) and correlation coefficients are computed. The advantage of this method is that it allows/eliminates systematic differences between the two series. However, the results can be interpreted with either of the two series as a reference, so this comparison technique will not yield unambiguous results. Instead, a direct comparison is opted for here, where the bias values reported for common passes as reported by an arbitrary QC center pair will be subtracted (cf. Figure 4) and simple, straightforward statistics will be computed. It should be noted that the QC centers may have developed/refined their analysis procedures over the course of time, and therefore allowance will be made for time-dependent answers, reflecting differences in quality. An indication of this is shown in Figure 6, which gives the rms-of-fit of orbital solutions on LAGEOS-1, as obtained by Delft University of Technology over the period 1985-2005; improvements in the quality of the orbital fit and therefore also in the bias detection capabilities are clearly visible.

## Results

A summary of these computations is given in Table 3: the rms values of the differences. Typically, some 20,000 common LAGEOS-1 and LAGEOS-2 passes went into the computation of a single entry in this table. It should be noted that individual biases of 100 mm and larger (in absolute terms) were ignored here for

various reasons: (i) they may be real in some cases, but not representative for a normal situation; (ii) they may be very weak because of a small number of observations during such a pass; and (iii) they may reflect problems with the model

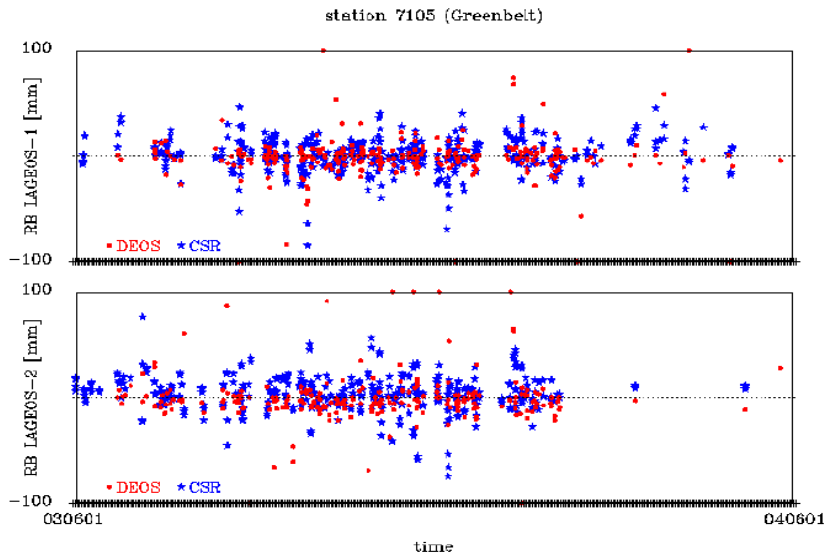


**Figure 4.** A comparison of bias values reported for common LAGEOS-1 passes over station Greenbelt by QC centers CSR and Delft, as an illustration of the scatter and uncertainties in these values (direct comparison).

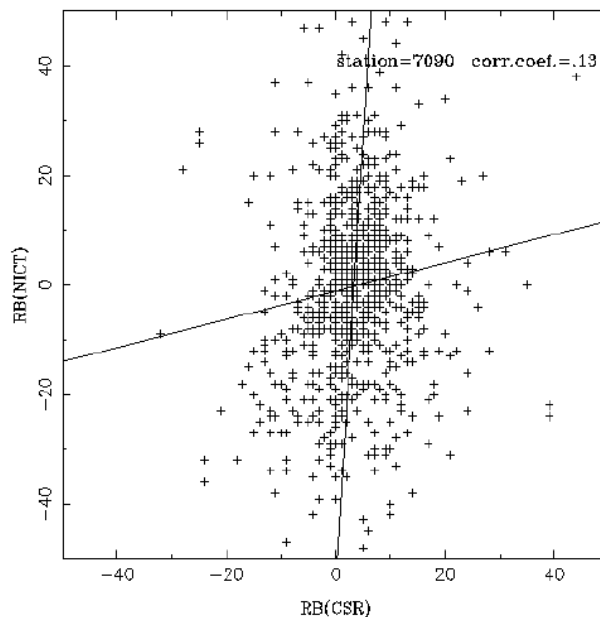


**Figure 5.** A comparison of bias values reported for common LAGEOS-1 passes over station Yarragadee by QC centers CSR and NICT, as an illustration of the scatter and uncertainties in these values (covariance-style comparison).

for station coordinates for the pertinent QC center. However, this represents a very small fraction of the total number of common passes. Another aspect to be noted is that the statistics have been computed in an unweighted fashion. Although passes with a relatively large number of normal points will lead to more stable (consistent) bias values, it is expected that this actually will average out, and straightforward statistics are given here only. After all that is what a station operator or manager is confronted with when reviewing the various bias reports.

As reported, the values have been computed for various periods: the years 2004 (when the Combined Bias Reports were initiated), 2005 and 2006. To better illustrate any trend, the rms differences are also shown in a graphical form: Figure 7.

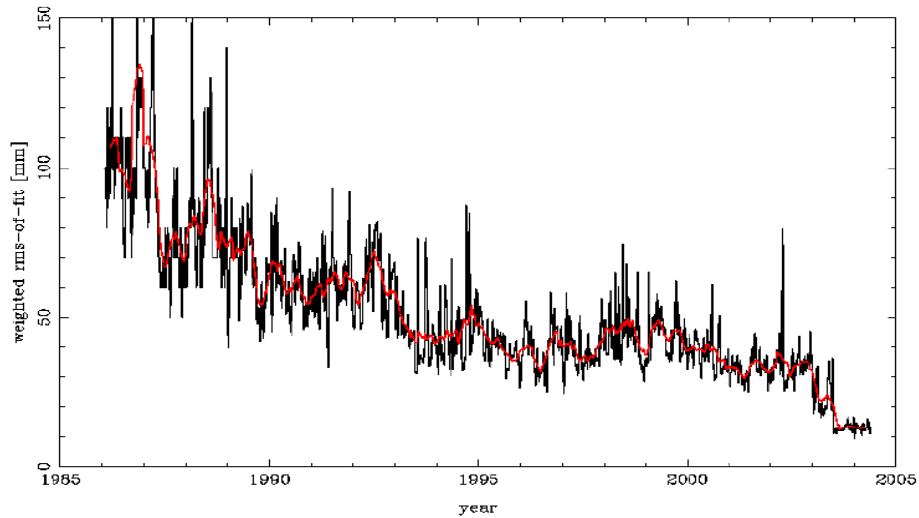


**Figure 6.** Overview of the LAGEOS-1 rms-of-fit of the weekly orbital computations as done by Delft University of Technology.

	DGFI	DUT	MCC	NICT	SAO
CSR	- / 26 / -	25 / 22 / -	28 / 25 / -	29 / 18 / -	34 / 21 / -
DGFI		- / 28 / 34	- / 29 / -	- / 29 / 28	- / 30 / 32
DUT			22 / 22 / -	25 / 22 / 21	24 / 22 / 22
MCC				26 / 25 / -	28 / 25 / -
NICT					32 / 26 / 21

**Table 3.** Statistics of the differences between bias values for common LAGEOS-1 and LAGEOS-2 passes observed by the global network of SLR stations, as reported by various pairs of QC centers. Entries are for 2004, 2005 and 2006, respectively. All values are in mm.

The discussion of the results is postponed until the next section. It is an unfortunate but real fact that the quality of the global SLR network is quite diverse: it is a mixture of top-quality stations and stations that do a little bit less in terms of performance. This might lead to the situation where the numbers reported in Table 3 and Figure 7 are indeed representative for the global network, but do not reflect the bias detection capabilities for the state-of-the-art stations properly. To that aim, the consistency computations have been repeated, but now for a subset of stations which has been given a preferential role in the derivation of the weekly official ILRS product on station coordinates and EOPs only: Graz, Greenbelt, Hartebeesthoek, Herstmonceux, McDonald, Monument Peak, Mount Stromlo, Riyadh, Wettzell, Yarragadee and Zimmerwald. These stations excel in terms of data quantity and quality, and it is expected that the bias values reported for these stations are more consistent than the values reported for the overall network. Results are presented in Table 4 and Figure 8, with similar definitions.

### Discussion

The numbers as reported in Tables 3 and 4 and illustrated in Figures 7 and 8 give a very clear message: on average, the reported range bias values are consistent at the level of about 20 mm when considering the total network of SLR stations, and at the

level of about 15 mm when considering the so-called AWG core stations only. If these numbers were to be reduced to an average quality verdict on a bias value reported for an individual pass in an individual analysis report, these numbers can be divided by  $\sqrt{2}$  (first order; one can argue about the level of formal correlation between the pairs of numbers).

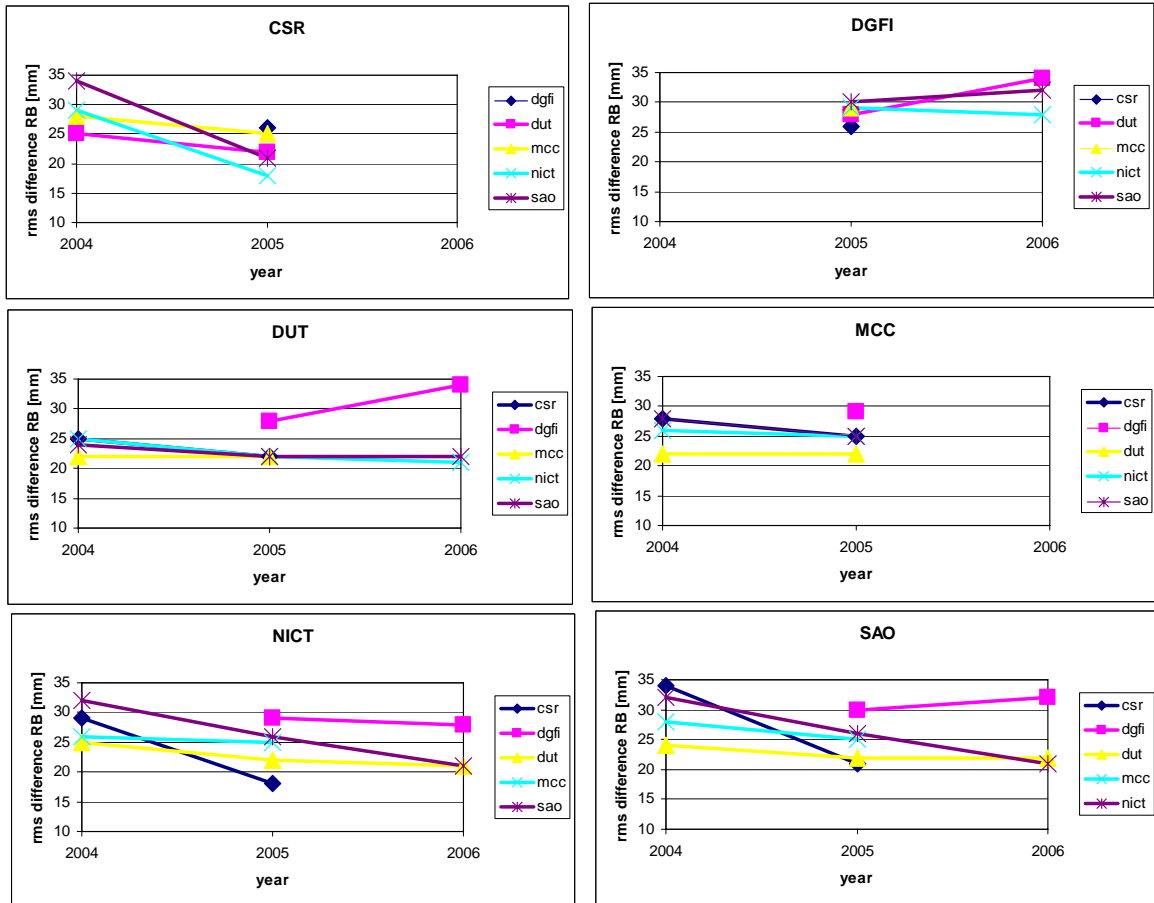


**Figure 7.** Statistics of the differences between bias values for common LAGEOS-1 and LAGEOS-2 passes observed by the global network of SLR stations, as reported by various pairs of QC centers. Entries are for 2004, 2005 and 2006, respectively. All values are in mm

The plots in particular show that the general trend of the agreement between QC center pairs is positive: the consistencies become better with time for most of them. A good illustration of this trend are all statistics involving NICT, where the level of agreement has gone down from about 30 mm (2004) to about 20 mm (2006) (Figure 7, all stations). Similar observations can be done for the AWG core stations only.

	DGFI	DUT	MCC	NICT	SAO
CSR	- / 22 / -	20 / 15 / -	20 / 15 / -	25 / 15 / -	29 / 17 / -
DGFI		- / 24 / 32	- / 26 / -	- / 26 / 25	- / 28 / 30
DUT			17 / 15 / -	22 / 18 / 14	22 / 18 / 18
MCC				23 / 19 / -	22 / 18 / -
NICT					29 / 23 / 18

**Table 4.** Statistics of the differences between bias values for common LAGEOS-1 and LAGEOS-2 passes observed by the so-called AWG core stations, as reported by various pairs of QC centers. Entries are for 2004, 2005 and 2006, respectively. All values are in mm.

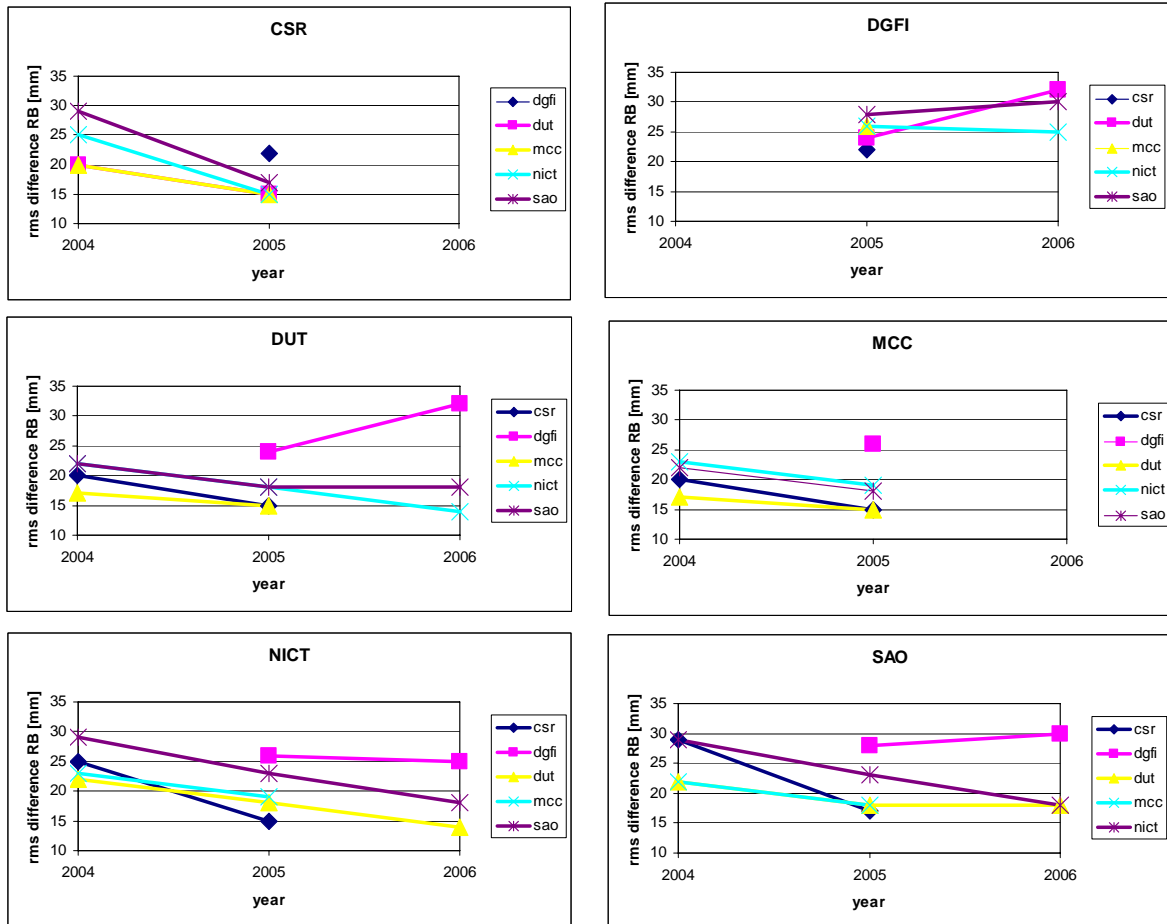


**Figure 8.** Statistics of the differences between bias values for common LAGEOS-1 and LAGEOS-2 passes observed by the so-called AWG core stations, as reported by various pairs of QC centers. Entries are for 2004, 2005 and 2006, respectively. All values are in mm.

Two points of concern remain: first of all, it is clear that the number of analysis centers involved in such analyses fluctuates quite a bit over time. In particular, the situation has become quite worrisome for 2006, with CSR and MCC not contributing anymore (and, although not visible, DUT in a similar situation since mid-2006) for various reasons. Every effort should be undertaken to improve this situation. Secondly, the plots also show that the trends are not so favorable for every QC center involved, and the consistency numbers get worse with time. This holds in particular for DGFI, and an effort should be started to remedy this.

Finally, coming back to the subject of the first part of the paper, the SLR network itself remains a continuous point of attention: only if the laser stations are distributed evenly on a global scale, can the space geodetic (and geophysical) community really take benefit from the unique capabilities of the technique to its fullest.

## References

- [1] Altamimi, Z., P. Sillard and C. Boucher: A new release of the International Terrestrial Reference Frame for earth science applications, *J. Geophys. Res.*, 107(B01), 2214, doi:10.1029/2001JB000561, 2002.
- [2] Gurtner, W., ILRS Combined Range Bias Report, [http://aiuas3.unibe.ch/ftp/slr/summary\\_report.txt](http://aiuas3.unibe.ch/ftp/slr/summary_report.txt), 2006
- [3] ILRS, [http://ilrs.gsfc.nasa.gov/working\\_groups/awg/awg\\_activities/awg\\_min\\_florence1999.html](http://ilrs.gsfc.nasa.gov/working_groups/awg/awg_activities/awg_min_florence1999.html), 1999.
- [4] ILRS, <ftp://cddis.gsfc.nasa.gov/pub/slr/products/pos+eop/>, 2006.

---

## The ILRS Standard Products: A Quality Assessment

G. Bianco<sup>1</sup>, V. Luceri<sup>2</sup>, C. Sciarretta<sup>3</sup>

1. Agenzia Spaziale Italiana, Centro di Geodesia Spaziale, Matera, Italy  
giuseppe.bianco@asi.it / fax: +39-0835-339005
2. e-Geos S.p.A., Centro di Geodesia Spaziale, Matera, Italy
3. Telespazio S.p.A., Roma, Italy

### Abstract

*In June 2004 the Space Geodesy Center (CGS, Matera, Italy) of the Agenzia Spaziale Italiana (ASI) has been selected by the International Laser Ranging Service (ILRS) as its Primary Official Combination Center for station coordinates and Earth Orientation Parameters.*

*From the beginning, the CGS has been providing the weekly operational combined ILRS solutions (SSC/EOP), also supporting the IERS B Bulletin production; moreover, CGS has produced the official ILRS contribution to ITRF2005, by combining the weekly solutions, from 1993 to 2005, submitted by the contributing ILRS Analysis Centers.*

*The CGS combination methodology relies on the direct combination of loosely constrained solutions. This methodology has been implemented and tested to handle site coordinates, site velocities, EOP, LOD coming from the same and/or different techniques.*

*The whole set of weekly combined solutions, those produced in support of ITRF2005 as well as the operational ones, is analyzed in detail in this contribution, to show the coherence and robustness in terms of global parameters as well as station coordinates.*

### Introduction

Soon after the establishment of the ILRS a strong need was felt to coordinate the work and combine the results of the various SLR data Analysis Centers (AC's) in order to define and distribute a series of "certified" ILRS products to the users community.

In 1999 the ILRS Analysis Working Group, chaired by Ron Noomen (TU Delft), outlined two Pilot Projects for the estimation of site coordinates and EOP, separately, from different AC solutions; the year after the two Pilot Projects were joined and the first results discussed. In 2003 the ILRS issued a formal Call for Participation for the generation of ILRS products,

In 2004 the ILRS AC structure was finalized and official delivery of standard products started; the CGS was selected as the Primary Official Combination Center, referred to as ILRSA, while DGFI was selected as Backup Official Combination Center or ILRSB.

In 2005 the ILRS contributed to the definition of ITRF2005 with its official time series.

### The ILRS Standard Products

Presently, the following six AC's regularly contribute to the production of the ILRS standard products by means of weekly solutions:

ASI, Agenzia Spaziale Italiana, I

BKG, Bundesamt fuer Kartographie und Geodaesie, D  
 DGFI, Deutsches Geodatisches Forschungsinstitut, D  
 GFZ, GeoForschungsZentrum Potsdam, D  
 JCET, Joint Center for Earth System Technology, USA  
 NSGF, NERC Space Geodesy Facility, UK

Those ACs have been recognized after passing the benchmark tests as requested by the AWG. Other institutes are now under test and on the way to become official ILRS Analysis Centers.

The standard weekly ILRS combined solutions (either the primary and the backup) are made available each Wednesday at CDDIS and EDC, together with the single contributing AC solutions. The complete time series, starting from 1993, is available at CDDIS and EDC. A backwards extension of the time series, back to 1980, is now under construction.

A complete description of standards and methods adopted in the combination is given in [Bianco et al, 2003].

### The ILRS coordinate solution in the ITRF 2000 and ITRF 2005

The first quality assessment has been done comparing the ILRS coordinate solution with the ITRF2000 as well as with the newly issued ITRF2005.

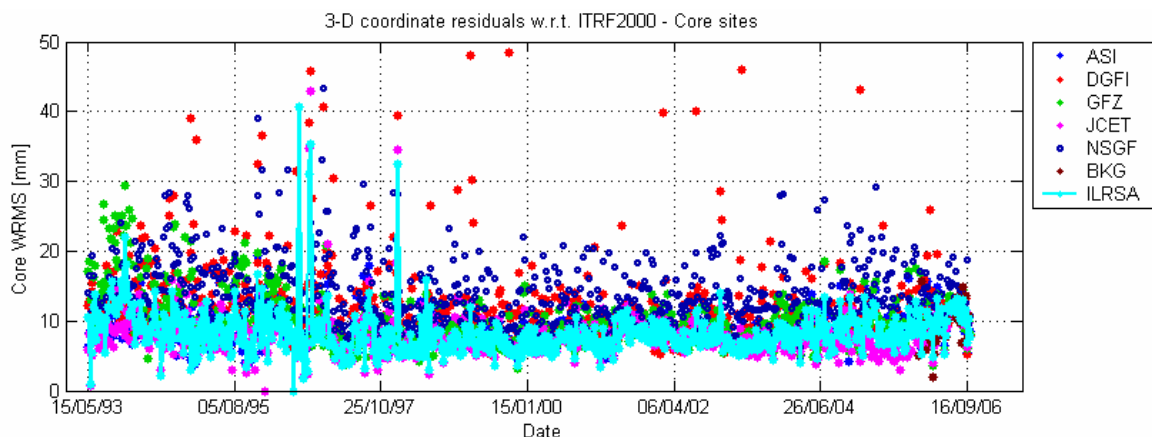


**Fig 1** Time series of weekly 3-D coordinate residuals w.r.t. ITRF2000 for ILRS core sites from individual AC solutions as well as from the combined ILRSA solution.

Generally speaking, the plot in Fig. 1 shows that the combined solutions represents a real improvement, in terms of consistency and dispersion, with respect to the individual AC solutions. The average 3-D residuals with respect to ITRF2000 are consistently at or below the 1 cm level, as confirmed by the plot in Fig. 2, which shows the 3-D coordinate residuals WRMS as a function of time.

It shows very clearly the fundamental role of the so called “core” sites (i.e., SLR stations with a consolidated tracking history in terms of data quantity and quality). The behavior of the total network worsens after year 2000 due to the introduction of several new observing sites which are not properly modeled in ITRF2000.

As expected, the situation improves with the ITRF2005, as shown if the plots in Figures 3 and 4 below. In particular, the new stations appear properly accounted for; moreover, the 3-D coordinate residuals for the “core” stations behave remarkably well, with an average value constantly below the 1 cm level.

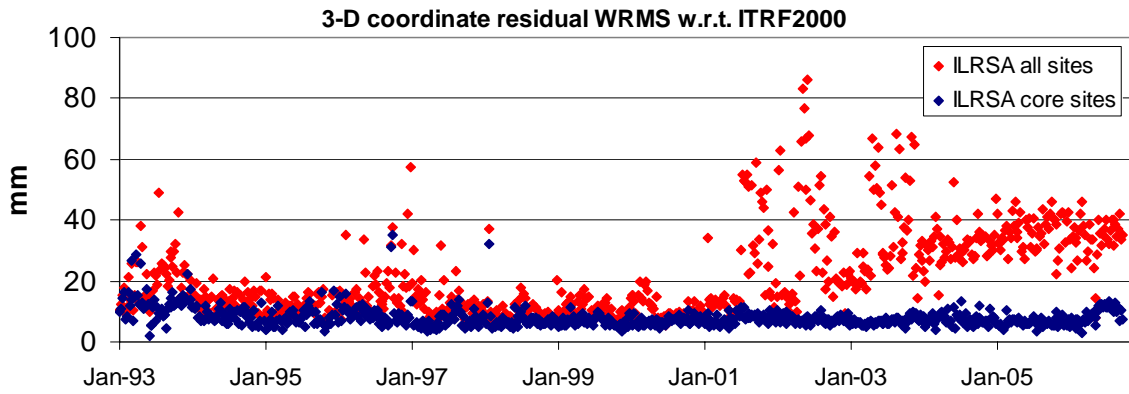


**Fig. 2** Time series of weekly 3-D coordinate residuals WRMS with respect to ITRF2000

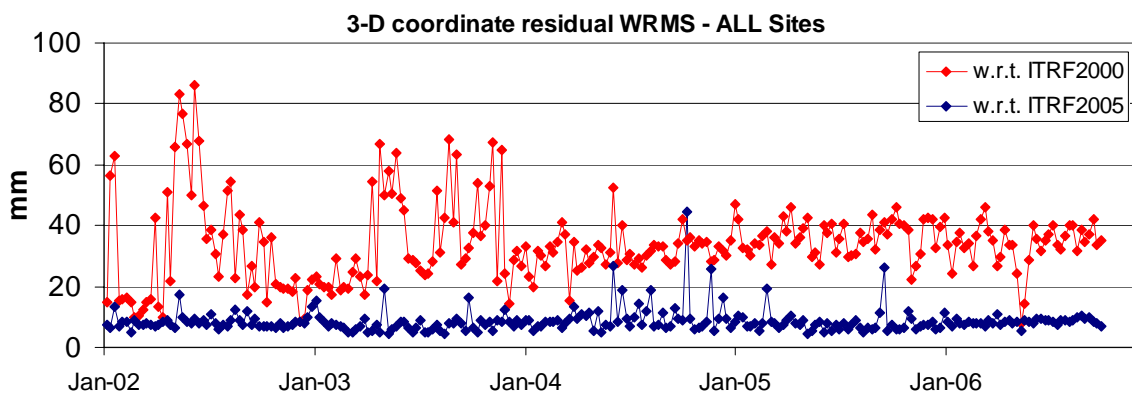


**Fig. 3** Time series of 3-D coordinate residual WRMS for all ILRS sites with respect to ITRF2000 and ITRF2005, as computed in the ILRSA combined solution

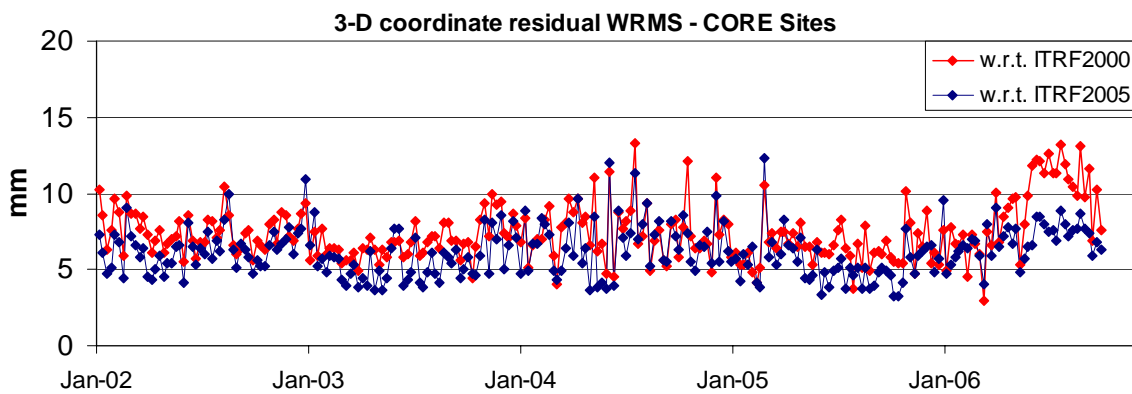


**Fig. 4** Time series of 3-D coordinate residual WRMS for ILRS “core” sites with respect to ITRF2000 and ITRF2005, as computed in the ILRSA combined solution

**ILRS TRF origin with respect ITRF 2000/2005 origins**

Another quality assessment has been done by looking at the time series of the 3-D distances of the ILRS Terrestrial Reference Frame origin with respect to another ITRF origin. Each TRF realized by the SLR stations in a loose solution places naturally its origin in the center of mass of the Earth: its Cartesian coordinate offsets from a conventional origin describe the geocenter location. This time series, often referred to as “geocenter motion”, is particularly interesting since it can be proposed as a new standard ILRS product.

The plots in Fig. 5 represent respectively the X, Y and Z components of the distance between the ILRS weekly origin with respect to the ITRF2000 and ITRF2005 origins, computed by roto-translations (“geometric” method) in the period 2002-2006. A clear annual signature is visible in all three components. The two series look pretty similar, with a slightly more evident drift in the Z component with respect to the ITRF2005 origin.

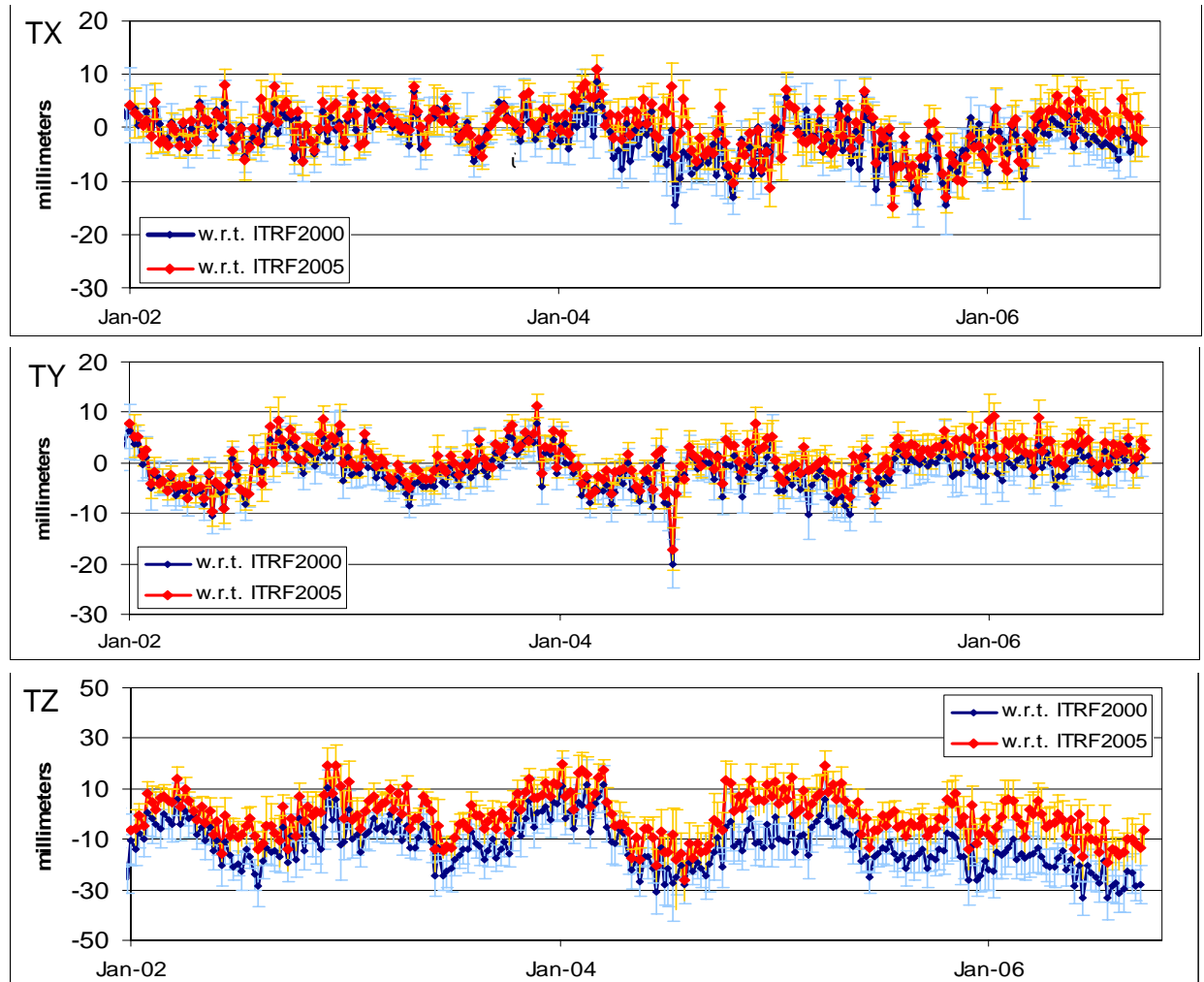


*Fig. 5 Time series of distance between the ILRSA geometric origin and the ITRF2000 and 2005 origins*

The translations of the ILRS TRF origin can also be obtained with a more rigorous data analysis strategy: through the estimates of the  $C_{10}$ ,  $C_{11}$ ,  $S_{11}$  geopotential coefficients, (“dynamic” method).

The plots in Fig. 6 show a direct comparison between the geometric and the dynamic ILRS TRF origin translations, with the latter obtained via the dynamic solution done by ASI. The behavior of the two time series is remarkably similar; the dynamic origin evolution looks smoother but the main features are present in both series.

This confirms that the geometric offsets, as defined by the standard ILRS combined solution, could be used to properly represent the geocenter motion.

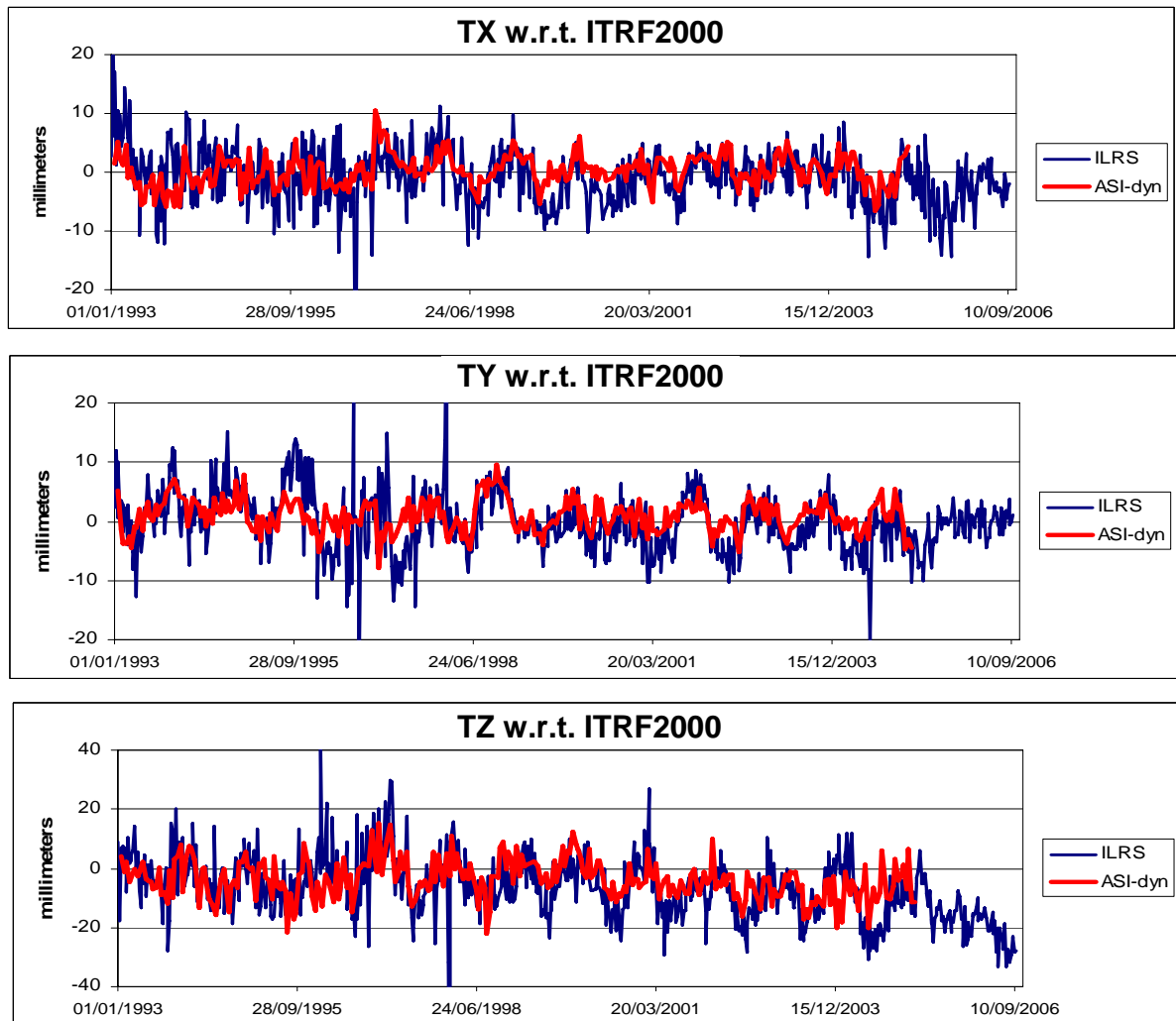


*Fig. 6 ILRSA geometric vs ASI dynamic geocenter motion.*

### The scale factor

Much debate has been generated soon after the publication of the ITRF2005, whose scale has been defined without taking into account the ILRS contribution, due to an apparent strange behavior of the ILRS scale itself.

However, based on our work, we do not find evidence of any strange effect in the ILRS scale, as shown in the plots hereafter, covering the period January 2002 to mid 2006.

The ILRS scale with respect to the ITRF2000 is nicely flat, while a clear trend shows up in the scale time series with respect to the ITRF2005.

The selection of the core sites to be used when comparing different reference frames is crucial and can introduce artifacts.

### Earth Orientation Parameters

In Fig. 8, ILRS X-pole, Y-pole and Length of Day (LOD) residuals with respect to the USNO “finals.daily” EOP time series, are plotted. The ILRS EOP products look pretty good and stable, with a WRMS of the residuals of the order of 0.25 milliarcseconds.

We've also made an external comparison between ILRS EOP's and those computed by other space geodetic services, namely IVS and IGS (CODE solution). The results for the Y component are shown in Fig. 9 below.

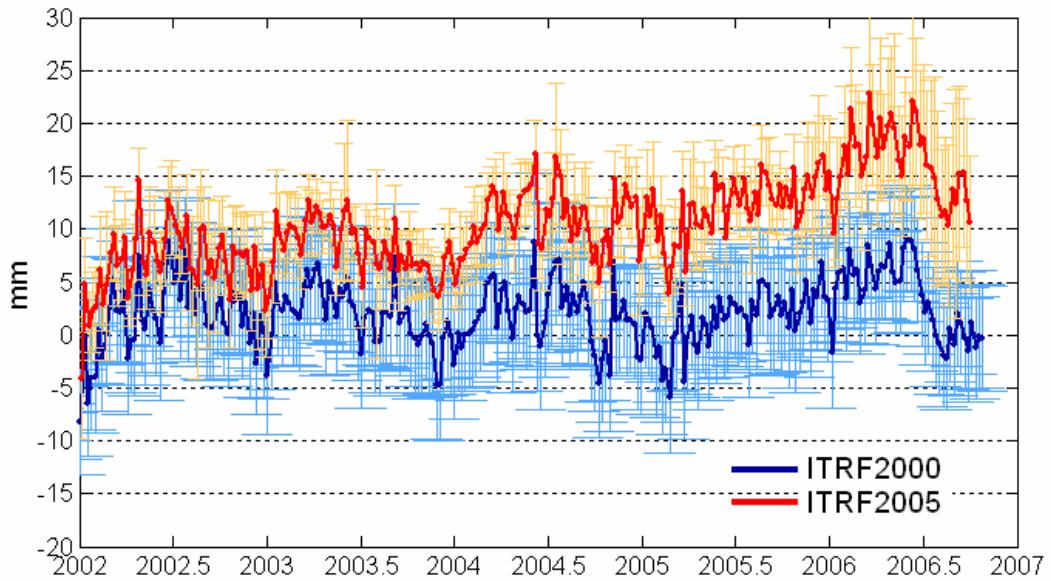


**Fig. 7** ILRSA scale with respect to ITRF2000 and ITRF2005

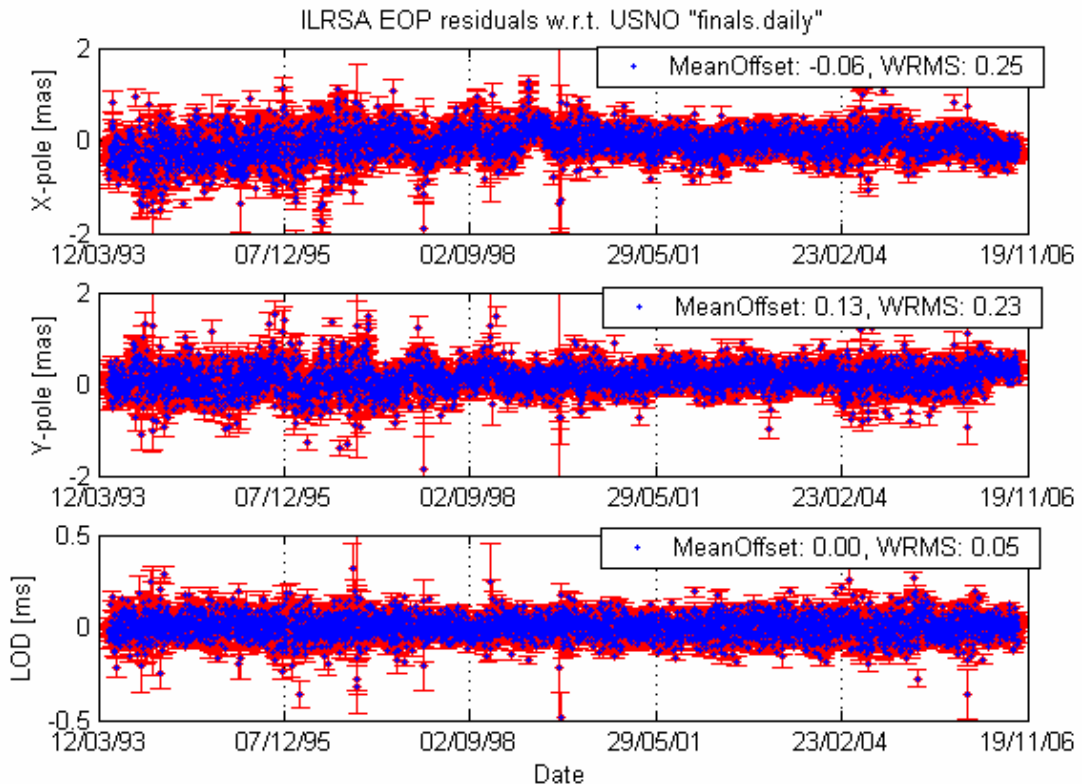


**Fig. 8** ILRSA EOP residuals with respect to USNO "finals.daily" EOP's

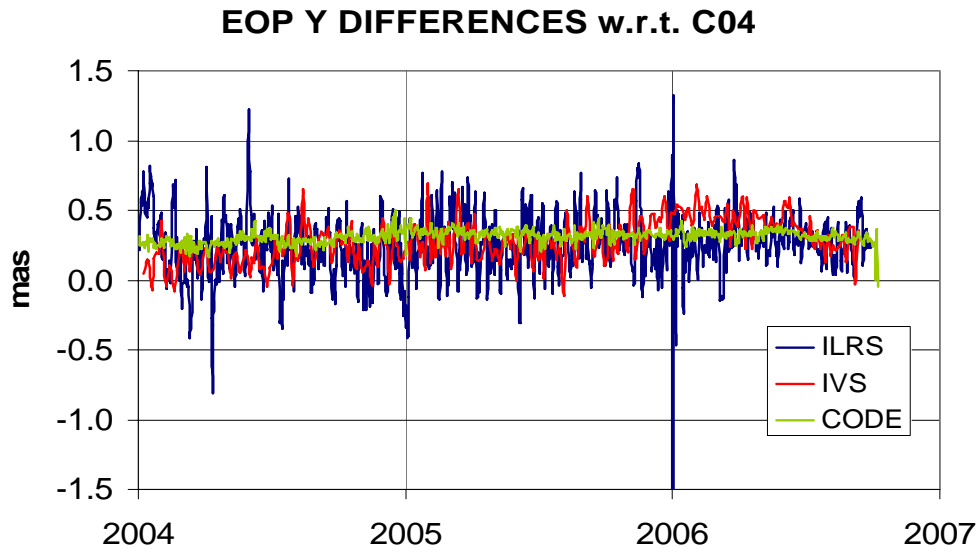


*Fig. 9 ILRSA EOP differences with respect to IERS EOPC04*

### Conclusions

After two years of continuous operations, the routine ILRSA combination production process is stable and reliable. The processing chain has been made almost completely automatic and has already demonstrated a high degree of dependability.

Other than for the definition of origin and scale, almost unique to SLR, the ILRS standard products are a very valuable monitoring tool for site coordinates and EOPs, with a very fast response time.

This work has also shown that the geocenter motion, geometrically derived from the weekly solutions, is reliable enough to be included among the future ILRS standard products.

### References

- [1] Bianco, G., Devoti, R., Luceri, V., 2003, Combination of loosely constrained solutions, Proceedings of the IERS Workshop on Combination Research and Global Geophysical Fluids (Munich, 18-21 Nov 2002), IERS Technical Note 30, 107-109, 2003

---

## Systematic range bias 2005-06

Toshimichi Otsubo<sup>1</sup>, Naoko Obara<sup>1</sup>

1. Kashima Space Research Center, National Institute of Information and Communications Technology, 893-1 Hirai, Kashima 314-8501 Japan.

Contact : [otsubo@nict.go.jp](mailto:otsubo@nict.go.jp) / Fax: +81-299-84-7160

### Introduction

Most of modern laser ranging systems potentially have 1-millimetre-precision measurement ability in a normal-point basis. However, when it comes to 1-millimetre ‘accuracy’, it has not been fully achieved yet and it is still a challenge for the International Laser Ranging Service (ILRS) network.

At National Institute of Information and Communications Technology (NICT), Kashima, Japan, we check the quality of laser ranging data from the whole ILRS network, in two folds. One is routine automated quality check analysis which gives quick alarms for large and obvious anomalies, and the other is precise residual analysis for sub-centimetre systematic range biases.

### Routine quality check analysis

We started the 3-satellite (two LAGEOS and AJISAI) routine bias report in 1997 (Otsubo and Endo, 1998) and enhanced it to the 7-satellite (plus STARLETTE, STELLA and two ETALON) analysis in 1999 (Otsubo, 2000). It was again significantly upgraded in May 2005 as follows.

Firstly, we further added satellites: ERS-2, JASON-1, ENVISAT, GPS-35, GPS-36, GLONASS-87, GLONASS-89 and GLONASS-95. Note that some of these satellites might be omitted from the analysis report in the case of failing a certain criteria in terms of data quality and quantity. Nevertheless, the analysis reports constantly include well more than 10 satellites. The increase of number of satellites and the variety of satellite altitudes will certainly help the ILRS stations easily point the problem and the cause.

We have switched the orbit analysis software from ‘concerto v3’ to ‘concerto v4’. The new version is almost compatible to the physical models recommended in IERS Conventions (2003). The station coordinates basically unchanged to ITRF2000, but those of new or significantly improved stations after the year 2000 were readjusted. Therefore the quality of our analysis reports should be more accurate.

We now publish the report every day, which used to be a week interval before May 2005. The report timing was also improved from 48-hour delay to 24-hour delay. Every morning in Japanese Standard Time (around 0 to 1 hr UT), a report covering up to two days before is being released. Such a quick reporting scheme became possible thanks to the rapid submission (typically within a few hours after the observation) and the rapid archive service (at CDDIS and EDC) of normal point data. The daily reports are available at our website and also via email. See figure 1 for previous website page. New website is: <http://www.science.hit-u.ac.jp/otsubo/slr/bias/> [ed].

The reports are distributed through the SLReport mailing list every Wednesday, and they are being sent to registered users even on a daily basis.

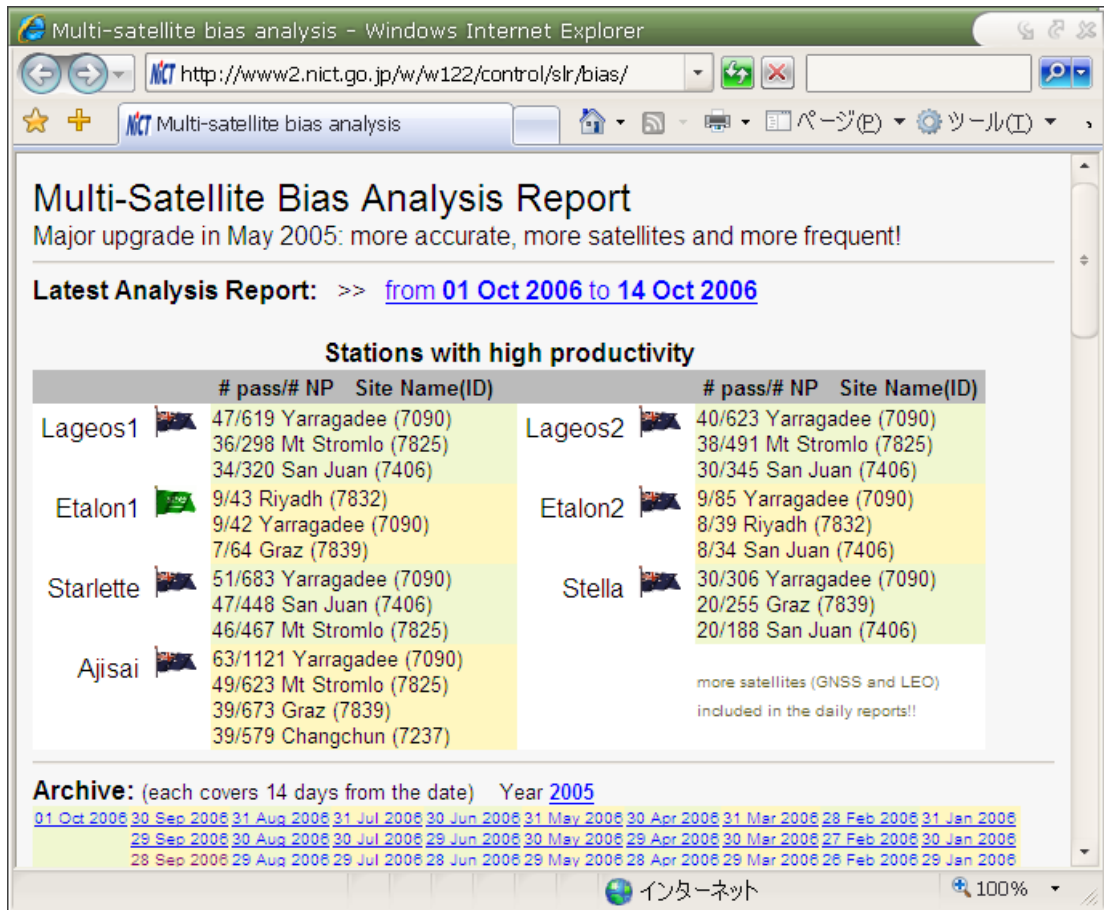


Figure 1. Multi-satellite bias analysis webpage at NICT.

### Range bias vs intensity

We have proposed a quality assessment method for the intensity-dependent biases (Otsubo, 2000). The post-fit residual data were sorted by the number of single-shot returns per normal point bin which should be strongly related with the signal intensity into a detector. If the detection signal intensity varies, and if the detection timing is dependent on it, there will be intensity dependent bias. Our previous studies also pointed out it is also related to the so-called target signature effect, which is now the major error source of laser ranging technique due to the reflection from multiple retroreflectors on board. The range measurement can differ, at maximum, by 4 to 5 cm for AJISAI and ETALON, and 1 cm for LAGEOS (Otsubo and Appleby, 2003).

We applied the same procedure to the 2005-2006 data set. Three sets of satellite types were chosen: LAGEOS-1 + LAGEOS-2, AJISAI, and STARLETTE + STELLA. For each satellite, the worldwide laser ranging data for 360 days from September 2005 to August 2006 were used for orbit determination. Orbits were solved for every 5 days for LAGEOS satellites and 2 days for others. The station coordinates and range bias were adjusted for all stations. The post-fit residual weighted rms of normal points was 1.0 to 1.2 cm for LAGEOS satellites and 1.5 to 2.5 cm for others.

The intensity dependent tests were carried out for most productive 24 stations during the period. The whole results are available at:

<http://www.nict.go.jp/w/w122/control/pod/bias-intensity-0506.pdf>

Fig. 2 (a) to (c) shows the three typical samples of them. The first case of Herstmonceux is the station where the return signal energy is almost strictly controlled to single photoelectron. This observation policy successfully results in the flat trend, that is, no intensity dependence seen for this station, in Fig. 2 (a). The Yarragadee station in Fig. 2 (b) represents good MCP stations. There is no intensity dependence larger than a few millimeters either. The typical result of (C-) SPAD stations is shown by Mt Stromlo in Fig. 2 (c). As the target signature studies suggested the strong signal makes the range measurement shorter. The AJISAI case is the largest in most cases, but a number of stations show significant trend (mostly negative) even for LAGEOS and STARLETTE + STELLA.

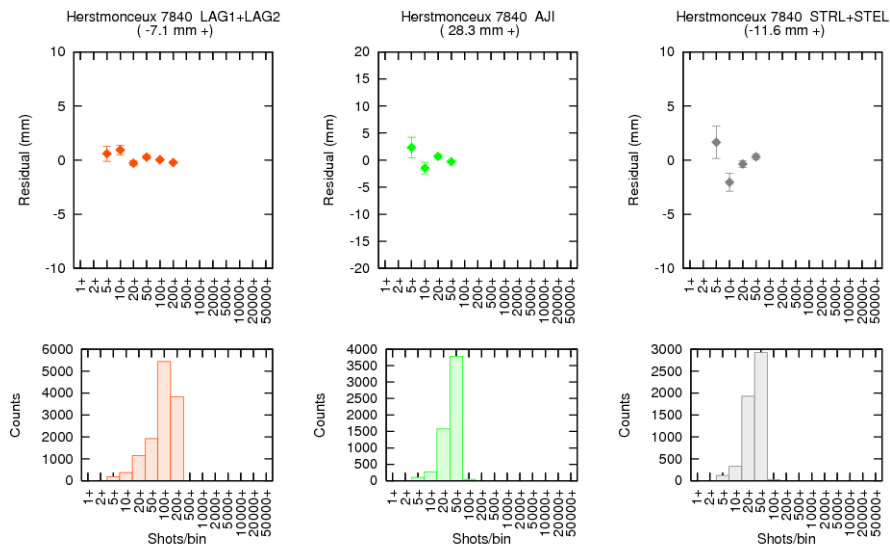


**Figure 2 (a).** Intensity dependence test. Single photon Herstmonceux station.

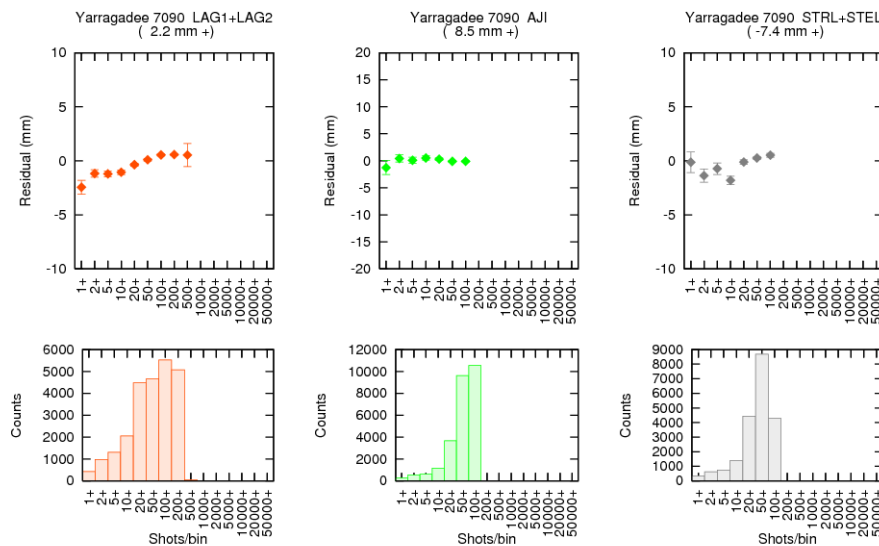


**Figure 2 (b).** Intensity dependence test. MCP Yarragadee station.

It is strongly recommended for every ILRS station to look into the result, and consider how the intensity dependent bias can be removed if it exists. As proven in previous

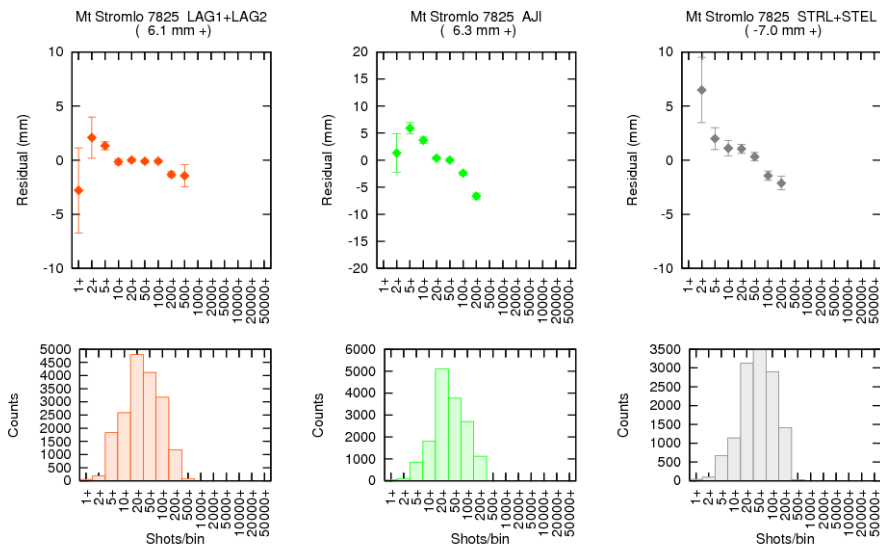


**Figure 2 (c).** Intensity dependence test. C-SPAD Mt Stromlo station.

studies (Otsubo and Appleby, 2004), the signal intensity is closely related to the elevation angle, and as a result the height component of station coordinates can be affected. This study probably underestimates the true intensity dependence. Note that the results from this study are just a guideline - it is the best to check the intensity dependence at each station, for example by inserting and removing the neutral density filter in front of the detector.

### Range bias vs applied system delay

The alternative approach is the use of the applied system delay (given in the ILRS normal point format) as a sorting parameter.

The applied system delay is the value to be subtracted from the raw range observations, and it is not constant. Therefore it is to be regularly observed by ranging to terrestrial targets, what we call ‘calibration’. There should not be any correlations between the range residuals and the applied system delay, in the ideal case. If there were, the station would have a systematic error in its ranging procedure to a terrestrial target or in its data processing stage.

We used the same set of the residual data as the previous section. At a number of stations, there have been jumps in the applied system delay itself probably due to some changes in optical or electronic path. Some stations seem to have multiple configurations (dual detectors, etc.) each of which gives different applied system delay. Such discontinuities themselves are not a problem at all as long as the reason is exactly known.

The bin size was set to the two-way range of 66 ps (1 cm in one-way distance). We applied the sorting procedure to the same 24 station as the previous section. The sorting procedure was chopped into a few portions for stations with large jumps. The graphs are also available at our website:

<http://www.nict.go.jp/w/w122/control/pod/bias-delay-0506.pdf>

(graphs for calibration dependent bias)

<http://www.nict.go.jp/w/w122/control/pod/delay-0506.pdf>

(auxiliary graphs for variation of applied system delay for the 1-year period)

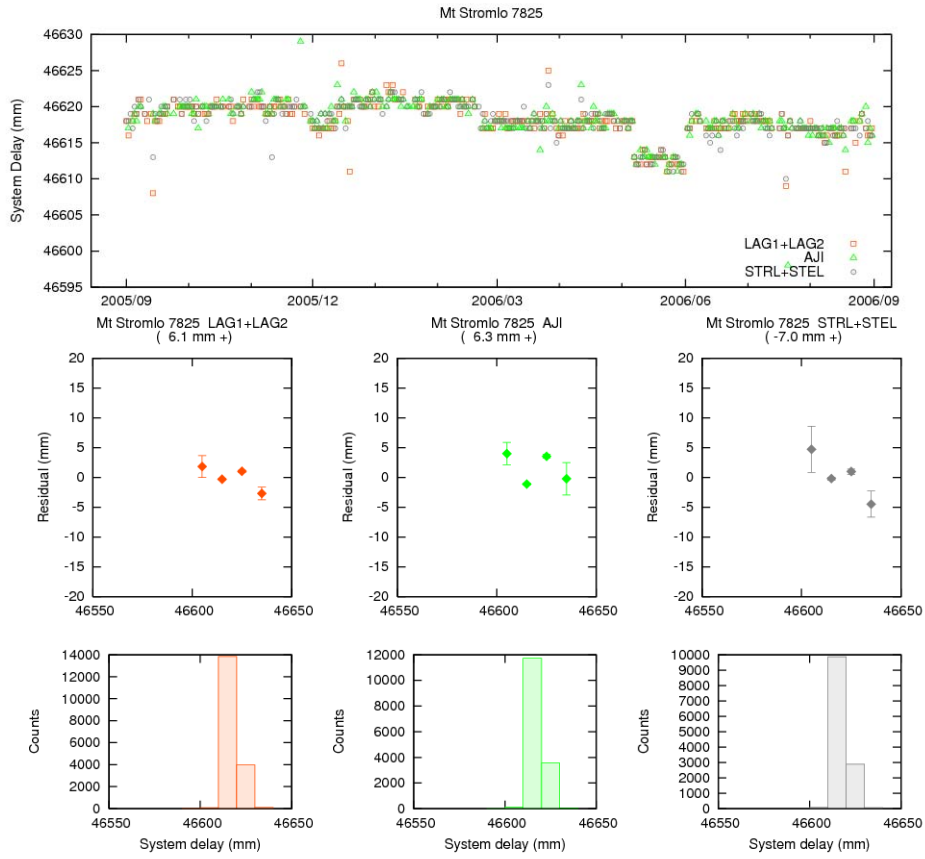


Figure 3 (a). Calibration dependence test. Mt Stromlo station.

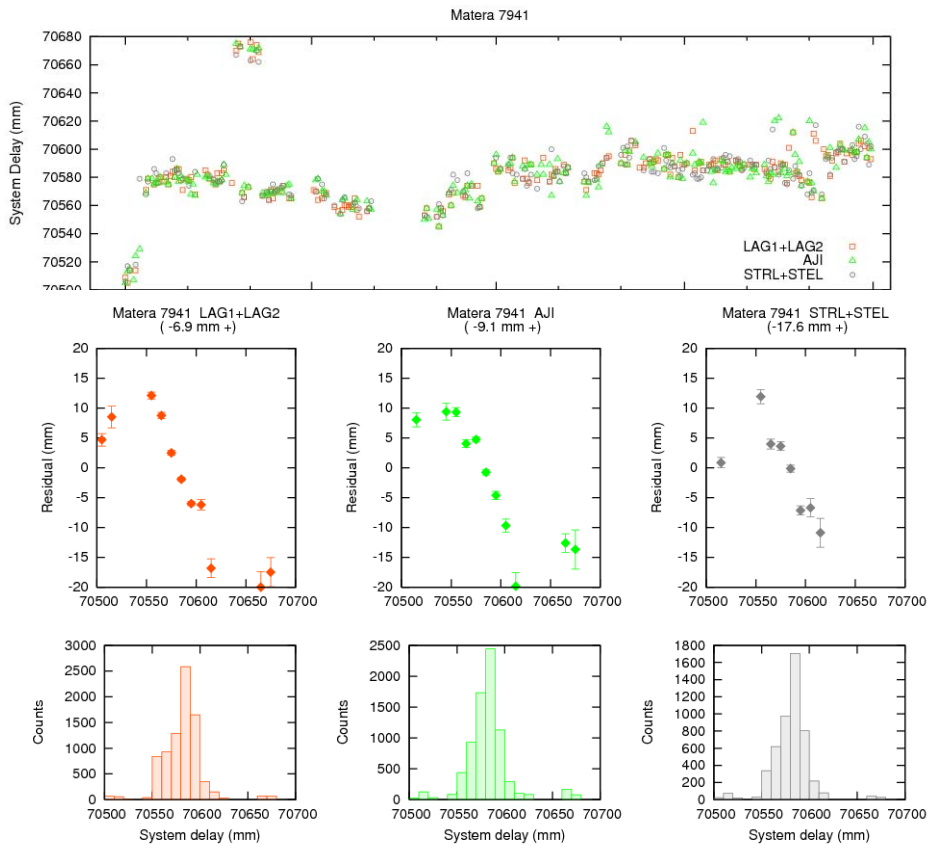


Figure 3 (b). Calibration dependence test. Matera station.

Two results are shown in Fig. 3 (a) and (b) among the 24 cases. The first case (Fig. 3 (a)) is probably the best one of all: Mt Stromlo. Its applied system delay has been very stable throughout the year, almost within  $\pm 1$  cm (top). There has been no significant calibration dependent bias (bottom). Such long-term stability of calibration ranging helps the long-term stability of satellite ranging. The next graph of Fig. 3 (b) shows those for Matera station. The stability of applied system delay is also good ( $\pm 3$  cm) for this station. However, there is a steep negative trend for all three types of satellites. A possible reason is that a part of the variation in calibration ranging might not be true and therefore the raw observation would be ‘wrongly calibrated’ by the calibration procedure.

The long-term variation of terrestrial target ranging is hardly separable from the seasonal or secular variation of station height. Therefore, the result from this approach has a risk of sending a wrong alarm if the station coordinates experience unmodelled effects like loading displacement. It is strongly recommended for each station to understand why the calibration measurement varies and strive to reduce the variation.

### Conclusions

In addition to the multi-satellite daily bias reporting system, we demonstrated the more precise ways for quality assessment of laser ranging data. We use the single shot returns per normal point bin, and the applied system delay, as a sorting parameter. Some correlations were found between the range data and these sorting parameters.

It is important to note that most of the information that is potentially useful to assess the quality is lost in the process of normal point generation. It is essential that each station performs extensive tests on site in order to eliminate any systematic bias and to keep the data quality stably high.

### References

- [1] Otsubo, T., and T. Endo, “Quick bias report for LAGEOS and AJISAI data,” Proc. 11th International Workshop on Laser Ranging, Deggendorf , 2, 650-653, 1998.
- [2] Otsubo, T., “New approach to quality check: multiple satellite and intensity dependence,” Proc. 12th International Workshop on Laser Ranging, Matera, CDROM, 2000.
- [3] Otsubo, T., and G. M. Appleby, "System-dependent Centre-of-mass Correction for Spherical Geodetic Satellites," Journal of Geophysical Research, Vol. 108, No. B4, 2201, doi:10.1029/2002JB002209, 2003.
- [4] Otsubo, T., and G. M. Appleby, "Centre-of-mass correction issues: toward mm-ranging accuracy," 14th International Laser Ranging Workshop, San Fernando, pp. 467-471, 2004.

## A reassessment of laser ranging accuracy at SGF Herstmonceux, UK

Philip Gibbs<sup>1</sup>, Graham Appleby<sup>1</sup> and Christopher Potter<sup>1</sup>

1. Space geodesy facility, Herstmonceux, East Sussex, UK.

### Introduction

*Gibbs et al (2007, these proceedings) reports on a major upgrade and expansion of capability at the Space Geodesy Facility, Herstmonceux, UK. A prerequisite of the laser ranging upgrade to kHz repetition rate is the in-house build of a ps-level precision event timer, based on Thales clock units and dubbed HxET. Extensive use has been made of HxET since it was completed during the summer of 2006 to calibrate the existing cluster of Stanford counters prior to making routine use of HxET. In particular, we are very interested in back-calibrating all the Herstmonceux data for the period 1994-present, during which time the Stanford counters had been exclusively used. In this paper we detail the results of this re-calibration, and also consider the effect the correction to our LAGEOS data will have on the published site coordinates in the ITRF.*

### Previous calibrations

Extensive tests on the linearity of the Stanford counters at satellite ranges, from a few to approximately 150ms were carried out by Gibbs (Appleby *et al*, 1999, Gibbs *et al*, 2002) using an early version of the Portable Pico Event Timer (P-PET, Hamal *et al*, 2007). The method used is to record start signals and subsequent noise events simultaneously by the P-PET and by the Stanford counter(s) that are under test. A hardware delay is used to move the average interval between start events and detected noise events from a few ms up to 150ms, the range encountered during real satellite ranging. For each event, comparison of the time interval as measured by each Stanford relative to that determined by the highly-linear P-PET, gives an estimate of the error in time interval determined by each Stanford. From this work, a correction table as a function of range was compiled and issued in SLRMail 0891 in 2002 January. The effective dates of application of the results are 1994 October to 2002 January and the magnitude of the corrections reaches 8mm. From 2002 February the corrections are applied at the station as part of pre-processing.

With the availability of HxET, these linearity tests were repeated during 2006 October; the results were found not to be significantly different from those determined in 1999 and 2001, confirming the ongoing validity of the correction table given in SLRMail 0891. The comparison between HxET and the three Stanfords in use at Herstmonceux (coded SRa, SRb and SRd) is shown graphically in Figure 1. The horizontal axis gives the time delay after which each set of measurement comparisons are made of 'flight time' as recorded by the Stanford counters and by HxET. The vertical axis records the mean difference of each Stanford-recorded flight time from that recorded by HxET. It is noted that SRd, the counter currently in use at the station, exhibits close-to linear behaviour over the entire time-range. Excursions from linearity of up to 100ps (15mm in range) are seen for the other two counters.

### New Calibrations

The availability of HxET has meant that more detailed measurements of non linearity effects can be made on the Stanford counters. In particular, we are interested in the behaviour at close ranges, within the first few micro-seconds. Time constraints on our previous experiments with the PPET precluded such a detailed study, and errors in

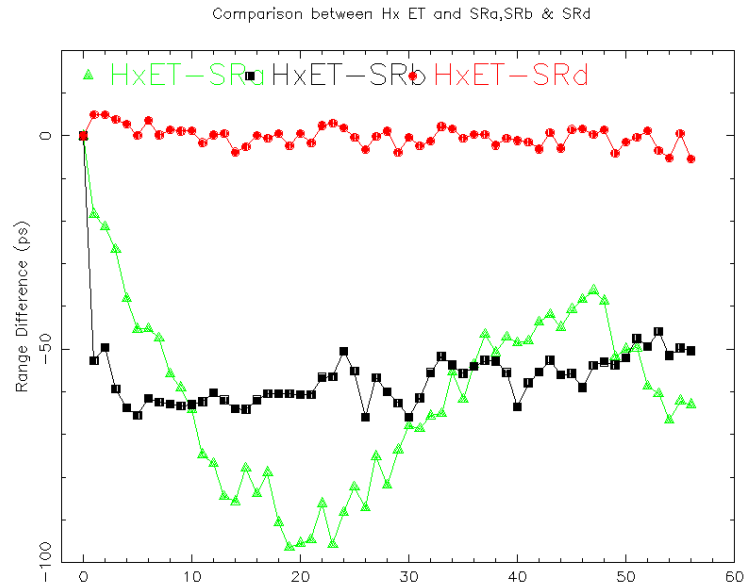
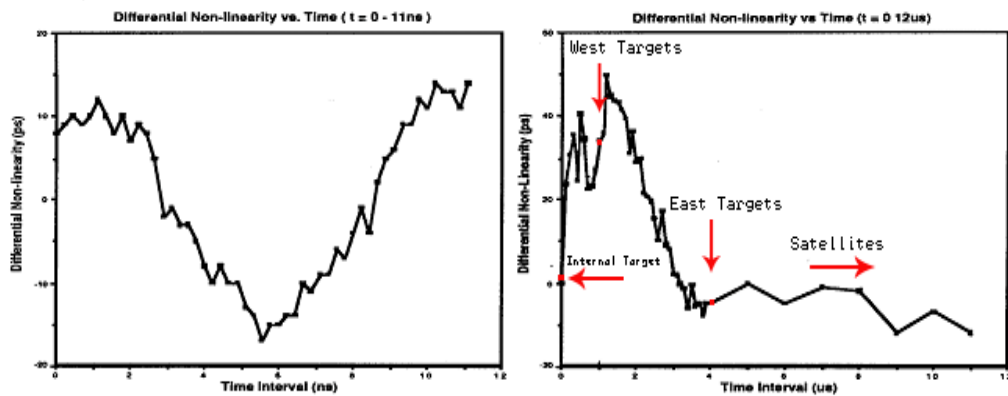


**Figure 1** SGF long-range linearity determination of three Herstmonceux Stanford counters relative to the event timer HxET.

this time-region will directly affect calibration ranging results and thus all satellite ranges from the station. We expect some significant effects in this region since the Stanford manual shows both high-frequency periodic signatures and more random departures from linearity in the critical range of about 1 micro-second, the distance of the prime SGF calibration target. A figure from the Stanford manual is reproduced here as Figure 2, with the time-range locations of the calibration targets marked. We carried out our tests on the behaviour of SRa, SRb and SRd against HxET in this critical range of from zero to 5 $\mu$ s; the results are shown in Figure 3 below and are to be compared with the Stanford manual results reproduced here in the right-hand plot of Figure 2.

In the range of from zero to 2 $\mu$ s the measured behaviour of our three Stanford counters is close to that expected from the specifications, with maximum departure from linearity of from 50 to 100ps, at a range of 1 $\mu$ s. Beyond a range of 2 $\mu$ s, the behaviour of the counters diverges. A probable explanation for the inter-counter scatter evident in these results is the high-frequency periodic structure shown in the

**Specification Guide**



Graph 1: Differential Non-linearity for time differences of 0 to 11 ns. This shows the residual non-linearity of the time-to-amplitude converters.

Graph 2: Differential Non-linearity for time differences of 0 to 11 $\mu$ s.

**Figure 2** Short-range non-linearity of Stanford counters as given in specification

specification (Figure 2, left-hand plot) and in our high-resolution results shown in Figure 4 where we find 22ns periodic effects (cf 11ns expected from specifications) of amplitudes up to 20ps (~3mm). This final result places a limit to the accuracy with which we will be able to determine corrections to range measurements made with the Stanford counters.

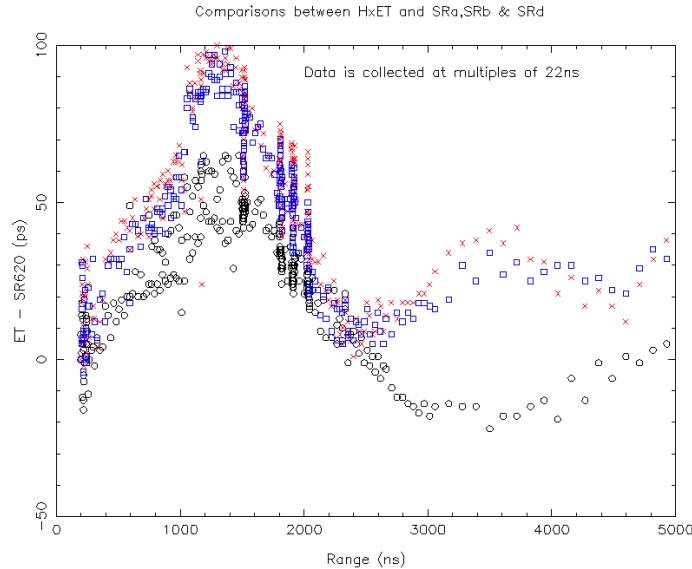


**Figure 3** SGF close-range linearity determinations of three Herstmonceux Stanford counters relative to the event timer HxET.

In summary, at the effective range of the SGF primary calibration target (890-930ps, dependent on electronic set-up), the non-linearity of the counters imparts an average of ~50ps error into the observed range; this value is dependent on the range itself and the uncertainty of the value is ~20ps due to the observed 22ns periodicity in the non-linearity function.

**Effect on LAGEOS data 1994-2006**

We have taken from Figure 3 the results for the appropriate counter and also recovered the actual calibration range as given in the ILRS normal point header of

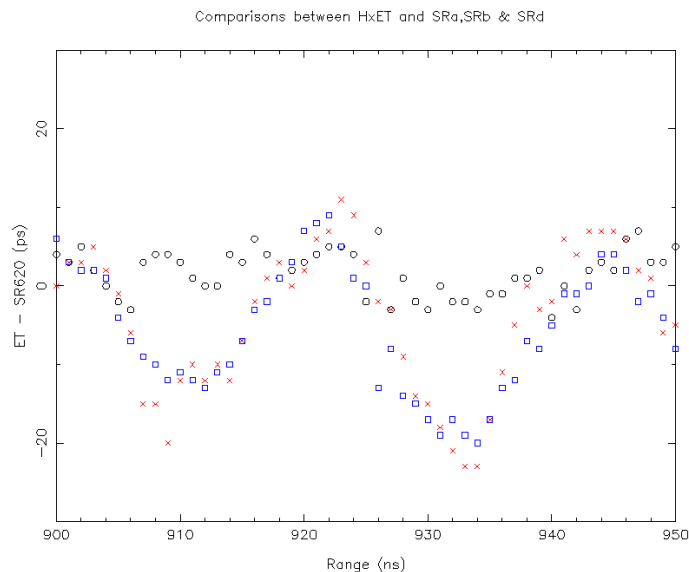


**Figure 4** Observed periodic behaviour in Stanford counters' error functions.

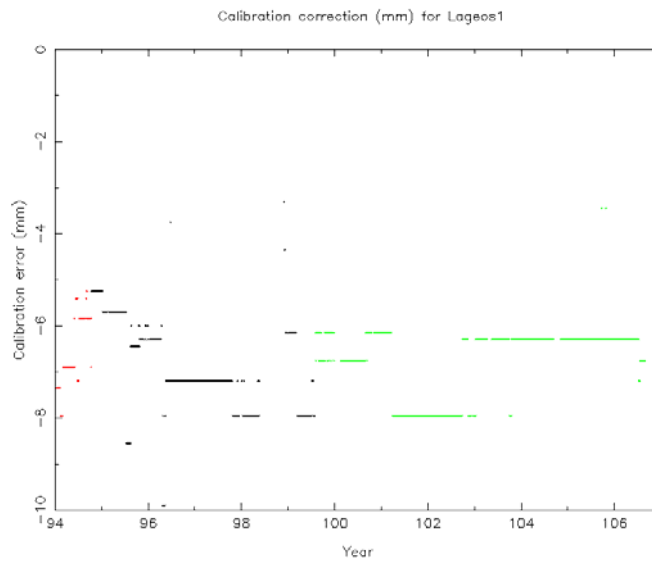


**Figure 5** Correction to calibration values used for LAGEOS during 1994-2006

SGF LAGEOS data for the period 1994-2006. From these values we have estimated the corrections in mm to be applied to our calibrations taken over that period. The results are displayed in Figure 5, where it is apparent that errors of between 5 and 8mm have been made to the calibration values. However, given our estimate of the uncertainty of these average values, we finally derive an average calibration error of  $7 \pm 2$  mm, and in the sense that the calibration correction is too large by that amount. During this re-assessment we also discovered that no account had been taken for the effect on total delay of a glass neutral density filter that is placed in the optical path during calibration but not during satellite ranging. This correction amounts to 1.5mm, again in the sense that the calibration correction derived from target-board ranging is too long. Therefore our calibration corrections in the period 1994-date are too long by  $8.5 \pm 2$  mm and thus calibrated satellite ranges short by the same amount. This correction, which affects all satellite data equally, is of course in addition to the range-dependent correction discussed under ‘previous calibrations’ above and announced for the period 1994 October to 2002 January in SLRMail 0891 in 2002 January.

Assuming that the corrections presented in SLRMail 0891 have been made to the Herstmonceux ranges, it is interesting to look at the implications for and evidence in geodetic solutions of this newly-discovered correction of  $8.5 \pm 2$  mm. The centre-of-mass (CoM) correction for LAGEOS for 7840 Herstmonceux single photon data is  $245 \pm 1$ mm (Otsubo and Appleby, 2003). However, in computing ITRF2000, the Analysis Centres used the ‘standard’ 251mm CoM for all stations, thus effectively *increasing* Herstmonceux ranges by 6mm and nearly cancelling the bias of -8.5mm present since 1994. Thus the coordinates (height) of Herstmonceux in ITRF2000 should have only a small bias from the true value, given that a range bias (RB) affects primarily the solution for height. Indeed, the mean of Herstmonceux LAGEOS 1/2 residuals in our daily QC based on fixed ITRF2000 coordinates is currently  $-11 \pm 2$ mm, close to the expected bias of -8.5mm. Thus it appears that the coordinates have not absorbed the range error and the full range bias remains. Further evidence comes from an analysis of LAGEOS 1/2 data between 1992 and 2006, where J Ries (personal communication, April 2006) finds a range bias of -10 to -12mm and a height change of  $\sim 7$ mm; from an analysis of LAGEOS 1/2 data in the period from 2001-

2005, Otsubo, Appleby, Gotoh and Kubooka (2006) find a range bias of -9mm, and a similar value for Etalon data.

For the ILRS combined product included in ITRF2005, the individual Analysis Centres used the correct value of 245mm for Herstmonceux's LAGEOS CoM, and did not solve for a bias for this station (AWG resolution at ILRS Fall Meeting, Eastbourne 2005). Thus it is likely that in particular station height will be in error in the ITRF2005. To test this, we apply the +8.5 mm range correction to LAGEOS 1/2 data for 2004, and solve simultaneously for correction to station coordinates as given in ITRF2005, and a range bias for 7840 Herstmonceux. On average, we find  $RB = +1 \pm 2$  mm and  $\Delta H = -5 \pm 1$  mm, implying that station height in ITRF2005 had absorbed half the RB and is in error by +5mm.

## Conclusion

All range data from 7840 Herstmonceux will from early 2007 be determined using HxET and will then be free of systematic error greater than 1 or 2mm. An SLRMail will announce the date and confirm that 8.5 mm should be *added* to all Herstmonceux satellite ranges from 1994 to that date, and re-iterate that the range dependent corrections given in SLRMail 0891 should also be applied for the period 1994 October to 2002 January. As a consequence of these counter problems, we estimate that the station height for 7840 Herstmonceux as given in ITRF2005 is approximately 5mm too large. We regret this long-term error that affects all laser data from Herstmonceux and encourage other stations, mostly among the EUROLAS sub-network, that use or have used Stanford counters, to investigate possible similar effects in their data. To this end, we will work with the ILRS Network and Engineering and Signal Processing Working Groups to calibrate the counters of all stations that are interested in collaboration.

## References

- [1] Appleby, G.M., Gibbs, P., Sherwood, R. and Wood, R., 1999. Achieving and maintaining sub-centimetre accuracy for the Herstmonceux single-photon SLR Facility, *Proceedings of Laser Radar Ranging and Atmospheric LIDAR Techniques II, Proc. SPIE Int. Soc. Opt. Eng.*, 3865, 52-63.
- [2] Gibbs, P., Potter, C., Sherwood, R., Wilkinson, M., Benham, D., Smith, V. and Appleby, G.M., 2007. Some Early Results of Kilohertz Laser Ranging at Herstmonceux, these proceedings.
- [3] Gibbs, P., 2002. Stanford Counter Comparison Results, Proceedings of EUROLAS Workshop 'Detecting and eliminating errors in the EUROLAS network', Herstmonceux, UK. [http://ilrs.gsfc.nasa.gov/reports/special\\_reports/eurolas\\_workshop.html](http://ilrs.gsfc.nasa.gov/reports/special_reports/eurolas_workshop.html)
- [4] Hamal, K., Prochazka, I. and Fumin, Y., 2007. Portable Pico Event Timer and SLR Control (P-PET-C) System, these proceedings.
- [5] Otsubo, T. and Appleby, G.M., 2003. System-dependent center-of-mass correction for spherical geodetic satellites, *JGR*, 108, no. B4, doi:10.1029/2002JB002209.
- [6] Otsubo, T., Appleby, G.M., Gotoh, T. and Kubo-oka, T., 2006. Potential TRF Improvements through better understanding of Laser Ranging Target Signature Effects, (abstract and oral presentation), *Geophysical Research Abstracts, Vol 8, EGU*.

---

## The Global SLR Network and the Origin and Scale of the TRF in the GGOS Era

E. C. Pavlis<sup>1</sup>

1. Joint Center for Earth Systems Technology (JCET), UMBC, Baltimore, MD, USA.

Contact: [epavlis@umbc.edu](mailto:epavlis@umbc.edu) / Fax: +1 410 455 5868

### Abstract

*Satellite Laser Ranging (SLR) data contribute to the realization of the Terrestrial Reference Frame (TRF), defining primarily its origin—geocenter, and in combination with VLBI, its scale. Both entities are fundamental in monitoring vital global change parameters, such as mean sea level, Earth rotation and orientation, etc. The Global Geodetic Observing System (GGOS), places the utmost importance on the development, maintenance and wide distribution of a TRF with very stringent attributes, an origin definition at 1 mm or better at epoch and a temporal stability of 1 mm/y, with similar numbers for the scale and orientation components. The stability, integrity and applicability of the TRF are directly related to the accuracy and fidelity with which mass redistribution can be observed or modeled during its development. Variations in the very low degree and order harmonics, produce geometric effects that are manifested as changes in the origin and orientation relationship between the instantaneous and the mean reference frame.*

*The unambiguous nature of SLR measurements and absence of significant biases, results in a very precise height determination, and thus the scale of the TRF. SLR has demonstrated millimeter level accuracy for weekly averages. Nevertheless, weather- or failure-induced changes in the network, and the small number and poor spatial distribution of the sites comprising the SLR network, generate additional signals aliased in the results. “Secular trends” seen in the recovered geocenter time series for example cannot be explained by any geophysical phenomena, and are primarily the result of these deficiencies of the present SLR network (poor geometry, lack of redundancy, N-S hemisphere unbalanced distribution, etc.). We investigate here through a number of alternate solutions the robustness of our results, using our SLR analyses spanning the past thirteen years.*

### Introduction

The Global Geodetic Observing System (GGOS), places the utmost importance on the development, maintenance and wide distribution of an International Terrestrial Reference Frame (ITRF) with very stringent attributes, an origin definition at 1 mm or better at epoch and a temporal stability of 1 mm/y, with similar numbers for the scale and orientation components (Pearlman et al., 2006). The stability, integrity and applicability of the TRF are directly related to the accuracy and fidelity with which mass redistribution can be observed or modelled during its development. Satellite Laser Ranging (SLR) data contribute to the realization of the Terrestrial Reference Frame (TRF), defining primarily its origin—geocenter, and in combination with VLBI, its scale. Both entities are fundamental in monitoring vital global change parameters, such as mean sea level, Earth rotation and orientation, etc., (Altamimi et al., 2002). The motivation behind this contribution was to examine the robustness of the ILRS (Pearlman et al., 2002) contribution to the ITRF in light of the forthcoming developments under GGOS and NASA’s effort to upgrade and integrate the space geodetic networks of the future.

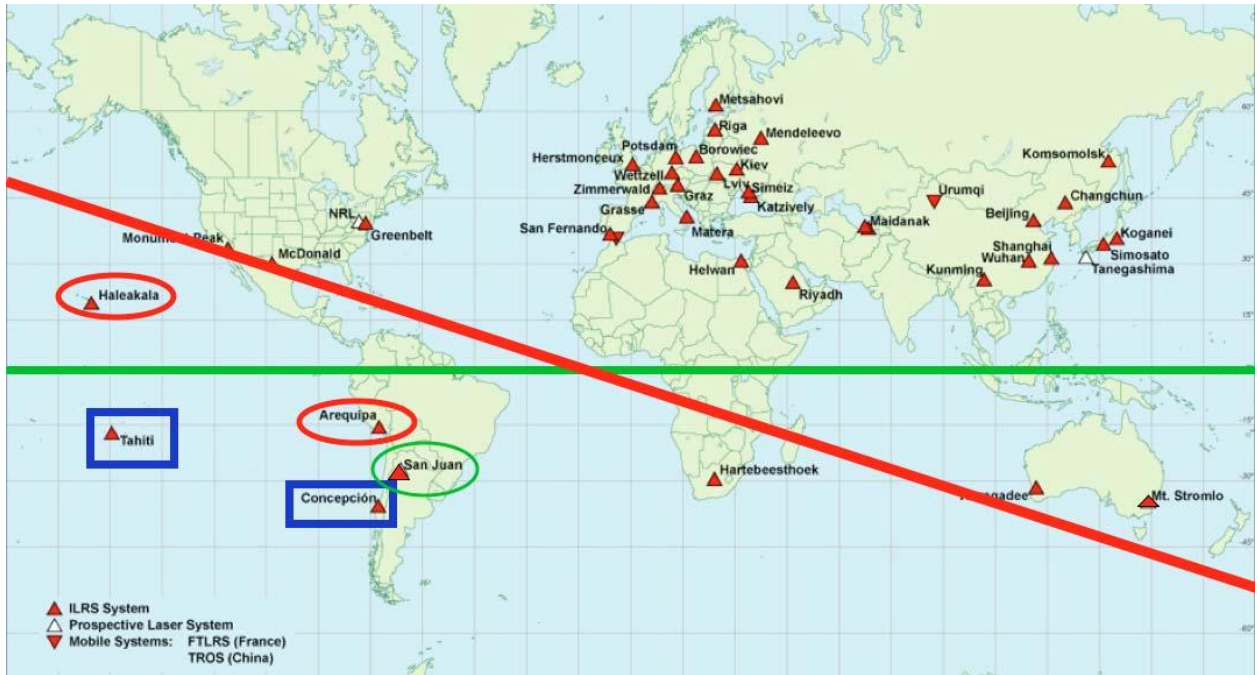


**Figure 1.** The current ILRS network with mark-ups of sites that were recently established (green), poor-yield southern hemisphere sites (blue), and sites that were shut down in 2004 (red).

### SLR contribution to ITRF

The SLR network never achieved an optimal, uniform distribution of stations globally (Figure 1). Furthermore, the closing of two key-sites, Arequipa, Peru and Haleakala, Hawaii in 2004 led to a disastrous lopsided distribution, where one-half the globe is totally void of any SLR observations! This eventually manifested itself in the SLR products as a serious and systematic degradation of the network scale as realized through the SLR observations. Aside from this recent degradation (which is addressed with the re-establishment of the closed down sites and improved performance for the others), this network has produced valuable TRF contributions over the decades. ITRF2000, (Altamimi et al., 2002), was a product that for the first time included a vast number of sites around the world and input from all geodetic techniques with rather strict and rigorous editing in its development. Weekly “geocenter” monitoring with respect to that frame yields a significant and systematic motion in the z-axis, at a rate of  $\sim 1.7 \pm 0.1$  mm/yr! Most of this is eliminated in the new realization ITRF2005, but not all. In particular, our SSC (JCET) L 06 analysis resulted in the following rates for the three axes:

$$\Delta x = -6.55 - 0.0848 \times (t-2000) + \text{periodic terms} \quad [\text{mm}]$$

$$\Delta y = 4.99 - 0.0898 \times (t-2000) + \text{periodic terms} \quad [\text{mm}]$$

$$\Delta z = 0.91 + 1.6981 \times (t-2000) + \text{periodic terms} \quad [\text{mm}]$$

The formal accuracy of these estimates is at 0.1 mm/y, however, without an independent estimate to compare, we have no sound way to calibrate this error. Interpreting these signals is even more difficult, since they can be caused by a number of different geophysical phenomena, none of which is easily or fully understood. Table 1 gives some estimates due the main sources that could cause such a systematic signal. It’s worth noting that recently, Peltier (private communication), has been able to develop models

for Greenland and Antarctica melting in recent times that support this level of “geocenter” motion, especially in the axial component.

*Table 1. Secular geophysical signals in the axial component of the “geocenter”.*

Source	Magnitude	Induced motion	Reference
Sea level	1.2 mm/y	$0.064 \pm 0.02$ mm/y	[2]
Ice sheets (G)	2 mm/y	$0.046 \pm 0.20$ mm/y	[2]
Tectonics	AMO-	$0.309 \pm 0.05$ mm/y	[2]
Postglacial rebound	ICE-3G	0.2 - 0.5 mm/y	[1]

(1) Marianne Greff-Leffitz (2000)

(2) Yu. Barkin (1997)

### Methodology

Our conjecture is that the remaining unaccounted-for motion is due to the evolving network, the uneven global distribution of the tracking sites with strong yields, and the poor coverage of some of the major tectonic plates. To test the effect of the “network evolution” we have performed a number of re-analyses of the data, defining TRFs from independent sub-sets of the data in various combinations. As for the effect of the lopsided distribution of the main tracking sites, a large-scale simulation is in progress, within a technique-wide coordinated effort to design the optimal space geodetic networks of the future. The initial results of this investigation will be available by late 2007. A third test involves the so-called effect of the “missing” historical SLR data, i.e. SLR data to LAGEOS prior to 1992. ITRF2000 contained that data, while ITRF2005 does not, due to its tight and firm release schedule. We have generated a TRF that includes the data obtained from LAGEOS since 1976. A comparison of this TRF to a similar one that does not include that data and spans exactly the same period with ITRF2005, should give some idea of whether the missing data contribute to the z-axis secular evolution or the scale difference observed between the SLR and VLBI contributions to ITRF2005.

### The effect of the “missing” historical SLR data on the SLR-definition of the scale

To test whether the addition of the “historical” LAGEOS data (1976 to 1992) to the definition of the TRF would eliminate the differences seen between the ITRF2000 and ITRF2005 realizations, we simply reduced that data and added them to the 1993 – 2005 data, generating a new TRF and comparing that through a 14-parameter similarity transformation to the two realizations, ITRF2000 and ITRF2005. The results are tabulated in Table 2.

Our solution is identical to neither ITRF2000 nor ITRF2005, although very close to both. This is expected of course since this is a SLR-only TRF and not a combination product with input from other techniques. Examining the differences in the scale and its rate, we notice that in the case of ITRF2000, our TRF indicates the same level of disagreement as it was originally seen between the SLR-only contributed inputs to this model. Similarly, we see the same for ITRF2005, and the combined difference is exactly what is seen when comparing one ITRF to the other. The fact that a TRF that contains the historical LAGEOS data shows similar differences to the ITRF2005 as does the one without that

data, indicates strongly that the lack of that data cannot be the main reason of the observed differences.

**Table 2.** Similarity transformation parameters between SSC (JCET) L 06 and ITRF realizations.

Parameter	SSC (JCET) L 06.97 vs. ITRF2000	SSC (JCET) L 06.97 vs. ITRF2005
$D_x$	-8.82 +/- 1.02 [mm]	1.25 +/- 0.91 [mm]
$D_y$	3.21 +/- 1.01 [mm]	8.37 +/- 0.91 [mm]
$D_z$	-5.65 +/- 0.95 [mm]	-6.59 +/- 0.86 [mm]
$D_s$	<b>0.52 +/- 0.15 [ppb]</b>	<b>-0.87 +/- 0.13 [ppb]</b>
$R_x$	-0.24 +/- 0.04 [mas]	0.05 +/- 0.04 [mas]
$R_y$	0.06 +/- 0.04 [mas]	-0.07 +/- 0.04 [mas]
$R_z$	0.15 +/- 0.03 [mas]	0.32 +/- 0.03 [mas]
$D_{x\text{-dot}}$	0.75 +/- 0.95 [mm/y]	-1.22 +/- 0.85 [mm/y]
$D_{y\text{-dot}}$	0.56 +/- 0.94 [mm/y]	1.37 +/- 0.85 [mm/y]
$D_{z\text{-dot}}$	3.10 +/- 0.73 [mm/y]	1.89 +/- 0.65 [mm/y]
$D_{s\text{-dot}}$	<b>-0.10 +/- 0.14 [ppb/y]</b>	<b>0.05 +/- 0.12 [ppb/y]</b>
$R_{x\text{-dot}}$	0.12 +/- 0.03 [mas/y]	0.12 +/- 0.03 [mas/y]
$R_{y\text{-dot}}$	-0.02 +/- 0.03 [mas/y]	0.02 +/- 0.03 [mas/y]
$R_{z\text{-dot}}$	0.02 +/- 0.03 [mas/y]	0.01 +/- 0.03 [mas/y]

In addition to the ‘geometric’ test of the scale implied by different spans of SLR data, we have also examined the dynamic definition of the scale, through the estimation of the  $GM_E$  constant from the different data sets. The SLR technique obtains the definition of the scale from the adopted speed of light in vacuum,  $v_c$ , however, because it involves satellite orbits, this scale should also be consistent with the size of the orbit as it is constrained by Kepler’s third law. With  $v_c$  fixed, we can monitor any changes in the intrinsic SLR scale through the estimation of  $GM_E$ . The historical data were reduced in three different ways (arc-lengths), in order to verify that this is also not a factor in the development of the TRF: fortnightly (F), monthly (M), and quarterly (Q) arcs. With each expansion of the arc-length, any unaccounted systematic errors in the description of the site-motions is smoothed out by averaging, since more data from other, non-affected sites contribute to the definition of the TRF over that interval of time. Table 3 indicates that a comparison of the  $GM_E$  estimates from these solutions to the value that we obtain from the weekly-arc (W) analysis for the 1993- 2005 period, shows no systematic difference, and certainly no scale change larger than the calibrated uncertainty of the estimates.

**Table 3.**  $GM_E$  estimates from two SLR data spans: 1993 – 2005 and 1976 – 2005.

Source of displayed $GM_E$	Value of $GM_E$
IERS Conventions 2003	398600.441500 x $10^9$ [ m <sup>3</sup> /s <sup>2</sup> ]
SSC (JCET) L 06 W 1993 - 2005	398600.441659 x $10^9$ [ m <sup>3</sup> /s <sup>2</sup> ]
SSC (JCET) L 06 F 1976 - 2005	398600.441634 x $10^9$ [ m <sup>3</sup> /s <sup>2</sup> ]
SSC (JCET) L 06 M 1976 - 2005	398600.441633 x $10^9$ [ m <sup>3</sup> /s <sup>2</sup> ]
SSC (JCET) L 06 Q 1976 - 2005	398600.441633 x $10^9$ [ m <sup>3</sup> /s <sup>2</sup> ]

We can reach two main conclusions from the above table: (a) the effect of the historical data in the intrinsic definition of the scale in SLR is at most at the level of 0.1 ppb, and (b) the effect of the arc-length used in the reduction of the data on the scale is even less significant, less than 0.002 ppb. A calibrated estimate of the accuracy of these estimates at the 99% level of confidence is 0.2 ppb or approximately 1.3 mm.

**Subset solution results**

We investigated the effect of the “evolution of the network” with the development of a number of TRFs from independent sub-sets of the data in various combinations (Figure 2). With only some thirteen years of data to work with, we went as far as  $\frac{1}{4}$  of the data, i.e. the smallest set of data spanned just over three years. This seemed to be marginally acceptable for a quality TRF, with six years being a comfortable minimum for a robust TRF product (specially for velocity estimates). We have two strategies in forming these subsets: (i) using similar amounts of data spanning the same period of time, and (ii) using the same amounts of data sampling totally different time periods. In the first case for example, we used  $\frac{1}{4}$  of the data to generate four different TRFs, each based on the weeks that span the same time-period, every subset formed by choosing every 4th week from the ensemble of all weeks available. In the second case, we also have four TRFs formed on the basis of approximately  $\frac{1}{4}$  the total data, but in this case we broke up the total interval in four equal-length intervals, so each TRFs is fit to data from a different period of time (and a different network with different conditions and performance).

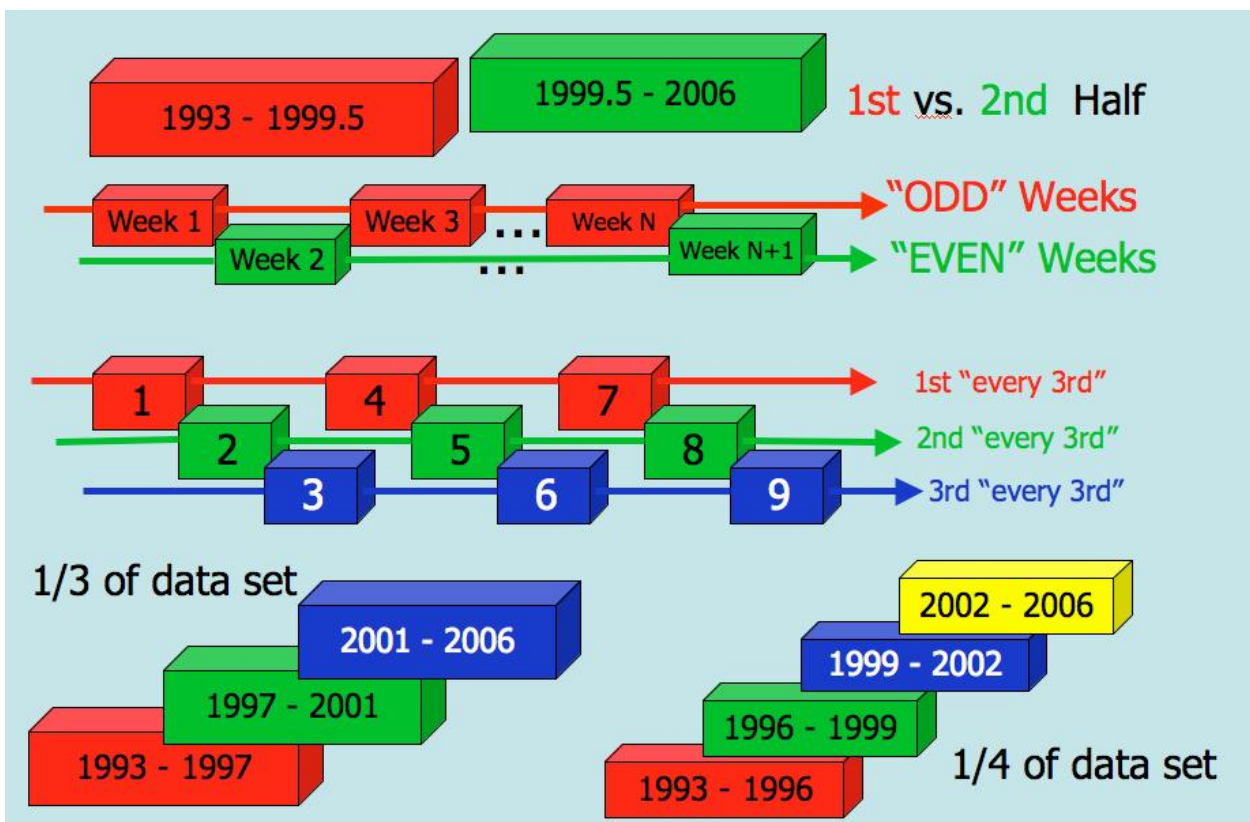


*Figure 2. The four groups of subset solutions used in this investigation*

Case	$\Delta X$ [mm]	$\sigma_{\Delta X}$ [mm]	$\Delta Y$ [mm]	$\sigma_{\Delta Y}$ [mm]	$\Delta Z$ [mm]	$\sigma_{\Delta Z}$ [mm]	3D $ \Delta $ mm	$\sigma_{3D\Delta}$ mm
3 <b>Odd</b>	-8.37	$\pm 10.91$	19.25	$\pm 10.78$	-4.20	$\pm 10.32$	<b>21</b>	$\pm 17$
4 <b>Even</b>	-12.62	$\pm 8.93$	5.15	$\pm 8.82$	-12.50	$\pm 8.44$	<b>18</b>	$\pm 16$
5 <b>@ 3rd</b>	-7.92	$\pm 18.84$	-3.87	$\pm 18.61$	3.56	$\pm 17.82$	<b>10</b>	$\pm 31$
6	-7.61	$\pm 8.66$	19.78	$\pm 8.56$	-15.33	$\pm 8.19$	<b>26</b>	$\pm 16$
7	-11.36	$\pm 10.41$	9.03	$\pm 10.28$	-11.58	$\pm 9.84$	<b>19</b>	$\pm 17$
8 <b>@ 4th</b>	-15.62	$\pm 21.76$	43.27	$\pm 21.49$	16.57	$\pm 20.57$	<b>49</b>	$\pm 36$
9	-17.75	$\pm 18.87$	16.31	$\pm 18.63$	-29.03	$\pm 17.84$	<b>38</b>	$\pm 33$
10	-6.61	$\pm 17.18$	-5.50	$\pm 16.97$	-11.56	$\pm 16.24$	<b>14</b>	$\pm 29$
11	-16.72	$\pm 12.01$	1.32	$\pm 11.86$	-9.92	$\pm 11.36$	<b>19</b>	$\pm 21$
1 <b>1/2</b>	-41.20	$\pm 35.82$	6.26	$\pm 35.38$	-10.10	$\pm 33.86$	<b>43</b>	$\pm 61$
2	1.74	$\pm 6.76$	8.06	$\pm 6.68$	7.28	$\pm 6.39$	<b>11</b>	$\pm 11$
12 <b>1/3</b>	-49.10	$\pm 22.39$	52.74	$\pm 22.11$	2.73	$\pm 21.16$	<b>72</b>	$\pm 38$
13	-3.07	$\pm 8.21$	-13.72	$\pm 8.11$	5.90	$\pm 7.76$	<b>15</b>	$\pm 14$
14	-16.95	$\pm 14.20$	5.72	$\pm 14.06$	4.28	$\pm 13.40$	<b>18</b>	$\pm 24$
15 <b>1/4</b>	-60.49	$\pm 23.68$	57.43	$\pm 23.39$	7.48	$\pm 22.39$	<b>84</b>	$\pm 40$
16	18.65	$\pm 31.40$	-57.81	$\pm 30.88$	-6.19	$\pm 29.50$	<b>61</b>	$\pm 53$
17	-0.27	$\pm 18.01$	-4.74	$\pm 17.79$	15.72	$\pm 17.03$	<b>16</b>	$\pm 31$
18	2.07	$\pm 12.29$	7.16	$\pm 12.18$	1.73	$\pm 11.60$	<b>8</b>	$\pm 21$

**Figure 3.** The four groups of subset solutions used in this investigation (top cases: same time-span, and bottom cases: disjoint time intervals).

We will limit the discussion of our conclusions to two items of importance to the ITRF: the definition of its origin and its axial rate. The results are summarized in Fig. 3, in terms of the differences in each component  $\Delta x$ ,  $\Delta y$ , and  $\Delta z$ , with respect to the solution obtained from the entire set of data. In order to facilitate their comparison we also formed a figure of merit, defined as the 3D positional difference, and formed as:

$$\Delta = \sqrt{\Delta x^2 + \Delta y^2 + \Delta z^2}.$$

We can draw several conclusions from this table:

- On average, each component is not determined to better than 6-8 mm (depends on time period)
- The 1993 to present data set is significantly non-uniform due to various factors
- There is a steady improvement over the years, however, we can see even 10-fold differences between different time-periods
- With the caveat that our calibrated error estimates are sufficiently realistic, and assuming that the second half of the 1993-2005 period is more representative of current network performance, we conclude that for a reliable definition of the origin of the TRF we need a data spanning more than ~6-7 years.

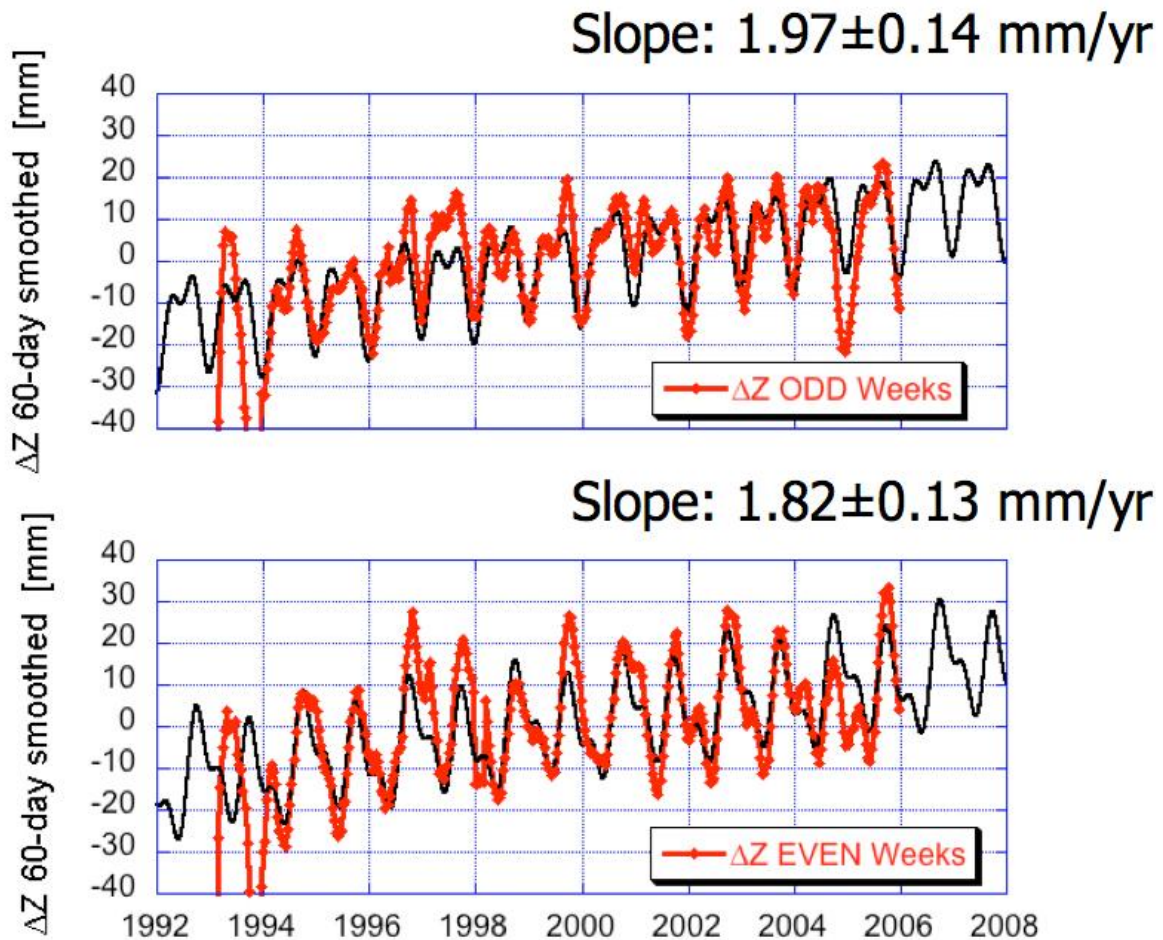


**Figure 4.** The time series of  $\Delta z$  (axial component of geocenter) from two independent subset solutions, each spanning the period 1993-2005.

With each subset solution we also obtained a time series of the weekly variations of the origin with respect to the geocenter. These were analyzed in a similar manner to the origin components themselves, i.e., in comparison to the series we obtain from our ensemble solution that spans the entire time period. The axial component is the only one that shows a significant secular trend, so we will use that in our example. Figure 4 gives an example of the recovered series and their fit to a model that includes a linear trend and three periodic terms, for the two subsets formed from the selection of the “even” and “odd” weeks (i.e. every other week used). The two subsets span the same time period with just one week “offset”, but each set has about half the data of the entire data set. It is apparent from these two cases that the secular trend recovered here is statistically insignificantly different from what we obtained from the entire data set (cf.  $\sim 1.7 \pm 0.1$  mm/y). There are differences though in the periodic components’ (not magnitude) and when we compare the results from subsets that span even smaller spans of data (less than half), then even the secular trend is not recovered correctly (sometimes we even get sign-reversals!). These observations lead us to the following conclusions:

- Secular trends from same size data span agree to 7-10%
- Secular trends from spans smaller than  $\sim 7$  years and different periods of time can differ up to 100%, indicating a highly non-stable network (shape, performance or a combination of both)
- The magnitude of the seasonal variations is stable when recovered from various subsets of the entire data set, but the phases seem to be sensitive to

that choice

- For the robust definition of secular trends and seasonal variations simultaneously, it is recommended that more than a decade of data (preferably from a stable network) be used.

### **Summary and future plans**

This study investigated the robustness of the definition of the origin and scale of the TRF from SLR data (only) and with the LAGEOS and LAGEOS 2 data available over the period 1993 to 2005. The conclusions we reached are that these data define the origin at epoch to no better than 10 mm. The monitoring of the secular motion of the origin depends strongly on the network evolution and its performance. For a robust estimate of temporal variations of the geocenter we need data sets that span a decade or more, with a stable network. In such cases, the secular trends can be estimated with an accuracy of about 10%.

For a complete rationalization of the observed error signatures and the performance of future networks, we need a set of very carefully controlled simulations (underway). Extension of this simulation to include the other techniques will give us the advantage to “negotiate” trade-offs between the techniques, since they all act in a complementary manner in the definition of the ITRF. This will allow better use of the available resources and full exploitation of the benefits from each technique.

### **References**

- [1] Altamimi, Z., P. Sillard, and Claude Boucher (2002), ITRF2000: A new release of the International Terrestrial Frame for earth science applications, *J. Geophys. Res.*, 107, NO. B10, 2214, doi:10.1029/2001JB000561
- [2] Pearlman, M.R., Degnan, J.J., and Bosworth, J.M., 2002. "[The International Laser Ranging Service](#)", *Adv. in Space Res.*, Vol. 30, No. 2, pp. 135-143, 10.1016/S0273-1177(02)00277-6.
- [3] Pearlman M., and co-authors (2005), Global geodetic observing system - Considerations for the Geodetic network infrastructure, 2005 IAG/IAPSO/IABO Joint Assembly, Cairns, Australia, August 22-26
- [4] Peltier, W. R., 2006, *private communication*.

## **FTLRS Ajaccio campaigns : operations and positioning analysis over 2002/2005**

F. Pierron<sup>1</sup>, B.Gourine<sup>2</sup>, P.Exertier<sup>1</sup>, P.Berio<sup>1</sup>, P.Exertier<sup>1</sup>, P. Bonnefond<sup>1</sup>,  
D.Coulot<sup>3</sup> and the Grasse/Ftlrs laser staff

1. Observatoire de la Côte d'Azur, GEMINI/UMR 6203-CNRS, Av N. Copernic, 06130 Grasse, France.
2. Centre National des Techniques Spatiales à Arzew (CNTS), Algeria
3. IGN, ENSG/LAREG, 6 et 8 Avenue Blaise Pascal, Cité Descartes, Champs-sur-Marne, 77455, France

### **Abstract**

*In the framework of JASON-1 project especially for Cal/Val aspects, Ftlrs has been deployed in Ajaccio for a six months campaign in 2005.*

*In the continuation of previous operations on the same site in 2002 the observations programs were carefully tuned to be pertinent on both aspects of scientific goals with new tools to optimize sky coverage for the data and technological issues like maintenance and operational costs.*

*In this paper, we'll present reports and results concerning station positioning with a very interesting combination of LAGEOS -1, -2, STELLA, and STARLETTE observations and comparison over 2002 and 2005 campaigns. An estimation of final accuracy will be discussed in such experiments of multi occupation site and operational issues will be commented.*

### **1. Introduction and Operational issues for Corsica campaigns**

*The Ajaccio site is the main calibration site of the satellite altimeters in the Mediterranean area*



*Typical setup of the station (Corsica 2002 and 2005 )*

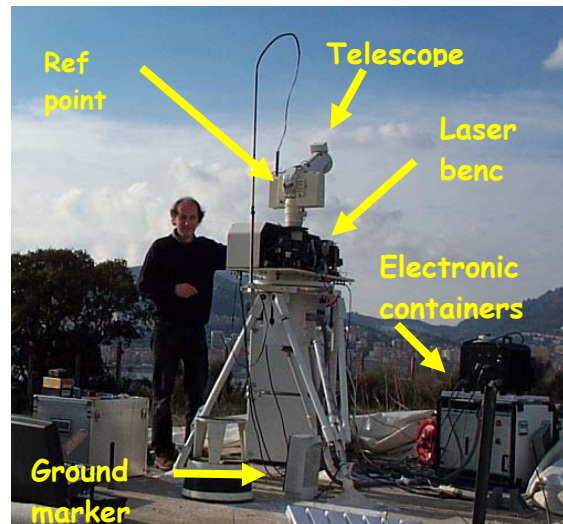
The SLR technique is the major contributor to the altimeter calibration: SLR data of the whole network are used to derive ultra precise orbit of altimeter satellites (in combination with DORIS and GPS data) and FTLRS conducts comparative laser distance measurements between the facility and satellite radar altimeters.

The objectives are the following :

- Absolute Sea level monitoring, altimeter calibration and orbit validation (CAL/VAL) of the Topex/Poseidon, Jason-1 and Envisat satellites from the Ajaccio site (Corsica-France)
- Estimation of the satellite altimeters biases and drifts

- Need for carrying out accurate SLR positioning from geodetic satellites observations

The FTLRS is a highly mobile Satellite Laser Ranging (SLR) system dedicated to the tracking of geodetic satellites equipped with retroreflectors. This instrument was developed by the Observatoire de la Côte d'Azur (OCA) and the Centre National d'Etudes Spatiales (CNES) in collaboration with the Institut National des Sciences de l'Univers (INSU) and the Institut Géographique National (IGN)



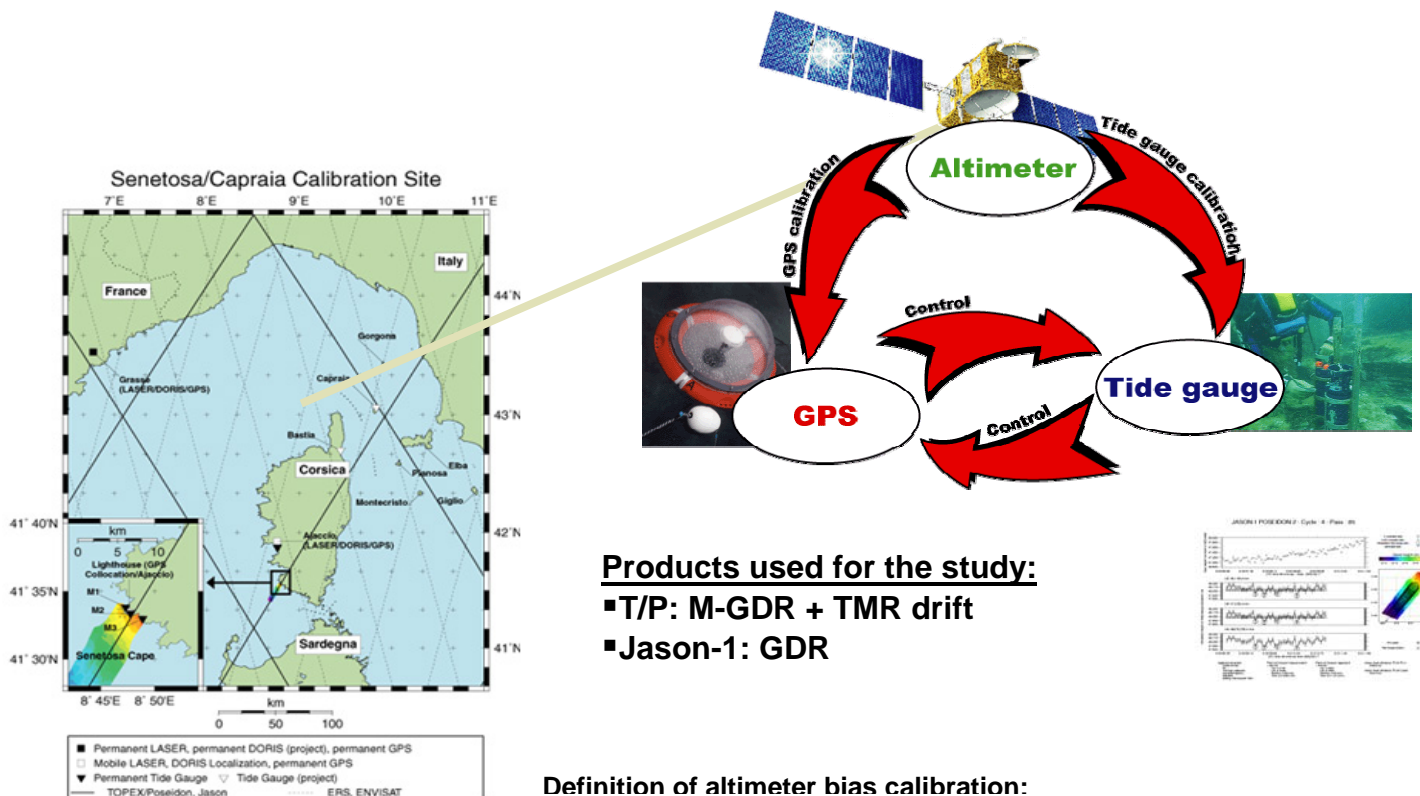
For these campaigns, Ftlrs system is deployed inside a French naval base near Ajaccio on a hill, close the sea and at some thirty kilometer from Senetosa Cape where are installed tide gauges and performed GPS buoys experiments near exact calibration point.

Two major campaigns have been organized at this site: January-September 2002 for 10 months and May-October 2005 for 5 months.

**Two major campaigns have been organized at this site: January-September 2002 for 10 months and May-October 2005 for 5 months.**

**2. Jason1 absolute calibration/validation configuration :**

- A geodetic site at Ajaccio with FTLRS settled for some months.
- An in-situ site at Senetosa cape under the track N°85.



**Products used for the study:**

- T/P: M-GDR + TMR drift
- Jason-1: GDR

**Definition of altimeter bias calibration:**

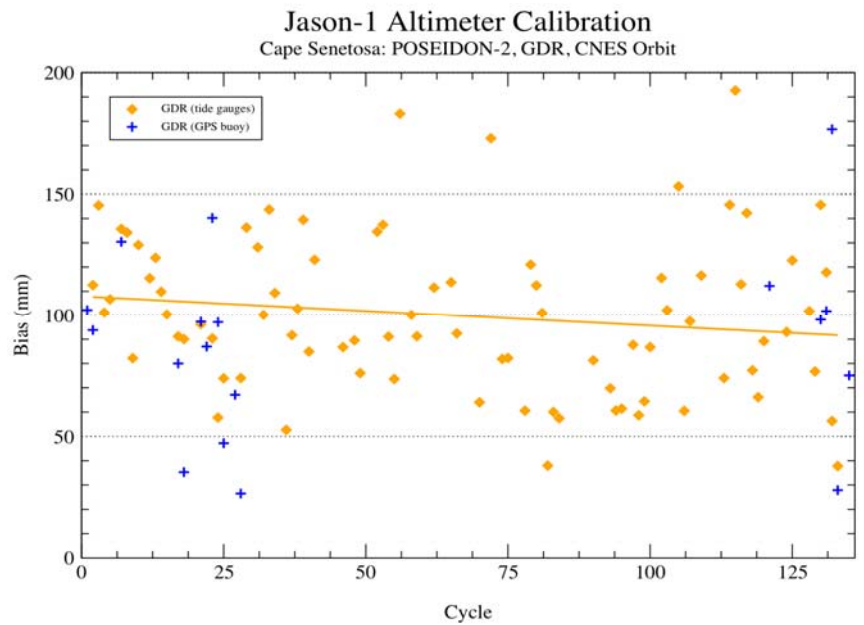
$$\text{sea height bias} = \text{altimeter sea height} - \text{in situ sea height}$$

Sea height bias < 0 meaning the altimetric sea height being too low (or the altimeter measuring too long)  
 Sea height bias > 0 meaning the altimetric sea height being too high (or the altimeter measuring too short)

The Senetosa site allows performance of altimeter calibration from tide gauges as well as from a GPS buoy.

At Senetosa POSEIDON-2 altimeter bias is  $+100 \pm 4$  mm, based on the whole set of GDR-A products (135 cycles).

The large negative trend is due to JMR (Wet Troposphere) in GDR-A and has been solved in recent analysis works



### 3. Scientific investigation for Positioning

#### ➤ Positioning with 4 geodetic satellites



**Lageos-1**  
**Lageos-2**

**Starlette**  
**Stella**



#### ➤ Goals of this positioning :

- To maintain geodetic accuracy of the FTLRS position in Ajaccio site (Corsica) between the two campaigns
- To provide high accuracy local orbits for the Jason-1 altimeter calibration

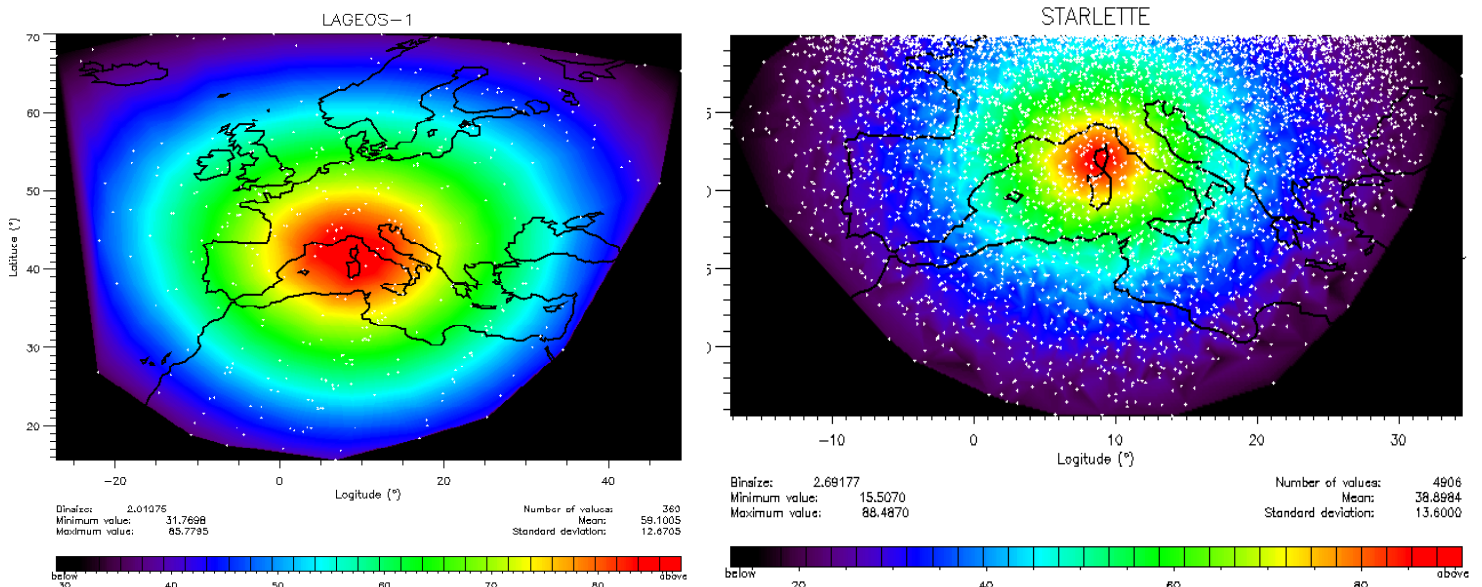
#### ➤ Main steps of the work methodology

- Orbit computation
- Positioning of the FTLRS Station with Multi satellite combination.

#### Npts data on the sky for 2005 campaign :

- High Elevation Orbiting Satellites:  
Few measurements on Lageos satellites, particularly at low elevation ( $40^\circ$ ), and irregular distribution of these data over the Ajaccio site
- Low Elevation Orbiting Satellites:  
Ten times more range data on Starlette/stella relative to Lageos, and homogeneous distribution of the range data over the Ajaccio site

The quality of FTLRS positioning is very dependent on the accuracy of orbits, and Starlette and Stella are more sensitive to remaining uncertainties in the dynamic models (gravitational and non gravitational effects).



**Maps of the range data distribution during the 2005 campaign (05 months) above Ajaccio site**

Since few years, thanks to new space mission like Grace, the community got an improvement of the gravity field models. The method in our analysis is to use an accurate field gravity model for the LEO computation and a multi-satellite combination.

**A. Parameters for orbit computation :**

-Gins software (developed by CNES)

-Dynamical models used :

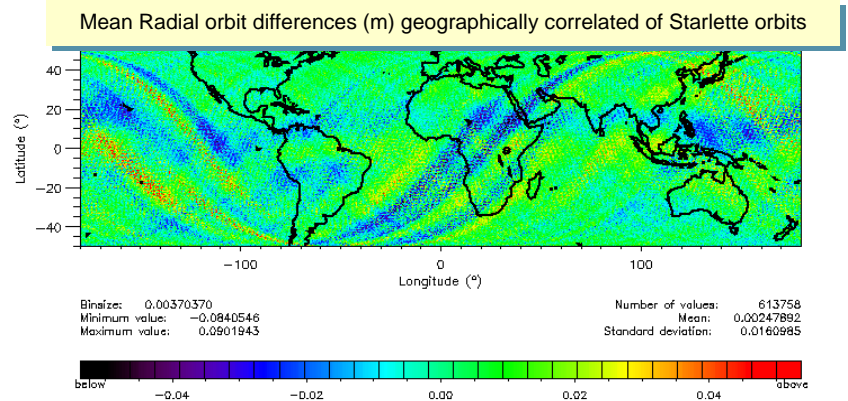
Model	Designation
Gravity field	<i>Grim5-c1 or Eigen-Grace03s</i>
Atmospheric pressure	<i>ECMWF</i>
Solar flow	<i>Acsol2</i>
Atmospheric Density	<i>Dtm-94bis</i>
Ocean tides	<i>Fes-2002</i>
Planets	<i>De403bdlf.ad.ibm</i>
Earth Orientation Parameters	<i>Eop-c04</i>

-Terrestrial reference frame : ITRF 2000

-Computation by successive arcs (9 days for Lageos 1/Lageos 2 and 6,5 days for Starlette/Stella ) with overlapping periods (1 day for Lageos 1/2 and 0,75 days for Starlette/Stella) allowing to control the orbits quality of successive arcs and to limit the “butterfly effect” on the arc computation.

-Effect of gravity field model :

On 32 arcs of Starlette/Stella in 2005, it appears that the Mediterranean area is less affected by a permanent effect.



The Lageos orbits are more precise and less affected by the change of gravity field model, but for Stella/Starlette, we have an improvement of orbit precision of +/- 5mm with Eigen-Grace03s model.

Satellite	2002 campaign		2005 campaign	
	GRim5-c1	Eigen-Grace03s	Grim5-c1	Eigen-Grace03s
LAGEOS-1	13	-	11	11
LAGEOS-2	10	-	10	09
Starlette	23	18	23	18
Stella	23	19	21	16

**B. Positioning of Ftlrs station :**

**-Matlo Software (developed by OCA) (Coulot 2005)**

This software dedicated to laser positioning (coordinates updates+ range bias/satellite) in a multi-satellite combination compute a global solution and Time series solution.

Range bias	$B_{LAG-1}$ (mm)	$B_{LAG-2}$ (mm)	$B_{STAR}$ (mm)	$B_{STEL}$ (mm)	Coordinate updates	$d\phi$ (mm)	$d\lambda$ (mm)	$dh$ (mm)	$\rho_{dh-Bias}$ (%)
Glob. Sol. (1)	+12.0	+12.2	-3.9	-6.4	Glob. Sol. (1)	+4.3 ± 0.6	-10.1 ± 0.6	+11.7 ± 1.8	94.4
Glob. Sol. (2)	+4.8	+4.6	-4.9	-4.9	Glob. Sol. (2)	+4.3 ± 0.5	-3.6 ± 0.4	+3.0 ± 1.4	94.4
7d. Sol. (1)	+11.7	+13.8	-4.6	-5.4	7d. Sol. (1)	+4.4 ± 0.6	-8.6 ± 0.5	+13.8 ± 0.6	55.4
7d. Sol. (2)	+4.9	+3.3	-5.6	-4.3	7d. Sol. (2)	+4.1 ± 0.4	-2.9 ± 0.4	+4.0 ± 0.4	55.4

The Main objective has been to reduce the correlation between the range bias and the vertical component. To do that, we compared a global solution (with coordinates and range biases estimated with the whole data) and 7 days solution (with bias/sat supposed constant remain estimated with the whole data). In the Global solution, the correlation remains to high between biases and dh, some parts of the bias may move to dh and vice versa.

**In the 7 days solution, the correlation decreases significantly (55%), this solution is finally held**

**C. Results and Analysis: adjusted Ftlrs parameters over 2002 & 2005 campaigns:**

with :

-Time series solution

-Eigen-Grace03s model

Coordinate updates	$d\phi$ (mm)	$d\lambda$ (mm)	$dh$ (mm)	$\rho_{dh-Bias}$ (%)
2002	-0.8 ± 0.7	+1.6 ± 0.7	+0.2 ± 0.8	55.8
2005	+4.1 ± 0.4	-2.9 ± 0.4	+4.0 ± 0.4	55.4

	Lageos-1 (mm)	Lageos-2 (mm)	Mean Lageos-1&2 (mm)	Starlette (mm)	Stella (mm)	Mean Starlette/Stella (mm)	Global mean (mm)
2002	-5	-7	-6	-13	-13	-13	-10
2005	+5	+3	+4	-5	-5	-5	0

- **The difference between Lageos and Starlette/stella biases** are probably coming from satellite signature and Ftlrs detection process.
- **adjusted values of Ftlrs range bias in 2002 campaign of -10 mm explained a posteriori:**
  - o Non linearity of Stanford chronometer not modelised at this epoch : -4.2 mm
  - o Geometrical path for external calibration not adjusted : - 3mm
  - **Total : 7.2mm**
- **The adjusted values of Ftlrs mean range bias for last campaign 2005 is very small and confirm agreement between analysis and technological corrections applied ( Stanford non linearity, ground target measurements,..)**

**D. Solved coordinates**

Geographical coordinates differences from (Exertier et al., 2004) solution:	Coordinates differences	$\Delta\varphi$ (mm)	$\Delta\lambda$ (mm)	$\Delta h$ (mm)
	2002	$+0.5 \pm 0.7$	$+2.7 \pm 0.7$	$-1.2 \pm 0.8$
	2005	$+4.1 \pm 0.4$	$-2.9 \pm 0.4$	$+4.0 \pm 0.4$

Stability :

Campaign	Number of solution	$\sigma_\varphi$ (mm)	$\sigma_\lambda$ (mm)	$\sigma_h$ (mm)	$\sigma$ (mm)
<b>2002</b>	28	14.6	13.1	10.5	<b>12.</b>
<b>2005</b>	20	7.5	12.3	10.5	<b>10.</b>

-Global mean of bias (-5mm): very close to the published one (-7mm)

-Coordinate updates values for 2002 and 2005 are at 3mm level in average relatively to previous solution.

-Coordinates differences are very small at level of residuals errors in the ITRF2000 velocities

-No significant differences between 2002 and 2005 coordinates (at level of the tectonic movement): FTLRS point is locally stable.

**4. Conclusion and Prospects:**

- **Multi-satellite combination** has allowed to palliate lack of measurements on high satellites
- The improvement of the dynamical models, notably of the terrestrial gravity field (thanks to the GRACE satellite data ( *Eigen-Grace03s*) has permitted a precise computation of the orbits, in particular for the low satellites, and so a more precise geographical positioning,
- **Interesting decorrelation (~ 40%)** is obtained between the range bias and the station vertical component, using the time series solution (MATLO),
- **The station position is stable** between the two observation campaigns,
- In conclusion, the FTLRS has allowed a **precise terrestrial positioning**. That confirms its importance for the absolute calibration process of oceanographic satellites.

---

## SLR-Based Evaluation and Validation Studies of Candidate ITRF2005 Products

Erricos C. Pavlis<sup>1,2</sup>, M. Kuzmich-Cieslak<sup>1</sup> and D. E. Pavlis<sup>3,2</sup>

1. Joint Center for Earth Systems Technology (JCET), Univ. of Maryland Baltimore County, Baltimore, MD, USA
2. NASA Goddard Space Flight Center
3. SGT, Inc.

Contact: [epavlis@umbc.edu](mailto:epavlis@umbc.edu) / Fax: +1 410 455 5868

### Abstract

*The recent release of candidate solutions for adoption of the new ITRF2005 International Terrestrial Reference Frame (ITRF) initiated numerous tests and comparisons over the past months. This presentation focuses on the evaluation tests we performed with the ITRF2005P and ITRF2005D products, primarily with Satellite Laser Ranging (SLR) tracking data. Since over two decades now, SLR tracking data contribute to the definition of the TRF, primarily in defining its origin and scale. LAGEOS 1 and 2 are the main targets contributing to this, and we use their data, as well as a limited number of independent data to gauge the improvement gained by going from ITRF2000 to either of the two new candidate solutions. An easy and immediate observation is that either of them is only slightly different from ITRF2000, in contrast to what was observed during the release of ITRF2000. This seems natural though, since ITRF2000 dealt with many problems observed with its predecessor and used a uniformly high quality input from nearly all techniques. We concentrate here on the differences between the two and the impact of such factors as the improvements in the analysis methodology, the underlying models, the use of IERS Conventions 2003, and the latest improvements in modelling SLR observations.*

### Introduction

Since over two decades now, SLR tracking data contribute to the development of the ITRF, primarily in defining its origin and scale. The release of ITRF2000 in 2001 ushered a new era of TRF quality and performance (Altamimi *et al.*, 2002). The recent (mid-2006) release of candidate solutions for adoption of the new ITRF2005 initiated numerous tests and comparisons over the past months. This presentation focuses on the evaluation tests we performed with the ITRF2005P (from IGN) and ITRF2005D (from DGFI) products, primarily with SLR tracking data. In contrast to what was experienced during the release of ITRF2000, the release of the new models did not bring about order-of-magnitude changes, but rather small adjustments and corrections, either for sites that appeared ‘after’ the release of ITRF2000 or whose ITRF2000 estimates were based on too limited a set of data for meaningful results.

### Initial tests for Precision Orbit Determination (POD)

As a first test of the two candidate models we looked at their performance on the LAGEOS and LAGEOS 2 data that were used in their development. From the initial tests on ITRF2005P, which was released first in early summer of 2006, it became obvious that the VLBI-consistent scale imposed on this model because of the observed scale discrepancy between SLR and VLBI, led to a TRF with inferior performance even on the SLR data that were used in its development.

When however we applied a scale adjustment to make it consistent with the intrinsic SLR scale or allowed for a scale adjustment in our tests, the two models performed very similarly, and only marginally better than ITRF2000, except for the few sites that either did not appear in ITRF2000 or had poor ITRF2000 estimates (Table 1).

**Table 1.** Weekly RMS values from the weekly operational ILRS products in comparison to the old (ITRF2000) and new (ITRF2005P), ITRFs (results courtesy Cecilia Sciarretta/Telespazio, S.p.A.).

Group RMS [mm]	ITRF2000	ITRF2005	ITRF2000	ITRF2005	ITRF2000	ITRF2005
	June 3, 2006		June 10, 2006		June 17, 2006	
All sites (24)	40	8	36	9	32	9.6
Core sites (16)	13	7	13	8	12	8

Several SLR analysts did similar POD tests and the main conclusion from all of these tests is that the new models perform very similarly, and not much different from ITRF2000, for the well-determined sites common to both TRFs. The POD tests we performed were limited to data from the period 2003 to 2006.5, and only for the sixteen (16) “Core SLR” sites as identified by the ILRS ACs’ operational procedures. A summary of the RMS of fit per site for either of the two new models and ITRF2000 are shown in Tables 2 (for LAGEOS) and 3 (for LAGEOS 2).

A quick observation from Tables 2 and 3 is that overall, ITRF2005D performs slightly better than ITRF2005P does, especially in the case of LAGEOS 2. Note that unlike ITRF2005P, ITRF2005D *does not* require any adjustment to its scale or scale rate in order to achieve this performance. Despite this fact, absent any substantiated errors in the development of ITRF2005D, and ignoring all official objections by the International Laser Ranging Service (ILRS), (Pearlman *et al.*, 2002), the final officially adopted model for ITRF2005 was a slightly modified version of ITRF2005P (without any changes with respect to the SLR-VLBI scale issue).

**The scale difference between ITRF2005P and SLR**

The scale difference between the new and old ITRF (about 1.4 ppb at 2000.0 or ~10 mm, and -0.15 ppb/y or -1 mm/y), intrigued all SLR analysts involved in the evaluation and validation of the new model. Several theories were formed and tested, all of them quickly eliminated following extensive and copious tests, in most cases cross-checked through repetition by more than one group. We list some of the more plausible ones here.

A possible error in the adopted value of  $GM_E$  was quickly discarded, since it would require an unreasonably large  $\Delta GM_E \approx 0.0025 \times 10^9$  or an equally unreasonable change in the CoM value for the two LAGEOS (~20 mm). Next, the differences in the submitted SLR contributions to ITRF2000 and ITRF2005 were examined closely. The

**Table 2. LAGEOS POD: Core sites' RMS of fit using ITRF2000, ITRF2005P and ITRF2005D, and differences. RMS in red (negative) indicates ITRF2005P performs better than ITRF2005D.**

SITE NAME	SITE ID	ITRF2000 (IGN)		ITRF2005P (IGN)		ITRF2005D (DGFI)	
		RMS [mm]	ARMS [mm]	RMS [mm]	RMS [mm]	RMS [mm]	ARMS [mm]
			2000-2005P		2005P-2005D		2000-2005D
BEIJING, PRC	7249	22.41	4.90	17.51	1.10	16.41	6.00
GRASSE, FRANCE	7835	10.45	2.54	7.91	-0.12	8.03	2.42
GFZ POTSDAM, DE	7836	13.11	2.60	10.51	-0.84	11.35	1.76
GRAZ, AUSTRIA	7839	9.46	1.48	7.98	-0.19	8.17	1.29
HALEAKALA, HI	7210	17.87	3.29	14.58	2.50	12.08	5.79
MLRO, MATERA, IT	7941	10.87	2.51	8.36	0.67	7.69	3.18
MLRS, TEXAS, USA	7080	13.54	2.00	11.54	1.11	10.43	3.11
YARRAGADEE, AUSTRALIA	7090	11.33	0.48	10.85	1.02	9.83	1.50
GGAO, WASHINGTON, DC	7105	12.35	1.14	11.21	-1.03	12.24	0.11
MON. PEAK, CA	7110	14.41	1.40	13.01	0.92	12.09	2.32
HARTESBESTHOEK, SA	7501	14.45	4.24	10.21	0.43	9.78	4.67
RGO, ENGLAND	7840	9.77	0.78	8.99	0.60	8.39	1.38
SALRO, SAUDI ARABIA	7832	12.59	2.53	10.06	-0.22	10.28	2.31
SIMOSATO, JAPAN	7837	17.13	2.58	14.55	-0.20	14.75	2.38
ZIMMERWALD, CH	7810	8.97	-0.86	9.83	0.51	9.32	-0.35
WETTZELL, DE	8834	11.36	1.75	9.61	0.34	9.27	2.09

**Table 3. LAGEOS 2 POD: Core sites' RMS of fit using ITRF2000, ITRF2005P and ITRF2005D, and differences. RMS in red (negative) indicates ITRF2005P performs better than ITRF2005D**

SITE NAME	SITE ID	ITRF2000 (IGN)		ITRF2005P (IGN)		ITRF2005D (DGFI)	
		RMS [mm]	ARMS [mm]	RMS [mm]	ARMS [mm]	RMS [mm]	ARMS [mm]
			2000-2005P		2005P-2005D		2000-2005D
BEIJING, PRC	7249	19.11	3.60	15.51	0.89	14.62	4.49
GRASSE, FRANCE	7835	10.58	3.47	7.11	0.34	6.77	3.81
GFZ POTSDAM, DE	7836	11.96	1.23	10.73	0.91	9.82	2.14
GRAZ, AUSTRIA	7839	8.63	1.34	7.29	0.30	6.99	1.64
HALEAKALA, HI	7210	16.33	3.61	12.72	1.68	11.04	5.29
MLRO, MATERA, IT	7941	10.60	2.37	8.23	0.62	7.61	2.99
MLRS, TEXAS, USA	7080	13.21	1.93	11.28	1.32	9.96	3.25
YARRAGADEE, AUSTRALIA	7090	10.87	0.09	10.78	2.22	8.56	2.31
GGAO, WASHINGTON, DC	7105	11.80	1.24	10.56	0.10	10.46	1.34
MON. PEAK, CA	7110	12.73	0.53	12.2	1.33	10.87	1.86
HARTESBESTHOEK, SA	7501	16.53	5.19	11.34	1.33	10.01	6.52
RGO, ENGLAND	7840	8.74	-0.08	8.82	1.15	7.67	1.07
SALRO, SAUDI ARABIA	7832	11.22	1.95	9.27	0.25	9.02	2.20
SIMOSATO, JAPAN	7837	17.35	3.10	14.25	-0.60	14.85	2.50
ZIMMERWALD, CH	7810	9.23	-0.09	9.32	0.90	8.42	0.81
WETTZELL, DE	8834	10.92	1.20	9.72	0.83	8.89	2.03

SLR contribution to ITRF2005 had some basic differences from what was submitted to ITRF2000:

- The new submission used the Mendes-Pavlis (2004) refraction model.
- Only the data spanning 1993 to end of 2005 were used instead of the 1976 -2000 that was used in ITRF2000.

The first difference was quickly discarded since the same SLR contributions were used in both ITRF2005 versions, P and D. Additionally, tests that were done to quantify the effect of the new refraction model (~0.4 ppb at most), gave no indication of any such large systematic scale differences between the two solutions with the character of the observed scale differences between the two TRFs. Considering the magnitude of the change in the VLBI-SLR scale difference between the two TRFs, a possibly missing relativistic correction in the formulation of the SLR-modeled time-delay advocated by Ashby (2003), was also investigated. Despite the close agreement in magnitude, this correction was also rejected as the cause of the scale differences, a

conclusion that was also supported by Ashby himself (2006, personal communication). The POD tests were extended to include other SLR targets with orbits markedly different from LAGEOS, such as JASON-1 and Starlette. A corollary benefit from these POD tests was that while LAGEOS data were satisfactorily reduced with the scaled version of ITRF2005P, Starlette data for example showed a slight degradation. This implies either a certain distortion in the ITRF2005P solution, or a significant error in the CoM value used for Starlette. The latter is highly unlikely, but cannot be outright discarded.

A final plausible cause investigated as a possible explanation was the fact that the SLR contribution to ITRF2005 did not contain the historical LAGEOS data from the period 1976-1992. To test this last theory, we reduced all of that data and generated solutions that included that data, which we later compared to the two ITRF2005 solutions. Figure 1 shows the LAGEOS data distribution (weekly resolution) for the ILRS network from 1976 to early 2006. It can be seen that there is no dramatic difference between the two networks that supported the two ITRFs.

The SLR data for the period 1976-1992 is certainly not of the same quality as for the recent years, and the network had undergone several upgrade stages during that period. The initial predominantly NASA-supported network from 1976 to 1980 was more of a research and test-bed outfit than an operational one. The two international MERIT campaigns in the early 80s forced the upgrade of the network, its expansion and strengthening with the addition of several stations outside North America and

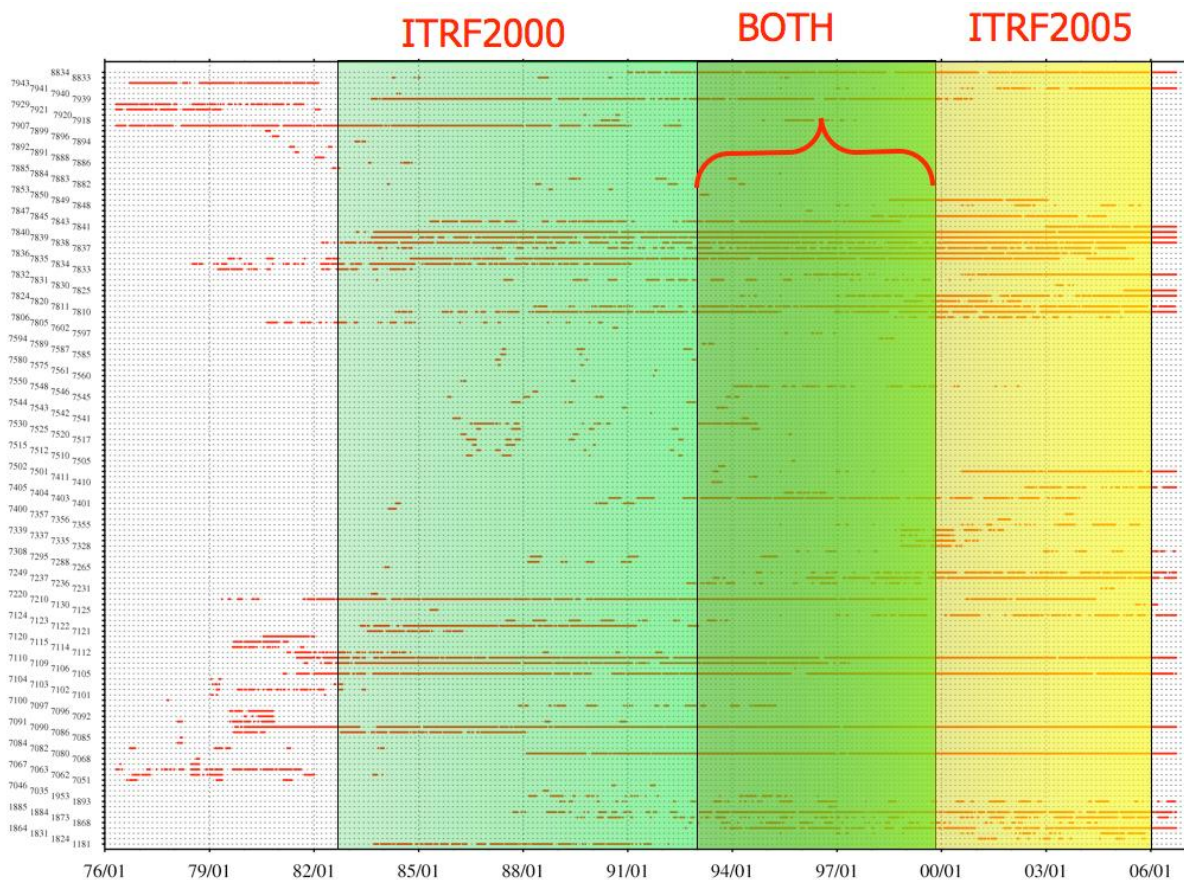


**Figure 1.** The LAGEOS and LAGEOS 2 data distribution for 1976 – 2006, and the portions used in the SLR submissions for the development of ITRF2000 (green) and ITRF2005 (yellow).

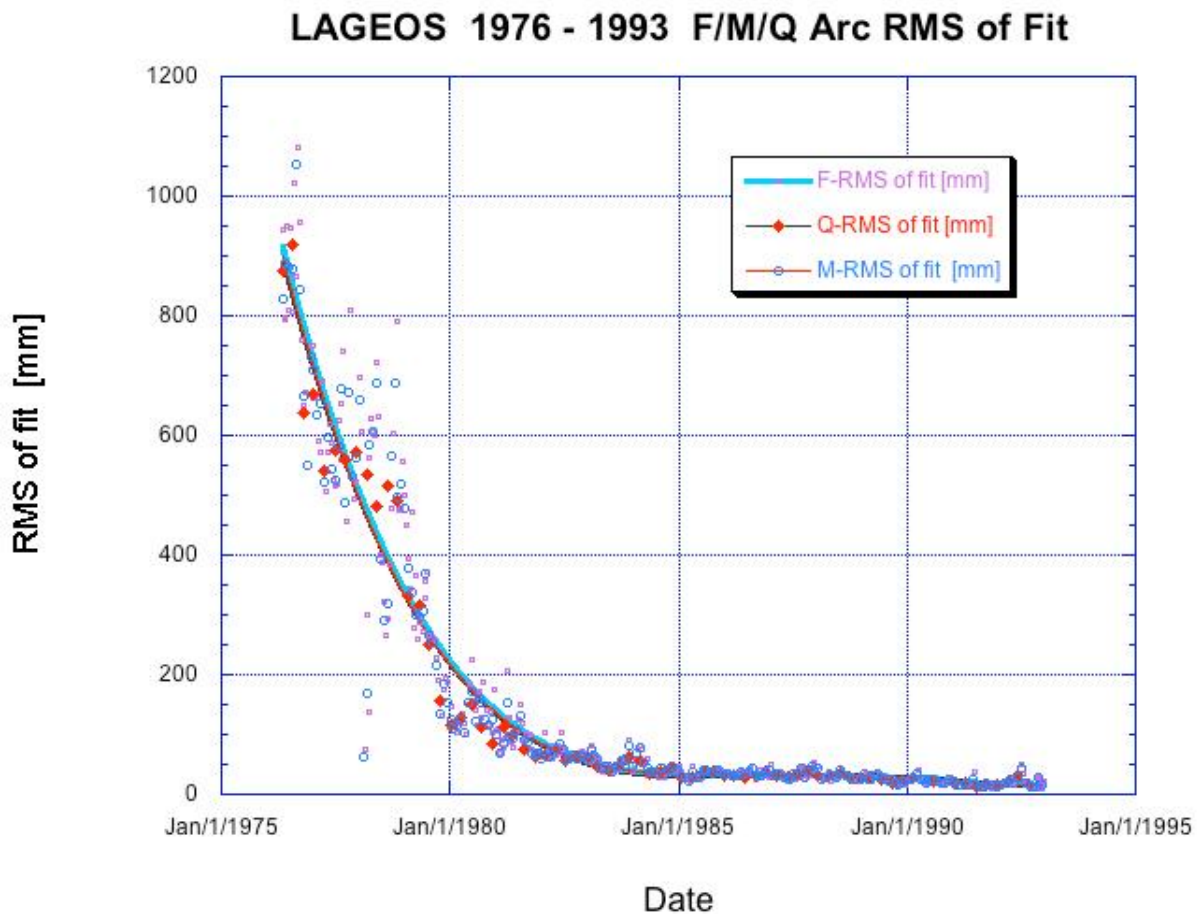


**Figure 2.** Orbital arc RMS of fit to LAGEOS data, 1976 – 1992. Results from reductions with three different arc-lengths are shown here, fortnightly (F), monthly (M) and quarterly (Q).

Europe, and ushered an era of operational mentality across continents, countries and agencies supporting these stations. As a result, the quality of the data improved by an order of magnitude, the quantity increased too, and internationally coordinated scheduling of operations was initiated for improved data yield. The result of these changes is reflected directly in the improved RMS of fit to the collected data, using the same models across all periods of time, as this is illustrated by the graph in Figure 2.

The development of TRFs that included the SLR data from the 1976-1992 period made little difference in their intrinsic scale and scale rate (~10% at most). On the other hand, it does improve the error statistics for sites that span both periods of time and it resulted in capturing in a single consistent frame all SLR sites that ever tracked either or both LAGEOS satellites. This result left the question about the SLR-VLBI scale difference in ITRF2005 open and unanswered, despite the fact that it eliminated a large number of serious candidate explanations.

### Recent (spring 2007) developments

During the 2007 General Assembly of the European Geosciences Union (EGU) in Vienna, Austria, MacMillan (2007) brought to the attention of the ITRF community the finding that the official International VLBI Service (IVS) submission to ITRF2005 had an error in the application of the pole tide, which generated a scale bias with respect to the true scale of ITRF.

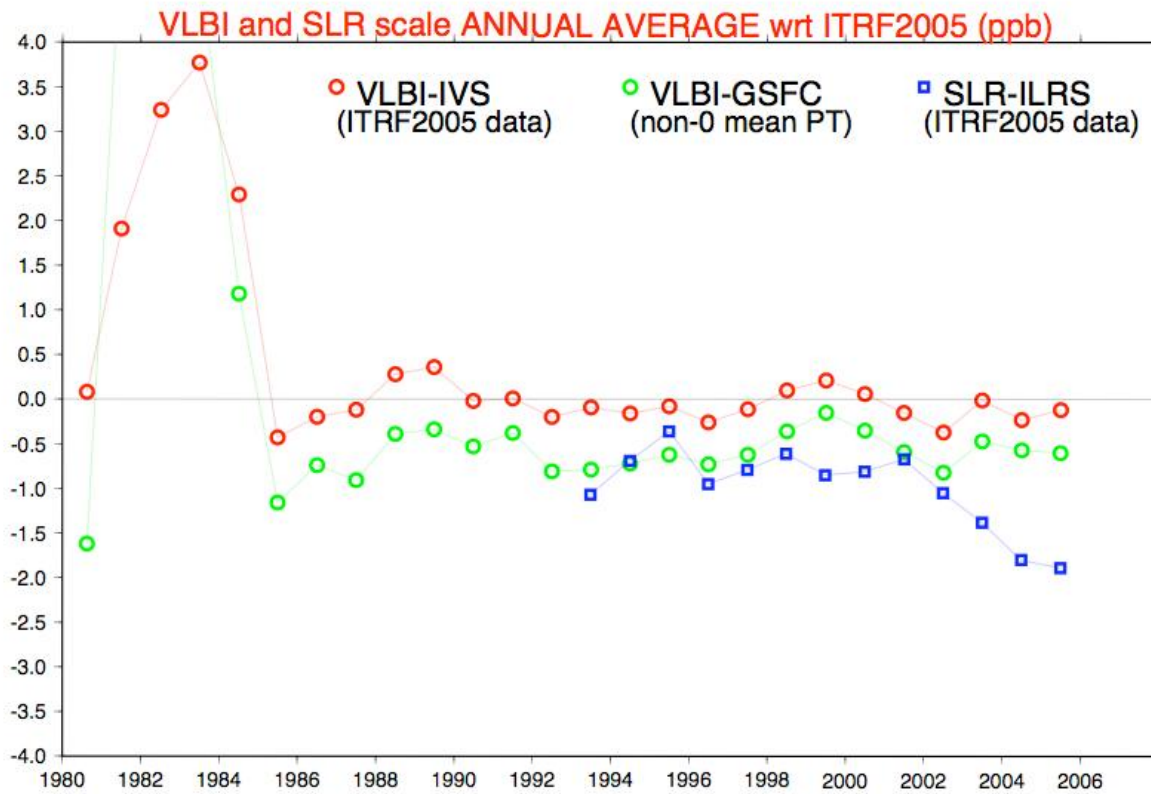


**Figure 3.** Time series of annual scale differences between various VLBI solutions and the SLR submission to ITRF2005, with respect to the ITRF2005 frame, (Altamimi, 2007).

After an exchange of corrected submission files, Z. Altamimi generated new test solutions that indicate that indeed, this error causes about 0.5 ppb scale bias between the SLR and VLBI frames of reference. This can be seen in the graph that Altamimi (2007) circulated via email on June 18, 2007, under the subject matter: “Pole tide effect on VLBI scale”. As you can verify from Figure 3, except for the period after 2004 when the SLR network covers only the one hemisphere of the globe, the scale difference between the two techniques is at the same level of discrepancy as it was during the development of ITRF2000. This means that there is really no reason for the exclusion of SLR from the definition of the scale of ITRF2005. The “significant” scale rate is also a result of the poor network configuration in the latter years and the consideration of some questionable site tie vectors (as pointed out by the DGFI combination center), and could have been dampened by appropriate weighting of the weekly contributions for that period of time, or editing of the ties (as DGFI did for ITRF2005D).

### Summary

The release of ITRF2005 in mid-2006 created a great commotion within the geodetic community with its departure from prior tradition, to adopt the scale implied by VLBI only, excluding SLR from the usual 50-50 sharing of this privilege. Additionally, the indication that SLR scale was not only off by more than 1 ppb from the true scale but also suffered from a significant rate change of -0.15 ppb/y, sent SLR analysts scrambling for answers. As we have seen here, none of the most plausible causes

could be found responsible for the observed discrepancy. The matter was never closed, and it was always suspected that in addition to the acknowledged effect of the deteriorating SLR network, either an error in another technique's submission were the cause, or the new way of constructing the ITRF, or a combination of all. The April 2007 findings of MacMillan's investigation in the VLBI scale definition explained for the most part the constant scale offset. The remaining scale rate effect seems to be the result of the new way the ITRF is constructed and the deterioration of the SLR network during 2004- 2006. The recent re-establishment of the SLR sites at Haleakala, Hawaii and Arequipa, Peru, and the new and improved re-analysis of the SLR data this year are expected to resolve many of these remaining issues and restore the faith of the ITRF community in SLR's unique ability to define the ITRF scale in the absolute sense.

## References

- [1] Altamimi, Z., P. Sillard, and Claude Boucher (2002), ITRF2000: A new release of the International Terrestrial Frame for earth science applications, *J. Geophys. Res.*, 107, NO. B10, 2214, doi:10.1029/2001JB000561
- [2] Altamimi, Z., (2007), email with subject matter "Pole tide effect on VLBI scale", June 18.
- [3] Ashby, N. (2003), Relativity in the Global Positioning System, *Living Rev. Relativity*, 6, , 1, available elect. at: <http://www.livingreviews.org/lrr-2003-1>, (revised 2007).
- [4] Ashby, N. (2006), private communication.
- [5] MacMillan, D. S. (2007), Determination of the reference frame scale with VLBI, Geophysical Research Abstracts, Vol. 9, 04545, 2007, 1607-7962/gra/EGU2007-A-04545.
- [6] Mendes, V.B., G. Prates, E.C. Pavlis, D.E. Pavlis, and R.B. Langley (2002), Improved Mapping Functions for Atmospheric Refraction Correction in SLR, *Geophys. Res. Lett.*, 29(10), 1414, doi:10.1029/2001GL014394.
- [7] Mendes, V.B., and E. C. Pavlis (2004), High-Accuracy Zenith Delay Prediction at Optical Wavelengths, *Geophys. Res. Lett.*, 31, L14602, doi:10.1029/2004GL020308.
- [8] Pearlman, M.R., Degnan, J.J., and Bosworth, J.M., 2002. "[The International Laser Ranging Service](#)", *Adv. in Space Res.*, Vol. 30, No. 2, pp. 135-143, 10.1016/S0273-1177(02)00277-6.

---

## **An Optimised Global SLR Network For Terrestrial Reference Frame Definition**

Ramesh Govind<sup>1</sup>

1. Geoscience Australia, Canberra, Australia

### **Abstract**

*It is a continuing debate on the current station distribution and geometry of the global SLR network. In order to design the optimum network for high quality geodetic products, a simulation study was undertaken. Data for previously closed or additional new stations was simulated and augmented into the existing available data set and the relevant geodetic parameters estimated. Weekly estimates of the degree one coefficients of the Earth's gravity field (centre of mass) is used as a measure of the influence of the simulated data with respect to the original solutions -- as determined from the observed data set. The simulated data, observed data, and the computation standards are described. On the basis of these results, an optimised global network of SLR stations is presented.*

## Performance of Southern Hemisphere Stations

John McK. Luck<sup>1</sup>

1. EOS Space Systems Pty.Ltd., Canberra, Australia

### Abstract

*The opening of the San Juan station in Argentina, and upgrades to other stations, has lifted the productivity of Southern Hemisphere stations to perhaps 40% of the global total, with a nice distribution in longitude. Various operational statistics will illustrate the improvements achieved up to the start of October 2006.*

### Introduction

The new San Juan station came on-line in March 2006, in collaboration with NAOC, Beijing. Its performance is highly impressive, and is significantly helping to satisfy the eternal cry for more SLR observations from the Southern Hemisphere.

At the same time, the BKG station TIGO at Concepcion, Chile has been upgraded to hectoHertz ranging with reliability enhancements, and has improved its output considerably in recent months. MOBLAS 8 at Papeete, Tahiti and MOBLAS 6 at Hartebeesthoek, South Africa are also making significant contributions. Of the Australian stations, MOBLAS 5 at Yarragadee continues to be the benchmark and workhorse station for the entire global SLR network, while the re-built EOS/GA station on Mount Stromlo is again one of the top performers.

Statistics for three 28-week time periods in Fig.1 and Table 1 show that data quantities from Southern Hemisphere stations have sustainably improved this year (2006). Other performance metrics are also displayed in this paper.

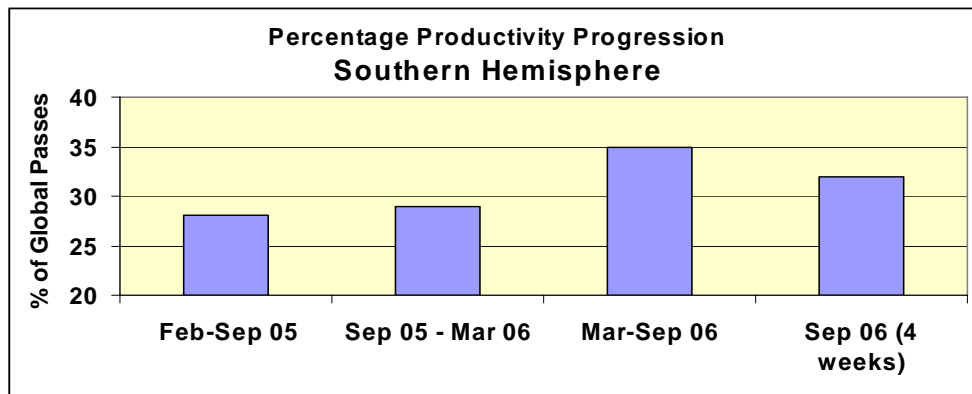


*Figure 1: Percentages of passes from Southern Hemisphere stations. Data extracted from CDDIS weekly SLRQL reports*

*Table 1: Pass percentages from S. Hemisphere stations, and also by ILRS Network*

Period	Southern Hemisphere	By Network (see (Luck, 2006))		
		WPLTN	NASA	EUROLAS
2005 Feb-Sept	28	38	15	46
2005 Sept – 2006 Mar	29	44	15	41
2006 Mar-Sept	35	42	16	41
2006 Sept 03-30	32	45	12	43

### Numbers of passes by station

In Fig.2, station totals are grouped by hemisphere. Some of the least productive Northern Hemisphere stations are not shown. Each point is a 28-week total.

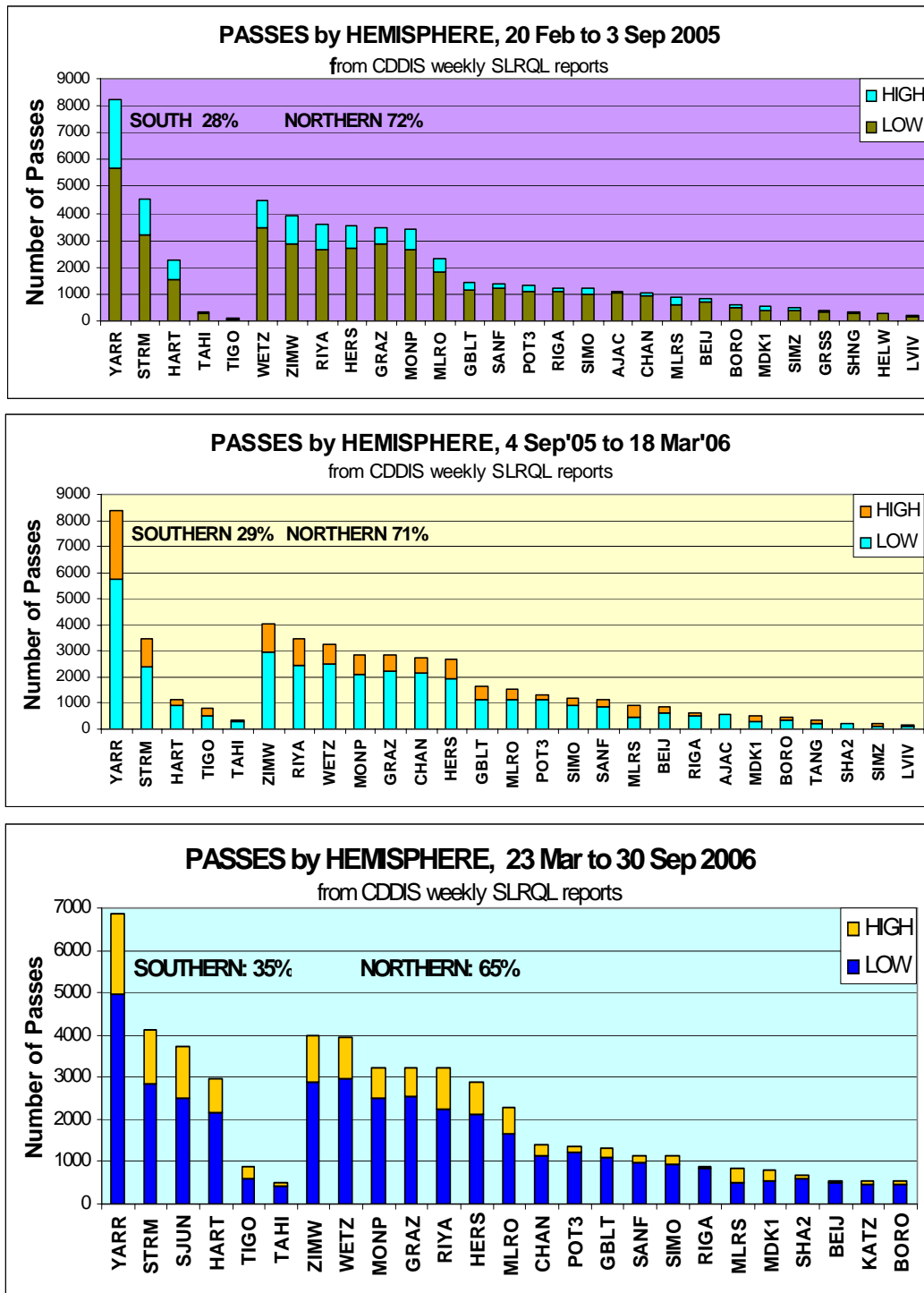


Figure 2: Station totals for three 28-week periods, grouped by hemisphere.

### Range bias stability

Fig.3 compares Southern and Northern Hemisphere stations for the RMSs since 19 March this year. They are the RMSs of range biases for LAGEOS I and II combined taken from NICT daily analysis reports, after some outlier editing.

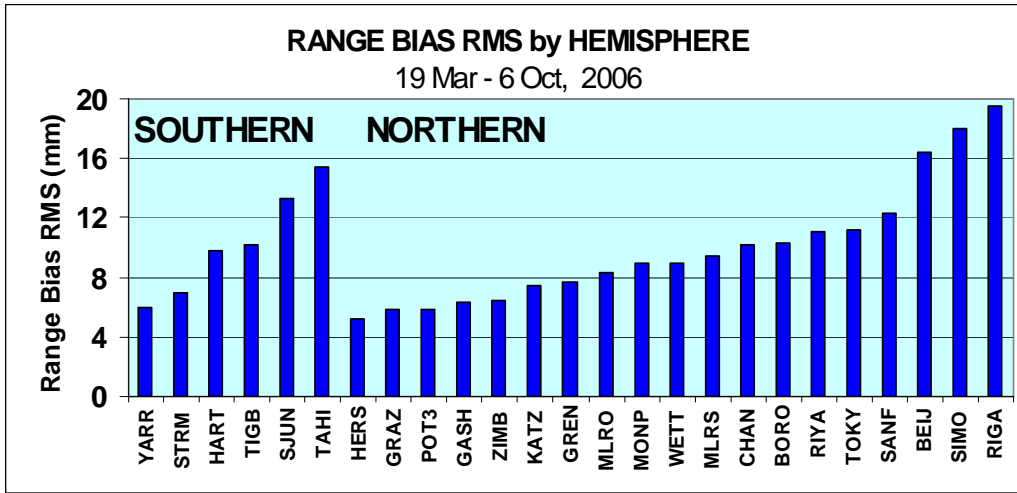


Figure 3: RMS of Range Bias per station per hemisphere, L1 & L2

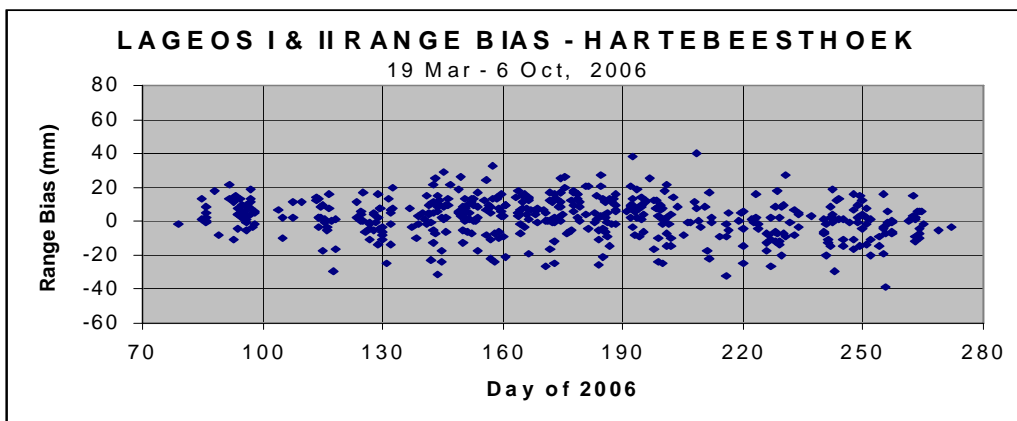
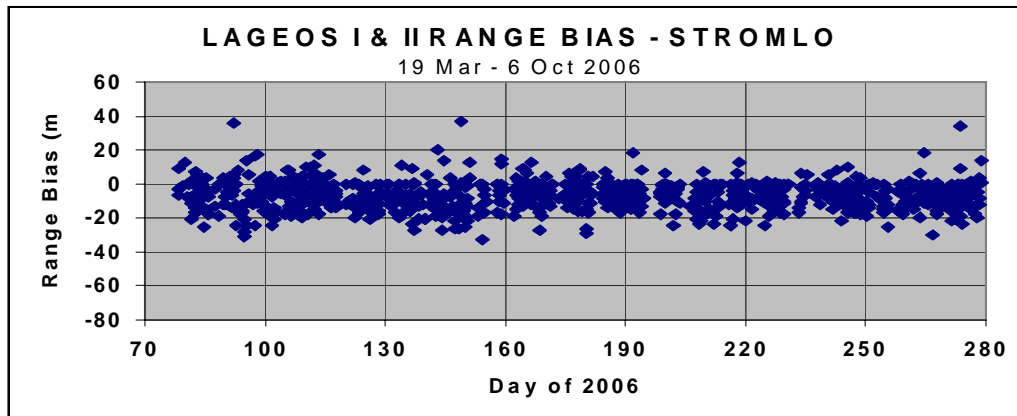
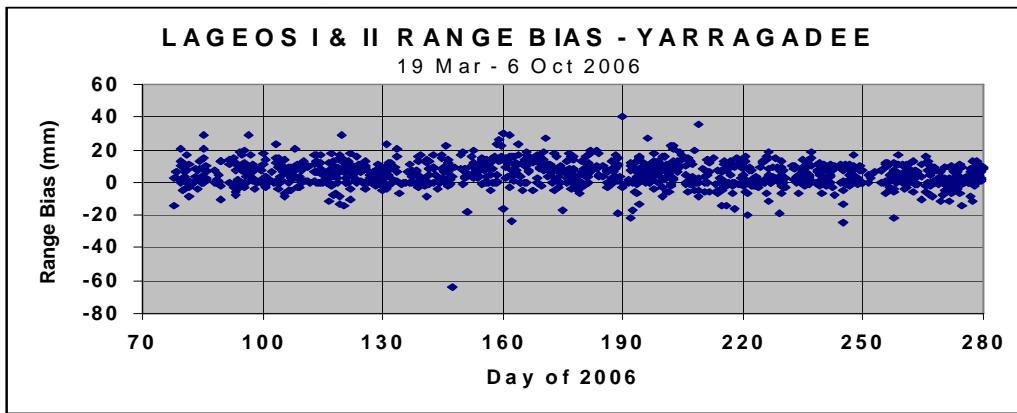
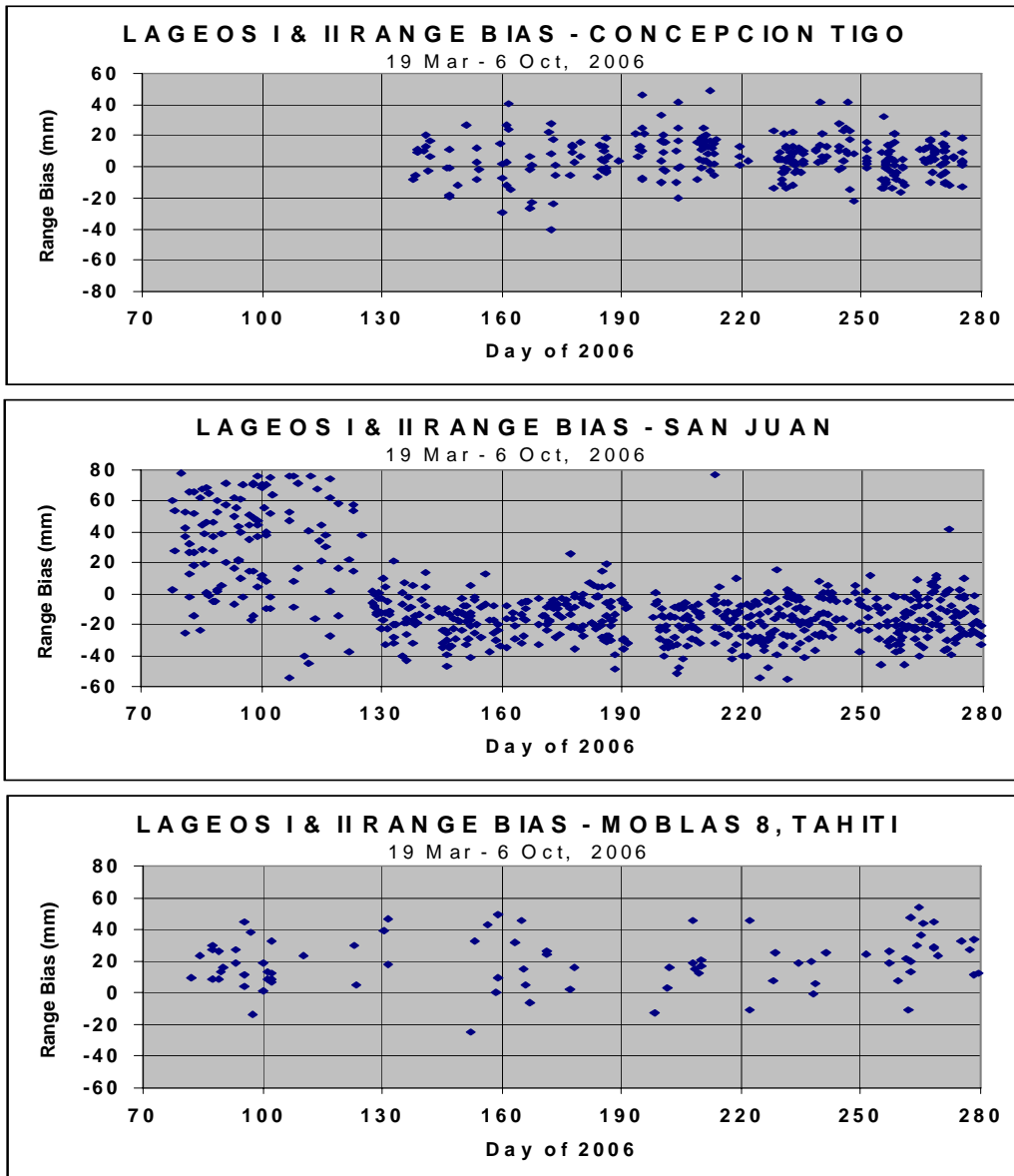


Figure 4a: Range Biases for LAGEOS I & II for Yarragadee, Stromlo and Hartbeesthoek .



*Figure 4b: Range Biases for LAGEOS I & II for Concepcion, San Juan and Tahiti.*

The time series for the 6 stations are shown in Figures 4a and 4b.

### **Normal points per pass**

This category reflects the observing efficiency of the stations, and is affected by skill in acquiring satellites and interleaving passes as well as factors like aperture, laser power, sun avoidance, priorities and bad weather. In general, a low ratio means more uncertainty in determining time bias, unless the few normal points are very well distributed throughout the pass. Fig 5 contrasts northern and southern hemispheres.

### **Normal point precision**

NP precision is calculated as the RMS of normal points about a trend-line fitted through the orbit residuals of the Analysis Centre's global solution. It is thus a measure of a station's internal consistency, and is affected by short-term variations in the station's observations, method of forming normal points, and errors in weather data as well as the Analysis Centre's methods of filtering and fitting. Fig.6 shows the results for the 28-week period Mar-Sep 2006 taken from the NICT daily analysis

reports, but only for passes containing at least four NPs, and Fig.7 shows the time-series for each station over the same period.

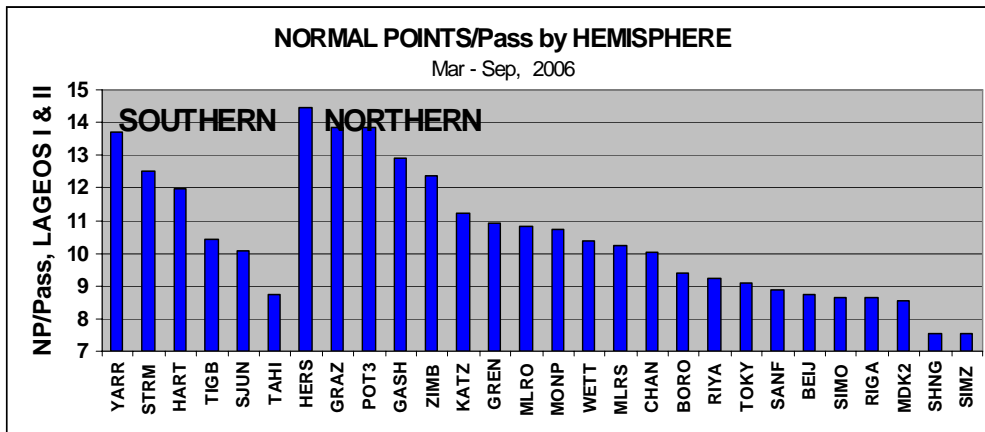


Figure 5: Normal points per Pass, LAGEOS I & II combined, extracted from NICT daily Analysis Reports. (Note truncated vertical scale - it looks worse than it is!)

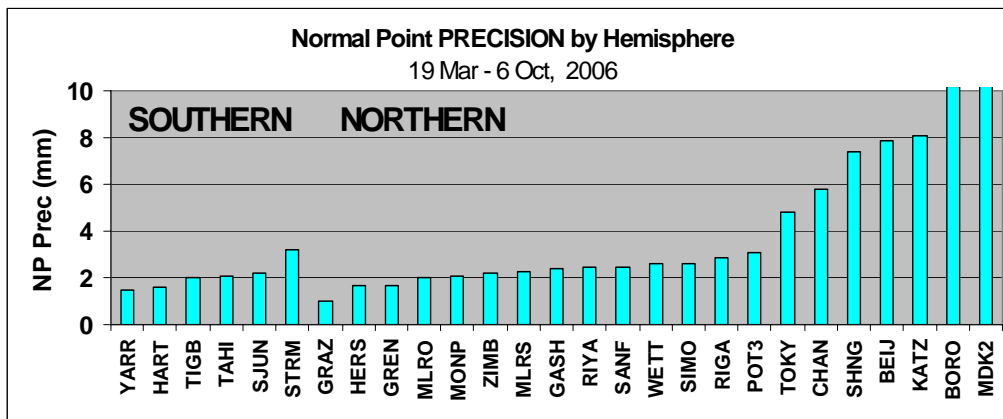


Figure 6: Normal Point Precisions Summary

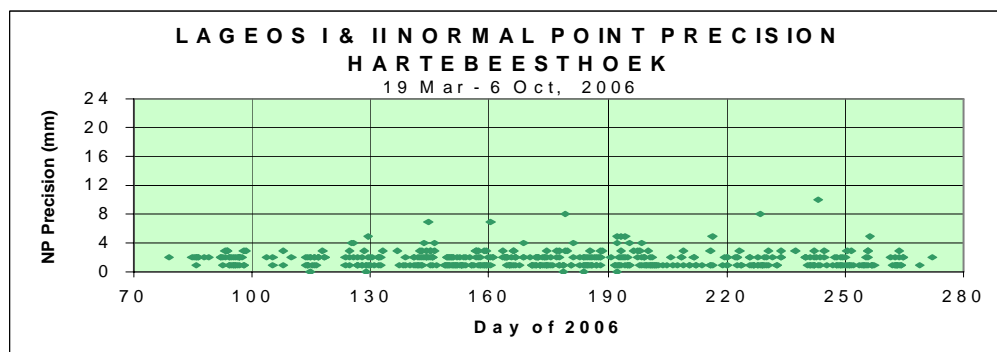
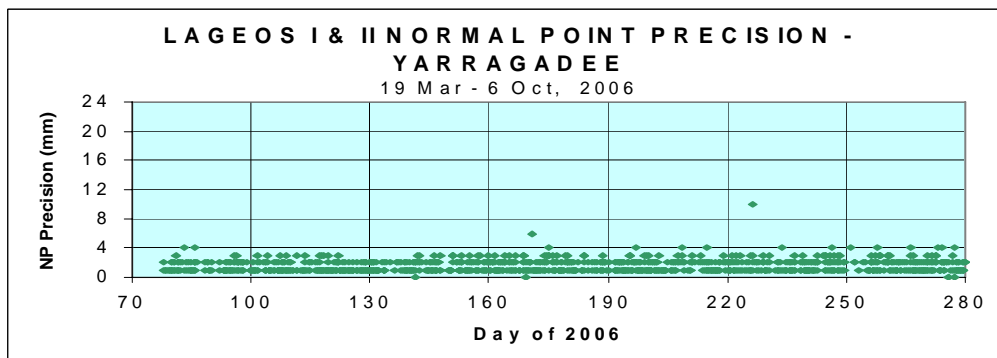
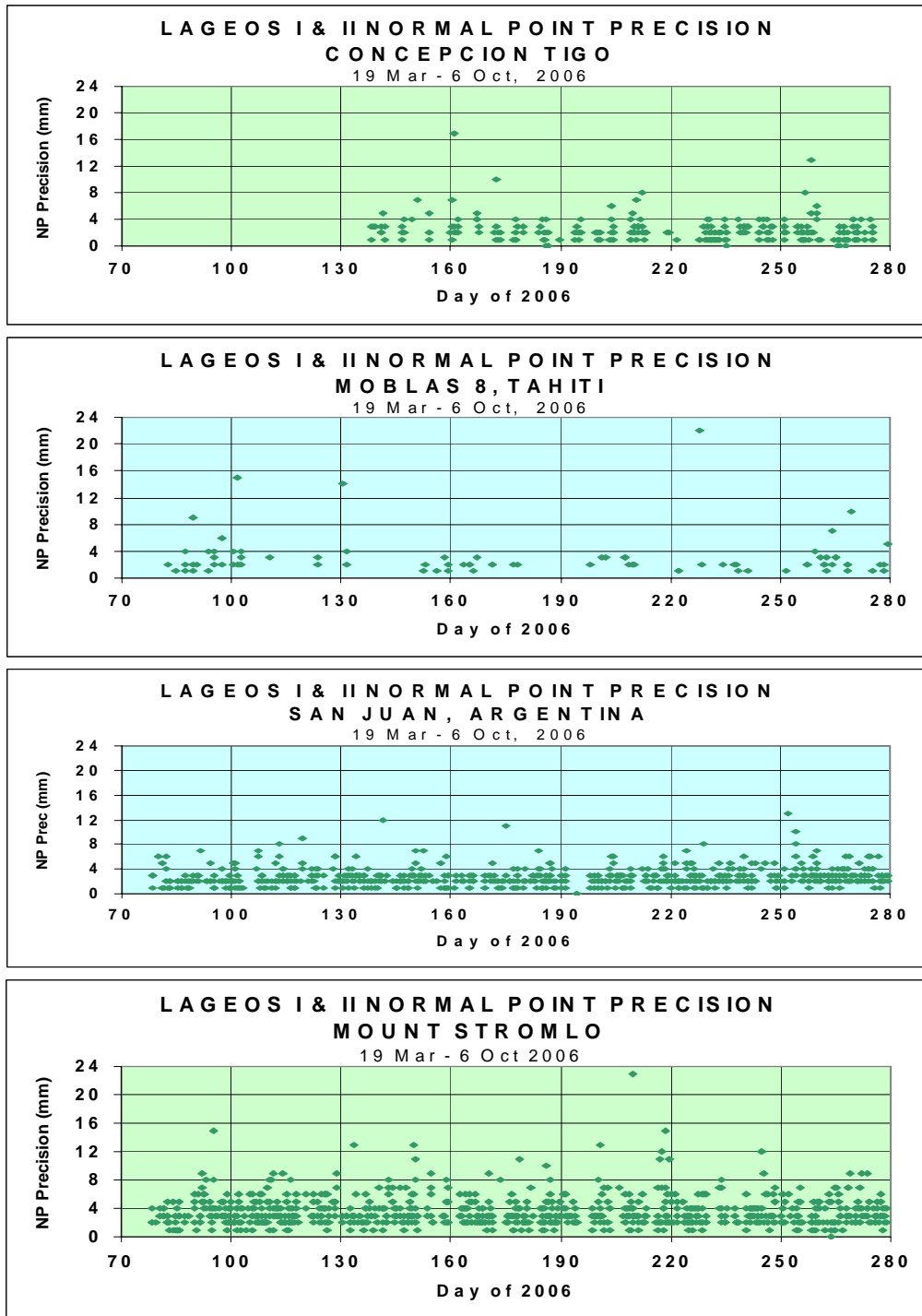


Figure 7a: Normal Point Precisions for Southern Hemisphere stations



*Figure 7b: Normal Point Precisions for Southern Hemisphere stations*

**System delay**

The system delays are the results of system calibration by pre- and/or post-pass ground target ranging, or equivalent. They have arbitrary values and are allowed to jump when, for example, cables are changed in the paths to the timing system, components in the optical path are moved, or other repairs and maintenance are performed. Otherwise, however, they should remain constant. In particular, they should not show drifts such as TIGO has been undergoing since about day 225 in Fig.8. The results in Fig.8 are from Ajisai entries in NICT daily analysis reports, with respect to the average system delay over the 28-week period.

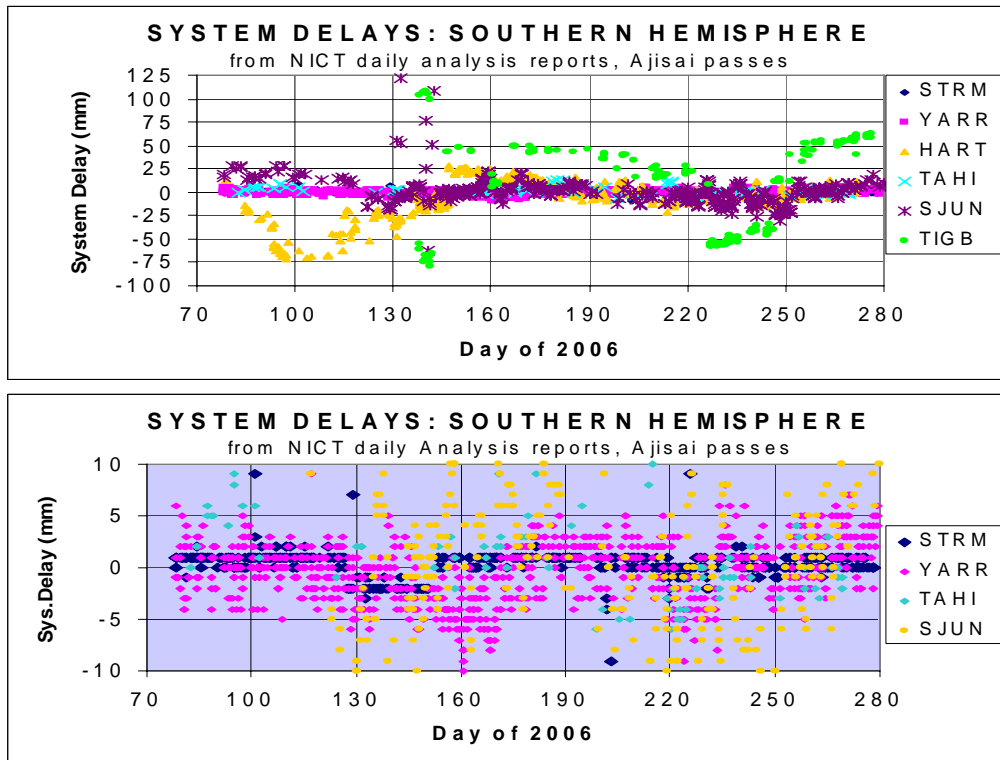


Figure 8: System Delays per pass (Ajisai). The lower plot is at expanded vertical scale.

## Conclusions

There has been a boom in Southern Hemisphere ranging in 2006, due mainly to the commissioning of the San Juan station, whose productivity is the more remarkable because it only observes at night-time. Tahiti only has limited day-time tracking.

The quality of ranging is comparable with Northern Hemisphere stations, too, although some stations show worrying trends in their system delay stabilities while Stromlo should be doing far better in its normal point precisions. The imminent resurrection of Arequipa, Peru should further enhance the Southern Hemisphere contribution to global SLR performance.

## Acknowledgements

The data used here were extracted from the CDDIS SLR Data Reports, courtesy Carey Noll, and from the NICT daily Multi-Satellite Bias Analysis Reports, courtesy Toshi Otsubo. These reports are produced on behalf of the International Laser Ranging Service (ILRS).

## Reference

- [1] Luck, J.McK.: "Performance of WPLTN Stations", these proceedings (2006)

## **The Evolution of SLR/LLR in Response to Mission Needs**

Peter Shelus<sup>1</sup>

1. University of Texas at Austin/CSR

### **Abstract**

*The response of the laser ranging network to the needs of the various missions over the past 40 years or so has been an evolving one. The targets have been varied and the science has been exciting. With the establishment of the International Laser Ranging Service (ILRS) and its Missions Working Group, this planning and coordination has been put on a much more formal basis. This presentation reviews some of the history, provides information on where we find ourselves right now, and tries to look a bit into the future as to where we wish to be.*

## Assessment of SLR Network Performance

Mark Torrence <sup>1</sup> and Peter Dunn <sup>1</sup>

1. SGT Inc, Greenbelt, Maryland, USA

### Abstract

*The SLR global performance report card is updated quarterly on the ILRS web-site and presents a broad view of the state of the network. The information summarized in that report can be treated in several different ways to clarify particular features. The usual expression of the station characteristics as a function of calendar time provides a method to monitor the evolution of the health of a station by considering the quantity of normal points collected, as well as the volume of full rate observations and the noise level of these data for each satellite. If the same variables are expressed as a function of local time, the distinction between day-time and night-time performance of a station is high-lighted. Satellite signature effects can be demonstrated by again plotting these same variables but as a function of range value, and this will also vary by station. We demonstrate the use of these alternative representations for all the stations in the network to many satellites and solicit ideas which could enhance the definition of the each observatory's contribution to the Global Network and the analyst's understanding of the data.*

### Introduction

The motivation for constructing graphs of station performance arose from an assessment of potential corner cube array design for HEO satellites. Looking at the SLR data as a function of local time and as a function of the satellite range may reveal station performance characteristics in SLR data such as whether patterns vary from year to year, and whether there are indications of satellite dependencies.

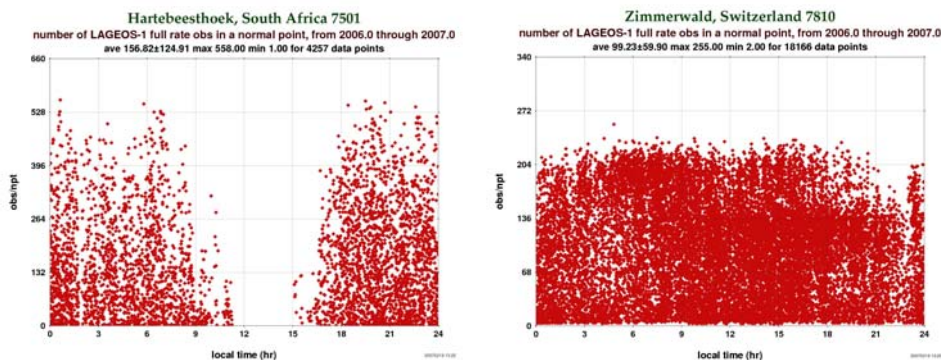


**Figure 1** Number of full rate observations in a normal point for Hartebeesthoek and Zimmerwald.

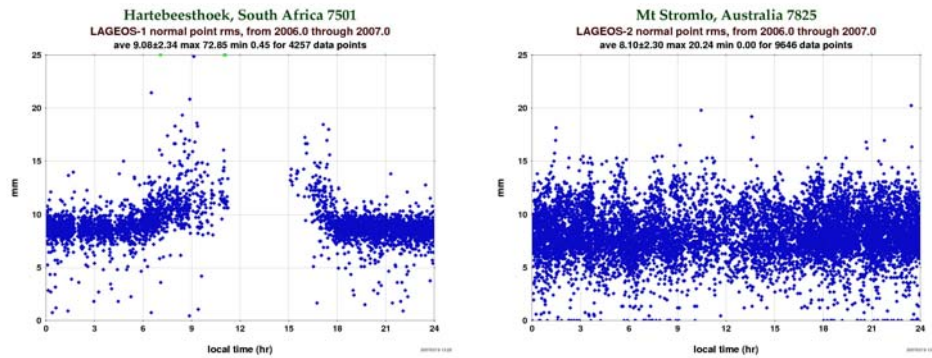


**Figure 2:** Normal point rms as function of local time for Hartebeesthoek and Mt Stromlo.

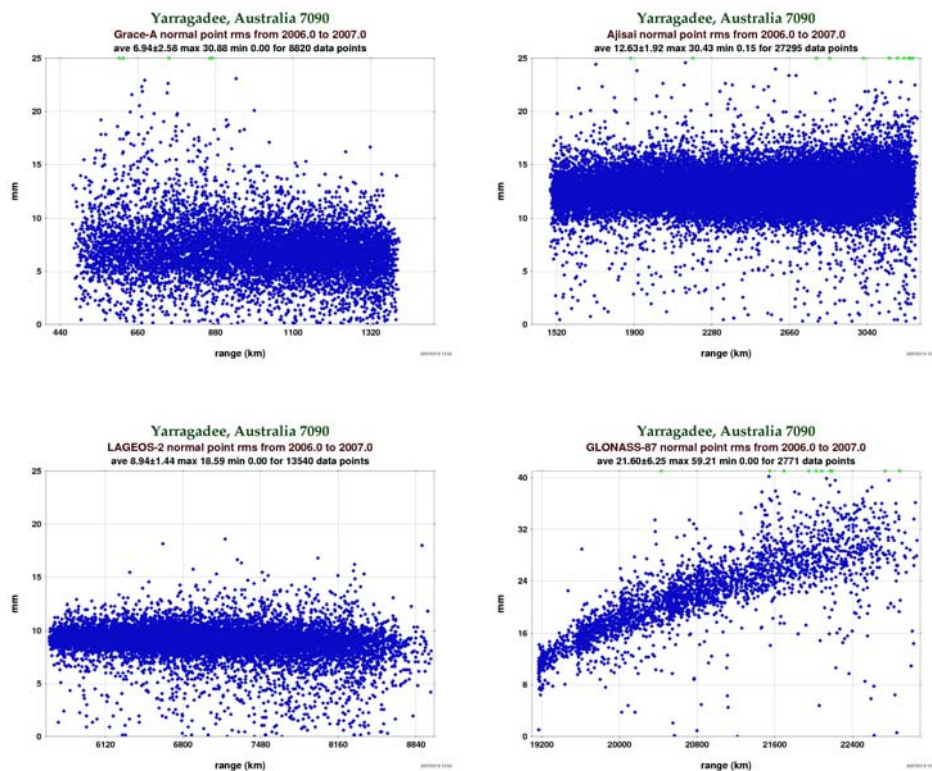


**Figure 3:** Normal point rms as function of range for Yarragadee for Grace-A, Ajisai, LAGEOS-2 and GLONASS-87.

The pattern seen in the normal point rms as a function of range for Yarragadee tracking GLONASS-87 is most probably due to the large array cross section of GLONASS-87 resulting in center-of-mass offset which is a function of viewing geometry.

See

[http://ilrs.gsfc.nasa.gov/cgi-bin/satellite\\_missions/select.cgi?sat\\_code=GL88&sat\\_name=GLONASS-88&tab\\_id=com](http://ilrs.gsfc.nasa.gov/cgi-bin/satellite_missions/select.cgi?sat_code=GL88&sat_name=GLONASS-88&tab_id=com)

Plots of this type will be available at the ILRS web site.

## Performance of WPLTN Stations

John McK. Luck<sup>1</sup>

1. EOS Space Systems Pty.Ltd., Canberra, Australia

### Abstract

*There have been significant upgrades to WPLTN stations in the last year. Performance statistics for each station will be presented, which may highlight where further improvements could be achieved.*

### Introduction

The working and developing stations which constitute the Western Pacific Laser Tracking Network (WPLTN) include Tokyo, Simosato and Tanegashima (Japan), Shanghai, Beijing, Changchun, Yunnan, Wuhan and the CTLRS (China), Yarragadee and Mount Stromlo (Australia), Riyadh (Saudi Arabia), Maidanak (Russia), and most recently the new Chinese-supplied station at San Juan, Argentina. In 2006, as well as the commissioning of San Juan, Shanghai moved to a new site and significant upgrades came to fruition at Simosato and Changchun. San Juan has been accepted as a member of WPLTN, and Yarragadee has dual membership with WPLTN and the NASA network.

These developments have produced a noticeable increase in the productivity and quality of the network as a whole. It is therefore timely to review its performance and to compare it with the NASA and Eurolas networks. (This paper was actually presented at the WPLTN General Assembly.)

For the purposes of this paper, Yarragadee is included in WPLTN, TIGO in Concepcion (Chile) and the Ukraine stations in Eurolas, and Hartebeesthoek and Tahiti in NASA. Data are shown in four periods – three 28-week periods spanning 20 Feb 2005 to 2 Sep 2006, and the 4-week period 3-30 Sep 2006 leading up to the Workshop. In many ways the data displays emulate the ILRS Quarterly Global SLR Performance Reports, arranged differently.

### Productivity

The numbers of passes summarized by network are shown in Fig.1 as percentages of the global totals. The increase since 2005 seems to be sustained, at the expense of the NASA network. Data were extracted from the weekly CDDIS SLR Data Reports.

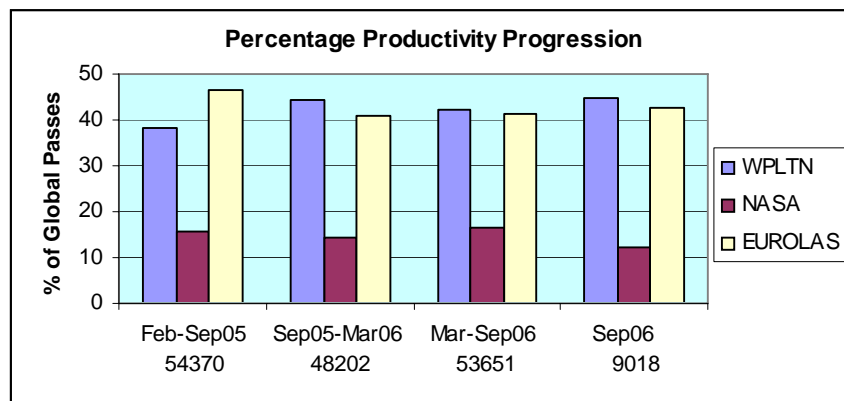


*Figure 1: Productivity comparison. The global totals of passes are on the bottom line.*

Fig.2 shows the numbers of passes per station per period, grouped by network.

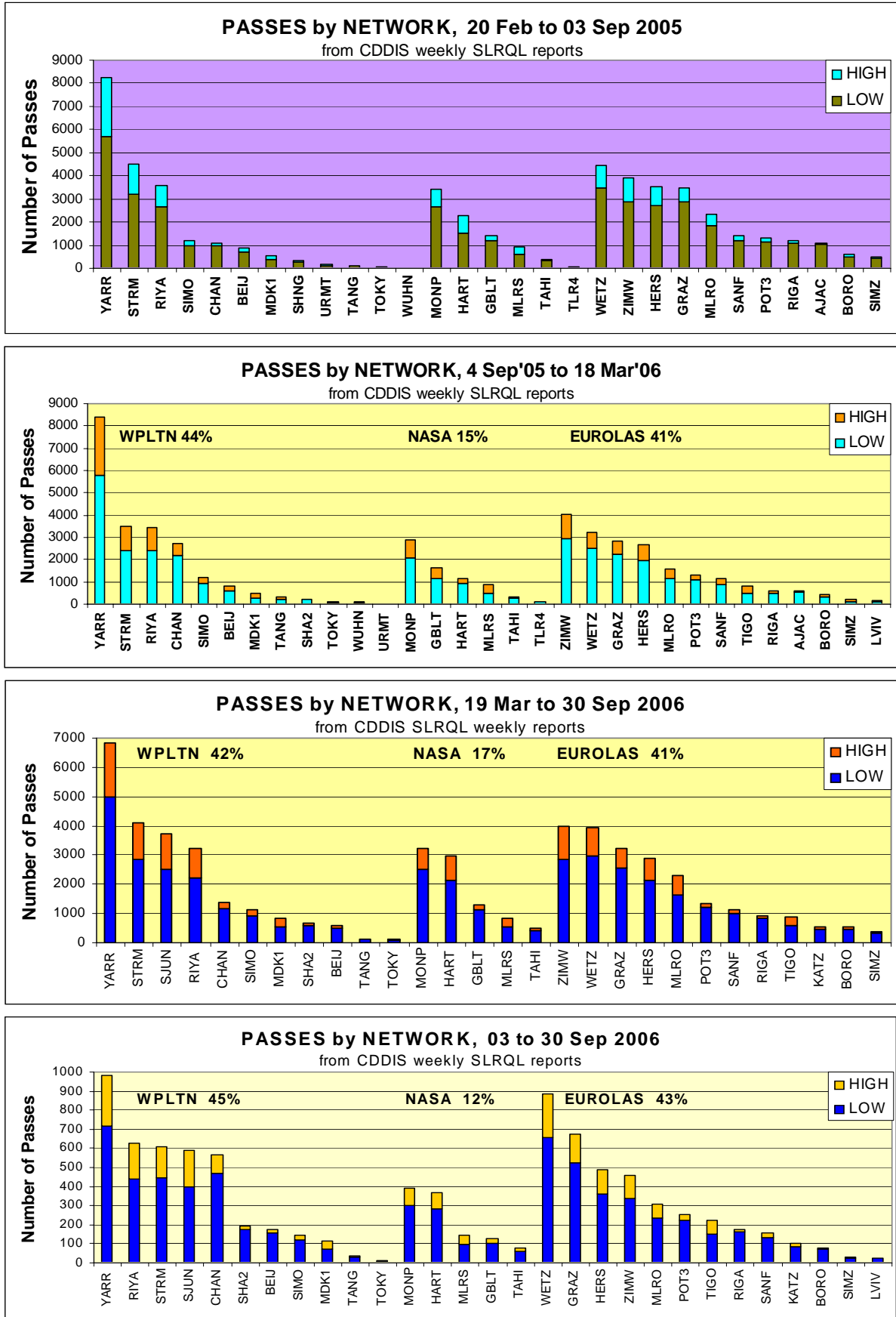
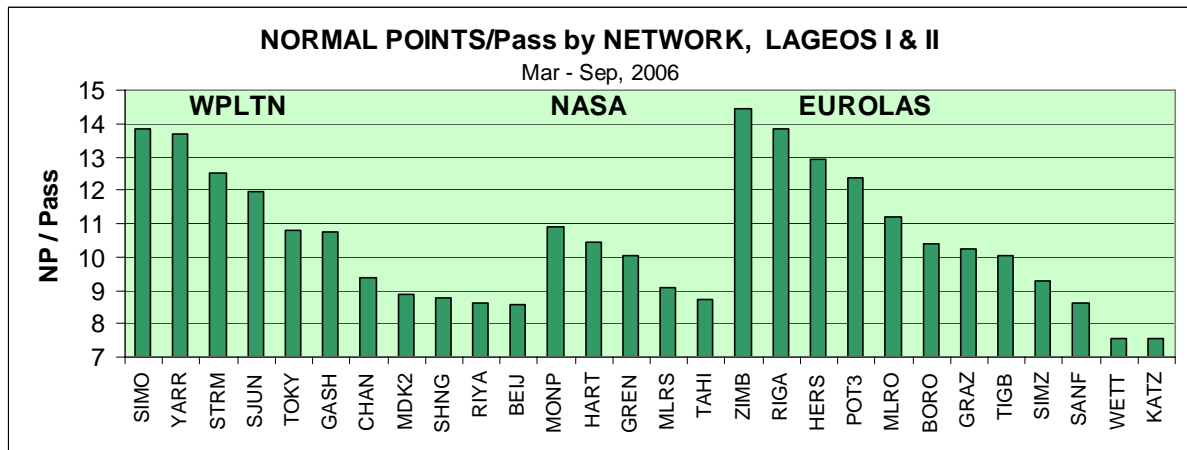


Figure 2: Numbers of passes per station in each of the four periods.

### Normal Points per Pass

This category reflects the observing efficiency of the stations, and is affected by skill in acquiring satellites and interleaving passes, as well as factors like aperture, laser power, sun avoidance, priorities, and bad weather. In general, low ratios mean more uncertainty in determining time bias, unless the normal points are very well distributed throughout a pass.



**Figure 3:** Normal points per pass in much of 2006.  
Data from daily NICT Multi-Satellite Bias Analysis Reports.

The best of the WPLTN stations are comparable with Eurolas. Stations with low ratios – in all networks! – should aim to improve coverage during passes.

### Normal Point Precision

For Fig.4, the average NP Precision values were calculated after removal of obvious outliers. Stations not shown were off-scale. The best stations achieve 2 mm, and 3 mm should be the aim. Clearly, several WPLTN stations and some from eastern Europe need to improve.

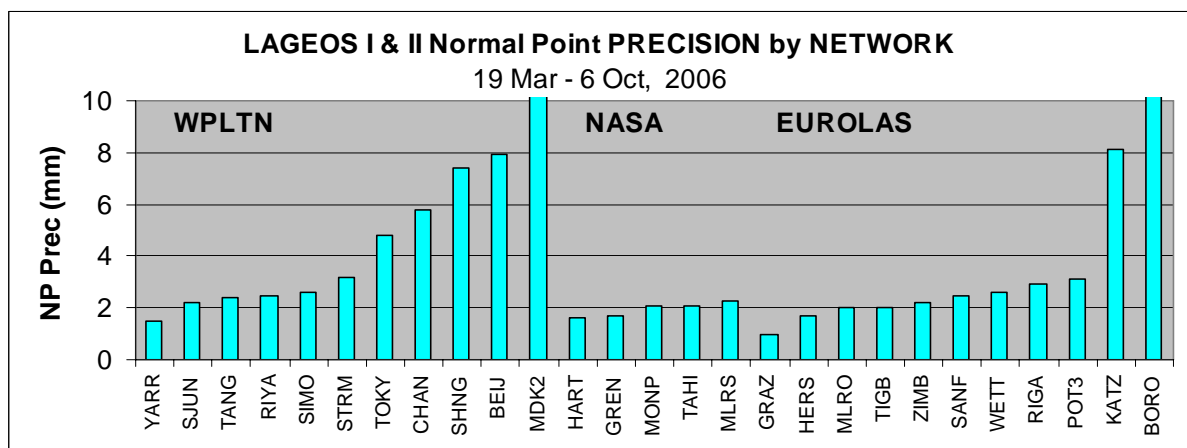


**Figure 4:** Average Normal Point Precisions for much of 2006.  
Data from NICT reports.

Time series graphs for some of the stations are shown in Fig.5. Only passes containing at least 4 Normal Points are plotted. Graphs for Yarragadee, Stromlo and San Juan are given in the companion ‘Southern Hemisphere’ paper (Luck, 2006).

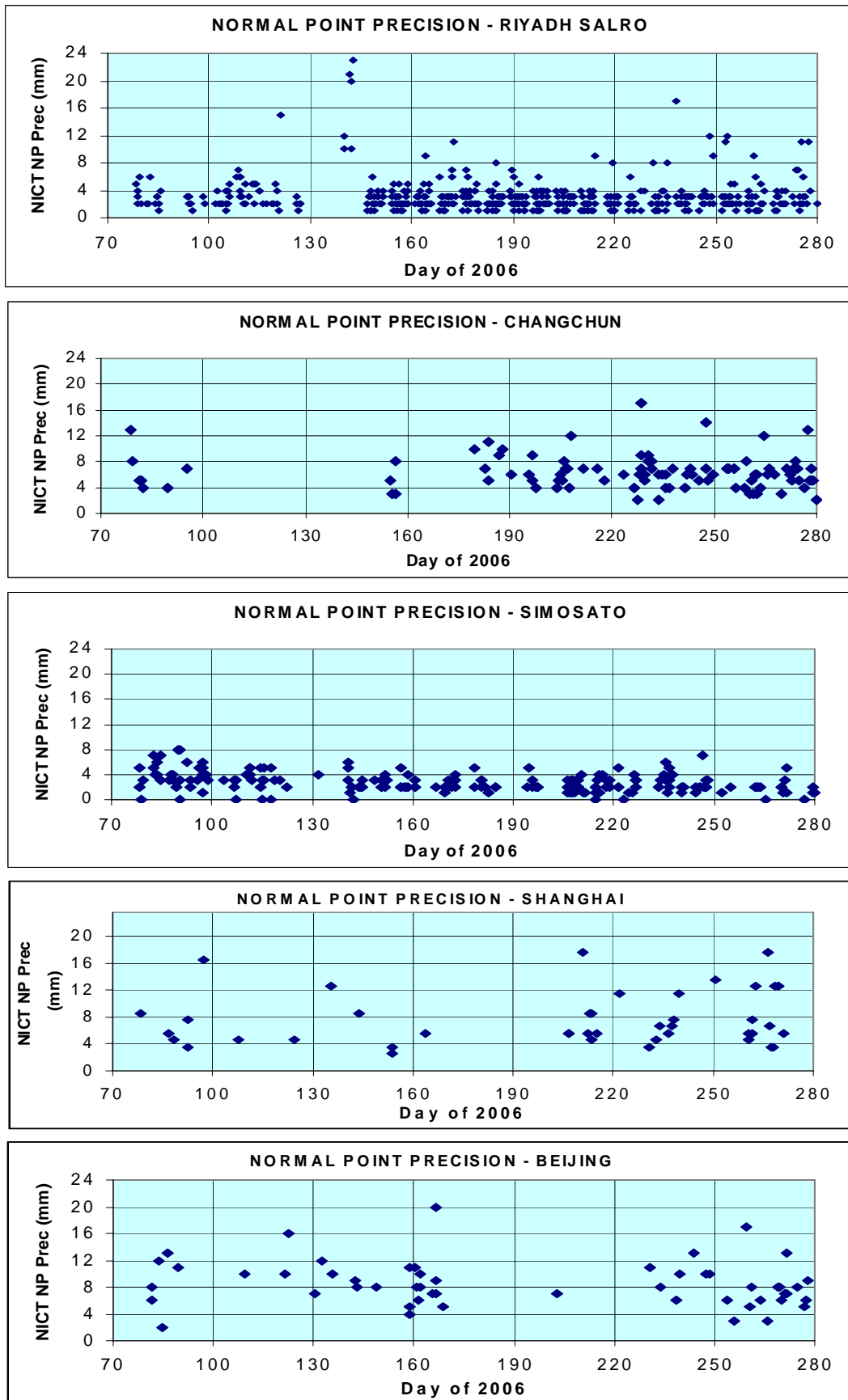


*Figure 5: Normal Point precisions for selected WPLTN stations. Data from NICT reports. See also (Luck, 2006)*

### Accuracy – Range Bias and System Calibration

More important than the precision of the measurements is their accuracy, i.e. how closely the numbers obtained reflect the true distances. There is no perfect way to assess accuracy, so we use range biases, which in a sense give a station's range errors against a sophisticated average over all stations using the satellites' orbits as constraints; and we use ground-target ranging to measure the system delays that are applied to the range measurements. Both these methods have drawbacks. Range biases depend upon the set of station coordinates and the processing philosophy adopted by any particular Analysis Centre. For ground-targets, the distance from invariant point to target must be measured with millimeter accuracy, and preferably be checked frequently by a technique such as MINICO (Luck, 2005).

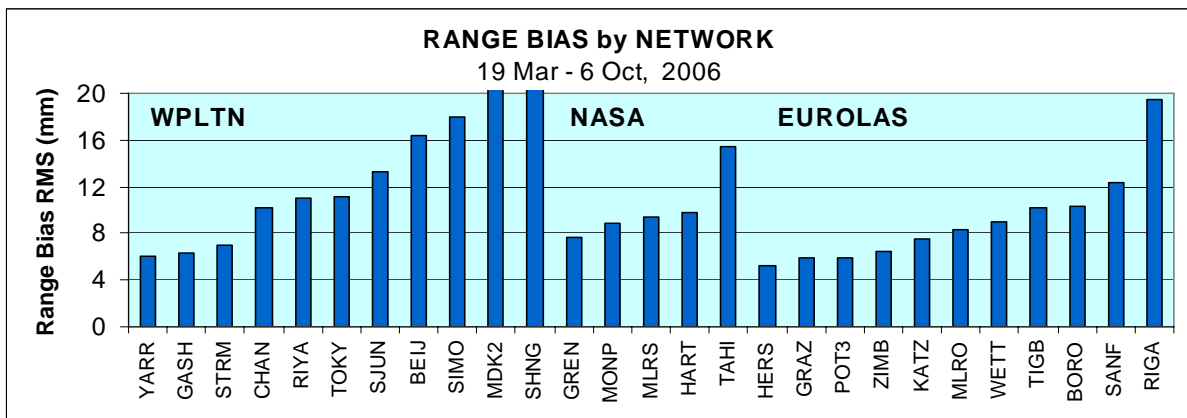


Figure 6: Range bias RMS about mean values by station. Data from NICT reports.

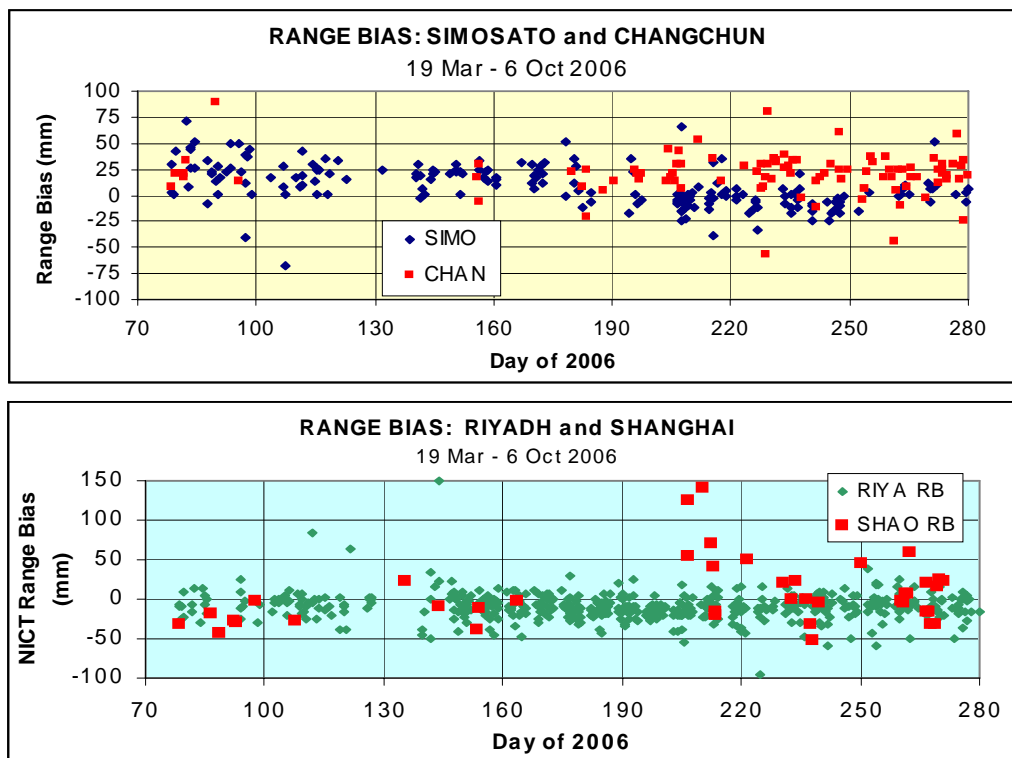


Figure 7: Range bias time series for reasonably productive stations. Data from NICT reports.

RMS variations of LAGEOS I & II range biases about their station means for a period in 2006 are shown in Fig.6, and time series for some of them in Fig.7. Yarragadee,

Stromlo and San Juan are shown in the companion “Southern Hemisphere” paper (Luck, 2006).

### System Delays

In Fig.8, the average system delay for each station has been subtracted from its values to clarify the comparisons. Large jumps, which are perfectly valid, occurred during the period at Simosato and Riyadh, so in Fig.9 they are adjusted to their piecewise averages.

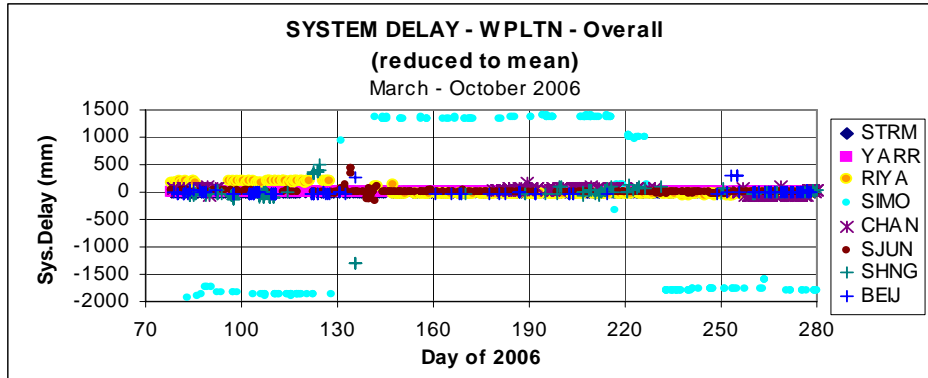


Figure 8: Relative system delays for productive stations. Data from NICT reports.

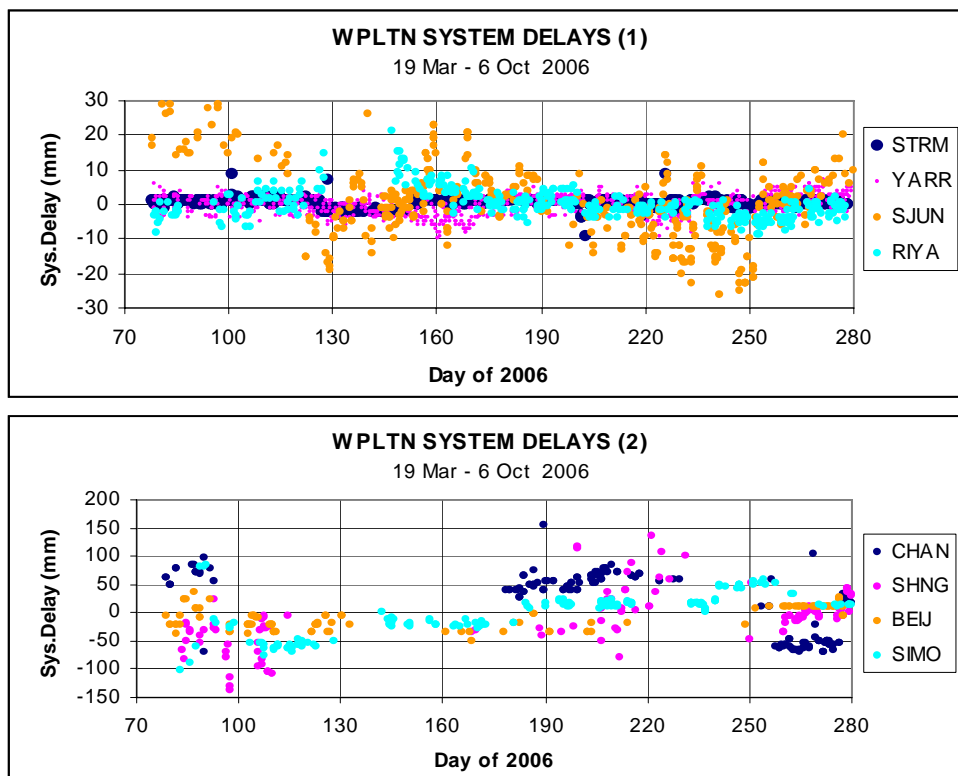


Figure 9: Relative system delays at different expanded vertical scales. Data from NICT Reports, AJISAI passes.

There is substantial scatter for most stations except Yarragadee, Stromlo and Riyadh, and drifts in several, most notably Riyadh and Simosato, which are even more worrying. Stations are strongly urged to investigate the causes of the scatters and drifts, because it is then likely that there are also large scatters and drifts within

passes. Fortunately, there is little evidence of correlations between range bias and system delay (although if there were, it should be easily fixed).

### **Conclusions**

The number of passes acquired by WPLTN stations has improved in the 12 months to October 2006, and now exceeds Eurolas. This is largely due to the commissioning of San Juan and upgrades at some other stations. Most stations now track GPS-35 & -36 successfully, at night. When stations like Changchun and San Juan achieve daylight tracking, the productivity ratios should improve even further.

The analysts prefer passes well tracked from observing horizon to observing horizon, or at worst that include segments near both horizons and at maximum elevation. NPs/Pass is a rough measure of how well this is achieved, but inspection of the NICT reports shows that sparse passes invariably fail to produce a Time Bias of decent quality, which indicates poor NP distribution. Fig.3 indicates that many stations (in all networks) need to improve this aspect of operations.

The quality of WPLTN stations, assessed by Normal Point precision and Range Bias RMS for LAGEOS I & II combined, is an area needing improvement, with only 5 stations showing NP precision better than 3 mm and 3 stations with Range Bias RMS below 8 mm. It is suggested that detailed attention to stabilizing system delays is needed at many stations.

*And if you think that this paper is just stating the bleeding obvious, then I have found by long and bitter experience that that is exactly what is sometimes needed!*

### **Acknowledgements**

The data used here were extracted from the weekly CDDIS SLR Data Reports, courtesy Carey Noll, and from the NICT daily Multi-Satellite Bias Analysis Reports, courtesy Toshi Otsubo. These reports are produced on behalf of the International Laser Ranging Service (ILRS).

### **References**

- [1] Luck, J.McK.: “*Five Target System Calibration*”, Proc. 14<sup>th</sup> International Laser Ranging Workshop, San Fernando, Spain. Boletin ROA No.5/2005, pp.311-321 (2005)
- [2] Luck, J.McK.: “*Performance of Southern Hemisphere Stations*”, these proceedings (2006)

---

## Archiving and Infrastructure Support at the ILRS Data Centers

C. Noll<sup>1</sup>, M. Torrence<sup>2</sup>, W. Seemueller<sup>3</sup>

1. NASA Goddard Space Flight Center, Code 690.5, Greenbelt, MD 20771, USA.
2. SGT, Inc., mark.h.torrence.1@gssc.nasa.gov
3. Deutsches Geodätisches Forschungsinstitut (DGFI), Marstallplatz 8, D-80539 Muenchen, Germany.

Contact: [seemueller@dgfi.badw.de](mailto:seemueller@dgfi.badw.de) /Fax: +49 89 23031-1240,

[Carey.Noll@nasa.gov](mailto:Carey.Noll@nasa.gov) /Fax: 301-614-6015

### Abstract

*Two global data centers have supported the International Laser Ranging Service (ILRS) since its start in 1998. The Crustal Dynamics Data Information System (CDDIS), located at NASA's Goddard Space Flight Center, and the Eurolas Data Center (EDC), located at DGFI, are active archives of laser ranging data and products derived from these data. The laser data sets consist of on-site normal points and full-rate data. The official ILRS products, currently station positions and EOP, are also made available to the user community through these data centers. Infrastructure support for the ILRS include reports of data holdings and quality, satellite predictions, and station configuration information. This presentation will describe this laser ranging archive available at the ILRS data centers and plans for future enhancements.*

### Data Center Archive Contents

Currently, the ILRS data and product archive consists of normal point and full-rate data, satellite prediction information, and site positions and velocities. Data since mid-1976 are available at the data centers; ILRS products from January 1993 to the present are also available.

Normal point data is the primary ILRS station data product, gradually replacing on-site sampled data and later full-rate data as the primary data product starting in 1991. Normal points are generated on-site very shortly after the satellite pass and transmitted within a few hours to the ILRS operations centers and, from there, to the ILRS data centers.

Full-rate data were the prime SLR product in the 1970's and early to mid 1980's. In the late 1980's, the normal point generation process was refined and normal points were obtained from the full-rate data during post-processing. In the 1990's, on-site normal point production became the accepted process. In the mid 1990's, the SLR/LLR CSTG subcommission agreed that there was no formal requirement for full-rate due to the transition and acceptance of on-site generated normal points as the prime and only station data product. Many stations, however, continue to provide full-rate data to the ILRS data centers since they are sometimes required for specific needs (e.g., center-of-mass analysis, retroreflector experiments, co-location analysis, etc.). Figure 1 summarizes the data holdings (full-rate or on-site normal point) of the CDDIS archive by year versus satellites tracked and network size.

The ILRS currently provides satellite predictions for the network in two formats: Tuned Inter-Range Vectors (TIRVs) and the newer Consolidated Prediction Format (CPF). The CPF is now considered the operational format for prediction providers and

network stations. However, TIRVs continue to be generated by the prediction providers and made available through email and at the data centers to accommodate stations that are continuing efforts to transition to the CPF.

The CPF information accurately predicts positions and ranges for a much wider variety of laser ranging targets than had been previously possible. Rather than using the tuned IRV's with an integrator, the new predictions provide daily tables of X, Y, and Z positions for each target which can then be interpolated for very accurate predictions. CPF provides an expanded format capability and greatly improves tracking on low satellites because the full modeling potential of the orbit computation at the prediction center will be passed on to the stations. Drag files and special maneuver files are no longer necessary. These predictions are available via email or via anonymous ftp from the data centers.

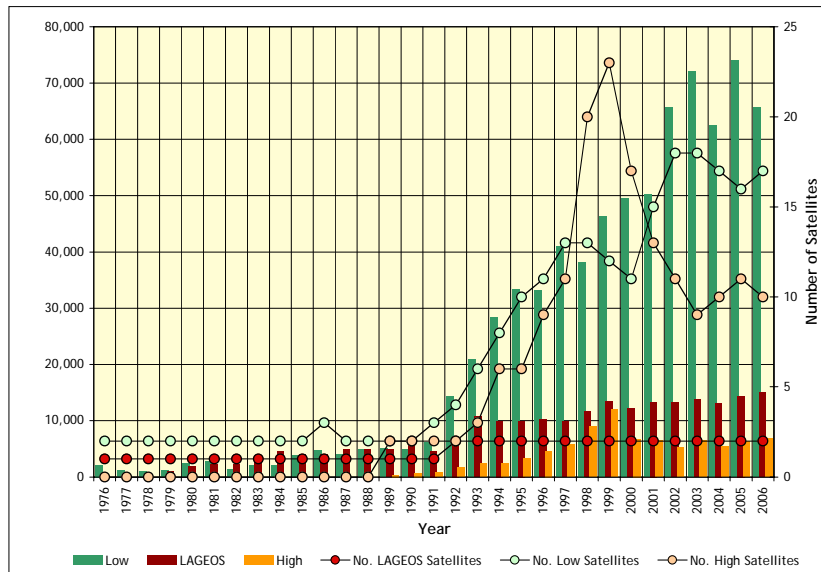


Figure 1. Laser ranging data volume by year

Six ILRS analysis centers (AC), ASI/Italy, BKG/Germany, DGFI/Germany, GFZ/Germany, JCET/USA, and NSGF/UK produce weekly solutions on LAGEOS-1 and -2 for global station coordinates and Earth orientation parameters (EOP). Each week, ASI (primary ILRS Combination Center) and DGFI (backup ILRS Combination Center) merge the individual AC solutions into the official ILRS Combination Product. This combination product is available every Wednesday via anonymous ftp from the data centers. The IERS uses this product for the multi-technique Combination Pilot Project and the Bulletin A EOP.

**Performance**

The ILRS Central Bureau staff has developed various reports and plots to monitor network performance. This information is updated on a frequent basis dependent upon the type of report. Station operators, analysts, and other ILRS groups can view these reports and plots to quickly ascertain how individual stations are performing as well as how the overall network is supporting the various missions. All plots and reports can be accessed through the station pages on the ILRS Web site at URL <http://ilrs.gsfc.nasa.gov/stations>.

The ILRS performance “report cards” are generated on a quarterly basis and show data volume, data quality, and ILRS operational compliance information. The

statistics are presented in tabular form by station and sorted by total passes in descending order. Plots of data volume (passes, normal points, minutes of data) and RMS (LAGEOS, Starlette, calibration) are created from this information and available on the report card Web site:

[http://ilrs.gsfc.nasa.gov/stations/site\\_info/global\\_report\\_cards/index.html](http://ilrs.gsfc.nasa.gov/stations/site_info/global_report_cards/index.html)

Example plots from the latest report card are shown in Figure 2.

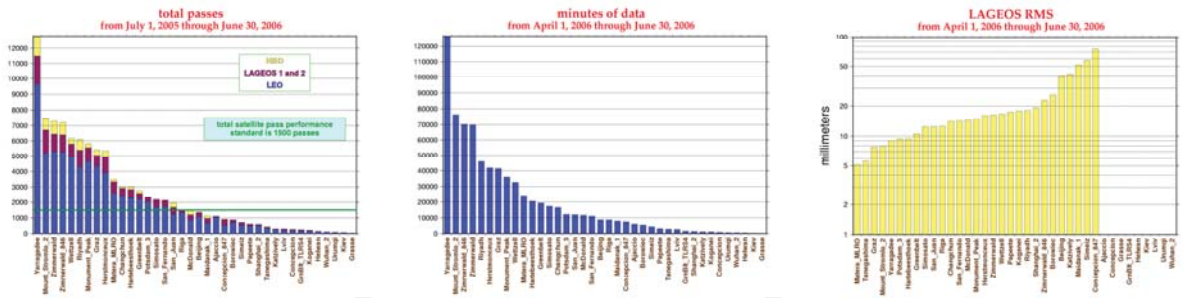


**Figure 2a.** Total passes for 2006q3 report card.

**Figure 2b.** Minutes of data for 2006q3 report card.

**Figure 2c.** LAGEOS RMS for 2006q3 report card.

A plot of the satellite ground tracks of the last seven days of geodetic satellite data is updated daily and available through the ILRS Web site at:

[http://ilrs.gsfc.nasa.gov/stations/recent\\_groundtrack.html](http://ilrs.gsfc.nasa.gov/stations/recent_groundtrack.html).

The plot, shown in Figure 3 for a week in November 2006, graphs the actual network ground tracks of Etalon, LAGEOS, Ajisai, Starlette, and Stella over the previous seven days based upon the archived normal point data.

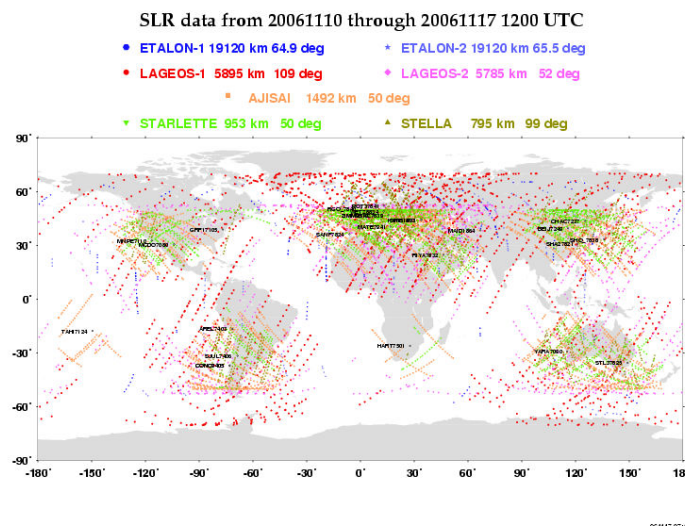


**Figure 3.** Plot of the satellite ground tracks of the last seven days of geodetic satellite data.

Plots of station performance and meteorological data are regularly generated. The plots are sorted by station and come in two forms: for data from the past year and for data since the year 2000. The information presented in these plots for each station in the ILRS network are: total number of normal points, total number of full-rate points, average number of data points per LAGEOS normal point, LAGEOS normal point rms, calibration rms, and system delay, and station temperature, pressure, and

humidity (as recorded in the normal point data). Examples of these plots for the Yarragadee station are shown in Figure 4. The plots are available through the individual station pages on the ILRS Web site (<http://ilrs.gsfc.nasa.gov/stations>).

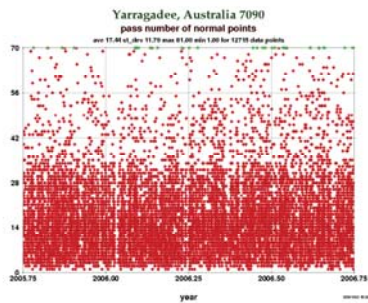


**Figure 4a.** Total number of normal points from Yarragadee for the past year.

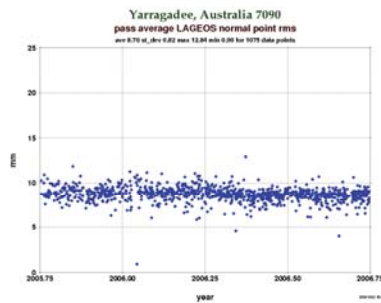


**Figure 4b.** Pass average LAGEOS normal point RMS from Yarragadee for the past year.

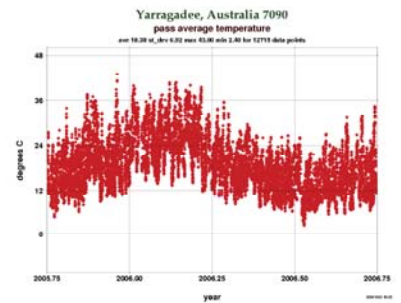


**Figure 4c.** Average temperature Yarragadee for the past year.

### Future Plans

Additional plots of station performance are under development for the ILRS Web site. These plots include statistics for all currently tracked satellites and all operational stations as a function of time; full-rate observations per normal point and normal point rms are also computed as a function of range and time. Examples of the new charts for the Yarragadee station are shown in Figure 5 below.

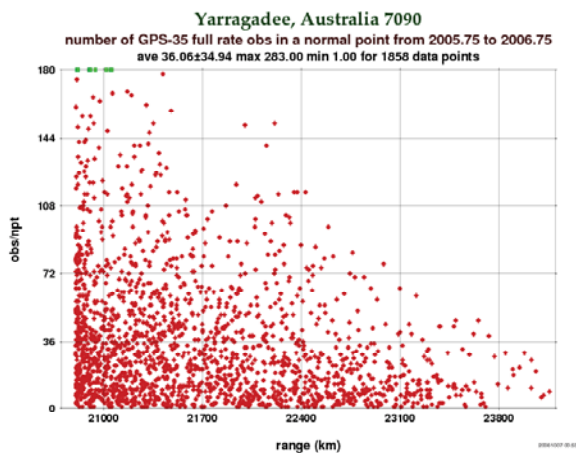


**Figure 5a.** Number of GPS-35 full-rate observations per normal point from Yarragadee for the past year.

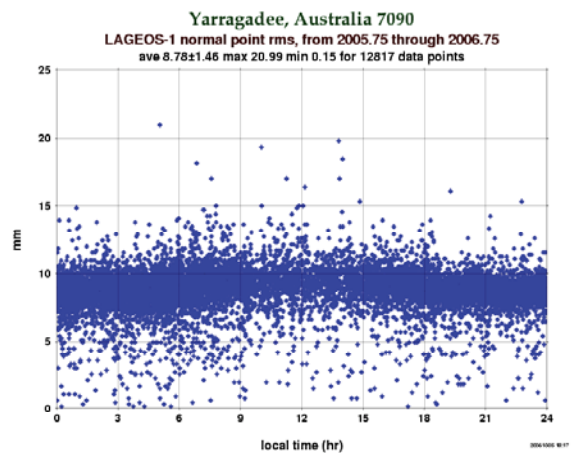


**Figure 5b.** LAGEOS-1 normal point rms from Yarragadee for the past year.

## **Minico Calibration of System Delay Calibration at Mount Stromlo SLR**

John McK. Luck<sup>1</sup>

1. EOS Space Systems Pty.Ltd., Canberra, Australia

### **Abstract**

*The MINICO method of ranging to four ground targets in rapid succession has been adopted as a nearly daily routine at Stromlo. In essence, it calibrates the range used for regular pre- and post-pass system delay calibrations. It also provides interesting information on the stability of the calibration pillars and of the telescope pier. There is a clear annual cycle of amplitude 1 mm in the results. The routine biennial precision ground survey was performed in August 2006. Its agreement, or otherwise, with the MINICO determinations of pier ranges will be presented.*

## A Summary of Observations of GioveA, taken from Mt Stromlo SLR Station

C.J. Moore<sup>1</sup>

1. EOS Space Systems Pty. Limited, 111 Canberra Ave., Griffith, A.C.T. Australia.

Contact: [cmoore@eos-aus.com](mailto:cmoore@eos-aus.com)

### Abstract

*A summary of satellite Giove A SLR data taken at Mt Stromlo over the period from May to August 2006 is presented, and some factors affecting tracking productivity are discussed. Although in a high earth orbit, Giove A has a large optical back scattering cross-section, and this has provided data for an empirical analysis of link budget factors which has allowed potential productivity gains to be assessed.*

### Introduction

The new Mt Stromlo SLR station has been in operation since December 2004 and data production has been reasonable and overall performance has been very good. Mt Stromlo productivity levels often exceed many other SLR stations. Nevertheless, improvements can be always be made, and this paper describes an analysis of the potential increases to productivity levels that may result from increased laser output energy, particularly as it applies to tracking Giove A and other high earth orbit satellites.

SLR productivity (i.e. detection of returns) of high satellites is particularly sensitive to environmental factors such as cloud, air mass water vapour content and photon noise during daylight hours. These high satellites include the Glonass and GPS satellites, Etalon 1 and 2 and the first Galileo test satellite, Giove A. Satellites such as Lageos 1 and 2 are also affected although to a lesser extent. To illustrate the relationships between laser energy and productivity from high satellites, an analysis of Giove A tracking at Mt Stromlo is presented, particularly taking into account actual availability of passes and their distribution with elevation.

<b>Total number of passes</b>	<b>77</b>	<b>100%</b>
<b>Number low elevation</b>	<b>11</b>	<b>14%</b>
<b>Number weather affected</b>	<b>33</b>	<b>43%</b>
<b>Number available</b>	<b>33</b>	<b>43%</b>
<b>Number attempted</b>	<b>21</b>	<b>27%</b>
<b>Number tracked</b>	<b>12</b>	<b>15%</b>
<b>Tracked/Possible</b>	<b>12/33</b>	<b>36%</b>

*Table 1 Productivity Metrics*

### Tracking Giove A

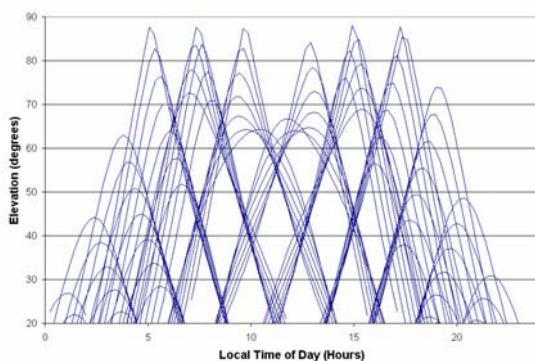


**Figure 1:** Giove A passes, June 1 to August 9, 2006

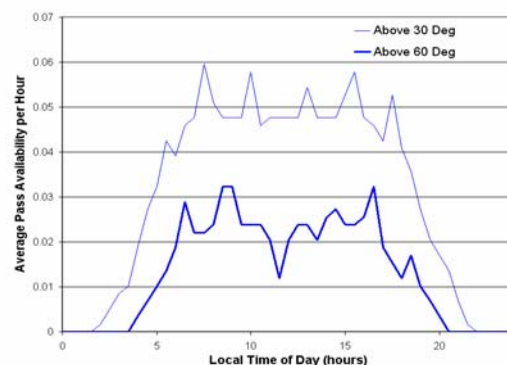


**Figure 2:** Giove A Pass Availability

Although Giove A was launched in December 2005, the ILRS was not requested to commence SLR tracking until late May 2006. The data from Mt Stromlo presented here are from observations taken from June 1st until August 9th (i.e. day 152 to 221). Table 1 summarizes the productivity statistics for this period and Figure 1 shows all of the available passes above the site's 20 degree horizon for this period.

By plotting pass elevations over 24 hour intervals, it was found that Giove A availability during the data period was on average not evenly distributed throughout the day. Figure 2 shows a frequency distribution plot (using time intervals of 0.1 hours) which indicated that there was a gap in passes during the period from approximately 18:00 to 04:00 local time (8:00 to 18:00 UTC) where passes were very sparse. There was also a significant reduction of very high passes in the middle of the day.

**Actual Productivity of Giove A at Mt Stromlo**

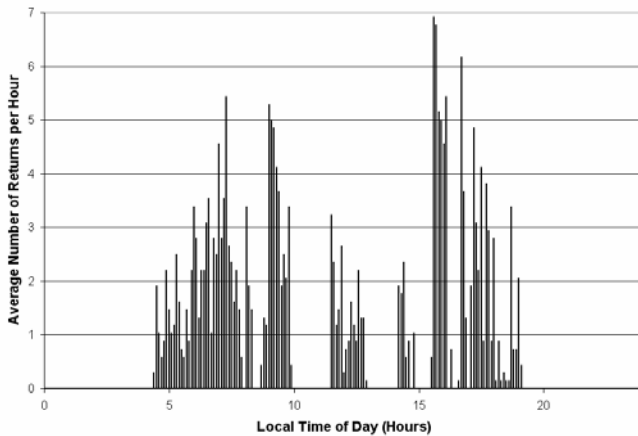


**Figure 3: Giove A Productivity**

While there are many factors affecting successful SLR tracking, it does appear that the distribution of available passes had influenced actual productivity of Giove A. Figure 3 shows the average distribution of number of successful (single-shot) returns over the course of a day, and as expected there were no passes tracked during the middle of the night. The impact of a

reduced number of very high passes in the middle of the day is also apparent. However other factors such as sun avoidance and increased daylight noise would have also contributed to reduced productivity.

Figure 2 illustrates that SLR returns were being obtained from a wide range of target elevations (and thus ranges). To assess how productivity was dependent on target elevation a link budget analysis was performed. The following sections describe this analysis and results obtained.

**Link Budget Analysis**

Estimation of the SLR link budget was made using the standard link budget formulae which determines the average number of detected photons (returns) per laser pulse,  $N_{pe}$ , as [1],

$$N_{pe} = \eta_q E_T \frac{\lambda}{hc} \eta_T G_T \sigma_{sat} (4\pi R^2)^{-2} A_T \eta_R \tau_A^2 \tau_C^2 \tag{1}$$

The transmit gain,  $G_T$  is given by  $G_T = \frac{8}{\theta_k^2} \exp\left[-2\left(\frac{\theta_p}{\theta_k}\right)^2\right]$

For Giove-A and Mt Stromlo SLR laser we set the detector quantum efficiency,  $\eta_q$ , to 20%, the transmit and receive path efficiencies,  $\eta_R$ ,  $\eta_T$ , to 90%, the laser pulse energy,  $E_T$ , to 13.5 mJ, the receive aperture area,  $A_T$ , to  $0.7 \text{ m}^2$ , the beam spread,

$\theta_p$ , to 1 arcsec, the pointing accuracy,  $\theta_K$ , to 2 arcsec and the usual values to wavelength,  $\lambda$ , Planck's constant,  $h$ , and speed of light,  $c$ . The atmospheric transmittance,  $\tau_A$ , was determined from an elevation dependent model [2] which gives transmittance at zenith of approximately 81% reducing to 72% at 20 degrees.

Clear skies were assumed, so that cloud transmittance,  $\tau_C$ , was set to 100%.

The Satellite back scattering cross section,  $\sigma_{sat}$ , for Giove A has been estimated to be in the order of  $46 \times 10^6 m^2$  (Dave Arnold, private communication).  $R$  is the distance from station to satellite (in meters) and is determined from orbit predictions.

The absolute value of estimated link budget is not critical and

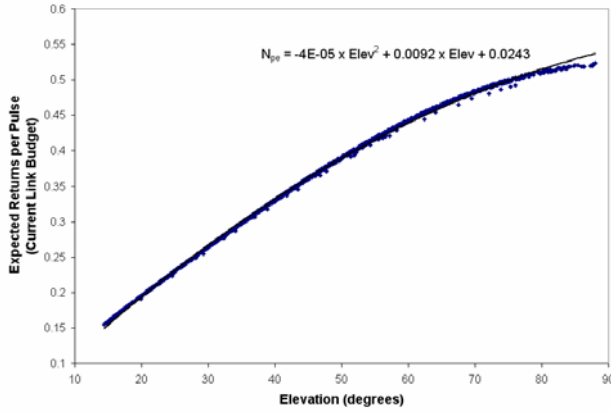


Figure 4: Link Budget versus Elevation

errors due to these assumptions do not affect this analysis. However, using these values, the average link budget estimates for Giove A against satellite elevation was calculated as shown in Figure 4. The polynomial regression line fitted to the average link budget estimates allows conversion or mapping between elevation, link budget estimates and hence laser energy. This equation is

$$N_{pe} = 0.0243 + 0.0092 \times Elev - 4 \times 10^{-5} Elev^2 \quad (2)$$

where the elevation,  $Elev$ , is valid over the range 15 to 85 degrees.

### Elevation Analysis

The mapping between link budget estimates and elevation allowed elevation to be used to provide a relationship between link budget estimates (i.e. laser power) and productivity. This analysis presents statistical analysis based on 5 degree elevation intervals from 20 degrees (the site horizon) to 90 degrees. For each elevation interval, the actual number of returns achieved (productivity) was normalized by the number of available passes in each interval to give the number of returns per pass.

The number of available passes per elevation interval is shown in Figure 5 and the productivity data for each elevation interval is shown in Figure 6. The second plot clearly illustrates that productivity falls with lower elevations (due to a decreasing link budget from an increasing range) and higher elevations (due to a lower number of available passes).

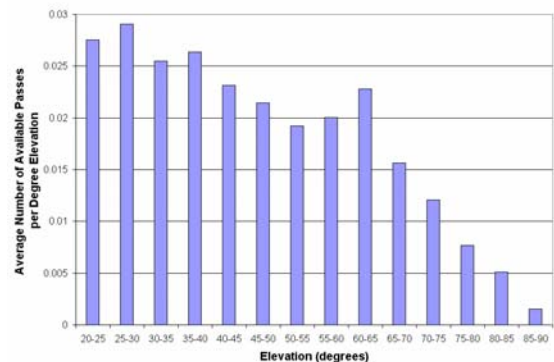
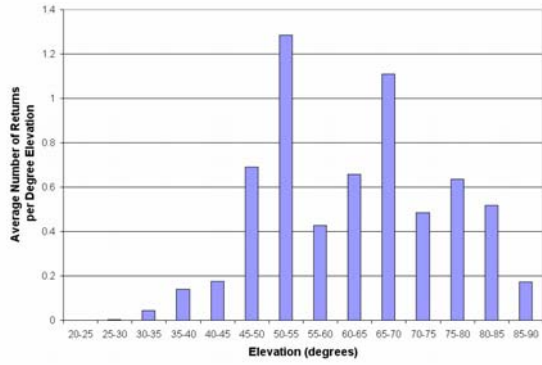
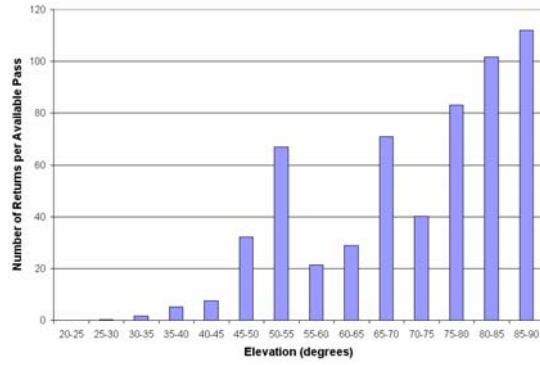


Figure 5: Available Giove A Passes versus Elevation

Hence a normalized productivity can be determined by dividing actual productivity data by the data availability. The results for Giove A are shown in Figure 7.



**Figure 6:** Giove A Productivity versus Elevation

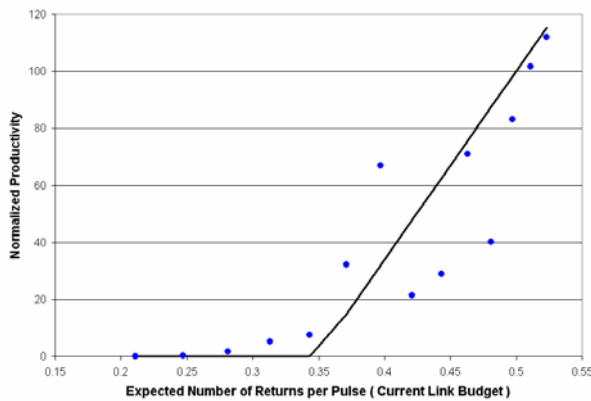


**Figure 7:** Giove A Normalized Productivity versus Elevation

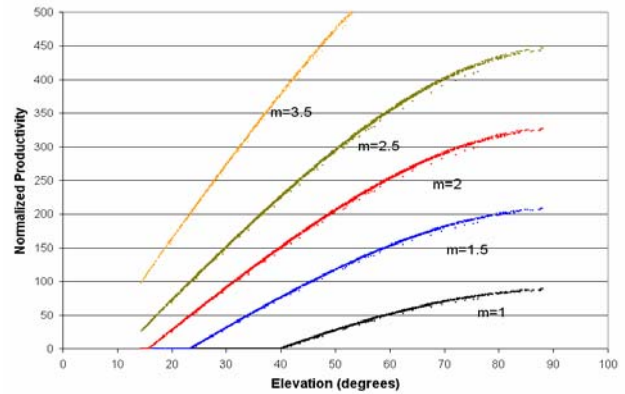
**Normalized Productivity**

Figure 7 illustrates that, all else being equal, more returns are expected when the satellite is at a higher elevation. Scatter in this data indicates that in practice other factors such as weather are influencing productivity. It also appears that below approximately 40 to 45 degrees elevation, few returns were being detected with the given laser power levels.

When returns were detected at the lower elevations, observation logs indicated that the atmosphere was particularly clear and clean of particles, and that a strong signal had already been detected, and the satellite was being tracked as it descended in elevation.



**Figure 8:** Normalized Productivity versus Link Budget



**Figure 9:** Normalized Productivity Gains

Using the conversion equation (2), normalized productivity can be compared to estimated link budget for each elevation interval. The results are shown in the Figure 8.

It appears that for link budget levels below 0.35 there is little or no productivity. For levels above 0.35, normalized productivity ( $\eta$ ) appears to increase linearly with estimated link budget. A regression equation gives

$$\begin{aligned} \eta &= 660 \times N_{pe} - 230 & N_{pe} > 0.35 \\ \eta &= 0 & N_{pe} < 0.35 \end{aligned} \tag{3}$$

Of course ideally, it should be expected that actual return rate is proportional to expected return rate. In practice, it appears that this may be the case once the link budget reaches some “threshold” value.

### Potential Productivity Gains

Equation (3) suggests that increasing the link budget (say by increasing laser power) to values less than 0.35 will give little or no improvement to productivity levels. However there should be significant gains by increasing link budget levels that are currently below 0.35 to values in excess of the 0.35.

Consider an increased link budget  $N'_{pe} = mN_{pe}$  which is a result of multiplying current levels by a factor of m. From equation (3) the actual normalized productivity rate is expected to be now  $\eta'$ , where

$$\begin{aligned} \eta' &= 660 \times mN_{pe} - 230 & mN_{pe} > 0.35 \\ \eta' &= 0 & mN_{pe} < 0.35 \end{aligned} \tag{4}$$

Figure 9 shows plots of increased normalized productivity depending on the link budget multiplier, m.

Using the data gathered on Giove A pass availability, as shown in figure 5, the effect of link budget increases on actual productivity can be determined. Figure 10 shows such productivity plots for various values of m. The heavy line with m = 1 is a smoothed curve using current data and is effectively equivalent to the plot shown in Figure 6.

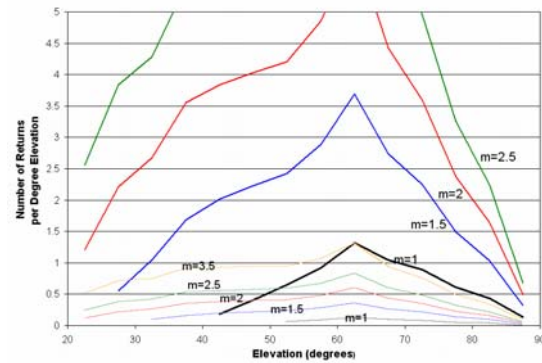


Figure 10: Productivity Gains

There are two sets of plots shown in Figure 10. The darker lines represent productivity increases based on current data while the lighter lines represent productivities assuming a factor of 10 (or 1 ND) loss in the number of returned photons. This factor is chosen to represent the loss when the enclosure glass window is installed and to account to some degree the effect of less than ideal sky conditions. The next section describes an analysis on the effect of the enclosure window, and for weak signals, it appears that a factor of 4 in link budget is required to compensate for the glass window.

It is clear that based on current data, increasing the link budget by 50% or 100% should make a substantial improvement to productivity including the possibility of obtaining reasonable number of returns from Giove A at elevations below 30 degrees. However, it is important that improved productivity levels can be maintained when the enclosure window is in place or when sky conditions deteriorate. Assuming a 1 ND loss, the second figure shows that an increase in link budget by a factor of 2 or more will be sufficient to maintain productivity at levels at least as good as current levels, and probably better at elevations below 40 degrees.

### Effect of Enclosure Window

The Mt Stromlo SLR station is designed to allow continuous and unmanned operations in all weather conditions. This is in part achieved by having a weather-proof telescope enclosure incorporating a glass window. Such a window has many advantages for operations, but will also attenuate the transmit and receive beams. An assessment of the net impact from operating through the glass window is presented from comparisons made with data obtained when there was no glass window in place, i.e. the glass window is exchanged with an “air window”.

**Near Field Target**

A comparison of measurements to calibration pier (at a range of approximately 92m) with and without the glass window in place are shown in the Figure 11. The mean difference between the signals is approximately 0.061 ns (in two way time of flight) consistent with having a window with glass thickness of 18.3mm.

For a given configuration (i.e. fixed laser power, ND filters etc.) and equal time periods the return rate with a glass window in place is 6.8% while in air the rate is 10.3%. Thus the difference in average return rate gives a loss of approximately 30%.

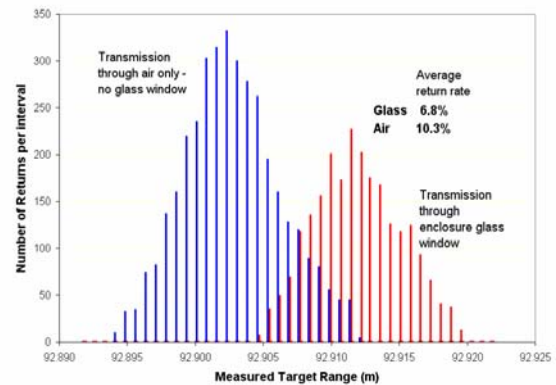


**Figure 11: Near Field Target Histogram**

**Far Field Targets**

Data from far field targets at ranges of 6,100 to 10,000 km allows a comparison of results for relatively good signals (Lageos 1) and weaker signals (Lageos 2). These satellites are used since comparisons are difficult using much higher satellites when fewer returns are available when the glass window is in place. The second and third plots show average return rates and return rate (suitably normalized by tracking periods) distributions for the two signal levels.

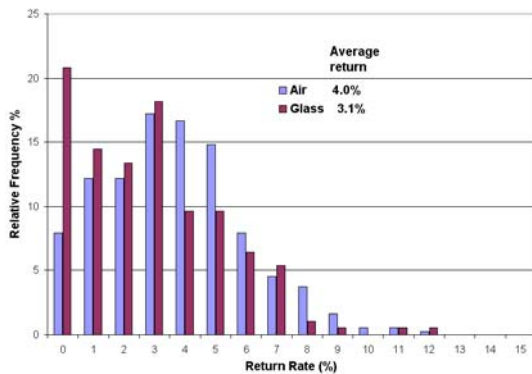


**Figure 12: Lageos 1 Return Rate Distribution**

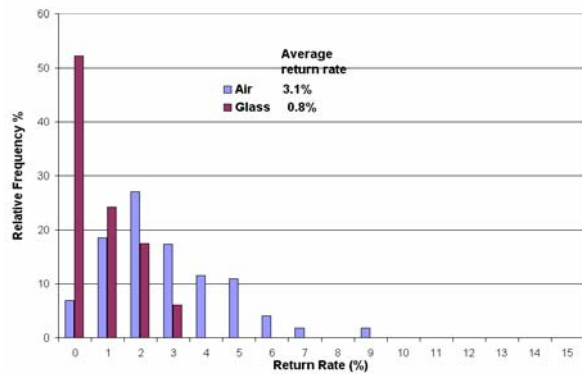


**Figure 13: Lageos 2 Return Rate Distribution**

**Good Return Signal**

When average return rate is relatively good, above 4% in air, the average return rate decreased to about 3% when the glass window was in place - indicating a 25-30% loss, similar to that for a near field target. The plot clearly demonstrates the relative decline in return rates above 3% when the window is in place and also the greater fraction of time there are no returns.

**Weak Return Signal**

When the return signal is weaker, in the case around 3% in air, the effect of the glass window is proportionally greater as illustrated in the third plot. In this case, the average return dropped to less than 1% when the glass was in place giving a loss of

over 75%. Return rates with the glass in place do not exceed 4% and there are no returns for at least 50% of the time.

### **Conclusions**

Mt Stromlo SLR station has successfully tracked Giove A for a number of months commencing in June 2006. A link budget analysis of the distribution of productivity data for this satellite with elevation has allowed an assessment of factors that may improve SLR productivity for Giove A (and other high earth orbit satellites).

Threshold effects associated with decreasing link budgets have been identified both during tracking of Giove A (e.g. with decreasing elevation) and also with Lageos 1 and 2 with transmission through air versus a glass enclosure window. Such threshold effects result in a rapid deterioration in detectable signal when return rates fall below approximately 3 or 4% for the current configuration at Mt Stromlo. Because of this threshold effect, it is possible that an increase in the link budget by a factor of two or better may lead to a substantial improvement in productivity. It is hoped that such an improvement can be demonstrated once the planned upgrade of the SLR laser power at Mt Stromlo has been implemented.

### **References:**

- [1] Degnan, J., Millimeter Accuracy Satellite Laser Ranging: A Review. Geodynamics Series 25.
- [2] Degnan, J., 1993. AGU Geodynamics Monograph Vol.25, p.139-140

## LASERS AND DETECTOR SESSION SUMMARY

Chairs: John Degan and Ivan Prochaska

The Czech Technical University reported the latest results on their space-qualified photon counting module for the Chinese Laser Time Transfer Project [Prochazka et al]. The silicon K14 SPAD has the following properties at 532 nm:

- Active area: 25 micron diameter
- Quantum Efficiency: 10%
- Timing Resolution: 75 psec
- Dark Count Rate: < 8 kHz @ 20°C
- Operating Temperature Range: -30°C to 80°C (no cooling)
- Power Consumption: <400 mW
- Mass: 4 g

In addition, it is highly resistant to solar and ionizing radiation (100 krad) damage and has an expected lifetime of greater than 10 years in space.

Andreev et al reported on a very different laser approach based on Stimulated Raman Scattering (SRS) pulse compression which produced 25 psec, 1 mJ pulses, at a 1 kHz rate and with good spatial mode quality ( $M^2 = 1.1$ ). Using a Nd:YAG Master Oscillator (MO) and three single pass Nd:YAG amplifiers in conjunction with a  $\text{Ca}_8\text{F}_{16}$  SRS cell, they generated 100 mJ, 350 psec pulses at 1319 nm. They used this radiation to pump a  $\text{Ba}(\text{NO}_3)_2$  SRS-MO and two SRS amplifier cells to obtain 50 mJ, 30 psec pulses at an eyesafe wavelength of 1530 nm and a 100 Hz rate. It was observed that the Raman conversion efficiency decreased noticeably at kHz rates for the higher peak pump powers.

Gao et al reported on diode-pumped lasers for tracking satellites and space debris. For SLR, 10 psec pulses are generated from a SESAM (Semiconductor Saturable Absorber Mirror) mode-locked laser oscillator, regenerative amplifier, and power amplifier. For debris tracking, they use two nanosecond pulses from a 230 Watt multistage system consisting of a single frequency oscillator, preamps, power amplifiers and SBS cells.

## Photon Counting Module for Laser Time Transfer Space Mission

Karel Hamal<sup>1</sup>, Ivan Prochazka<sup>1</sup>, Lukas Kral<sup>1</sup>, Yang Fumin<sup>2</sup>

1. Czech Technical University in Prague, Brehova 7, 115 19 Prague 1, Czech Republic,
2. Shanghai Observatory, Chinese Academy of Science, 80 Nandan Road, Shanghai, China

Contact: [prochazk@troja.fjfi.cvut.cz](mailto:prochazk@troja.fjfi.cvut.cz)

### Abstract

*We are presenting the results of research and development of the Single Photon Avalanche Detector (SPAD) for application in a Laser Time Transfer (LTT) space mission.*

*For the joint project with the Shanghai Observatory, Academy of Sciences of China, we have developed the detector package dedicated for the project of synchronizing the hydrogen maser-based time scales by laser pulses. The technology demonstrator of a dual detector has been built and tested in our labs. The main parameters are: detection efficiency 10% at 532 nm, timing resolution 80 psec, dark count rate 8 kHz, non gated operation. The detector's active area is 25  $\mu\text{m}$  in diameter. The total mass, including bias stabilizing circuit, is 2 grams, and the total power consumption is below 0.5 Watt per detecting channel. The detector can be operated in a wide range of temperatures ranging from  $-30^{\circ}\text{C}$  to  $+60^{\circ}\text{C}$  without any additional temperature control.*

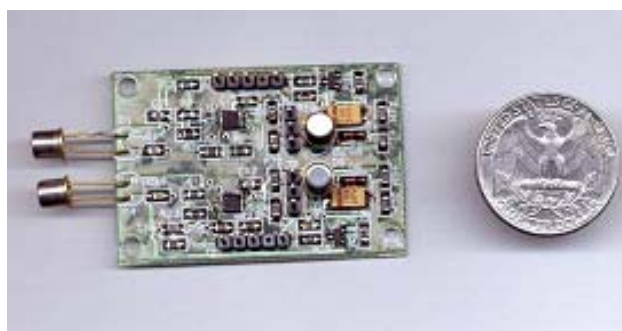


**Figure 1:** *The technology demonstrator of the dual photon counting detectors. The detection chips (protective caps installed for handling) are on the left.*

*The ruggedness of the detector is superb. Optical power of 2 mW has been focused onto a sensitive area while the detector has been biased for 8 hours. No detectable degradation has been experienced. The overload tolerance negates the need for any mechanical Sun protection shutter in space. The recovery time from optical overload to full functionality is less than 0.1 second. The detector package has been successfully integrated into the LTT timing electronics and the pre-flight test was performed in China during the period July-September 2006.*

## GOALS

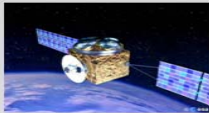
- Fast photon counting detectors for the Laser Time Transfer space mission, China
- BACKGROUND  
the K14 SPAD detectors have been launched onboard MARS 96 (Russia) and NASA Mars Polar Lander (USA) space missions
- REQUIREMENTS
  - low mass, power, bias voltage
  - high radiation in - sensitivity (> 5 years in space)
  - high temperature range
  - extreme optical damage threshold (full Solar flux, no shutter)



Prochazka, Hamal, Kral, Yang Fumin, Canberra, October 2006

## „LTT Module in Space”, China, 2007-2008

- GOALS
- to synchronize the rubidium clocks in space, hydrogen masers in a future.
- Laser Time Transfer (LTT) between space and ground
- employing the existing China Satellite Laser Ranging network consisting of 5 fixed and 2 mobile systems
- required ~ 100 ps timing accuracy
- expected accuracy improvement >> 10x over RF techniques



Prochazka, Hamal, Kral, Yang Fumin, Canberra, October 2006

## Detector Requirements - version LTT China

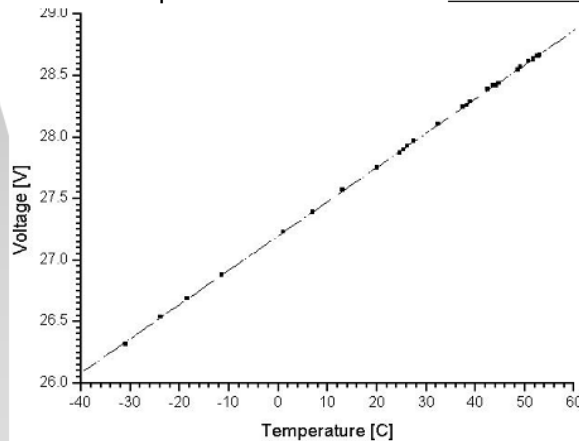
- single photon timing K14 SPAD chips  
two channels
- aperture 25  $\mu\text{m}$  each
- timing resolution < 100 psec
- power, mass < 2 W , 100 grams
- operating temperature -30 ... +60°C
- lifetime in space > 5 years
- high opt. damage threshold direct exposure to the Sun (!!)  
in a focal plane of 2 mm aperture collecting optics  
no Sun safety shutter will be installed
- design & construction 3 months (!) 😊



Prochazka, Hamal, Kral, Yang Fumin, Canberra, October 2006

## SPAD Bias Temperature Control

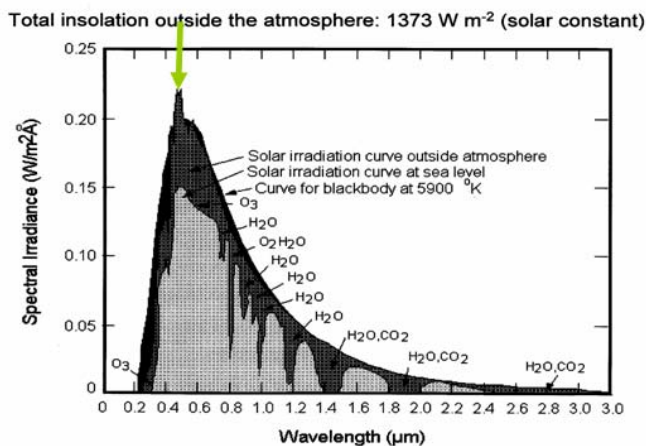
- SPAD break down voltage 29 Volts
- bias accuracy required 100 mV
- temperature range requested -30 ... + 60° C
- no temperature control or cooling
- SPAD break voltage temperature drift - 30 mV / K
- => temperature controlled bias circuit



Prochazka, Hamal, Kral, Yang Fumin, Canberra, October 2006

## Optical Damage Threshold

### Solar Spectrum



Source: The University of Texas at Austin, Center for Space Research

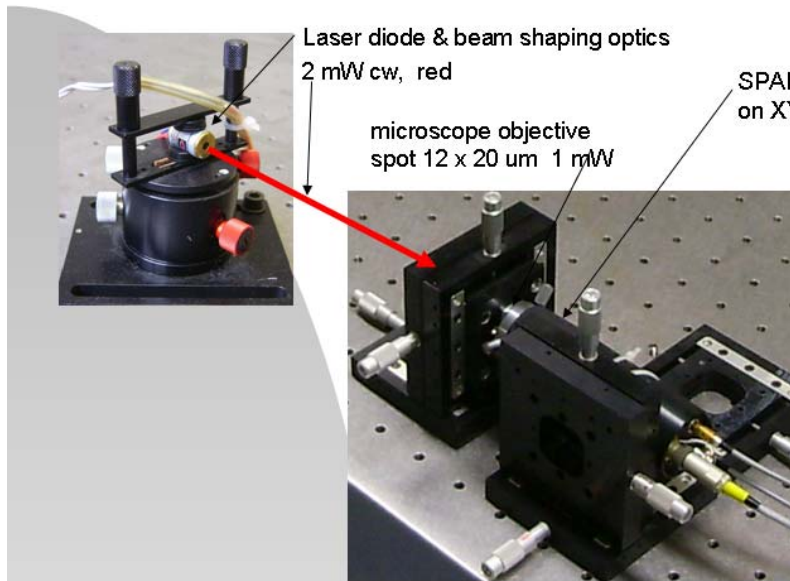
- Irradiance 0.2 W/m<sup>2</sup>/0.1 nm @ 532nm wavelength
- receiver
  - aperture 2 mm
  - f / d ~ 1.0
  - field of view ~ 0.5°
  - entire Solar disc
- bandwidth 100 nm
- blocking glass filter
- => 1 mW max. on SPAD

Surprisingly, the total flux on the detector aperture is not exceeding 1 mW /100 nm for any aperture (!), due to the field of view limitation.

Larger telescope is not capable to focus all the incoming Sun light onto small SPAD aperture.

Prochazka, Hamal, Kral, Yang Fumin, Canberra, October 2006

## Optical Damage Tests

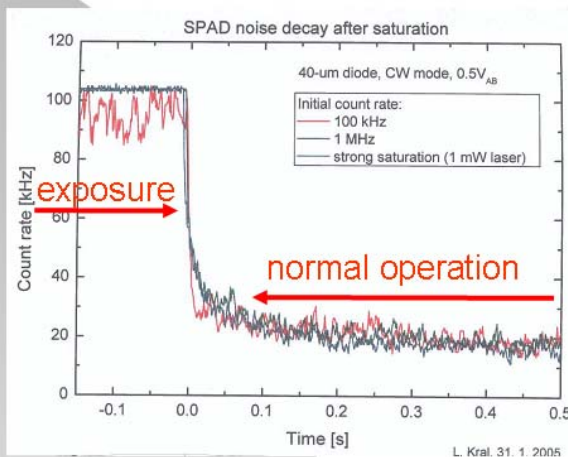


- exposure tests :
- no bias 3 x 8 hr
- biased 3 x 8 hr

- NO detectable detector degradation after all optical irradiation tests
- Any size telescope with SPAD detector may be pointed toward the Sun without the damage ( $< 100$  nm bandwidth)

Prochazka, Hamal, Kral, Yang Fumin, Canberra, October 2006

## Optical Saturation Recovery



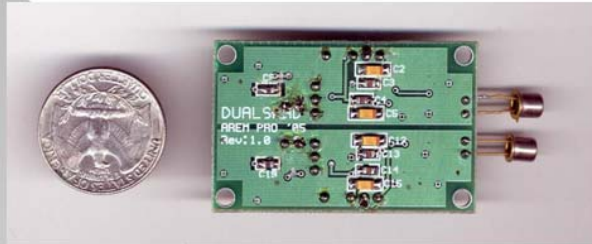
- Detector operation recovery after strong optical signal exp.
- detector illumination
  - ambient light 100 kHz
  - attenuated laser 1 MHz out of range when illuminated
  - full laser 1 mW NA out of range when illuminated
- instrument time constant  $\sim 0.02$  s

- Detector recovery time after saturation is well below 100 ms
- within this time, the dark count rate drops to 1.1 times the standard value

Prochazka, Hamal, Kral, Yang Fumin, Canberra, October 2006

## Photon Counting Module for Space Mission LTT

Technology demonstrator  
Prague, March 2005

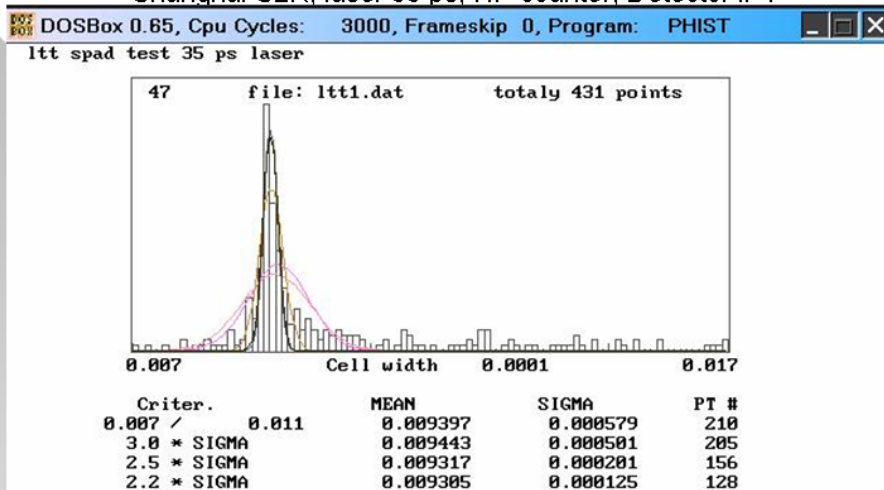


Detector package sample  
for pre-flight tests  
Shanghai, China, July 2006

Prochazka, Hamal, Kral, Yang Fumin, Canberra, October 2006

## SPAD Timing Resolution Tests, Shanghai July 2006

Shanghai SLR, laser 35 ps, HP counter, Detector # 1



- Jitter detector # 1 125 psec
- detector # 2 120 psec
- Detection delay difference 440 +/- 20 psec

Prochazka, Hamal, Kral, Yang Fumin, Canberra, October 2006

## Dual Single Photon Counting Module Detector Technology Demonstrator - Specifications

- configuration dual photon counting detector based on Silicon K14 SPAD
- quenching active
- active area circular 25  $\mu\text{m}$  diameter
- quantum efficiency  $\sim 10\%$  @ 532 nm
- timing resolution 75 psec
- dark count rate  $< 8\text{ kHz}$  @  $+20^\circ\text{C}$
- operating temp.  $-30 \dots +60^\circ\text{C}$   
no cooling, no stabilisation
- power consumption  $< 400\text{ mW}$
- mass 4 grams
- optical damage th. full Solar flux 100 nm BW,  $> 8\text{ hr}$
- lifetime in space  $> 10\text{ years}$



Prochazka, Hamal, Kral, Yang Fumin, Canberra, October 2006

## CONCLUSION Photon Counting Module for Space Mission LTT

- the Technology Demonstrators have been completed  
Prague, March 2005



- the Flight Unit detector version has been completed  
Shanghai, July 2006
- Solar flux resistant using moderate wavelength filtering
- radiation resistant, 100 kRads without parameter change  
=> lifetime in space  $> 10\text{ years}$
- pre-flight tests, Shanghai, Beijing, fall 2006

Prochazka, Hamal, Kral, Yang Fumin, Canberra, October 2006

---

## **Picosecond lasers with Raman frequency and pulsewidth conversion for range finding**

N.F. Andreev<sup>1</sup>, E.A. Grishin<sup>2</sup>, O.V. Kulagin<sup>1</sup>, A.M. Sergeev<sup>1</sup>, M. Valley<sup>3</sup>

1. Institute of Applied Physics, Nizhny Novgorod, Russia
2. Institute for Precision Instrument Engineering, Moscow, Russia
3. Sandia National Laboratories, Albuquerque, USA

### **Abstract**

*We review design issues for short-pulse lasers with Brillouin and Raman pulse compression and frequency conversion. In particular, scheme and material development has enabled us to provide output pulsewidth of 25 ps by SRS at a repetition rate of 1 kHz. Also, advantages of advanced laser ranger based on eye-safe high-power laser are discussed.*

### **Introduction**

Solid-state lasers generating high power picosecond pulses are attractive for a wide range of applications. Conventional mode-locked lasers with complex scheme emit ps pulses of widened spectral width at low pulse energies (less than 1  $\mu$ J) [1-3]. Slightly higher energies are produced by microchip lasers with passive [4] and active [5] Q-switch. Such laser may generate pulses as short as 56 ps [5] with high repetition rate. However, the pulse energy in this case is not higher than a few  $\mu$ J if  $\tau \leq 500$  ps. In both cases such pulses require further amplification in regenerative and multipass amplifiers. But a direct amplification of picosecond pulses is complicated and negatively affects the quality of the beam. The other method to increase the peak power of laser pulses is to use the pulse compression via Stimulated Raman and Brillouin Scattering (SRS and SBS) [6-8].

We present here the results of using SBS and SRS for an efficient temporal compression and frequency conversion of Q-switched laser pulses for range finding systems. High conversion efficiency and simple optical approach make this method rather attractive for the pulses up to several picoseconds. But there non-linear optical pulse compression was applied in pulsed lasers with low repetition rate. Earlier experiments were submitted where for the first time SBS pulse compression technique for diode-pumped solid state lasers (DPSSL) has been demonstrated [9].

It is known that the pulse compression ratio of up to  $\sim 17 \div 20$  could be achieved in the optimal pumping geometry of SBS. Besides pulse compression, the phase conjugation (PC) and beam cleanup by SBS have been widely employed in the double-pass laser amplifiers. However, the spatial-temporal distributions and energetic stability of output Stokes pulses dramatically degrades for the pump pulses approaching  $\sim 3$  ns due to unwanted self-focusing or SRS in conventional SBS-active liquids, such as  $\text{CCl}_4$ ,  $\text{SnCl}_4$ , and  $\text{D}_2\text{O}$ . Therefore the short pulses of  $\sim 160$  ps duration and  $\sim 0.3$  mJ energy attained presently in SBS-compressors by neglecting poor energy stability and accompanied by thermal and diffraction distortions introduced by subsequent multi-pass amplifiers.

It is shown here that SBS-cell filled by high purity heavy fluorocarbons  $\text{C}_8\text{F}_{18}$  is capable to maintain order of magnitude higher intensities of pump radiation without

the risk of optical breakdown. This allowed us for the first time to incorporate SBS-compressor into the scheme of double-pass amplifier and employ it as phase conjugate mirror for the beam cleanup. As a result, the exceptionally smooth and diffraction-free Gaussian beam has been achieved at the output of SBS-compressor. Moreover extraordinary high reflectivity ( $>97\%$ ) of novel SBS-mirror allows efficient energy extraction from double-pass amplifier.

This scheme has been incorporated into custom design Nd:YAG lasers (see Fig.1) for plasma and ultrafast flow dynamic research. High-quality spatial and temporal distributions are assured by a two-pass Nd:YAG amplifier with SBS-compressor. The MO is protected by Faraday isolator from unwanted backward high-intensity amplified Stokes radiation.

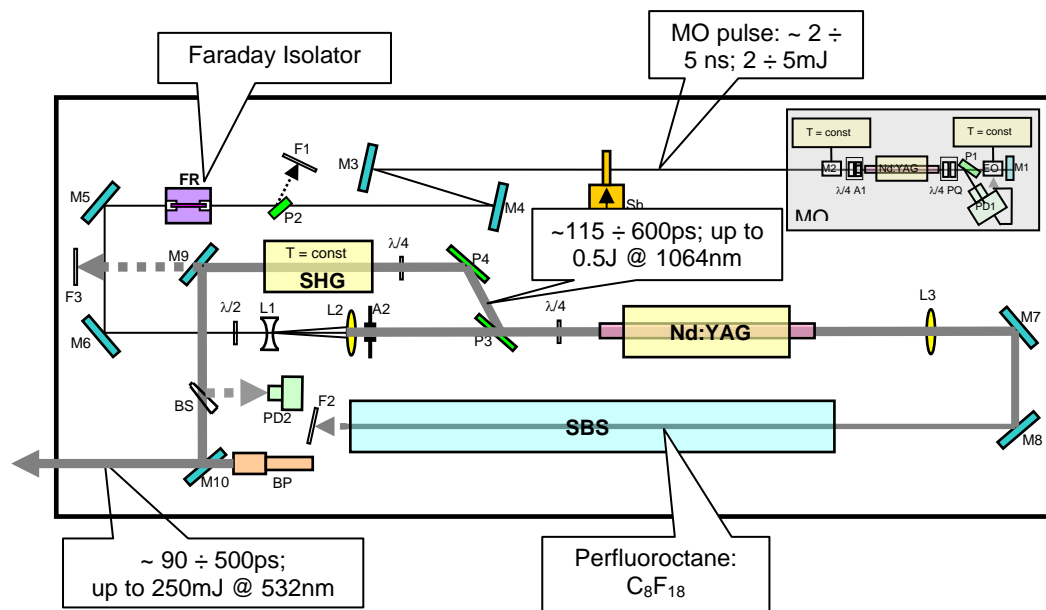


**Fig.1.** Schematic of the laser with the SBS compression stage

In optimised SBS focusing geometry laser provides output pulses of  $\sim 100$ ps at 532nm. RMS energy stability of output laser pulses at 532nm (114ps; 90mJ) was  $\pm 2.5 \div 3\%$ ; temporal jitter  $< 100$  ps (RMS deviation) respectively the signal of fast electrical trigger.

The subsequent solid-state SRS-compressor based on  $\text{Ba}(\text{NO}_3)_2$  crystals combined with SBS-compressor allows us to increase compression while ensuring a diffraction-limited output Stokes beam as well as to get output wavelength in a wide range (in particular, in eye-safe range), because of high value of Raman frequency shift. As a result of these investigations, a robust and reliable Nd:YAG laser (see Fig.2, as it is at the operational site for SLR) for satellite ranging has been created. This laser was installed in Altay Optical\ Laser Center of Institute for Precision Instrument Engineering.

Here the laser pulses with a pulse width of 3 ns and energy of 1 mJ come from a master oscillator (MO) to the power amplifier (laser heads PA1 and PA2). A Faraday rotator FR was installed between the MO and the power amplifier to protect the MO from residual backward radiation. After positive lens L2, we have got a collimated beam with a diameter of about 7 mm, which is a bit smaller than the diameters of Nd:YAG rods (8 and 10 mm) in the laser heads. After the first pass through laser heads PA1 and PA2 a laser pulse is reflected in the SBS-cell. Then the laser pulse

passes second time through quarter-wave plate, changes its polarization into orthogonal and leaves the power amplifier with the help of a polarizer. A two-stage SRS pulse compressor was used to provide high efficiency of laser energy into the picosecond region.

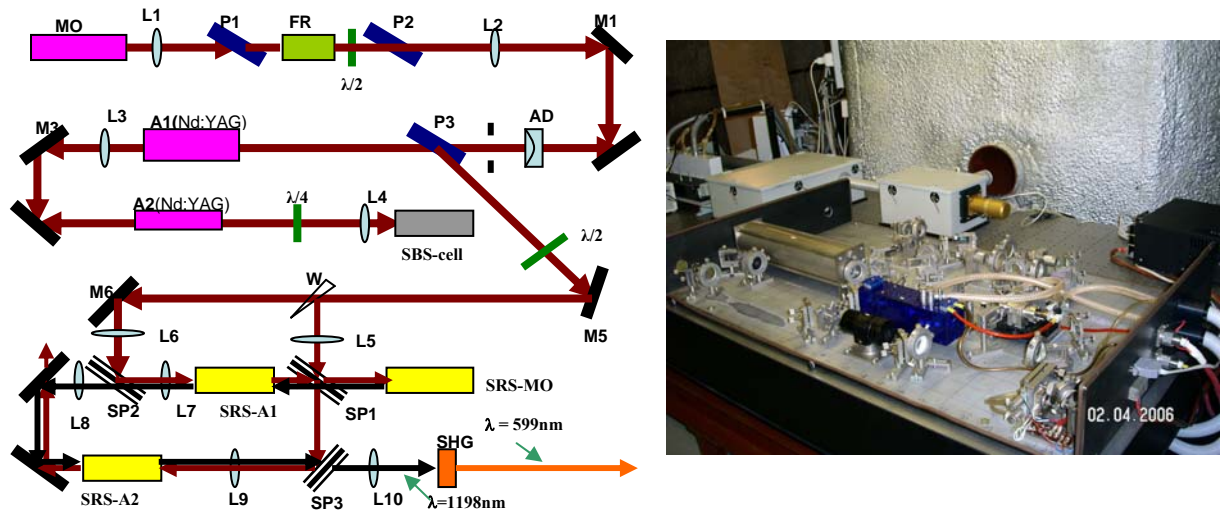


*Fig.2. Scheme and view of the laser with the SBS and SRS compression stages*

On the input to Raman compressor a beam-splitter **W** (a glass wedge) after our Nd:YAG laser reflects about 0.5% of laser output to pump the Raman oscillator. The remaining radiation is sent to pump crystals of the first Raman amplifier by a mirror **M6** and a spectrum-splitter **SP2**. The first Raman amplifier is placed between two spectrum splitters **SP1** and **SP2** - dichroic mirrors which are transparent for the Stokes wavelength of 1198 nm and high-reflected for the 1064 nm pump. For optimal time matching between pump and Raman pulses, the both Raman amplifiers were shifted along optical axes. When pulse compression conditions are met, 100 mJ 30 ps pulses will be generated at appropriate repetition rates, i.e., the Raman pulses' width is more than 10 times narrower compared to that of the pump pulses, as was measured at the previous stage of the project. After the first Raman compression stage, the conversion efficiency of pump radiation to the Raman output is about 10-20%. It is due to a comparatively low output energy from the Raman oscillator ( $\sim 0.01$  mJ) and the length ( $\sim 7-8$  cm) of the Raman amplifier crystals relative to the pulse width. The conversion degree was increased by up to 50% - 60% by arranging an additional path of counter-running Raman and pump beams through the second Raman amplifier. As a result, the laser produces spectrally limited pulses of 30 ps duration and  $\sim 100$  mJ energy at 1198 nm with RMS energy stability of 4%. Moreover, the second harmonic generation was used at the laser output to meet requirements of ranger system specification. In this case we have got output laser energy of 50-55 mJ in 25-30 ps pulses at 599 nm.

Also, an eye-safe high-power Raman picosecond laser is developing now for a project of an advanced laser ranger. Next to atmospheric turbulence, range is the dominant source of uncertainty in acquired laser ranger and tracker Time Space Position Information data. State-of-the-art ranging systems have an operating range and accuracy far below the needs for performance testing and model validation. A new, eye-safe, long operating range, accurate (order of cm) ranger will be developed using an ultrashort pulse (e.g., picosecond) laser system in conjunction with time-of-flight

measurement methods. This laser has the similar scheme as in Fig.2, but a four-pass power amplifier with three laser heads is used instead of two-pass one with two laser heads in Fig.2. In this case Nd:YAG MOPA scheme produces pulses (pulse width  $\sim 0.35$  ns) of energy up to 100 mJ at 1319 nm to pump Raman compressor scheme. The Raman compressor produces Stokes output pulses with wavelength of 1530 nm and picosecond pulse width. As a result of the development of the eye-safe picosecond Raman laser, we achieved the following set of parameters: output of 25-30 ps pulsewidth and 50 mJ pulse energy at 1530 nm and repetition rate of 100 Hz.

Further, Raman compression in the field of two counterpropagating pump beams has been studied for the first time both theoretically and experimentally [10]. It was shown that this geometry allows further increasing the compression ratio of incident laser pump pulses up to 150. To check it experimentally, we used a diode pumped electro-optically Q-switched Nd:YAG laser as a pumping source for the solid-state SRS pulse compressor based on  $\text{Ba}(\text{NO}_3)_2$  crystals (see a lower/left corner of Fig.3). This laser (Master Oscillator for Raman compressor stage) produced single longitudinal mode near-diffraction-limited pulses of 3.3 ns duration and 3 mJ energy at a pulse repetition rate of 1 kHz.

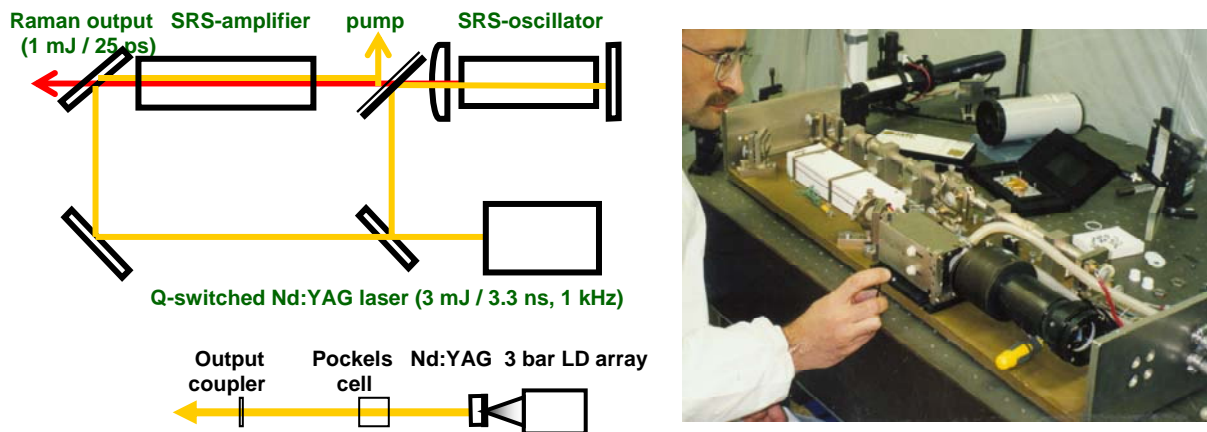


*Fig.3. Scheme and view of 1-kHz diode-pumped Raman laser*

Then the beam-splitter after the Nd:YAG laser reflected 20% of laser output to pump the SRS-oscillator. The rest laser radiation was sent to pump crystals of the SRS-amplifier. It was placed between the couple of dichroic mirrors which were transparent for Stokes wavelength 1198 nm and high-reflected for the 1064-nm pump. The high-reflected mirror for the both wavelengths was placed close to output from the SRS-generator. The alignment of its reflection in back direction provided the SRS threshold decrease by some times. It depended on focusing sharpness and pulse width. For the optimal time matching of pump and Raman pulses the SRS-amplifier was shifted along optical axes. With the carefully adjusted focusing of pump pulses into the crystal we obtained “pump – to Raman” energy conversion efficiency as high as 53% (for 1 kHz). When pulse compression conditions were held, 0.8 mJ - 1 mJ, 25 ps - pulses were generated at 1 kHz repetition rate, Raman pulses’ width being narrower than that of the pump by more than 100 times. Output beam was near-Gaussian shape, i.e. the beam quality was close to the diffraction limit. However, in the “pulse compression mode” the pump to Raman conversion efficiency dropped to 28%. It was caused by the insufficient total length (25 cm) of crystals in the SRS-amplifier

relatively to pulse width. However, the conversion energy efficiency could be increased by the arranging an additional opposite-directed pass of Raman and pump radiation through the SRS-amplifier.

Earlier, to our knowledge, the SBS and SRS pulse compression has not been practically studied for high repetition laser pulses typical for diode-pumped solid state lasers.

As a conclusion, the short pulse lasers with non-linear optical pulse compression are very attractive for laser ranging applications because of appropriate set of output parameters, the scheme simplicity and reliability.

## References

- [1] J. Aus der Au, G.J. Spuhler, T. Sudeyer, *et al.* "16.2-W average power from a diode-pumped femtosecond Yb:YAG thin disk laser" *Opt. Lett.* **25**, pp. 859-861 (2000).
- [2] T. Beddard, W. Sibbet, D.T. Reid, *et al.* "High-average-power, 1-MW peak-power self-mode-locked Ti:sapphire oscillator" *Opt. Lett.* **24**, pp. 163-165 (1999).
- [3] Z. Liu, S.Izumida, S. Ono, *et al.* *Appl. Phys. Lett.* **74**, 3622 (1999).
- [4] B. Braun, F.X. Kartner, G. Zhang, *et al.* "56-ps passively Q-switched diode-pumped microchip laser", *Opt. Lett.* **22**, pp. 381-383 (1997).
- [5] J. Zayhowski and C. Dill III. "Diode-pumped passively Q-switched picosecond microchip lasers", *Opt. Lett.* **19**, pp. 1427-1429 (1995).
- [6] D. Neshev, I. Velchev, W.A. Majeovski, *et al.*, "SBS-pulse compression to 200 ps in a compact single-cell setup", *Appl. Phys. B*, **68**, pp. 671-675 (1999).
- [7] V. Gidrauskas, A. Dement'yev, E.Kosenko and A.Rodin, "The SRS-amplification of picosecond Stokes pulses", *Journal of Applied Spectroscopy*, **60**, pp 266-272 (1994).
- [8] A.N.Mal'shakov, G.A.Pasmanik and A.K.Potemkin, "SRS-compression of 1ns laser pulses in SnCl<sub>4</sub>", *Quantum Electronics*, **27**, pp. 1024-1027 (1997).
- [9] A.A. Shilov, G.A. Pasmanik, O.V. Kulagin, K. Deki. "High-peak-power diode-pumped NdYAG laser with a Brillouin phase-conjugation pulse-compression mirror" *Opt. Lett.* **26**, pp. 1565-1567 (2001).
- [10] O.V. Kulagin, A.K. Kotov, G.A. Pasmanik. "Stimulated Raman scattering in counterpropagating pump beams – threshold decrease and pulse compression" *CLEO Pacific Rim, Proceedings*, v.2, p.475, (2003)

## **Advanced Solid State Laser Systems for Space Tracking**

Yue Gao, Yanjie Wang, Ben Greene, Craig Smith, Amy Chan,  
Andrew Grey, Josh Vear, Mark Blundell

1. EOS Space Systems Pty.Ltd., Canberra, Australia

### **Abstract**

*A new generation of advanced solid state laser systems has been developed at EOS for space tracking applications.*

*A completely diode pumped laser system consisting mode-locked laser oscillator, regenerative amplifier, power amplifier and non-linear device with 10 pico-second pulse width has been developed for satellite laser ranging.*

*A multi-stage and multi-channel completely diode pumped laser system consisting single frequency oscillator, pre-amplifiers, power amplifiers, SBS cells and imaging relays with 2 nano-second pulse width and 230 W output power has been developed for tracking space debris.*

*Both systems have been in service for more than 2 years with excellent performance and reliability.*

## **ALTIMETRY SESSION SUMMARY**

Chair: Frank Lemoine

With the successful return of data on missions such as Mars Global Surveyor, Clementine, Near Earth Asteroid Rendezvous (NEAR), and ICESAT, laser altimeters have been revealed as an essential tool for planetary exploration and Earth monitoring. This session included three papers on aspects of laser altimetry and a fourth paper demonstrating laser communications. Michaelis et al. reviewed the design for BELA, or the Bepi-Colombo Laser Altimeter. This instrument, onboard the Bepi-Colombo spacecraft would globally map Mercury with a 1 m /10 Hz instrument (100 m footprint, 300 m spacing) starting in 2019. Degnan et al. discussed second-generation photon counting imaging lidars. Second generation systems have flown on aircraft (1 km altitude) providing 15-20 cm resolution and contiguous coverage. Future systems could provide high-resolution topographic mapping even from orbital altitudes. Jirousek et al. presented the design of a timing system technology demonstration with sub ns resolution. The range gate delay width was 40 ns; the repetition rate was 24 Hz max, and the unit mass was 2.5 kg. The system was based on tested technology and developed in less than 3 months. Burriss et al. presented the results of a demonstration of laser communications at sea. Live video and other data were transmitted on a 125 Mbps fast Ethernet ship-to-ship link over distances of up to 11 nautical miles.

---

## Second-Generation, Scanning, 3D Imaging Lidars Based on Photon-Counting

J. Degnan, D. Wells, R. Machan, E. Leventhal, D. Lawrence, Y. Zheng,  
S. Mitchell, C. Field, and W. Hasselbrack

1. Sigma Space Corporation, 4801 Forbes Blvd., Lanham, MD 20706 USA  
Contact: [John.Degnan@sigmaspace.com](mailto:John.Degnan@sigmaspace.com) /Fax +01-301-577-9466

### Abstract

*Sigma Space is building a new generation of 3D imaging/polarimetric lidars based on photon-counting for use in small aircraft or mini-UAV's. The most recent system is designed to provide contiguous, high resolution (15 cm horizontal, 3 cm vertical) 3D volumetric images of the underlying terrain on a single overflight from an altitude of 1 km. Based on prior experiments with a first generation NASA prototype system and significant technological improvements, the second generation instruments are expected to have greatly enhanced spatial resolution, areal coverage, and ability to penetrate atmospheric haze, tree canopies, and even water columns for underwater imaging.*

### Introduction

In 2001, a prototype photon-counting laser altimeter was developed by NASA Goddard Space Flight Center [Degnan et al, 2001]. This first generation NASA system flew at altitudes up to 6.7 km and, using single photon returns in broad daylight, successfully recorded high resolution images of the underlying topography including soil, low-lying vegetation, tree canopies, water surfaces, man-made structures, ocean wave structures, and moving vehicles. The lidar was able to see the underlying terrain through trees and thick atmospheric haze (even when onboard cameras and personnel could not) and performed shallow water bathymetry to depth of a few meters over the Atlantic Ocean and Assawoman Bay off the Virginia coast. An external conical scanner, combined with the aircraft motion, allowed the generation of 3D images as in Figure 1.

### Second Generation Lidar

Sigma Space Corporation is presently developing a more compact and higher capability second generation 3D imaging and polarimetric lidar for high resolution

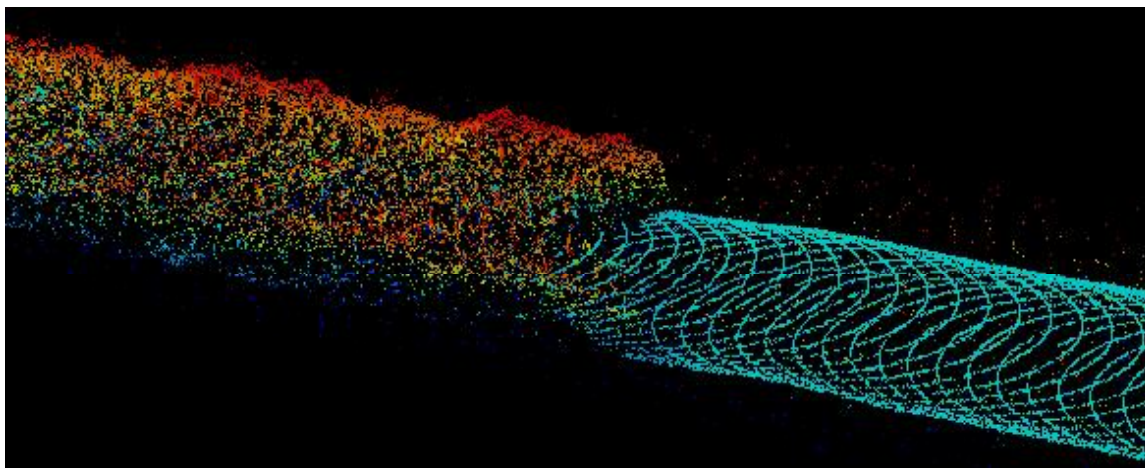


**Figure 1:** 3D image of a forest edge obtained in daylight by the 1<sup>st</sup> generation NASA photon-counting microlaser altimeter. (Courtesy Jan McGarrv. NASA/GSFC)

surveying and surveillance from a low altitude, mini-UAV. The shared transmitter is a passively Q-switched Nd:YAG microchip laser oscillator operating at a nominal fire rate of 20 kHz and producing 380 mW of output power at 1064 nm. The photon-counting imager operates at pulse rates up to 22 kHz with approximately 142 mW of frequency-doubled output power at 532 nm; the 238 mW of residual 1064 nm power

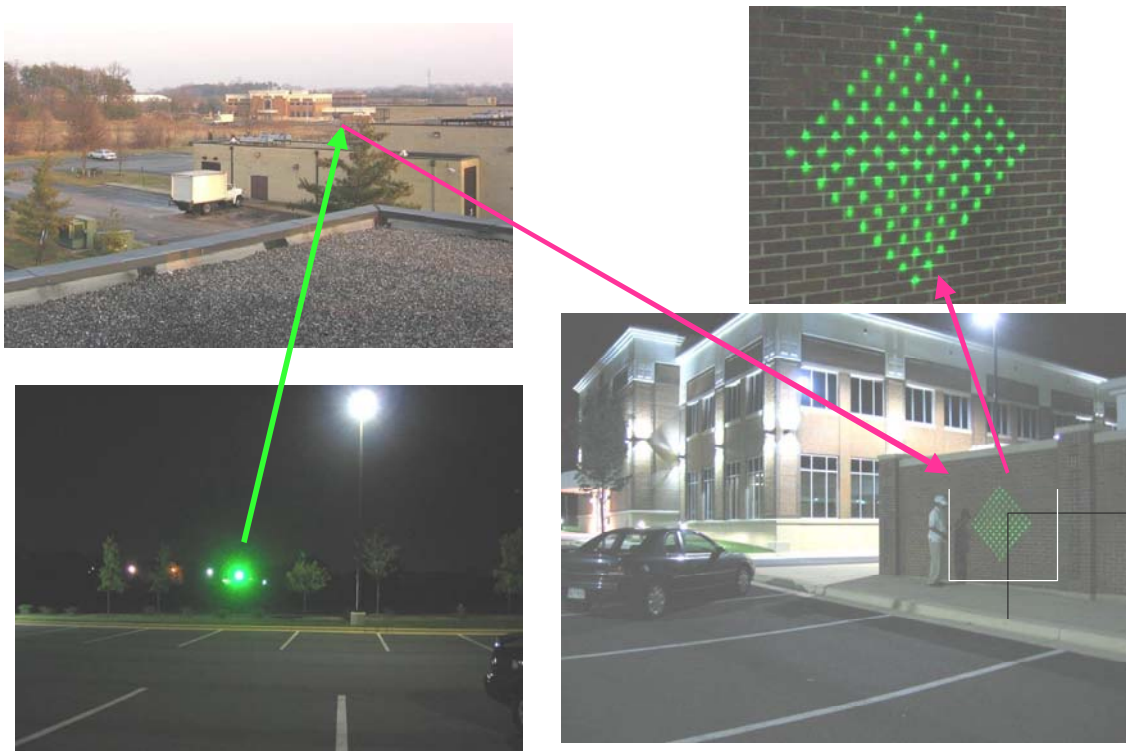


**Figure 2:** Counter clockwise from top left: View of target area (most distant building) from the Sigma rooftop; lidar beam as viewed from the target area; projection of holographically altered Gaussian beam on a brick wall at a distance of 250 m; closeup of 10x10 array of beamlets on the brick wall.

is allocated to polarimetry. Since the green wavelength is near the peak transmission of water, it is suitable for undersea imaging applications. The imager is designed to provide a contiguous, high resolution 3D topographic/volumetric map during a single overflight of the ground scene. From 1 km altitude, the scanner has a swath width of 150 m, a horizontal resolution of 15 cm, and an expected vertical (range) resolution of less than 3 cm. A Holographic Optical Element (HOE) breaks the spatially Gaussian laser beam into a 10x10 array of quasi-uniform eyesafe spots at the target (see Figure 2). The 100 individual far field spots from the HOE are then imaged by the receive optics onto individual anodes of a 10x10 GaAsP segmented anode microchannel plate photomultiplier. The output of each anode is input to one channel of a 100 channel, multistop amplifier/discriminator/timer. Presently, 50 multiple-stop timing channels can be accommodated by one amplifier/discriminator and one Time-of-Flight (TOF) Printed Circuit Board (PCB). The prototype timer has a demonstrated  $\pm 100$  picosecond timing ( $\pm 1.5$  cm range) resolution, a multistop capability with a 2 nsec recovery time per channel (corresponding to a capability to resolve objects separated by 30 cm or more in a single pixel for a single laser fire), and an ability to transfer up to 2.2 million ranges per second to onboard memory for long term storage and post-flight processing. Thus, each laser pulse produces a 100 pixel 3D volumetric image of

a 1.5 m x 1.5 m ground area. The individual images are then mosaiced together via the platform velocity and the action of a highly flexible dual wedge optical scanner synchronized to the laser pulse train.

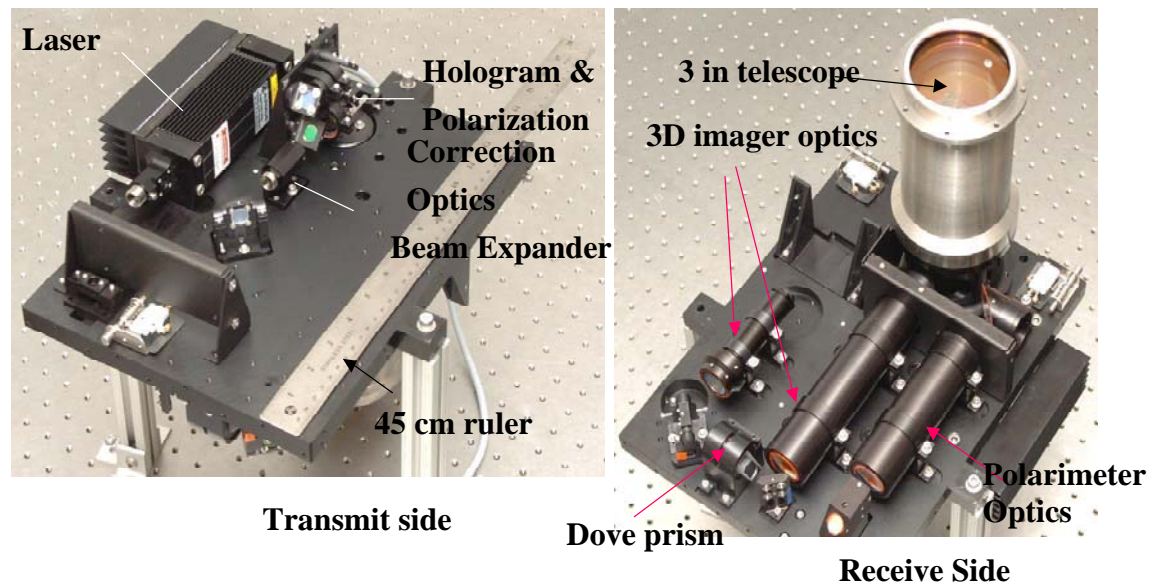


**Figure 3:** Optical bench and telescope for second generation 3D imaging and polarimetric lidar. An 18 inch (45cm) ruler is shown for reference

The transmitter and two receivers (imaging and polarimetry) share a common, 3 inch diameter afocal telescope and optical scanner. This allows the transmitter and receiver to have a common, but narrow, field of view (FOV) to aid in noise rejection and ensures that the imaging and polarimetric data are geographically coregistered. The polarimeter uses the residual laser power (~238 mW) at 1064 nm and two single element detectors to detect two polarization components (although the optomechanical design can accommodate up to 4 NIR detectors for a full determination of the Stokes parameters). Thus, the polarimeter has a nominal horizontal spatial resolution of 1.5 meters. A photo of the lidar optical bench (excluding scanner) is shown in Figure 3. The swath and scan frequency of the dual wedge optical scanner in Figure 4 are tailored to provide contiguous coverage of a ground scene in a single overflight [Degnan and Marzouk, 2003]. The highly flexible servo controller is capable of independently locking the phase and rotation rate of each wedge to the multi-kHz laser pulse train for an infinite variety of precision patterns. These include linear raster scans at various angles to the flight path and conical scans of varying cone angle as well as 2-dimensional rotating line or spiral scans, which might be useful for slow-moving aircraft, helicopters or hovering UAV's. Examples of a 1D linear scan at 45° to the flight path and a 2D rotating line scan are shown in Figures 5a and 5b respectively. The phase locking capability causes the laser beam to be laid down in precisely the same positions with each scan, thereby eliminating the need to record, store, and transfer the scanner wedge positions on each laser fire and greatly reducing data storage and handling. The measured scan repeatability is about 0.07 pixels or about 1 cm at an altitude of 1 km.

The 3D imaging and polarimetric lidar consists of two parts – an optical head and a supporting electronics box. The optical head measures approximately 33 cm x 30 cm x 43 cm and houses the optical bench in Figure 3 (transmitter, imaging and polarimetric optics and detectors, telescope, laser gyros and inclinometer for attitude

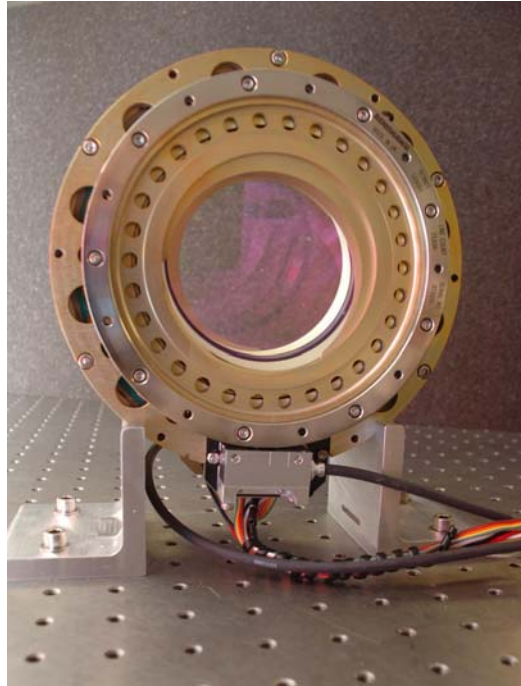


**Figure 4:** Photo of the direct drive dual wedge annular ring scanner developed under the NASA JIMO program. The annular ring motors have cryogenic and vacuum compatible counterparts suitable for space use.

determination, etc) plus the external dual wedge scanner in Figure 4, the MCP/PMT gating PCB, and the Amplifier/Discriminator/Timer PCB boards. The electronics box has a volume of 0.027 m<sup>3</sup> and houses the scanner electronics, GPS receiver, Reference Oscillator and Timing Distribution Circuits, Navigation and Imaging/Polarimeter Data Acquisition Modules, the laser power supply, and various DC/DC converters and voltage regulators. The manner in which the entire lidar system fits within the forward electronics bay of an Aerostar mini-UAV is illustrated in Figure 6.

### Summary

Photon-counting altimeters are extremely sensitive and highly efficient, requiring only one photon per range measurement, and, with multistop capability, can be operated day or night with large temporal gate widths for monitoring large elevation changes or simultaneously detecting the tops of tall buildings and city streets or tall treetops and the underlying terrain. Post-detection Poisson filters easily extract the signal from the solar background [Degnan, 2002]. The ability to penetrate obscurants (ground fog, vegetation, water) on a single shot (i.e. without “staring” at a scene while multiple pulses are fired) was demonstrated in the NASA prototype [Degnan et al, 2001]. This penetration capability was the result of the single photon sensitivity and the rapid multiple stop capabilities of the range receiver and will be substantially enhanced in our second generation instruments due to a factor of 12 increase in the effective signal photoelectrons received per ground pixel (~3 pe vs 0.25 pe in the NASA prototype).

Since the laser fires at a rate higher than necessary for contiguous coverage, the 3 pe/pixel is accumulated during multiple interrogations of the pixel during the scan, i.e. typically 3 interrogations at 1 pe which results in a higher probability of detection (~99%) than 3 pe for one interrogation (95%). The integration of a dual wedge scanner in the 2<sup>nd</sup> generation systems will eliminate the gaps in coverage previously observed with a single wedge conical scanner (see Figure 1) and provide contiguous coverage on a single overflight.

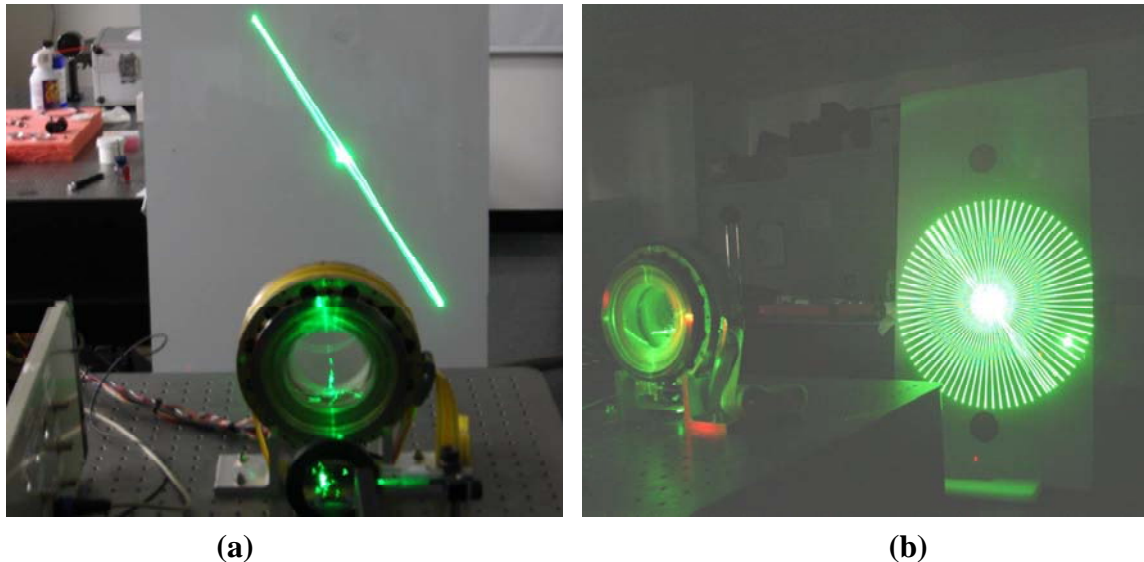


**Figure 5:** NASA prototype Direct Drive Internal Scanner generating (a) a linear scan and (b) a rotating line scan on a near field screen. Both scan types were run at 18 Hz and synchronized to a nominal 9 kHz Q-switched microchip laser pulse train. The slight bowing of the linear scan in (a) is due to near field displacement of the beam in the optical wedges but collapses to a true line in the far field. The non-uniformity of the rotating line scan at the 4 o'clock and 10 o'clock positions is due to a slight overlap of two consecutive rotating line scans.

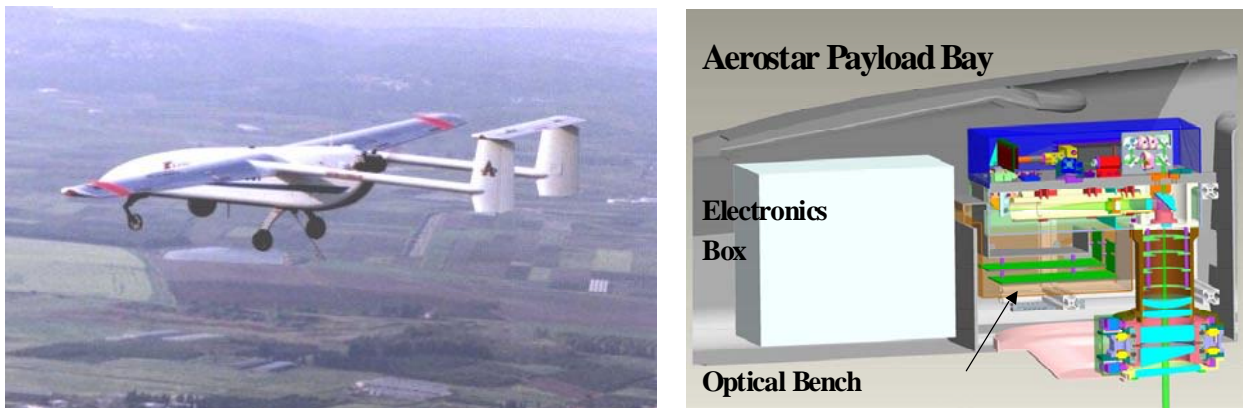


**Figure 6:** (a) Aerostar mini-UAV in flight; (b) Packaging of the 3D imaging/polarimetric lidar within the nose electronics bay.

### Acknowledgement

The work presented here was partially supported by USAF Phase II SBIR PO FA8650-05C-1817, Technical Officer: Richard D. Richmond, AFRL, Wright Patterson AFB OH 45433 and by NASA Contract NNH05CC68C, Technical Officer, Dr. Curt Niebur, NASA HQ, Washington DC 20546.

### References

- [1] Degnan, J., "Photon-Counting Multikilohertz Microlaser Altimeters for Airborne and Spaceborne Topographic Measurements", Journal of Geodynamics (Special Issue on Laser Altimetry), pp.503-549, November, 2002.
- [2] Degnan, J. and J. Marzouk, 2003 "An inexpensive 3D imaging lidar for contiguous decimeter resolution topographic mapping from a high altitude aircraft", Proc. AMOS 2003 Technical Conference, Maui, HA, Sept. 8-13, 2003.
- [3] Degnan, J., J. McGarry, T. Zagwodzki, P. Dabney, J. Geiger, R. Chabot, C. Steggerda, J. Marzouk, and A. Chu, "Design and performance of an airborne multikilohertz, photon-counting microlaser altimeter", Int. Archives of Photogrammetry and Remote Sensing, Vol. XXXIV-3/W4, pp. 9-16, Annapolis, MD, 22-14 Oct. 2001.

---

## **The BELA - The first European Planetary Laser Altimeter: Conceptional Design and Technical Status**

Harald Michaelis<sup>1</sup>, Tilman Spohn<sup>1</sup>, Jürgen Oberst<sup>1</sup>, Nicolas Thomas<sup>2</sup>,  
Karsten Seiferlin<sup>2</sup>, Ulrich Christensen<sup>3</sup>, Martin Hilchenbach<sup>3</sup>, Ulrich Schreiber<sup>4</sup>

1. Deutsches Zentrum für Luft- und Raumfahrt, Institut für Planetenforschung, Berlin, Germany.
2. Physikalisches Institut, Universität Bern, Switzerland.
3. Max-Planck Institut für Sonnensystemforschung, Katlenburg-Lindau, Germany.
4. Forschungseinrichtung Satellitengeodäsie der Technischen Universität München, Wetzell, Germany.

### **Abstract**

*The BepiColombo Laser Altimeter (BELA) is the first European laser altimeter for planetary exploration which has been selected by ESA for flight aboard ESA's Bepi Colombo mission to planet Mercury. A consortium led by the Physikalisches Institut Bern and Institut für Planetenforschung (DLR-Berlin, Germany) will develop a laser altimeter based on the classical principle of laser pulse time of flight measurement. The instrument is based on a longitudinally pumped Nd:YAG laser with 50mJ pulse energy and pulses of about 3ns duration, operating nominally at 10Hz repetition rate. The BELA requirements, the conceptional design, the technical development activities and their status are presented during the workshop.*

### **Introduction**

BepiColombo is the European Space Agencies (ESA) cornerstone mission to the planet Mercury. It consists of two orbiters, the Mercury Planetary Orbiter (MPO) and the Mercury Magnetospheric Orbiter (MMO). Among the instruments that have been confirmed is the Bepi Colombo Laser Altimeter (BELA). BELA's primary goal is:

- develop a full topographic map of the planet with an accuracy (goal) of 1m to support geomorphologic studies,
- explore Mercury's interior structure by joint analysis of topographic, gravity and rotation data,
- determine elastic properties of the planet by measurements of tidal deformation
- measure surface albedo and roughness,
- support spacecraft navigation.

### **Main Requirements**

The instruments key requirements are:

- Global topographic mapping with height accuracy of 10m wrt. COM (goal: 1m),
- Surface spacing 300m (shot to shot),
- High detection probability (>70%) up to 1000km,
- Laser footprint <100m.

The detection probability is defined by the PFD, the probability that a random noise fluctuation in the pulse detection chain is misinterpreted as a laser echo.

These requirements have to be fulfilled under the harsh environmental conditions at Mercury. The main design drivers for the instrument are:

- high thermal- and solar flux,

- to guarantee an alignment stability of a few arc seconds
- cosmic radiation levels,
- low resources (e.g. mass)

The main demands come from the high thermal flux (that is as high as  $10\text{kW/m}^2$ ) and the high Temperature of Mercury, which can reach surface temperatures of up to  $700\text{K}$ . The total instrument mass must not exceed  $12\text{kg}$ , which limits the size of the receiver and the laser transmitter.

### Technical Approach and Design

The BELA instrument consists of the receiver and the transmitter part which will be developed by institutions from Switzerland, Germany and Spain. The architecture of the instrument is shown in Figure 1.

The receiver telescope with the detector, the laser head and the beam expanding telescope are assembled on the so called Baseplate (BP) unit. The laser head, (OAB), is fibre pumped by the pumped-diode unit (PDU) which is controlled by the laser electronics (LEU). The main electronics of BELA including rangefinder electronics, data processing electronics, transmitter electronics (START-pulse detection and digitization) and the power supply are accommodated in a common electronics box,(ELU).

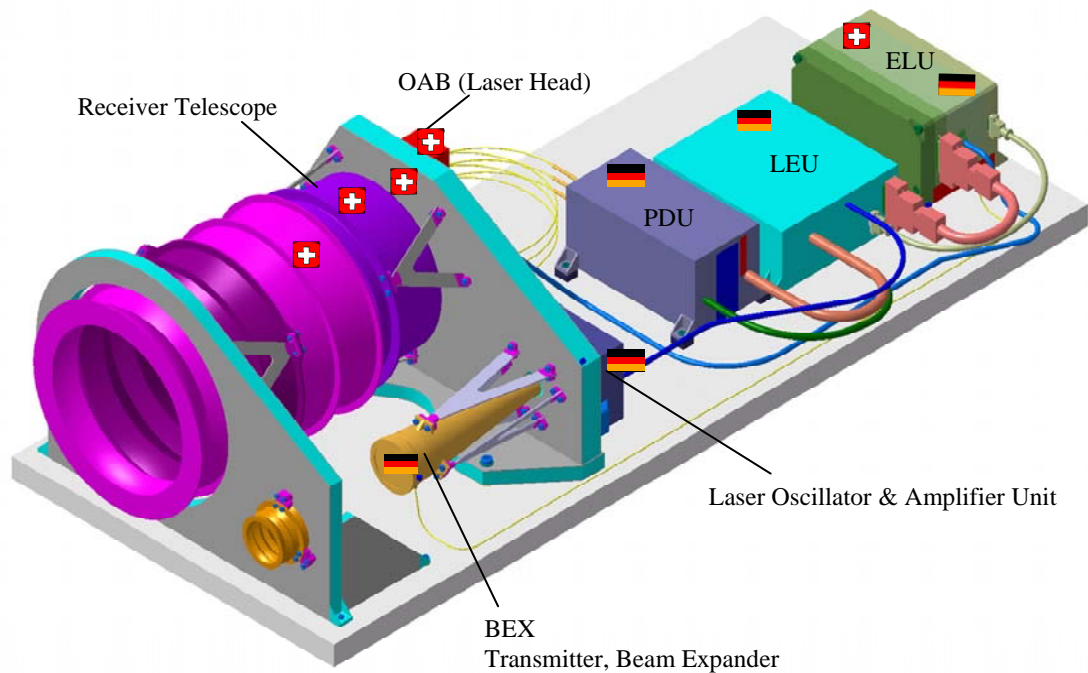


**Figure 1:** Main Components of the BELA Laser Altimeter

The main characteristics of the envisaged instrument are:

- 20-25cm lightweight telescope (1kg) with large baffle for thermal protection,
- backend optics with  $1\text{nm}$  filter /FWHM) and  $>80\%$  transmission,
- high sensitive (low noise) APD detector,
- $50\text{mJ}$ ,  $3\text{ns}$  diode pumped Nd:YAG laser,  $10\text{Hz}$  nominal repetition rate,
- $50\text{mm}$  (20x) beam expander with  $\sim 50\text{m}$  footprint @  $1000\text{km}$ ,

- common E box (ELU) with receiver-, START electronics and LEON-3 processor, power converter, thermal controller,
- 12kg, 33W (nominal).

The instrument's characteristics were derived by performance simulations according to the following parameter spreadsheet (see Table 1).

**Table 1:** BELA parameter set for performance simulation

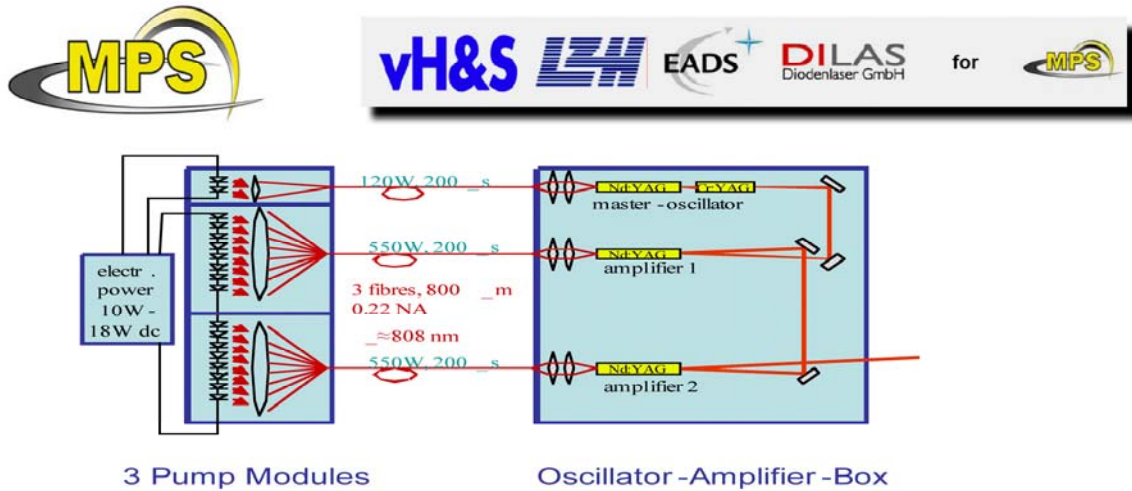
Parameter	Symbol	BELA
<u>S/C</u>		
Destination		Mercury
Altitude	$H$	400-1500 km
Pointing uncertainty	$\delta\phi$	25 $\mu$ rad
<u>Laser transmitter</u>		
Pulse energy	$E_r$	50 mJ <sup>a</sup>
Pulse width	$\delta_0$	3.4 ns <sup>b</sup>
Wavelength	$\lambda_T$	1064 nm
1/e <sup>2</sup> beam divergence	$\theta_T$	25 $\mu$ rad <sup>c</sup>
Repetition rate	$\nu_T$	10 Hz
Collimator efficiency	$\epsilon_T$	0.80
<u>Receiver optics</u>		
Aperture radius	$r_R$	125 mm
Focal length	$f_R$	1250 mm
Field of view	$\theta_{FOV}$	200 $\mu$ rad <sup>c</sup>
Optical efficiency	$\epsilon_{RO}$	0.70 <sup>d</sup>
Filter transmission	$\epsilon_{RF}$	0.80
Filter bandpass	$\delta_{RF}$	0.42 nm <sup>b</sup>
<u>Detector</u>		
Quantum efficiency	$\epsilon_{QE}$	0.38
Gain	$M$	150
Excess noise index	$\chi$	0.25
Surface dark current	$I_{DS}$	20 nA <sup>a</sup>
Bulk dark current	$I_{DB}$	50 pA <sup>a</sup>
<u>Electronics</u>		
TIA Bandwidth	$B_0$	20 MHz
ADC sample period	$T_R$	12.5 ns
Noise floor	$\delta I_{NF}$	1.0 pA Hz <sup>-1/2</sup>

The most critical parameters are the laser pulse energy, the aperture of the receiver telescope and the performance characteristics of the detector (quantum efficiency, noise). It was estimated that the instrument will be capable of meeting the performance requirements, PFD<0.1 out to a height of 1050km and a height accuracy measurement of down to 1m for a reasonable set of observing conditions.

Key instrument components are presently in development for performance verifications and testing. One key component, the laser units has already been designed and fabricated by MPS and German industry (Laser Zentrum Hannover e.V., DILAS GmbH, Mainz, Von Hoerner & Sulger, Schwetzingen) as a prototype model, which is shortly described below.

### The BELA-Laser

The optical design of the BELA laser is based on the concept of Nd:YAG laser crystals for the oscillator and the two amplifier stages, which are longitudinally pumped with GaAs diodes around 804 to 808 nm (@298K). The simplified block diagram of the laser head (OAB) and the pump diode unit (PDU) is shown in Figure 2.



The BELA instrument requirement is to have 3 fibre coupled pump sources (called modules); two of them shall deliver 550W ex fibre each for amplifier pumping while the third has to deliver 120W ex fibre for oscillator pumping. The diodes for oscillator pumping shall be available in cold redundancy, which means that two bars will be operated and two other bars can be used alternatively (not sketched).

**Figure 2:** Block diagram of the laser head (OAB) and the pump diode unit (PDU)

The OAB is optically pumped via three fibre optics cables between the OAB and the PDU. The output pulse energy of the laser is 50mJ at 3ns pulse duration (measured) and a firing of 10Hz (nominally). The control and the current supply of the laser are provided by the Laser Electronics Unit (LEU). The main parameters of the laser are summarized in Table 2.

**Table 2:** Laser Main Characteristics

Parameter	Unit	Value/Description
Material		Nd:YAG
Wavelength	nm	1064.x
Pulse Energy	mJ	50 (EOL)
Pulse frequency	Hz	10 (nominal)
Pulse Duration	Ns	3
M2		<1.6 (measured: 1.3)
Q-switch		Passive
Laser Pump		Longitudinal
Efficiency (electro-optical)	%	5.2 (measured)

The first Prototype Model of the laser is shown in Figure 3.



**Figure 3:** BELA Laser Prototype Model-1

Further key components that are presently in development are only shortly listed below:

***Beam Expander (BEX)***

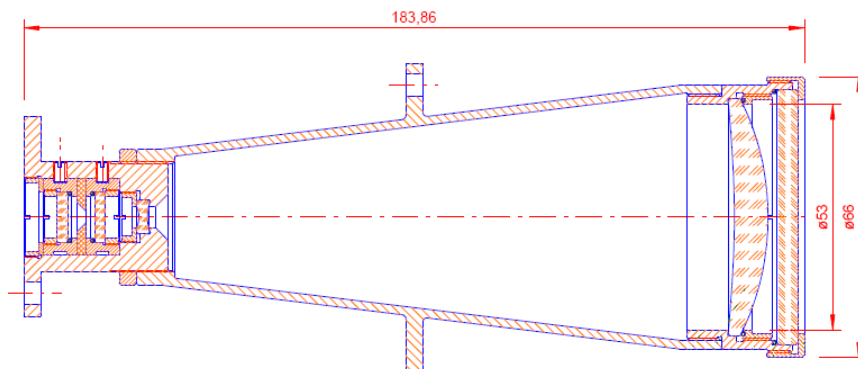


**Figure 4:** Opto-mechanical layout of the BELA Beam Expander (BEX)

The BELA beam expander (Prototype Model) is based on an aspheric lens design for the exit-lens in order to prevent a double-lens and to save mass. The beam direction can be slightly adjusted by wedge prisms at the entrance of the beam expander. The BELA-BEX has a nominal beam expansion ratio of 20. A fibre-optics interface is foreseen for optical detection of the START-pulse.

***START Electronics***

The START electronics has two functions:

1. detection of the START-pulse, which will be fed to the rangefinder electronics
2. digitization of the START-pulse for energy and shape measurement of the outgoing pulse

The block diagram of the START electronics and the first prototype is shown in Figure 5 and Figure 6 respectively.

The components of the receiver: telescope (incl. base plate), baffle, detector and rangefinder electronics are presently in development in Switzerland, lead by the University of Bern (Nicolas Thomas and Karsten Seiferlin).

### Conclusion and Outlook

The BELA team is in process to design the first European laser altimeter for planetary exploration which has been selected by ESA for flight aboard of ESA's Bepi Colombo mission to planet Mercury. Numerical models have been developed to assist with design tradeoffs and definition of operational modes. Key components like the laser have been developed as prototype model and further units are in fabrication (beam expander, receiver telescope, detector electronics).

The Forschungseinrichtung Satellitengeodäsie der Technischen Universität München (Wetzell) and DLR are presently in process to design a first performance demonstrator which is based on the BELA prototype models and commercial components with a performance characteristics close to BELA. This performance demonstrator will be used for functional and performance verification of BELA by satellite laser ranging, and it will be used as a transponder demonstrator.

### Acknowledgement

The authors would like to thank Reinhard Roll (MPS), Daniele Piazza and Kurt Gunderson (UBE) and the BELA team members of DLR Berlin (Mrs Kerstin Rösner, Wolfgang Bresch, Thomas Behnke, Matthias Tschentscher, Alexander Lichopoj, Kay Lingenauer, Rolf Schrödter) for their contribution to the present design, simulation and test of BELA components.

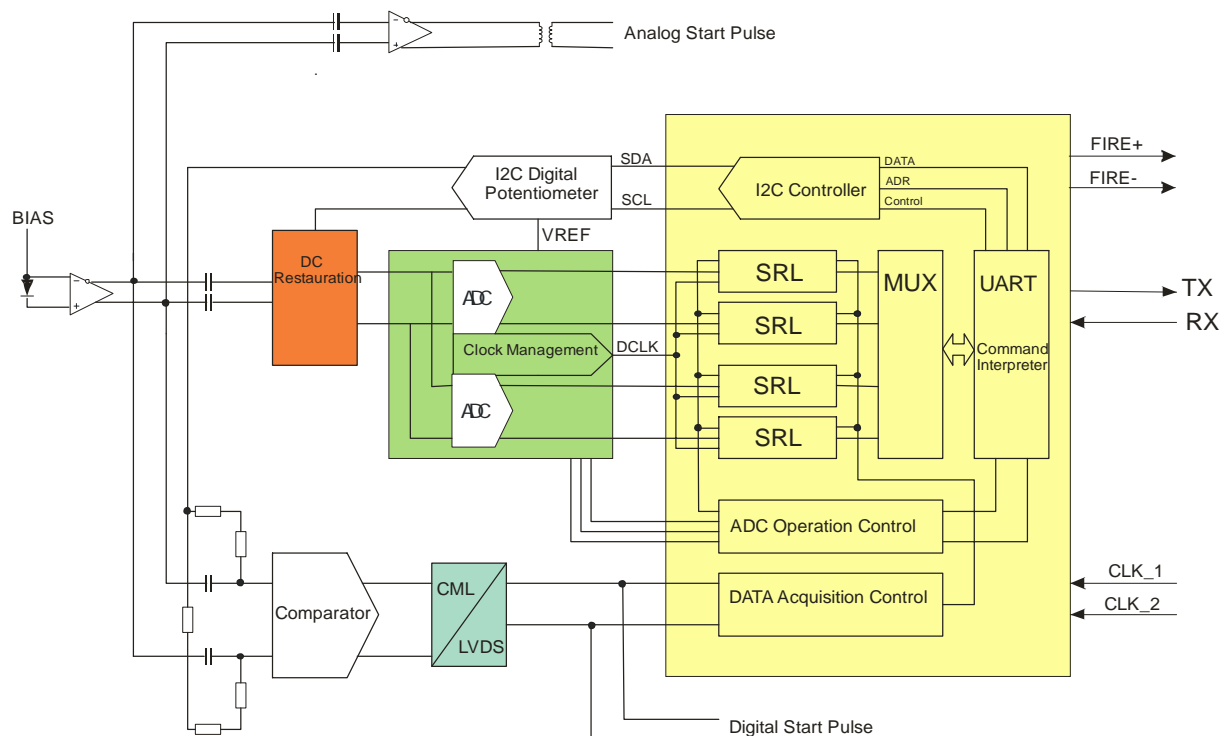


**Figure 5:** Block Diagram of the START-Electronics

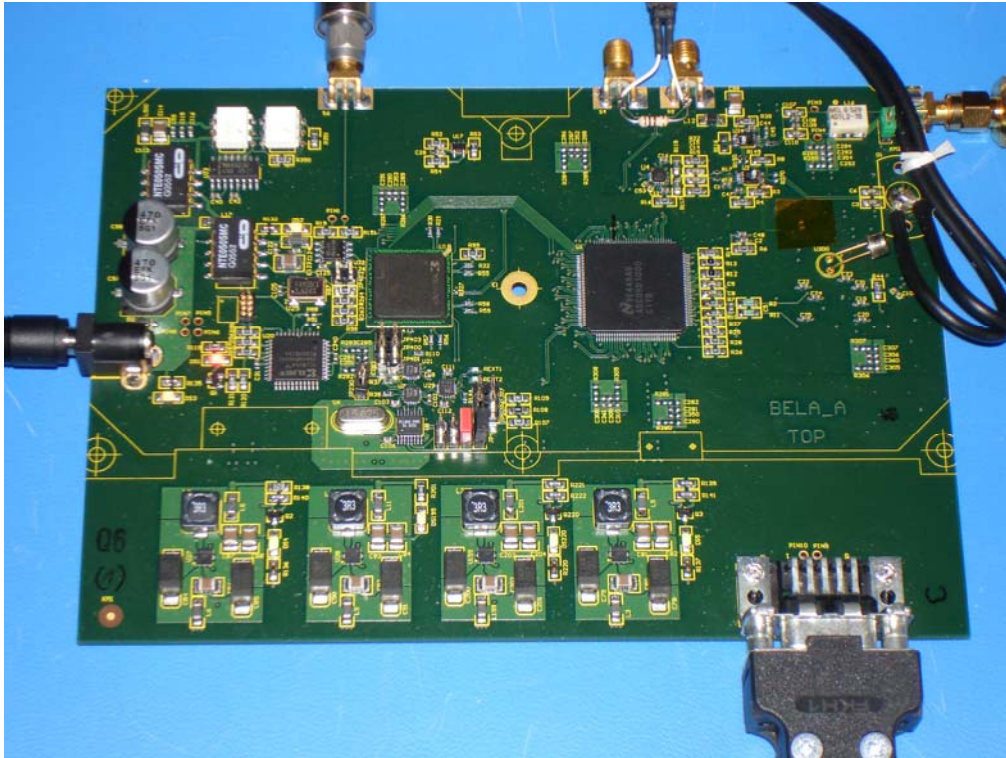


*Figure 6: Prototype of the START Electronics*

---

## Timing System for the Laser Altimeter for Planetary Exploration Technology Demonstrator

P. Jirousek<sup>1</sup>, I. Prochazka<sup>1</sup>, K. Hamal<sup>1</sup>, M. Fedyszynova<sup>1</sup>, U. Schreiber<sup>2</sup>,  
H. Michaelis<sup>3</sup>, Yang Fumin<sup>4</sup>, Huang Peicheng<sup>4</sup>

1. Czech Technical University in Prague, Brehova 7, 115 19 Prague 1, Czech Republic
2. TU Munich, Germany
3. DLR Berlin Adlershof, Germany
4. Shanghai Observatory, Chinese Academy of Science, China

Contact: [prochazk@troja.fifi.cvut.cz](mailto:prochazk@troja.fifi.cvut.cz)

### Abstract

*We are presenting the design, construction and tests of the timing system for the Bepi Colombo Laser Altimeter (BELA) technology demonstrator. BELA Timing System (BTS) is an universal timing system for laser ranging in ground-ground, air-ground and ground-satellite experiments. It is dedicated to measure precise time interval with subnanosecond resolution. The device for advanced range gating is included. The unit is interfaced to a host personal computer via a serial data link for control, two way data transfer and diagnostics.*

*The entire BTS has been designed and constructed on the basis of the Portable Calibration Standard (PCS) for satellite laser ranging, which has been developed in our labs within the last ten years. To reduce the complexity, costs, weight and power, considering the modest timing resolution requirements, the sub-nanoseconds instead of picoseconds resolution of the time intervals, the timing part of the original device has been replaced by the Mini counter. The overall design philosophy, the operational control software, the epoch timing, the range gate generation have been preserved along with the concept of the host computer software package for data acquisition, control and data analysis including the communication protocol, data and command formats etc. The use of well tested concept of both the HW and SW enabled to shorten the design, construction and testing phase of the final device down to several weeks.*

*The BTS consists of the Mini Counter module, the epoch timing and range gate generator module, the control processing unit, the input / output circuits and of the power supplies. The entire control logic hardware including the epoch timing and range gate generator and the input/output board logic is based on the FPGA (ispGAL) programmable logical arrays. There is a significant array capacity still available for future functional extensions and device upgrades, the arrays are field programmable. This fact ensures the maximum device flexibility and upgradability. The main parameters are : resolution 0.25 ns, linearity and stability better than 0.1 ns and 0.1 ns per K and per hour resp. The laser fire epoch resolution is 100 ns, the range gate is programmable in 40 ns steps. The device is small (2 kg), low power, it is capable to operate 3 hours on eight AA batteries.*

## Goals

- Technology demonstrator of a Compact Laser Rangefinder applicable in future space projects :
  - Mercury planet altimetry
  - Lunar altimetry and surface mapping
  - on-board optical transponder(s) for Earth orbiter(s)
  - airborne range finder
  - ground based Satellite Laser Ranging (SLR)
- Main altimeter parameters:
  - one meter ranging precision
  - multiphoton approach
  - diode pumped laser, ns pulses,
  - modular construction
  - existing / available technology

Jirousek, Prochazka, Hamal, Fedyszynova, Schreiber, Michaelis, Yang, Huang, Canberra 2006

## Philosophy

- Technology demonstrator of a Compact Laser Rangefinder
- modular construction
- existing / available technology
- test bench at the Satellite Laser Ranging site Wettzell, WLRS
- applicable in various ground and space projects :
  - Mercury planet altimetry
  - Lunar altimetry and surface mapping
  - on-board transponder for Earth orbiters
  - ground based Satellite Laser Ranging (SLR)
  - airborne range finding

Jirousek, Prochazka, Hamal, Fedyszynova, Schreiber, Michaelis, Yang, Huang, Canberra 2006

## Schedule & responsibilities

July 31 st	decision, proposal, quotation	CTU Prague
August 31st	DLR acceptance, contract	DLR
October 30	first version operational	CTU Prague
November	on-site testing	CTU / DLR
November 30	delivery	CTU
December 15	integration at DLR	CTU / DLR

Jirousek, Prochazka, Hamal, Fedyszynova, Schreiber, Michaelis, Yang, Huang, Canberra 2006

## Altimeter Timing System Requirements

- GENERAL  
universal timing system for laser ranging with sub-ns resolution
  
- FUNCTIONS
  - determining the epoch of laser fire
  - measuring the time-of-flight of the laser pulse
  - generating the range gate pulse for the echo signal detector
  - data acquisition and process control.
  
- PROPERTIES
  - compact, low power (battery operated), low cost
  - based on field - proved components HW & SW
  - simple to integrate into final device

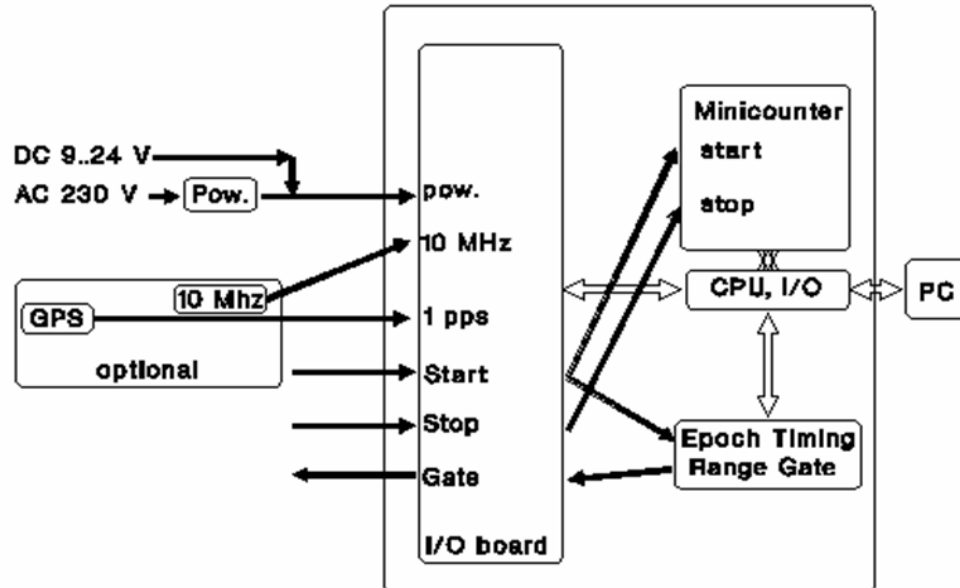
Jirousek, Prochazka, Hamal, Fedyszynova, Schreiber, Michaelis, Yang, Huang, Canberra 2006

## Altimeter Timing System Concept

- Based on P-PET hw and sw concept, the Dassault modules are replaced by integrated TDC chips .
  
- The timing system consists of the range counter module, the epoch timing and range gate generator module, the control processing unit, the input / output circuits and of the power supplies.
  
- The entire control logic hardware, epoch timing, range gate, and input/output board is based on the FPGA (ispGAL) programmable logical arrays.  
This ensures the maximum device flexibility and upgradability.

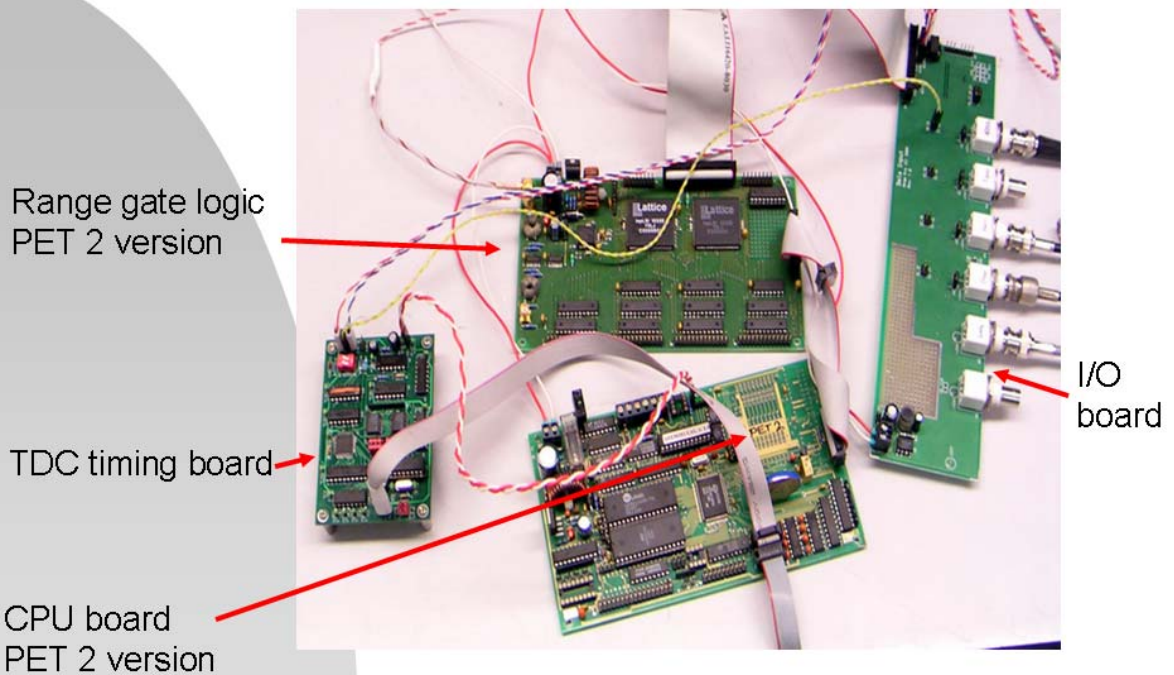
Jirousek, Prochazka, Hamal, Fedyszynova, Schreiber, Michaelis, Yang, Huang, Canberra 2006

## Timing System Technology Demonstrator Block scheme



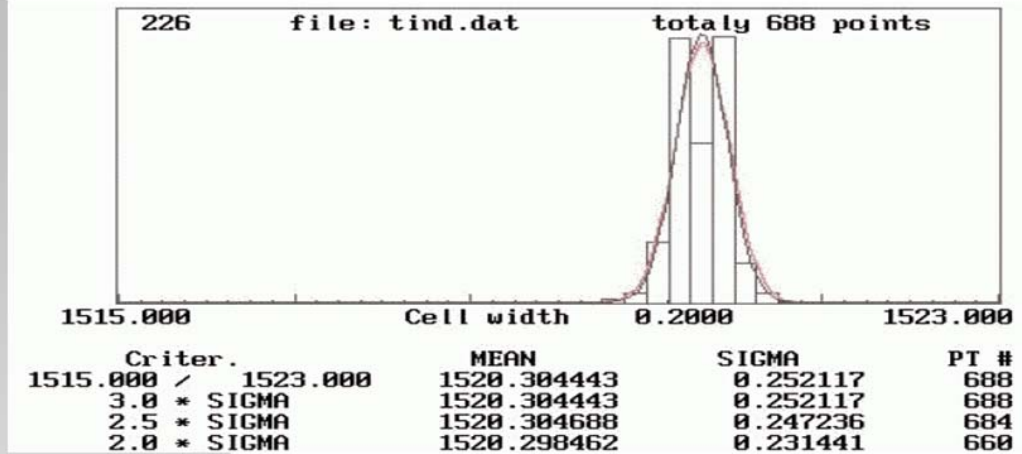
Jirousek, Prochazka, Hamal, Fedyszynova, Schreiber, Michaelis, Yang, Huang, Canberra 2006

## Timing System Technology Demonstrator Electronics boards



Jirousek, Prochazka, Hamal, Fedyszynova, Schreiber, Michaelis, Yang, Huang, Canberra 2006

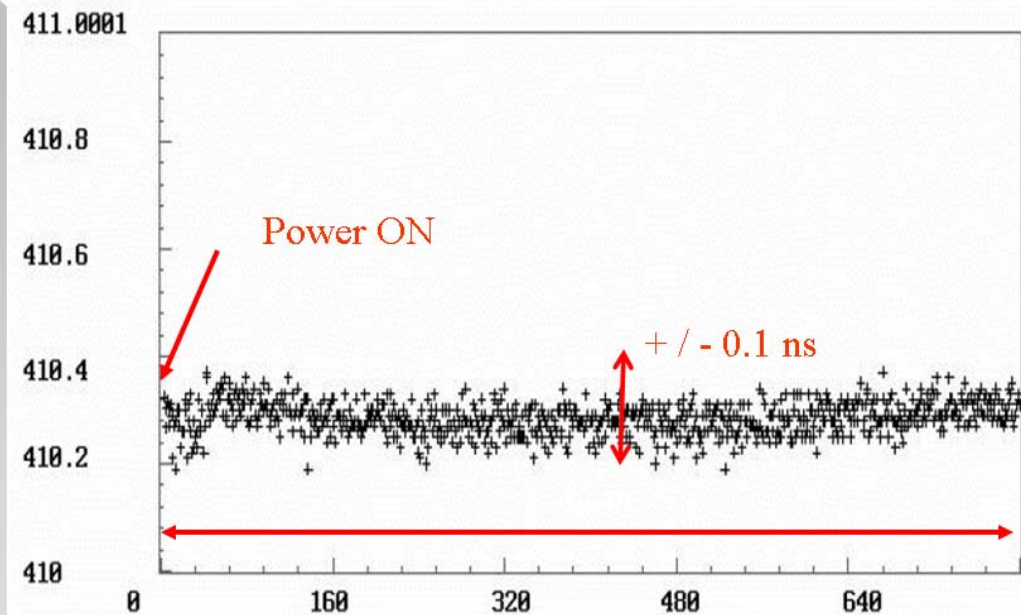
## Timing System Technology Demonstrator Temporal resolution



measured time 1.52  $\mu$ s  
 the timing resolution of 0.25 ns  
 normal data distribution

Jirousek, Prochazka, Hamal, Fedyszynova, Schreiber, Michaelis, Yang, Huang, Canberra 2006

## Timing System Technology Demonstrator Long-term temporal stability



Jirousek, Prochazka, Hamal, Fedyszynova, Schreiber, Michaelis, Yang, Huang, Canberra 2006

## Timing System Technology Demonstrator Parameters

- universal timing system for laser ranging with sub-ns resolution



- resolution, precision 0.25 ns, 0.25 ns rms
- non-linearity, stability < 0.1 ns, < 0.1 ns/hour
- range gate delay, width 40 ns steps
- repetition rate 24 Hz max.
- mass 2.5 kg
- power DC 9-38 V, 7 VA  
> 3 hr operation on AA cells (8x)

Jirousek, Prochazka, Hamal, Fedyszynova, Schreiber, Michaelis, Yang, Huang, Canberra 2006

## Altimeter Timing System Technology Demonstrator Conclusion

- the universal timing system for laser ranging:  
ground-ground, air-ground and ground-satellite  
with sub-ns resolution has been developed and tested
- simple to implement:  
SW package identical to PET devices
- based on tested technology and components  
development period < 3 months :-)
- In perspective the Altimeter Timing System may be applied  
in deep space laser transponder experiments

Jirousek, Prochazka, Hamal, Fedyszynova, Schreiber, Michaelis, Yang, Huang, Canberra 2006

## **A Compact Low Power Altimetry Laser For Lunar Applications**

Thomas Varghese<sup>1</sup>, Ralph Burnham<sup>2</sup>

1. Cybioms Corporation, 607 Autumn Wind Way, Rockville, MD 20850
2. Fibertek Inc., 510 Herndon Parkway, Herndon, VA 20170

### **Abstract**

*A very compact 10 mJ, 10 Hz, 4ns laser with greater than a billion shots capability is being developed for lunar altimetry applications for a mission projected for 2008. The altimeter will complement other scientific payloads of the mission that includes Terrain Mapping Camera with stereo imaging capability, Hyper-Spectral Imager, and a Low Energy X-ray spectrometer. The laser design exploits the advances in technologies, capabilities, and lessons learned from the NASA Risk Reduction Laser program, Calipso, and others. The Engineering Model and Flight Model are discussed.*

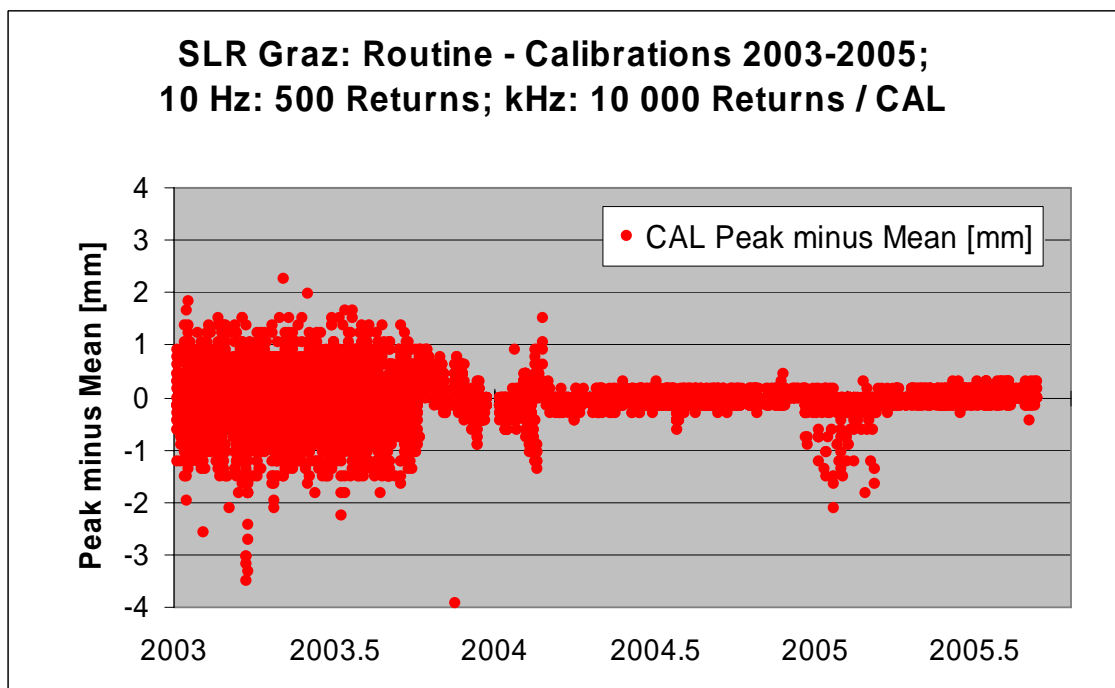
## KILOHERTZ SESSION SUMMARY

Chairs: Georg Kirchner, Graham Appleby

Talks / presentations given:

- Hamal et al: Portable Pico Event Timer and SLR Control System
- Gibbs et al: Early Results of kHz SLR at Herstmonceux
- Degnan et al: LC Optical Gate for Monostatic kHz SLR System
- McGarry et al: SLR 2000: The Path Towards Completion
- Kirchner et al: Spin Parameters of AJISAI and GP-B from kHz SLR
- Kucharski et al: Lageos-1 Spin Determination from kHz SLR
- Kirchner et al: Measuring Atmospheric Seeing with kHz SLR

In addition: kHz SLR has a lot of unique advantages; just as an example, the graph below shows the significant improvement of the Peak-Minus-Mean value, when going from a standard 10-Hz system (old Graz SLR) to a kHz system; please note that such a statistical improvement is a necessary requirement if we want to think / talk about “mm-SLR” ☺



---

## Portable Pico Event Timer and SLR Control (P-PET-C) System

Karel Hamal<sup>1</sup>, Ivan Prochazka<sup>1</sup>, Yang Fumin<sup>2</sup>

1. Czech Technical University in Prague, Brehova 7, 115 19 Prague 1, Czech Republic
2. Shanghai Observatory, Chinese Academy of Science, 80 Nandan Road, Shanghai, China

Contact: [prochazk@troja.fifi.cvut.cz](mailto:prochazk@troja.fifi.cvut.cz)

### Abstract

*We are reporting design, construction and parameters of the Portable Pico Event Timer and SLR Control (P-PET-C) System. It has been developed as a self-consistent system dedicated for the millimeter precision satellite laser ranging systems operating at high repetition rates up to 2 kHz. It provides real time control, measurement, data acquisition and data processing of the advanced satellite laser ranging station. It consists of the PET-C hardware and the software package. The system hardware has been developed on the basis of the Pico Event Timer (P-PET), which has been employed in laser ranging stations in Wettzell, Germany, TIGO Chile and in Portable Calibration Standard, a world wide accepted reference for pico-event timing for millimeter laser ranging. These systems have been operated at numerous stations around the world, including China, without any single failure for more than 8 years of continuous operation. The event timing is based on space qualified Dassault units no adjustment or re-calibration is needed. The 200MHz frequency generator was developed in FH Deggendorf. The real time control, measurement, data acquisition and data processing interface is based on the codes developed and operated at the satellite laser station in Graz, Austria, which is world first station operating a high repetition rate millimeter precision laser system. The real time control and data acquisition is provided by the built in PC. The first field operation was performed at the SLR Shanghai, China, 2006.*

## Portable Pico Event Timer and SLR Control (P-PET-C) System

### Goals

- Portable Pico Event Timer and SLRControl 2kHz
- Self-consistent portable unit
- Built in PC
- Dassault Timing Units
- Range Gate Generator
- T/R Pulse Overlap Avoidance
- Dedicated for Portable Calibration Standard 2k

K.Hamal,I. Procházka, Yang Fumin, 15th ILRS Workshop,Canberra,2006

## Portable Pico Event Timer and SLR Control (P-PET-C) System

SLR Workshop

Freq module  
Deggendorf

2 kH SLR PC Card  
Graz

Pico Event Timer (P-PET)

Portable Pico Event Timer  
and SLR Control (P-PET-C) System

London 1998

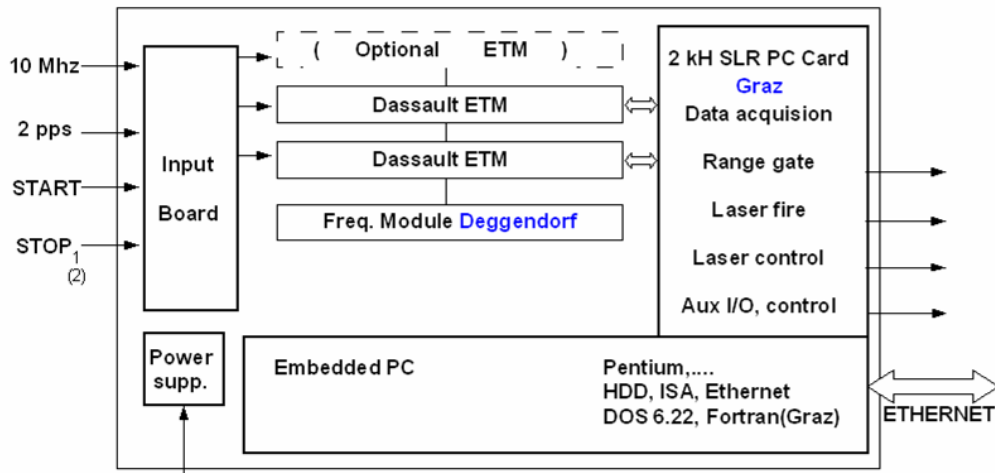
Prague, Shanghai 2006



K.Hamal,I. Procházka, Yang Fumin, 15th ILRS Workshop,Canberra,2006

Portable Pico Event Timer and SLR Control (P-PET-C) System

## P-PET-C Block Scheme



K.Hamal, I. Procházka, Yang Fumin, 15th ILRS Workshop, Canberra, 2006

Portable Pico Event Timer and SLR Control (P-PET-C) System

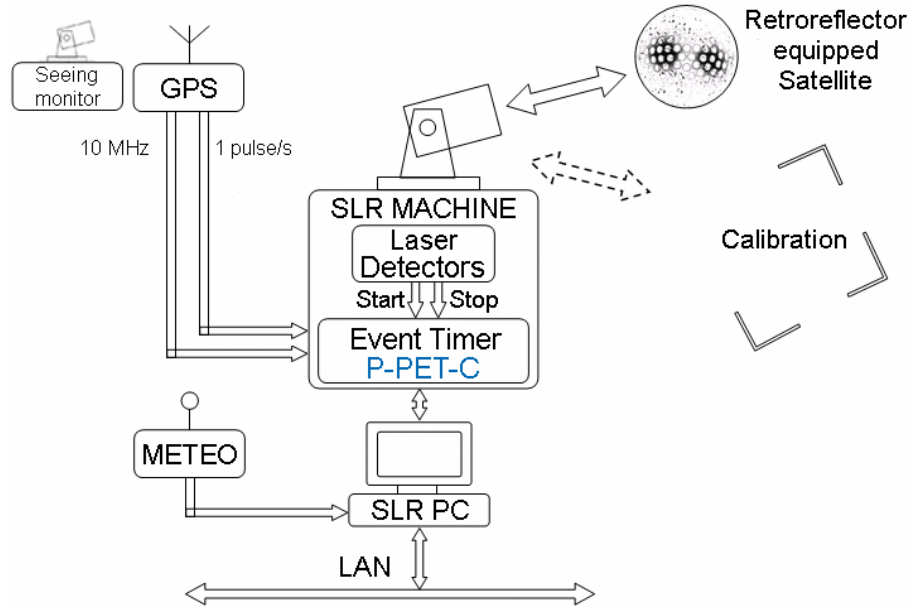
## Parametres

timing principle	event timing
timing resolution	1.2 ps
precision	3 ps
timing stability	better than 1 psec / K, / hour
maximum repetition rate	2 kHz
range gate	1 ns steps pulses "in space" maximum time un-limited
processes under control	epoch and range timing, range gate laser fire, laser control echo energy monitor interfacing T/R pulses collision avoidance additional epoch timing devices optional I/O
computer	built in, industrial PC
software package	Fortran :-) code, DOS 6.22 field upgradable
dimension / mass / power	19' rack unit, 12' high / 30 kg / 200 W

K.Hamal, I. Procházka, Yang Fumin, 15th ILRS Workshop, Canberra, 2006

Portable Pico Event Timer and SLR Control (P-PET-C) System

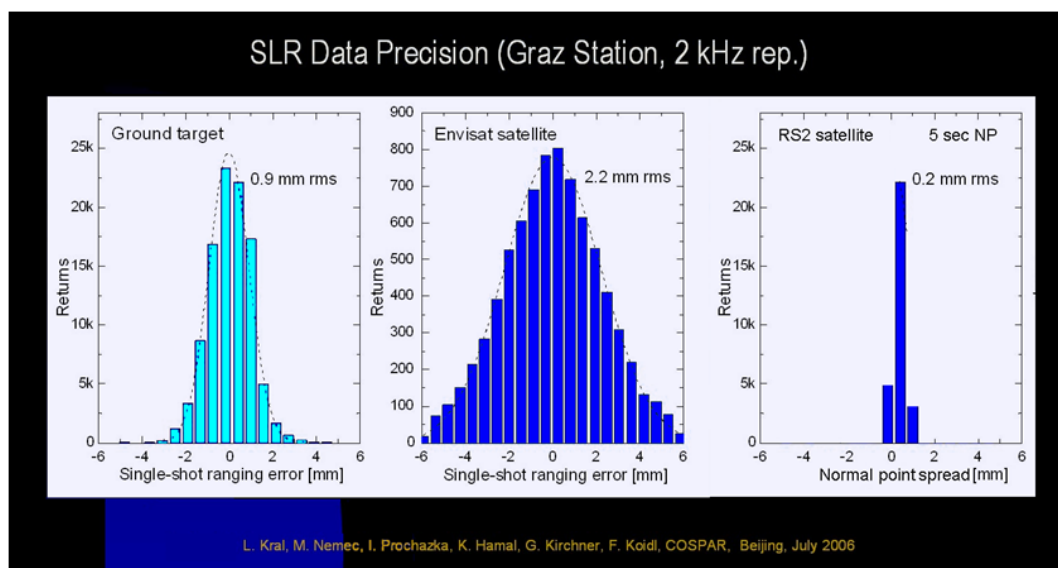
# Portable Calibration Standard



K.Hamal, I. Procházka, Yang Fumin, 15th ILRS Workshop, Canberra, 2006

Portable Pico Event Timer and SLR Control (P-PET-C) System

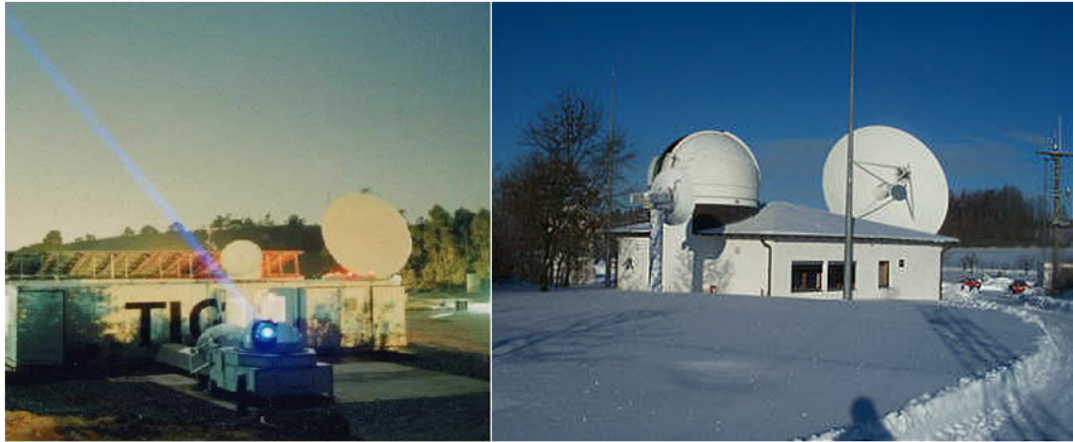
# Expected parameters: Equal Graz



K.Hamal, I. Procházka, Yang Fumin, 15th ILRS Workshop, Canberra, 2006

## Portable Pico Event Timer and SLR Control (P-PET-C) System

Permanent installations of the PET timing technology



SLR station TIGO operated in  
Concepcion Chile,

WLRSS , Satellite Laser Station  
Wetzell, Germany

PET4 operational since 1999.

PET4 operational since 1998

**8 years no recalibration, no adjustment**

K.Hamal, I. Procházka, Yang Fumin, 15th ILRS Workshop, Canberra, 2006

## Portable Pico Event Timer and SLR Control (P-PET-C) System

### Conclusion

- 2kHz
- SLR control system
- Built-in PC
- Portable
- 8 years – no recalibration, no adjustment

- |                  |     |     |    |      |
|------------------|-----|-----|----|------|
| • Ground         | RMS | 1   | MM | Graz |
| • Satellite ERS2 | RMS | 2,8 | MM | Graz |
| • Normal Point   | RMS | 0,2 | MM | Graz |

- Price

K.Hamal, I. Procházka, Yang Fumin, 15th ILRS Workshop, Canberra, 2006

Portable Pico Event Timer and SLR Control (P-PET-C) System  
Shanghai indoor test, July 2006



K.Hamal, I. Procházka, Yang Fumin, 15th ILRS Workshop, Canberra, 2006

Portable Pico Event Timer and SLR Control (P-PET-C) System  
Shanghai outdoor test, July 2006



40W 2J

K.Hamal, I. Procházka, Yang Fumin, 15th ILRS Workshop, Canberra, 2006

---

## Some Early Results of Kilohertz Laser Ranging at Herstmonceux

Philip Gibbs, Christopher Potter, Robert Sherwood, Matthew Wilkinson,  
David Benham, Victoria Smith and Graham Appleby

1. NERC Space Geodesy Facility, Herstmonceux Castle, Hailsham, UK, BN27 1RN.

Contact: [pgib@nerc.ac.uk](mailto:pgib@nerc.ac.uk)

### Abstract

*As part of its support of an upgrade and expansion of capability at the UK Space Geodesy Facility, the UK Natural Environment Research Council has provided funding to enable in-house development of kHz-rate laser ranging at the site. The scientific justification for this upgrade included the expectation of an increase in single shot precision furnished by the much shorter laser pulse-length, an increase in normal point precision from compression of a greater number of raw data points and much more rapid target acquisition via rapid searching.*

*The upgrade has proceeded in stages. Before we were able to consider kHz ranging we needed an event timing device able to record epochs of multiple events at kHz rates. To this end we built in-house the Herstmonceux Event Timer (HxET), which is based on three modules supplied by Thales. Following completion of HxET in August 2006, the device was thoroughly tested and found to agree with expectations in terms of linearity and precision. With HxET in place we were able to make our first tentative steps by late September into kHz calibration and satellite ranging. This paper presents some of our early problems and successes.*

### Basic Requirements for Kilohertz ranging

- A kHz laser.
- An event timer to record epochs of laser firing and detector triggering. This must be able to record epochs to an accuracy of a few picoseconds.
- A computer system(s) able to read ET, control the laser, display data and archive the data at kHz rates.
- Software to extract weak return signals from the higher noise levels generated by a C-SPAD running at kHz rates.
- Reduction software that can cope with the new features displayed in kHz data.

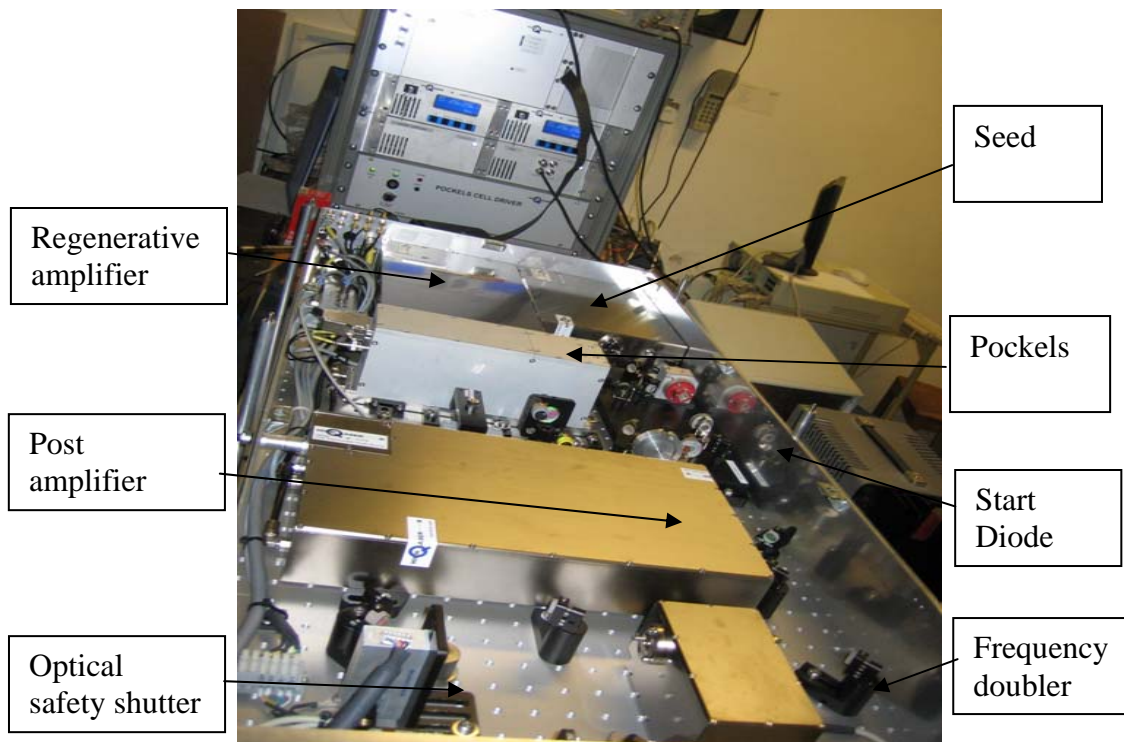
### kHz Laser

Preparation for a kHz laser system began in 2003 with a visit to the SLR station in Graz, Austria. Graz had at that time recently purchased a kHz laser and was in the process of validating. This visit proved to be exceedingly useful in providing background knowledge necessary for the specification of a laser for the SGF. In 2004 final specifications for the kHz laser system were agreed and suppliers sought. The specification included a final output wavelength of 532nm with a pulse width of 10 – 15 ps at 1 – 2 kHz and a beam quality ( $M^2$ ) better than 1.5. The ability of the laser to fire at ~10Hz to enable a smooth validation/transition from the old system to the 2 kHz system was also considered important. Other factors needed were the ability of the laser to fire on a shot by shot, variable rate basis under computer control, the ability of all the safety systems (lid locks, door interlocks and radar system) to be able to communicate with and inhibit firing, and the ability of the laser system to recover well after one of the frequent power cuts experienced at the SGF.

Given these specifications, a tender exercise identified two potential systems from High Q Lasers of Austria; one generating a power output of 0.4 mJ at 532nm and the second being capable of 1mJ at 532nm. With these power outputs the link budget calculations, to estimate return rates using a given laser system, were favourable. The following table shows our estimates for the link to the Lageos satellites in daytime, assuming an average amount of cirrus and a horizontal visibility of a poor 8km. The percentage value is the return rate of photons detected by the C-SPAD and the number in brackets is the resultant number of returns per 2-minute normal point:

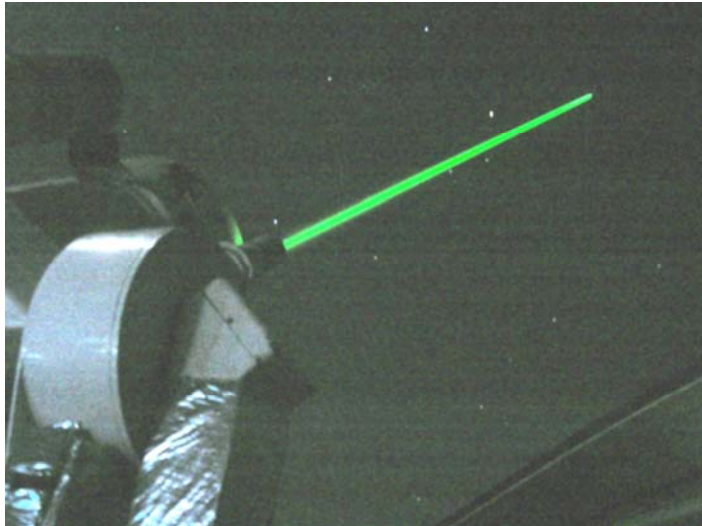
Elevation	90°	50°	30°	25°
0.4mJ, 2kHz:	20% (12000);	8% (4000);	1% (500);	0.3% (150)
1.0mJ, 1kHz:	50% (15000);	19% (6000);	2% (700);	0.7% (150)

Following these calculations and financial considerations the 0.4mJ system was deemed sufficient but an extra long housing was ordered to enable possible future modification of the laser with an extra amplifier unit.



In summary, the specifications for the kHz laser are as follows:

- Nd: Vanadate picoREGEN laser from High-Q Lasers
- Pulse energy 0.5mJ at 532nm at 1kHz  
0.4mJ at 532nm at 2kHz
- Repetition rates of between 10 and 2000 (although large changes may require realignment). To date rates between 100 and 2000 Hz have been used without re-alignment.
- Pulse width is 10ps FWHM at 532nm.
- Upgradeable to >1mJ at 532.
- Firing predictability to 6ns.
- Typical lifetime of pump diode in excess of 10000 hours
- Beam quality – TEM<sub>00</sub> M<sup>2</sup><1.5



Shown here is a picture of the kHz laser at night

### **Event timer**

A decision was made in 2004 to replace our SR620 timers with a timing system which would be linear across the range of times being measured and also be usable for a Kiloherz system. After investigating various options it was decided to build in-house an event timer with 3 Thales modules (1 clock module and 2 timing modules). The design of HxET included providing power supplies for each module plus some fifteen other power supplies, building an interface between the modules and the ranging computer, the ability to have start and stop signals as either NIM or TTL, and 1pps signal. It also had to include an onboard 1 kHz signal to monitor the difference between the two timing modules. The timer was completed in late July 2006 and ready for use soon after.

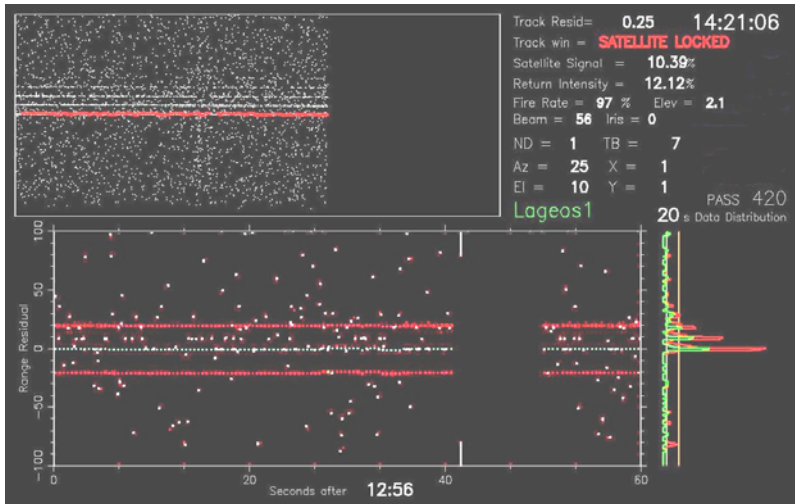
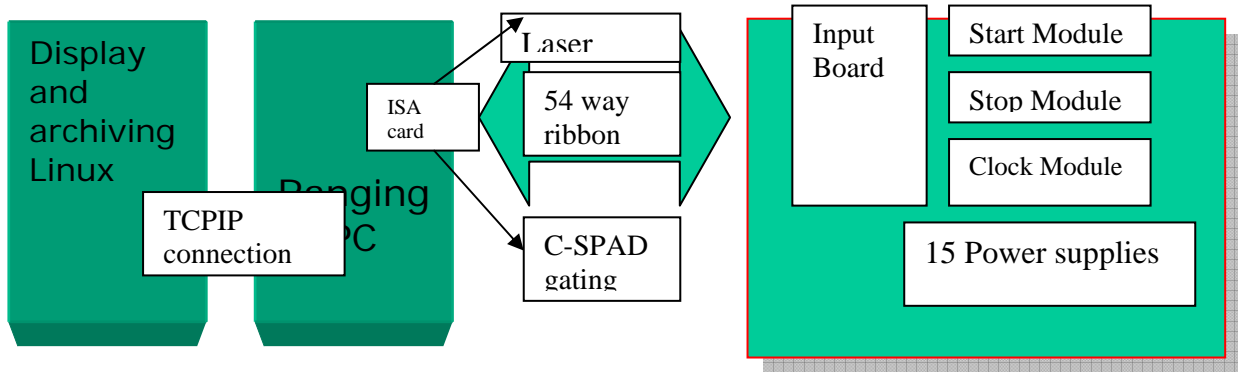
Initial tests of HxET using a split signal to the start and stop channels resulted in a total jitter of 7ps. If we assume an equal contribution from both the start and stop channels, this result gives a jitter of 5ps for each, in agreement with the specifications for the modules. Tests were also carried out using HxET to determine the behaviour of our SR620s across the whole timing range from local targets to the GNSS satellites; the results agreed with the results of previous identical tests carried out between PPET and the SR620s (Florence 1998). This we believe shows that there is agreement between PPET and HxET and that HxET is linear across the full range of current timing measurements. This calibration work is the subject of a further paper in these proceedings (Gibbs, Appleby and Potter, 2007).

### **Computer configuration.**

The station computer configuration is as shown below. It comprises a Linux machine that is used to display and archive the data and run the reduction processes. This machine receives in real-time the data from the ranging PC (running under DOS) using TCPIP. The ranging PC communicates with HxET via a Programmable ISA card that was supplied to us by the GRAZ group. The ISA card also controls the Laser and arms the C-SPAD. The ranging PC also controls the telescope tracking, the safety radar, laser beam divergence and an iris in the receive optical path, as well as determining average return rate in real-time and maintaining a single photon return level via a neutral density wheel.

### **Real Time Display**

Recognising that moving to kHz ranging will significantly reduce the signal to noise



The display process runs on a Linux platform using a TCP-IP connection to the dedicated ranging PC. The display shows long term and short term range gate O-C values as well as a histogram of user defined time span to plot the intensity profile of the data.

ratio of the recorded data, early preparations were made to upgrade the display software. Previously, detection of track in the O-C real-time data within the range gate was aided by the known profile of the semi-train. The high rate data, lack of a semi-train and reduced satellite return signal associated with the low energy laser would make this procedure far more difficult, both for the observer and for the software.

The histogram technique is a very good indicator of the presence and the strength and stability of a satellite return signal and is used for automatic real-time track detection. The technique was developed and implemented for the 13Hz system with the eventual goal of preparing for kHz ranging. The 13Hz laser profile is an initial pulse followed by a significant semi-train, so to avoid tracking the wrong pulse within the semi-train a second histogram was designed in which later pulses are folded in to enhance the initial pulses. This technique exaggerates the first pulse and allows it to be continually tracked. The original (green) and altered (red) histogram profiles can be seen at the bottom right corner of the image above.

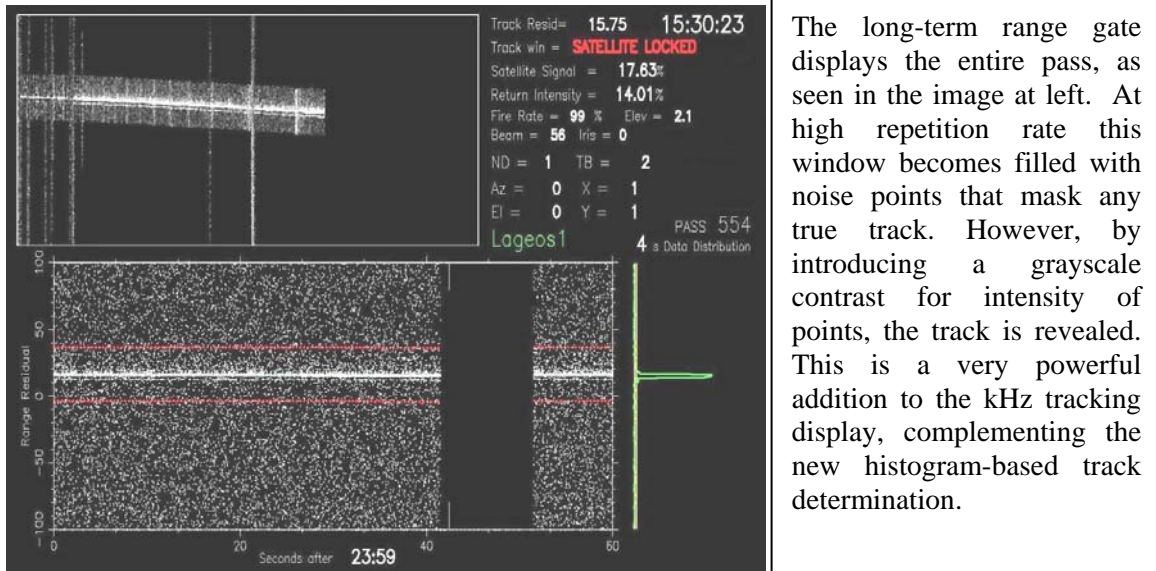
A confirmed satellite track is defined by a histogram bin reaching a level of 3-sigma above the background noise in the range gate. Two 3-sigma uncertainties for this track detection are calculated from the instantaneous histogram peaks and from peaks in short blocks of data over the histogram time period. If the satellite signal is strong and stable the software 'locks' onto the track. Once the satellite is locked, the track uncertainties are reduced to 2-sigma and only peaks falling within the newly-defined track window are considered as possible track.

The kHz laser has one dominant pulse and can be tracked with a single histogram. The high firing rate also means that a shorter histogram time span is sufficient, but additionally the histogram can pick out a weak intermittent track if it is given a longer

time span. From experimentation the software can lock on to a 1% satellite return signal with a 3 second time span and lock onto a 2% signal with a 2 second time span.

**First Results**

Testing of HxET and a full range of comparison tests between HxET and the SR620s were completed in late September 2006. Once completed, we designed the simplest possible software/hardware package that would enable us to obtain some high-rate satellite data as quickly as possible. To this end we simply used a pulse generator to

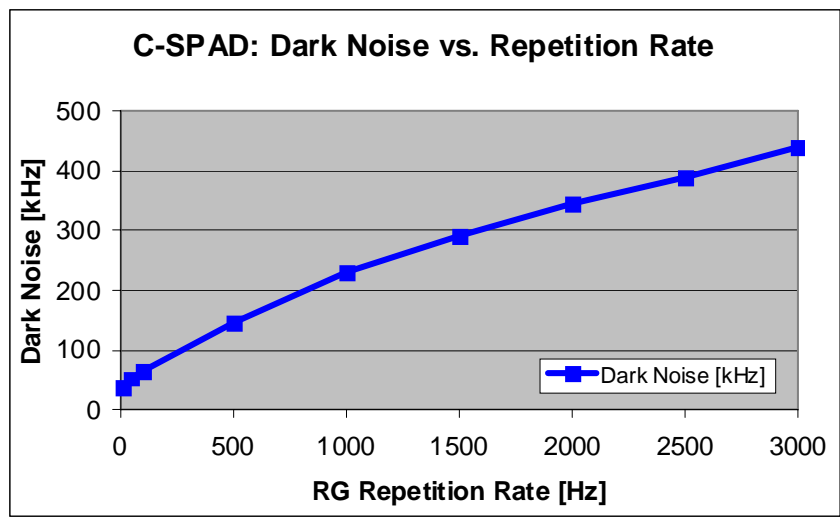


The long-term range gate displays the entire pass, as seen in the image at left. At high repetition rate this window becomes filled with noise points that mask any true track. However, by introducing a grayscale contrast for intensity of points, the track is revealed. This is a very powerful addition to the kHz tracking display, complementing the new histogram-based track determination.

fire the laser at approximately 2kHz. This simple system meant that we had no ‘collision’ control and as a result periods of high noise can be seen clearly in the data displayed below. We also did not attempt automatic control of return level (although manual control was still available) – in truth we were just happy to see that we were getting data. After just one week we had a software package that could collect data at kHz rates without any losses and then tried observing both in daylight and at night.

During the daytime we were able to track successfully all satellites from Lageos’ heights and lower except for Champ and Grace. At night we were able to range to all the ILRS satellites, again except Champ and Grace. These exceptions were caused by a software problem which has subsequently been solved.

One of the first things that was noticed was that many more noise events were detected than had been expected; initial tests indicated a noise increase of about a

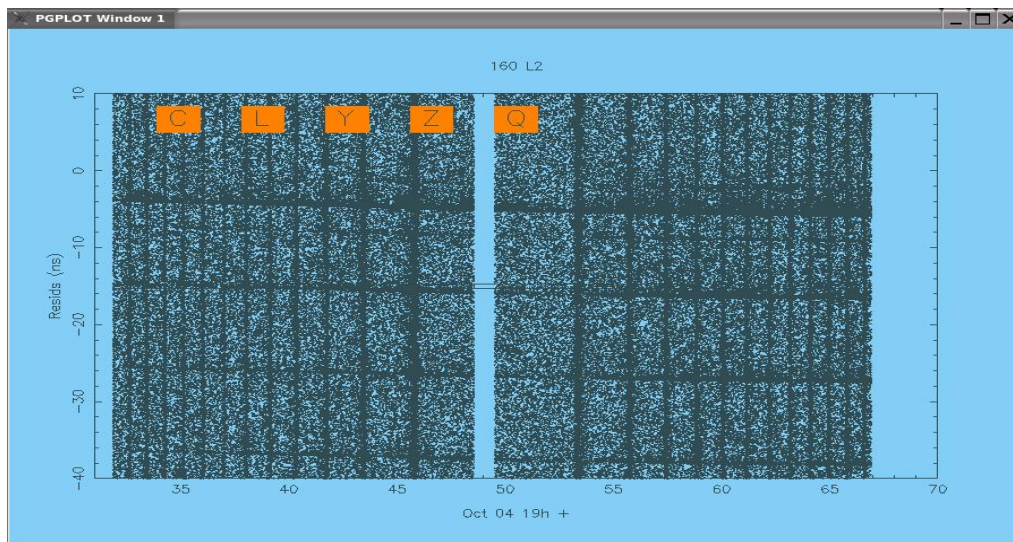
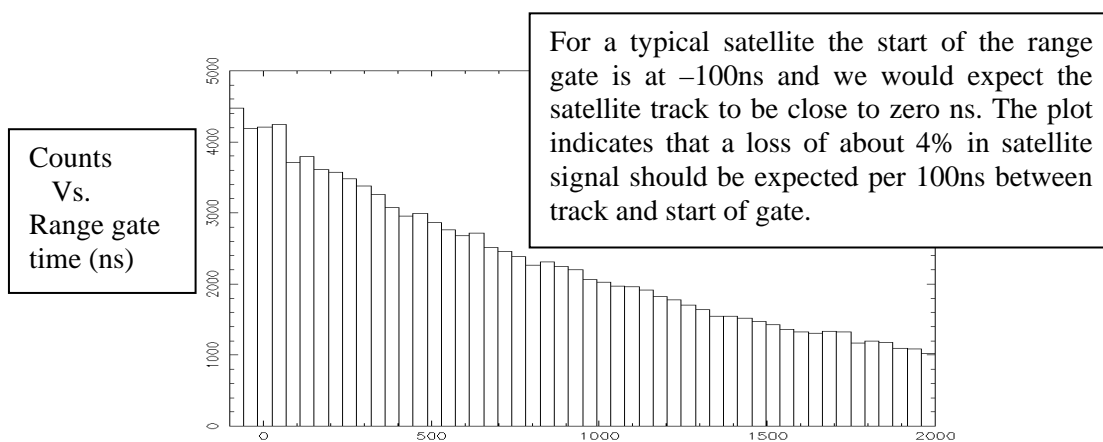


factor of 7 between tracking at 10Hz and at 2kHz. This appears to be due to an increase of dark noise in the C-SPAD as a function of arming rate. This effect had been discovered and quantified by the Graz group, and below is a plot provided by Graz of their results for C-SPAD noise vs. repetition rate.

To estimate the effect this increase of noise would have on our system we examined a histogram of noise collected at 2kHz.

### Results from LAGEOS

Shown below is a plot of range O-C for Lageos-2 from October 4<sup>th</sup> 2006. Present is a number of interesting features. Clearly seen are the ‘collision’ periods when there are overlaps between incoming return pulses (C-SPAD gated on) and spurious detections of backscatter from outgoing laser light. Also apparent are pre-pulses and spurious other pulses because at the time of the observation the laser pockels cell was not optimally tuned. The uppermost O-C track represents the primary return signal.



Having collected kHz data the next step was to use our current 10Hz reduction system to check whether there are any significant differences in the data, primarily in systematic effects that may compromise its quality.

The current reduction system comprises the following steps:

1. Extract a data set by a combination of linear and polynomial fitting to the raw O-C data. A minimum limit to the data set of  $\pm 0.75\text{ns}$  about the zero mean is imposed by the software to prevent the reduction being biased by the observer.

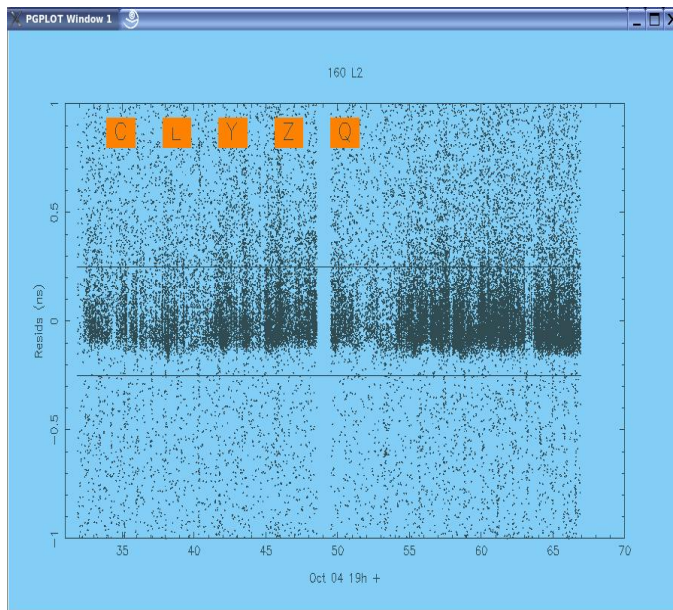
2. Fit an orbit to the extracted data, iteratively rejecting residuals at a 3-sigma level;
3. Remove this orbit from the entire raw data set and reject at 5-sigma level (yes 5);
4. Fit a smoothing function to this data set, rejecting at 2.5-sigma, using the routine DISTRIB that was produced and made widely available by A. Sinclair (SLRmail 0008).

### Extraction of Data.

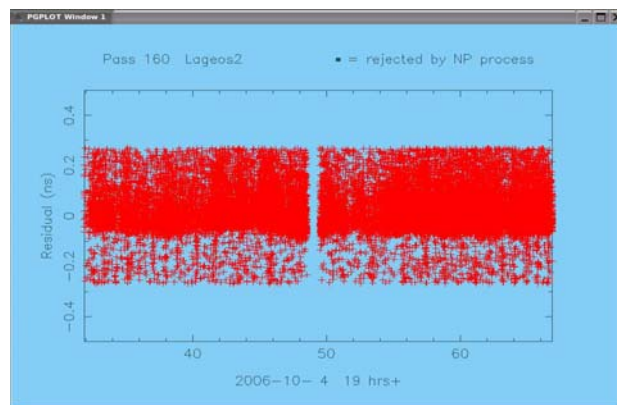
Below is a plot of the initial data set from which the observer will select the data to be passed to the orbital solution.

### Gaussian Fit

Having selected the data as shown in the above plot an orbit is fitted to it. The orbit is then removed from the whole data set and residuals rejected at 5-sigma. We then need to know if this data set is different for the 10Hz and kHz systems



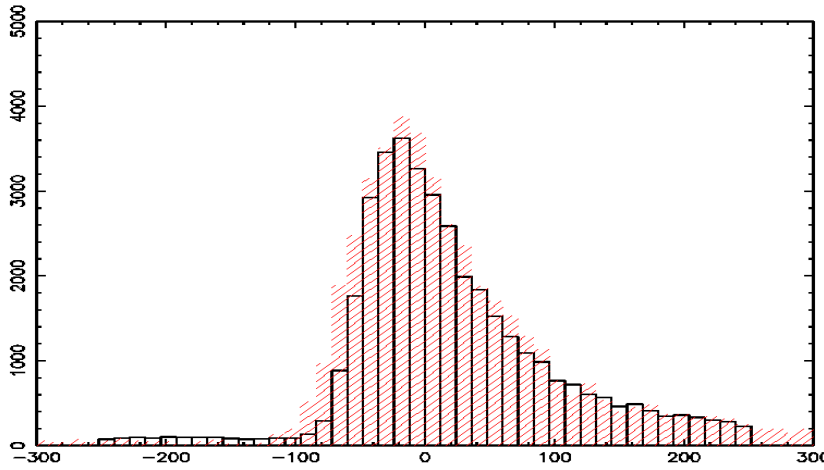
With the increase in background noise apparent at kHz rates it was felt that keeping at least  $\pm 0.75\text{ns}$  of data would introduce too much noise in the preliminary signal extraction. We are currently experimenting with a reduced restriction of  $\pm 0.25\text{ns}$  as shown in the plot, although the observer has the option of overriding these limits. In fact, better predictions, better software and higher-precision data means there is much less scatter in the residuals.



Pictured here is the data set after removing a best-fit orbit and rejecting residuals at a 5-sigma level. Apparent is a “significant” amount of noise below the track and some structure above the track. But is this behaviour significantly different to our current system?

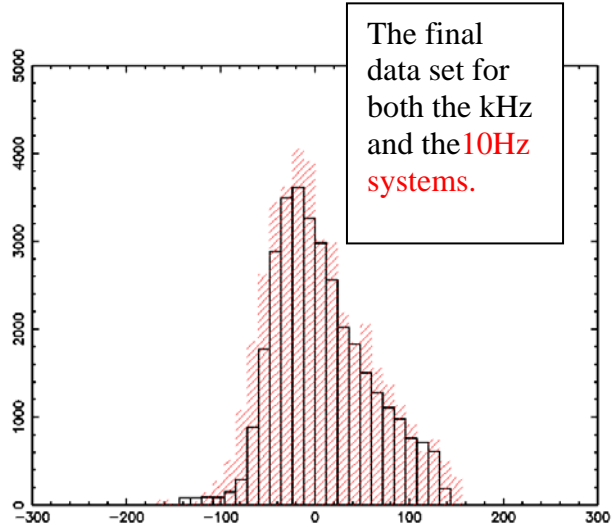
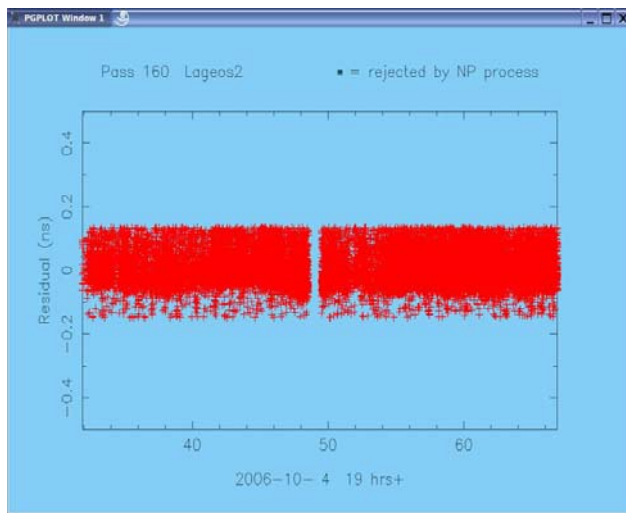
At first glance it would appear that our reduction process is producing the same results for Lageos from both systems, but we have started a more detailed analysis in order both to define a robust reduction process and also to derive an accurate centre of mass correction. Previous work (Otsubo and Appleby, 2003) found that uniquely for the Herstmonceux single-photon system a Lageos centre of mass correction (CoM) of 245mm should be applied (cf 251mm for high-energy ILRS systems). It is important that once our new kHz data becomes available to the analysis community that we have also determined an accurate CoM correction, which may well be a few mm

different from the current 10Hz value. This ongoing work will be reported elsewhere, but the plot below shows the result of an initial investigation of the detailed post-reduction O-C distribution. The rapid rise of the leading edge is as expected and is a result of the short pulse length of the kHz laser, as suggested in the discussions above.



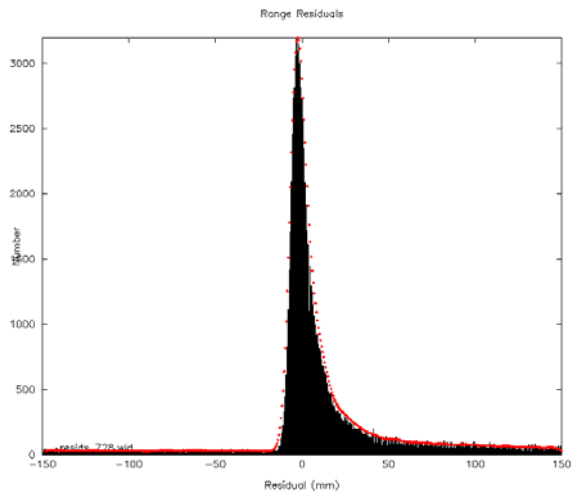
The distribution of the residuals from the two systems is very similar since the Lageos response dominates. As expected, the 10Hz data appears to be slightly broader as the timer and laser contributions are larger:

10Hz:	35ps for SR620
	100ps for laser
KHz:	7ps for HxET
	10ps for laser



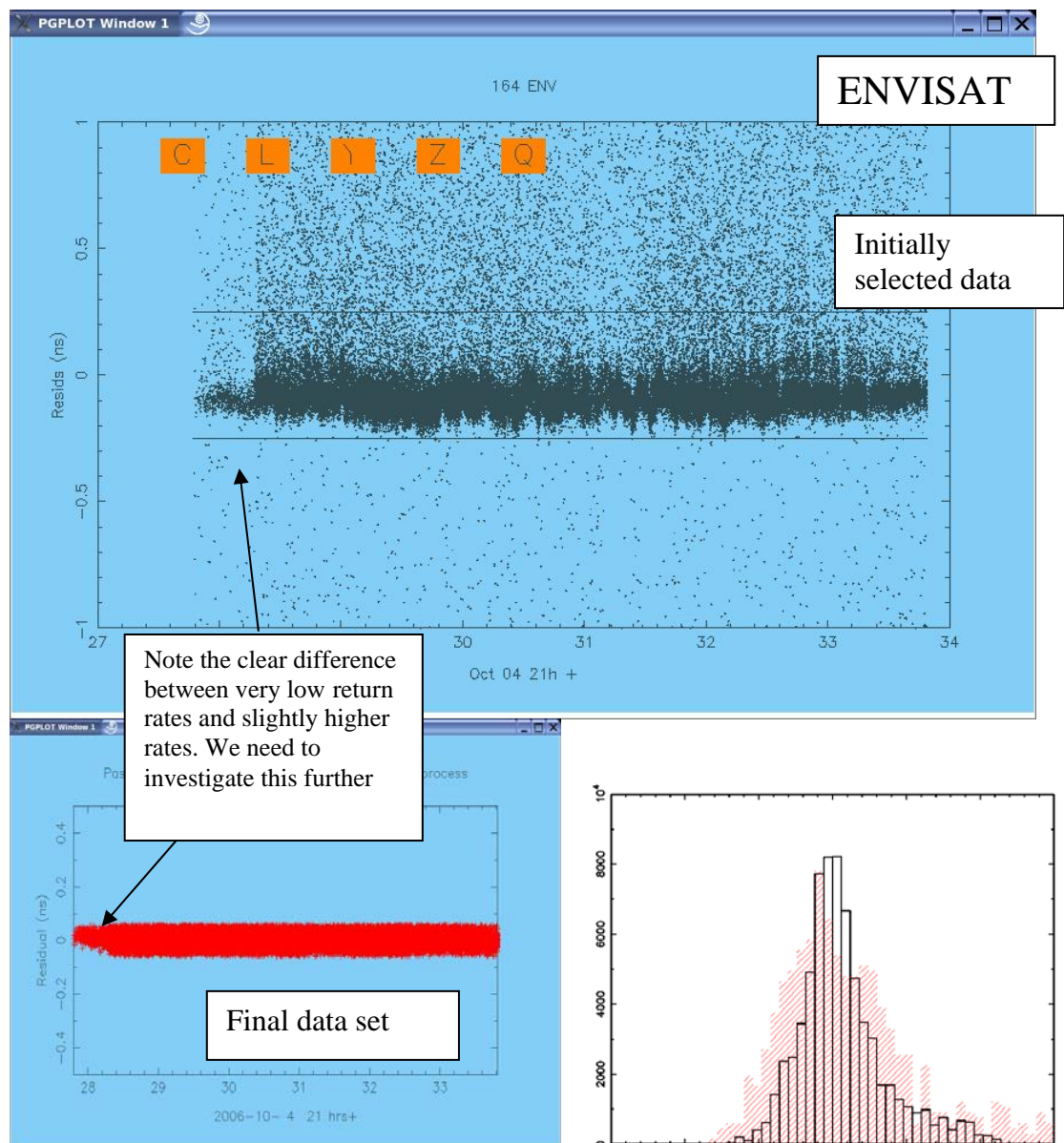
The final data set for both the kHz and the 10Hz systems.

*Shown above is the final data set for Lageos. There is clearly some noise below the track and the sharp cut off of dense data above may well have removed real observations.*



The smoothing function fitted to the distribution is shown in red, and will be used in an asymmetric filtering process to remove primarily leading-edge noise and in a model to determine an accurate CoM value.

## Results from a small-array satellite (ENVISAT).



### Conclusion

The SLR system at the UK Space Geodesy Facility is at an advanced stage of upgrade to kHz repetition rates, and incorporates a very accurate event timer. Paramount in the upgrade plans is that on-site reduction of the new data should not introduce any discontinuity into the long series of high quality laser data from the site.

### Acknowledgement

We would like to thank the staff of the Institut for Space Research, Observatory Lustbuehel at Graz, Austria for their help and encouragement during the development of our kHz system at Herstmonceux.

### References

- [1] Gibbs, P., Appleby, G.M. and Potter, C.P., 2007. A re-assessment of laser ranging accuracy at SGF, Herstmonceux; *these proceedings*.
- [2] Otsubo, T. and Appleby, G.M., 2003. System-dependent centre-of-mass correction for spherical geodetic satellites, JGR, vol. 108, doi:10.1029/2002JB002209.

---

## Performance of a Liquid Crystal Optical Gate for Suppressing Laser Backscatter in Monostatic Kiloherz SLR Systems

John J. Degnan and Daniel Caplan

1. Sigma Space Corporation, 4801 Forbes Blvd., Lanham, MD 20706 USA.

Contact: [John.Degnan@sigmaspace.com](mailto:John.Degnan@sigmaspace.com) / Fax:+01-301-577-9466

### Abstract

*Some of the unique blocking features required by SLR2000 included a large aperture (15 mm), arbitrary polarization returns, a rapid 2 kHz cycle time, long and flexible blocking periods (up to 10% of each 500 microsecond interval between pulses), and adequate switching speeds to minimize data loss. After evaluating numerous potential approaches to optical gating, we determined that the use of a liquid crystal optical gate (LCOG) afforded the best overall protection. We have successfully implemented a 2 kHz LCOG which provides a 50 microsecond "blocked" interval, a 450 microsecond "unblocked" interval, a 10 microsecond rise and fall time on the blocking interval, approximately 90% transmission in "unblocked" mode, and a 659:1 reduction in backscattered radiation in "blocked" mode. Furthermore, the LCOG adapts readily to time shifting of the outgoing pulse.*

### Introduction

Since SLR2000 operates at a 2 kHz fire rate, multiple pulses are in the air at all times and, at various times within a given satellite pass, reflected signal photons arrive at the SLR2000 telescope at the same time a subsequent transmitted pulse is exiting the system. We refer to these events as "collisions". Since the range gate is open for some period surrounding the expected signal arrival time, the sensitive detector is exposed to backscattered laser radiation from both the instrument and the local atmosphere while in a high gain mode. In principle, backscatter from the atmosphere can be observed for up to 10% of the 500 microsecond laser fire interval. During this time, backscattered photons can cause significant charge transfer from the photocathode to the anode and, since the lifetime of a photocathode is dependent on the number of coulombs transferred, unsuppressed laser backscatter is a potentially life-limiting mechanism. In addition, since SLR2000 is designed to correct telescope pointing by balancing the photon returns in the four ranging detector quadrants, we believe that backscattered photons can interfere with the performance of the pointing correction algorithms by biasing the pointing error in the direction of the transmitter point ahead.

The quadrant segmented anode microchannel plate photomultiplier (MCP/PMT) in SLR2000 has recently been upgraded in order to achieve a factor of 3 to 5 improvement in detection efficiency and sensitivity. The bialkali photocathode tube built by Photek Inc. has been replaced by a significantly more expensive Hamamatsu tube with a less mature but higher efficiency (30% to 40%) GaAsP photocathode. In order to protect the tube from backscattered laser radiation and extend photocathode life, SLR2000 incorporates two design features. The first feature involves periodically changing the laser repetition rate to avoid "collisions" between outgoing pulses and incoming signal photons. This eliminates backscatter during the most critical period when the detector is gated "on", minimizes data loss, and helps to prevent corruption of the quadrant detector pointing correction. We have recently investigated the inclusion of an optical gate which acts as a second layer of defense by

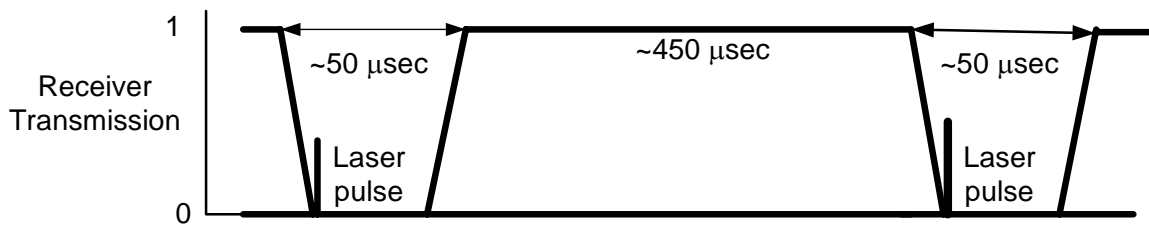


**Figure 1.** Performance of the ideal optical gate for suppressing laser backscatter in SLR2000 operating at a 2 kHz rate.

suppressing backscatter impinging on the photocathode even during less critical times when the detector is gated “off”. The ideal performance of the “ideal optical gate” is illustrated in Figure 1. To minimize loss of signal while providing maximum protection, a successful optical gate in SLR2000 must possess the following characteristics:

- Operate at SLR2000 2 kHz laser fire rate,
- Accommodate the 13 mm receiver beam diameter on the optical bench,
- Block atmospheric backscatter for up to 50 microseconds following laser fire,
- Provide high backscatter extinction in blocked mode,
- Provide high signal transmission in unblocked mode,
- Provide a fast transition between blocked and unblocked modes,
- Accommodate variable fire rate used to avoid “pulse collisions”,
- Can take advantage of linearly polarized light in two SLR2000 receiver channels if necessary.

We considered various approaches to optical gating including mechanical, electro-optical, acousto-optical, and liquid crystal and rated them with respect to transition speed, aperture, transmission, and ability to provide a long “open” mode. Liquid crystal gates were found to have the best overall performance with electro-optical being deemed less appropriate due to the need to maintain high voltages on the crystals for long periods of time. Our conclusions are summarized in Table 1.

**Table 1.** Comparative performance of various optical gating approaches.

Gating Approach	Speed	Aperture	Transmission	Gate Duration
Mechanical	Poor	Poor	Excellent	Poor
Electro-optic	Excellent	Good	Good	Poor (2-3 kV)
Acousto-optic	Good	Poor	Fair	Good
Liquid Crystal	Good	Good	Good	Good ( $\pm 30V$ )

## Experiment

The Liquid Crystal Optical Gate (LCOG) takes advantage of the fact that, in SLR2000, the received signal is split based on polarization. This is a consequence of our unique passive Transmit/Receive switch which permits the transmitter and receiver to share the entire telescope aperture simultaneously while experiencing low loss in either path [Degnan, 2004]. In a typical configuration, the LCOG normally acts as a time dependent polarization rotator placed between two crossed polarizers. The first polarizer defines the input polarization. Relatively low voltage ( $< \pm 30$  VDC) waveforms applied to the crystal align the liquid crystals and rotate the propagating light in a time dependent manner. The action of the second polarizer on the rotated light creates the time varying transmission function of the gate.

As will be described later, the current SLR2000 receiver configuration uses uncrossed polarizers in each receiver leg although crossed polarizers could be employed with a relatively minor design change. For this reason, we conducted our laboratory tests with both crossed and uncrossed polarizer pairs. The signs of the waveform voltages were chosen accordingly to approximate the performance of the ideal gate depicted in Figure 1. Figure 2 provides a block diagram and photo of our test setup.

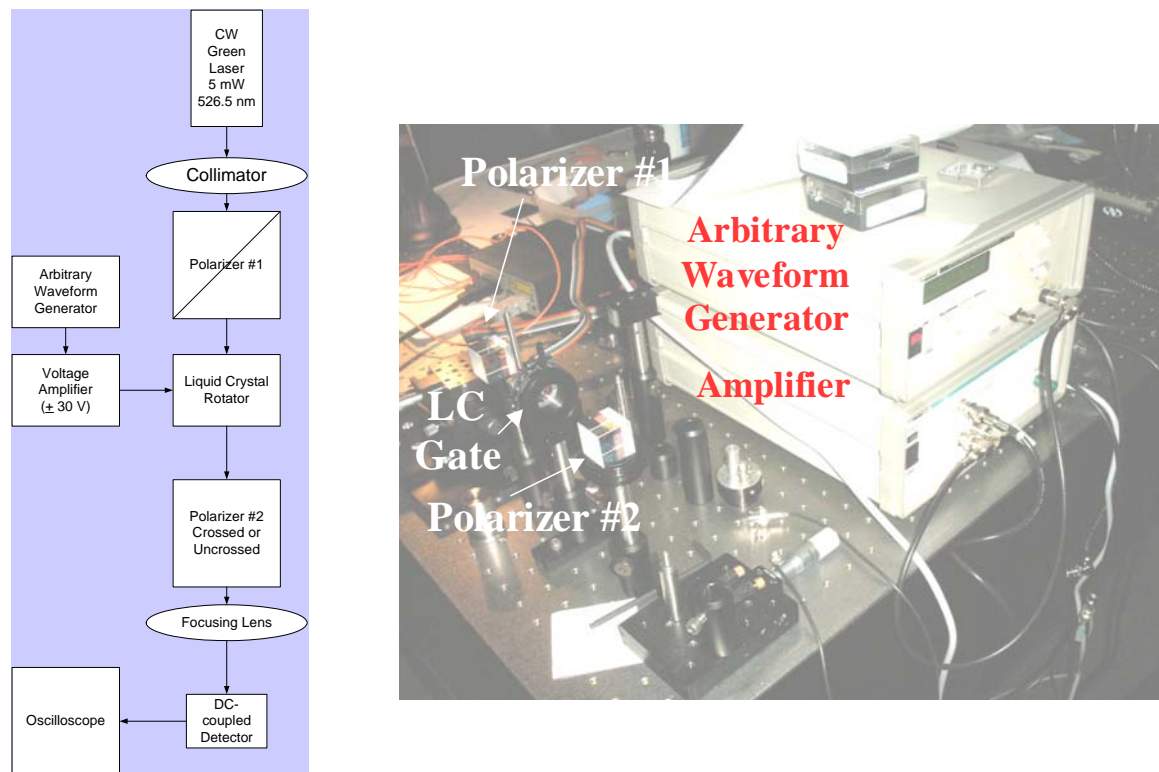


**Figure 2:** Block diagram and photo of the laboratory test setup.

The required waveform was programmed into a high bandwidth Arbitrary Waveform Generator (AWG) and iterated to best approximate the ideal transmission function. The low voltage output of the AWG was amplified to the required  $\pm 30$ VDC by a separate amplifier module and applied to the flying leads of the Liquid Crystal Rotator manufactured by Boulder Nonlinear Systems, Inc. . Collimated light from a CW green laser was passed through the LCOG and focused onto a DC-coupled detector whose output was displayed on an oscilloscope. Prior to inserting the Liquid Crystal Rotator (LCR), the extinction of the crossed CVI cube polarizers was measured to be 6222:1 in reasonable agreement with the specified value of 10,000:1 and demonstrated the

sensitivity of our measurement approach. A summary of the peak optical gate transmissions and extinctions obtained with different polarizer combinations is given in Table 2. Not surprisingly, the best extinction of 659:1 during “closed” periods was obtained with the normal crossed polarizer configuration whereas the P/P and S/S configurations, corresponding to the current SLR2000 receiver configurations (see Figure 4), provided significantly poorer extinctions of 164:1 and 82:1 respectively. The transmission of the gate during “open” periods was comparable in all cases, varying over a narrow range between 89.3% and 92.1%.

*Table 2. Summary of experimental transmissions and extinctions for various configurations of crossed and uncrossed polarizers.*

Polarizer 1	Liquid Crystal Gate	Polarizer 2	Transmission (gate open)	Extinction (gate closed)
P	No	S	NA	6222:1
P	Yes	S	89.3%	659:1
P	Yes	P	91.3%	164:1
S	Yes	S	92.1%	82:1

Temporal waveforms obtained for the gate with crossed polarizers, as registered in different channels of the oscilloscope, are shown in Figure 3. The “optimized” drive voltage waveform to the LCR, corresponding to the orange curve, is being repeated at the 2 kHz rate of SLR2000. The purple curve, corresponding to the optical detector output, is a good approximation to the “ideal” transmission waveform in Figure 1, where the gate is closed for 50 microseconds and open for 450 microseconds and shows a fast transition between the two states (< 10 microseconds). The upper green curve is the purple curve viewed at high resolution and clearly shows the rapid reversal in the transmission trend as the drive waveform voltage to the LCR changes sign.

It is worthwhile to point out certain required characteristics of the drive waveform. The integral of the waveform over one cycle must equal zero, i.e. the positive area under the waveform must equal the negative area. If the average is not zero, any ions present in the liquid crystal will migrate to the surfaces resulting in a build-up of charge. This will effectively keep the liquid crystal pinned in that state [Bauchert, 2004]. Furthermore, during the “open” mode, one must apply a slight residual positive voltage (~2 to 3V) which holds the molecules in their transmissive state and prevents them from becoming randomly oriented and thereby reducing the transmission when the switch is “open”. The width of the blocking gate is determined by the combined widths of the positive and negative going pulses. Because of the zero integral

condition over the full 500 microsecond cycle, the temporal width of the negative drive pulse is necessarily less than that of the positive pulse.

### Integration into SLR2000

Figure 4a shows the current SLR2000 receiver configuration where the incoming light is split into s and p polarizations and then recombined on a final polarizer before impinging on the quadrant MCP/PMT. Note that, without the LCR, the polarization of the light is preserved during recombination at the final polarizer. Thus, using the results in Table 2 for uncrossed polarizers, one can project a mean transmission of 91.7% for the open gate and a mean extinction of 123:1 for unpolarized light entering the receiver. Significantly better performance is obtained if a mirror is placed to the left of the combining polarizer as in Figure 4b and the drive voltages to the LCR are reversed. The expected extinction rises significantly to 659:1, and the transmission decreases only slightly to 89.3% for unpolarized input.

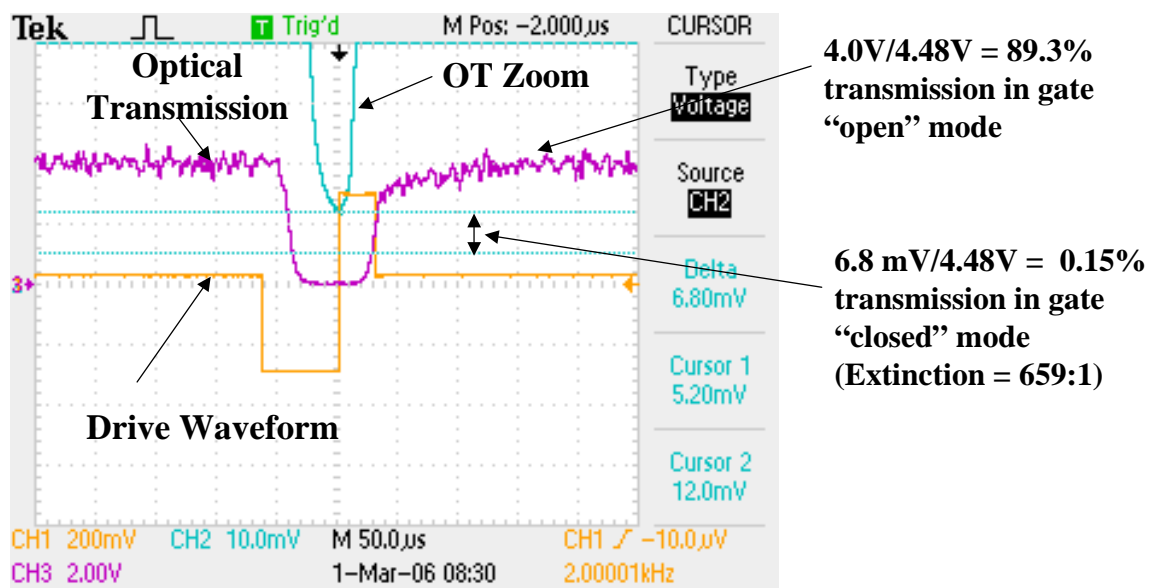


**Figure 3:** Oscilloscope traces obtained during transmission/extinction experiments with the normal crossed polarizer configuration. The drive waveform to the LCR is indicated by the orange trace. The purple trace gives the optical transmission from “open” to “closed to “open”. The narrow green trace at the top of the figure is a high vertical resolution version of the purple trace and shows the rapid reversal in the optical transmission trend at the point where the sign of the applied LCR voltage is suddenly reversed.

### Summary

We have demonstrated that liquid crystals, when used as a 90° polarization rotator between two cube polarizers, can:

- reduce the amount of laser backscatter by 2 to 3 orders of magnitude in the “closed” state while exhibiting high transmission (~90%) in the “open” state,
- operate at few kHz rates,
- handle large aperture beams (~15 mm),
- switch states in less than 10 microseconds with low voltage (<±30V),
- produce flexible gate waveforms of arbitrary shape and duration,
- work in tandem with variable laser fire rates to avoid “collisions” between incoming and outgoing pulses.

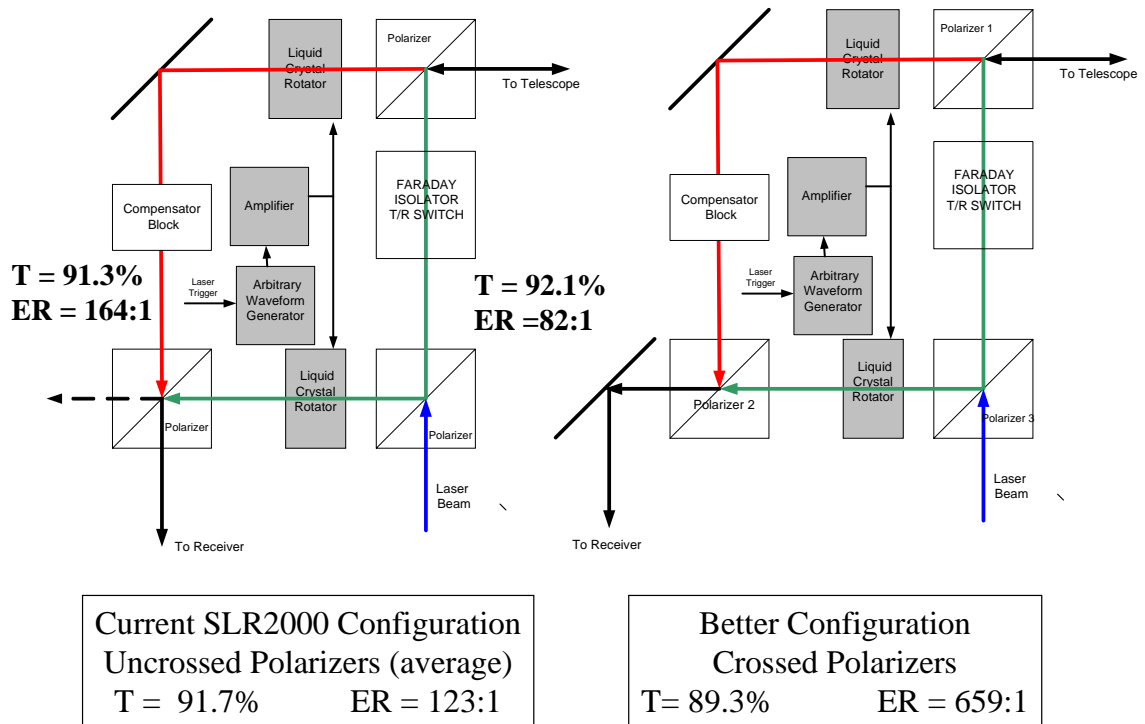


**Figure 4:** (a) With LCR's installed in both legs of the current SLR2000 receiver and unpolarized signal, the mean transmission and extinction would be 91.7% and 123:1 respectively; (b) a minor modification of the SLR2000 receiver configuration would result in 89.3% transmission and 659:1 extinction.

We close with certain precautions in the use of these devices. The liquid crystal medium is sandwiched between two optical substrates. Care must be taken when mounting the LCR's to avoid stressing the delicate interface. The voltage to the unit must not exceed the  $\pm 30$ VDC maximum or serious damage to the interface may result. Also, as mentioned previously, in designing the drive waveform, the voltage over one repetition cycle must average to zero.

**References**

[1] Bauchert, K., Boulder Nonlinear Systems, private communication, 2004.  
 [2] Degnan, J., "Ray Matrix Approach for the Real Time Control of SLR2000 Optical Elements", Proc. 14<sup>th</sup> International Workshop on Laser Ranging, San Fernando, Spain, June 6-10, 2004.

---

## SLR 2000: The Path toward Completion

J. McGarry, T. Zagwodzki

1. NASA / Goddard Space Flight Center.

Contact: [Jan.McGarry@nasa.gov](mailto:Jan.McGarry@nasa.gov)

### Abstract

*After years of programmatic and technical issues, SLR2000 is finally receiving the manpower and money needed to solve the final technical challenges. This paper describes the progress that has been accomplished over the past year and discusses the final steps that we will take in the coming year to make the system operational.*

### Introduction

SLR2000 is the prototype for NASA's Next Generation of Satellite Laser Ranging (SLR) Systems. It was originally designed to be completely automated, eye-safe, with a lower cost of operation, a high reliability, and an accuracy comparable to the existing NASA MOBLAS systems [Degnan(1)]. After many years where funding was low, in 2006 SLR2000 development was given a higher priority and more funding.

Much progress has been made in the last year. The system is now tracking low earth orbiting (LEO) and LAGEOS satellites, able to acquire and track most LEOs relatively easily, although the returns are not yet optimized. The system timing, pointing and ranging capability, and accuracy have been tested using MOBLAS-7 return pulses. The software is more robust and the system is more repeatable. We believe that the system is within a year of final collocation with MOBLAS-7.

### Recent system developments.

An optical shutter was designed and built by SigmaSpace and installed in the system to reduce the laser backscatter on the detector [Degnan(2)]. In a single telescope common optics transmit-receive system the photomultiplier tube (PMT) is exposed to a significant amount of laser backscatter within its field of view (FOV) as the pulse leaves the system. Even though the PMT is gated off during the laser fire this illumination stresses the photocathode and may shorten its lifetime. Mechanical choppers or shutters were investigated but deemed too problematic for operation at 2 KHz. The solution was an optical shutter in the form of two liquid crystal (LC) polarizing filters, one installed in each leg of the transmit-receive switch which reduce the backscatter by two orders of magnitude (Figure 1).

A new higher quantum efficiency (QE) quadrant PMT was installed in the system. The comparison with the previous detector is shown in the following table.

	<u>Photek(PMT210)</u>	<u>Ham(R4100U- 74-M004C)</u>
MCP stages	2 plates	2 plates
Active diameter	10mm	6mm
Photocathode	S20	GaAsP
Q.E.*	12%	33%
DC current Gain	$1 \times 10^6$	$2.6 \times 10^5$
PMT HV bias	-4700V (nom.)	-2250V (nom.)

The relative sensitivity improvement of the Hamamatsu tube over the Photek tube was estimated during an Etalon track to be approximately 5:1. Additional loss in Photek

sensitivity is surmised to be due to aging or degradation of the photocathode over many months of SLR operation.

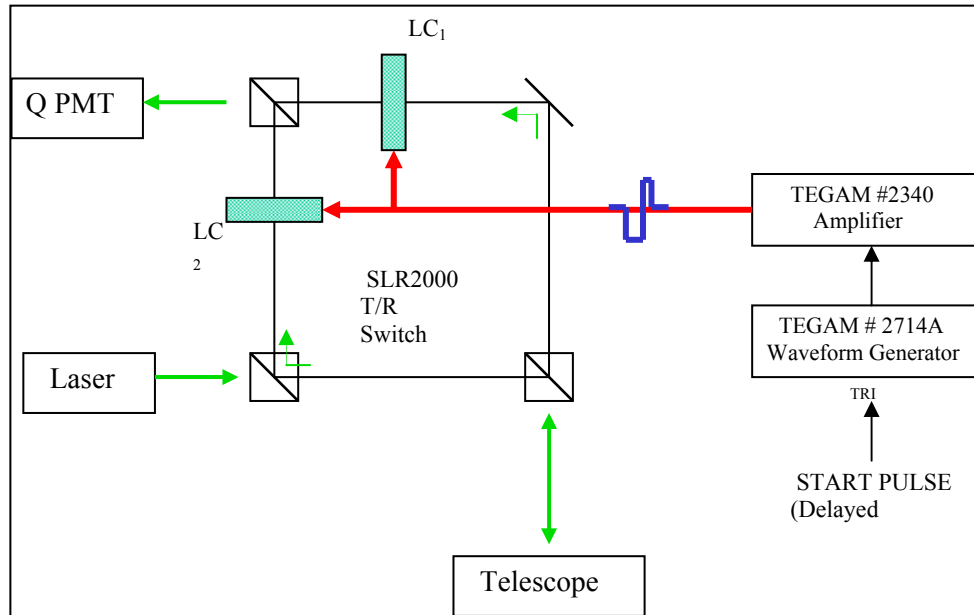


**Figure 1:** Optical bench with Liquid Crystal Shutter in both legs of T/R switch

A laser beam expander was replaced in the system to both control the laser divergence and to give adequate knowledge of the divergence setting. This expander was designed and built by SigmaSpace [Degnan(3)]. Originally the laser transmitter beam divergence could not be adjusted without de-focusing the common beam expander for the receiver. The resultant FOV change in the receiver adversely effected control of background noise and vastly complicated tracking. The solution was to develop a beam expander mechanism which operates solely on the laser transmit beam (independent of the receive path) and which could be focused to accommodate the 10 to 30 arcsecond (full angle) desired beam width.

The Risley prism laser point-ahead optics are now operational in the system [McGarry]. The Risley wedge pair is used to steer the transmit beam ahead of the telescope receive path and put the center of the transmit laser beam directly on the target. The telescope can then be pointed behind to center the receive FOV about the return light. This then allows the FOV to be closed to 10 arcseconds, which reduces the optical noise and allows use of the quadrant detector information to correct the telescope pointing. The Risley optics have successfully undergone testing with an off-line software package. The operational software package interface to the Risleys will be verified in the next few months.

The software now controls the Laser Pulse Repetition Frequency (PRF) to avoid fire/return collisions [Titterton]. This is needed due to the common optics design of the system. Only two different fire intervals are needed for any of the ILRS tracked satellites. The values of the two fire intervals are dependent upon altitude:

- Low Earth Orbiting (LEO): 500 and 510 microseconds
- LAGEOS: 500 and 502 microseconds
- High Earth Orbiting (HEO): 500 and 501 microseconds

The PRF switching is currently being successfully used in all satellite ranging. Figure 2 shows how the laser PRF changes during the course of a LEO (left plot) and LAGEOS (right plot) pass.

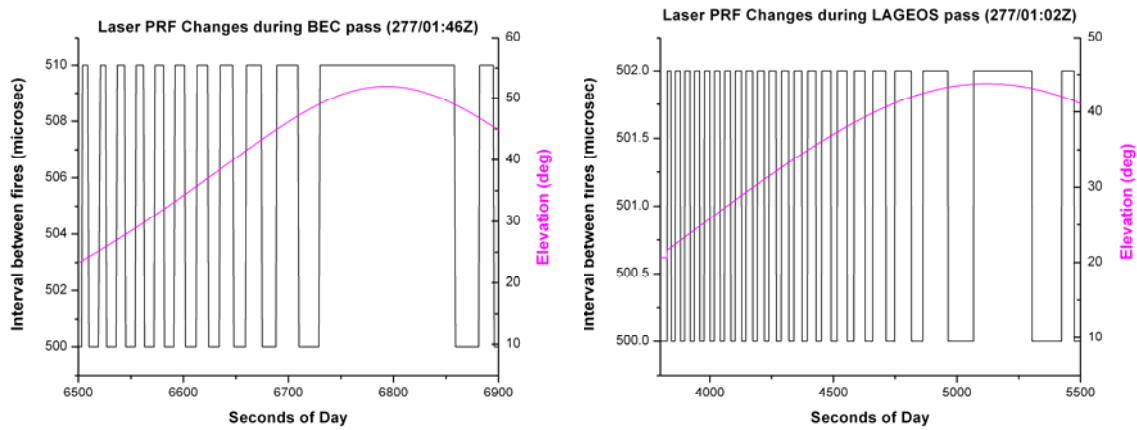


**Figure 2:** Examples of laser PRF changes during two passes. The left plot is BEC and the right plot is LAGEOS.

The new Q-Peak laser was installed into the system. The energy of the previous laser (an earlier Q-Peak version) had degraded to the point where it was transmitting only about 60 microJoules per pulse. The newer laser transmits approximately 120 microJoules per pulse.

Both the star camera (for star calibrations) and the sky camera (for sky condition) failed during 2006 and have been replaced. The star camera had been in use for approximately ten years. The new star camera is the Santa Barbara Instrument Group (SBIG) ST-402ME CCD imaging camera. The CCD chip is 9 microns square with 765 x 510 pixels. It is a low noise, high QE camera with a USB 2.0 interface. It greatly increases the star sensitivity from our old camera, where the dimmest useable star was around magnitude 3.5. The SBIG camera in SLR2000 can resolve better than 8<sup>th</sup> magnitude stars. The new star camera has been installed and is operational.

The sky camera failed after about five years of more or less continuous operation. The new sky camera is the Jenoptik VarioCam InfraRed (8 – 13  $\mu\text{m}$ ) camera. It has an uncooled sensor with a 320 x 240 pixel resolution and a Fire-Wire interface. The new sky camera is installed and working but has not yet been incorporated into the operational software.

### Testing with MOBLAS-7

To checkout the system timing, pointing and receive electronics, we took many passes with MOBLAS-7 acting as the transmitter for SLR2000. These tests took two forms: (1) transferring the receive time from the MOBLAS-7 discriminator to the SLR2000 event timer with a cable running between the systems (start/stop via cable), and (2) receiving the actual return light with the SLR2000 quadrant detector. In both cases the MOBLAS-7 fire time was transferred to SLR2000 via cable.

Analysis showed (1) good pointing for SLR2000 (these tracks required no biases to maintain the returns), (2) comparable results between MOBLAS-7 and SLR2000 for data RMS when the cable was used to transfer the MOBLAS-7 fire times, and (3) in general a higher return rates for HEO satellites at SLR2000, due to its single photon detection capability. Examples of the full rate data RMS for various passes are given in the table below.

Figure 3 shows an example of the LAGEOS return rates for MOBLAS-7 and SLR2000 with MOBLAS-7 providing the fires for both systems and SLR2000 receiving the return light with the quadrant detector.

LAGEOS RMS (mm)

MOBLAS-7 Start/Stop via cable: 10

SLR2000 quadrant detector: 25 – 40

ERS-2/ENVISAT RMS (mm)

SLR2000 quadrant detector: 20 – 25

GLONASS-87 RMS (mm)

MOBLAS-7 Start/Stop via cable: 15

SLR2000 quadrant detector: 35 - 45

ETALON RMS (mm)

SLR2000 quadrant detector: 50 – 60

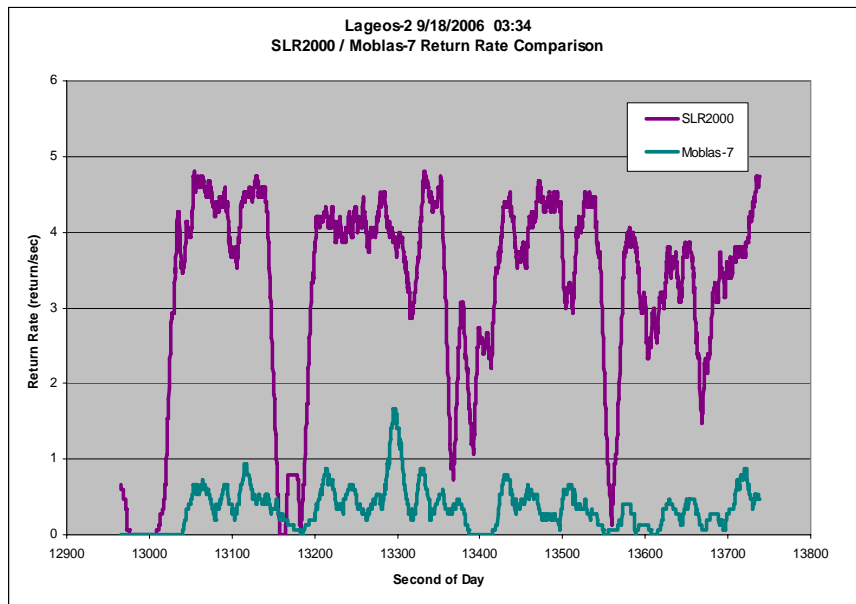


**Figure 3:** LAGEOS return rates for SLR2000 (top curve) and MOBLAS-7 (bottom curve) when MOBLAS-7 was used as laser transmitter (5Hz) for both systems.

**Satellite ranging with the 2 kHz eyesafe laser**

In the last several months SLR2000 has been ranging to satellites using its own eye-safe 2 kHz laser and pointing the telescope ahead. This configuration removes the need for the Risleys to point the laser ahead, but prevents daylight operation due to the need to keep the receiver field of view open to 25 arcseconds to cover the point-behind angular deviation from the point-ahead.

We have tracked many low earth orbiting satellites as well as a portion of a few LAGEOS passes. The pass RMS values remain relatively high due to our relatively wide pulse width laser (250 picoseconds). An example of the raw data from a STARLETTE pass is shown in Figures 4.

**Path to Completion**

Our immediate goal for 2007 is to increase our return rate from LAGEOS when ranging with our 2 khz eye-safe laser. We also need to return to our operational configuration where the telescope is pointed behind (toward the receive light) and the Risleys are used to point the laser ahead of the target. In this configuration we will work on finishing the closed-loop tracking. We expect our return signal rate to increase measurably when the system is closed-loop tracking.

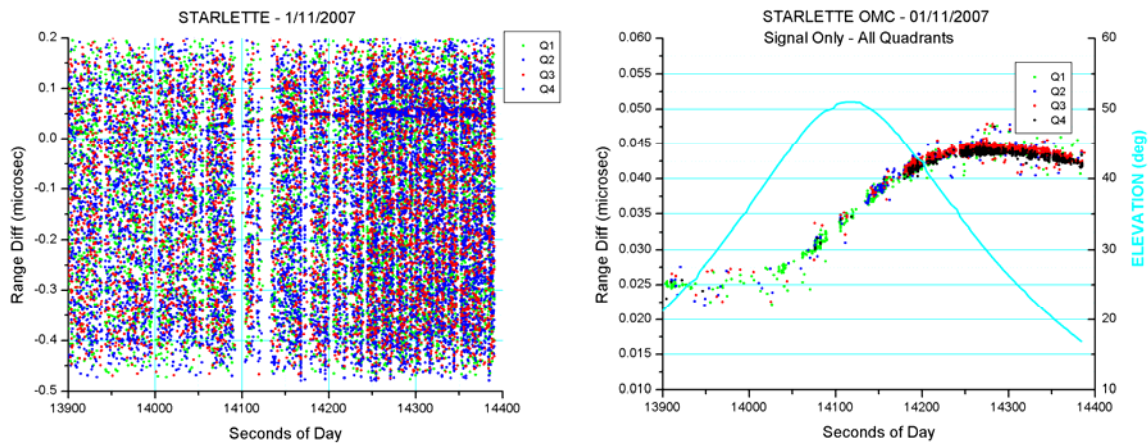


**Figure 4:** STARLETTE pass on 1/11/2007. Left plot shows entire range window with signal and noise. Right plot is of signal only (as determined by signal processing).

Along with this work, a new in-house laser is being built by Barry Coyle and colleagues. This 2 khz laser is expected to have a less than 200 picosecond pulse width with a 100 microJoule to 2 milliJoule variable per pulse output energy. This laser, which will enable us to track the higher satellites (in particular GPS), is expected to be delivered near the end of 2007. Our goal is to complete the SLR2000 prototype system in calendar year 2007 and perform a collocation with MOBLAS-7 in early 2008.

### Acknowledgements

The authors would like to thank John Degnan, who developed the concept of SLR2000 and who led the development of this system until recently, for both his original idea and for his continued and unfailing support of this effort. We would also like to thank the SLR Network Manager, David Carter, for his support of our work, and Michael Pearlman who, as chairman of the ILRS Central Bureau, has been a steadfast proponent of SLR2000. We would also like to acknowledge the SLR2000 team, whose efforts were instrumental in SLR2000's progress: Christopher Clarke, John Cheek, Peter Dunn, Howard Donovan, Mike Heinick, Julie Horvath, Anthony Mallama, Anthony Mann, Donald Patterson, Mike Perry, Randall Ricklefs, Mark Torrence, Susan Valett, and Thomas Varghese. This work is being performed with funding from NASA's Science Mission Directorate.

### References

- [1] Degnan, J., J. McGarry, and T. Zagwodzki, "SLR2000: An Inexpensive, Fully Automated, Eyesafe Satellite Laser Ranging System," Proceedings of 10<sup>th</sup> International Laser Workshop on Laser Ranging Instrumentation, Chinese Academy of Sciences, Yang Fumin (ed.), 367-377, Shanghai, 1996.
- [2] Degnan, J., and D. Caplan, "Performance of Liquid Crystal Optical Gate for Suppressing Laser Backscatter in Monostatic Kiloherz SLR Systems", in this Proceedings.
- [3] Degnan, J., G. Jodor, and H. Bourges, "Adaptation of a Commercial Beam Expander for Automated Transmitter Beam Size and Divergence Control in the SLR2000 System", in this Proceedings.
- [4] McGarry, J., T. Zagwodzki and J. Degnan, "SLR2000 Closed Loop Tracking with a Photon-Counting Quadrant Detector," Electronic Proceedings of 13<sup>th</sup> International Workshop on Laser Ranging, Ron Noomen (ed.), Automation and Control Session, Washington, DC, 2002.
- [5] Titterton, P., H. Sweeney, and D. Leonard, "System/Usage Impact of Operating the SLR2000 at 2 kHz," Proceedings of the 11<sup>th</sup> International Workshop on Laser Ranging, 426 – 437, Deggendorf, 1998.

---

## Determination of AJISAI spin parameters using Graz kHz SLR data

Georg Kirchner, Walter Hausleitner, and Elena Cristea

1. Austrian Academy of Sciences, Institute for Space Research, Graz.

Contact: [Georg.Kirchner@oeaw.ac.at](mailto:Georg.Kirchner@oeaw.ac.at) ; [Walter.Hausleitner@oeaw.ac.at](mailto:Walter.Hausleitner@oeaw.ac.at) ;  
[Elena.Cristea@oeaw.ac.at](mailto:Elena.Cristea@oeaw.ac.at)

### Abstract

*Using the Graz full rate kHz SLR data, we determined the spin rate and spin direction of the satellite AJISAI as well as its slow down between 2003/10 and 2005/06. The high density of the kHz data results in a precise scanning of the satellite's retro-reflector panel orientation during the spin motion. Applying spectral analysis methods, the resulting frequencies allow identification of the arrangement of the involved laser retroreflector panels at any instant in time during the pass. Using this method, we calculated the spin rate with a high accuracy (RMS of  $4.03 \times 10^{-4}$  Hz), and the slow down of the spin rate during the investigated period with a magnitude of 0.0077497 Hz/year. We obtained these results from routine SLR tracking data, i.e. day and night observation, without any additional hardware.*

### Introduction

The Japanese geodetic satellite AJISAI, launched on August 13, 1986 into a 1500 km circular orbit with a 50° inclination, is a passive sphere with a diameter of 2.15 m [1]. The surface is covered with 318 sunlight reflection mirrors for visual tracking and 120 laser retro reflector (LRR) panels each carrying 12 corner cube reflectors for SLR [2] (see Fig. 1). The satellite's axial rotation causes the mirrors to produce visible flashes of reflected sunlight, which are observable on Earth [4]. This in principle allows a precise determination of the spin rate, but, however, requires dedicated photometric equipment at the ground station. Furthermore, these observations can only be made during night time, and for limited time spans where the satellite is illuminated by the Sun. This method was applied for AJISAI in Japan only in the frame of a few campaigns.

AJISAI was put into orbit with an initial spin rate of 40 rpm, and with the spin axis parallel to the Earth's rotation axis. With the method of photometric timing an axial rotation of 0.67 Hz was measured after launch [5], slowing down to 0.57 Hz by October 1997 [2].

In the present study AJISAI's spin rate has been investigated using the full rate kHz SLR observations of the Graz laser station and was determined to be 0.5064 Hz in July 2005. The main reason for this slowdown is the eddy current resulting from an interaction between the satellite's metallic parts and the Earth's magnetic field [2].

While standard SLR measurements are usually done at a 5 or 10 Hz repetition rate, the SLR station Graz was upgraded and is operating a 2 kHz laser system since October 2003. Due to the capability of detecting return pulses with as few as a single photon, the return rate from AJISAI comes close to 100 %, even with the low energy per shot 400  $\mu$ J) of the Graz SLR system. The 2 kHz repetition rate produces up to 1 million measurements per AJISAI pass, which has a duration of typically 16 minutes. This amount of data represents a very dense temporal sampling of the satellite's rotating surface, which allows an accurate determination of the spin parameters.

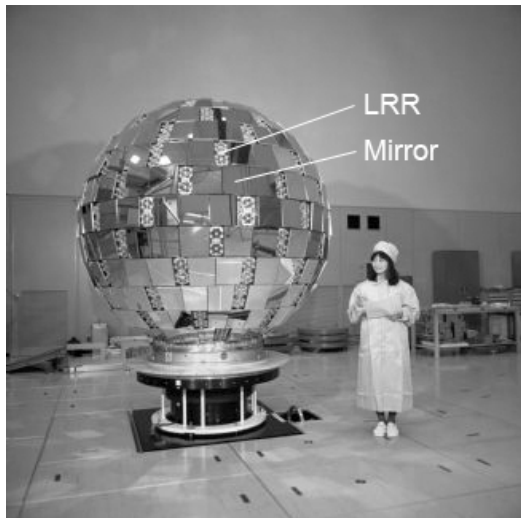


**Fig. 1.** Geodetic satellite AJISAI.

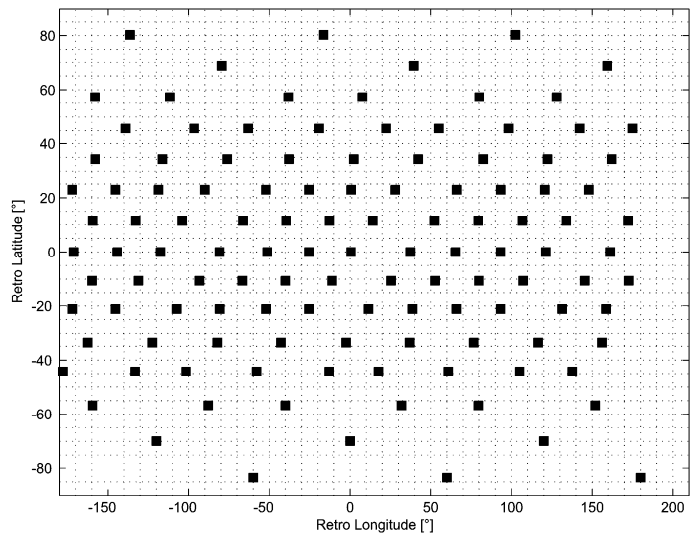


**Fig. 2.** Schematic distribution of the LRR panels

The LRR panels are almost uniformly distributed over the surface, arranged in 15 latitudinal rings [2]. There are 5 rings with 12 LRR's, 4 rings with 9 LRR's, 2 rings with 6 LRR's, and 4 rings with 3 LRR's each. The schematic distribution of these LRR panels in terms of latitude and longitude is shown in Fig. 2.

### Ranging Simulations

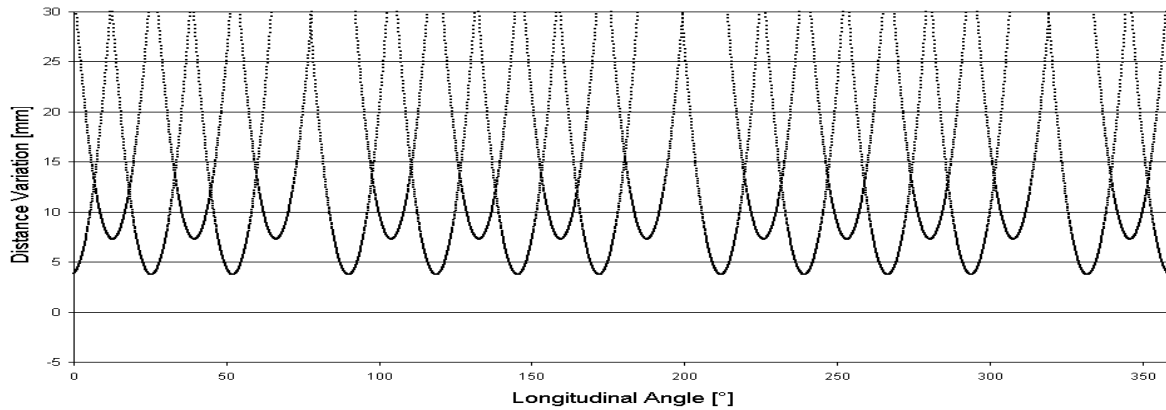
Due to the axial rotation of AJISAI and the well separated reflector panels, the distance from the observer to each panel varies periodically. The periods are given by the spin rate of the satellite and the number of panels of the involved ring. The amplitudes depend on the dimension of the sphere, the distance between the panels and on the incidence angle of the laser beam. Based on the known location of each reflector panel on AJISAI [6], a ranging simulation was made which clearly shows the expected periodic distance variation.

Fig. 3 shows a full 360° rotation viewing with an incident angle of  $-18.125^\circ$  from the satellite's equator, which contains 12 reflector panels, consisting of 3 groups with 4 panels each. The distances between these 3 groups are slightly larger than the distances between the panels within each group (Fig. 2). The resulting pattern shows the corresponding peaks, with 3 larger gaps (at  $100^\circ$ ,  $220^\circ$  and  $340^\circ$  longitude) in between.

### Spectral analysis of kHz data

In order to verify these simulation results, using the Graz kHz SLR measurements, we calculated a reference orbit from the standard SLR predictions and subtracted the calculated value from the measured distance. A low order polynomial was approximated and subtracted from the residuals in order to remove the remaining low-frequency part (approx. a few minutes in time) of the observations, but keeping the high-frequency variations (less than a few seconds) originating from the rotating reflector panels.

Fig. 4 shows range residuals for a 2 s interval (1 full revolution) of a routinely observed AJISAI pass.. The residual plot clearly shows the bigger gaps (longer ranges) due to the larger distances between the 3 groups as well as small variations in



**Fig. 3.** Simulated distance variations of LRR panels at a laser beam incidence angle of  $-18.125^\circ$  latitude. The non-symmetric LRR arrangement (Fig. 2) causes the slightly irregular distribution in both the simulation (Fig. 3) and in the ranging residuals (Fig. 4).

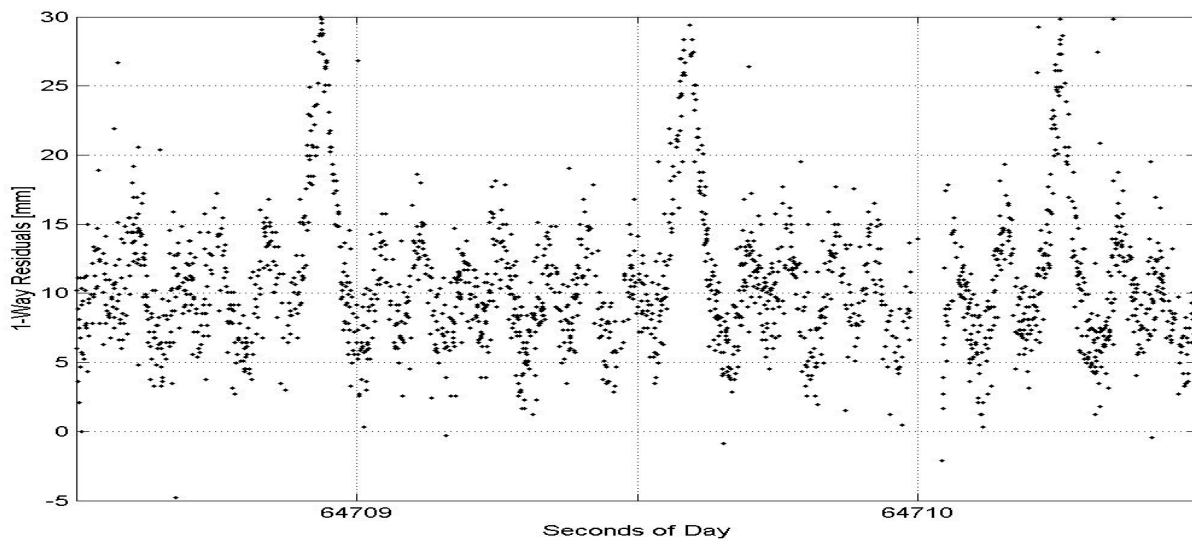


**Fig. 4.** Full rate 1-way range residuals during one full rotation of AJISAI (DOY 122/2005) for comparison with the simulation shown in Fig. 3

between due to 2 different rings. This residual analysis coincides well with the corresponding simulation shown in Fig. 3.

#### **Frequency Analysis using FFT versus Lomb**

Usually, SLR systems do not reach a 100 % return rate, even in good weather conditions. Due to the resulting gaps, the measurements are in general not equidistant in time and therefore the Fast Fourier Transform (FFT) method cannot be directly applied for a frequency analysis. In order to use FFT for the given AJISAI range residuals, the data gaps may be interpolated, but, however, this may induce new frequencies and decrease the accuracy of the results [8]. In [2], the Lomb method for spectral analysis of non-uniformly distributed data was suggested as a useful alternative. This method can handle non-equally spaced data and provides an approximation of the spectrum using the least-squares method.

#### **Connecting Frequencies with AJISAI Geometry**

Applying the Lomb method to the residuals of a 10 seconds interval of an AJISAI pass (see Fig. 5), a number of spectral peaks due to the distance variations can be seen clearly. The frequencies of 1.5, 3.1, 4.6 and 6.1 Hz are multiples of AJISAI's basic

spin rate of about 0.5105 Hz in January 2005, and the number of LRR panels (3, 6, 9 or 12) of the involved ring. The higher frequencies of 7.57, 9.09, 10.60 and 12.12 Hz are generated by simultaneous contributions of LRR of two or more adjacent rings. For instance, the clear spectral peak at 12.12 Hz in Fig. 5 cannot be associated with any single ring, but is produced by the combination of two 12-retro rings.

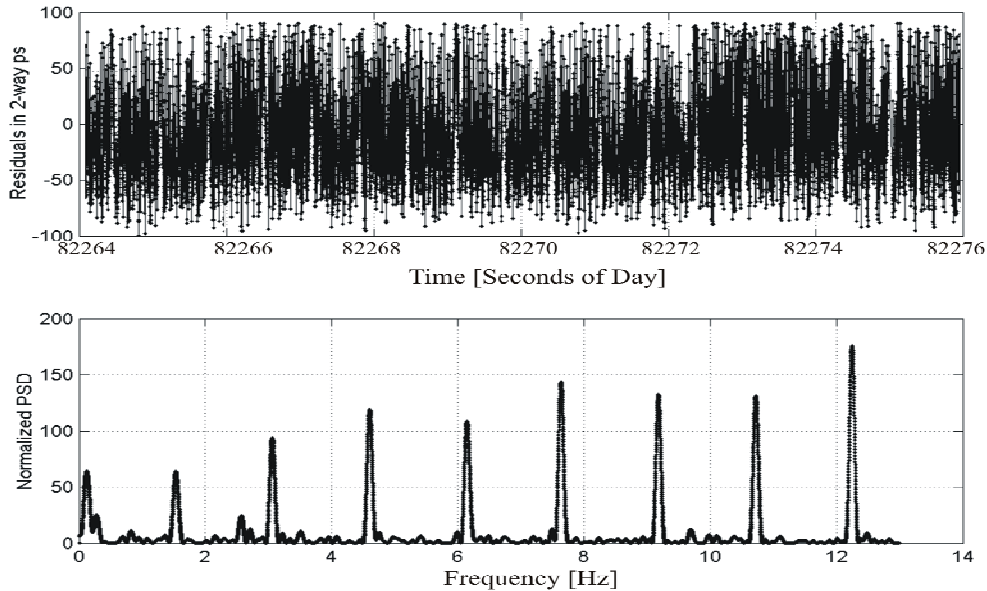


**Fig. 5.** *Twelve seconds interval of 2-way residuals in time and frequency domain (DOY 019/2005, multiple rings visible).*

### Spin rate slow down

It was shown that each calculated frequency corresponds to a specific number of LRR panels. The ratio between frequency and the number of panels of the corresponding ring gives the exact spin rate of AJISAI. The frequency generated by the 3 LRR rings was not used for spin rate calculations, because they generate lower spectral power and lower resolution than the 6, 9 or 12 LRR rings.

For the frequency analysis we selected only passes with high data density ( $> 300$  k returns) observed between 2003/10 and 2005/06. From these passes we used only data of a 1.5 minutes interval centered at the closest approach, containing more than 40 k returns, in order to keep the computation time within reasonable limits (a 3 GHz PC still needed 5 days to analyze the 195 selected passes).

Because the measured spin rate is an apparent spin rate it was corrected for the apparent effect in order to get the sidereal spin rate (see details below). The resulting spin rates for this time span show a well defined slow down rate of 0.0077497 Hz / year (Fig. 6), coinciding well with AJISAI's spin rate slow down calculated for 1997-1999 [2].

### Apparent Spin and Spin Direction

The apparent spin rate of a satellite observed at any site on Earth is affected by the axial spin as well as by its orbit around the Earth and by the Earth rotation itself. Therefore the apparently measured spin has to be corrected for these effects, in order to obtain the sidereal spin of AJISAI.

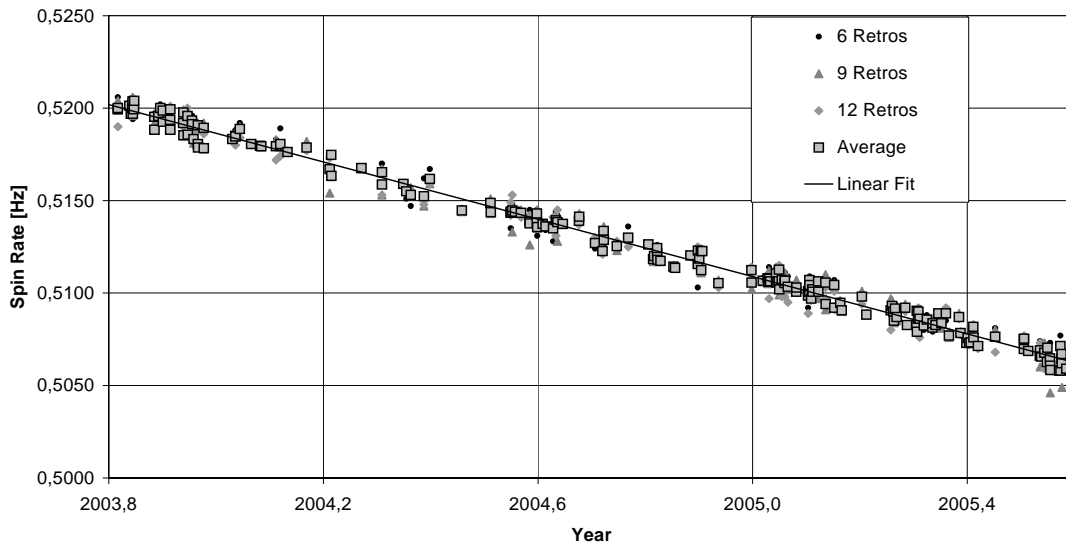


**Fig. 6.** AJISAI spin rate decrease determined from the averages of 6, 9 and 12 retro ring spin rates for 195 passes between 2003/10 and 2005/06. The linear fit to these average values yields a slow down rate of 0.0077497 Hz / year, with a standard deviation of 0.000403 Hz.

As an example, we calculated the spin rate of an AJISAI pass of 2005/01/19 (again for a period of 1.5 minutes around the closest approach). However, in this case, we selected only short slots of 12 seconds (containing at least 5000 residuals), calculated the spin rate with the same approach as above, then shifted the slot time by 6 seconds, and repeated the procedure.

This results in a clearly visible – apparent – increase of the spin rate near the maximum elevation ( $71.9^\circ$  for this pass) as shown in Fig. 7, where the values are given together with the corresponding calculated apparent spin rate. The clearly visible outliers at about 82050, 82150 and 82250 seconds can be correlated with according ring transitions, identifiable by detailed analyses of the residuals. The results confirm the high sensitivity of kHz SLR data for the determination of satellite spin rates.

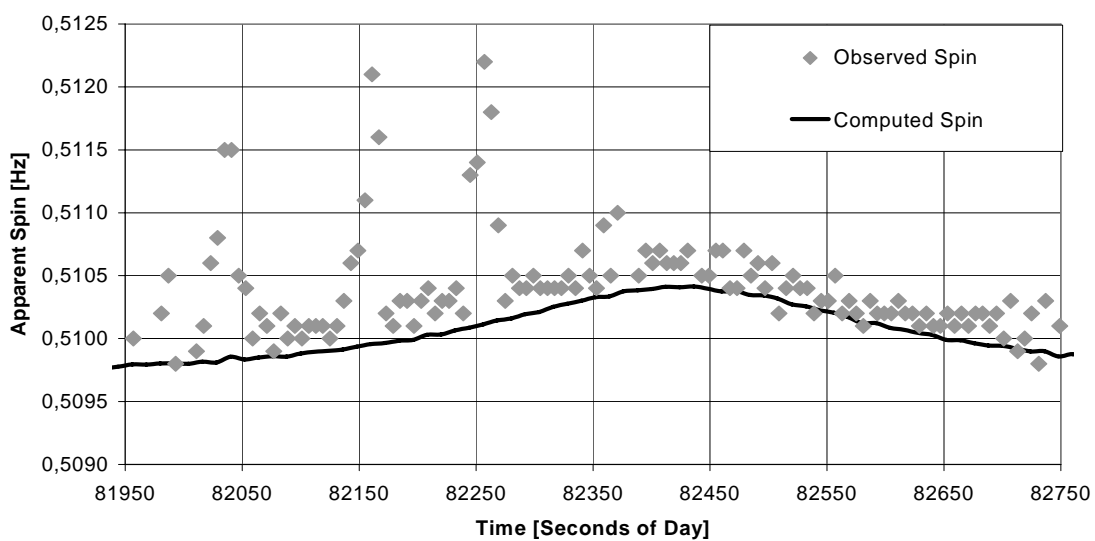


**Fig. 7.** Apparent spin motion as observed from the SLR site. Measured rates (diamonds) vs computed values (solid line).

We assume that the spin direction of AJISAI a priori is not known. From sequences of observed LRR ring transitions in most passes we have evidence that the spin axis is still at least approximately parallel to the Earth axis. Because the closest approach (CA) of the selected pass was at about  $160^\circ / 71.9^\circ$  (as seen from Graz), and the apparent spin shows a slight increase (Fig. 7) at CA, we can conclude that AJISAI is spinning in a clockwise direction.

## References

- [1] T. Otsubo, J. Amagai, and H. Kunimori, "The center of mass correction of the geodetic satellite AJISAI for single-photon laser ranging", IEEE Transactions on Geoscience and Remote Sensing, Vol. 37, No. 4, July 1999.
- [2] T. Otsubo, J. Amagai, H. Kunimori, and M. Elphick, "Spin motion of the AJISAI satellite derived from spectral analysis of laser ranging data", IEEE Transactions on Geoscience and Remote Sensing, Vol. 38, No. 3, May 2000.
- [3] International Laser Ranging Service (ILRS) Home Page: <http://ilrs.gsfc.nasa.gov> .
- [4] R. Wood, T. Otsubo and R. Sherwood, "Lageos 2 spin rate and orientation", [http://cddisa.gsfc.nasa.gov/lw13/docs/papers/target\\_wood\\_1m.pdf](http://cddisa.gsfc.nasa.gov/lw13/docs/papers/target_wood_1m.pdf)
- [5] T. Kanazawa, "Determination of the rotation phase angle and the rotation period of AJISAI(II)" in Proc. 70th meeting Geodetic Soc. Of Japan, Kyoto, Japan, 1988, pp. 51-52.
- [6] T. Uchimura, Personal communication, July 2005, ( [uchimura.takashi@jaxa.jp](mailto:uchimura.takashi@jaxa.jp) )
- [7] M. Sasaki and H. Hashimoto, "Launch and observation program of the experimental geodetic satellite of Japan", IEEE Transactions on Geoscience and Remote Sensing, Vol. GE-25, No. 5, September 1987.
- [8] N. R. Lomb, "Least-squares frequency analysis of unequally spaced data", Astrophysics and Space Science 39, p. 447-462, 1976.

## New Methods to Determe Gravity Probe-B Spin Parameters using Graz kHz SLR Data

Georg Kirchner, Daniel Kucharski, Elena Cristea

1. Austrian Academy of Sciences, Institute for Space Research, Graz.

Contact: [Georg.Kirchner@oeaw.ac.at](mailto:Georg.Kirchner@oeaw.ac.at) ; [Walter.Hausleitner@oeaw.ac.at](mailto:Walter.Hausleitner@oeaw.ac.at) ;  
[Elena.Cristea@oeaw.ac.at](mailto:Elena.Cristea@oeaw.ac.at)

### Abstract

*Using kHz data of the SLR station Graz, spin parameters of the satellite Gravity Probe B (GP-B) are derived; these include spin period and its change over a 1.5 year period, as well as spin direction, and spin axis orientation. The results are compared to the actual data sets - as determined by the GP-B mission itself – thus allowing independent confirmation of the kHz SLR derived results.*

### Introduction

GP-B was launched on April 20<sup>th</sup>, 2004, into a polar orbit at 640 km altitude. During its measurement phase, the spacecraft was spinning slowly - with about 77.5 seconds / revolution - around its central axis, defined by a telescope at one end, and the laser retro reflector (LRR) array at the other end. Its orientation was maintained always to point with high accuracy to the star IM-Pegasus; the direction to this star is measured with the on-board telescope with a stability of 0.1 milliarcseconds per year [1] (ed.).

The LRR array (Fig. 1) on GP-B consists of 8 retro reflectors in a ring-like formation, and a central LRR [2]. While such an arrangement only spreads standard SLR measurements, the high resolution of kHz SLR allows to scan the single reflectors, to identify their motion due to the spin of the satellite, and to derive all GP-B spin parameters from kHz SLR data.

### Spectral Analysis of kHz Slr Data

The spectral analysis of kHz SLR data is based on residuals obtained by subtracting the calculated, predicted orbit, from the measured distances. Fitting a low order polynomial to these residuals allows elimination of outliers, but keeps the oscillating signal of the eight rotating LRR's (Fig. 2, top).

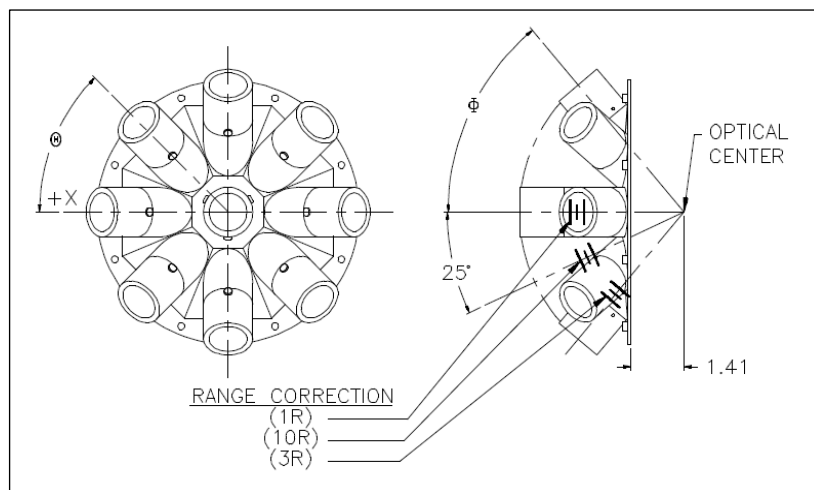


**Fig. 1:** GP-B Laser Retro Reflector (LRR) Design

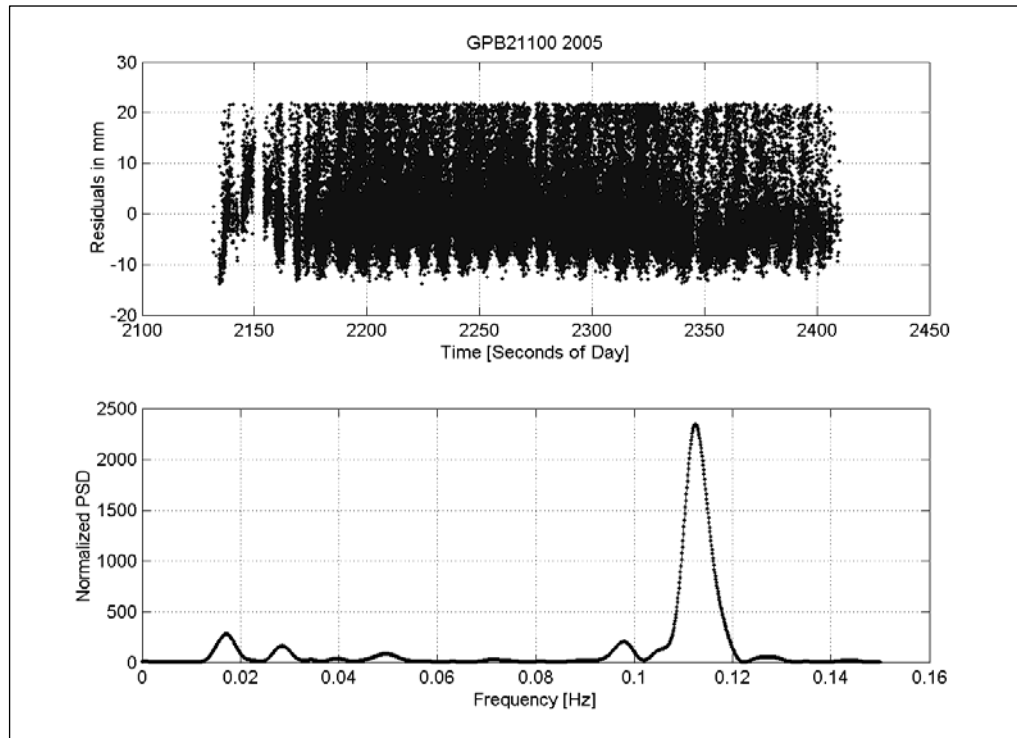


*Fig. 2: Residuals of a 280 seconds segment of a GP-B pass of DOY 211/2005 (top); frequency spectrum generated by these residuals (bottom).*

The Lomb method of spectral analysis was suggested in [3] alternatively to the Fast Fourier Transform (FFT), allowing for non-equally spaced data, as it is the case for such SLR measurements. The FFT could still be used if the data gaps were interpolated, but this would introduce unwanted frequencies. Therefore the Lomb method was preferred.

Taking into account the known inertial spin period of GP-B (77.5 seconds per revolution) during phase A (Fig. 3), and the 8 retro reflectors per revolution, we selected passes with at least 100 seconds to analyze a minimum of 10 oscillations, to get reliable results for the spectral power (Fig. 2, bottom).

This spectral power varies from pass to pass, with the data gaps and the length of the pass being the main corrupting factors. The analysis has been performed also on selected intervals of the longer passes, with high data density, as an additional verification of the frequency obtained for the complete pass.

### Spin Period Trend

From all GP-B passes measured by Graz kHz SLR, we selected those with more than 50,000 returns per pass. Applying the Lomb analysis to these passes, we found three different regions of spin periods after the initialization period, as soon as SLR measurements started (Fig. 3, top): phase A: from 10.08.2004 until 6.09.2005, the mean spin period was about 77.5 seconds; phase B: the spin period changed to about 125 seconds; after 11.01.2006 (phase C), the spin period analysis shows an unstable behavior, as expected after termination of the active phase of the GP-B experiments (Fig. 3, top). Comparing the SLR derived spin periods with the GP-B based data set for phase A (Fig. 3, bottom), the RMS of the differences is 4.99 seconds.

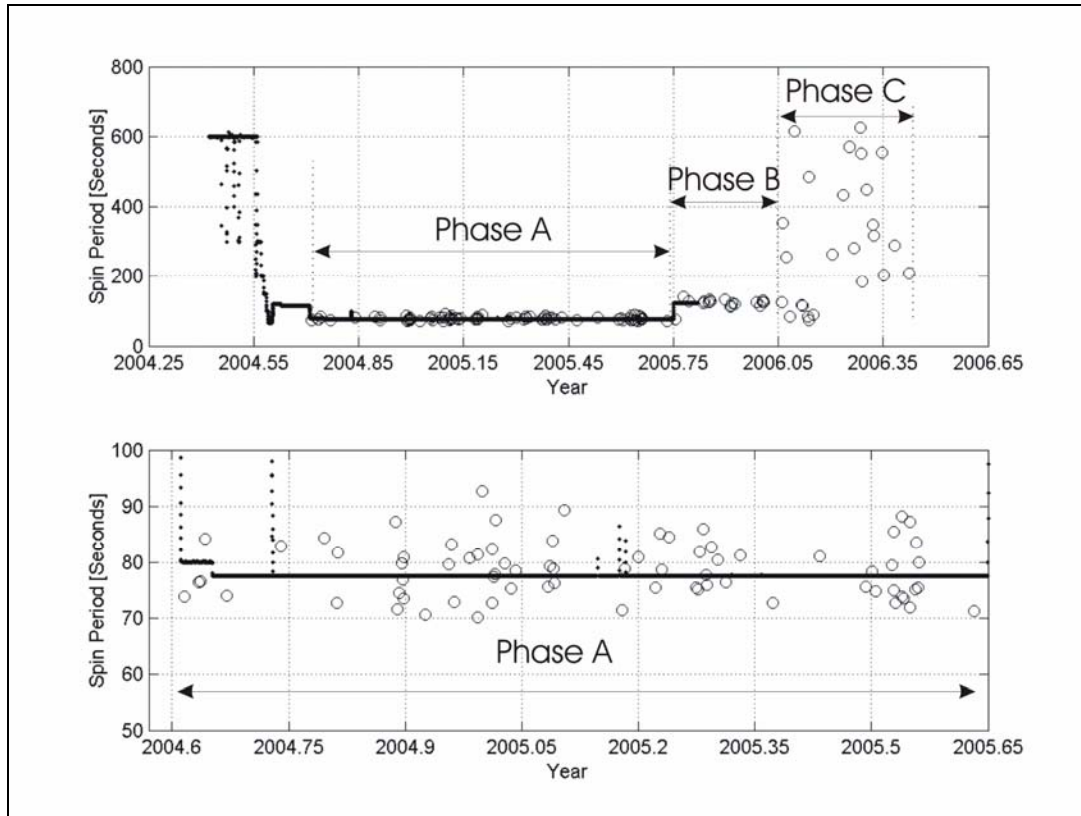


**Fig. 3.** GP-B spin period variations. Dots indicate spin periods as measured on-board; circles (o) show results of kHz SLR spectral analysis. Bottom: Expanded view for phase A, showing RMS of 4.99 seconds.

### Apparent Spin

Although the spectral analysis already yields clear results – coinciding with the GP-B on-board measured data sets (Fig. 3) -, the accuracy is not as expected: the frequency peak (Fig. 2, bottom) is well defined, but rather broad; and the RMS of the differences between kHz SLR based periods and the on-board spin measurements (Fig. 3) amounts to rather high 4.99 seconds for phase A.

Simulating the measured GP-B passes, using all known parameters (GP-B orbit, Earth rotation, fixed pointing of GP-B to IM-Pegasus, inertial GP-B spin period as measured by the spacecraft itself, geometry of the retro reflectors, as well as their range corrections, etc.), the influence of the apparent spin - the satellite’s spin as observed from Earth – was identified as the main reason (Fig. 4). GP-B’s spin period is about 77.5 seconds; because the satellite moves along its orbit considerably during this time, the apparent spin period for even the short part (151 seconds) of the pass in Fig. 4 changes from initial 72.8 seconds (9.1 x 8 retro reflectors) to 70.4 seconds (as determined from peak-to-peak distances; Fig. 5). This change in apparent spin period is the main reason for the mentioned inaccuracies in the spectral analysis. In addition, the change of the incident angle of the laser beam causes a decrease of the “modulation depth”, as indicated by the line in Fig. 4.

### Spin Period Determination Using Simulation

Due to the low spin rate of GP-B, it is not possible to apply the apparent spin directly to the spectral analysis results, as it has been done in [4]; we therefore checked other

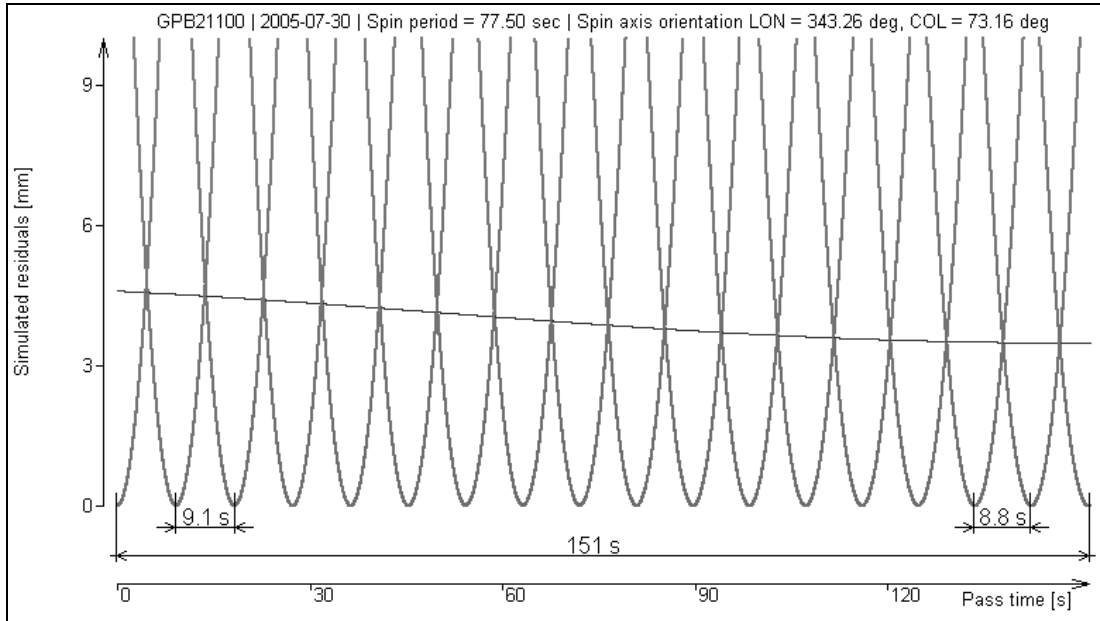


**Fig. 4.** Simulation of GP-B pass DOY 211/2005; spin period slightly changing due to apparent spin. The line shows the decreasing “modulation depth” during the 151 seconds.

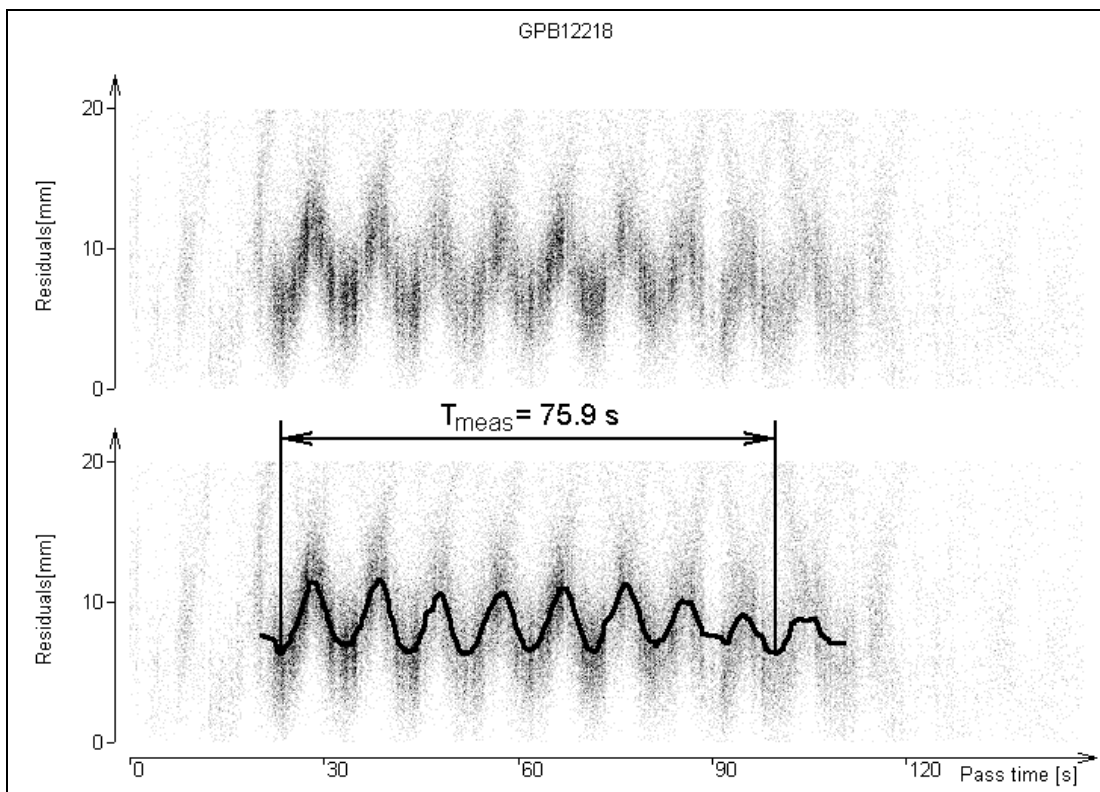


**Fig. 5a:** GP-B pass of DOY 122 / 2005, Top: Residuals; about 79200 points in 151 s; bottom: solid line: averaging; 75.9 s from first to last peak ( $T_{meas}$ ).

methods to calculate more accurate, inertial spin periods for GP-B using our kHz SLR data.

The simulations, as described above, proved to be a good and powerful tool: for each measured pass, we determined the time period from first to last peak (Fig. 5a,  $T_{meas}$ ); the same pass was simulated also (Fig. 5b,  $T_{sim}$ ); however, the inertial spin period of

GP-B was used here as parameter, varying its value from  $-50$  to  $-100$  seconds, and from  $50$  to  $100$  seconds, in steps of  $0.01$  seconds. If the estimated and the true inertial spin periods coincide, the measured and the simulated  $T$  values for the same epoch times should be the same. In Fig. 6, the differences  $T_{meas} - T_{sim}$  for 100 phase A passes are plotted, allowing for both spin directions. The zero-crossings of these differences determine the inertial GP-B spin periods.

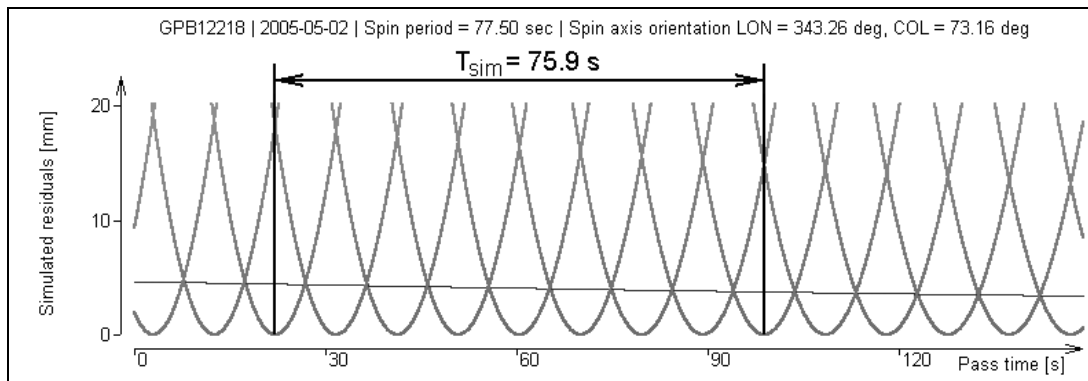


**Fig. 5b:** Simulation of same pass of DOY 122 / 2005:  $T_{sim}$  is same as  $T_{meas}$  at same epoch time, when simulating with inertial spin period of 77.50 seconds.

Applying this method to 86 GP-B passes of phase A (selected to contain at least 5 peaks), the resulting spin period values coincide well with spin data as measured by GP-B (Fig. 7a); the accuracy of the resulting inertial spin period is improved now, with an RMS value of 0.98 seconds (Fig 7b).

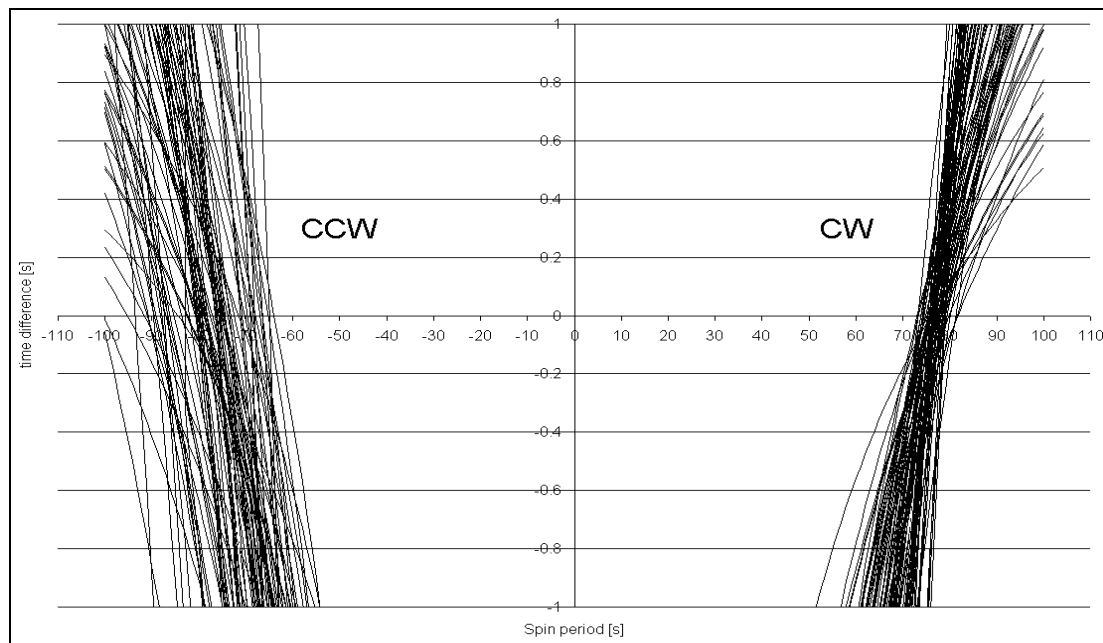


**Fig. 6:** Differences between  $T_{meas}$  and  $T_{sim}$  for 100 passes of phase A; CCW (left) and CW (right) spin directions have been simulated.

### Determination of Spin Direction

We define clockwise (CW) and counter clockwise (CCW) spin direction here as the spin of the spacecraft when looking on the LRR in pointing direction of GP-B. This spin direction of GP-B is a priori not known to us. To determine it using the kHz SLR

data, both spin directions were simulated (Fig. 6).

The results in Fig. 6 indicate that GP-B spins CW, because the spread of the result here is much less than for the CCW simulation.

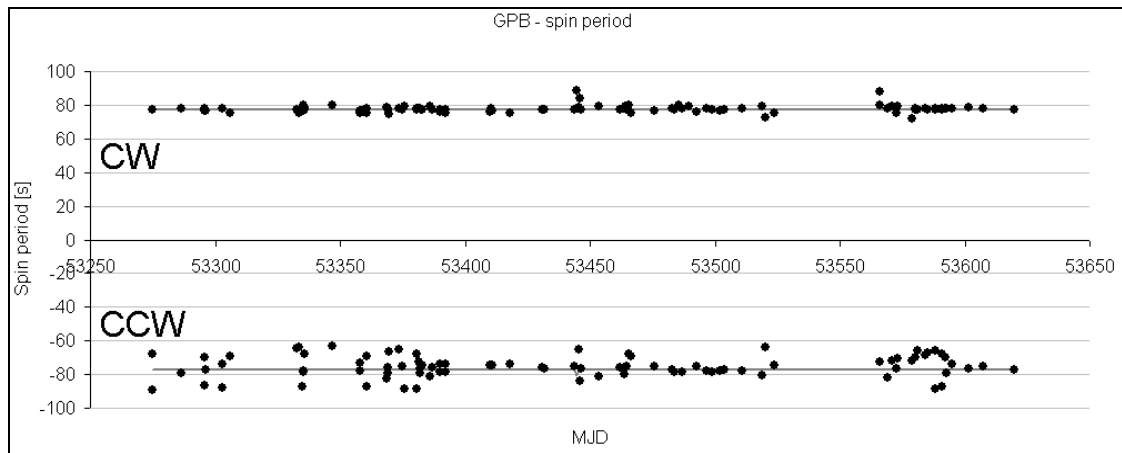


**Fig. 7a:** GP-B spin period for 86 passes during phase A; positive values are for CW spin, negative for CCW spin assumed; solid lines at  $\pm 77.5$  seconds indicate results of on-board spin measurements.

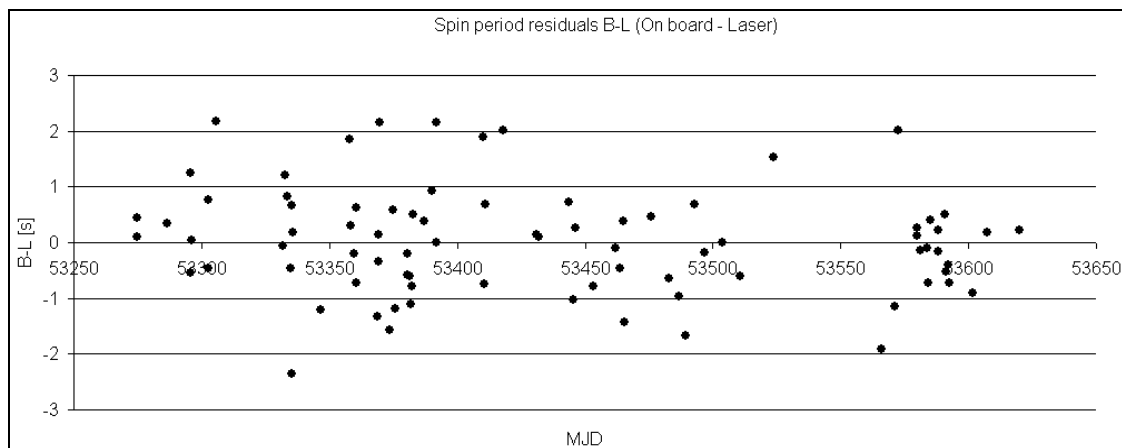


**Fig. 7b:** Spin period for 86 passes of phase A with at least 5 peaks: differences to on-board spin period measurements; RMS of differences is 0.98 seconds.

### Determination of Spin Axis

Due to their periodically varying distances as seen by the SLR measurements, the eight laser reflectors generate specific patterns within the return data set, with a “modulation depth” depending on the incident angle between laser beam and GP-B’s axis (Fig. 8).

This change of the modulation depth within the pass can be used to evaluate the incident angle (Fig. 8, bottom) and thus at least one orientation angle of the satellite. However, this method proved to be more inaccurate than expected, mainly due to the limited resolution of the modulation depth determination; the instrumental jitter of about 3 mm RMS of the Graz kHz SLR system for GP-B is not really adequate to determine the modulation depth variations of 0 to 6 mm with sufficient accuracy.

Looking for a more suitable method to determine spin axis, the comparison between simulations and measurements once more proved to be appropriate. For this purpose, the returns from the 9<sup>th</sup> or central retro reflector, which are vaguely visible in a few

passes, were used additionally (Fig. 9). Fitting a parabola to these returns, and determining the minimum value of the oscillations of the other 8 retro reflectors (Fig. 10), allows to fix the minimum distance between the upper and the lower curve (D), and the corresponding epoch time.

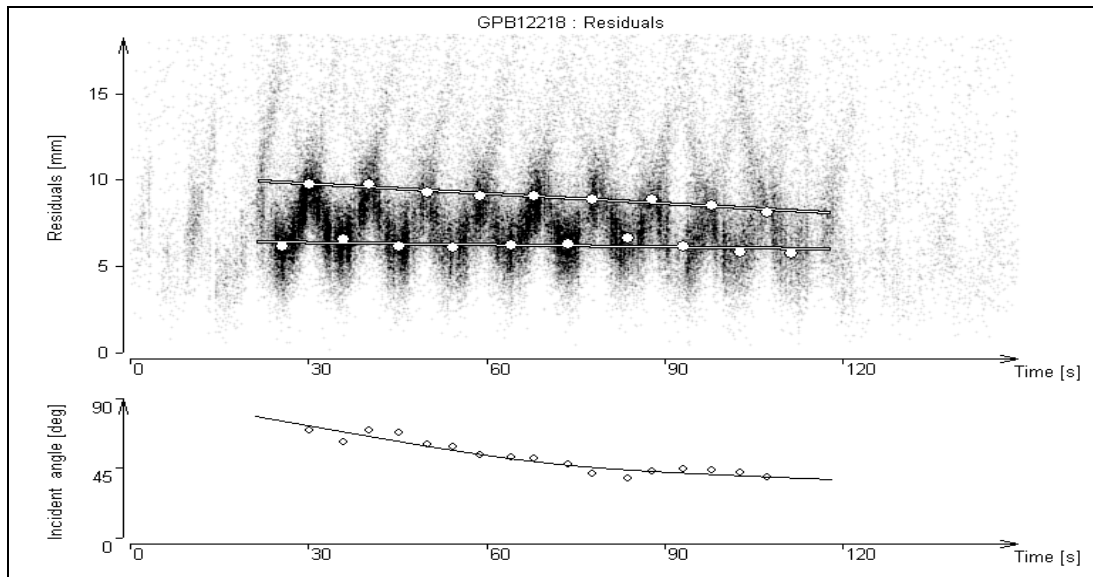


**Fig. 8:** GP-B pass of DOY 122 / 2005: “Modulation depth” decreases during the pass (top); applying the known geometry of the retro reflectors, the incident angle of the laser beam can be determined (bottom).

Running now simulations for this pass, spin axis longitude and colatitude (i.e. spin axis direction) were varied in steps of  $1^\circ$  each; for each spin axis direction, the spin period was calculated with the same method as described above. The goal was to find a combination spin period and spin axis direction, so that epoch time differences (between 9<sup>th</sup> retro parabola minimums of measurement and simulation) and range differences D (between simulations and measurements) are zero or close to zero.

Fig. 11 plots these differences between simulations and measurements; on the X-axis the differences in epoch time, on the Y-axis the differences in the distances D are shown; each line (set of points) represents solutions for different spin axis longitudes, and each point on these lines represents a solution for different spin axis colatitudes. The lowest line indicates a longitude of  $320^\circ$ , step size is  $1^\circ$ ; zero for epoch and range differences means that the correct spin axis angles have been used in the simulation, as well as the correct inertial spin period; using this rough graph, the approximate longitude solution is between  $340^\circ$  and  $341^\circ$ , and the approximate colatitude between  $73^\circ$  and  $74^\circ$  (Fig. 11, left).

Using these values as boundaries for a more detailed simulation run with step sizes of  $0.1^\circ$ , we get about  $341.4^\circ$  for longitude, and  $73.3^\circ$  for colatitude, at an inertial spin rate of 77.42 seconds (Fig.11, right).

Two more GP-B passes were analyzed in this way, and the spin axis parameters determined; all results were coinciding with the on-board values with good accuracy (Table 1): standard deviation of the differences is  $1.6^\circ$  for colatitude,  $1.77^\circ$  for longitude, and 0.6 seconds for spin period.

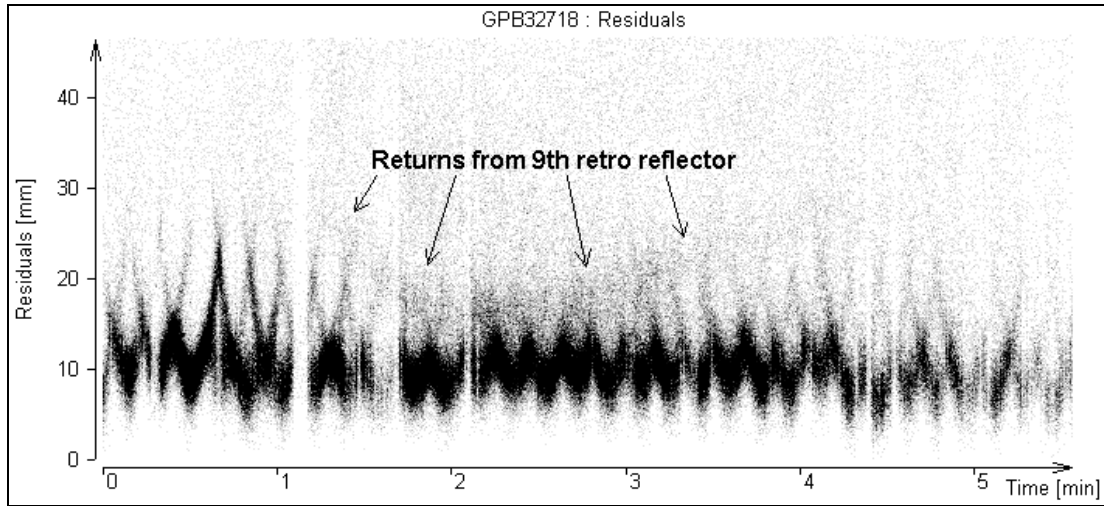


**Fig. 9:** GP-B pass of DOY 327/2005: Vaguely visible returns from 9<sup>th</sup> retro.

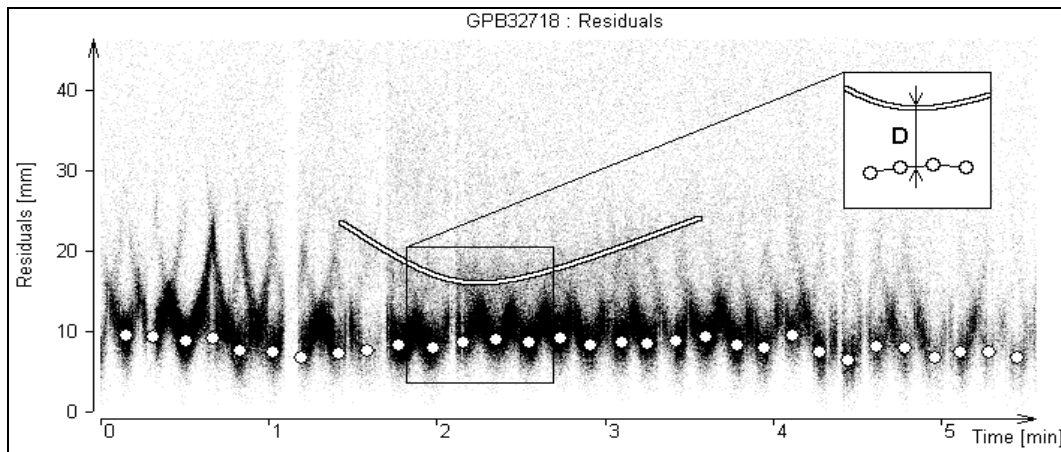


**Fig. 10:** Parabola fitted to 9<sup>th</sup> retro returns, gives epoch time and value of “D”

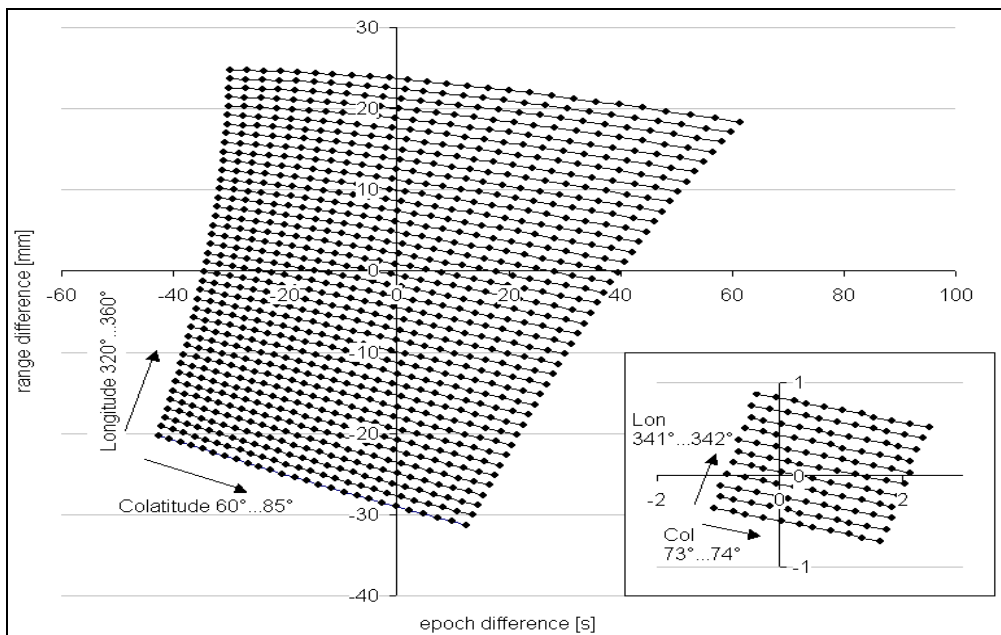


**Fig. 11:** Simulations for Longitude and Latitude values of GP-B Spin Axis, varied in 1°-steps (left); same with 0.1° steps around ZERO (right)

**Table 1: Comparison of complete spin parameters for 3 GP-B passes.**

Pass date	Colatitude [deg]		Longitude [deg]		Spin period [s]	
	Calculated	IM-Pegasus	Calculated	IM-Pegasus	Calculated	On board measurements
2004-11-22 18:06	73.3	73.16	341.4	343.26	77.42	77.48
2005-04-04 9:23	71.7	73.16	339.9	343.26	76.30	77.53
2005-07-29 1:48	74.9	73.16	341.2	343.26	77.05	77.48

## Conclusions and Future Aspects

Using only kHz SLR data to derive spin parameters of satellites, opens completely new possibilities and areas for present and especially for future missions; larger separations between the individual elements of the retro reflector arrays automatically would increase the resulting accuracy. Suitable LRR geometries - to allow the identification of returns from single retro reflectors - enables complete spin axis determination from kHz SLR measurements. To get a more uniform distribution of returns from retro reflectors at different locations on the satellite, it would be easy to attenuate all echoes to the single photon level, resulting e.g. in the GP-B case in a much clearer identification of the 9<sup>th</sup> retro returns (Fig. 9, 10).

As more such kHz SLR stations will be operational in the very near future (Herstmonceux in the UK, SLR 2000 in USA), the availability of kHz SLR data sets will increase, allowing even more accurate spin parameters determination. As the satellite's payload for SLR is only a passive retro array, without any need for power supply or transmission bandwidth – and without major concerns about operational life time - , it might be a good main or backup device to obtain independently spin parameters of satellites, in addition to its main task of precise orbit determination via SLR.

## Acknowledgment

The authors would like to thank Paul Shestopole of Stanford University for providing the on-board GP-B spin rate data.

## References

- [1] GP-B Home Page: <http://einstein.stanford.edu/>
- [2] LRR Manufacturer Home Page: <http://www.iteinc.net/>
- [3] T. Otsubo, J. Amagai, H. Kunimori, and M. Elphick, "Spin motion of the AJISAI satellite derived from spectral analysis of laser ranging data", IEEE Transactions on Geoscience and Remote Sensing, Vol. 38, No. 3, May 2000.
- [4] G. Kirchner, W. Hausleitner, E. Cristea, "AJISAI Spin Parameters Determination using Graz kHz Satellite Laser Ranging Data", IEEE Transactions on Geoscience and Remote Sensing, Vol. 45, No. 1, January 2007.

---

## LAGEOS-1 spin determination, using comparisons between Graz kHz SLR data and simulations

D. Kucharski<sup>1</sup>, G. Kirchner<sup>2</sup>

1. Space Research Centre, Polish Academy of Sciences, Borowiec, ul. Drapalka 4, 62-035 Kornik, Poland.
2. Space Research Institute, Austrian Academy of Sciences, Lustbuehelstrasse 46, A-8042 Graz, Austria.

Contact: [kucharski@cbk.poznan.pl](mailto:kucharski@cbk.poznan.pl) / Tel. +48 61 817 01 87;  
[Georg.Kirchner@oeaw.ac.at](mailto:Georg.Kirchner@oeaw.ac.at) / Tel. +43 316 873 4651

### Abstract

*kHz SLR data contains unique information about the measured targets; this information allows e.g. determination of spin parameters (spin period, spin direction, spin axis orientation) of various satellites, using various methods for different spin periods / satellites: Spectral analysis for spin periods of 2 s (AJISAI (Kirchner et al, 2007)), simulations for spin periods of 77.5 s (GP-B), and comparing simulation results with kHz data for very long spin periods like LAGEOS-1 (about 5000 s).*

*For the long LAGEOS-1 spin periods, we developed a method to calculate spin axis orientation and spin period from Graz kHz SLR data. This method is based on simulation of returns from each retro reflector, with spin period and spin axis orientation as input parameters. Varying these parameters, the simulation generates retro tracks similar to those seen in the kHz SLR data; comparing simulated and measured tracks, allows determination of spin period, and spin axis orientation. Applying this method to a set of LAGEOS-1 passes - covering a period of 178 days - shows also the slow change of the LAGEOS-1 spin axis direction with time.*

**Keywords:** *satellite laser ranging, LAGEOS-1, satellite spin*

### Introduction

LAGEOS-1 and LAGEOS-2 are identical satellites in circular orbits, about 5,900 km above Earth's surface. Both satellites are spheres with 60 cm diameter, covered with 426 cube corner reflectors (CCRs) arranged in 20 rings symmetrically with respect to the satellite equator (Fitzmaurice et al., 1977). Because the satellites are totally passive, their orbital motions are affected only by the natural perturbations. In this paper, we analyse only kHz SLR data of LAGEOS-1, due to its very low spin rate.

Perturbations can be of gravitational, non-gravitational (for example: Yarkovsky effect, Yarkovsky-Schach effect) or magnetic nature. SLR distance measurements to the satellites allow precise determination of these orbital perturbations and consequently identification of their origin. The more accurately we can determine the effect of perturbations, the more reliably we can obtain the geodynamical parameters of the Earth, and the relativistic effects in the near space (Ciufolini and Pavlis, 2004). It is expected that a detailed knowledge of LAGEOS-1 spin behaviour should improve the accuracy of such analysis, and will help to identify and confirm the source and magnitude of the (unknown) perturbations, which are introduced presently as empirical accelerations in actual models.

Up to now two methods were used to calculate spin parameters of LAGEOS satellites: frequency analysis of full rate SLR data (Bianco et al, 2001) and analysis of

photometric observations. The frequency analysis works well if the spin rate is not too low (e.g. 23.5 s for LAGEOS-2 in May 2000 gives good results in Bianco et al, (2001), but is not applicable anymore for larger spin periods, like the expected 5000 s for LAGEOS-1 in 2004 (Andres et al., 2004). Photometric measurements of LAGEOS-1 spin parameters were performed until 1997, when they were ceased because of a too low spin rate. In total, 57 photometric observations were carried out for this satellite (Andres et al., 2004), which allowed verification and improvement of the models of its spin motion. The most accurate model describing changes in the parameters of LAGEOS-1 spin is LOSSAM (Andres et al., 2004). According to this model, LAGEOS-1 started the third phase of its life in 1999, where the influences on spin parameters by magnetic, gravitational and non-gravitational torques are of the same order of magnitude. Bertotti and Iess (1991) have predicted that at this phase LAGEOS-1, having reached an extremely low spin rate, will start tumbling more and more, rapidly changing orientation of the spin axis, with chaotic dynamics.

### SLR Graz kHz laser measurements

Usually, SLR stations measure distances to satellites with laser repetition rates of 5 or 10 Hz. The Graz SLR station was the first station to measure with a laser repetition rate of 2 kHz (Kirchner and Koidl, 2004). Because of the very short 10 ps laser pulses, and the single photon detection system, the measurements are not only very precise (2–3 mm single shot RMS), but also allow identification of retro – reflector tracks in the data, easily seen due to their slightly different distances.

After a successfully measured satellite pass, the differences between measured and predicted distances are calculated. From these residuals the systematic trends are eliminated, e.g. by using polynomials; plotting these residuals (Fig. 1), different tracks from various retro-reflectors (or groups of them) can be identified easily. Residuals of nearer satellite prisms are on the bottom (satellite front), and residuals originating from more distant prisms are more towards the top in this figure.

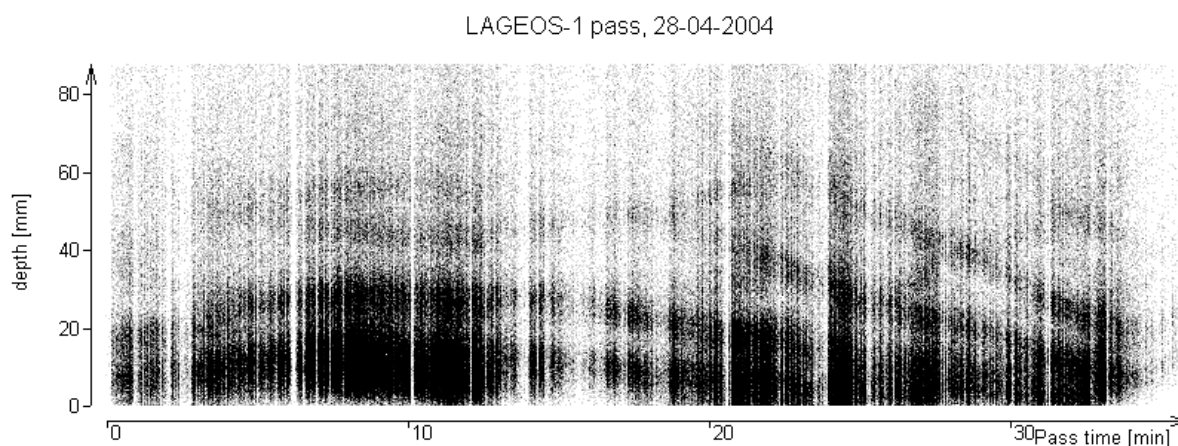


*Fig. 1. Range residuals of a LAGEOS-1 pass, measured by Graz kHz SLR system, 28-04-2004, 2 a.m. (P1)*

The residuals plotted in Fig. 1 refer to a LAGEOS-1 pass of April 28<sup>th</sup>, 2004 (P1). During the 35 minutes of the pass, more than 500,000 returns were measured. The majority of the returns come from the nearest retro-reflectors; the detection probability for returns from more distant retro – reflectors on the satellite’s sphere is decreasing. The reason for this effect is the geometry between the incident laser beam and the CCR. Total internal reflection of LAGEOS-1 optical retro - reflectors depends

on the angle between the incident laser beam and optical axis of the CCR as well as on the azimuth angle giving the direction of the incident beam about the normal to the front face of the CCR (Arnold, 1979; Otsubo and Appleby, 2003).

### Identification of the single prism tracks – the method

The tracks in Fig. 1 are due to the passage of retro – reflectors through the field of view of the telescope; thus they contain information on the satellite spin (Arnold et al., 2004). To recognize spin parameters out of the geometry of these spin tracks we developed a new method based on simulations of SLR measurements. The model used in these simulations is divided into two parts. The first part (macro-model) contains the Earth’s rotation, the site position in ITRF2000 (Altamimi et al., 2002) and the orbital motion of the satellite. The second part (micro-model) contains the retroreflector-array arrangement and the range correction function (Fitzmaurice et al., 1977). In present study the model does not contain CCR transfer function (Arnold, 1979). The range correction function describes the photon’s time of flight delay when the photon is going through the glass of the CCR. This correction depends on refractive index of the glass and the angle of incidence.

The geometry of range residuals distribution depends on spin parameters of the satellite: spin axis orientation and spin period. To calculate spin parameters it is necessary to determine epochs of the spin tracks and their tilt angles. The pass shown on Fig. 1 contains horizontal and tilted CCR tracks.

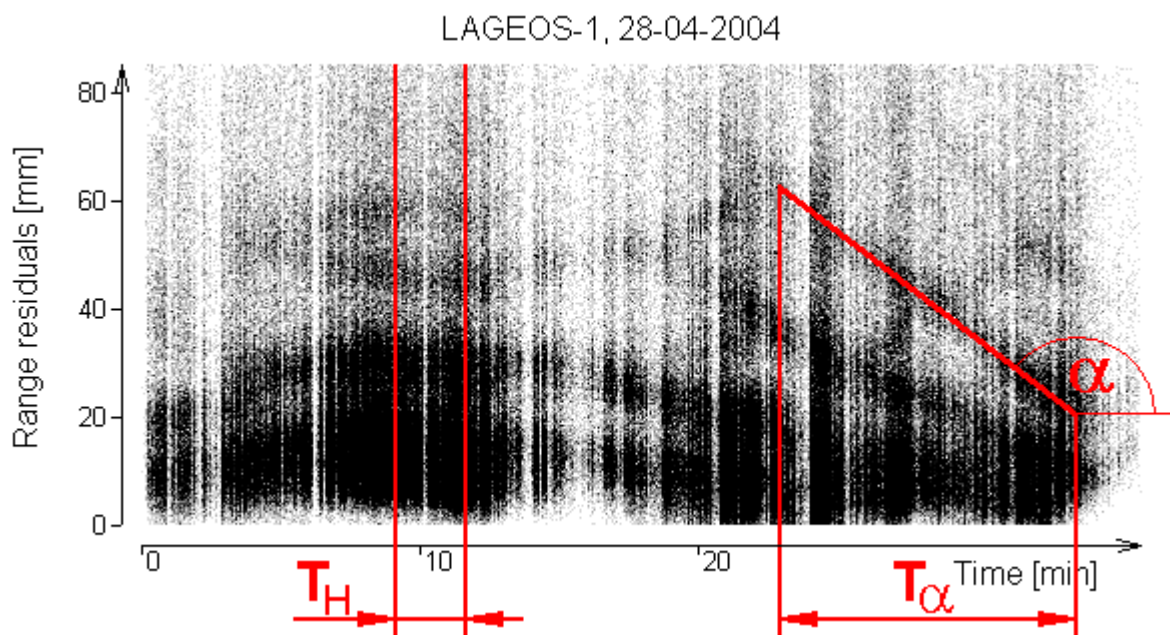


**Fig. 2.** Range residuals distribution:  $T_H$  - epoch range of horizontal tracks,  $T_\alpha$  - epoch range of  $\alpha$ -tilted track, pass start 28-04-2004, 2 a.m.

By using simulations it is possible to generate range residuals for every CCR distributed over the visible satellite’s surface. Figure 3 presents examples of simulated CCR’s trajectories for different spin parameters of the pass presented on Fig 2. For both charts spin period remains the same, but the second case was generated for different spin axis orientation: both angles (longitude and co-latitude) were increased by  $10^\circ$ . The geometry of the CCRs trajectories is very sensitive for spin parameters.

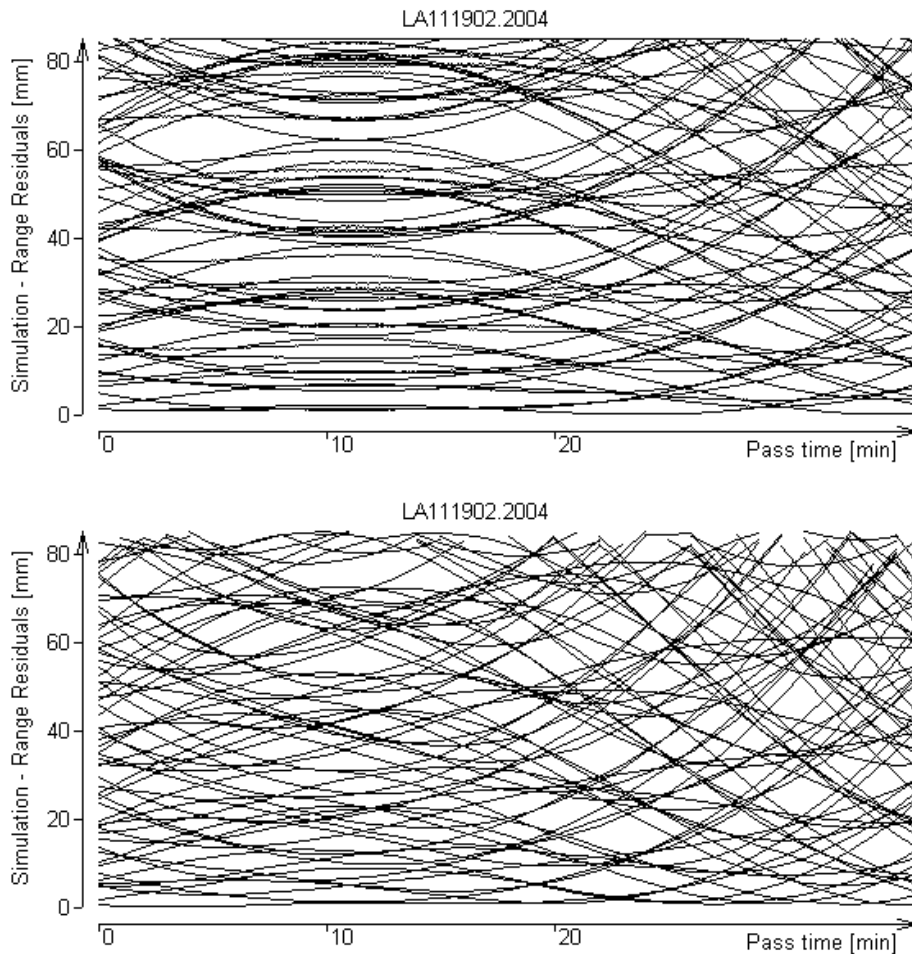


**Fig. 3.** Simulations of the CCR's trajectories for the pass presented on fig 1, for both cases spin period stays constant, but spin axis orientation for the bottom situation is shifted by  $10^\circ$  in longitude and colatitude.

### Spin parameters determination

The LAGEOS-1 pass shown in Fig. 2 (P1) shows two significant kinds of range residuals distribution - horizontal and  $\alpha$ -tilted - which allows determination of the satellite's spin rate. LOSSAM predicts a spin period of about 5,000 s for LAGEOS-1 for the first half of 2004. Therefore we simulated range residuals for the pass P1 for spin periods  $T_S$  from  $-8,000$  s to  $-3,000$  s and from  $3,000$  s to  $8,000$  s with 50 s steps, and for all spin axis orientations with  $1^\circ$  steps.

Figure 4 shows results of simulations for all possible spin axis orientations (longitude and colatitude), for a spin periods of  $T_S = -6,000$  s and  $T_S = 6,000$  s. The top chart presents amounts (right scale - color bar) of  $\alpha$ -tilted spin tracks in  $T_\alpha$  epoch range for all spin axis orientations, the middle chart presents amounts of flat spin tracks in  $T_H$  ( $T_\alpha$  and  $T_H$  are given for the pass presented on Fig. 2). During all simulations the algorithm was searching for simulated  $\alpha$ -tilted CCR tracks within  $\alpha \pm 5$  deg. The bottom charts (Fig 4) show the sum of the top and the middle charts, evaluated pixel by pixel; as can be seen, for some spin axis orientations both kinds of spin tracks can exist. Such common spin axis orientation areas are the biggest for  $-6,000$  s (counter-clockwise rotation) and  $6,000$  s (clockwise rotation), therefore those spin periods were chosen for further investigation.

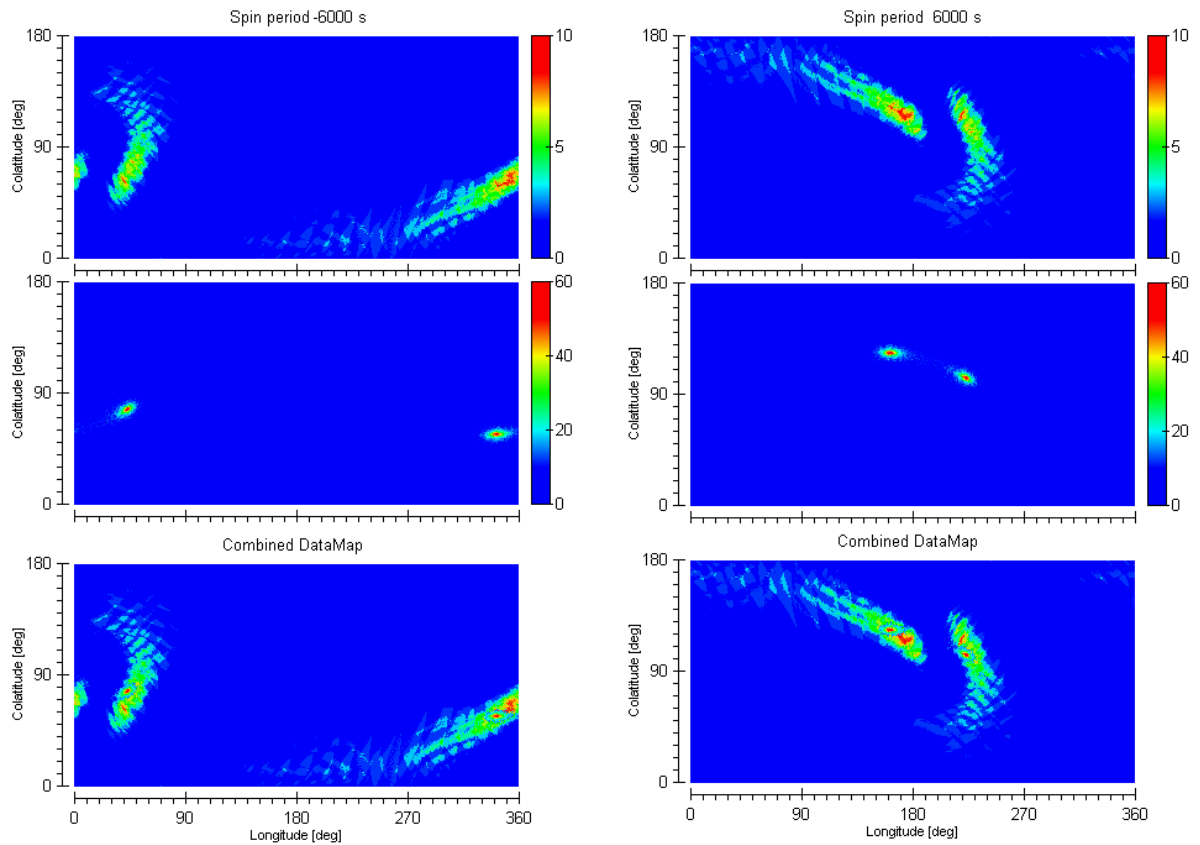


**Fig. 4.** Simulation results for spin period of  $T_S = -6000$  s (left) and  $T_S = 6000$  s (right); Top: Amounts of  $\alpha$ -tilted spin tracks; Middle: Amounts of horizontal spin tracks; Bottom: Sum of Top and Middle, pixel-by-pixel

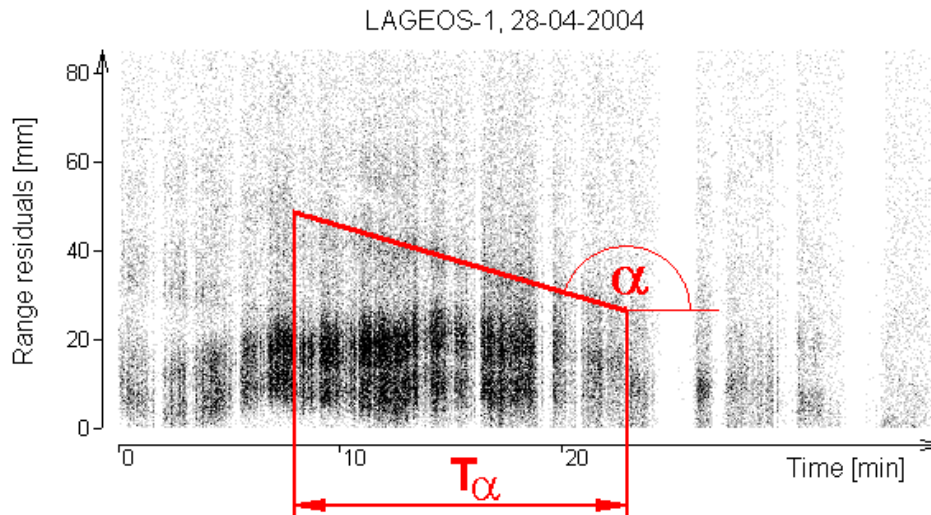


**Fig. 5.** Range residuals of LAGEOS-1 pass tracked 12 hours later (P2), pass start 28-04-2004, 2 p.m.

For both spin periods it is possible to detect two different solution areas (Fig. 4, the bottom charts), due to the symmetrical arrangement of the CCRs over the surface of the satellite. After processing four solutions were obtained, two for CW and two for CCW spinning. To identify which is the real one we used a LAGEOS-1 pass (P2) tracked 12 hours after the main pass (P1) – Fig. 5.

Supposing that spin parameters of the satellite will not change significantly during 12 hours (from pass P1 to pass P2), one of the solutions determined for P1 should be the solution also for pass P2. Figure 6 presents three charts; the top one shows spin axis orientation solution for P1 and the middle chart for P2. The bottom chart shows common area of solutions for these two passes (pixel by pixel comparison); the appropriate spin axis orientation for both P1 and P2 was calculated as a mean value of this area.

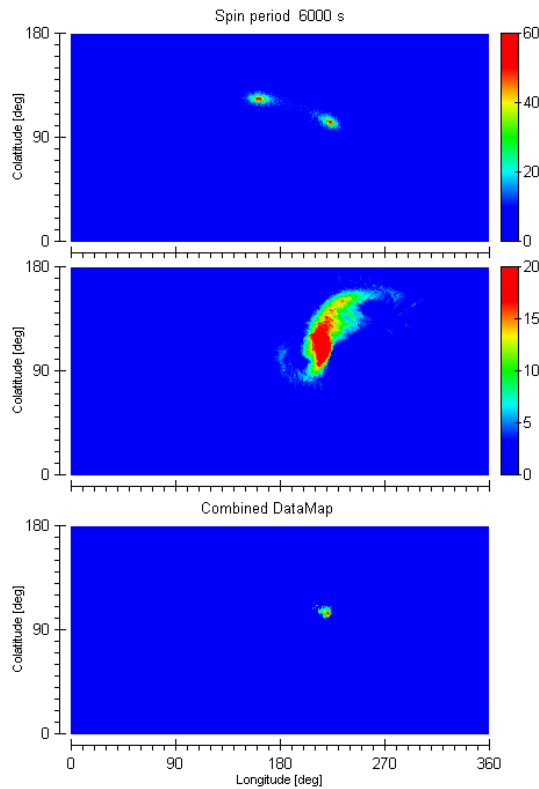


**Fig. 6.** Simulation - results; Top and middle: solutions for passes P1 and P2; Bottom: common area of the solutions

Using this pass-to-pass method reduces the amount of possible solutions from four to one; the spin parameters of LAGEOS-1 calculated from these two passes are: spin period (CW)  $T_S=6,000$  s, spin axis orientation: colatitude=103.8 deg, RMS=3.66 deg, longitude=224.2 deg, RMS=3.76 deg. All parameters are expressed in the J2000 inertial reference frame.

This pass-to-pass method was used to process 33 passes during 178 days of year 2004. Figures 7 and 8 present results for colatitude and longitude of spin axis orientation. The results were obtained for spin period  $T_S=6,000$  s, mean value of RMS for all colatitude results is  $RMS_{COL\_mean}=5.87$  deg, and for longitude  $RMS_{LON\_mean}=7.19$  deg.

For both angles the scatter around the fitted trend function is visible and has similar magnitude. That may be caused by inaccuracy of the used method or even by chaotic changes of the spin axis precession. The trend function of colatitude values shows sinusoidal decreasing during the investigated time period, while the longitude angle is more stable.

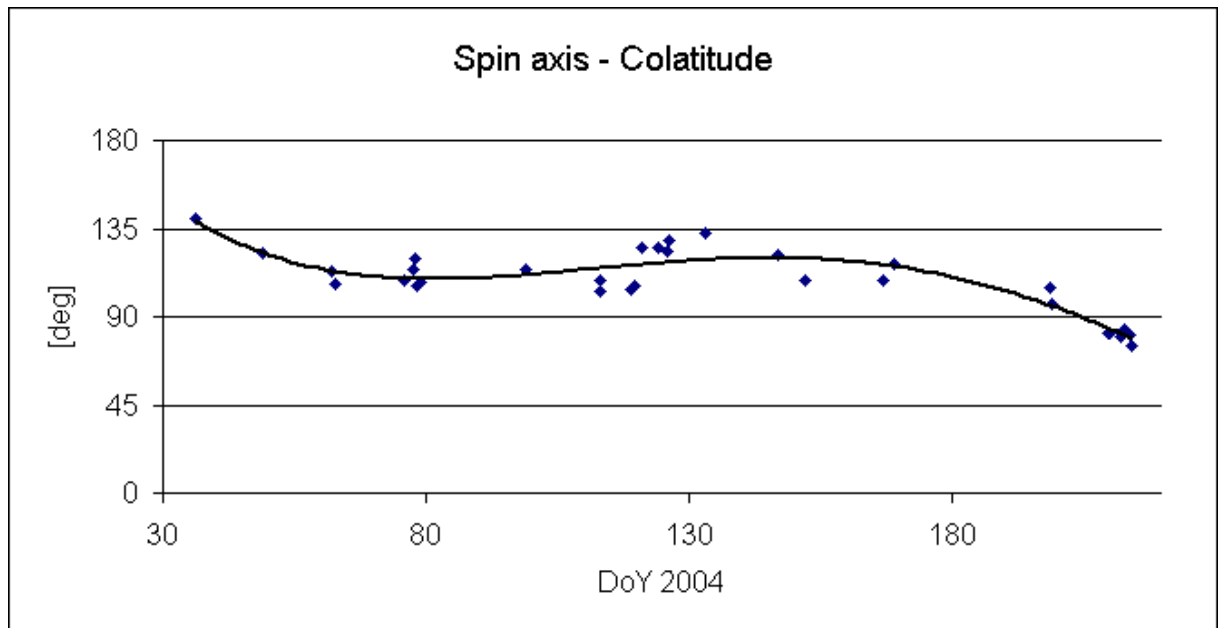


**Fig. 7.** Time-series of colatitude angle observations of the spin axis of LAGEOS-1, and trend function

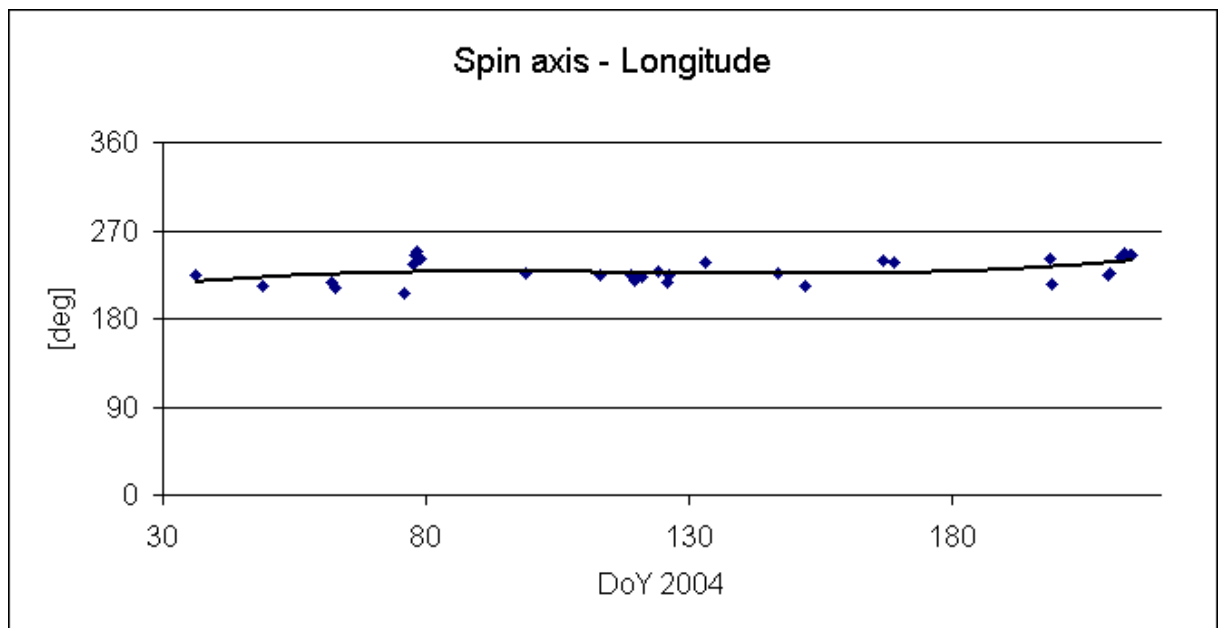


**Fig. 8.** Time series of longitude angle observations of the spin axis of LAGEOS-1, and trend function

### Conclusions

The analysis presented in this paper identifies spin tracks in kHz SLR measurements to LAGEOS-1, and uses them to fully determine the spin parameters of this very slowly spinning satellite. This was possible by identifying the geometry of the observed tracks and looking for similar geometries in simulations generated for various spin parameters. This process allows to find several possible solutions, but with the pass-to-pass method it is possible to find a single common solution for two consecutive passes. This method can be applied only when spin parameters do not change significantly between the two analysed passes. Only one out of 33 investigated

passes contains both horizontally and  $\alpha$ -tilted CCR tracks, which are both necessary to determine the spin period of the satellite. The simulation model used for presented investigation is missing CCR energy transfer function, thus obtained results contain additional error. The transfer function will be taken into account with next version of the model and then analysis process will be repeated.

The accuracy of our method is a few times worse than that of photometric measurements. However, for long spin periods kHz SLR measurements and this simulation-based method is the only source of information about spin parameters of LAGEOS-1.

kHz SLR measurements, as started for the first time at the Graz SLR station, have opened new possibilities, allowing determination of the satellite spin parameters when all other methods fail. Additionally, the expected increase of the number of kHz SLR stations in the near future will improve the accuracy of spin parameter determination by a few orders of magnitude.

### Acknowledgments

This work has been supported by the Ministry of Science and Information of Poland under grant No. 4T12E 062 29.

### References

- [1] Altamimi, Z., Sillard, P., Boucher, C. ITRF2000, A new release of the International Terrestrial Reference Frame for Earth science applications, *J. Geophys. Res.* 107(B10), 2214, 2002
- [2] Andrés, J. I., Noomen, R., Bianco, G. et al., Spin axis behavior of the LAGEOS satellites, *J. Geophys. Res.*, 109(B6), B06403, doi:10.1029/2003JB002692, 2004
- [3] Arnold, D., Method of calculating retroreflector-array transfer functions, Spec. Rep. 382, Smithsonian Astrophys. Obs., Cambridge, Mass., 1979
- [4] Arnold, D., Kirchner, G., Koidl, F., Identifying single retro tracks with a 2 kHz SLR system – simulations and actual results, 14th ILRS Workshop, 2004
- [5] Bertotti, B., and L. Iess, The rotation of LAGEOS, *J. Geophys. Res.*, 96(B2), 2431–2440, 1991
- [6] Bianco, G., Chersich, M., Devoti, R. et al., Measurement of LAGEOS-2 rotation by satellite laser ranging observations, *Geophys. Res. Lett.*, 28(10), 2113–2116, 2001
- [7] Ciufolini, I., Pavlis, E., A confirmation of the general relativistic prediction of the LenseThirring effect, *Nature*, 431, 958-960, 2004
- [8] Fitzmaurice, M.W., Minott, P.O., Abshire, J.B. et al., Prelaunching testing of the Laser Geodynamic Satellite (LAGEOS), NASA Technical Paper 1062, NASA, 1977
- [9] Kirchner G., Hausleitner W., Cristea E., "Ajisai Spin Parameter Determination Using Graz Kilohertz Satellite Laser Ranging Data", *IEEE Trans. Geosci. Remote Sens.*, vol. 45, no. 1, pp. 201-205, Jan. 2007
- [10] Kirchner, G., Koidl, F., Graz KHz SLR System: Design, Experiences and Results, 14th ILRS Workshop, 2004
- [11] Otsubo, T., Appleby, G., System dependent center-of-mass correction for spherical geodetic satellites, *J. Geophys. Res.*, 108(B4), 2201, doi:10.1029/2002JB00209, 2003

---

## Measuring Atmospheric Seeing with kHz SLR

Georg Kirchner<sup>1</sup>, Daniel Kucharski<sup>2</sup>, Franz Koidl<sup>1</sup>, Jörg Weingrill<sup>1</sup>

1. Austrian Academy of Sciences, Institute for Space Research, Graz
2. Space Research Centre, Polish Academy of Sciences, Borowiec, Poland

Contact: [Georg.Kirchner@oeaw.ac.at](mailto:Georg.Kirchner@oeaw.ac.at) ; [kucharski@cbk.poznan.pl](mailto:kucharski@cbk.poznan.pl) ; [Franz.Koidl@oeaw.ac.at](mailto:Franz.Koidl@oeaw.ac.at) ; [Joerg.Weingrill@oeaw.ac.at](mailto:Joerg.Weingrill@oeaw.ac.at)

### Abstract

*During night-time kHz SLR operation in Graz, we use an ISIT camera to see satellites, stars, and also the backscatter of the transmitted kHz laser beam (Fig. 1). This backscatter image of the laser beam shows a beam pointing jitter in the order of several arcseconds, caused by the actual atmospheric conditions (“Seeing”).*

*Using real time image processing, we determine the area of this beam pointing jitter, and derive the actual astronomical seeing values. These values depend not only – as usual for optical astronomy - on actual atmospheric conditions and on elevation of telescope, but also on the angular speed of telescope motion. In addition, the seeing values are considerably bigger (worse) during winter time, when – due to heating and poor isolation of the Graz observatory - the air above the observatory roof is significantly more turbulent than during the other seasons.*

*This beam pointing jitter due to atmospheric turbulence can reach a similar magnitude as the laser beam divergence; it spoils our pointing accuracy, affecting our return rate especially from higher satellites. To reduce these effects, we are planning to use a fast steering mirror, which is controlled by the ISIT image derived laser beam pointing offsets.*

### Introduction

The ISIT camera observes the backscatter of the transmitted laser beam; the image is transferred into the PC via a standard frame grabber. The software (written in C++) now uses the brightness of each pixel, to find out the borders of the laser beam image, and to determine the coordinates of the peak. The offset of the peak from the center (as defined by the illuminated reticle, visible in Fig. 1), is kept as a result for each processed image. This image processing at present is running with 25 Hz, and can handle each ISIT image.

The offsets of the laser beam pointing show variations in the several arcsecond range, and with frequencies between few Hz up to 25 Hz.

### Possible reasons for the Laser Beam Pointing Jitter (other than atmosphere)

To verify that this jitter in laser beam pointing is NOT caused by the laser itself, we installed a Laser Beam Monitor at the exit window of the laser box (Fig. 2).

A mirror reflects a small portion of the laser beam ( $\ll 1\%$ ) on a CCD chip; the CCD image is monitored by a PC, with up to 30 fps; for each image, the PC calculates the center coordinates (X/Y) of the laser beam, and stores single frame center coordinates and / or averaged values. This data sets (Fig. 3) show that the pointing stability of the laser at the output window of the laser box is in the order of a few microrad ( $\ll 1''$ , more or less within the measurement accuracy); there is no indication of a laser beam induced pointing jitter, as seen in the atmospheric backscatter images. The only visible effect is a very fast (few seconds) warm-up time at start of firing (Fig. 3)

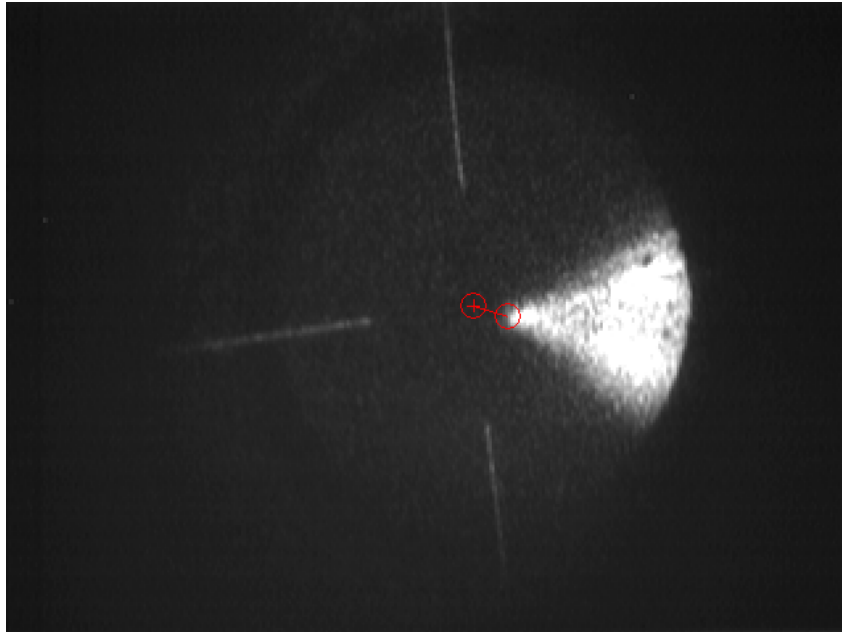


*Fig. 1: ISIT image, with laser beam backscatter, laser beam peak as determined by image processing, and its offset from the center. This offset shows a pointing jitter due to atmospheric turbulence*

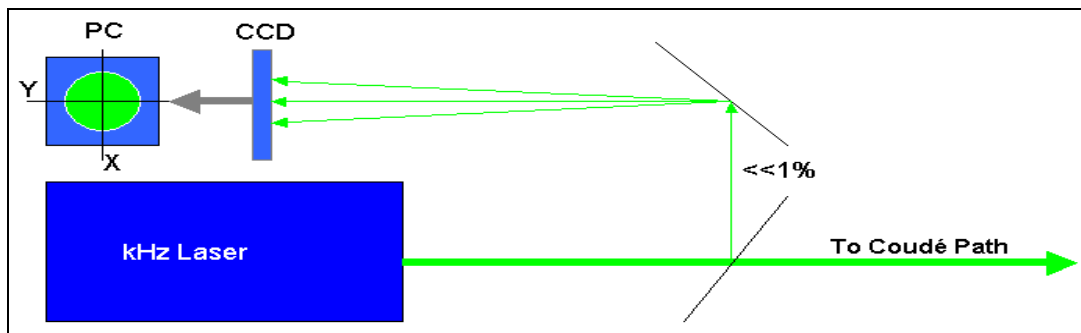


*Fig. 2: Laser Beam Monitor*

Another possibility for the observed laser beam pointing wobble is the mount itself; but tests with fixed mount showed the same wobble of the laser beam pointing.

**Laser Beam Pointing Jitter: It is due to atmosphere !**

We concluded that the Laser Beam Pointing Jitter is caused by atmospheric micro-turbulences (atmospheric “seeing”); after talking with astronomers working in Graz, we expected seeing values of about 2-4 arcseconds as an average, with expected frequencies from a few Hz up to a few 10 Hz.

However, our measurements usually showed higher seeing values, ranging from about 3” up to more than 8”; there are several reasons for that:

- The fast moving SLR telescope, instead of a more or less constant pointing (or only slow moving) astronomy telescopes; the atmospheric conditions during SLR tracking are therefore changing much faster;
- Heating of the – almost NON-isolated – observatory in cold winter nights; the leakage causes heating of the surrounding air, which heavily degrades seeing; and most astronomy work at the Graz observatory is done usually in autumn, with almost NO heating of the rooms;

- SLR in Graz is usually done down to  $10^\circ$  elevation and lower, where seeing values are increasing.

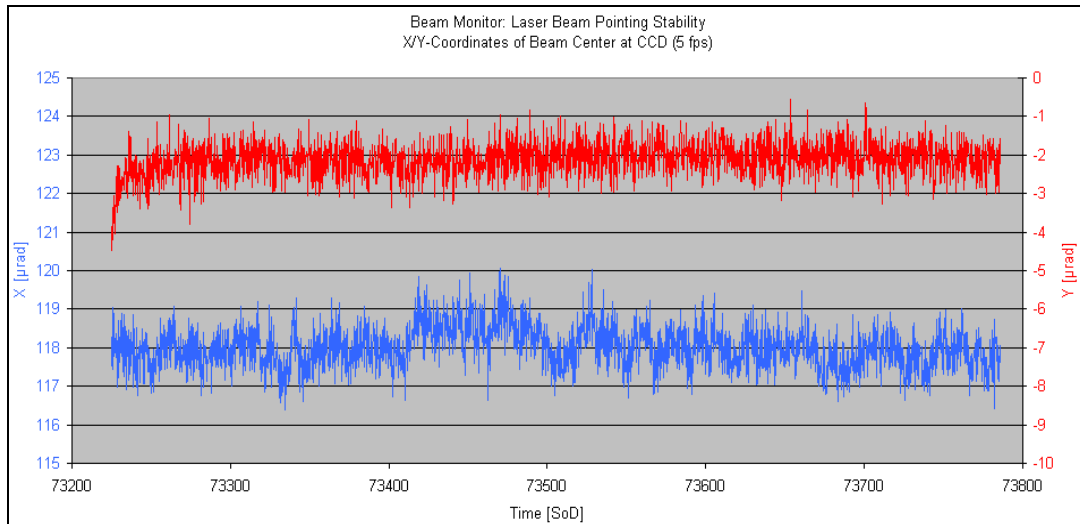


*Fig. 3: X/Y coordinates of Laser Beam Center, 10 minutes of routine SLR operation.*

### What are the effects for SLR ?

The minimum laser beam divergence of SLR Graz is about  $5''$ ; with a pointing jitter caused by seeing values up to  $3''$  to  $8''$  (and sometimes worse) the “hit rate” or pointing accuracy will decrease (Fig. 4), reducing the return rate.

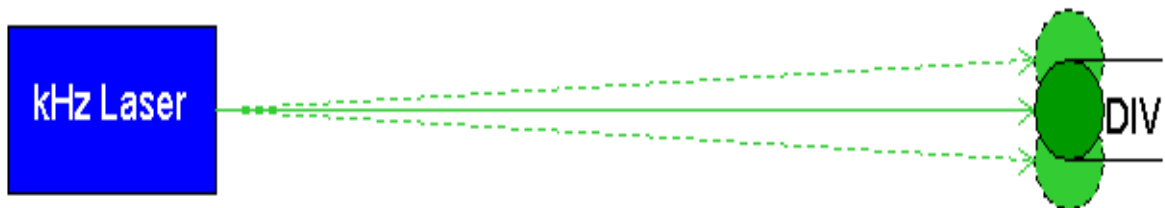


*Fig. 4: Atmospheric turbulences cause laser beam jumping*

### Verifying the Seeing Values

To check and verify the seeing values, as measured by the beam pointing jitter, we used the standard DIMM (Differential Image Motion Monitor; Hartmann – Shack) method: With an additional, standard telescope we observed e.g. the polar star; a mask with 2 small holes at a specified distance is placed at the entrance pupil of the telescope (Fig. 5); a CCD (defocused; placed with some offset from the focal plane) monitors the 2 spots created from the star light and the two holes; all images are stored on the PC.

The atmospheric turbulences cause the dual star images to move relatively to each other; this relative motion is measured in the PC, and allows calculation of the atmospheric seeing values.

A typical result of such seeing measurements is shown in Fig. 6; showing an average seeing value of  $3''$  to  $4''$ ; it was made in summer time (no heating), at  $45^\circ$  elevation (polar star) and with constant pointing (star).

### Seeing Values Derived from kHz Laser

Using the ISIT-Camera and the image processing programs- as described at the beginning - we monitored the atmospheric seeing values automatically during routine

SLR operation for several months; due to the method, we were able to collect seeing values along each tracked pass, and to correlate it with azimuth and elevation of each pass. As an example, an AJISAI pass with about  $50^\circ$  maximum elevation is shown in Fig. 7; tracking started / stopped at about  $10^\circ$  elevation; the correlation between elevation and seeing is obvious for this pass; however, other passes showed sometimes completely different values. Such a different pass is shown in Fig. 8: an ENVISAT pass, with a maximum elevation of  $<30^\circ$ , starts with the usual decrease of the seeing value with increasing elevation; however, it then shows a significant INCREASE.

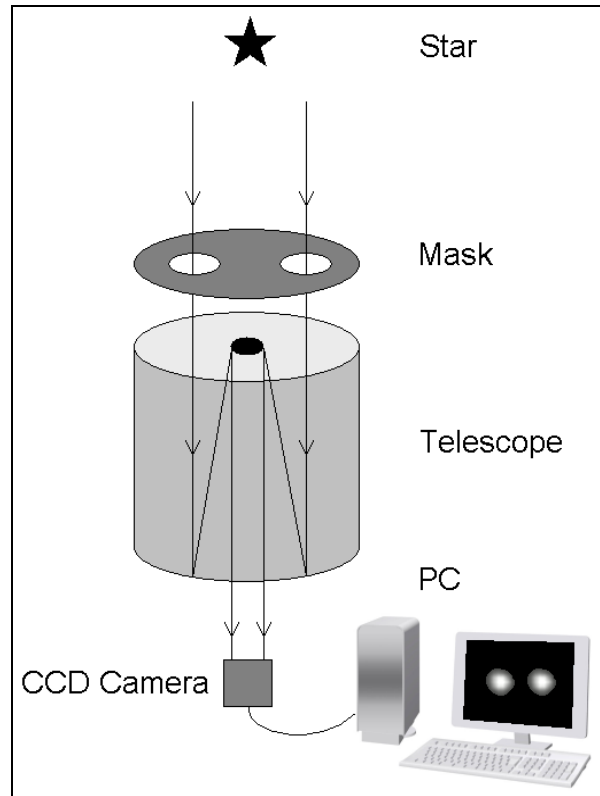


**Fig. 5:** *Differential Image Motion Monitor (DIMM) / Hartmann – Shack method.*

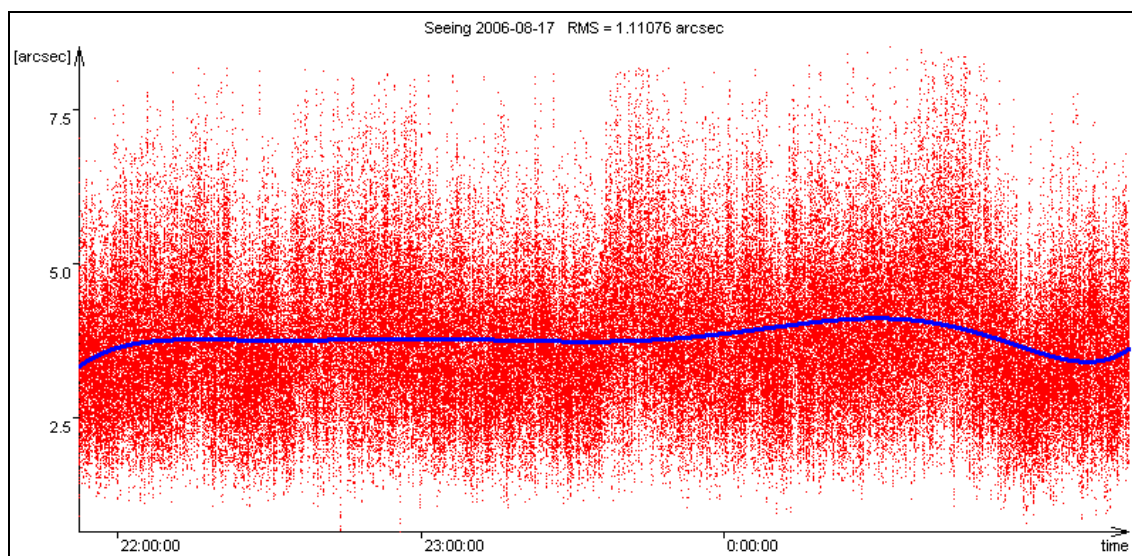


**Fig. 6:** *Seeing Values measured with DIMM: Summer night, polar star used.*

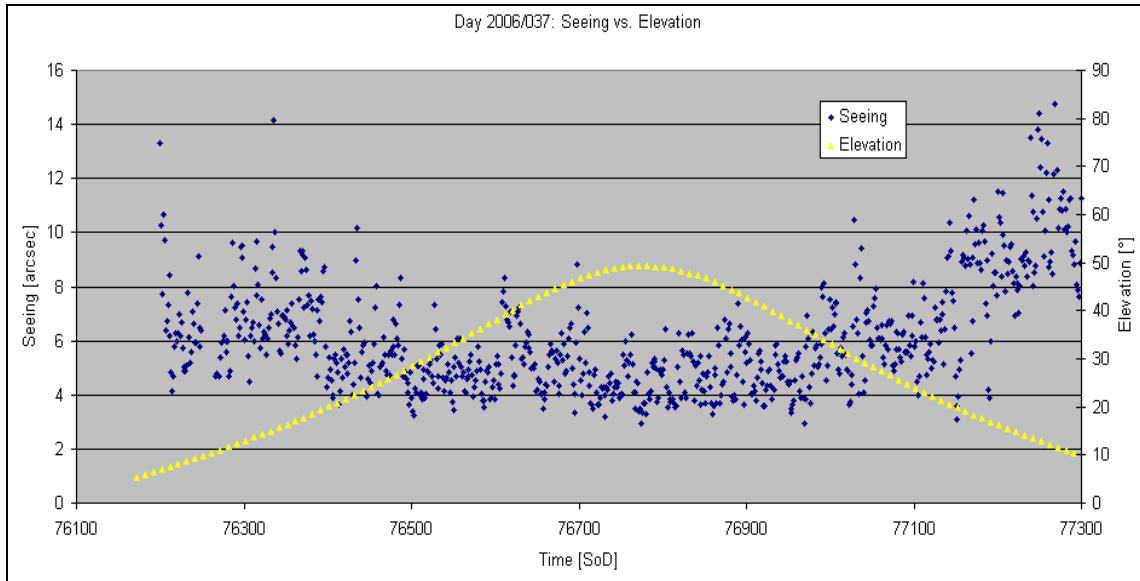


**Fig. 7.** Ajisai: day of year 2006 / Day 037: Seeing changes with elevation.

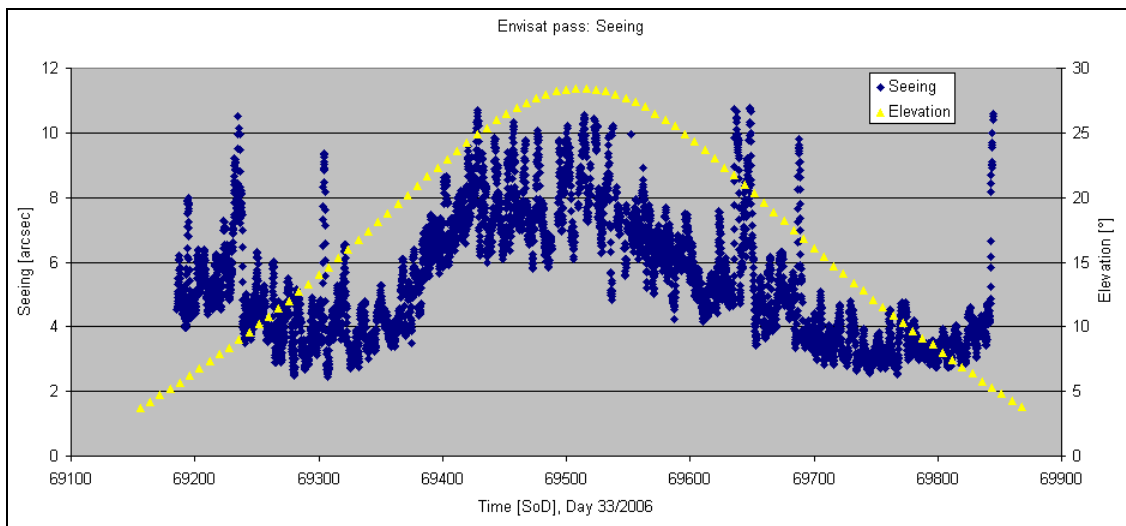


**Fig. 8:** Envisat: day of year: 33, < 30° Elevation

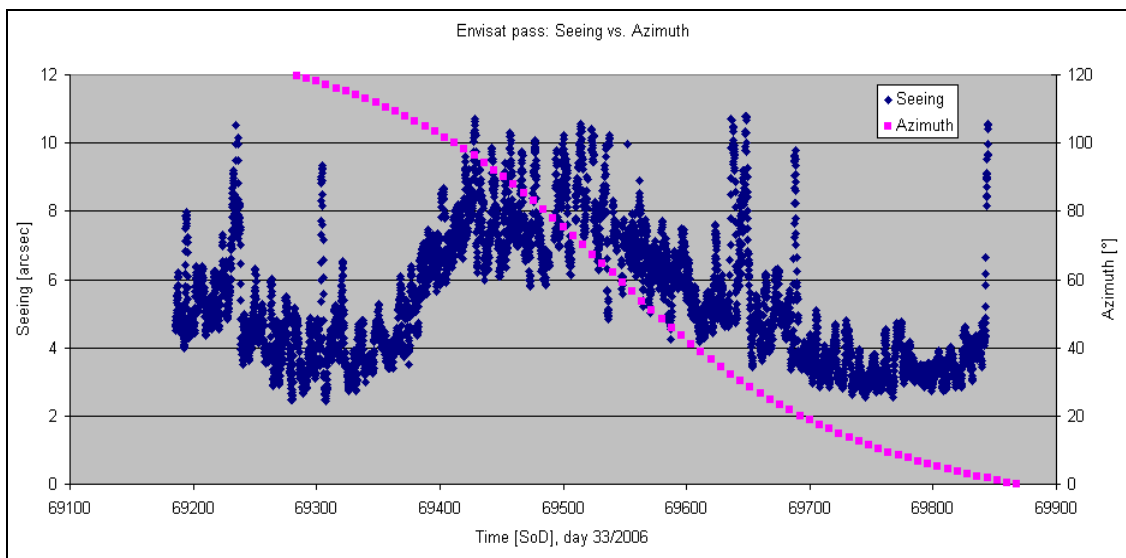


**Fig. 9:** At 90° Azimuth: => Obs. Roof, Heating Influence

The explanation for such a strange behaviour: At this time we started to track (at 90° azimuth) along / above the observatory, where the leakage of the heated building caused increasing turbulence, and hence increasing seeing values (Fig. 9).

**Future plans:**

We will continue to monitor atmospheric seeing values along the laser beam path during routine SLR operation at night; at least we should get some valuable statistics about the seeing values at the observatory (no such records exist here up to now). In addition, there are plans to install a Fast Steering Mirror (FSM) at the laser bench, to be able to compensate at least partially the beam pointing jitter, using the actual pointing offsets of the laser beam as derived from the ISIT images as control input to the FSM. The goal is to increase return rate from high satellites, like GPS, Giove etc.